FOR LOAN TO MO STAFF ONLY.

METEOROLOGICAL OFFICE
145726
- 7 MAY 1985
c
LIBRARY

ADVANCED LECTURES 1985

THE CLIMATE OF THE WORLD

BY

C K Folland and D E Parker

Advanced lectures delivered by C K Folland to the Scientific Officers Course 1-7 March 1985.

ORGS UKMO

National Meteorological Library
FitzRoy Road, Exeter, Devon. EX1 3PB

3 8078 0006 6039 1

INDEX

1. INTRODUCTION TO WORLD CLIMATE I

2. INTRODUCTION TO WORLD CLIMATE II

3. CLIMATE FORCING AND FEEDBACK PROCESSES I

4. CLIMATE FORCING AND FEEDBACK PROCESSES II

5. RECURRING NON-SEASONAL CLIMATE VARIATIONS

6. CLIMATES OF THE PAST I - EARLY EARTH TO PLEISTOCENE ICE AGES

7. CLIMATES OF THE PAST II - 15000 BP TO THE LITTLE ICE AGE

8. CLIMATES OF THE PAST III - INSTRUMENTAL PERIOD

9. CARBON DIOXIDE AND CLIMATE VARIATION

LECTURE 1 INTRODUCTION TO WORLD CLIMATE - I

Summary

This introductory lecture discusses the physical approach to climate studies. The WMO World Climate Program (1980-2000) is introduced; this program already provides a focus for many activities relating to climate research and the use of climate knowledge and data for practical purposes.

1. Introduction

There are several complementary approaches to the study of climate. A traditional image of climate is the one often presented at school. In the preface to his book 'Climatology' (9th Edition 1961) (1) the famous Reading University geographer Professor Austin Miller wrote 'The nature of the relief, the vegetation, the habits of the people, their architecture and their occupations will be attuned to the prevailing rainfall and temperature conditions and it is the response rather than the cause which the geographer wishes to know'. This is still the main approach of the many 'human' geographers who wish to use climate data to explain the development of society and industry in the context of the physical environment. It is nevertheless a legitimate use of climate data, paralleled by the wide-spread use of climate data by industry and agriculture for planning. Here understanding how climate operates is much less important than the goal of collecting and validating climate data to provide reliable analyses of that data tuned to user's needs. However a qualitative understanding of climate is still very desirable when deciding on the choice of appropriate statistics and of suitable data; nowadays many of the analyses needed are far removed from the calculation of simple climatic averages. This 'applied' climate activity is important in several branches of the Meteorological Office.

Over the last few decades, research into the physical basis of climate and more recently its variability has become increasingly feasible and productive due to developments in meteorological theory, computers and thus in meteorological models. In addition, our ability to collect and validate reliable worldwide data has considerably increased. Research into the mechanisms and behaviour of climate is essential if useful climate predictions are to become possible, especially the prediction or simulation of the consequences of increased carbon dioxide and the persistent and socially disruptive droughts endemic in parts of the tropics. In the following lectures most emphasis will be placed on the physical approach to climate.

2. What is climate?

The Scientific Plan for the World Climate Research Programme (2) provides several useful definitions:-

- Weather is the manifestation of a state of the atmosphere at a particular instant in time and the evolution of this state through the generation, growth and decay of individual transient (synoptic scale) disturbances.

- Climate is the synthesis of weather over the whole of a period long enough to establish its statistical ensemble properties (mean values, variances, probabilities of extreme events ...) and is largely independent of any (particular) instantaneous atmospheric state. A climatic state is described by these statistical properties.

- Climate change (or climate signal) is measured by the difference between mean values of a climatic parameter or statistic, i.e. the difference between climatic states.

- Climate variability is measured by the deviations of monthly, seasonal and annual values from the mean value of the climatic state established over an ensemble of such periods. The differences from the mean associated with an individual event are called anomalies.

For the purposes of these lectures a given 'climate' would normally be measured over a period of decades (30 years is a 'standard' period). Climate variability is in principle a manifestation of the variations of time-averaged weather that contribute to a given climate eg the fact that last January was markedly different to the previous January would usually reflect 'variability' but if the average temperature for the last 30 Januarys was markedly different from the average temperture of the preceeding 30 Januarys, we could legitimately talk about climate change. Climate 'variability' of course includes a stochastic component due to transient variations associated with weather.

3. The World Climate Programme

In 1974 the Executive Committee of WMO decided that it was important for WMO to take a lead in promoting studies of climate changes and their impact on the natural environment and on food production. So, jointly with ICSU, the International Council of Scientific Unions, they arranged a high level scientific and technical World Climate Conference in 1979 which represented the climate sensitive branches of national economies including agriculture, energy, water resources, fisheries and health (3). They reviewed knowledge of climatic change and variability and their implications for human activities. There followed an outline plan and basis for the World Climate Programme (WCP) 1980-1983 (WMO 540) (4).

WMO's role is to support and help co-ordinate national activities, not to run them. They have set up a World Climate Programme Office within the Office of the WMO/ICSU Joint Planning Staff at Geneva and have established a Joint Scientific Committee (JSC) with ICSU to provide, amongst other things, scientific guidance for the international aspects of the World Climate Research Programme which is a sub-unit of WCP. The JSC determines the main research objectives and facilitates the exchange of information between scientists.

The World Climate Program is divided into 4 main sections:-

a. World Climate Data Program (WCDP)

It might be thought that the voluminous data being collected to support weather forecasting should also be sufficient for climate studies. Indeed the data collected for weather forecasting including that archived in the form of initialised meteorological fields is increasingly valuable for climate studies. Nevertheless elucidation of many of the processes essential to understanding climate fluctuations or climate change as well as monitoring how the climate is currently behaving require much more atmospheric data from above the oceans and remote land areas than are presently available. Even more importantly, reliable worldwide measurements of data from the ocean surface and from the depths of the ocean are badly needed. The study of climate change demands long, homogeneous, records. If we are to make more progress with observational studies of climate change not only must the future coverage of atmospheric, land surface and ocean data be more complete but we must be able to make use of existing historic data. Much of this is not at present easily accessible nor has it been properly validated. So major goals of WCDP are improvement of future observational coverage of the atmosphere and the boundary surfaces and here satellite data will be vitally important. Also, it is hoped to organise the identification and assembly of lengthy climate data sets covering the last 100 years and as complete a set as possible of atmospheric, ocean and land-surface data for about the last 30 years. Figure 1 from (5) gives an indication of the proposed management of this program.

b. World Climate Applications Program (WCAP)

Specific goals of WCAP are to enlighten people and policy-makers concerning the value of applying climate data to socio-economic problems and to ensure this knowledge is available. Examples include agriculture, water, energy and health. In fact such applications are already quite highly developed in some countries eg in UK. In UK climate data is extensively used to aid agriculture eg to advise on irrigation and the need for preventive measures for disease control, to design oil rigs to guard against extremes of wind and waves and to design and simulate the behaviour of storm water sewers and culverts in a cost-effective way etc. Clearly these activities are appropriate in many parts of the world. Figure 2 provides an example of a practical application of climate data to agriculture; Fig 1.2 can be used, with additional information, to decide where in England and Wales it may be cost effective to grow maize to make a form of silage to feed animals in the winter.

c. World Impact Studies Program (WCIP)

This is a more open ended program that seems to come nearest to the 'geographers' approach to climate. The main objectives are to study the impact of climate variability and climate changes on the main economic activities in society (eg agriculture, transport, land use and water resources) and the way that society reacts to these fluctuations with emphasis on the range of impacts in different human societies throughout the world. These societies might be chosen for their different levels of development and different natural environments.

d. World Climate Research Program (WCRP)

This is the most important unit of the World Climate Program from the point of view of these lectures. This program developed from the Global Atmospheric Research Program of the 1970's. It main objectives (see 2) are bold: to determine to what extent climate can be predicted and the extent of man's influence on climate. The primary approach for meeting these objectives is based on the use of physical-mathematical models (eg general circulation models) capable of simulating and eventually (perhaps) predicting climate fluctuations and changes. The program is divided into three streams:-

(1) Stream 1

This stream is meant to establish the basis for long-range weather forecasting ie the prediction of weather anomalies on time scales of 1-2 months (perhaps a little more). Thus the development of long-range weather forecasting is now elevated in an international context to a primary concern of meteorology and climatology. For those interested in more detail, reference (6) gives an up to date picture of developments and further references.

(2) Stream 2

This stream aims at predicting variations of global climate over periods of several years. This is an even bolder aim and a special sub-program of the World Climate Research Program called TOGA (Tropical Oceans and Global Atmospheric Research Program) has been set up which formally commenced on January 1st 1985. This program recognises the crucial role that anomalies in the circulation and heat content of the tropical oceans have on interannual climate variability. It also recognises the fact that variations in the temperature of the upper layers of the tropical oceans for example can to some extent be understood and modelled without, at this stage attempting to model the remainder of the global ocean in full detail. This strategy is a consequence of current ideas about the dynamics of the tropical oceans. Here the Coriolis force is weak giving rise to several dynamical processes which differ from those in mid latitudes and whose effects tend to be confined to the tropical oceans.

(3) Stream 3

This stream aims at studying the patterns of climate fluctuation and variation over several decades or more and assessing the potential response of climate to man-made or natural influences. For example, these influences might be the increase of carbon dioxide in the atmosphere or slow changes in the large scale global ocean circulation. Thus a key sub-program will be the World Ocean Circulation Experiment (WOCE) planned for the 1990's.

Figures 1.3 to 1.5 give examples of why these 3 research activities are in principle challenging and interesting. Figure 1.3 shows that nearly 50% of the detrended variance of temperatures in Central England (when the annual cycle is removed) in a recent 5 year period occurred on time scales of 10 days to 2 months. Can we predict some of this 'Stream 1' variance? There are many commercial and industrial concerns who would find it useful if we could do this. Figure 1.4 shows that fluctuations in many meteorological parameters occur in the Pacific region which are coherent from season to season and year to year and which fluctuate on time scales of a few years. Can we predict these 'stream 2' time-scale fluctuations. These may be linked (lecture 5) to many irregularly recurring tropical anomalies, including drought in east Australia and floods in coastal Equador and north Peru. Figure 1.5 shows that average Northern Hemisphere near surface land temperatures have almost certainly fluctuated appreciably over the last century (stream 3). There have also been roughly parallel quite large variations in atmospheric circulation patterns and in ice cover in some regions. Is this a real effect? If confirmed these fluctuations need to be understood if we are to predict the consequences of say large increase in carbon dioxide over the next century with any accuracy. A stimulating introduction to the three streams is given in chapter 1 of 'The Global Climate' edited by J T Houghton.

4. Relationship between climate and general circulation

I shall frequently refer to the Met O 20 advanced lectures on General Circulation. There is no hard and fast rule for the difference between the two sets of lectures; however Tony Slingo's and Andrew Lorenc's lectures emphasise the physical causes and principles underlying atmospheric circulation. My lectures will have a similar background but are more concerned with the observed behaviour of statistical ensembles of weather events (climate) and the reasons for that behaviour. I will also have an eye on the question: how could we predict these variations? So my lectures will emphasise the near surface environment that affects man, animals and plants. Of course the atmosphere is 3-dimensional and discussion of 'higher' climatic matters will be brought in as necessary.

5. Methods of studying climate

(a) Empirical methods

Most (but not all) scientific knowledge is based on observations. We usually need to make observations to develop theories or choose between competing alternatives. Much empirical work on climate is basically 'detective' work which attempts to find out how the atmosphere and oceans behave on longer than synoptic time scales as few theories yet exist for such behaviour. Outstanding examples of important climate fluctuations which have been discovered empirically are the remarkable 17 year sequence of droughts in the Sahel region of Africa (1968-date) whose continued persistence since the well known initial drought sequence of 1968-1974 was only verified in 1982 (8) but whose consequences are now painfully obvious (Figure 6). On a shorter time scale there is a tendency for the extratropical north Pacific/north American/subtropical west Atlantic atmosphere to adopt a special 'PNA' pattern of variation on time scales of weeks in the winter half year. This variation has an equivalent-barotropic structure in the vertical and seems to be distinct from synoptic scale variability as it exhibits the characteristics of a stationary wave with a non-zonal orientation. (Figure 1.7). This atmospheric 'regime' was discovered about 50 years ago by Walker and Bliss (9), confirmed quite recently by Wallace and Gutzler (10) and is now found to exist in several atmospheric general circulation models (AGCMs) eg (11). The PNA pattern seems to be one of several internal atmospheric modes that can be self stimulated within the atmosphere or in AGCM's but might also be preferentially stimulated (or suppressed?) by external forcing eg due to sea surface anomalies etc (Fig 1.7). These wave-like patterns are sometimes called teleconnections as the fluctuations of a given variable at a selected location eg 500 mb height, tend to be persistently positively or negatively correlated with those at selected distant locations. Teleconnections have long been used in long range forecasting.

6. Synoptic climatology

This is a branch of climatology which up to recently has been the province of the empiricist. There are many definitions of the subject but in essence it tries to provide explanations or predictions of regional or local climates in terms of large scale fluctuations of the atmosphere. Only one book purely devoted to synoptic climatology has been published so far (12), written before the use of AGCM's started to make an impact on the subject. The 'synoptic method' involves the study of patterns of variation at fixed times or averaged over fixed intervals is quite powerful and was used, in the near instantaneous mode, to provide the foundations of practical weather forecasting prior the extensive use of mathematical forecasting models. A technique of synoptic climatology is to classify time-averaged circulation patterns into 'types' which have markedly different consequences for regional surface weather or reflect (sometimes only hopefully) different physical generating mechanisms. So the PNA pattern mentioned above would be a good example of a 'circulation type'. Other examples of circulation types include the 4 basic 'elementary circulation mechanisms' of Dzerdzeevski (see p164 of ref (12)) (with 41 sub-units) that attempt to summarise different patterns of extratropical Northern Hemisphere circulation. These patterns were developed to help long-range forecasting in Russia (Figure 1.8). A local example is the catalogue of the so called 'Lamb' types of daily surface circulation patterns over UK whose aggregate over long periods has often been found useful in climate studies and in long-range forecasting for UK (13). Figure 1.9 gives examples of Lamb types.

7. Climate Modelling

This subject has been extensively discussed in the last few advanced lectures on general circulation. A recent development has been the interactive use of synoptic climatological methods and AGCM's to study short time scale climate fluctuations. The best example so far is the ongoing, extensive, international study of the El Nino/Southern Oscillation (eg 14) where AGCM and OGCM (ocean GCM) experiments have been firmly guided by a series of climatological investigations (eg 15). However some of the results of the GCM experiments already go beyond what would soundly be deduced from available observations (see Lecture 5 in this series). In this way the modelling results stimulate new ways at looking at the observations allowing interactive studies to flourish. This is the approach increasingly being adopted in Met O 13.

8. Summary

I have tried to introduce the vast range of climate studies and why they are important. In the next lecture we shall explore in outline present-day climates of the major regions of the world including some features of their interannual variability.

LECTURE 1 REFERENCES

1. A.A. Miller (1961) Climatology. Methuen.

2. WMO (1984) Scientific Plan for the World Climate Research Programme. WCRP Pub. Series No. 2. WMO/TD No. 6.

3. WMO (1979) Proceedings of the World Climate Conference, Geneva, 12-23 February 1979. WMO No. 537.

4. WMO (1980) Outline plan and basis for the World Climate Programme 1980-83. WMO No. 540.

5. WMO (1983) Plan for the World Climate Data Program. WCP-59.

6. WMO (1984) Report of the Session of the Commission for Atmospheric Sciences Working Group on Long-Range Weather Forecasting Research. WMO LRF Research Pub. Series No. 4.

7. Houghton, J.T.(Ed) (1984) The Global Climate. Cambridge University Press.

8. Lamb, P.J. (1982) Persistence of Sub-Saharan drought. Nature, 299, pp 46-7.

9. Walker, G.T. and Bliss, E.W. (1932) World Weather V. Mon. Roy. Meteor. Sci., 4, pp 53-84.

10. Wallace, J.M. and Gutzler, D.S. (1981) Teleconnections in the geopotential height field during the Northern Hemisphere Winter. Mon. Weath Rev., 109, pp 784-812.

11. G-Q Qiu and S.K. Esbensen (1984) Teleconnection patterns simulated by the OSU AGCM. Climatic Res. Inst. Report No. 51. Oregon State University, Corvallis, Oregon.

12. Barry, R.G. and Perry, A.H. (1973) Synoptic Climatology. Methuen.

13. Lamb, H.H. (1972) British Isles Weather types and a register of the daily sequence of circulation patterns 1861-1971. Met. Off. Geophys. Mem. No. 116. HMSO.

14. Proceedings of 16th Liege Conference on Ocean Hydrodynamics (1985) Elsevier (in press)

15. Rasmusson, E.M. and Carpenter, T.H. (1982) Variations in Tropical Sea Surface Temperature and Surface Wind Fields associated with the Southern Oscillation El Nino. Mon. Weather Rev., 110, p 354-383.

Figure 1.1: Data Management and Archiving Centres

Building Blocks of a Co-ordinated Distributed Climate Data Management System

Data Category	National	Specialized or Regional	Global or International
Synop. Met.: Surf. Marine, Upper-air	NMC/NCC	RMC	WMC
Surface climate Precipitation	Nat. Services, Nat. Agencies		
Oceanography	Nat. Centres	SOC/RNODC	WDC
Marine Met. - Logbook obs.	Nat. Services	Responsible Members (8)	Members
Surface Radiation	Nat. Services Res. Inst.		WMO Centre
Glaciology, Snow and Ice	Nat. Agencies Res. Inst.		WDC, PSGF WGI
Atmos. Comp., CO_2, O_3, Chemistry, Pollution, Aerosol	National BAPMoN		WDC (Ozone) BAPMoN
Hydrology	National and Sub-national		
Agriculture - Meteorology	National and Sub-national		
Agriculture - Agronomy	National and Sub-national		
Land surface, Vegetation, Crops, Soil, etc.	National and Sub-national		
Satellite	Nat. Services Res. Inst.	Regional	
Proxy	Research Groups	Specialized Data Banks	
Solar and extra-terr. radiation	National Services	Specialized Institutes	WDC
Res. Expt. data sets-Meteorology	National Services	Special Centres	WDC
Other types of data: Mean Sea Level Gravimetry Earth tides Ionosphere Seismology Tsunamis Geomagnetism Paleomagnetism Volcanology	National Services		ICSU Centres

International Service for Information on Data Sources

USERS, WCRP, WCAP, WCIP

Acronym: INFOCLIMA (not yet established)

USERS WCRP, WCAP, WCIP

BAPMoN = BACKGROUND AIR POLLUTION MONITORING NETWORK (WMO)
RNODC = RESPONSIBLE NATIONAL OCEANOGRAPHIC CENTRE
PSGF = PERMANENT SERVICE ON GLACIER FLUCTUATIONS

NMC = NATIONAL METEOROLOGICAL CENTRE
NCC = NATIONAL CLIMATOLOGICAL CENTRE
RMC = REGIONAL METEOROLOGICAL CENTRE
WDC = WORLD DATA CENTRE
WGI = WORLD GLACIER INVENTORY
SOC = SPECIALIZED OCEANOGRAPHIC CENTRE

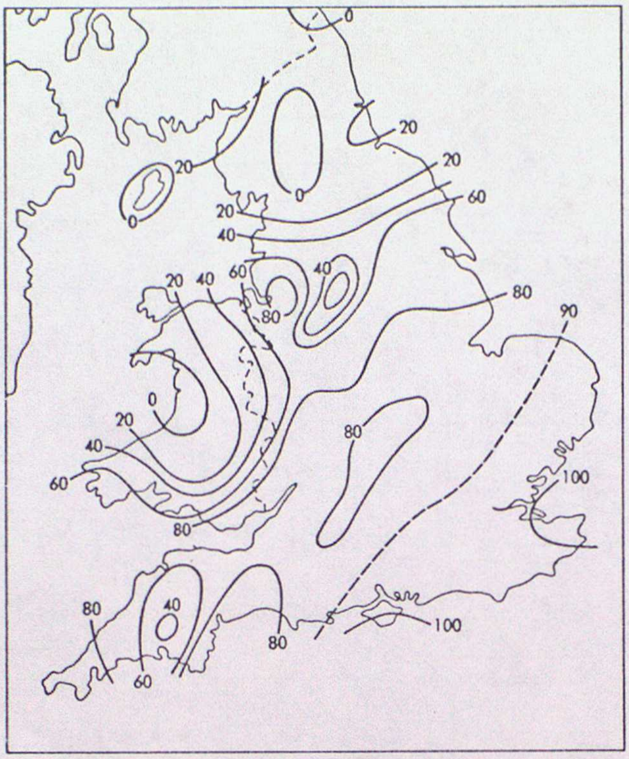
0
20
20
20
60
20
0
0
20
40
20
40
60
40
80
80
90
0
20
40
60
80
80
100
80
40
0
80
100
80
60

Figure 1.2 Percentage of years suitable for making Tower Silage from maize in England, Wales and the Isle of Man.(From Hough 1978.)

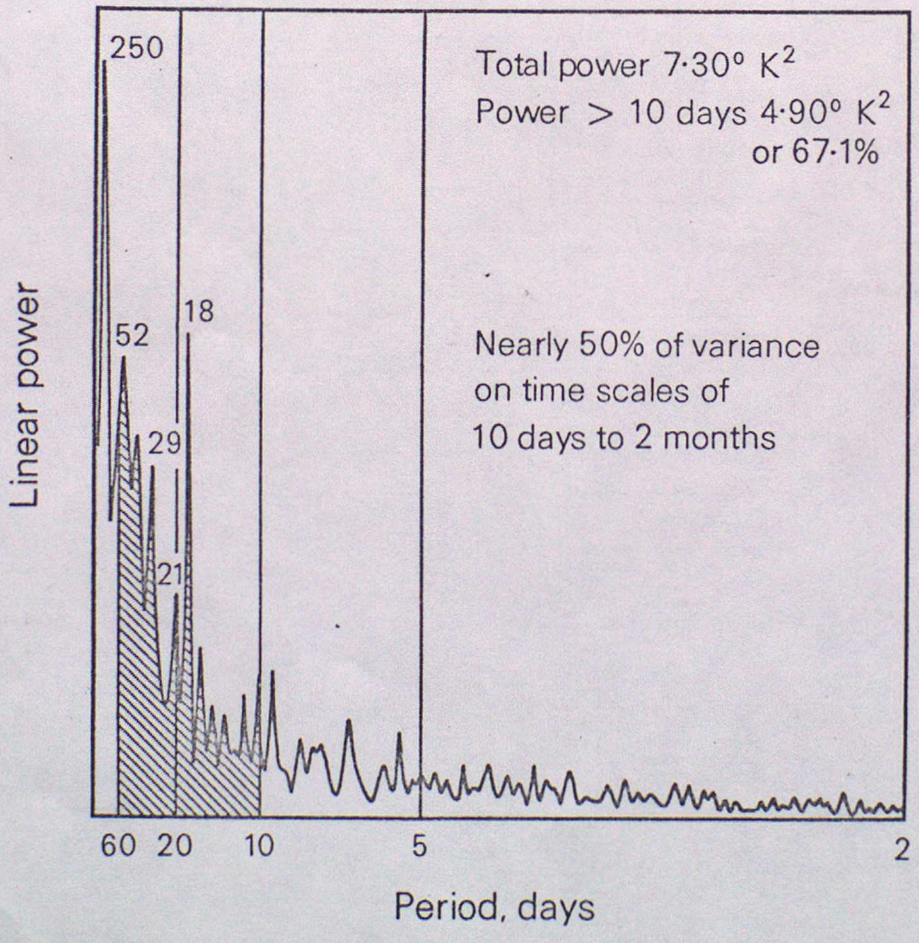

Fig. 1.3 Power spectrum of daily central England temperature (1976-1980) with annual cycle removed

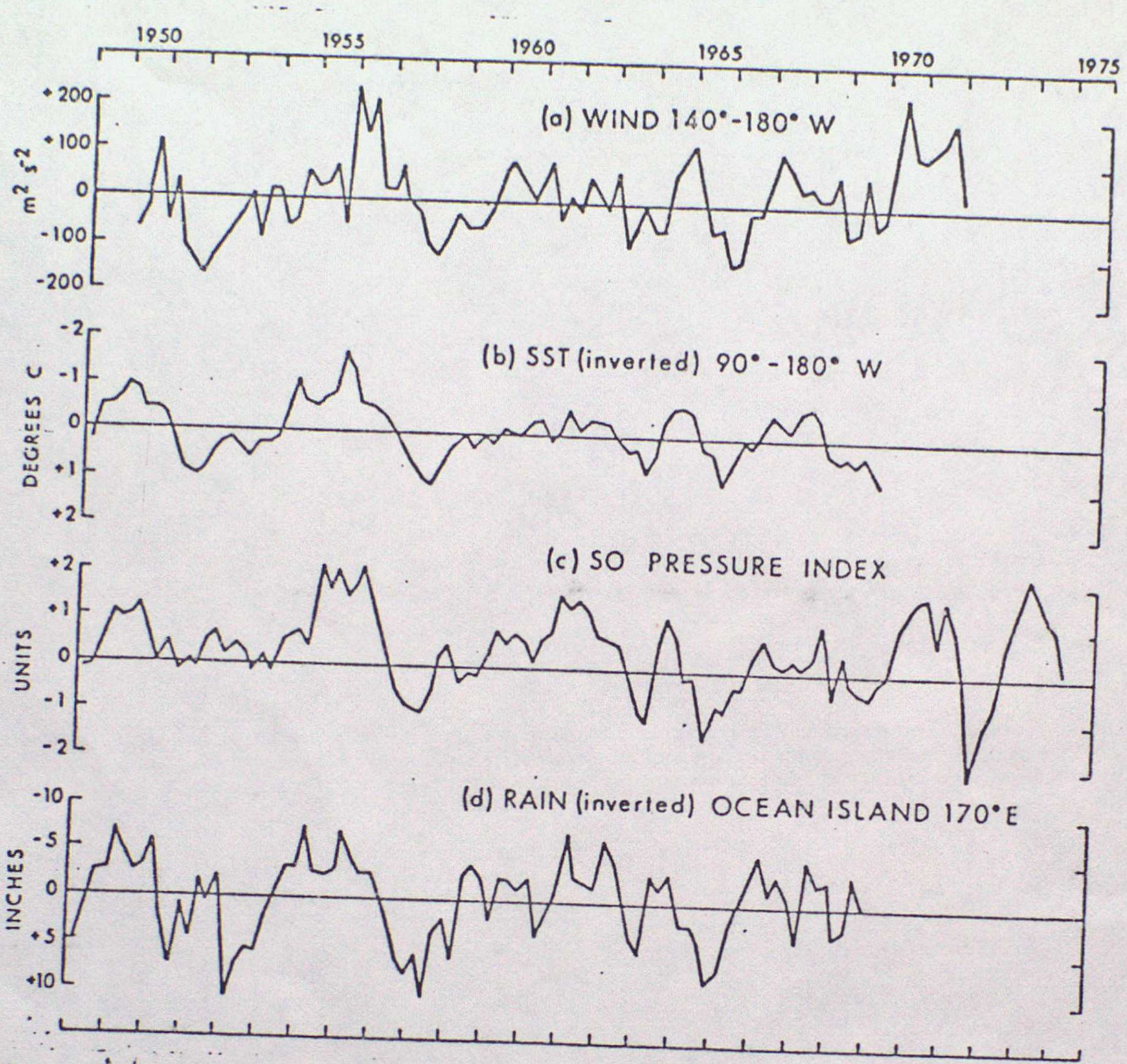

Figure 1-4. Parameters of the Southern Oscillation (after Wright 1977), showing interannual variations.

a) Zonal component of wind stress, 4N-4S 140-180W, seasonal anomalies relative to 1950-1969 mean (after Wyrtki 1975);

b) Sea-surface temperatures 10N-10S, 90-180W, seasonal anomalies relative to 1949-1969 mean;

c) Southern Oscillation seasonal pressure index; (South east Pacific — N. Australia / Indonesia)

d) Rainfall at Ocean Island ($0^{o}52'$S, $169^{o}35'$E), mean monthly anomalies for each season relative to 1950-1969 mean.

Ticks along the top and bottom margins denote the northern autumn of the year immediately preceding.

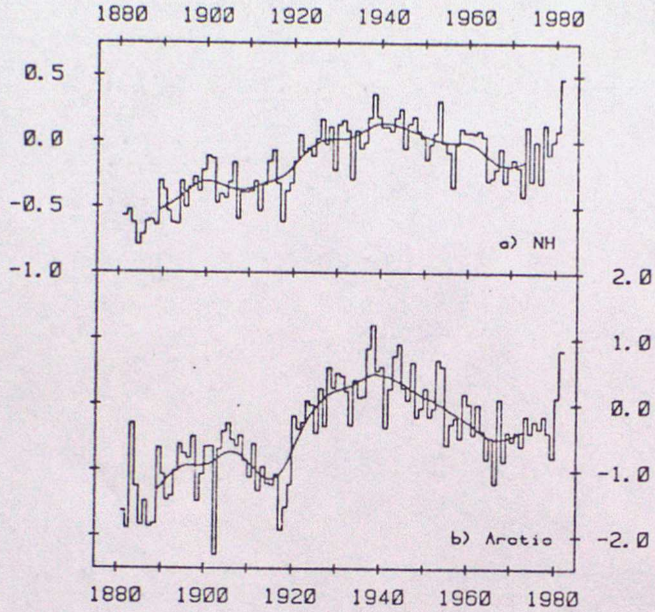

A

Figure 1·3 Annual means of surface air temperature for the Northern Hemisphere and for the Arctic (expressed as departures in °C from the 1946–1960 reference period). Data for 1981 are included in this figure but have not been analyzed. The smoothed curves show the data smoothed with a binomial filter designed to suppress variations on time scales of less than 20 years

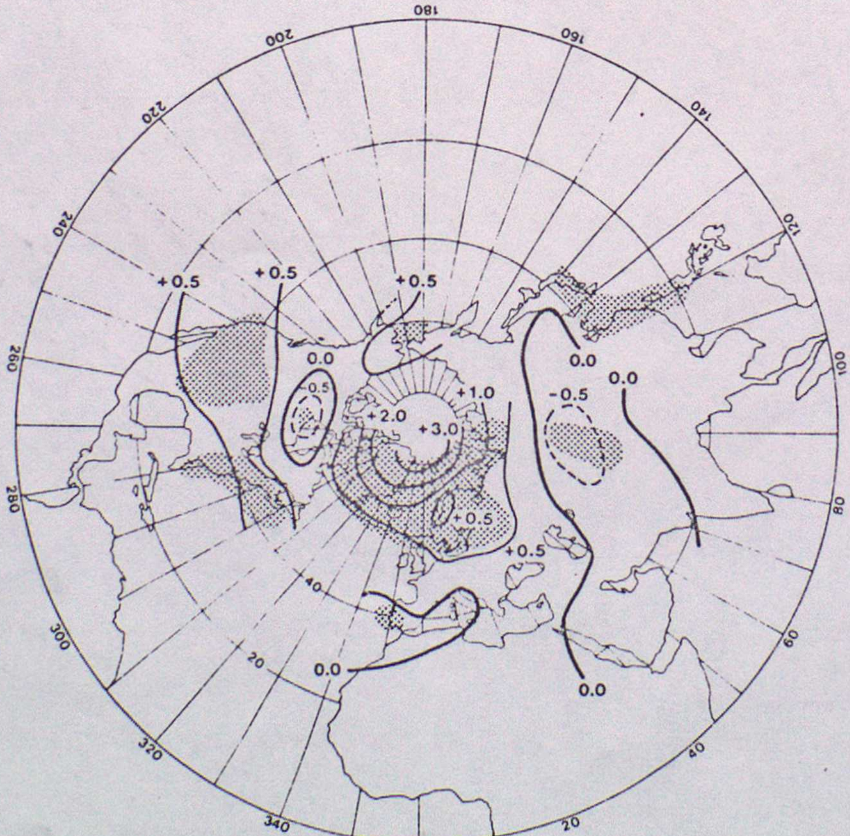
180
200
160
220
140
240
120
260
100
280
80
300
60
320
40
340
20
360
+0.5
+0.5
+0.5
0.0
-0.5
+1.0
+2.0
+3.0
0.0
0.0
-0.5
+0.5
+0.5
40
20
0.0
0.0

B

Linear trend of gridpoint temperatures over the period 1917–1939 (°C/y×10^{-1}). Shaded areas are significant at the 5 per cent level

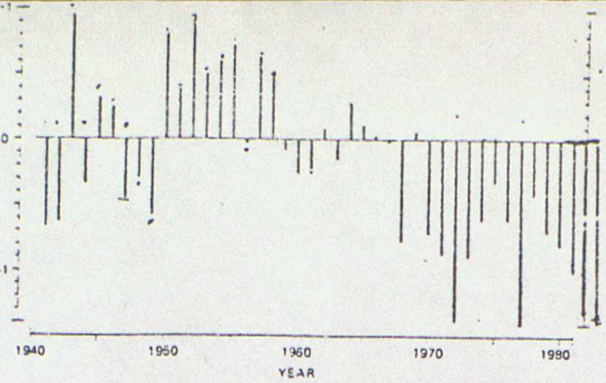

Fig. 1.6 1941-81 time series of the yearly average of the normalized rainfall departures (σ) for 14–20 Subsaharan stations west of 9°E. Kraus[13], and Faure and Gac[19] suggest that the largely dry epoch at the start of the time series (1941–49) commenced no more than a year or two earlier. The 1969 value of +0.06 is a correction of the −0.11 value published earlier[21].

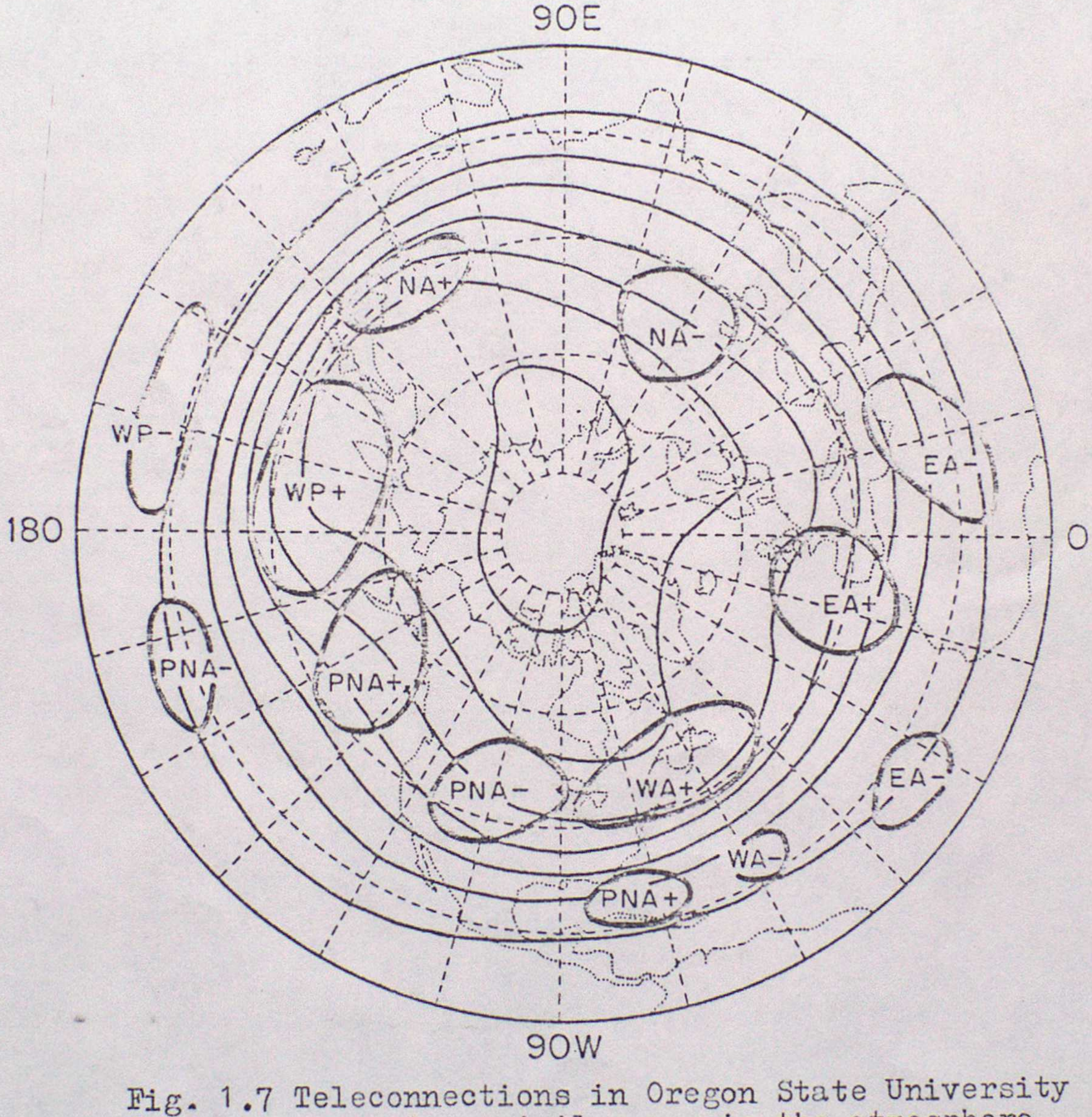

Fig. 1.7 Teleconnections in Oregon State University AGCM also seen in a similar way in the atmosphere (Winter)

The "centers of action" of the teleconnections in the simulated 400 mb height field. The isopleths of the ±0.6 correlation coefficient between each of the five pattern indices and the 400 mb height anomaly field are indicated by heavy lines.

"PNA" is the Pacific North American Pattern

"WP" is the West Pacific Pattern

"EA" is the East Atlantic Pattern

"WA" is the West Atlantic Pattern
"NA" is the North Asian Pattern

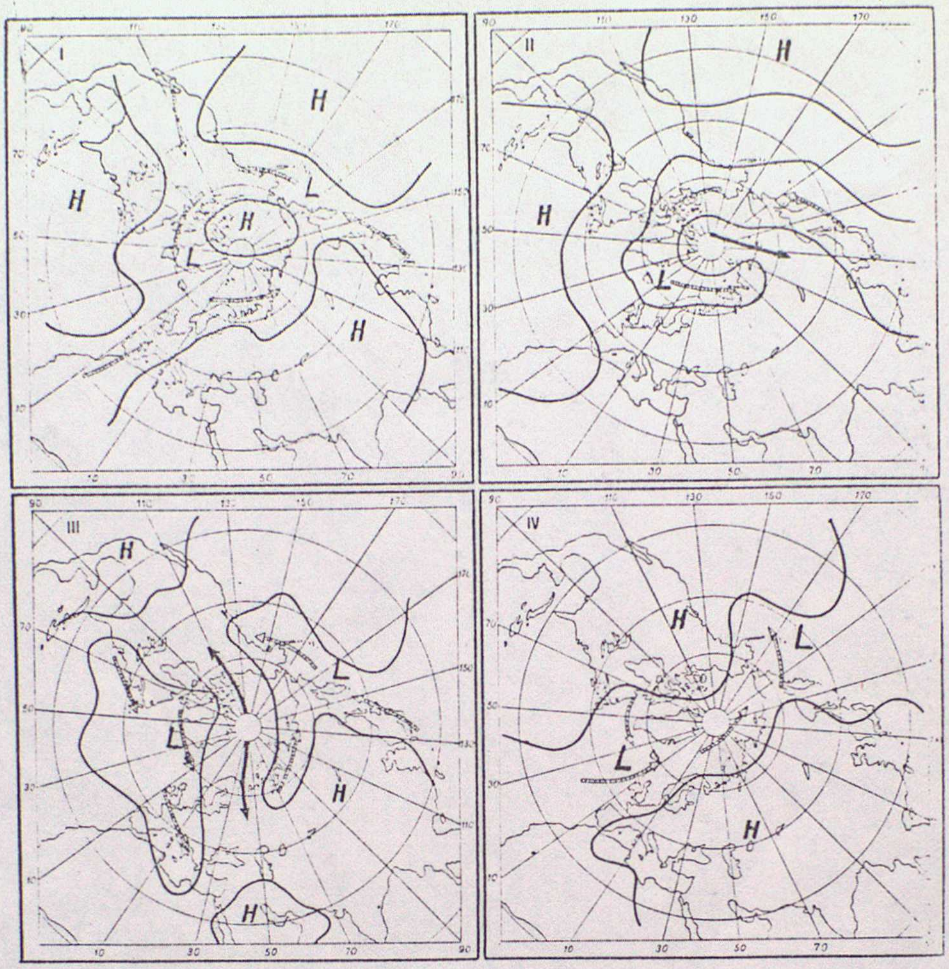

FIG. 1.8 Four principal groups of circulation types over the Northern Hemisphere. ⟹ Cyclone tracks; ⟶ anticyclonic tracks; L—Areas of cyclonic activity; H—Areas of anticyclonic activity

I. Ring of depression tracks around pole and some advection from the South-mainly zonal type.

II. Mainly zonal but strongly meridional in one sector (ie blocking tendency)

III. Generally meridional-strong interchange of warm and cold air-general blocking tendency.

IV. Strong flux of warm air toward pole in one sector with depressions moving near central Arctic (Atlantic sector favoured in Winter)

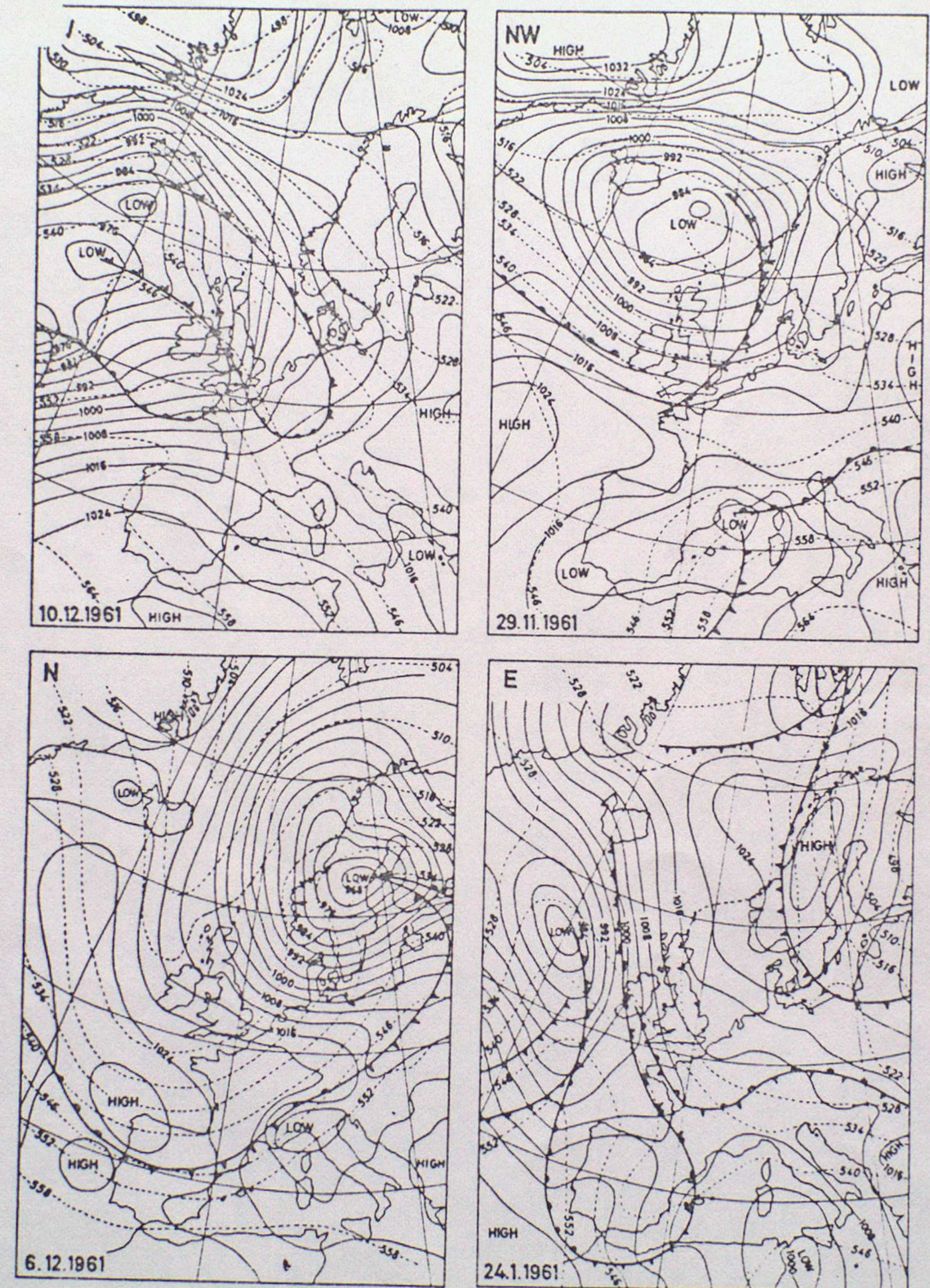
W
10.12.1961
NW
29.11.1961
N
6.12.1961
E
24.1.1961
HIGH
LOW

Figure 1.9 Examples of Lamb (W) Westerly; (NW) North Westerly; (N) Northerly (E) Easterly

FOR LOAN TO MET OFFICE STAFF ONLY

METEOROLOGICAL OFFICE
145727
- 7 MAY 1985
LIBRARY

ADVANCED LECTURE NO 2

INTRODUCTION TO WORLD CLIMATE - II

2.1 Introduction

The lectures on General Circulation (GC) have shown that ideas of a simple symmetric atmospheric circulation are far from correct but nevertheless useful. Fig 2.1A shows an idealised wind circulation for the globe while Fig 2.1B gives a more realistic picture where the central role of the mid-latitude transient eddies is shown. Fig 2.2 is a representation of the N Hemisphere mean meridional circulation: the strong upward motion at the ITCZ (whose position is variable) is shown, helping to give rise to a Hadley cell to the north with descending motion around 30°N (further north in summer). A "Ferrel" cell is shown further north still: it is the net result of eddy activity in mid-latitudes on several time-scales. Finally there is a more doubtful Polar cell.

Even in the Tropics, a simple picture of dominant mean motion resulting from a Hadley cell is rather misleading: besides eddy motions, there are a substantial set of more or less east-west circulations whose east-west components are called "Walker" cells (Fig 2.3). These cells are thought to be driven by the strong longitudinal variations of thermal forcing near the equator. The most prominent cell has a rising branch over and near the Tropical W Pacific in northern winter extending over SE Asia in the northern summer. The descending branch occurs over the cool tropical east Pacific just to the west of S America. Fig 2.4 shows, from Newell et al (1974)(1) estimates of the mean mass flux in the Walker circulation cells: the strongest mass fluxes are only a little less than those in the Hadley cells in Spring and Autumn (GC Lecture 2 Fig 2.4).

A partial explanation of these cells, which affect precipitation in equatorial regions very strongly, lies in the geography of tropical continents and oceans. Fig 2.5 shows the January and July climatological mean SST (for 1951-80) derived from the Meteorological Office Historical Sea Surface temperature data set (MOHSST) (2). In the tropical Pacific and the tropical Atlantic there is a west-east surface temperature gradient. In the Pacific, the difference in SST at 10°S between 150°E and the S American coast is about 6-7°C in January (southern summer) and almost 10°C in July. In the Pacific, these longitudinal SST differences are comparable to those between the Equator and nearly 30°S in the same seasons, which of course help to drive the regional Hadley circulation. Not surprisingly, convective activity is usually very weak or non-existent in the tropical east Pacific south of the Equator but this situation is apparently rather unstable and a dramatic warming of the east tropical Pacific can sometimes occur (the ENSO events, lectures 4 and 5). The result of these mean motions is that air-flow trajectories in the tropics are far different from those that could be derived from the simple picture of a meridional Hadley cell.

Fig 2.6 shows a map of global ocean currents which helps to explain the SST variations. The currents are of course driven mainly by the pattern of surface winds (Fig 2.7). The tropical anticyclonic ocean gyres are driven by the trade-wind circulations to the south and the westerlies to the north. These gyres are associated with strong, warm western ocean

ORGS UKMO
National Meteorological Library
FitzRoy Road, Exeter, Devon. EX1 3PB
3 8078 0007 8109 8

boundary currents: the Gulf Stream (GS) and Kuro Shio (KS) in the N Hemisphere, and in the S Hemisphere the Brazil (BC) and Agulhas (AG) currents (the latter off S Africa). Eastern boundary currents are cold: the Canary (west of N Africa) and Californian (CC) currents in the N Hemisphere and the very cold Humboldt (HC) and Benguela (BC) currents in the S Hemisphere. So it is not surprising that SST is very low, for example, off Peru though upwelling of water from below is an additional factor in all cold currents in tropical regions. Upwelling results from an off-shore Ekman drift which is driven by the prevailing off-shore winds. In the Indian Ocean, currents tend to reverse in direction with the seasons and are driven respectively by the SW (Summer) and NE (Winter) monsoons.

2.2 Seasonal variations of atmospheric circulation

The climate of the world can only be understood by including the seasonal variations in atmospheric circulations, snow and ice etc.

2.2.1 January and July pressure and wind fields

Important features in Fig 2.7-2.8 are:-

January - Note the subtropical highs; the low pressure trough of the ITCZ near to or south of the Equator; the intense Siberian high with surface air streaming away from it. Being a cold high, the Siberian high decreases in intensity with height and is overlain by the midlatitude westerlies. In the N Pacific and N Atlantic there are deep lows (the Aleutian and Iceland lows).

In the S Hemisphere (Summer) the subtropical highs form an almost continuous belt, with centres over the cool oceans; heat lows dominate the three main continental land masses.

July - The northern subtropical highs are further north with considerable PMSL differences between land and sea in the same latitudes; heat lows exist over the southern United States, the Sahara, and most prominently, southern Asia. The Iceland low is still present but rather weak but there is now very little sign of the Aleutian low, the east Pacific high being placed surprisingly far to the north. Fig 2.7 shows that the ITCZ moves further away from the Equator over land than over the oceans. Being largely the result of vertical convective processes, the tropical lows shown in Fig 2.8 decrease in intensity with height unlike the Iceland low, which merely slopes to the west with height.

Note that the ITCZ lies where the trade winds meet. When this is far from the Equator, the air that crosses the Equator turns southwesterly in direction due to the change in direction of the Coriolis force, though a westerly component sometimes develops before the Equator is crossed, eg over the Indian Ocean in July. Fig 2.9 shows that the picture of a single ITCZ moving North over the Indian Ocean in summer is far from correct. The apparent double ITCZ structure, if that is what it is, is poorly understood but is the subject of current research. A possible explanation is that individual zones of tropical convergence tend to occur above individual absolute SST maxima if those maxima exceed about 27-28°C (Gadgil

(1984)(3)). On Fig 2.5 for mean July SST, there is a suggestion of a SST maximum near the southern of the two convergence zones as well as a further maximum adjacent to the coast of the Indian sub-continent.

2.2.2 Upper level flow

2.2.2.1 Tropics and Sub-tropics

Figs 2.10 and 2.11 show the 850 mb and 200 mb streamlines during Dec-Feb and June-Aug. At 850 mb, the anticyclonic centres over the oceans are clearly seen in both seasons, overlain by a strong westerly flow at 200 mb. In June-Aug a strong warm anticyclonic centre is seen at 200 mb over N India/Tibet, with cyclonic motion at 850 mb. This vertical structure is the result of convective heating over N India and heating of the Tibetan plateau (height 4000-5000 m) resulting in a high-level warm anticyclone giving a strong 200 mb easterly flow to its south which extends all the way from the tropical W Pacific to the tropical Atlantic. At the surface, the flow is reversed and is mainly westerly. Over coastal W Africa Fig 2.7B indicates a south westerly flow at the surface though at 850 mb Fig 2.10 suggests a more south to south-easterly flow. A problem in this region (see later) is that interannual and longer time scale variability has been very large in recent decades so different, rather short, data periods may give different results. In the S hemisphere in Dec-Feb, a monsoon-like heat low over S Africa at the surface (cyclonic centre marked C) is overlain by a warm 200 mb anticyclonic centre; there is a similar feature over the Bolivian Plateau. To the north and north east of the latter feature, there exists strong 850 mb north westerly flow over W Brazil and W Argentina which is evident also in June-Aug. This north-westerly tropical circulation is thought to depend on the fact that the Andes form a sharp physical western barrier to flow over these regions (4). This is the only tropical region in the S Hemisphere where low level tropical north westerlies are common (except perhaps near Papua-New Guinea in northern winter).

2.2.2.2 Mid-latitudes (500 mb)

GC lecture No 4 (its Figs 4.1) shows the 500 mb flow in the N Hemisphere with its attendant ridges and troughs. Please refer to that lecture. Here it is worth mentioning that the S Hemisphere 500 mb flow is more symmetrical but there is a marked tendency to a broad trough over the Southern Ocean between about 30°W and 40°E. This feature is associated with long-term SST and air temperature averages up to 5°C below the average for their latitude between 50°-60°S (Hoflich) (1984) (5). Fig 2.12 (below Fig 2.9) shows the S Hemisphere 500 mb flow in January (summer). Between about 40°S and the S Pole 500 mb FLOW is of similar strength to that in the N Hemisphere winter in a similar latitude band (which of course includes the same month). In the S Hemisphere the strength of the flow in local winter hardly changes. This occurs because the surface temperature gradient between equator and pole scarcely alters through the seasons.

2.3 Mean seasonal snow and ice variations

Ice and snow are an important feature of the mean seasonal variation of climate (Fig 2.13A). Taken together the region of permanent sea and land ice in the N Hemisphere is currently slightly smaller than that in the

S Hemisphere, but the maximum seasonal extent of ice and snow in winter is much larger in the N Hemisphere. Sea ice around Antarctica fluctuates from a typical minimum extent of 2.5 x 10^6 km^2 (Feb/March) to a typical maximum of 15 x 10^6 km^2 (September) (note that the area of Antarctica itself is 14 x 10^6 km^2). Over the N Hemisphere the typical minimum extent of sea ice is about 8 x 10^6 km^2 (September) with an additional 1.8 x 10^6 km^2 contributed by Greenland. However the maximum extent of ice and snow together is apparently about 55 x 10^6 km^2 in the N Hemisphere (February) (Untersteiner) (1984) (6). There are pronounced interannual fluctuations of N Hemisphere snow and ice extent (see Fig 2.13B from Hahn (1981)(7). Reliable measurements of fluctuations in Antarctic sea ice on time scales of several years are just beginning to emerge (Chiu) (1983) (8). Reliable satellite plus conventional assessments of global seasonal cryospheric extent only began about 1974.

2.4 Climate classification and world climate

In one lecture I cannot attempt to cover the climate of the whole world in detail. I shall briefly discuss climate classification and then select a few main regions for discussion. I shall also mention some lesser known but perhaps thought-provoking habits of regional climates.

2.4.1 Climate classification

The climate of even a small area is composed of a large number of locally-varying climate elements and it is nearly impossible for two places to have identical climates. So condensation and ordering is needed to facilitate analysis and explanation. Classification consists of recognising important characteristics which individuals have in common and grouping the individuals into a few classes or types in order to establish generalisations.

Classifications can be based on the way climates are generated or on their effects eg their effects on surface vegetation or specialised problems like the reliability with which maize can be grown in UK discussed in Lecture 1. In fact applied classifications are now numerous but are usually of main interest to specific users, though as a result many useful climatic maps of extremes or the frequencies of given thresholds of rainfall amount, temperature, wind speed etc have been produced.

The genetic type of classification appeals to meteorologists but it must be simple and there is a danger that the facts of climate may be forced into a preconceived and not wholly appropriate genetic structure. Empirical classification starts from the observed facts but the basis of division can be arbitrary and its validity depends of course on the use to which it is put.

The best known empirical classification is that due to W Koppen. A considerable number of Koppen's climatic types and subtypes do in fact coincide with broadscale features of the general circulation which allow the numerous and important deviations from a "standard" world pattern to be realistically highlighted. Koppen's system is known throughout the world and was the result of half a century's study and refinement. His classification is quantitative and is based upon annual and monthly means of temperature and precipitation; it accepts native vegetation as the best expression of climate so that many of the climate boundaries are selected with vegetation limits in mind. It recognises that plant development depends on available water as well as on temperature so that precipitation and evaporation are included in the classification scheme. Because evaporation measurements are not usually available, evaporation is estimated from temperature and precipitation. Many authors have proposed modified schemes based on Koppen's scheme; they mostly differ in the method of expressing the available water for plant growth. Appendix 1 to this lecture describes Koppen's scheme in detail and has been taken from Trewartha and Horn (1980) (9). It is interesting that Koppen's scheme has already been used to help interpret the results of an AGCM experiment (Manabe and Holloway)(1975)(10).

Fig 2.14 shows a climate classification scheme due to Critchfield (11) which is rather like a simplified version of Koppen's system or Trewartha's scheme, and we shall use Critchfield's scheme as a background for our description of world climate. Three main climatic classes are defined (subjectively, not rigorously) in terms of monthly mean temperatures (basically according to freedom from frost and the length of the growing season) with an extra highland climate class which includes all temperature classes and can occur anywhere in the world. Arid climates are a subgroup of the three main types where precipitation is less than potential evaporation. Like most schemes, Critchfield's scheme subdivides classes according to whether or not there is a dry season and when in the year it occurs (except for highland climates). Fig 2.15 shows a map of mean annual world precipitation which will be a useful background to the following descriptions.

2.5 Description of selected world climates

2.5.1 Tropical climates

Consider first the air flowing around the oceanic cells of the sub-tropical high pressure belt centred about 25-35°N and S. The air flowing toward the equator on the eastern side of the cells and not far from the latitude of the centre of the cells is stable and dry and strongly subsides due to the large-scale divergence caused by the Hadley cell. This gives rise to a low level temperature inversion Riehl (1979) (Fig 2.16). As a result the eastern half of the sub-tropical oceans has a sunny and fairly dry climate so that islands such as the Canaries tend to be arid, though orographic precipitation on high mountains can be considerable. The subsidence also gives rise to extremely arid coastal regions on the western sides of the continents in latitudes 20-30°N and S such as the Kalahari and Chile-Peruvian deserts and the western margin of the Sahara.

The dry Equator-ward moving air picks up heat and moisture from the sea, so that the trade-wind inversion steadily rises as the air turns more and more to the west. The air beneath the Trade-wind inversion becomes deeper and more unstable and increasingly subject to convection. Riehl (1979)(12) shows theoretically and from observations that the trade wind inversion is not a physical barrier: sinking and diverging air from above descends through the inversion as shown in Fig 2.16, the descending motion being forced by the large scale divergence around the high pressure cell. The descending air is mastered as it sinks; thus the inversion rises as more air is incorporated beneath it. The air becomes quite rapidly warmer and moister because sea temperatures also tend to rise towards the western halves of the tropical oceans.

As the air approaches the Equatorial trough of low pressure, it meets the corresponding flow from the other hemisphere and is subjected to strong convergence and lifting, and so creates the great deep convective cloud systems of the ITCZ. Although the Trade Winds are mostly dry, fair-weather winds on the eastward and poleward sides of the high pressure cells, their Equatorward and western sectors are subject to synoptic-scale disturbances including tropical storms in the western sectors if SST is high enough and the latitude exceeds about 8°. So the amounts of cloud and precipitation in the west are considerably greater though most rain falls near the ITCZ itself. Most of the energy released in the upward branch of the Hadley cell re-enters the lower atmosphere well away from the Equator so a considerable amount of latent heat energy is conveyed towards the Equator by the trade winds (thus the trade winds tend to "heat the equator"). Upward motion in the region of the ITCZ is confined at any one time to small areas concentrated in mesoscale convective systems which have a bewildering range of sizes which are poorly understood. The ITCZ follows the annual path of the vertical midday sun but moves much further in some longitudes than in others, tending to move most over continents. So a fundamental division of tropical humid climates is between those regions near the Equator which have considerable rainfall all the year round (tropical wet climates or equatorial rain climates) and those which have a pronounced dry season in the local winter when the ITCZ has moved well away or even into the other hemisphere so that the region is subject to subsidence from the sub-tropical anticyclone (tropical wet and dry climates).

This difference of climate has a great influence on vegetation and marks the difference between the jungles, the hardwood forests and swamps of the Congo or the Amazon basin, south east Asia and parts of Central America and the lighter more deciduous forests and tree studded grasslands often called savannah which are typically located to the north and south of the equatorial region. Good examples of savannah exist in South Central Brazil, northernmost South America and in tropical Africa. It is not certain whether the existence of savannah is always caused by drought conditions in winter or whether it is caused by the frequent fires that sweep the grasslands from which trees do not recover. It is interesting that man himself in recent centuries may have inadvertently created apparently natural savannah. New savannahs are now being deliberately created, especially around the edges of the Amazon jungle.

Much work on the General Circulation and climate concentrates on the tropical and equatorial zone: this is the major source of energy for the atmosphere and it covers about 40% of the world. It is also one of the zones about which least is understood. It was once thought that tropical climates were simple and followed regular patterns but this is now known to be far from correct. Most importantly, the details of the climates are not easily explained especially their tendency to pronounced inter-annual variability.

Africa probably provides the best examples of the expected arrangement of climate zones of the tropics so we shall look at the structure of the atmosphere over West Africa where the arrangement of climates zones is simplest. Please refer to Fig 2.7, 2.8, 2.10 and 2.18 and note the following:-

a. The S Hemisphere south east Trade Winds cross the Equator to become moist, south westerlies (sometimes called "monsoon" air). (Fig 2.7B).

b. The north east Trade Winds over the Sahara originate from near the Mediterranean (and their specific humidity is fairly low). (Fig 2.7B).

c. The ITCZ does not normally move south of the Equator in the longitude of W Africa even in winter because the tropical S Atlantic Ocean is relatively cool. This means that the Gulf of Guinea coastal region is wet in the winter.

d. Further east in tropical Africa, the behaviour of the ITCZ becomes more complex especially in Ethiopia, Kenya and Uganda. It is much affected by the high mountains and plateaux of this region and in summer by the Indian monsoon circulation. So this is a poorly understood region - one of the earth's "problem climates".

The vertical structure of the atmospheric flow in the tropical W African region in August and some of its interannual variability is shown as a function of latitude in Fig 2.18A and B (Newell and Kidson (1984)(13)). These diagrams show the zonal and meridional components of the wind through the depth of the atmosphere for two sets of recent years. In one set the Sahel region (Region 5 south of the Sahara desert in Fig 2.14) was wetter than normal and in the other set it was dryer than normal. Referring to Fig 2.10, we would expect to see, north of about 5°S, fairly strong upper level easterlies extending from the Asian monsoon circulation. These easterlies are clearly present in both sets. In the years marked wet, the upper easterlies are slightly stronger than in the years marked dry but the sample is too small to be sure of this. Lower down, there is a pronounced easterly jet near 700-800 mb near 20-25°N which is more pronounced in the dry years. This result is probably real and due to an enhanced low-level thermal gradient between the wet regions near the coast and the more than usually dry region of the North Sahel. This dryness should give rise to more sensible heating of the ground and thus warm the lower layers of the atmosphere. A low-level south westerly flow is evident in both wet and dry years between 10°S and 20°N but is markedly less deep and certainly is less strong in the dry years. In fact the ITCZ annually reaches 20-22°N where practically no rain falls; the boundary between the northerly and southerly components of the flow near the ground in August does not seem to vary greatly between wet and dry years. However Fig 2.18B suggests that the flux of warm, moist air from the S Atlantic is weaker in the dry years.

The detailed mechanisms of rainfall release near the ITCZ are complex and ill understood but certainly not solely accomplished by the random occurrence of isolated thunderstorms. Fig 2.19, taken from Riehl (1979), shows a typical organised synoptic disturbance, known as an "easterly wave", which was observed during GATE (The GARP Atlantic Tropical Experiment of 1974). When viewed from a satellite, easterly waves can look like a very large mesoscale "cloud cluster" though there are other types of cloud cluster. In Fig 2.19 the winds are south west to the south of the trough line and north easterly to the north so diagrams of seasonal mean conditions like Fig 2.18A and B are the net result of many individual synoptic features. Referring back to Fig 2.14, we can see several nearly parallel climatic zones in W Africa. Zone "4" is the western Sahara desert where rainfall is always rare; zone "5" is the Sahel which is placed north of about 10°N in the west of W Africa but which tends to be located a few degrees to the south further east. The Sahel depends, as discussed above, for its rainfall on the northward movement of the ITCZ into the region in July-Sep. Area "3" is fairly wet most of the year as it is affected by the ITCZ, or the moist unstable air just to its south, much of the time. The small area "5" in south Togo is sufficiently far enough south in summer to escape much influence from the ITCZ so has a summer dry season. The very wet region "2" around Liberia and Sierra Leone is an anomaly probably partly caused by local convergence due to mountains just inland from the coast, otherwise it would be like area "3".

Atypical of these latitudes is the dry zone of tropical East Africa near the Indian Ocean coast that stretches from about 4°S to at least 10°N. This region has been the subject of much study. The Indian summer monsoon flow strongly affects this region and the moist easterlies experienced by other continental eastern margins near the equator are replaced by a south-south westerly flow that seems to be relatively dry but does not penetrate very far inland. The lack of rain in the south Somalia/Kenya desert region in southern summer seems to be related to an airstream which is derived from an anticyclone over Arabia rather than from the warm ocean but the lack of rain in northern Somalia in the northern summer does not have an adequate explanation. Perhaps the strong seasonal upwelling of cold water offshore near 10°N during the Indian south westerly monsoon season plays a part in the dryness, in addition to the dry southerly airflow.

I shall not discuss the Indian or other monsoon in more detail: please see R Riddaway's 1980 Advanced Lecture (14). In passing one might note that much of India is classed by Critchfield (Fig 2.14) as a tropical wet and dry climate though the dry season on much of the west, mountainous, coast is short and there is enough soil moisture during the dry months to support tropical rain forests. The true tropical wet climate starts further east in Burma. A typical example of this climate is enjoyed by Belem at the mouth of the Amazon. The mean temperature of every month is close to 26°C while average monthly rainfall varies between about 100 and 450 mm. Sunshine averages 5.5-6 hrs a day. So even here a short dry season exists and in fact only restricted areas of the equatorial regions have a uniformly wet climate eg in the western Amazon basin and in western Colombia on the other side of the Andes north of the Equator. This extraordinary climate, which is hardly understood, is uniformly extremely wet (see the area marked 12 in Fig 2.14); Fig 2.19 shows daily rainfall for the year 1928 which totalled 7089 mm and was remarkably uniformly distributed through the year. By contrast there is a small, heavily populated, dry area in NE Brazil (the "Nordeste") (Fig 2.21) whose climate is again ill-understood but which is being intensively studied (Hastenrath et al) (1984) (15). Much hardship is quite regularly caused by excessive drought.

Turning to an ocean climate, the "desert islands" just south of the Equator in the central and eastern Pacific stretching from near the dateline to the Galapagos Islands represent one of the most extraordinary of world climates. These islands stretch a quarter of the way round the world and owe their unusual dryness to the fact that a cool sea is normally maintained by the wind circulation so that the ITCZ is almost always north of the Equator. The cool sea near the Equator seems to be maintained by Ekman divergence. However, every few years the ITCZ moves over the area for much of the high-sun season and the sea becomes very warm giving intense convective activity. Indeed the sea surface temperature maximum viewed in the meridional direction tends to move over the islands. Average yearly rainfall totals of 500-700 mm are quoted for many of the islands but this hides the fact that in dry years perhaps only 50-150 mm fall and in the few wet years there may be as much as 2500 mm. These fluctuations are now known to be intimately related to the ENSO phenomenon which happens sufficiently often that these islands could be truly said to have a bi-modal "almost intransitive" non-seasonal climate (see Fig 1.4 Lecture 1, and Lecture 5).

Before leaving the tropics, we might note some interesting features of highland tropical climates. Tropical glaciers are surprisingly numerous eg there are many in the tropical Andes, several in Africa in the Ruwenzori Mountains of Uganda and on Mounts Kenya and Kilimanjaro above about 4500 m. Surprisingly there is even a 7 km ice cap in the Star Mountains of W Irian, Indonesia known as the Caarstenz Glacier (16). This glacier exists at a height of about 4500-5000 m despite being surrounded by the warmest SST in the world. However at about 15°-25°S in the Andes no glaciers are found at these or even much higher levels. The determining factor here is lack of precipitation and lack of cloudiness so only very small glaciers are found above 6000 m. By contrast in the cloudy Andes of Equador near 0° one glacier extends down to almost 4300 m. Many tropical glaciers are slowly receding and may not be in equilibrium with the current tropical climate.

2.5.2 Subtropical climates

2.5.2.1 Mediterranean climates

On the western margins of the continents in both hemispheres there are regions where summer is dominated by the anticyclones of the desert zone (ie the descending branch of the Hadley circulation); these anticyclones are particularly stable being on the eastern cool sides of the subtropical oceanic circulation. However in winter these areas come under the influence of mid-latitude travelling cyclones and are consequently much wetter with changeable weather. These are the areas of Mediterranean climate, characterised by (1) a concentration of the year's rainfall in winter and sometimes in autumn, while the summers are mainly dry, (2) they have warm to hot summers and mild winters, (3) there is abundant sunshine especially in summer. The five regions where the Mediterranean climate occurs are fairly similar: the border lands of the Mediterranean Sea stretching for 2500 km into Eurasia, the coastal strip of central and southern California, central Chile, the south western tip of Africa and parts of southernmost W Australia, S Australia and Victoria.

In California and Chile the Mediterranean climate ends abruptly at high mountains 100-300 km inland with mountain-induced desert on the eastern side. The remaining continents of the S Hemisphere only just reach the appropriate latitudes while the Mediterranean Sea itself acts as a cool-season convergence zone and route for winter depressions. In this respect the Mediterranean is different from the other areas and some of these depressions penetrate well into Asia in winter.

It might be thought that Mediterranean summer climates would always be hot but in coastal S California and Central Chile cold offshore currents (see Fig 2.5 and 2.6) keep coasts 10°C or more cooler than inland and more than this by day. The coasts have frequent fogs and low stratus and strong sea breezes set in because of the contrast in afternoon temperature with the hot interior. In the poleward parts of these regions occasional winter frosts occur and as the winter of 1984-5 showed on the Riviera snow may on rare occasions reach down to the coast. (Eastern Spanish beaches in January 1963).

2.5.2.2 Eastern sides of continents

The subtropical eastern sides of continents receive, in summer, unstable or neutral tropical maritime air as subsidence in the subtropical anticyclone on the western side of the oceans is weak and the boundary layer is moist. This favours abundant summer rain from convective activity aided by the development of tropical storms, some of which gain the structure of mid-latitude depressions as they pass over or near these regions. There is also a tendency for monsoon circulations to develop, especially in south east China and to some extent in the south east United States. This climate is represented in all 3 southern continents, ie S Brazil, East Australia and SE South Africa. It differs from the Mediterranean type by having tropical humid climates instead of tropical hot dry climates on the equatorial side. These tropical humid regions provide a source of sultry heat in summer rather than the dry heat that exists adjacent to the Mediterranean climates.

In the N Hemisphere, a severe continental climate exists on the poleward side which can bring intense cold in winter for brief spells. For example, Nanking in eastern China at 31°N has occasional severe snow storms and frequent frosts in winter. Even further south, occasional very low night minima are a feature of the climate of central and northern Florida. Summers are hot, the monthly mean temperature averaging 24-27°C or slightly higher, with high accompanying humidity from the dominating tropical maritime air, giving rather oppressive nights. Annual rainfall is relatively high (1000-1500 mm is typical) and tends to be concentrated towards the summer and autumn seasons, when tropical cyclones are most frequent and when cold fronts moving from the north-west can give very heavy precipitation, especially in USA.

The area of south east Asia affected by this climate has complicated, ill-understood climate. In winter the subtropical branch of the jetstream flows around the southern slopes of the Himalayas, while the polar-front jet moves to the north of the Tibetan plateau; both meet in an upper convergence zone over China. This upper convergence zone leads to subsidence over inner China and therefore to generally fine weather in winter. The two jet streams tend to reinforce each other over Japan, forming part of the very strong E Asian trough and giving extremely high wind speeds which can regularly reach 100 m/sec at the 200 mb level. In summer the subtropical jet stream flows to the north of Tibet and so the upper convergence zone over China disappears. In Japan an early summer rainfall maximum occurs, the "Bai-U" rains, followed by a later summer maximum. Fig 2.22 gives a schematic picture of the surface wind fields over SE Asia in summer (SW monsoon) and in winter (SE monsoon).

2.5.3 Mid-latitude climates

2.5.3.1 General Discussion These are dominated by the influence of the upper westerlies and their attendant troughs and ridges, and on the western sides of the continents the surface westerlies also dominate. So the natural subdivision is into maritime and continental climates. The maritime climates are found on the extreme western sides of N America, over much of Europe, and in the S Hemisphere in Southern Chile, in Tasmania and over most of New Zealand. Truly continental climates are found (in the N Hemisphere) either well inland or on the eastern sides of the continents where extreme seasonal variations of temperature result from their leeward location and the influence of summer monsoonal wind systems. Patagonia in Southern Argentina has some of the characteristics of an eastern mid-latitude climate but the continent is too narrow for the temperatures to be extreme while the influence of the Andes renders the climate extremely dry.

The mid-latitude oceanic climates mostly lie poleward of 40° and stretch well towards the poles because of the influence of warm or for their latitude relatively warm ocean currents. In N and S America the climates occupy very narrow belts only 200-300 km wide with an extraordinarily rapid transition zone to dry climates to the east. For example in parts of Northern Oregon and S Washington states the transition from the mid-latitude to the inland dry climate can be accomplished in a day's walk. The major characteristics of this oceanic climate are cool summers, mild winters, changeable weather, considerable cloudiness, and mostly adequate rainfall at all seasons. The seasonal emphasis in rainfall tends to be towards late autumn and winter on the extreme western margins, and late summer and early autumn further inland. Over north west Europe, there is a tendency for late spring to be driest, due to a peak frequency of blocking anticyclones at that season. Nevertheless seasonal rainfall deficiency does not cause a dormant period for plant growth.

Unusual aspects of the mid-latitude oceanic climate include the rather dry summers in the north west United States probably caused by the northerly extension of the N Pacific high over the Gulf of Alaska and the exceptionally mild winters over large areas of W Europe and the coastal fringe of Norway beyond the Arctic Circle, caused by the openness of these regions to the warmth of the eastern N Atlantic. The oceanic margins also exhibit a strong decrease of temperature with altitude and thus in the length of the summer growing season. The tree line in NW Scotland is at about 1000 ft though man has removed some of the remaining trees and it appears to be almost at sea level. The low tree line is partly a result of the exceptional windiness of the climate.

The Chilean mid-latitude climate is one of the cloudiest in the world as frequent depressions in the stormy sub-Antarctic summers and winters (see Fig 2.12) meet the formidable, steep, highland barrier of the southern Andes. The combination of extreme cloudiness, heavy precipitation and steep mountains has created one of the most remarkable climatically-caused phenomena in the world. Fig 2.23 and Charles Darwin's words (17) speak eloquently:- "In Eyre's Sound, in the latitude of Paris, there are immense glaciers, and yet the loftiest neighbouring mountain is only 6200 feet high. In this Sound, about fifty icebergs were seen at one time floating outwards, and one of them must have been at least 168 feet in total height. Some of the icebergs were loaded with blocks of no inconsiderable size, of granite and other rocks, different from the clay-slate of the surrounding mountains. The glacier furthest from the Pole, surveyed during the voyages of the Adventure and Beagle, is in lat 46° 50', in the Gulf of Penas. It is 15 miles long, and in one part 7 broad, and descends to the sea-coast. But even a few miles northward of this glacier, in the Laguna de San Rafael, some Spanish missionaries encountered "many icebergs, some great, some small, and others middle-sized," in a narrow arm of the sea, on the 22nd of the month corresponding with our June, and in a latitude corresponding with that of the Lake of Geneva!"

These glaciers, descending from the vast mid-latitude Patagonian ice-sheet, set Darwin thinking about the causes of the ice ages in subsequent pages of "Voyage of the Beagle".

The mid-latitude temperate continental climates (here defined as having a cold month under 32°F) exhibit a cold winter, with a durable snow cover, and a warm summer season, so that the annual range of temperature is large. In the maritime climate the temperature of one winter is much like that of another, but wide deviations from the normal seasonal temperature are characteristic of continental mid-latitude climates (as much as 10°C in extreme climates). Summer is the season of maximum rain, which is mostly convective.

A feature of some northern hemisphere mid-latitude climates is "blocking" which is a strong influence on UK weather variations. Fig 2.24 from Lejenas (1983) (18) shows the longitudinal variation of blocking in the N Hemisphere. In the S Hemisphere blocking is rarer but not uncommon near New Zealand for instance. The effect on weather over a month or a season can be surprisingly large. Fig 2.25 show two contrasting "blocked" and "westerly" Januaries over NW Europe (Folland (1983) (19)). The reasons for blocking are currently an area of much research.

2.5.3.2 Continental anticyclones

Blocking is, superficially, a result of stationary large amplitude ridges in the westerlies: anticyclones associated with the block have a warm core. In winter, the Eurasian and N American continents have cold anticyclones as a prominent feature of the climate: they are situated to the west of the regional climatological mean upper troughs (see GC Lecture 4). These cold anticyclones do not extend very far into the troposphere but bring intensely cold weather to the eastern half of the continents. The Siberian anticyclone is firmly sited well away from the western seaboard and is thus relatively undisturbed by mid-latitude depressions. However the

N American winter anticyclone tends to be sited over or to the east of the Rocky Mountains and it is not as stable a feature as the Siberian high, often being disrupted by depressions moving in from the west so that the winter weather of Central and Northern USA is decidedly changeable. Surges in the Siberian anticyclone can bring intense cold to Japan and even to south China (a subtropical climate) so that even Hong Kong has suffered air frost in winter (22°N).

2.5.4 Climates

The essential feature of a dry climate is that the potential annual water loss through evapotranspiration at the earth's land surface exceeds the annual gain from precipitation. Thus dry climates do not have a constantly replenished ground water. Fig 2.14 shows that arid climates cover a broad latitude band and occupy a considerable part of the earth's land surface. The deserts are usually surrounded by semi-arid lands (called steppes in Asia) where rainfall is very unreliable.

2.5.4.1 Typical types of desert climate

The tropical dry climates lying at about 20 or 25°N and S with their northern and southern margin at about 15° and near 35°. These climates coincide fairly closely with subsiding branch of the Hadley cell. The deserts do not reach the eastern coasts of continents (usually) because in these regions the subtropical anticyclones are much less stable. There are two types of semi-arid regions around these deserts: those that lie on the equatorial side and experience rainfall at the time of high sun due to the northward progression of the ITCZ, and those that lie on the poleward side of the desert and receive rain from the mid-latitude westerly circulation in winter. In N Africa, parts of the Atlas Mountains and Tunisia can receive 500-800 mm of rain. Typical desert rainfalls are much less (Cairo 30 mm in a year; Yuma, Arizona 80 mm; Calama, northern Chile usually no rainfall in the year). Average summer temperatures are about 30-35°C so maxima are as a rule near 40-45°C, and in the winter months a mean of 10-15°C is typical. In northern highland margins snow may fall and lie and mean winter temperatures may be similar to those of UK but with a much larger daily range. In the Central Asia deserts, winter temperatures are much lower (northern Tibet, China, parts of Mongolia).

2.5.4.2 Western ocean margins of dry climates

Here cool ocean currents strongly affect air temperature which can be as much as 10°C lower than normal for the latitude with a small annual range. There are surprising features of these dry oceanic climates, particularly their exceptional dryness eg in northern Chile. Lettau and Lettau (20) has shown that along the western margin of the Chilean desert the juxtaposition of very cold sea and intensely heated land gives rise to a low level jet stream which flows from south to north (Fig 2.26). This is considered to arise from a sea breeze type circulation which is so strong that it persists, less strongly, by night and thus all the time. If this circulation was spun up from rest as a "sea breeze" the Coriolis force would strongly influence it after a few days. Thus the wind tends to blow northwards parallel to the coast in geostrophic equilibrium with high pressure to the west and low pressure to the east but with a sea breeze circulation cell superimposed. The subsiding component of this sea breeze component occurs over a narrow band of ocean immediately adjacent to the coast and is thought to give rise to the long thin, cloudless strip of ocean off the Chilean coast often seen on satellite photographs. So air moving in this jet undergoes a corkscrewing, helical type of motion. The additional effects, if any, of the jet (500 m) on rainfall are not clear.

2.5.5 Climate of the S Pacific and S Ocean 150E-70W

This is the region least well observed but it is large in extent, covering 120° of longitude, and has some unexpected features. Fig 2.27 shows that in addition to the expected features which can be deduced from Fig 2.8-2.12, there is a zone of cloudiness and cyclogenesis stretching from near the Equator across the whole width of the Pacific to mid-latitudes. Thus the ITCZ in the tropical W Pacific appears to be directly connected with the westerlies near Cape Horn. This "South Pacific Convergence Zone (SPCZ)" shows up as a cloud band which stretches south east across the S Pacific (Fig 2.28) and represents convergence of air between the almost permanent anticyclone near Easter Island in the eastern Pacific and the more mobile anticyclones to the east of Australia and New Zealand. Detailed studies (Fig 2.28) show that there is a high frequency of cyclogenesis along this cloud band at least as far south as 40°S with a maximum near 150°W between about 25°S and 35°S. Of course the data are poor and details are uncertain. Some AGCM's reproduce this feature quite well, though it has not yet been much studied even in the models. An exception is a recent paper by James and Anderson (1984) (21) who discuss a similar but less permanent feature that may exist in the S Atlantic and does exist in the ECMWF model. Streten and Zillman give an extensive description of the climate of the S Pacific Ocean in Climate of the Oceans (reference containing (5)).

Another peculiar feature of the southern oceans, including the S Pacific region, is that the mean latitude of the depression belt around Antarctica varies semi-annually (Fig 2.29). This fluctuation is related to a more general semi-annual variation of circulation in the S Hemisphere (Hsu and Wallace (1976) (22)).

2.6 Summary

This long lecture has tried to show that the climate of the world and its variability is very interesting, complex and nowhere completely understood. It is a fitting subject for the World Climate Research Programme. I recommend the 15 volumes of the "World Survey of Climatology" for those who require factual detail on specific regions.

Acknowledgement

I have drawn freely from Mr D Jones 1982 Advanced Lecture 2.

REFERENCES

1. NEWELL et al (1974) The General Circulation of the Tropical Atmosphere. Vol 2, p151, MIT Press.

2. MINHINICK J AND FOLLAND C K (1984) The Meteorological Office Historical Sea Surface Temperature Data Set. Met O 13 Branch Memo No 137.

3. GADGIL S et al (1984) Ocean-atmosphere coupling over monsoon regions. Nature, 312, p141-143.

4. SCHWERTFEGER W (1976) Introduction to the Climate of Central and South America. In World Survey of Climatology; Climate of C and S America. Ed: W SCHWERTFEGER, Vol 12.

5. HOFLICH O (1984) Climate of the S Atlantic Ocean. In World Survey of Climatology; Climate of the Oceans. Ed: E van Loon, Vol 15, pp1-192.

6. UNTERSTEINER N (1984) The cryosphere. In The Global Climate. Ed: J T Houghton, Cambridge University Press.

7. HAHN O G (1981) Summary requirements for GCM's for observed snow and ice cover data. In Snow Watch 1980 Ed: G Kukla et al. World Data Centre A for Glaciology.

8. CHIU, L S (1983) Variation of Antarctic Sea Ice: an update. Mon Weath Rev, 111, pp578-580.

9. TREWARTHA G T AND HORN L H (1980) An introduction to climate. 5th Edition. McGraw-Hill.

10. MANABE S AND HOLLOWAY S (1975) The seasonal variation of the hydrologic cycle as measured by a global model of the atmosphere. J Geophys Res, 80, pp 1617-1649.

11. CRITCHFIELD, H J (1983) General Climatology. 4th Edition. Prentice-Hall.

12. RIEHL H (1979) Climate and weather in the tropics. Academic Press.

13. NEWELL R E AND KIDSON J W (1984) African mean wind changes between Sahelian Wet and Dry periods. J Clim, 4, pp 27-33.

14. RIDDAWAY R W (1980). Monsoons. In Advanced Lectures, 1980, on "Some aspects of dynamical meteorology". Unpublished: available from Met Office College.

15. HASTENRATH S et al (1984) Toward the monitoring and prediction of N E Brazil droughts. Q J Roy Met Soc, 110, pp 411-425.

16. McALPINE et al (1983) Climate of Papua and New Guinea. CSIRO. Aust Nat Univ Press.

17. DARWIN C (1979) reprint of "Voyage of the Beagle" (p 235). J M Dent.

18. LEJEAS H (1983). Characteristics of northern hemisphere blocking as determined from a long time-series of observational data. Tellus, 35A, pp 350-362.

19. FOLLAND C K (1983) Regional-scale interannual variability of climate - a north west European perspective. Met Mag, 112, pp 163-183.

20. LETTAU H H AND LETTAU K (Eds) Exploring the World's driest climate. Inst for Env Studies Rep 101, Univ of Wisconsin, pp 182-248.

21. JAMES I N AND ANDERSON T (1984) The seasonal mean flow distribution of large-scale weather systems in the southern hemisphere: the effects of moisture transports. Q J Roy Met Soc, 110, pp 943-966.

22. HSU C P AND WALLACE J M (1976) The global distribution of the annual and semi-annual cycles in sea-level pressure. Mon Weath Rev, 104, pp 1597-1601.

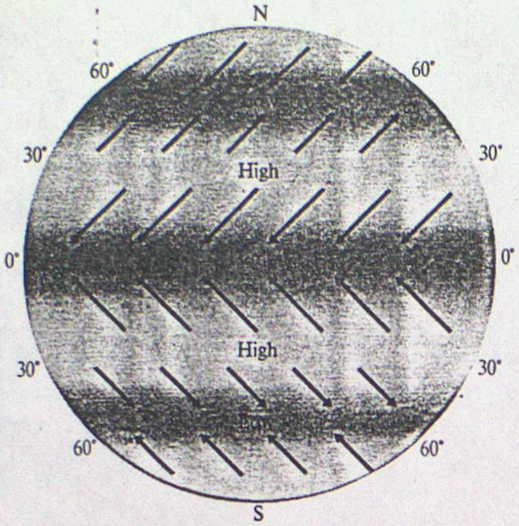
N
60°
60°
30°
30°
High
0°
0°
High
30°
30°
Low
60°
60°
S

Fig. 2.1. Idealized pattern of pressure and winds over the surface of the globe.

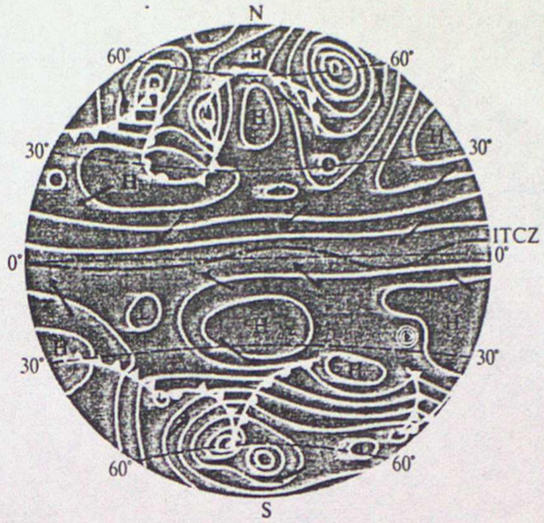
N
60°
60°
30°
30°
H
H
H
ITCZ
10°
0°
H
30°
30°
60°
60°
S

Fig. 2.1.B Typical distribution of pressure systems, winds and fronts near an equinox.

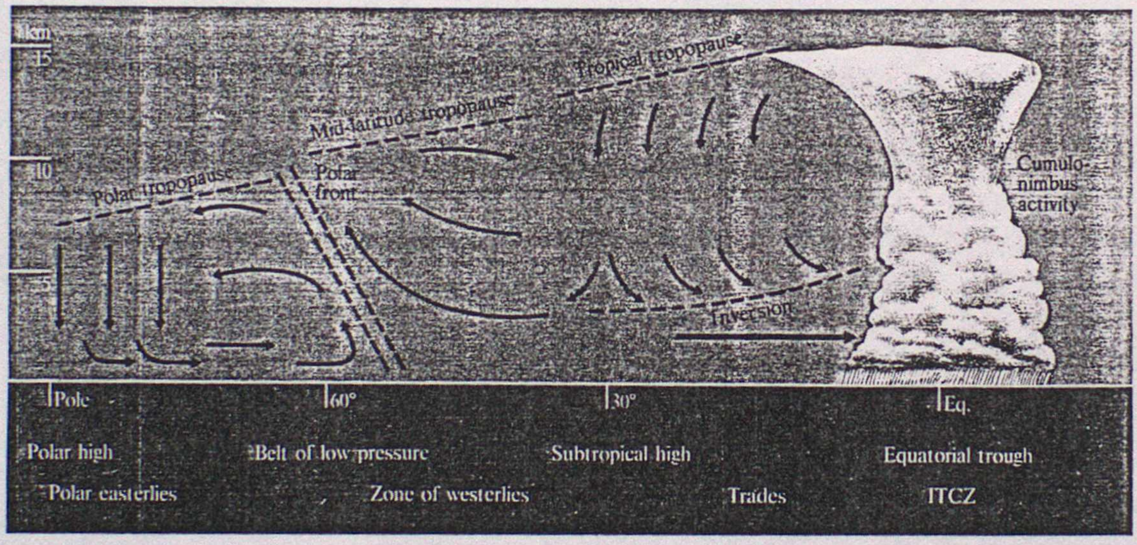
km
15
10
5
Tropical tropopause
Mid-latitude tropopause
Polar tropopause
Polar front
Cumulonimbus activity
Inversion
Pole
60°
30°
Eq.
Polar high
Belt of low pressure
Subtropical high
Equatorial trough
Polar easterlies
Zone of westerlies
Trades
ITCZ

Fig. 2.2 Schematic representation of the atmospheric general circulation, in vertical section from polar regions to the equator.

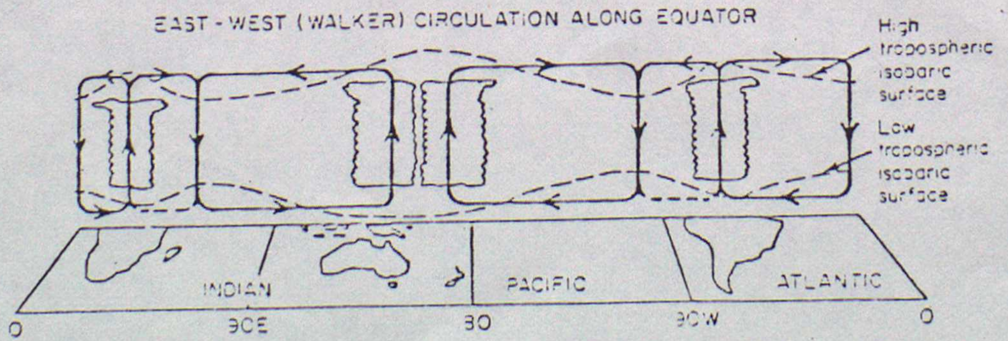
EAST - WEST (WALKER) CIRCULATION ALONG EQUATOR
High tropospheric isobaric surface
Low tropospheric isobaric surface
INDIAN
PACIFIC
ATLANTIC
0
90E
180
90W
0

Fig.2.3 Schematic view of the equatorial symmetric planetary scale features. Regions of ascent correspond to locations C in Fig. 9.2. Note the dominance of the Pacific Ocean - Indonesian cell which is referred to as the Walker Circulation. (From J. Zillman, private communication.)

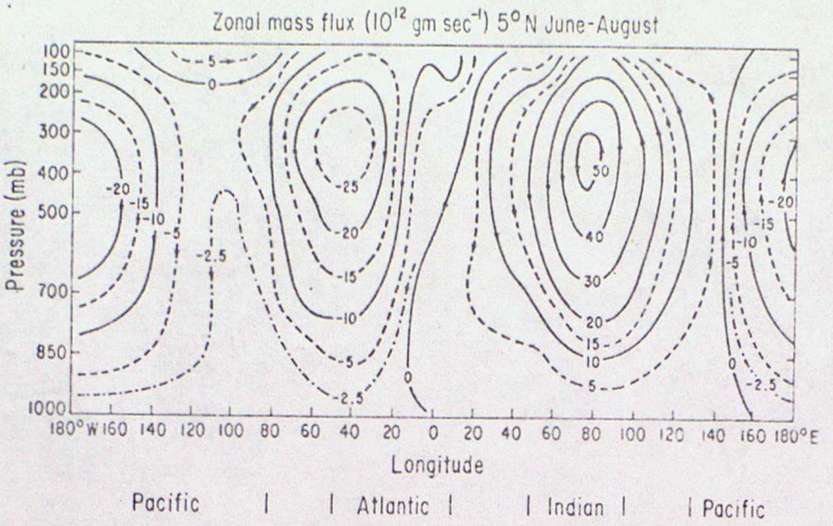

Fig. 2.4 A representation of the zonal mass flux, averaged over the region 0°–10°N for June–August. Contours do not correspond to streamlines, but give a fairly good representation of the velocity field associated with the Walker circulation. [From Newell *et al.* (1974), "The General Circulation of the Tropical Atmosphere," Vol. 2, p. [illegible] Fig. 9.3; reproduced by permission of the MIT Press.]

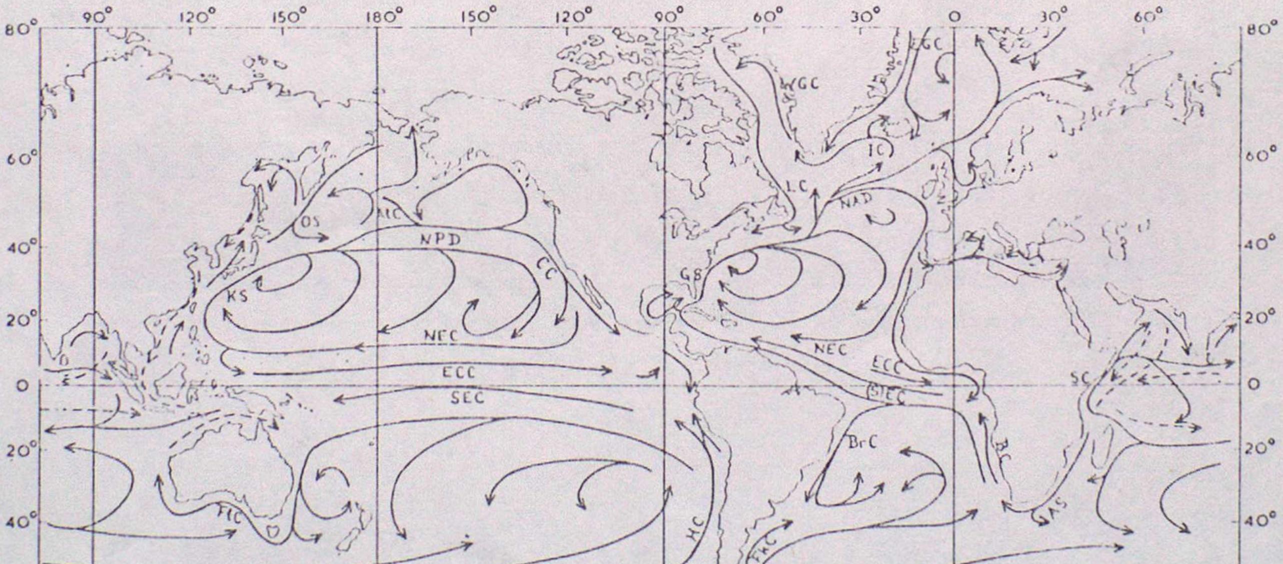

90° 120° 150° 180° 150° 120° 90° 60° 30° 0 30° 60°
80° 60° 40° 20° 0 20° 40° 60° 80°
EGC
WGC
IC
LC
NAD
OS
AC
NPD
CC
KS
GS
NEC
ECC
SEC
SC
BrC
BC
AS
HC
FKC
EAC
WWD
EWD

FIG 2.6 Main surface currents of the oceans.
(The abbreviations for the names of the currents are expanded in Table 8.2.)

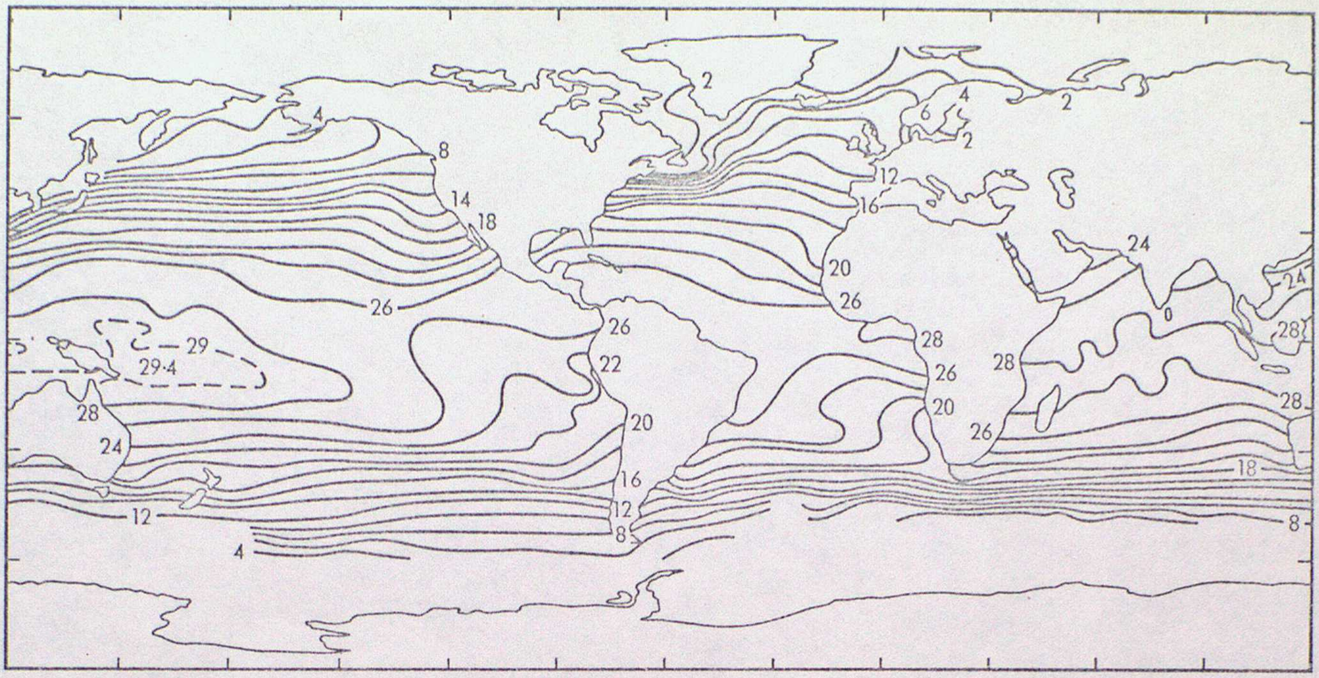
2
4
6
4
2
2
8
14
18
12
16
24
24
20
26
26
26
28
26
0
28
28
29
29·4
22
28
20
20
26
28
24
18
16
12
12
8
4
8

Average sea surface temperature (1951-80), January (Based on MOHSST 3)

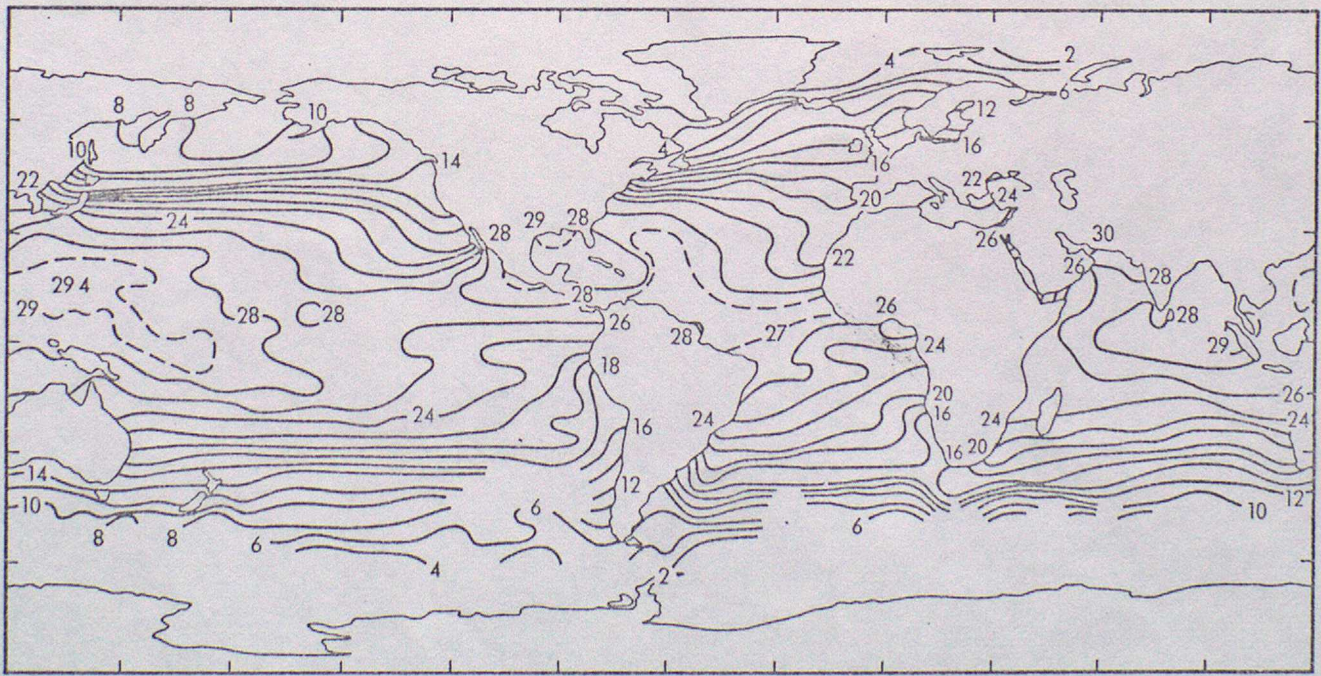
8
8
10
10
22
14
24
28
29
28
4
2
4
6
12
16
16
22
24
20
26
30
26
28
29 4
29
28
C28
28
28
26
18
28
27
22
26
24
20
16
16
20
24
16
24
26
24
29
12
10
14
10
8
8
6
6
4
6
2

Average sea surface temperature (1951-80), July (Based on MOHSST 3)

DO 3723

Fig. 2.5

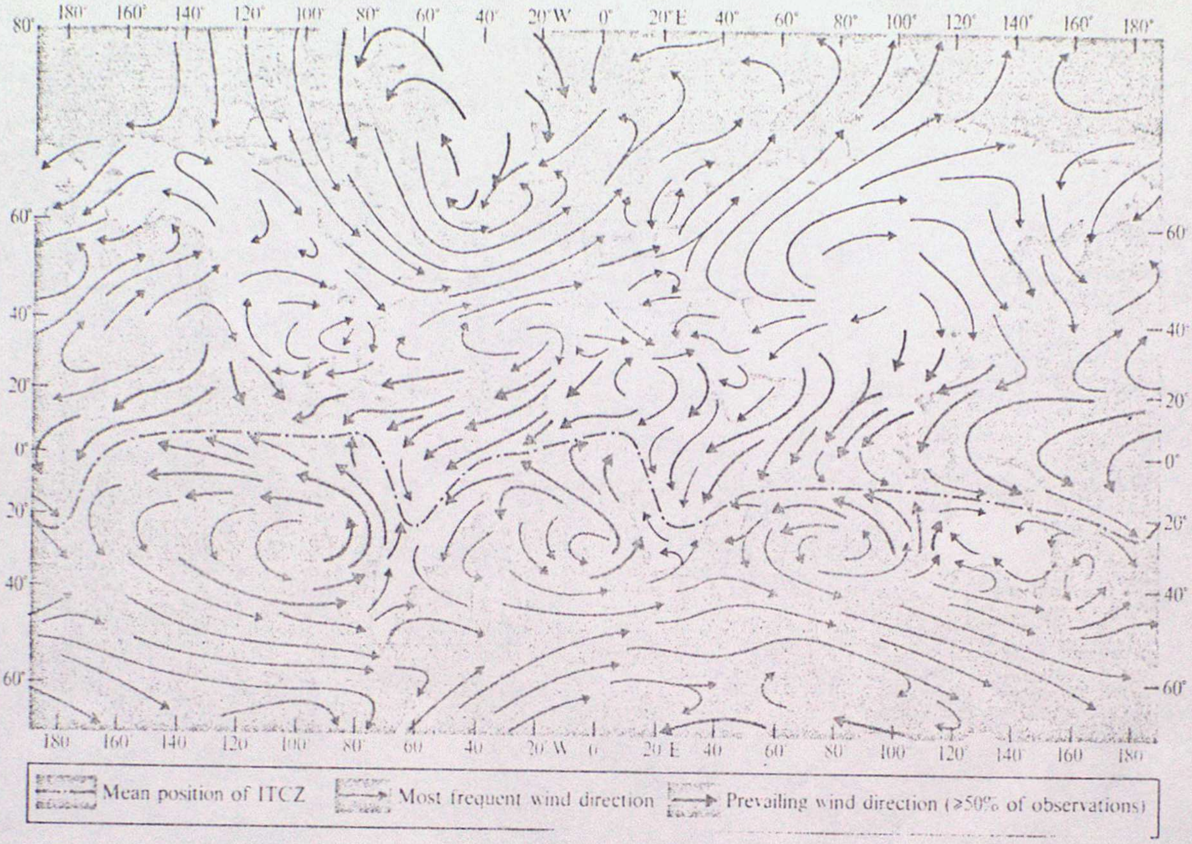

180° 160° 140° 120° 100° 80° 60° 40° 20°W 0° 20°E 40° 60° 80° 100° 120° 140° 160° 180°
80° 60° 40° 20° 0° 20° 40° 60°
Mean position of ITCZ
Most frequent wind direction
Prevailing wind direction (≥50% of observations)

Fig.2.7A Surface winds and ITCZ January

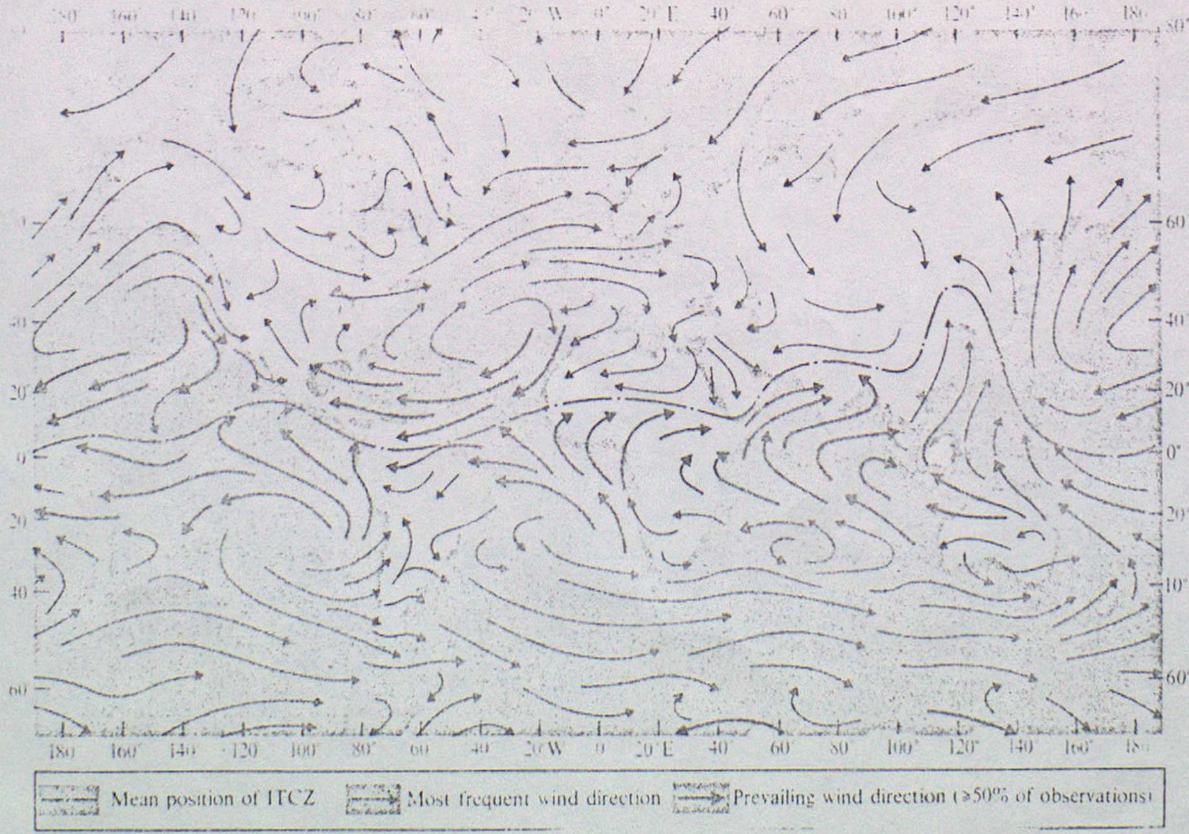

180 160 140 120 100 80 60 40 20 W 0 20 E 40 60 80 100 120 140 160 180
60° 40° 20° 0° 20° 40° 60°
Mean position of ITCZ
Most frequent wind direction
Prevailing wind direction (≥50% of observations)

Fig.2.7B Surface winds and ITCZ July

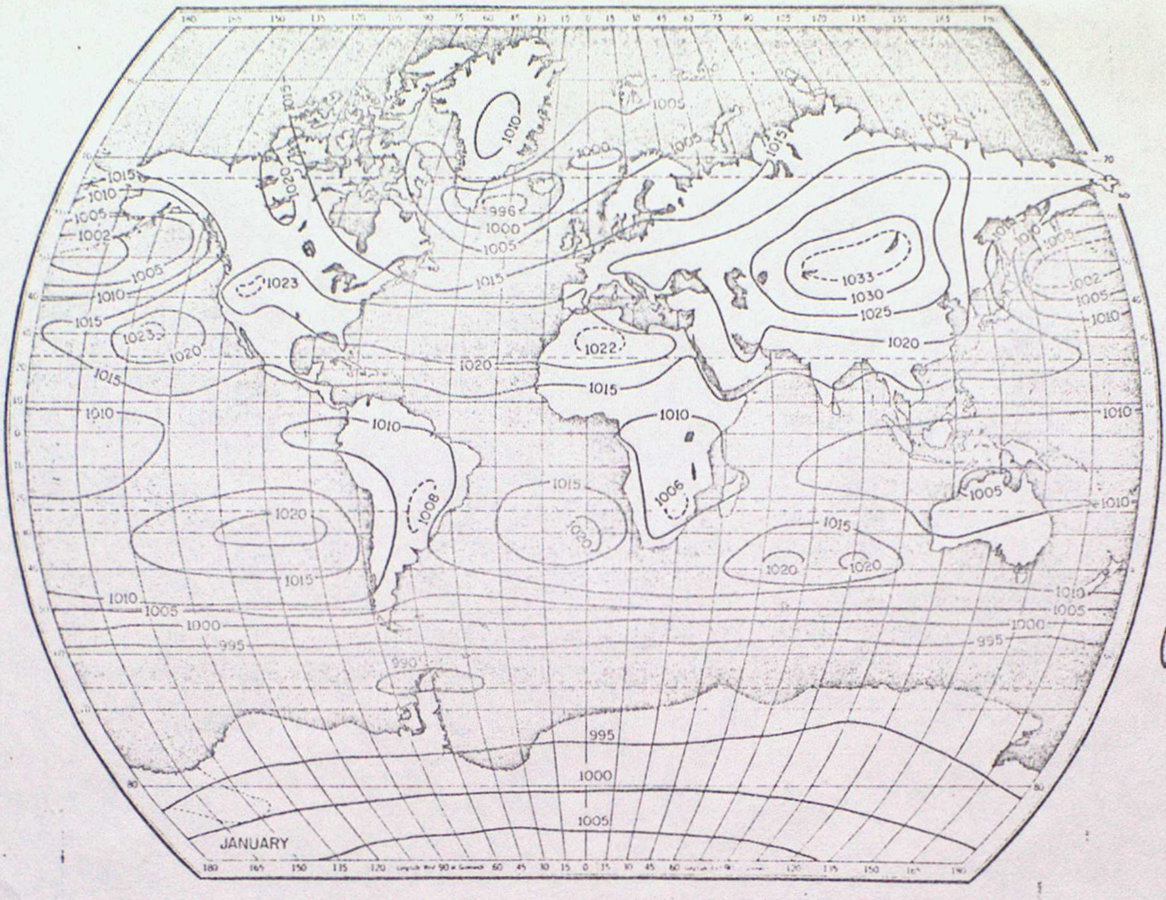
JANUARY
1010
996
1000
1005
1015
1023
1020
1022
1033
1030
1025
1006
1008
995
990

A

World sea-level pressure (mbs) in January. (Modified Van der Grinten projection.)

FIG 2.8

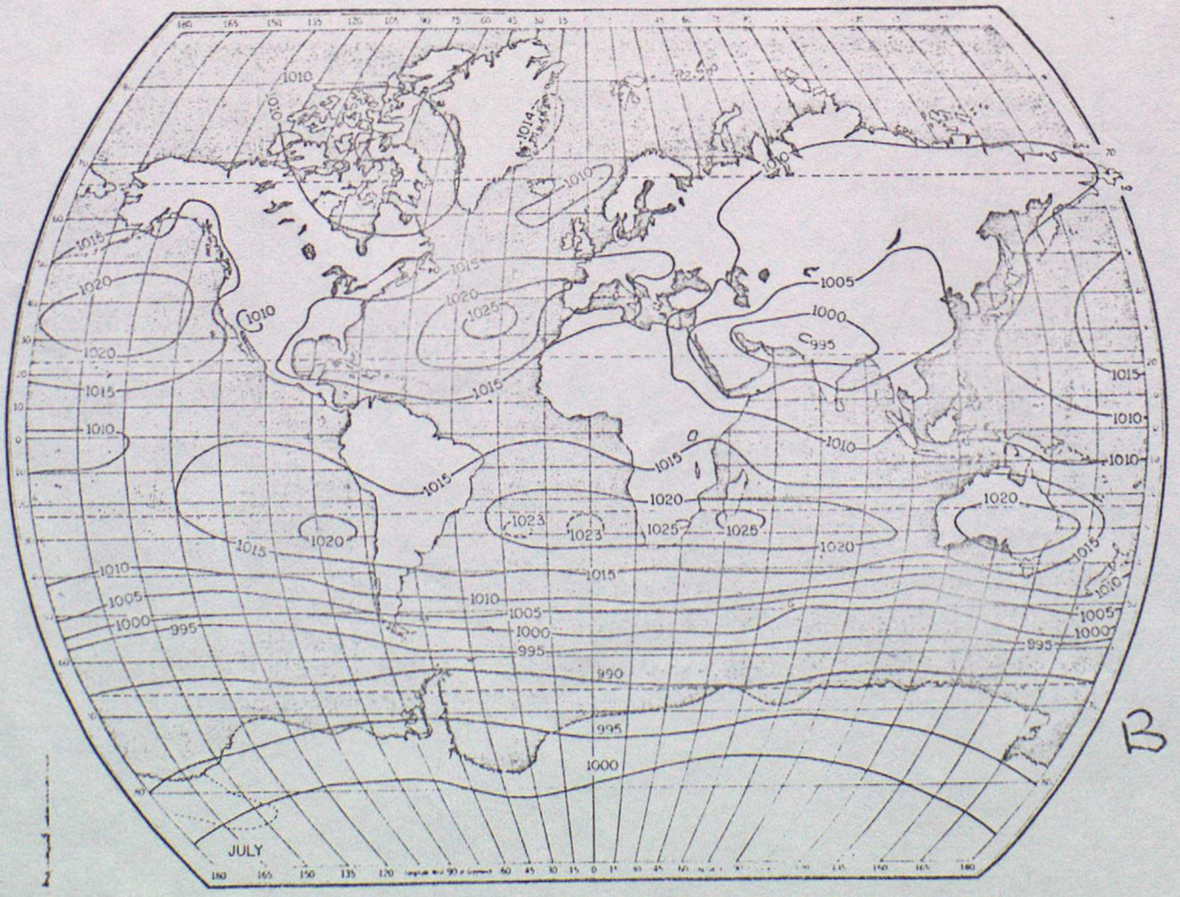
JULY
1010
1014
1015
1020
1025
1005
1000
995
1023
990

B

World sea-level pressure (mbs) in July. (Modified Van der Grinten projection.)

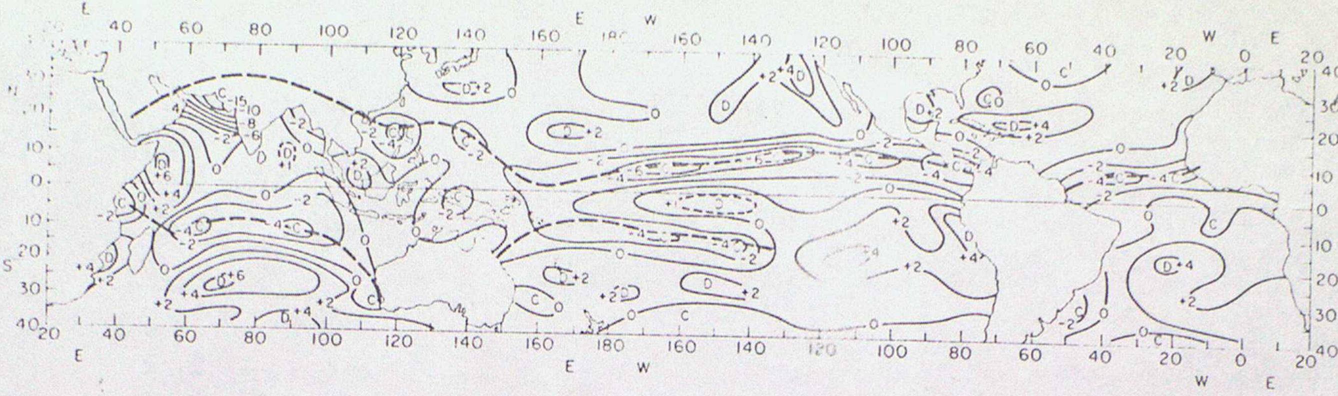
40
60
80
100
120
140
160
180
160
140
120
100
80
60
40
20
0
20
E
W
N
S
C
D
+2
-2
+4
-4
0

Fig. 2.9 Chart of mean horizontal velocity divergence ($10^{-6}s^{-1}$) for July over the oceans. ITCZ position is dashed

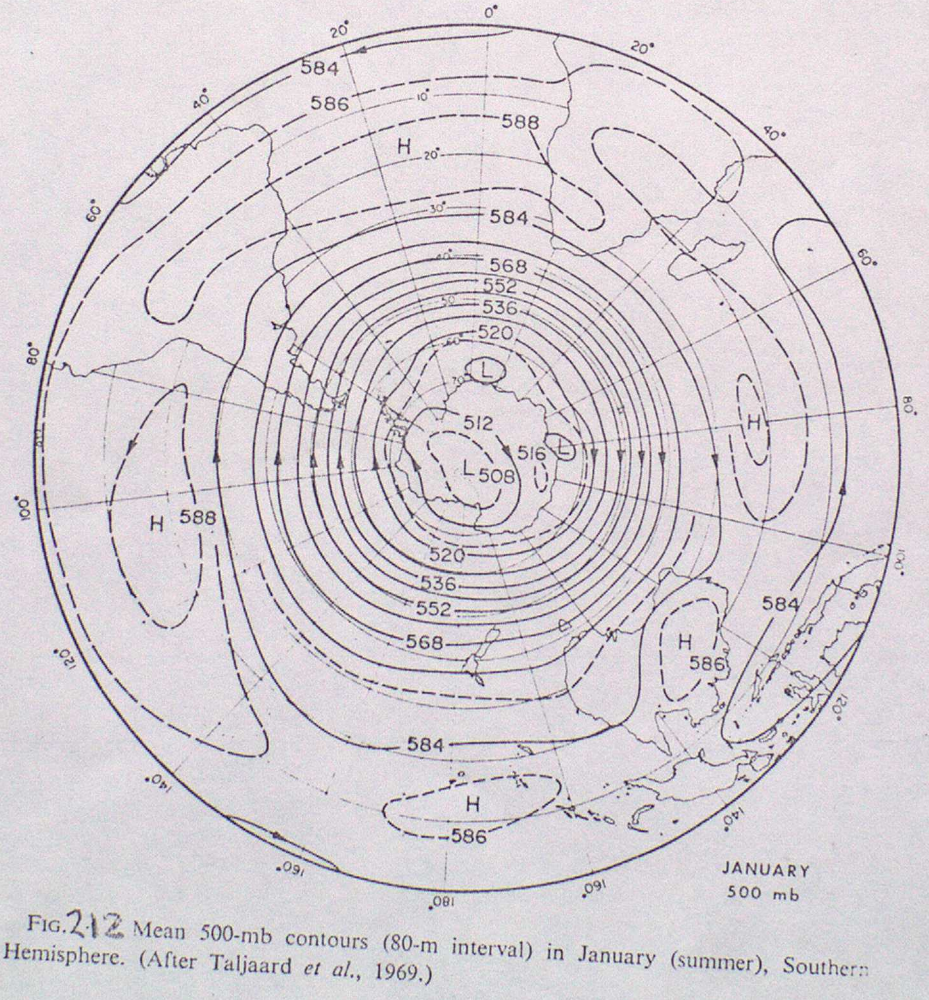
0°
20°
40°
60°
80°
100°
120°
140°
160°
180°
584
586
588
H
L
568
552
536
520
512
516
508
JANUARY
500 mb

FIG. 2.12 Mean 500-mb contours (80-m interval) in January (summer), Southern Hemisphere. (After Taljaard *et al.*, 1969.)

STREAMLINES 850mb DEC-FEB

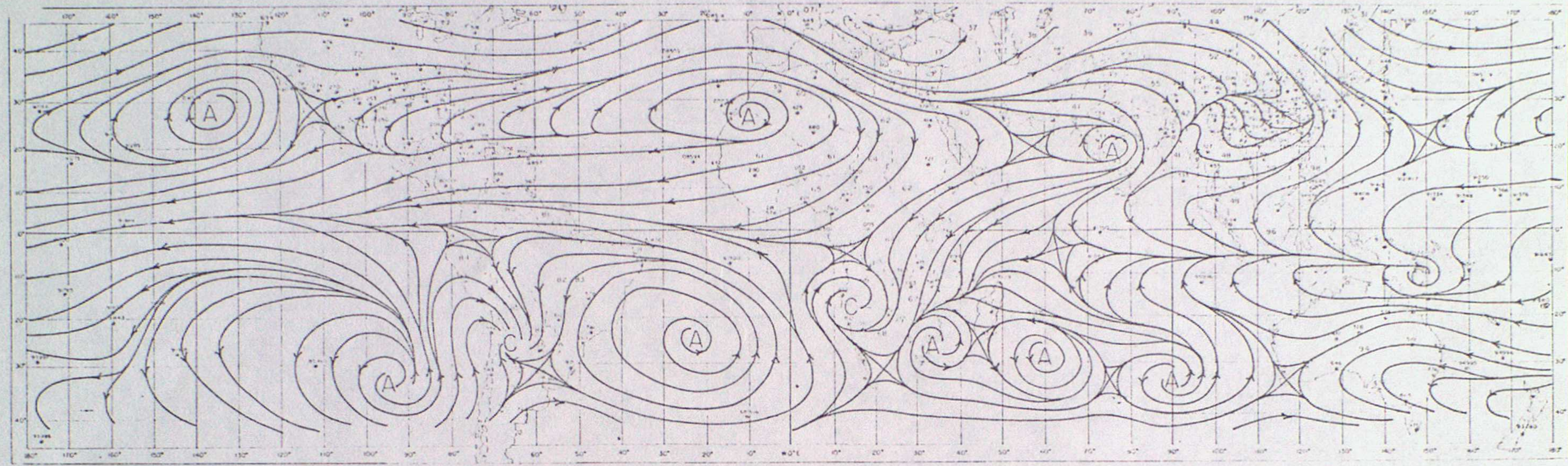
A
A
A
A
A
C
C
A
A
A
A
A

FIG 2.10

STREAMLINES 200mb – DECEMBER – FEBRUARY

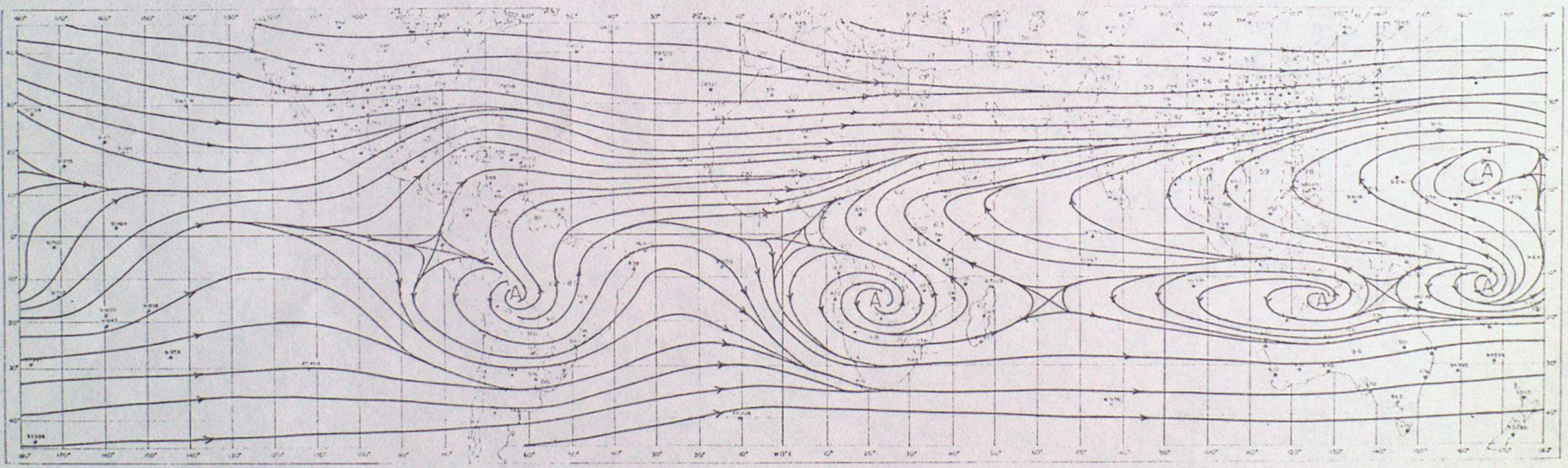

STREAMLINES 850mb JUN-AUG

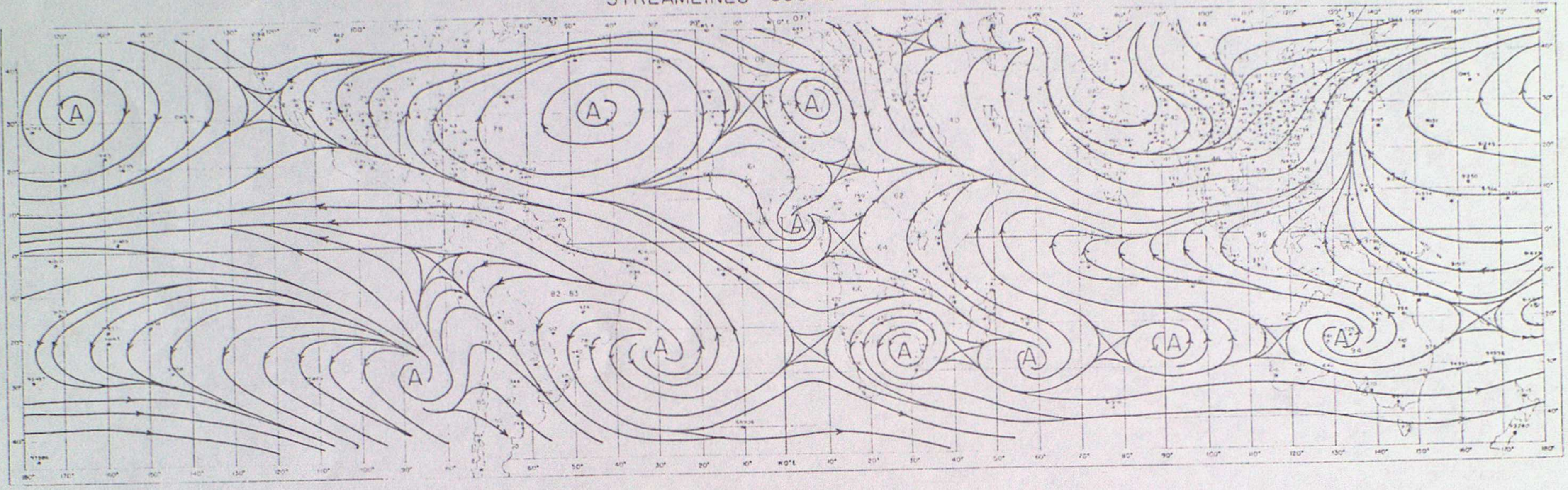
A
A
A
A
A
A
A
A
A
A
A

FIG 2.11

STREAMLINES 200mb JUN-AUG

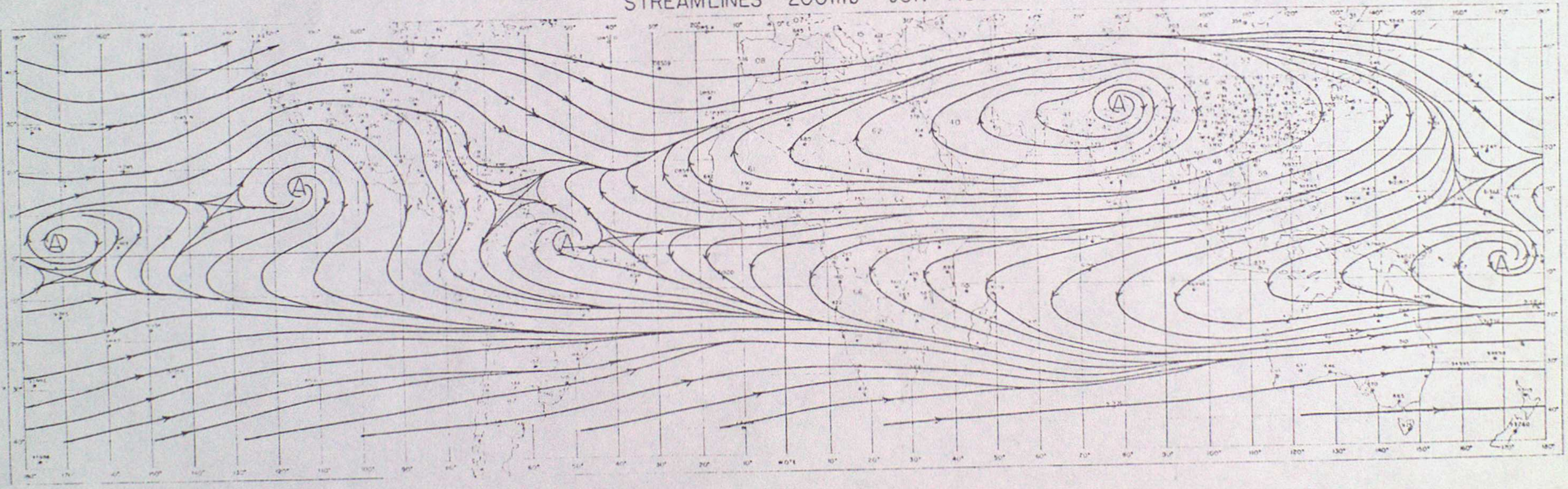

(*a*) Snow and ice in the northern hemisphere at their minimum and maximum extent. (*b*) Snow and ice in the southern hemisphere at their minimum and maximum extent (from Meier, 1983). It should be noted that the summer sea ice extent in Fig. 8.1 appears larger than the corresponding value shown in Table 8.1. The reason is that sea ice 'edge' or 'boundary' are definable only in the context of the method by which the data were obtained or by the purpose for which the data are to be used. The best set of data for Antarctic sea ice was derived from passive microwave images (ESMR on NIMBUS 5, beginning in December 1972). For reasons of accuracy and unambiguous interpretation of these data, the ice limit was taken to be at concentrations of > 15%, which tends to make the total ice extent appear large. Ships reporting the encounter with ice are likely to place the 'ice margin' at a far higher concentration.

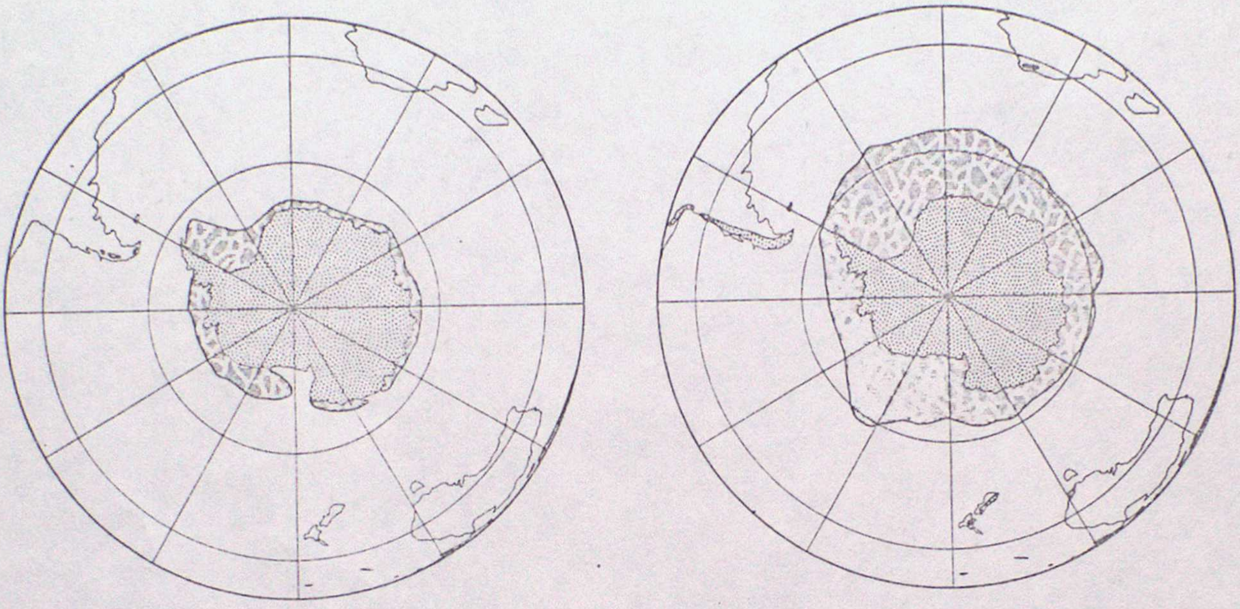

(*a*)

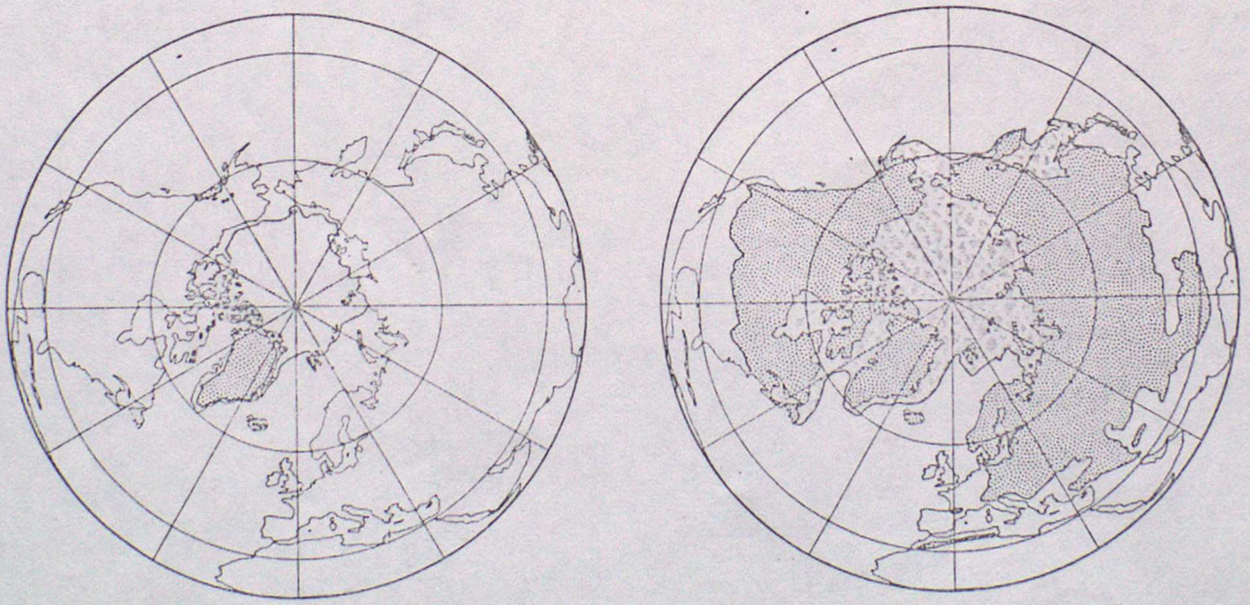

(*b*)

FIG 2.13A

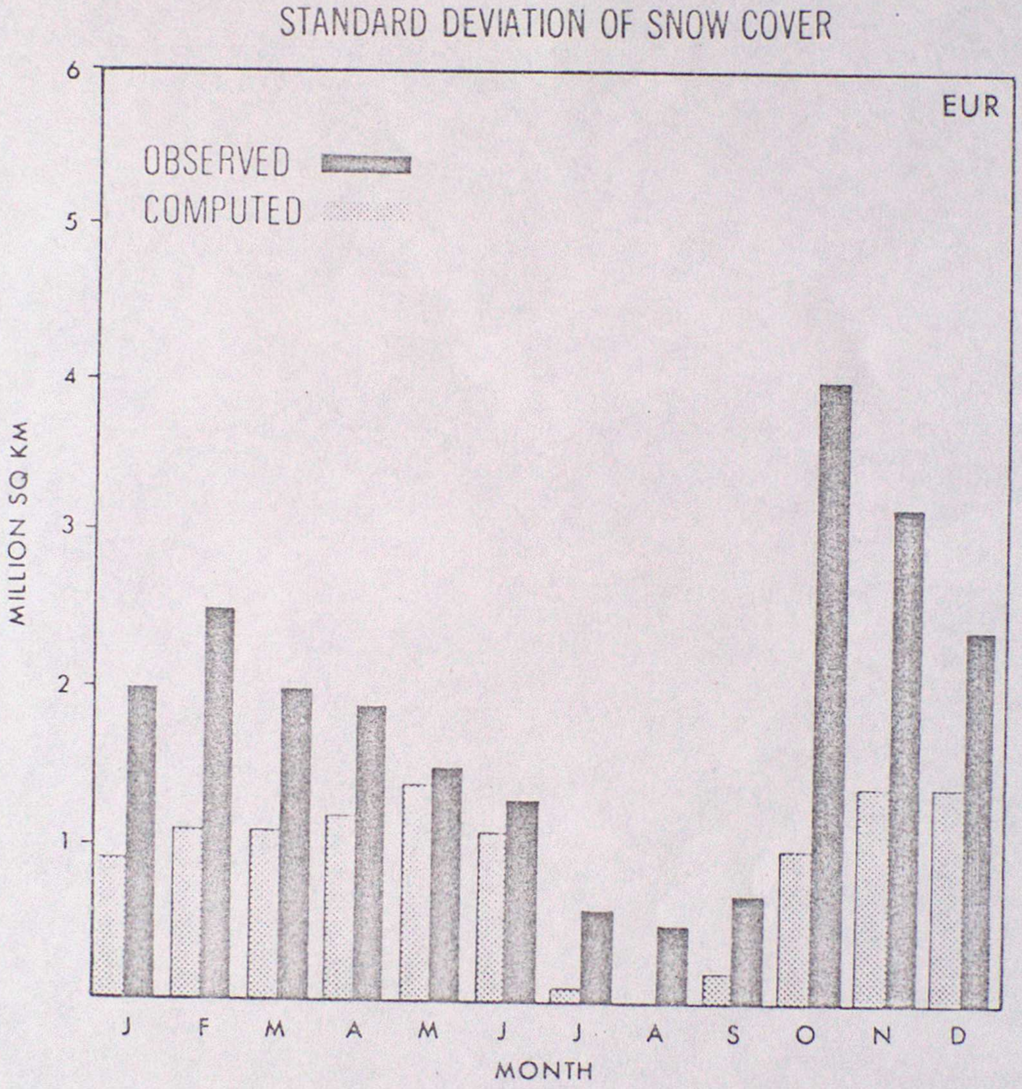

Fig.2.13B Standard deviation of monthly mean snow cover of Eurasia as observed (Matson, personal communication) and as computed by the GCM.

FIG 2.14

CLIMATES OF THE WORLD

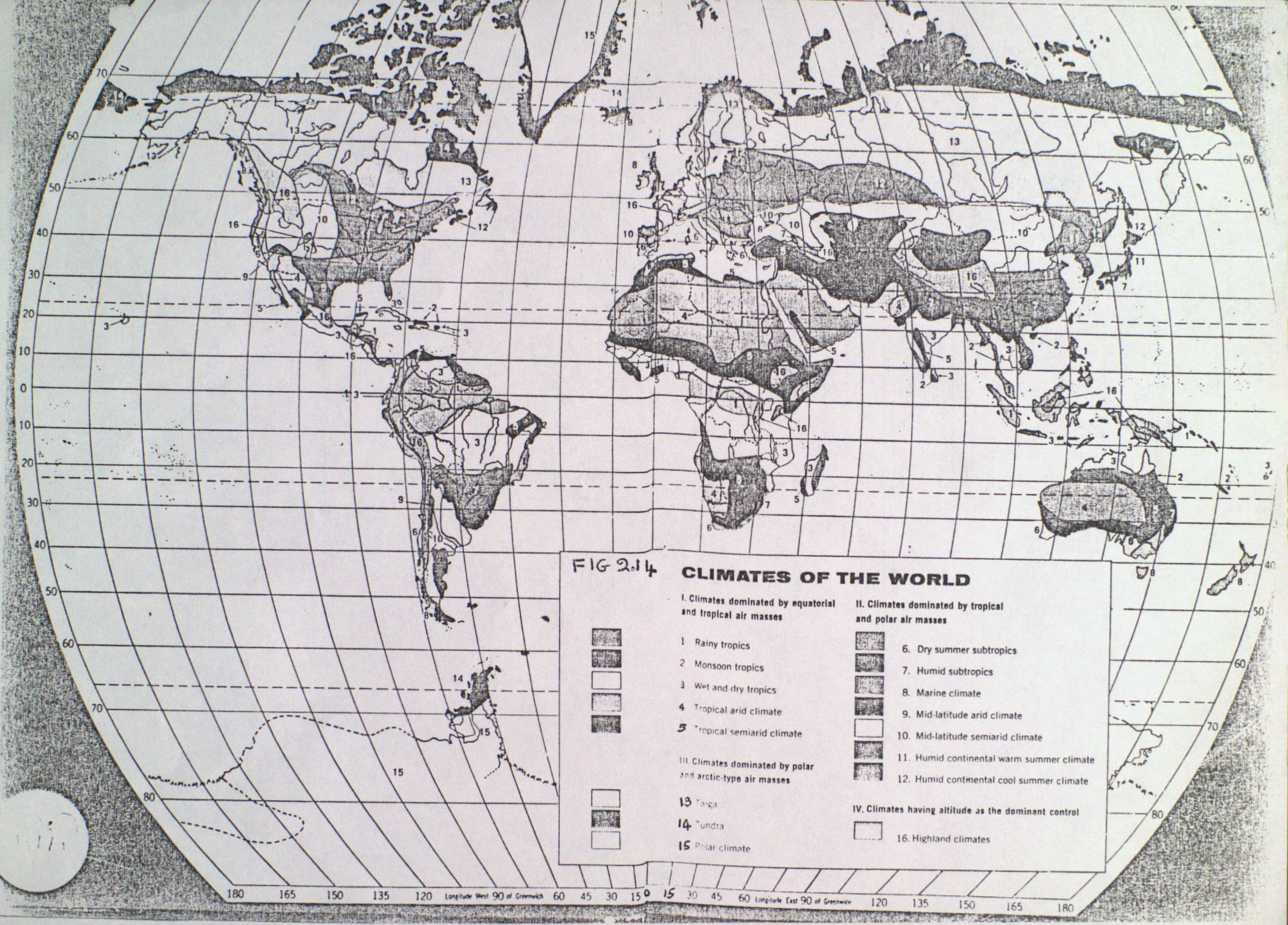
I. Climates dominated by equatorial and tropical air masses
1 Rainy tropics
2 Monsoon tropics
3 Wet and dry tropics
4 Tropical arid climate
5 Tropical semiarid climate
II. Climates dominated by tropical and polar air masses
6. Dry summer subtropics
7. Humid subtropics
8. Marine climate
9. Mid-latitude arid climate
10. Mid-latitude semiarid climate
11. Humid continental warm summer climate
12. Humid continental cool summer climate
III. Climates dominated by polar and arctic-type air masses
13 Taiga
14 Tundra
15 Polar climate
IV. Climates having altitude as the dominant control
16. Highland climates
180
165
150
135
120
Longitude West 90 of Greenwich
60
45
30
15
0
15
30
45
60
Longitude East 90 of Greenwich
120
135
150
165
180
70
60
50
40
30
20
10
0
10
20
30
40
50
60
70
80

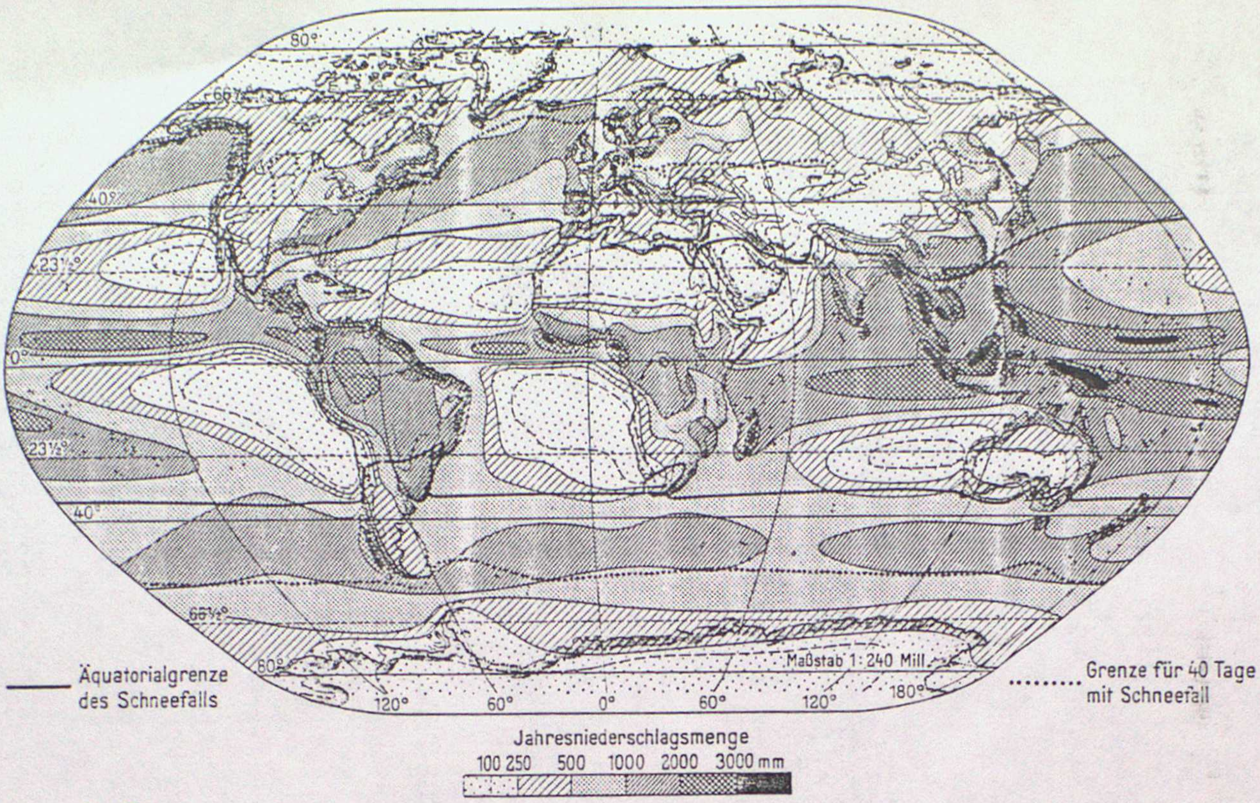
80°
66½°
40°
23½°
0°
23½°
40°
66½°
60°
120°
60°
0°
60°
120°
180°
Maßstab 1:240 Mill.
Äquatorialgrenze des Schneefalls
Grenze für 40 Tage mit Schneefall
Jahresniederschlagsmenge
100 250 500 1000 2000 3000 mm

FIGURE 2.15 Average annual precipitation over the earth (Jahresniederschlagsmenge) in mm. Also shown are the equatorward limits of snowfall (Äquatorialgrenze des Schneefalls) and the limits for 40 days with snowfall (Grenze für 40 Tage mit Schneefall). (*From Meinardus and Moller.*)

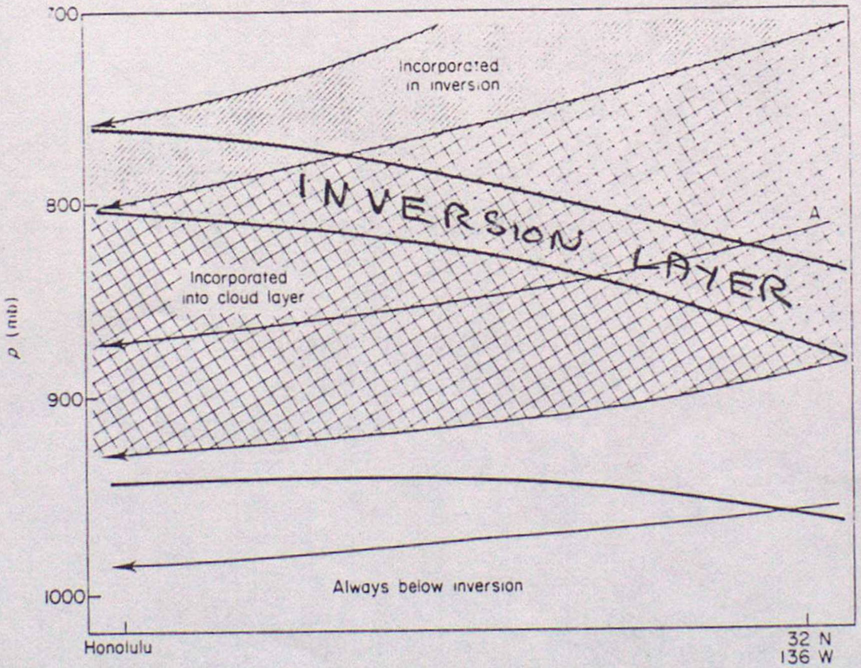
700
800
900
1000
p (mb)
Incorporated in inversion
INVERSION LAYER
A
Incorporated into cloud layer
Always below inversion
Honolulu
32 N
136 W

Fig 2.16 The flow of mass through the trade inversion.

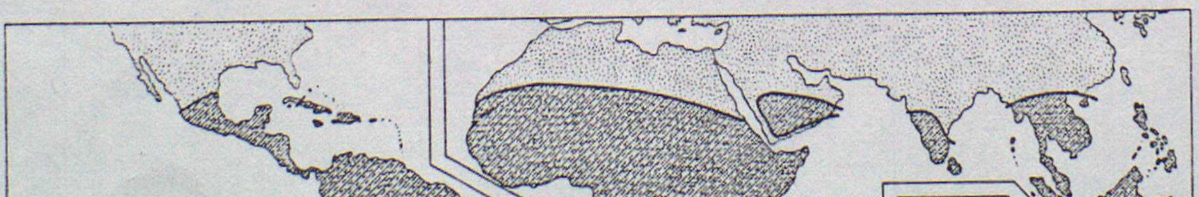
Land areas where average daily range of temperature exceeds annual range

FIGURE 2.17 distinctive feature of most tropical climates is that average *daily* range of temperature exceeds average *annual* range. (*After Troll*)

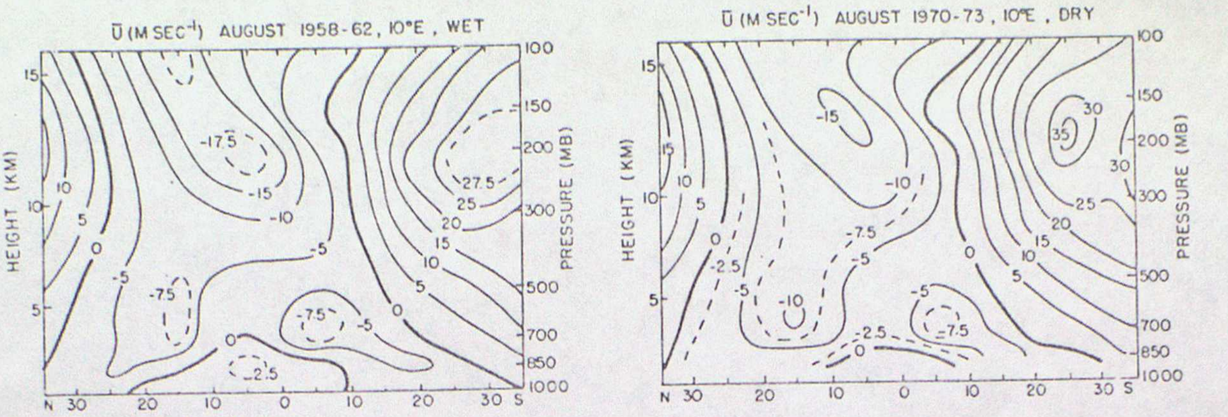

FIG 2.18A

Fig . Meridional cross-sections along 10°E of mean zonal wind for August 1958–1962 and August 1970–1973. Units: m s^{-1}

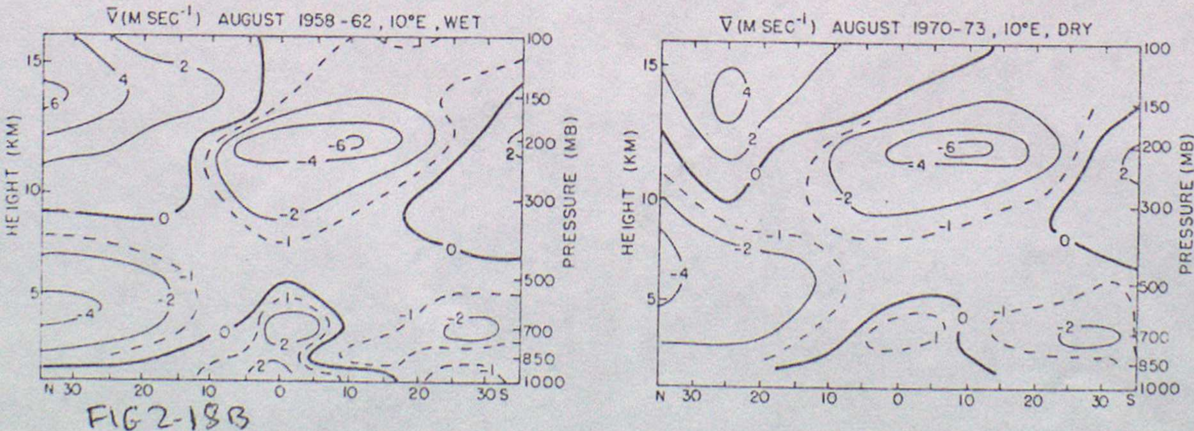

FIG 2-18B

Meridional cross sections along 10°E of mean meridional wind for August 1958–1962 and August 1970–1973. Units: m s^{-1}

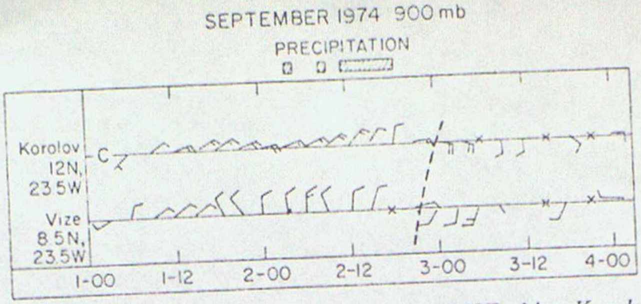

A

Three-hourly 900 mb winds (knots) at the USSR ships *Korolov* and *Vize*. 1-3 September, 1974. Dashed line marks trough passage moving from east to west. Precipitation periods at *Vize*: shaded boxes.

FIG 2.19 A

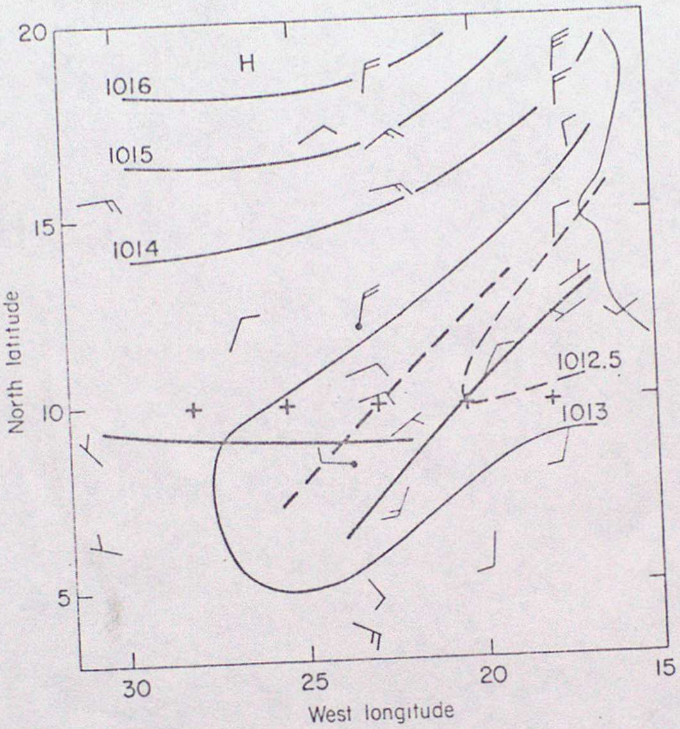

B

FIG 2.19B Surface map for the GATE area, 2 September, 1974, 1200 GMT. Winds in knots, pressures and isobars in millibars. Heavy solid lines: moving wave in easterlies oriented northeast-southwest, equatorial trough oriented east-west. Dashed line: position of trough 12 hours later. Crosses: 12-hourly trough positions at latitude 10°, 2-4 September, 00 GMT.

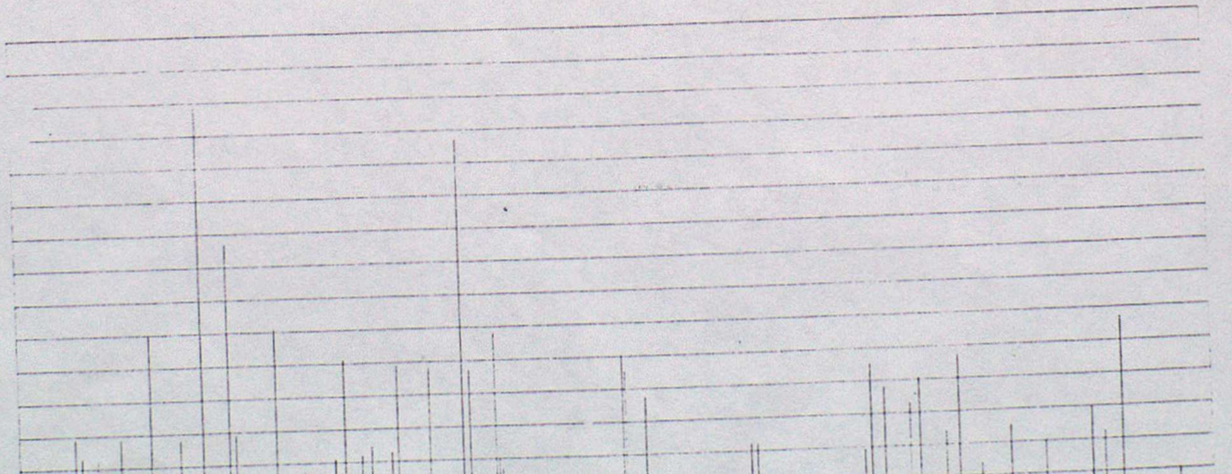

FIGURE 2.20 Daily rainfall amounts for one year (1928) at Andagoya, an *Ar* station in western Colombia inland from the Pacific coast. Here the average annual rainfall is exceedingly heavy (7089 mm: 282 in), and no month is dry. In 1928, there were only 48 days on which no rain fell. (*After M. Hendl,* Einführung in die physikalische Klimatologie. *Band II*)

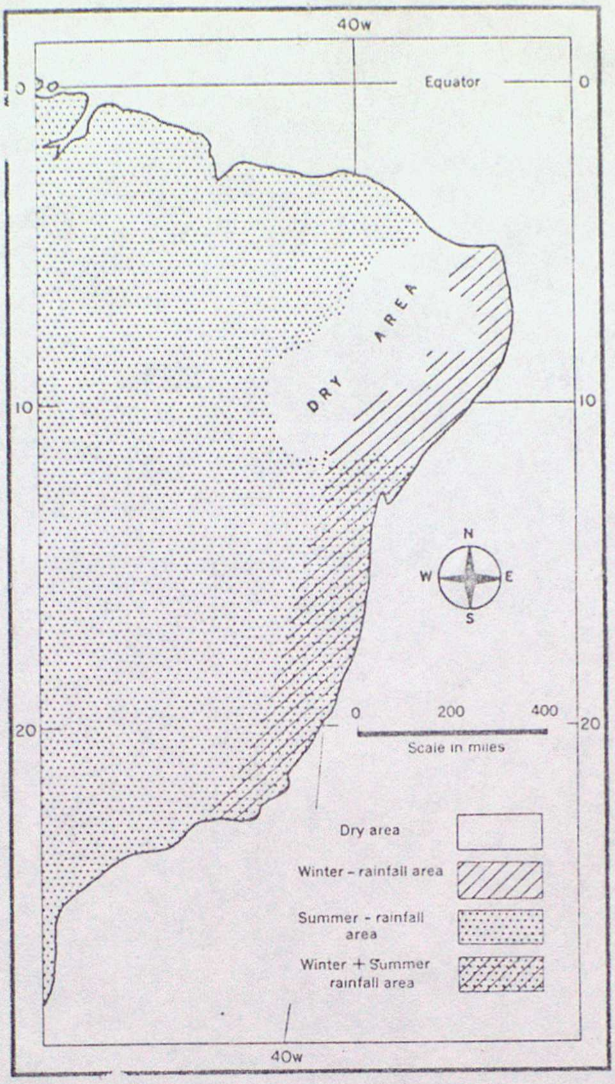
40w
Equator
0
10
20
DRY AREA
N
W
E
S
0
200
400
Scale in miles
Dry area
Winter - rainfall area
Summer - rainfall area
Winter + Summer rainfall area
40w

FIGURE 2.21 The dry area in eastern Brazil occupies an intermediate position between the winter-rainfall region to the east and south and the strong summer-rainfall region to the interior and west. It normally escapes the full effects of the disturbances which produce these contrasting seasonal rainfalls. (*From Trewartha,* The Earth's Problem Climates)

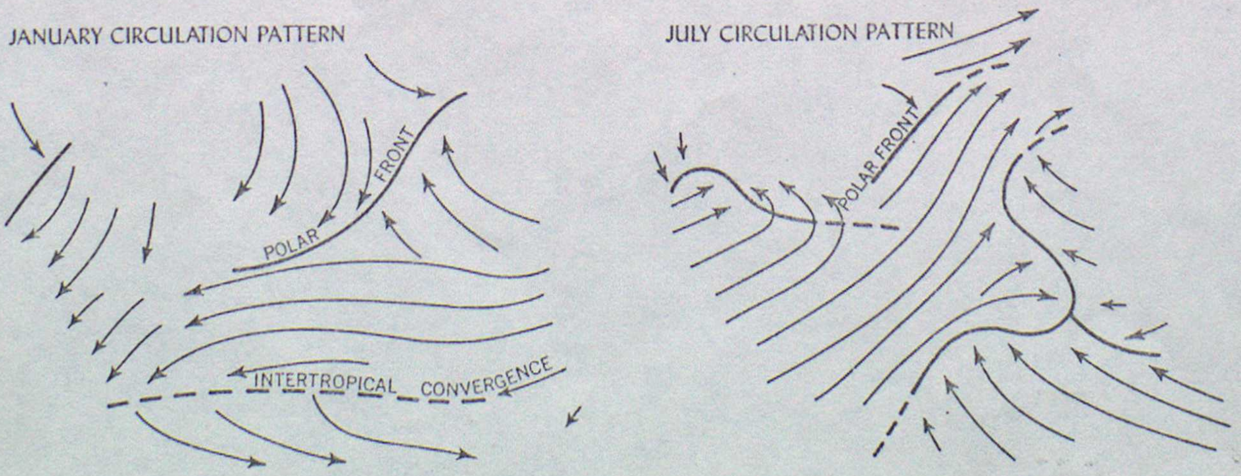
JANUARY CIRCULATION PATTERN
POLAR FRONT
INTERTROPICAL CONVERGENCE
JULY CIRCULATION PATTERN
POLAR FRONT

FIGURE 2.22 Principal elements of the low-level circulation patterns over eastern and southern Asia in the cold and the warm seasons. (*After Thompson, Watts, Flohn, and others. From Trewartha,* The Earth's Problem Climates, *University of Wisconsin Press, Madison, Wis.*)

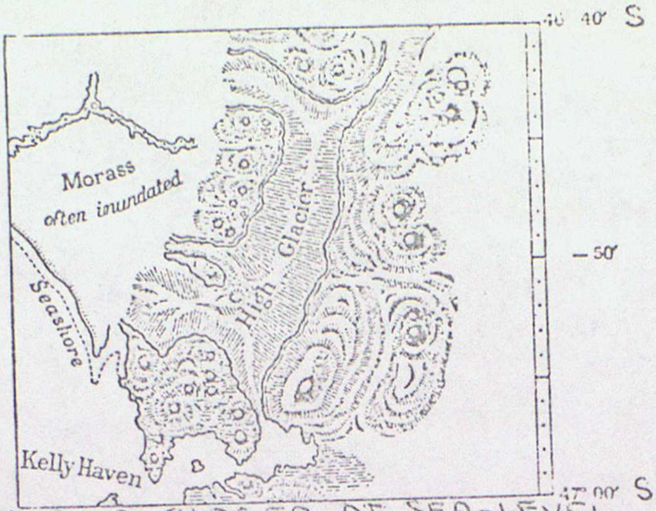
46°40' S
Morass
often inundated
High Glacier
Seashore
Kelly Haven
— 50'
47°00' S

FIG 2.23 GLACIER AT SEA-LEVEL

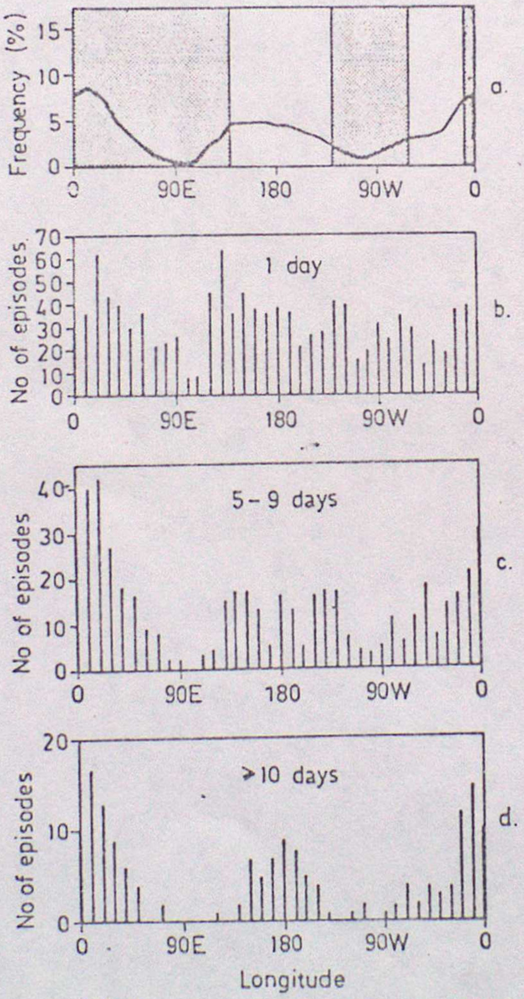

Fig.2.24 Longitudinal variation of blocked 500-mb flow averaged over the whole year. Continents are shaded. (b–d) Frequency distribution of blocking episodes as a function of longitude. 1950–1979. Duration 1 day (b), 5–9 days (c) and >10 days (d).

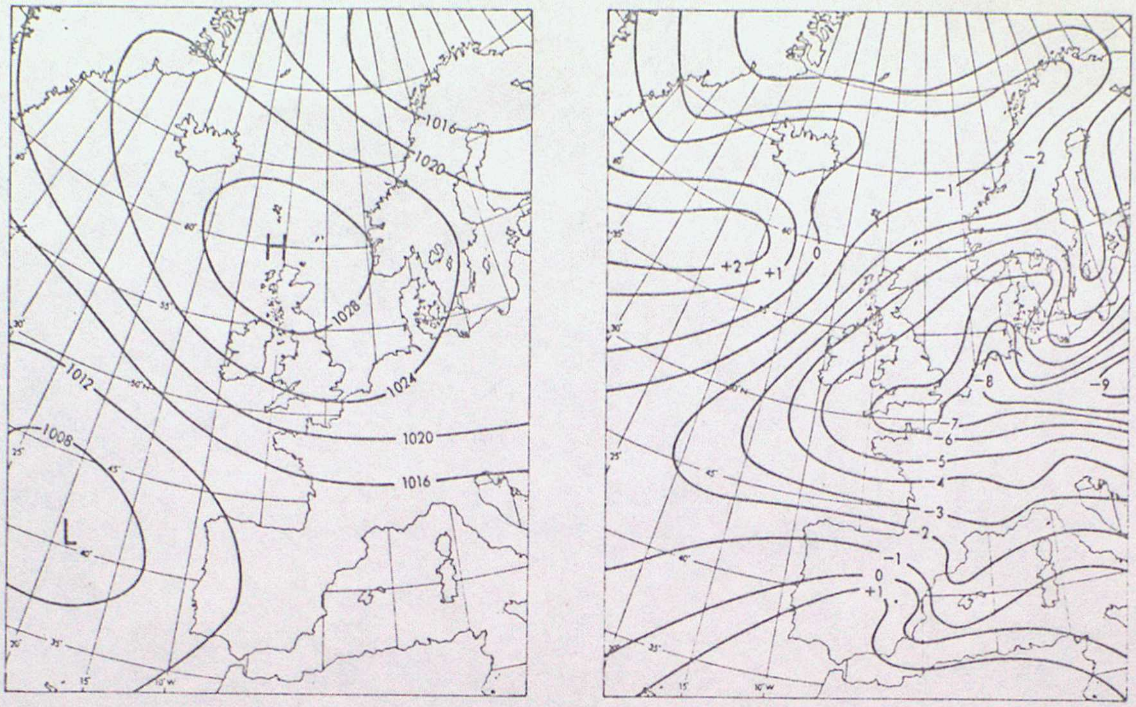

1016
1020
H
1028
1024
1012
1020
1016
1008
L
−2
−1
+2
+1
0
−8
−9
−7
−6
−5
−4
−3
−2
−1
0
+1

(a) (b)

A

Fig 2.25 (a) Average pressure (mb) at mean sea level, January 1963.
(b) Average screen-level temperature anomaly (°C), January 1963. (Anomalies mainly from 1931–60 station averages.)

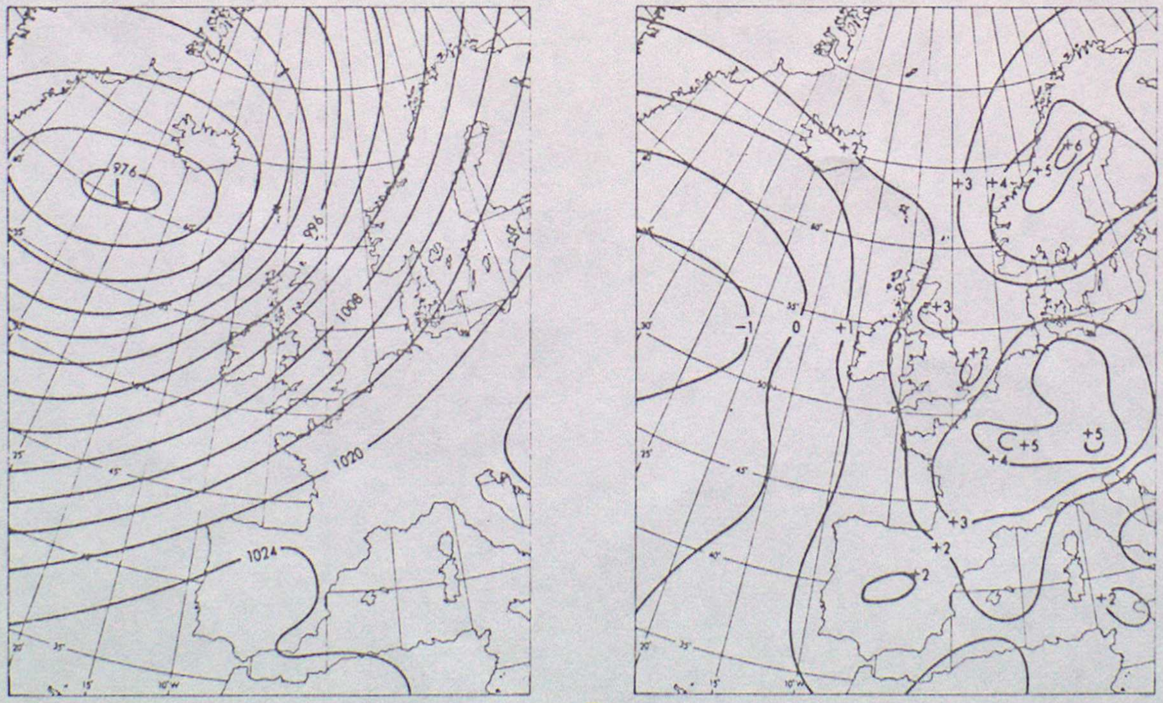

976
L
996
1008
1020
1024
+2
+3
+4
+5
+6
−1
0
+1
+3
+2
+5
+5
+4
+3
+2
+2
+2

(a) (b)

B

Fig (a) Average pressure (mb) at mean sea level, January 1974.
(b) Average screen-level temperature anomaly (°C), January 1974. (Anomalies mainly from 1931–60 station averages.)

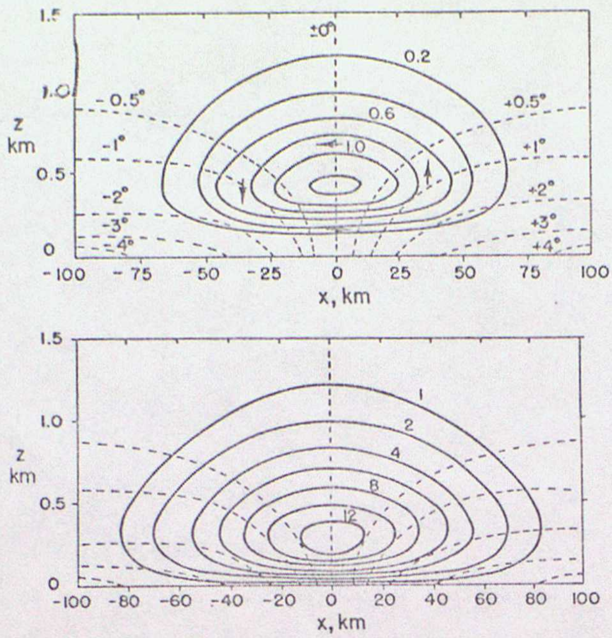

FIG. 226 Vertical cross sections oriented perpendicular to a Southern Hemisphere low-latitude coastline (land to right of 0 km). Upper panel: Deviations of temperature °C (dashed lines) from the temperature at the coastline. A sea breeze circulation results (flow is parallel to solid lines, in sense of arrows). Lower panel: Solid lines are isotachs (lines of equal wind speed in m/s) showing a low level jet from the south (i.e., into the page). (*Courtesy of H. H. Lettau, "Explaining the World's Driest Climate," in H. H. Lettau and K. Lettau (eds.),* Exploring the World's Driest Climate. *Institute for Environmental Studies, Rep. 101, University of Wisconsin, Madison, Wis., 1978, pp. 182–248*)

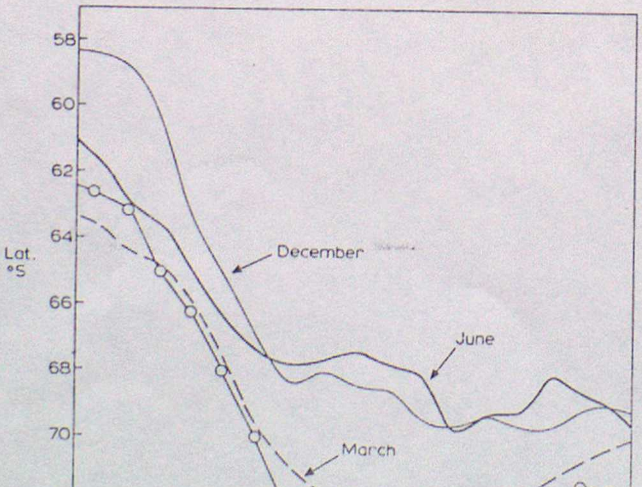

FIG 2.29 Mean latitude of the axis of the Antarctic trough in indicated months (1972 – 1977). (Data from STRETEN, 1980.)

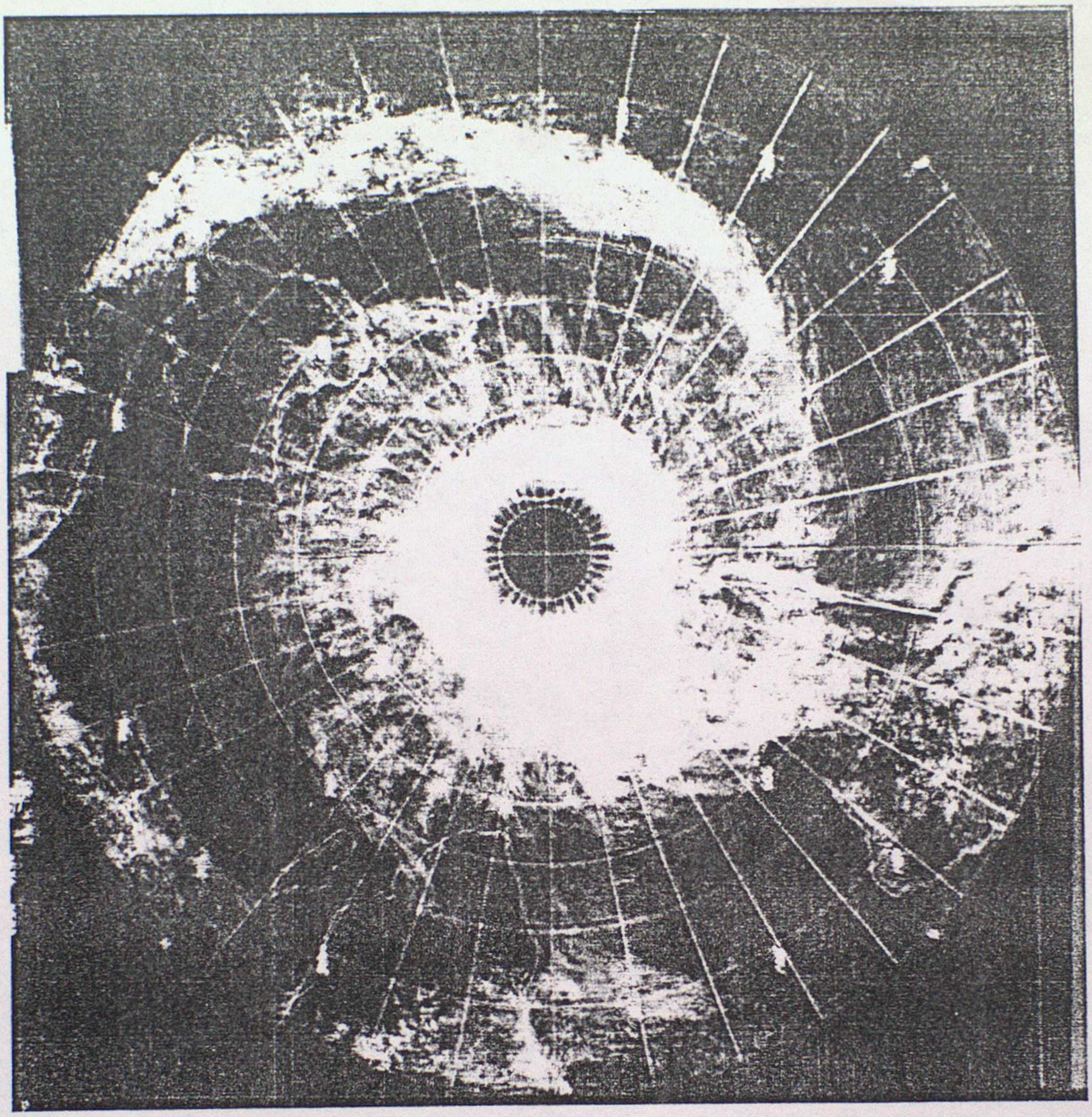

FIG 2.27 Averaged Southern Hemisphere cloud imagery (visible range) 1 – 15 October 1967, showing South Pacific cloud band. (After KORNFIELD and HASLER, 1969.)

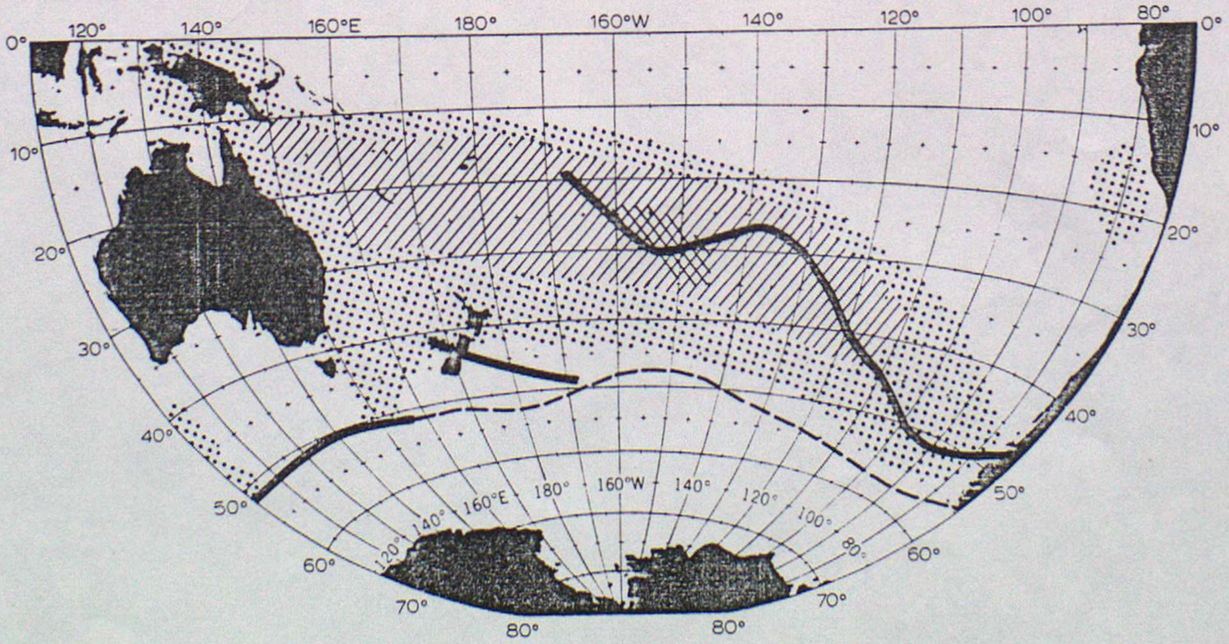
120°
140°
160°E
180°
160°W
140°
120°
100°
80°
0°
0°
10°
10°
20°
20°
30°
30°
40°
40°
50°
50°
60°
60°
70°
70°
80°
80°
120°
140°
160°E
180°
160°W
140°
120°
100°
80°

FIG 2.28 Percentage frequency of 5-day averaged mosaics having axes of major cloud bands within a 5°-lat. by 10°-long. area for spring and autumn (stippled >10%; hatched >20%; cross-hatched >40%), after STRETEN (1973a). Axes of zones of highest frequency of early cyclonic development for the same seasons is shown by the full line (after STRETEN and TROUP, 1973).

APPENDIX TO LECTURE 2

Köppen's world-wide classification system

Climates are ranged in the following main groups:

A	Tropical rain climates
B	Arid climates
C	(Warm) temperate rain climates
D	Boreal forest and snow climates
E	Cold snow climates (treeless)

A, C and D are all essentially tree climates; **BS** is the steppe grassland climate; **BW** defines the (warm) deserts (W standing for desert-waste/*Wüste*); E climates are those of the tundra and polar desert.

Subdivisions are designated as follows:

s	Summer dry season In group **A** climates confined to exceptional areas such as lee-sides of islands in the Trade Wind zone. In groups **C** and **D** the wettest month of the year must have $\geqslant 3$ times the average rainfall of the driest month.
w	Winter dry season Group **A** climates are only designated **Aw** when at least one month normally has <60 mm rainfall. In groups **C** and **D** the wettest month of the year is required to have $\geqslant 10$ times the average rainfall of the driest month.
s′, w′	Special cases of summer or winter dry season climates, where the chief rains come in late summer–autumn.
x	Climates where the early summer is wet, late summer fine.
s″, w″	Special cases of summer or winter dry season climates, where the rainy season is split – i.e. has two peaks, with another, short dry season in between.
f	Moist climates, with no marked dry season.
m	Monsoon climates, with only a short dry season in the winter half-year.

On this system the chief types of climate appearing on the world map (fig. 11.8) are defined as follows:

Tropical rain climates

Mean temperature of the coldest month in all cases $>+18°$C.

Af Driest month has on average $\geqslant 60$ mm rain.

Am Driest month <60 mm but rainfall in the rainy season compensates this enough to allow forest.

Driest month R	60	40	20	0 mm
Required yearly R	1000	1500	2000	2500 mm

(**Af** and **Am** are both characteristically accompanied by tropical evergreen rain-forest.)

Aw Driest month <60 mm; annual rainfall insufficient to compensate.
(**Aw** produces Savanna.)

Arid climates

Defined by (i) $R < 2T + 28$ where summer is the season with most rain.
or (ii) $R < 2T + 14$ where there is no season with more liability to rainfall than another.
or (iii) $R < 2T$ where winter is the season with most rain.

In these formulae R is the average rainfall for the year in centimetres; T is the average yearly temperature (°C).

BS $R \geqslant T + 14$ for summer rain areas
$R \geqslant T + 7$ where there is no season with more liability to rain than another
$R \geqslant T$ for winter rain areas
(In **BS** climates the vegetation ranges from bush to grassland.)

BW $R < T + 14$ for summer rain areas
$R < T + 7$ where there is no season with more liability to rainfall than another
$R < T$ for winter rain areas
(**BW** produces desert.)

Temperate rain climates

Mean temperature of the coldest month between +18°C and −3°C.

Cs Wettest (winter) month of the year has $\geqslant 3$ times the average rainfall of the driest (summer) month.
(**Cs** is typically accompanied by evergreen broad-leafed forest.)

Cf No marked dry season.
Sub-types:
Cfa Hot summers: warmest month > + 22°C
Cfb Warm summers: at least 4 months > + 10°C
Cfc Cool summers: only 1–3 months > + 10°C.
(**Cfa** and **Cfb** vegetation generally deciduous broad-leafed forest, but in areas with very mild winters evergreen broad-leafed forest.
Cfc vegetation needle-tree forest.)

Cw Wettest (summer) month has $\geqslant 10$ times the rainfall of the driest winter month.
(**Cw**, occurring mainly on mountain heights above **Aw** climates, produces evergreen forest vegetation.)

Boreal forest and snow climates

Mean temperature of the warmest month > + 10°C, coldest month < − 3°C.

Dw Wettest (summer) month has $\geqslant 10$ times the average precipitation of the driest (winter) month.

Df Less seasonal difference in the average downput of rain and snow.
Sub-types:
Dfa and **Dwa** Hot summers: warmest month > + 22°C
Dfb and **Dwb** Warm summers: at least 4 months > + 10°C
Dfc and **Dwc** Cool summers: only 1–3 months > + 10°C.
(**Dfa, Dfb, Dwa, Dwb** climates go with deciduous (broad-leafed) forest.
Dfc, Dwc go with needle-tree forest.)

D climates and their vegetation are only found in the northern hemisphere, where the great continents provide the requisite conditions.

Cold snow climates

Mean temperature of the warmest month < + 10°C.

ET Mean temperature of the warmest month > 0°C.
(**ET** vegetation is tundra, dwarf tree species and mosses.)

EF (sometimes called simply **F**).
Mean temperature of the warmest month <0°C.
Brief thaws and rain can occur, but have little or no effect on the long-term condition of the surface.
(No vegetation in **EF** climates: polar desert.)

Further letters are sometimes used to distinguish particular climates and subdivisions of the KÖPPEN types:

d	coldest month < −38°C
g	Ganges type climate, warmest month before the summer solstice, height of summer rainy
h	hot: yearly mean temperature > +18°C
i	isothermal: difference between warmest and coldest months < 5°C
k	cold-winter climate: yearly mean temperature < +18°C, but warmest month > +18°C
l	lukewarm, even warmth: all months between +10 and +22°C
n	foggy
n′	moist, but not foggy: with mean summer temperatures over +24°C designated **n″**, over +28°C **n‴**
t′	Cape Verde Islands type: warmest in autumn
t″	Sudan type: coolest month just after the summer solstice.

It may be held that the types of climate covered by group **C** embrace too wide a range, and that the cooler temperate climates where birch forest (or mixed birch and pine) constitutes a large element should be distinguished from those of the domain of oak forest where the average temperature of the warmest month is generally about +15°C or over.

The proportions of the Earth's surface classified as falling within KÖPPEN's various types at the present day are estimated as follows:

	Portion of land surface	*Portion of total surface*
A	20%	36%
B	26%	11%
C	15½%	27%
D	21%	7%
E	17%	19%

KÖPPEN's classification can be criticized because it makes no mention of the level of incoming radiation and allows only indirectly and crudely for differences in the rate of evaporation. But these criticisms apply equally to most other classifications.

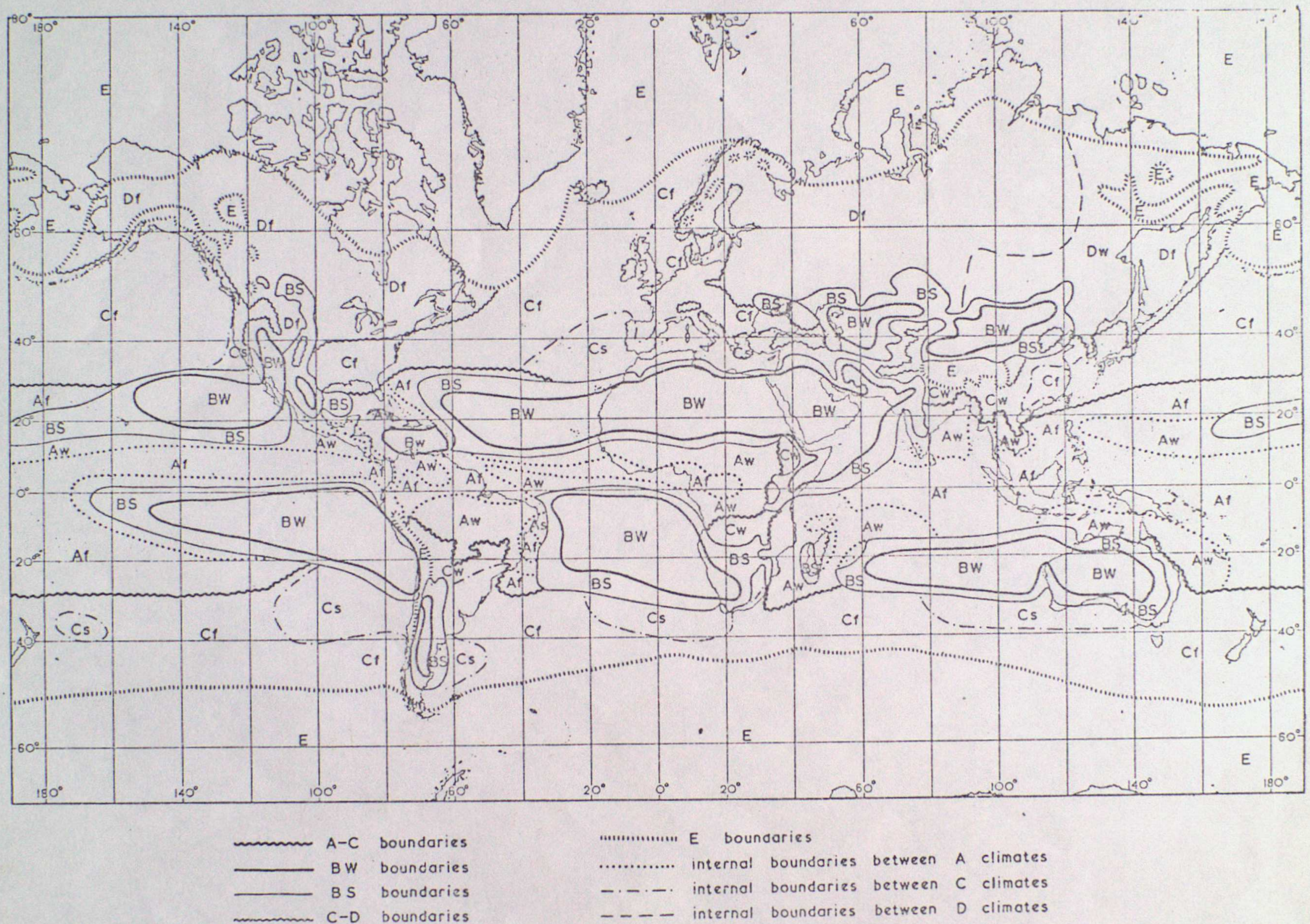
A–C boundaries
BW boundaries
BS boundaries
C–D boundaries
E boundaries
internal boundaries between A climates
internal boundaries between C climates
internal boundaries between D climates
180°
140°
100°
60°
20°
0°
20°
60°
100°
140°
180°
80°
60°
40°
20°
0°
20°
40°
60°
E
Df
Dw
Cf
Cs
Cw
BS
BW
Af
Aw

Fig. 2A | Köppen's world classification of climates.

FOR LOAN to M. O. Staff only

METEOROLOGICAL OFFICE
145727
- 7 MAY 1935
LIBRARY

LECTURE 3 - CLIMATE FORCING AND FEEDBACK PROCESSES I - FORCING FROM ABOVE

PART I - Variations in Solar Radiation and climate variability

3.1.1 Earth's climate is in principle sensitive to fluctuations of solar radiation if they persist for sufficient lengths of time. The average flux of energy from the sun at the mean radius of the earth is called the solar constant S and is about:-

$$S = 1370 \pm 15 \text{ Wm}^{-2}$$

Now the average flux of solar radiation received on the earth is, if R is the earth's radius:-

$$E_S = \pi R^2 S$$

The area of the earth's surface is $4\pi R^2$ so the average amount of energy received by the earth-atmosphere system is

$$S/4 = 342 \pm 4 \text{ Wm}^{-2}$$

It is easy to see that if the axis of rotation of the earth was normal to the plane intersecting the sun and all points in the earth's orbit, E_S would vary between a maximum ($S = 436 \text{ Wm}^{-2}$) at the equator to zero at the poles. However the tilt of the earth's rotation axis from this position is currently 23.44°. This results in large seasonal variations in radiation, though the simple calculation above is quite accurate close to the equator. Fig 3.1 shows the current zonally averaged radiation balance of the earth; the seasonal variations are shown in Fig 3.1 of lecture 3 on the General Circulation. A fraction $\alpha = 0.3$ (approximately) of the radiation is reflected or scattered; this fraction is called the albedo. Figs 3.2 and 3.3 are a good guide to the surface albedo of the world with and without clouds. So the effective temperature of the earth is given by

$$\sigma T_e^4 = (1-\alpha)S/4 \qquad (1)$$

T_e is approximately the mass-weighted temperature of the atmosphere, subject to some modification by dynamical processes. The sensitivity of T_e to S is shown by differentiating equation (1)

$$4\sigma T_e^3 \Delta T_e = \frac{\partial T_e}{\partial S} \Delta S + \frac{\partial T_e}{\partial \alpha} \Delta\alpha \qquad (2)$$

If a 1% increase in S was accompanied by a 0.01 decrease in α due to the associated melting of snow and ice, or perhaps a reduction in low-cloudiness, we obtain:-

$$T_e = 1.5°\text{C}/1\% \text{ change in S}$$

ORGS UKMO
National Meteorological Library
FitzRoy Road, Exeter, Devon. EX1 3PB

3 8078 0006 6040 9

If $\Delta\alpha = 0$ then ΔT_e is only 0.6°C/1% change in S. So the sensitivity of the climate to S strongly depends on any associated changes in albedo. The ice/snow component of the feedback between solar radiation and climate is often called the ice-albedo feedback but its magnitude is uncertain Nevertheless the climate system is very sensitive to long-lasting small changes in S.

3.1.2 Change of S

Does S actually change? Astronomers can say little about the fluctuations of S on short time scales but they believe it varies on geological time scales. Current theories suggest that S progressively increases as the sun gets older so that its value was perhaps 30% less 4 thousand million years ago than now. This question will be discussed in lecture 6.

Leaving aside the regular change of nearly 7% in radiation flux between January and July due to the fact that the earth currently moves in an elliptic orbit with eccentricity 0.0167, there are recent measurements of very small changes in S from the Solar Maximum Mission spacecraft. Fig 3.4 (Hudson (1983) (1)) shows rapid variations in S measured by a cavity radiometer at a time of high solar activity (when many sunspots are sometimes visible on the solar disk). Although the mean absolute value of S shown in Fig. 3.4 (1368.2 Wm^{-2}) is in fact only accurate to about ± 0.5% (± 7 Wm^{-2}) the relative changes in S are believed to be accurate to ± 0.1% (say ± 1 Wm^{-2}). The variations in Fig 3.4 approach four times this size and have a typical range of 0.2% over say a 10 day period. These variations have been shown to be due to 'sunspot blocking'; ie if there are many sunspots visible from the earth they block the solar radiation at least temporarily, since sunspots are cooler than the remainder of the surface of the sun (the sunspot temperatures are typically about 4000°C rather than the normal 6000°C, and warmer areas (formulae) sometimes surrounding sunspots do not compensate). Thus the radiation from the very small area covered by sunspots is reduced by a multiplying factor of $(4 / 6)^4$, about 0.2. These measurements are the first that indicate a real variation in the solar constant, though of course by very small amounts on short time scales. Fig 3.5 shows an imaginative but plausible reconstruction of variations of S over the last century from these observations, past sunspot data and a few other assumptions. The variations in Fig 3.5 seem insufficient or at least to last insufficiently long to have much effect on climate. Solar activity and the number of sunspots vary on several timescales eg 11 years, about 80 years and possibly longer time scales(2) (Fig 3.6). These variations of solar activity are also associated with fluctuations in the intensity of ultra violet radiation so that ultra violet radiation intensity increases as solar activity increases.

Many authors have in the past associated widespread cooler climates with a lack of sunspots and thus by implication a lower solar constant(eg during the Maunder "minimum" of the Seventeenth century shown in Fig 3.6) when sunspots may have been virtually absent. So recent satellite measurements of S paradoxically only confuse ideas about the relationship between sunspots, variations in the solar constant and climate variations (see Lecture 8). Gilliland (1983) (3) has claimed to detect small changes in solar radius on a dominant time scale of 76 years using measurements of uncertain homogeneity made by astronomers since the mid-nineteenth century. He tentatively associates a larger radius with an enhanced solar radiation flux etc. Unfortunately this kind of evidence has to be seriously considered until the time comes when accurate measurements of the solar constant made over many years are available. Fortunately such measurements are still being made by satellites.

3.1.3 Changes in the distribution of solar radiation on earth with the seasons

Changes in the seasonal distribution of radiation occur on long time scales due to fluctuations in the orbit of the earth. Assuming no intrinsic change in S, the changes in orbit are accompanied by very small apparent changes in S because the mean earth-sun distance changes only by small amounts. However seasonal values of radiation received at given latitudes on earth change much more. The fact that the earth's orbit has varied in a systematic way in the past was first calculated by Laplace (1798)using Newton's laws of motion and of gravity. The variations were calculated in great detail, with suggestions for their climatic consequences, by the Yugoslav mathematician Milutin Milankovitch (4). Fig 3.7 shows the three basic types of orbital variation that occur, discussed in detail by Berger (5):-

(1) The eccentricity of the earth's orbit changes on timescales close to 10^5 years between values of about $e = 0$ and $e = 0.06$. The current value of e is 0.0167.

(2) The angle of tilt of the earth's spin axis ('the obliquity of the ecliptic') relative to the plane passing through all points on the earth's orbit (plane of the ecliptic) varies on a timescale close to 41×10^3 years. The angle is defined to be zero when the earth is imagined to be in an 'upright' position with its spin axis normal to the ecliptic. At present the angle, q, = 23.44° but fluctuates with variable amplitude between limits of about 22° and 24.5° and is at present decreasing on average by about 0.01°/60 years.

(3) The time of year when the earth is closest (perihelion) and furthest (aphelion) from the sun varies on timescales in the range $19\text{-}23 \times 10^3$ years. These changes are called the 'precession of the equinoxes' and are often measured by an angle, θ between the position of the earth in its orbit at the time of the N hemisphere autumn solstice and the position at perihelion. At present, the earth is at perihelion on approximately Jan 3rd so this angle is now 102°.

Fig 3.8 shows the computed changes in seasonal radiation at different latitudes for the last 10^6 years.Superimposed on these slow changes are much smaller, faster, changes in the geometry of the earth's orbit largely due to the orbit of Jupiter and variations in the moon's orbit which occur on timescales of decades to centuries (Fig 3.9) (6).

Are these longer timescale (tens of thousands of years) radiation changes important? They are sufficient to alter the July radiation in the Northern Hemisphere through a range of at least 20% in most latitudes even though there is negligible change (0.2%) in the total mean annual radiation. (Least average radiation is received when the orbit is circular). An increase of summer radiation would warm the summer climate, balanced of course by a decrease in winter radiation which should tend to cool the winter climate and so increase the seasonal contrast. Changes in atmospheric circulation should result: eg the monsoons might tend to be more vigorous if summer radiation is more intense in the Northern Hemisphere and the ITCZ might move further north. At present summer radiation is relatively weak, though not especially so. Although the earth is furthest from the sun in July, e is fairly low. Thus the earth does not get as far away from the sun in Northern Hemisphere summer at present as it did in some previous epochs. However if radiation decreases in summer and winters are still cold enough some areas which lose their snow in summer when summer radiation is high may retain it when summer radiation is low. Albedo will increase and amplify any cooling effect. In this way snow fields and ice sheets might grow given other favourable circumstances.

A simple test calculation was carried out by Mason.(1976) (7) who showed that the deficiency of radiation in N Hemisphere summer between 83000 and 18000 BP may have been just enough to balance the latent heat of fusion produced when the ice sheets are thought to have grown, between those dates, to their maximum size. He also calculated that the increase in summer radiation from 16000 BP to 6000 BP was just enough to provide the latent heat of fusion required to melt the amount of ice that is believed, from geological evidence, to have disappeared between these two dates (90% of the difference between the volume of ice-age ice and that which exists now). As Mason was at pains to point out, the calculation was over-simple and on their own the radiation deficiencies and excesses seemed insufficient to guarantee the waxing and waning of the ice sheets. On the other hand, the variations in summer radiation were of the correct order of magnitude to make a substantial contribution, given other favourable "positive feedback"processes. So it is very important to identify these other processes. On shorter timescales the 'Milankovitch' radiation changes are not entirely negligible; since the High Middle Ages (1200 AD) the flux of solar radiation incident on the atmosphere around the summer solstice at the North Pole has decreased by nearly 0.5%.

3.1.4 The equilibrium sensitivity of earth's climate to changes in S can be studied in an instructive if preliminary way using simple 'energy balance' models. Appendix I prepared by David Carson for the 1982 Advanced Lectures discusses simple models and their approach to calculating the consequences of changes in S and in carbon dioxide. The results of many of these calculations are thought-provoking even if they turn out to be somewhat misleading. Figure 13 of Appendix I shows that a reduction of S by a few per cent might cause the earth to become completely glaciated; subsequent increase in S of at least 30% might be needed to melt the ice that has formed. These conclusions do indicate the potential sensitivity of climate to S in the presence of albedo feedback and the likely non-linearity of the response of the climate system.

In lecture 6 we shall discuss the effects of the Milankovitch radiation variations in more detail and the hypothesis that they are the pace-makers of the ice-age - interglacial fluctuations that have occurred quite regularly over the last 2-3 million years.

II. CARBON DIOXIDE AND THE GREENHOUSE EFFECT

3.2.1 Carbon dioxide is present in only small amounts in the atmosphere but is increasing by about 0.5% a year at present (current concentration is about 340 parts per million by volume (ppmv)). Carbon dioxide is important since it strongly absorbs long-wave radiation and re-emits it, so is radiatively very active in the climate system. The following discussion is only schematic and is oversimplified in many ways. It is adapted from Gill (9) and applies to carbon dioxide, water vapour and other (lesser) 'greenhouse' gases.

Consider a greenhouse formed by placing a horizontal thin sheet of glass above the ground (Fig 3.10). Let this glass be nearly transparent to solar radiation (assume it absorbs a small fraction s), but much less transparent to terrestial radiation. Suppose the glass and ground are initially cold. Let a downward flux, I, of solar radiation commence. Most of I will reach the ground; assuming the ground is a black body (ie has zero albedo), the ground will warm up to a temperature Tg and emit long-wave radiation with a flux U given by Stefan's law:-

$$U = \sigma T_g^4 \qquad (1)$$

Now let a fraction e of U be absorbed by the glass. The glass will warm up and emit a flux of radiation B. Equilibrium is reached when on both sides of the glass the upward and downward fluxes of radiation are equal.

Thus

$$I = (1-e)\,U + B \qquad \text{above the glass} \qquad (2)$$

$$(1-s)\,I = U-B \qquad \text{below the glass} \qquad (3)$$

It is easy to show that

$$\sigma T_g^4 = I \left[\frac{1 - s/2}{1 - e/2} \right] \qquad (4)$$

If s was zero and e = 1 then

$$\sigma T_g^4 = 2\,I \qquad \text{from} \quad (4)$$

or B = I so the flux received by the ground would be twice the solar flux.

T_g would increase by a factor $\Delta T_g = 2^{1/4} = 19\%$. Now s is about $1/5$ for present conditions and if this was true when e = 1 then $\Delta T_g = 16\%$. An increase of 19% would correspond to a temperature rise of about 50°C above the condition where e=0, if the albedo was zero; as the average amount of energy incident per unit area of the earth's surface is about $I = 342\ \mathrm{Wm}^{-2}$.

and $\sigma = 5.7 \times 10^{-8}$ Wm^{-2} K^{-4}, so Tg = 278°K and δTg = 53°C. In practice T_g would be considerably less than 331°K because e < 1 and because of atmospheric readjustments including the fact that some of I is converted to latent heat.(see Appendix I) This provides a 'radiative-convective' equilibrium ie the atmosphere above the ground takes up some of the extra heat.

Of course, the 'glass' is in reality distributed continuously in the vertical and water vapour is an important greenhouse gas which is very variable in concentration geographically (see Lecture 9). A point to note is that the addition of a greenhouse gas to the atmosphere does not necessarily leave the effective solar radiation received by the earth-atmosphere system unchanged eg if changes to the earth-atmosphere albedo also result. If we include the effect of the albedo α of the earth-atmosphere system and replace the net solar radiation received by the ground by $(1-s)(1-\alpha)I$ (ignoring αS^2) and the net downward solar radiation above the glass by $I(1-\alpha(1-s)^2)$ we obtain approximately:-

$$\sigma T_g^4 = I \left[\frac{1 - \frac{(s+2\alpha-3\alpha s)}{2}}{1 - e/2} \right] \qquad (5)$$

Here we arbitrarily attribute the albedo (due to ground and clouds) to the whole layer below the 'glass' so Tg is not really the ground temperature. If α decreases as e increases, σT_g^4 will increase at a faster rate. This could happen if snow and ice melted or low cloudiness decreased. Under present day conditions where nominally T_g = 287°K, s=0.2 and α = 0.3, equation (5) gives approximately e = 0.8 for carbon dioxide ozone , water vapour and other trace greenhouse gases together. Thus, schematically, $\sigma T_g^4 = 1.1I$ which implies that the long-wave radiation B incident on the ground from above is about 0.6I. So U-B = 0.5I at the surface. Figure 3.11 summarises the current radiation balance of the earth-atmosphere system. This shows that the direct loss of long-wave radiation from the surface is 0.2I, the remaining 0.3I being first converted to sensible and latent heat in the lower atmosphere and then lost as long-wave radiation once precipitation has occurred.

Lecture 9 discusses the physical basis and evidence for the potential effects of carbon dioxide in the climate system in more detail and Lectures 6 and 7 indicate its possible role in past climatic changes.

PART III - Variations in volcanic dust in the stratosphere

3.3.1 From time to time huge volcanic eruptions of the explosive kind create world-wide veils of finely-divided dust causing optical effects such as a reddened sun or moon or halo effects around the sun like Bishop's rings. During an eruption, carbon dioxide and water vapour are ejected into the stratosphere with, very often, compounds of sulphur such as H_2S and SO_2 in gaseous form. The quantity of carbon dioxide ejected in a typical eruption is thought to be only about 0.01 ppmv, so the addition of carbon dioxide to the atmosphere is minute compared to the current rate of annual increase (1.5 ppmv). Likewise the heat output is, in relative terms, minute. It has long been considered that the dust vented from a huge volcanic eruption that reaches well into the stratosphere could affect climate. This was thought to be likely because:

(a) Estimates of surface temperature over widespread parts of the globe often showed a drop after (but also, disturbingly often, before) a huge volcanic eruption.

(b) The measured intensity of the direct solar beam was always reduced though the diffuse radiation usually increased to partially compensate.

The classic book on volcanic dust and climate is by Humphreys (1940) (10), whose ideas are instructive and not wholly outdated. An extensive description of the development of observational studies of volcanic dust and climate effects is given by Lamb (1972) (10). Fig 3.12 from (10) shows examples of historical measurements of monthly average values of the strength of the direct solar beam, while Fig 3.13 shows a graph of historic worldwide average temperatures derived by Koppen (see p 410ff of (10)). The timing of the largest volcanic eruptions is shown on the diagrams. Lamb has devised a "dust veil" index to measure the climatologically most important eruptions which is partly based on observations of the optical effects of the dust but also on the worldwide fall in surface temperature (as far as it can be judged) following a given eruption (Lamb (1970) (12). This subjective index suggests that the eruptions of Tambora (1815) (Indonesia), Coseguina (1835) (Nicaragua), Krakatoa (Indonesia) (1883) and Agung (Indonesia) (1963) (Fig 3.14) were among those most likely to have affected surface temperatures since the beginning of the nineteenth century, prior, that is, to the recent eruption of El Chichon (see later). On a millenial time scale, Fig 3.15, from Lamb (1972), shows an apparent association between the reconstructed extent of sea-ice near Iceland and volcanic eruptions in Iceland.

3.3.2 Controversy concerning volcanic dust and climate

The problem of whether the apparent associations between volcanic activity and climate exist continues to be controversial. The main reasons are:-

(a) There is sufficient uncertainty about the physics of the interaction between volcanic dust and solar and terrestrial long wave radiation that the sign of the effect of stratospheric volcanic dust on surface temperature is uncertain and may vary from eruption to eruption.

(b) The net effects depend crucially on the size distribution and chemical constitution of the dust, which may vary between eruptions.

(c) It has not yet proved possible to use an AGCM with a realistic stratosphere and using what would now be regarded as the essential physics of the radiative interactions, to attempt to simulate the climatic effects of volcanic dust. In any case, the simulated response of the oceans could be crucial as the volcanic effects may stay in the stratosphere for several years.

It is now thought that the reason why past ground measurements have indicated long-residence times for stratospheric dust, despite the appreciable scavenging that must exist due to dynamical interactions between troposphere and stratosphere, concerns the fact that some of the "dust" is formed after the eruption. Sulphur gases (H_2S, SO_2 etc) formed during the eruption may slowly combine with stratospheric water vapour to produce reflective, aqueous droplets of a typical diameter 1 µm or less whose terminal velocities are very low. So the quantity of sulphur gas and possibly sulphur particles ejected in an eruption is now thought to be very important. Lamb (1972) shows terminal velocities for spherical particles of several radii (Table 3.3.1).

TABLE 3.3.1

Stratospheric residence times for volcanic dust

(Total times taken to fall through still air to tropopause at (*a*) 17 km, (*b*) 12 km)

Particle diameter	*Initial height (km)*	(*a*)	(*b*)
2 µm	40	25 weeks	41 weeks
	30	21 ,,	37 ,,
	25	16 ,,	31 ,,
	20	7 ,,	23 ,,
1 µm	40	1·9 years	3·1 years
	30	1·6 ,,	2·8 ,,
	25	1·3 ,,	2·4 ,,
	20	0·6 ,,	1·7 ,,
0·5 µm	40	7·8 years	12·5 years
	30	6·5 ,,	11·3 ,,
	25	5·0 ,,	9·7 ,,
	20	2·2 ,,	6·9 ,,

3.3.3 El Chichon

In April 1982 a very violent, explosive eruption occurred in S Mexico from the volcano El Chichon (the "lump on the head") situated at 17°N 93°W. Fig 3.16 from (13) shows how the dust from that explosion circled the globe in about 1 month in a narrow band between 15°-25°N. Winds were easterly, and accelerating, at the 25-30 km level where much of the dust initially resided because the summer stratospheric circulation was just getting underway. At Hawaii (Central Pacific 19°N) directly under the cloud direct solar radiation was reduced by up to 30% in the months following the eruption, a reduction offset, but not completely, by an increase in diffuse solar radiation. (Coulson et al (1982)) (14). The measurements indicated that in the visible spectrum at a wavelength of 0.55 µm the dust produced a mean optical depth T of 0.25. Optical depth is defined as

$$F = F_O e^{-T}$$

F_O is the incident flux and F is that part of the flux that emerges below the dust layer without absorption or being scattered ie it only measures the reduction of direct radiation. Balloon and other measurements suggested that much of the cloud a few months after the eruption was composed of droplets of 75% sulphuric acid and 25% water with a mode radius of about 0.3 µm (MacCracken and Luther (1984) (15) give details). By July the dust cloud, now at a height of between 20-25 km, reached Italy and became visible to the naked eye on a few evenings in August 1982 around Bracknell, with some unusual sunsets. Referring back to Table I, droplets near a radius of 0.3 µm have such very low terminal velocities so that dynamical and other processes are likely to be important their removal from the stratosphere. It has yet to be shown that El Chichon has affected global surface temperatures (which in fact rose soon after the eruption, due to El Nino (see lecture 5)).

3.3.4 Heating of stratospheric dust layer

It is not completely obvious that a volcanic dust cloud should get hotter than its environment. The particles may be so small that solar heating is negligible and their radiative properties could be such that infra-red radiation from below also has little effect. Newell (1981) (16) claimed to have detected a heating of the dust cloud produced by Agung (1963) by several degrees centigrade. Theoretical work has recently suggested that a heating of several degrees is possible for the likely sizes and chemical constituents of volcanic dust, mainly due to the absorption of infra-red radiation from below. Parker and Brownscombe (1983) (17) cautiously concluded that the El Chichon dust cloud was heated near the equator between 30-50 mb by several degrees centigrade. Fig 3.17A (from Ref (17)) shows stratospheric temperatures at several levels in 1980-82 derived from the NOAA 6 Stratospheric Sounding Unit and Microwave Sounding Unit. Of the levels sampled, that at 50 mbar shows the largest temperature increase from 1980-81. Fig 3.17B (again from Ref (17)) shows the 30 mb temperature anomalies in August 1982 from radiosonde data. A complicating factor in this and the Agung studies is that anomalous warming was expected in both 1963 and 1982 within 15°N or S of the equator below the descending, westerly, phase of the stratospheric "quasi-biennial oscillation" (QBO) (see Lecture 5). An analysis by Labitske and et al (18) of the 50 and 30 mbar temperatures between 1964 and 1982 strongly suggests that the QBO contributed only a part of the 1982 warming. Nevertheless the observed temperature anomaly maximum near the equator in Fig 3.17B, rather than at the latitude of the main dust cloud (20°N), is probably a result of the additional influence of the QBO.

3.3.5 A schematic, simplified, model of effects of volcanoes on surface temperature

Although literature on the modelling of the physical effects of volcanic dust on the surface temperature is in some diagreement, there is an emerging picture of the important physical processes. However the sign of the effect of volcanic dust in the surface energy balance is difficult to determine because there are two important competing physical effects and a host of smaller ones. The most important opposing effects are:-

(a) The dust layer reflects solar radiation, tending to cool the surface of the earth.

(b) The dust layer absorbs terrestrial radiation, tending to warm the surface of the earth.

Absorption of solar radiation can be significant but is now thought to be fairly small at least in some volcanic eruptions.

Fig 3.18 shows a simple schematic model (which cannot be used to make predictions). Because we shall estimate the perturbation of the surface energy balance due to stratospheric dust we will not explicitly include the effects of carbon dioxide and other greenhouse gases which are assumed to be fixed. Imagine solar radiation I passing down through the dust layer; a fraction rI is reflected to space and lost while the remaining fraction tI = (1-r)I is transmitted to ground either as direct or diffuse radiation. Here we have assumed no absorption of solar radiation by the dust layer itself, which is not quite correct. The transmitted radiation, It, reaches the "ground" and a fraction αIt, is reflected upward (in principle α is not quite the same as for the "non dust" case as more of the solar radiation is diffuse and less is direct). On reaching the dust layer again, an amount of reflected radiation $t(\alpha It)$ is lost and an amount $r(\alpha It)$ is reflected down. So the initially reflected solar radiation is multipally -reflected between dust layer and ground with rapidly decreasing intensity. The initial loss of solar radiation to the system, rI, is to some extent "made up" as the expected loss from the ground in the absence of dust due to a finite non-zero value of α is reduced. However the total radiation absorbed by the ground cannot quite reach the initial amount transmitted (It).

Now also assume that a fraction b of the long-wave radiation U lost from the surface (partly indirectly from the troposphere itself - see section 2) is absorbed by the dust layer without further reflection.

Then we find that the radiation absorbed by the ground I_G is:-

$$I_G = (1-\alpha)tI \; (1+r\alpha+r^2\alpha^2+\ldots)$$

or $$I_G = \frac{(1-\alpha)tI}{1-r\alpha}$$ after summation

Similarly the solar radiation lost through the dust layer to space after multiple reflection is:-

$$I' = rI+t^2\alpha I \; [\; 1+r\alpha+\ldots]$$

or $$I' = rI\left[\frac{+t^2\alpha I}{1-r\alpha}\right]$$

We can now calculate the value of I_G . The radiation balance at the ground is:-

$$-B+U = I_G \qquad (1)$$

The radiation balance above the dust layer is

$$B+(1-b)U = I-I' \qquad (2)$$

Adding (1) and (2) and substituting for I_G and I' we find

$$U = \left[\frac{2}{2-b}\right] \quad I \quad \left[\frac{1-r-\alpha+\alpha r}{1-r\alpha}\right]$$

Now if $t = 1$ and $r = 0$, ie no dust layer exists, we found in section 2 that $U = (1-\alpha)I$. So the net change ΔU in the long-wave radiation lost eventually by the ground when a dust layer is interposed is:-

$$\Delta U = I(1-\alpha) \quad \left\{ \left[\frac{1 + {}^b/_2}{1 - r\alpha}\right] (1-r)-1 \right\} \qquad (4)$$

Now $U = oT_g^4$ as in section 3.2, so $\Delta U = 4oT_g^3\Delta tg$.
Table 3.1 shows calculations of equilibrium values of Δtg, assuming tg = 287°C, for reasonable values of t and b (where of course the effects of additional surface evaporation etc are neglected). References (15), (19), (20) give a discussion of the detailed physics and its uncertainties and suggestions for values of t and b and their effects on surface temperature.

TABLE 3.3.2 EQUILIBRIUM TEMPERATURE CHANGES AT THE SURFACE FROM THE SCHEMATIC MODEL, °C

1. b = 0

α	t = 0.99	t = 0.97	t = 0.95
0	-0.6	-1.9	-3.1
0.3	-0.3	-0.9	-1.6
0.6	-0.1	-0.3	-0.5
0.8	0.0	-0.1	-0.1

2. b = 0.02

α			
0	0.0	-1.3	-2.6
0.3	0.1	-0.5	-1.1
0.6	0.2	-0.3	-0.3
0.8	0.1	+0.1	0.0

Even if the magnitudes are incorrect, it is seen that the sign of the change in surface temperature is very sensitive to t and to b and also to α. These results qualitatively agree with existing ideas, despite the crudeness of the model. So a cooling due to volcanic dust is less likely where α is high but small changes in b, the coefficient that measures the absorption by the dust of long-wave radiation, can easily change the sign of a surface temperature response. Ref (20) agrees that eruptions are likely to produce varying surface temperature responses due to differences in particle size or chemical composition even if their dust clouds are similar in extent and optical depth. Also the temperature changes in Table 3.1 would also usually be much reduced near the surface due to the thermal inertia of the oceans; so bigger temperature changes are more likely higher in the atmosphere. Fig 3.19 from Ref (20) is a simple (but very uncertain) calculation allowing for these effects. In Lecture 8 we briefly consider whether it is likely that volcanic dust has really affected surface and tropospheric temperature since about 1850.

References

1. HUDSON, H S (1983) Variations of the Solar Radiation Input. Weather and Climate responses to solar variations. Ed: B M McCormac, Colorado Ass. Univ. Press. pp 31-41.

2. EDDY, J A (1983) A Historical review of solar variability weather and climate. Ibid. p1-15.

3. GILLILAND, R L (1981) Astrophys. J, 248, pp 1144-1155.

4. MILANKOVITCH, M (1941) Kanon der Erdbestrahlung und seine Andwendung auf das Eiszeitenproblem. Royal Serb Acad., Spec Publ. 133, Belgrade pp1-633. Trans. 1969 by Israel program for Scientific Translation, US Dept of Commerce.

5. BERGER, A (1984) Accuracy and frequency stability of the Earth's orbital elements during the Quaternary. Milankovitch and Climate Pt I: Ed. A Berger et al, pp 3-40. D. Reidel Pub. Co.

6. BORISENKOV, YE. P, TSVETKOV, A V and AGAPONOV, S U (1983) On some characteristics of insolation changes in the past and the future. Climatic Change, 5, pp 237-244.

7. MASON, B J (1976) Toward the understanding and prediction of climate variations. Q.J. Roy. Met. Soc., 102, pp473-498.

8. NATIONAL RESEARCH COUNCIL (1982) Solar Variability, Weather and Climate. Ed: J Eddy. Studies in Geophysics Ser., Geophys. Res. Board. National Academy Press.

9. GILL, A E (1982) Atmosphere-ocean dynamics. Academic Press.

10. HUMPHREYS, W J (1940) Physics of the air. 3rd Edition. Reprinted by Dover (1964).

11. LAMB, H H (1972) Climate, Present, Past and Future. Vol 1, Methuen.

12. LAMB, H H (1970) Volcanic dust in the atmosphere. Phil Trans, Roy Soc, A, 266 (No 1178) pp 426-538.

13. ROBOCK, A and MATSON, M (1983) Circumglobal Transport of the El Chichon volcanic dust cloud. Science, 221, pp 195-197.

14. COULSON, ET AL (1982) Lidar and Optical Polarisation Measurements of Stratospheric Cloud at Hawaii presented at the Fall AGU Meeting, San Francisco. Dec 7-15 1982, Eos, 63, p 897.

15. MacCRACKEN, M C and LUTHER, F M (1984) Radiative and climate effects of the El Chichon eruption. Proc of Fifth Amer. Met. Soc. Conf. Radiation, 31 October-4 November 1983, Baltimore MD.

16. NEWELL, R E (1981) Further studies of the atmospheric temperature change produced by the Mount Agung volcanic eruption in 1963. J. Volcanology and Geoth. Res., 11, pp 61-66.

17. PARKER, D E and BROWNSCOMBE, J L (1983) Stratospheric warming following the El Chichon volcanic eruption. Nature, 301, pp 406-408.

18. LABITSKE, K et al (1983) Temperature effects on the stratosphere of the April 4, 1982, eruption of El Chichon, Mexico. Geophys. Res. Letters, 10, No. 1, pp 24-26.

19.. POLLACK, J et al (1976) Volcanic Explosions and Climatic Change: A theoretical assessment. J. Geophys. Res, 81, No. 6, pp 1071-1083.

20. CHOU et al (1984) Climate Studies with a multilayer energy balance Model, Pt III: Climate impact of stratospheric volcanic aerosols. J. At. Sci., 41, pp 759-767.

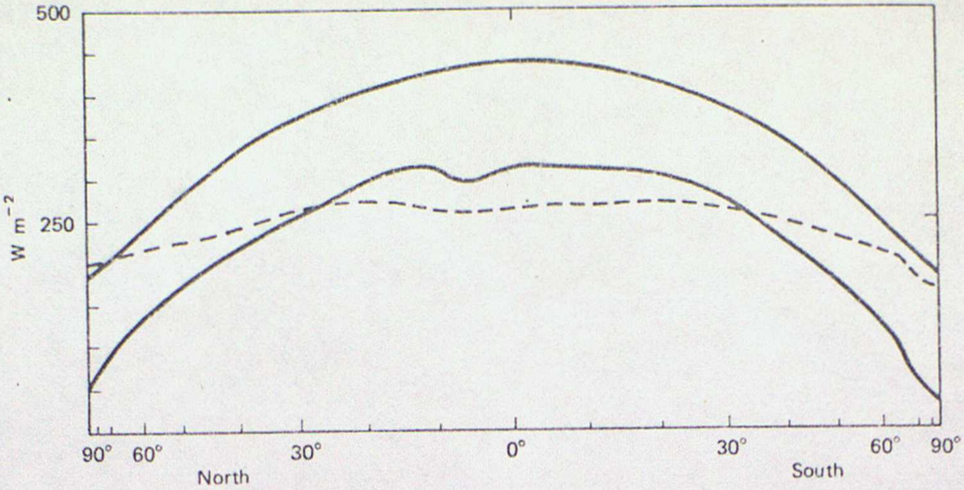

Fig. 3.1. The radiation balance of the earth. The upper solid curve shows the average flux of solar energy reaching the outer atmosphere. The lower solid curve shows the average amount of solar energy absorbed; the dashed line shows the average amount of outgoing radiation. The lower curves are average values from satellite measurements between June 1974 and February 1978, and are taken from Volume 2 of Winston *et al.* (1979). Values are in watts per square meter. The horizontal scale is such that the spacing between latitudes is proportional to the area of the earth's surface between them, i.e., is linear in the sine of the latitude.

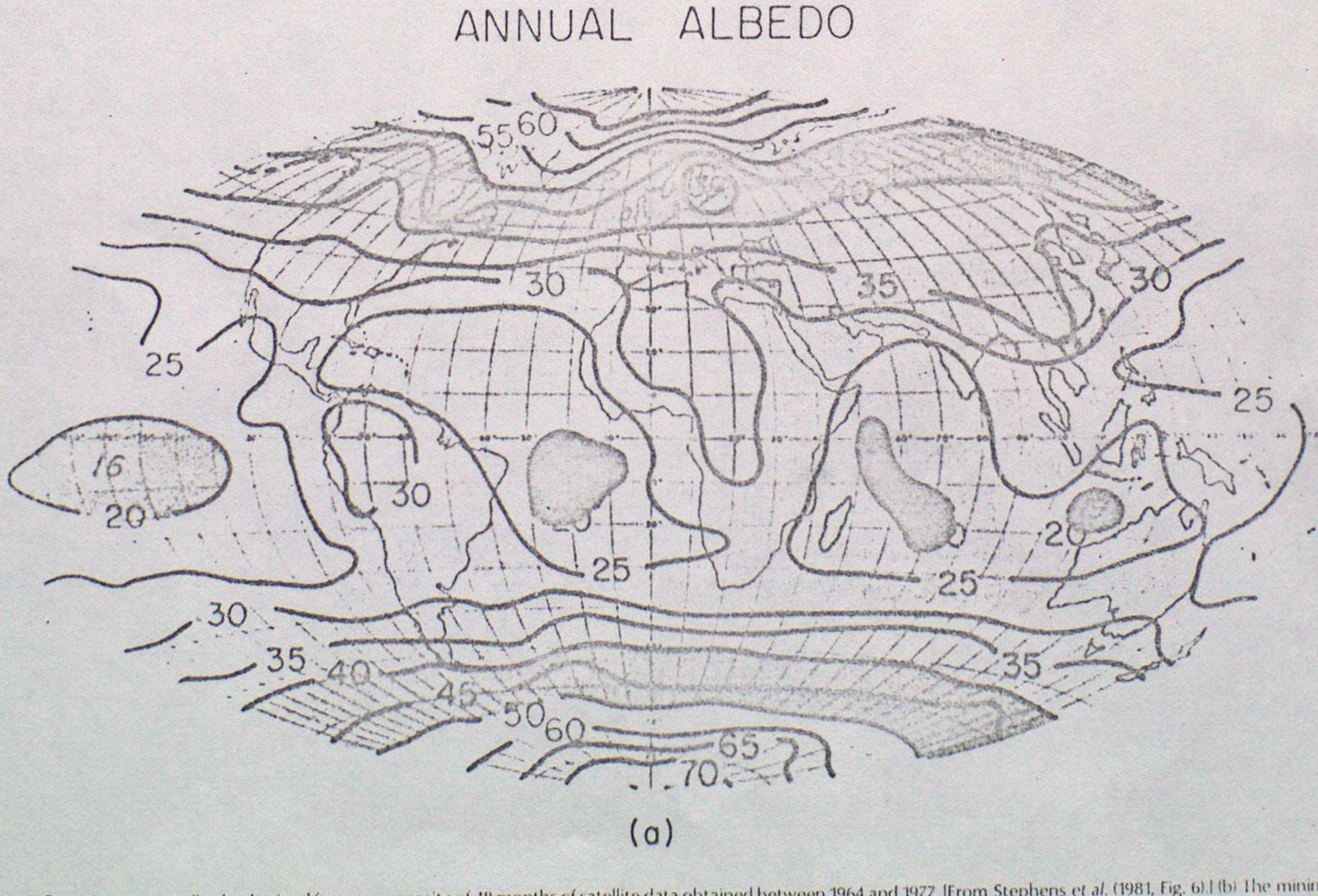

(a)

Fig. 3.2 (a) The average albedo obtained from a composite of 48 months of satellite data obtained between 1964 and 1977. [From Stephens *et al.* (1981, Fig. 6).] (b) The minimum albedo of the earth from Nimbus 3 satellite measurements in 1969–1970. [From Raschke *et al.* (1973, Fig. 23).]

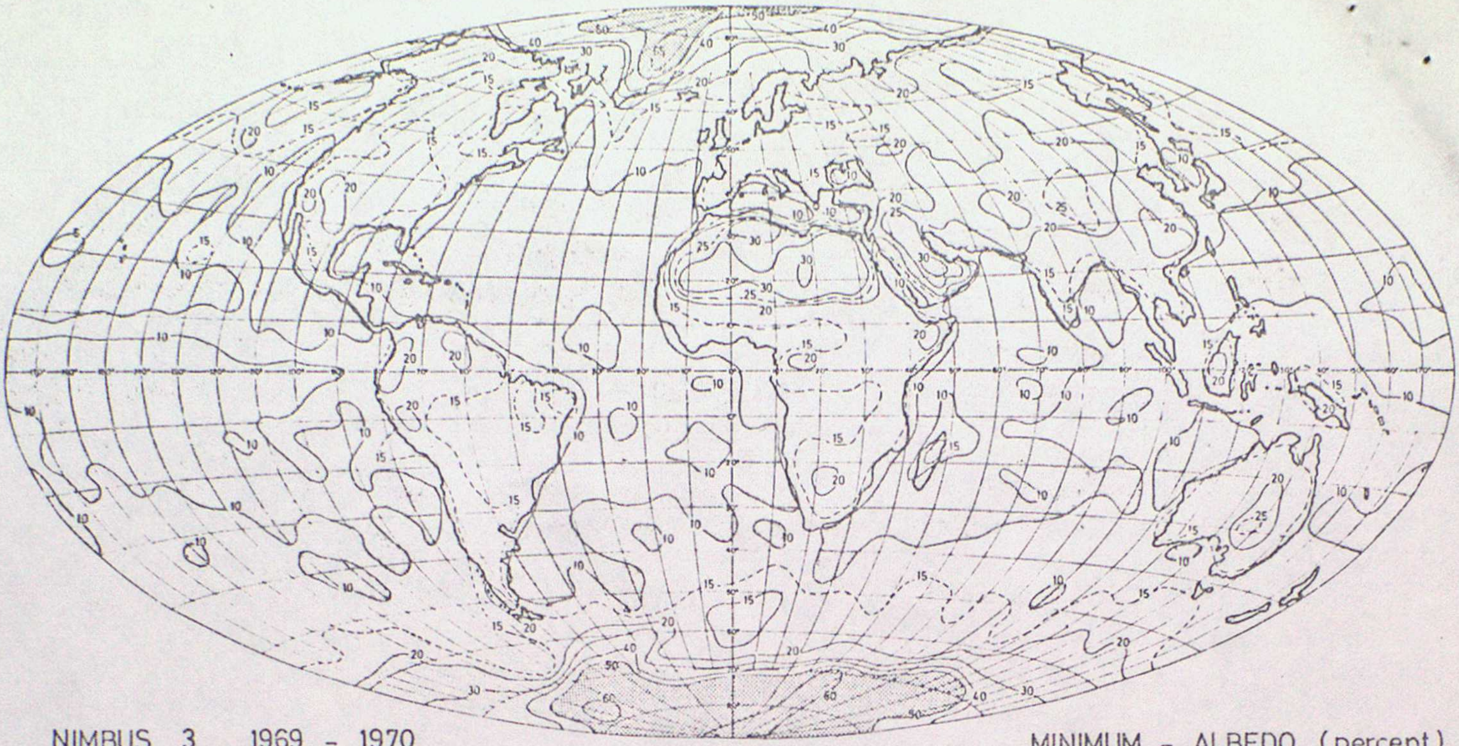

NIMBUS 3 1969 - 1970 MINIMUM - ALBEDO (percent)

(b)

Fig. 3.3. (continued)

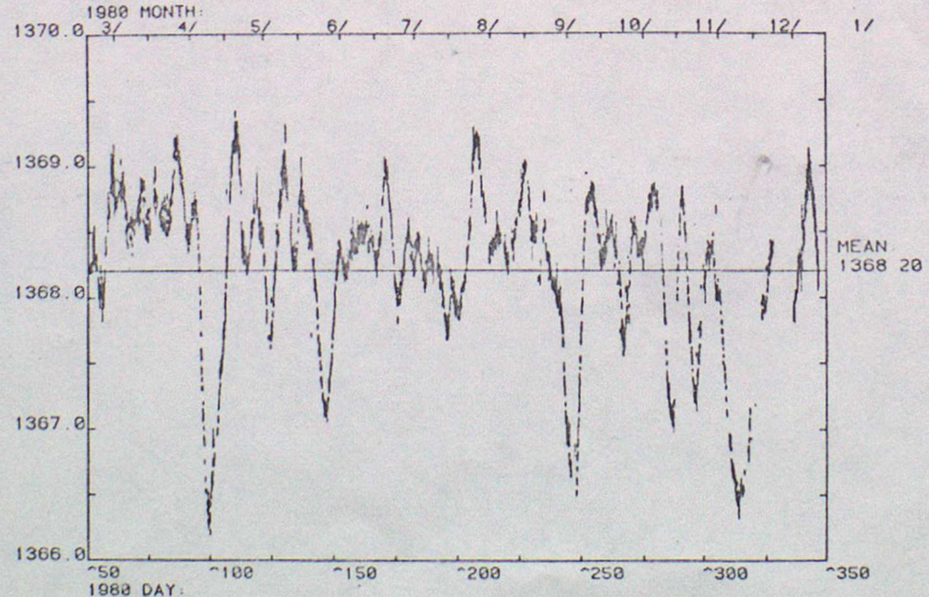

SMM/ACRIM RESULTS * ORBIT MEAN VALUES AND THEIR UNCERTAINTIES

Figure 3.4. Total solar irradiance ($W\ m^{-2}$) as measured by the active cavity radiometer onboard the SMM (Willson, 1982). Each point represents the average of data for one orbit (~96 min); the observed standard deviation for each point is on the order of 15 ppm. The large dips are associated with the crossing of the solar disk by large sunspot groups.

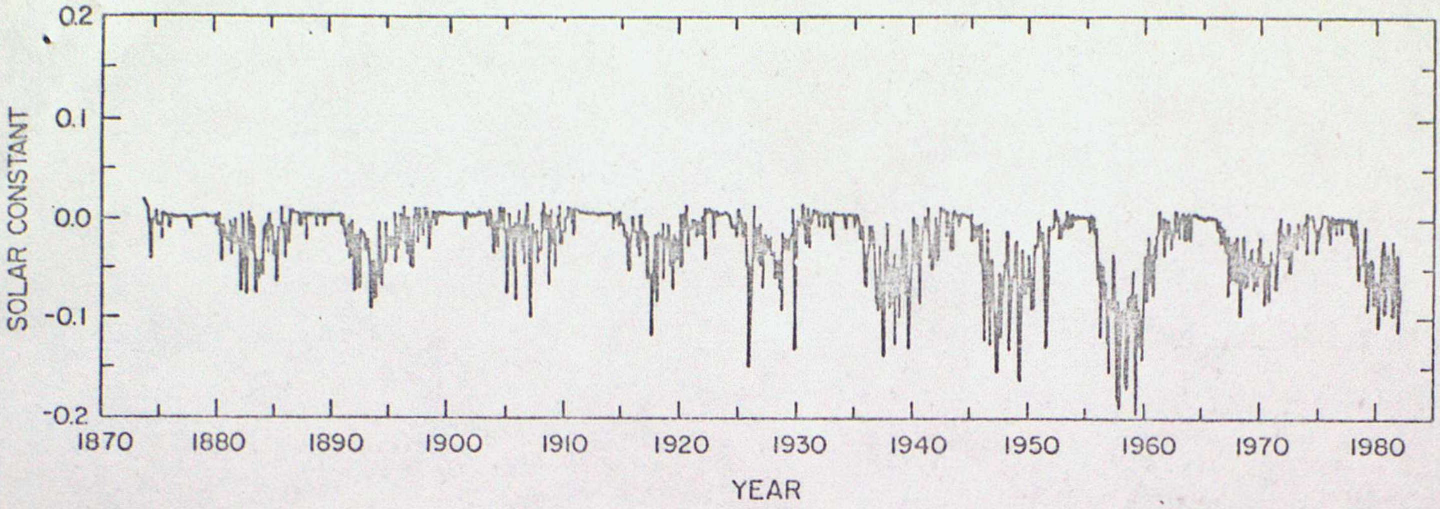

Figure 35 Calculated monthly mean variations in solar luminosity (in percent deviation from quiet Sun level) for the period 1874–1981 (from Hoyt and Eddy, 1982). Energy blocked by sunspots is assumed to be stored for at least six mo, consistent with observations made on the SMM spacecraft.

GURE 3. 6 Annual mean sunspot numbers, 1610–1979. During the Maunder Minimum, solar activity (as measured by sunspot number) fell to an unprecedented low level for approximately 70 years centered about 1670 (from Eddy, 1979).

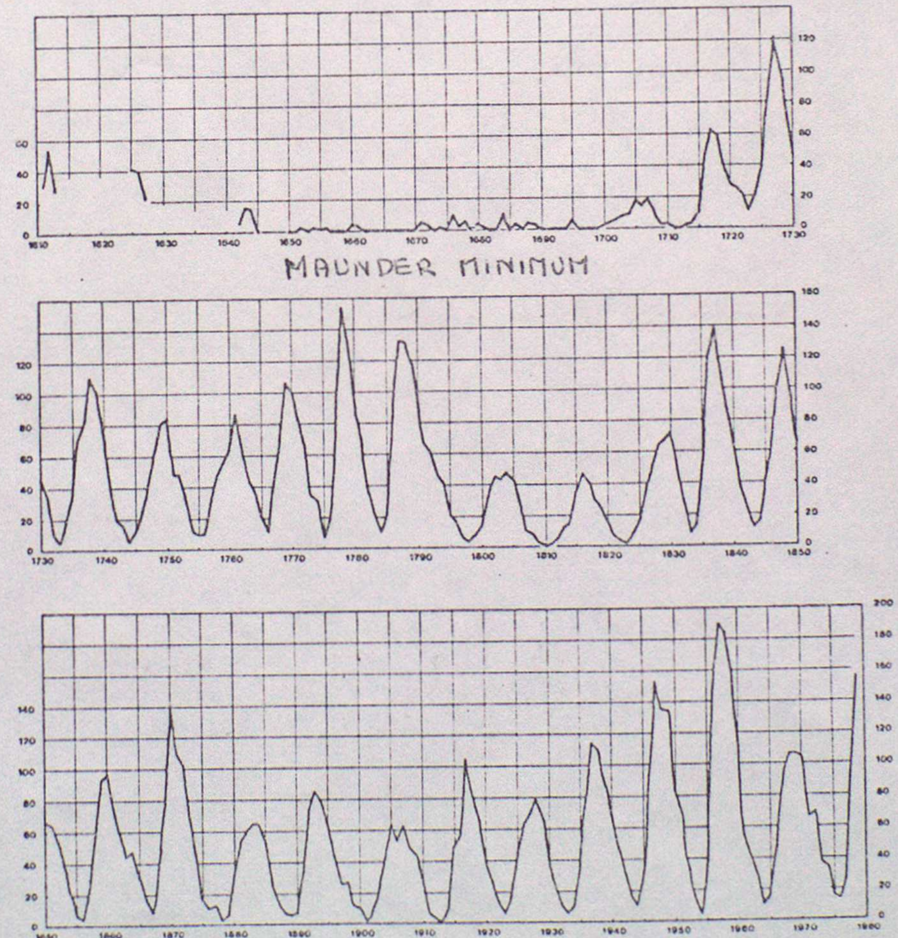

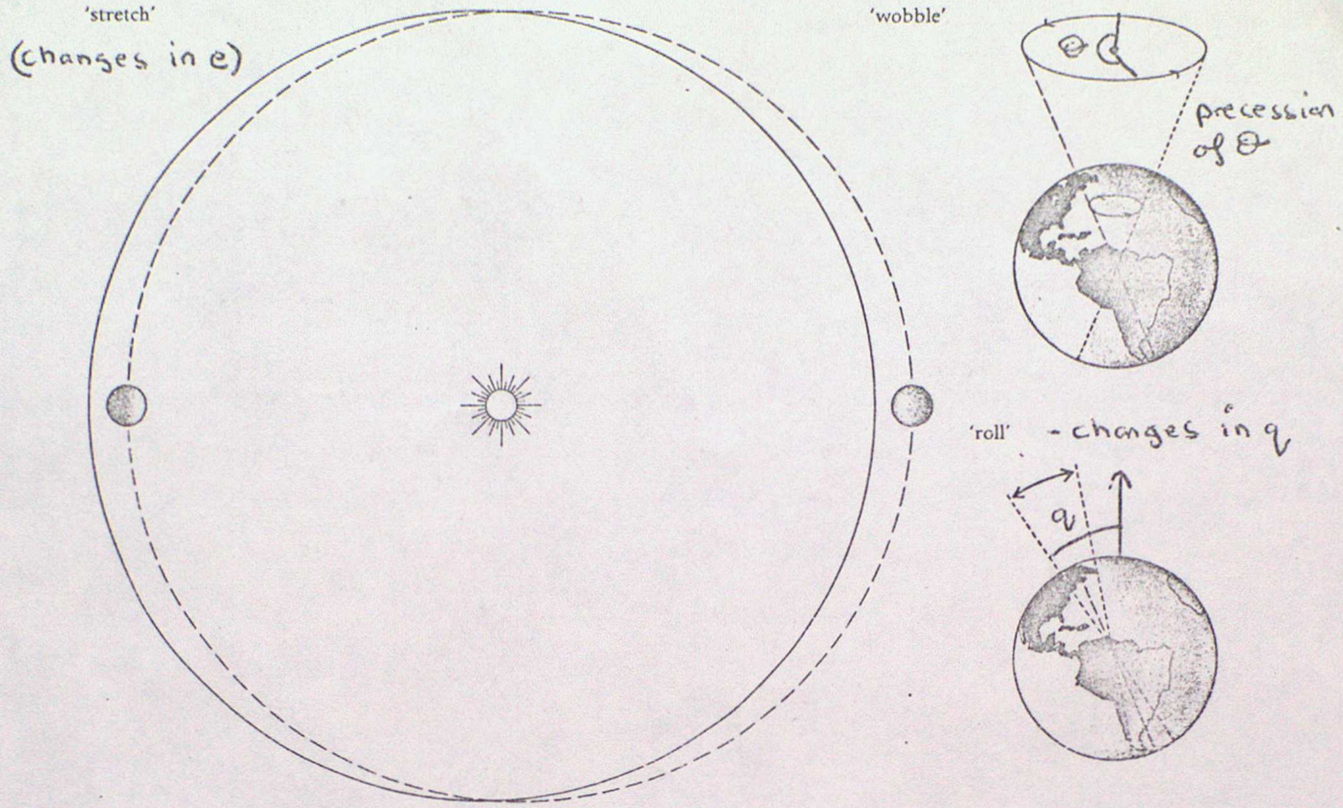
'stretch'
(changes in e)
'wobble'
Θ
precession of Θ
'roll' - changes in q
q

FIG 3·7

1 = 85°N
2 = 55°N
3 = 25°N
4 = 5°N
5 = 25°S
6 = 55°S
7 = 85°S

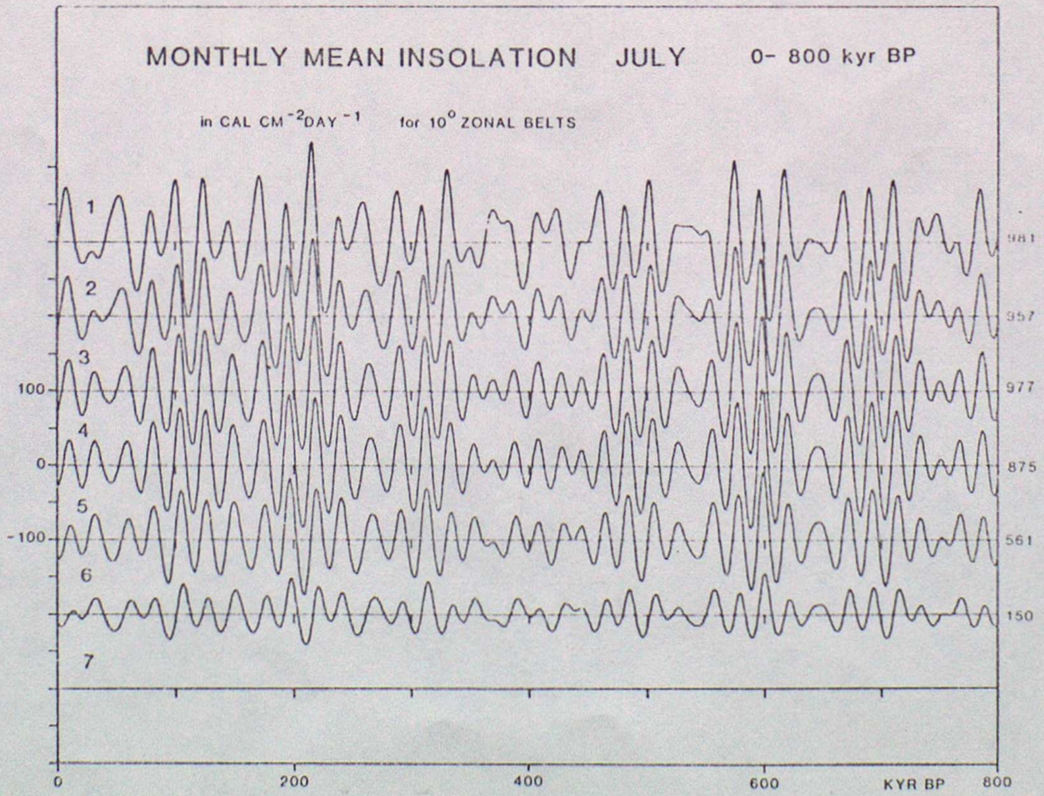

FIG 3.8

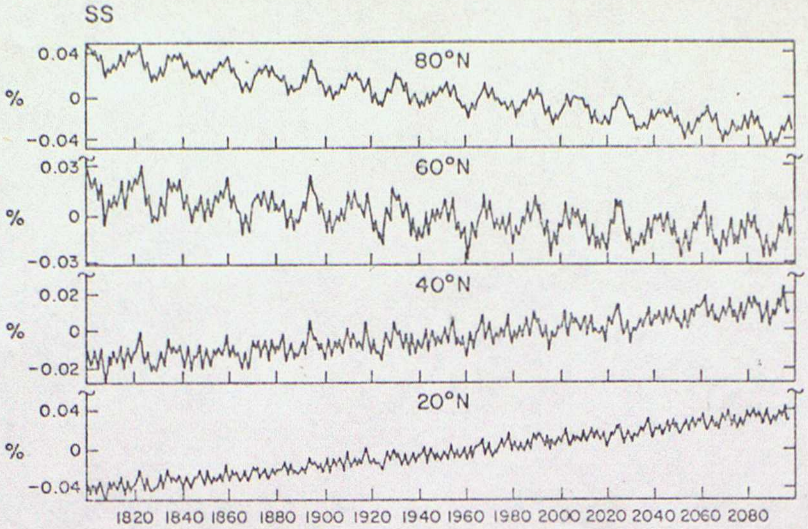

Fig.3.9 Relative insolation at summer solstice calculated for selected latitudes of the Northern Hemisphere for the period A.D. 1800–2100, as percent variation from the mean.

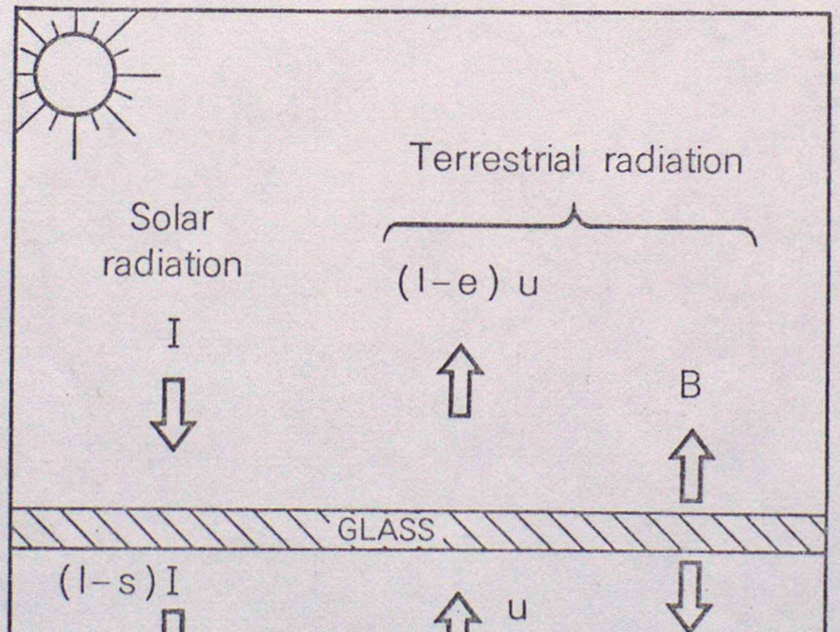
Solar radiation
I
Terrestrial radiation
(I−e) u
B
GLASS
(I−s) I
u
B
GROUND

Fig. 3.10 The 'Greenhouse' effect

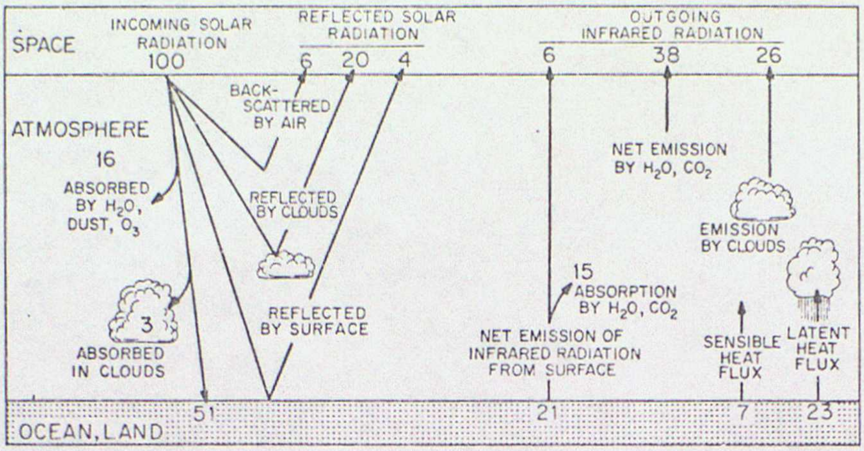
SPACE
INCOMING SOLAR RADIATION
100
REFLECTED SOLAR RADIATION
6
20
4
OUTGOING INFRARED RADIATION
6
38
26
BACK-SCATTERED BY AIR
ATMOSPHERE
16
ABSORBED BY H2O, DUST, O3
REFLECTED BY CLOUDS
NET EMISSION BY H2O, CO2
EMISSION BY CLOUDS
3
ABSORBED IN CLOUDS
REFLECTED BY SURFACE
15
ABSORPTION BY H2O, CO2
NET EMISSION OF INFRARED RADIATION FROM SURFACE
SENSIBLE HEAT FLUX
LATENT HEAT FLUX
51
21
7
23
OCEAN, LAND

Fig.3.11 Radiation balance for the atmosphere. [Adapted from "Understanding Climatic Change," U.S. National Academy of Sciences, Washington, D.C., 1975, p. 14, and used with permission.]

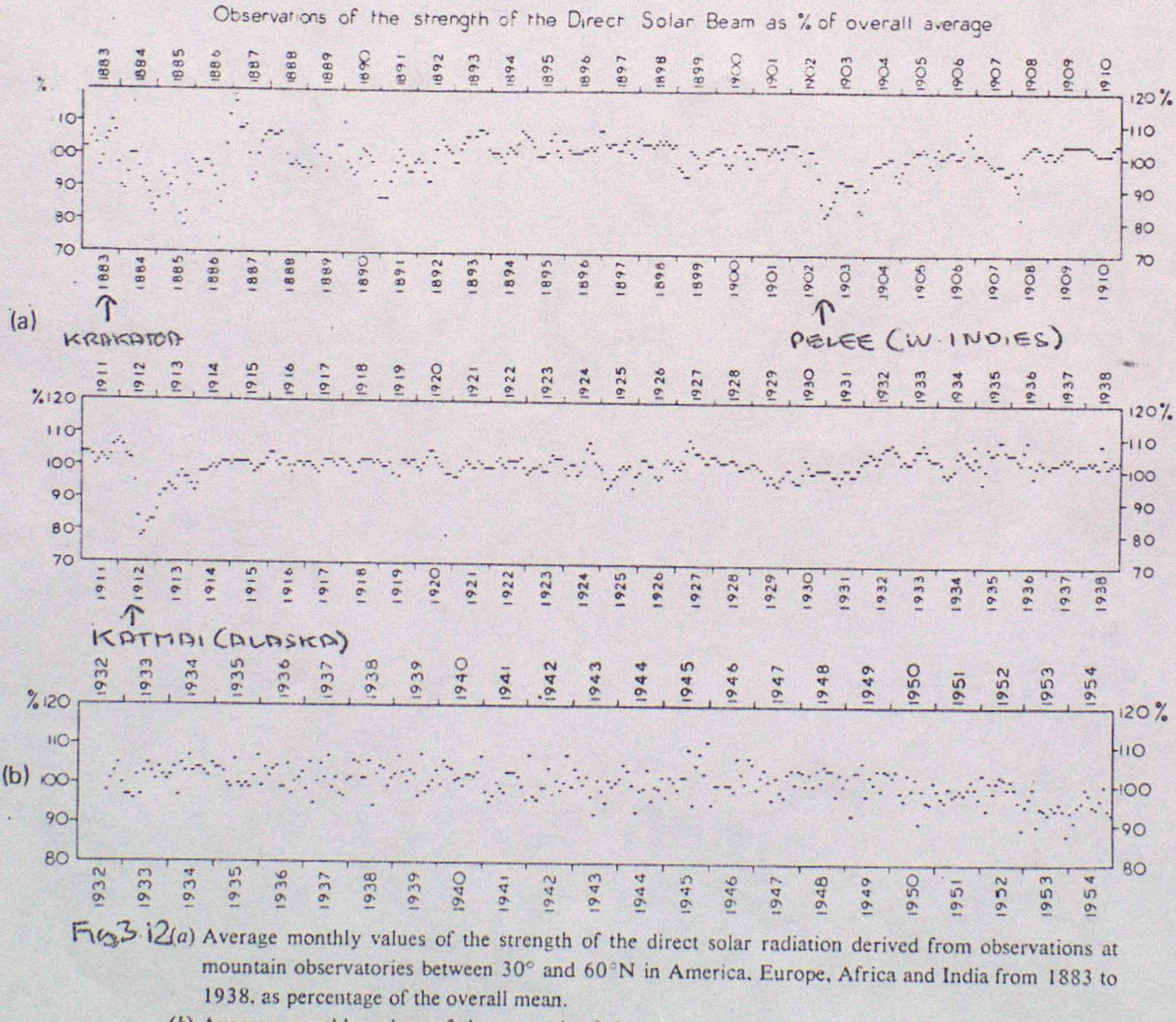

Fig3.12(*a*) Average monthly values of the strength of the direct solar radiation derived from observations at mountain observatories between 30° and 60°N in America, Europe, Africa and India from 1883 to 1938, as percentage of the overall mean.

(*b*) Average monthly values of the strength of the direct solar radiation derived from observations at Matsumoto (36°15'N, 137°58'E) and Shimizu (32°47'N, 132°58'E) in southern Japan from 1932 to 1954, as percentage of the overall mean. (from Lamb 1972)

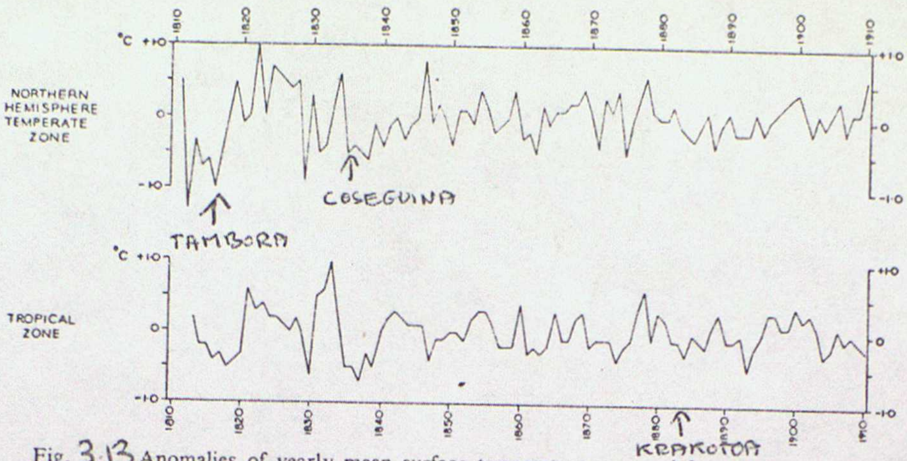

Fig. 3·13 Anomalies of yearly mean surface temperature averaged for certain areas, from 1815 to 1910:

(*a*) Northern hemisphere temperate zone

(*b*) Tropical zone

Unsmoothed yearly values.

Standard deviations of the yearly values here plotted:

Northern temperate zone (land stations) 0·38°C.

Tropical zone (land stations) 0·29°C.

(*After* KÖPPEN *1873, 1914.*)

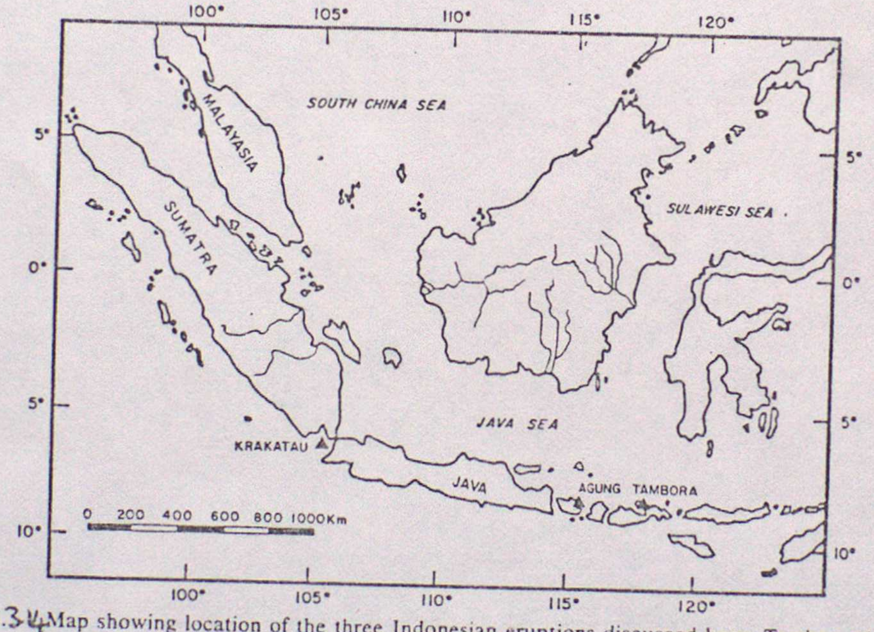
100°
105°
110°
115°
120°
5°
0°
5°
10°
SOUTH CHINA SEA
MALAYASIA
SUMATRA
SULAWESI SEA
JAVA SEA
KRAKATAU
JAVA
AGUNG
TAMBORA
0 200 400 600 800 1000Km

FIG. 3·14 Map showing location of the three Indonesian eruptions discussed here: Tambora (1815), Krakatau (1883), and Agung (1963). (triangles).

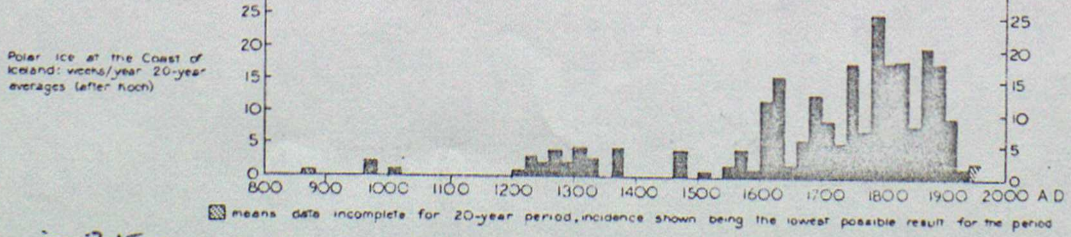

Fig. 3·15 Great volcanic eruptions in Iceland and incidence of Arctic sea ice in that area since A.D. 870.

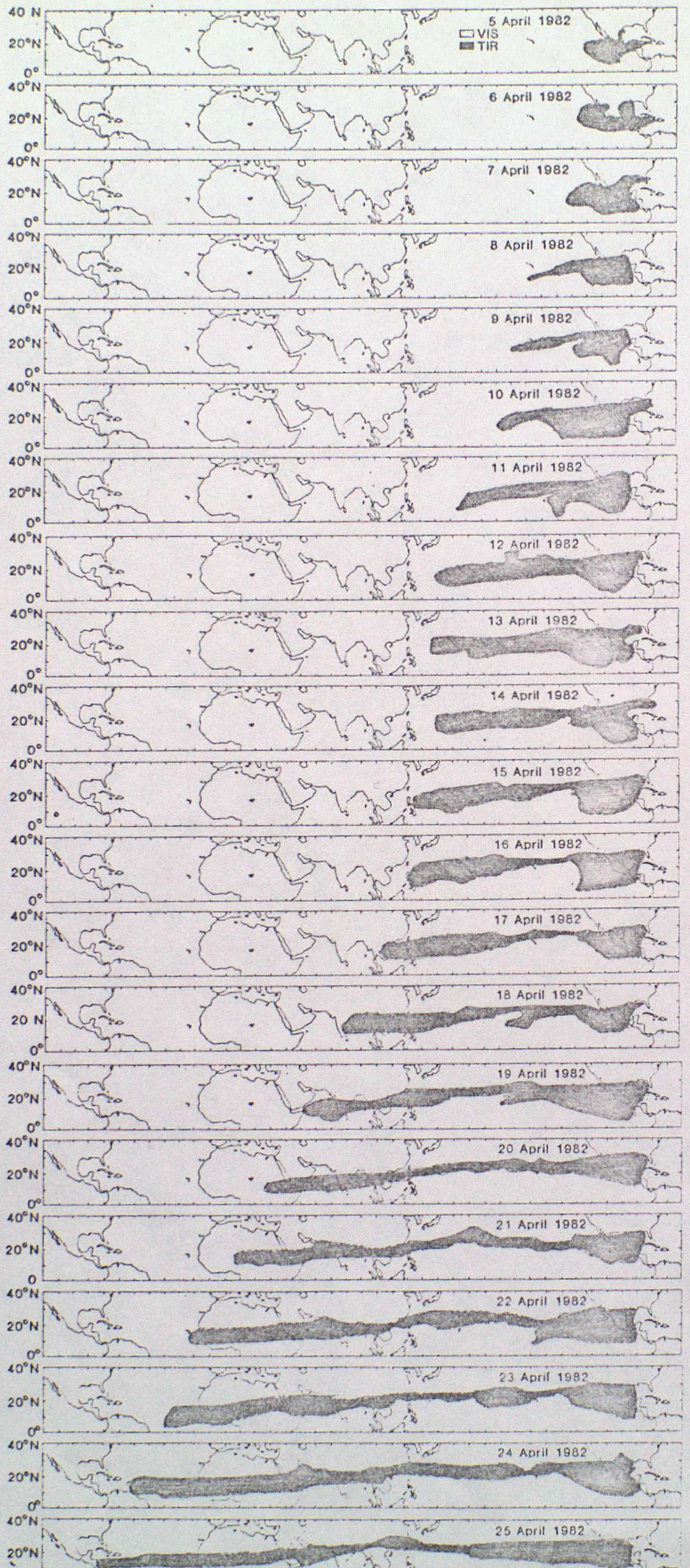
5 April 1982
☐ VIS
▨ TIR
6 April 1982
7 April 1982
8 April 1982
9 April 1982
10 April 1982
11 April 1982
12 April 1982
13 April 1982
14 April 1982
15 April 1982
16 April 1982
17 April 1982
18 April 1982
19 April 1982
20 April 1982
21 April 1982
22 April 1982
23 April 1982
24 April 1982
25 April 1982
40 N
40°N
20°N
20 N
0°
0
120°W
80°W
40°W
0°
40°E
80°E
120°E
160°E
160°W
120°W
80°W

Fig 3.16 Location of the dust cloud from the El Chichón eruption as observed with visible (*VIS*) and thermal infrared (*TIR*) imagery. Portions of the cloud to the right of 180° are plotted at 0000 GMT. Portions to the left of 180° are plotted at 1500 local time. Dash-dot lines indicate difficulties in observing the exact location of the edge of the cloud.

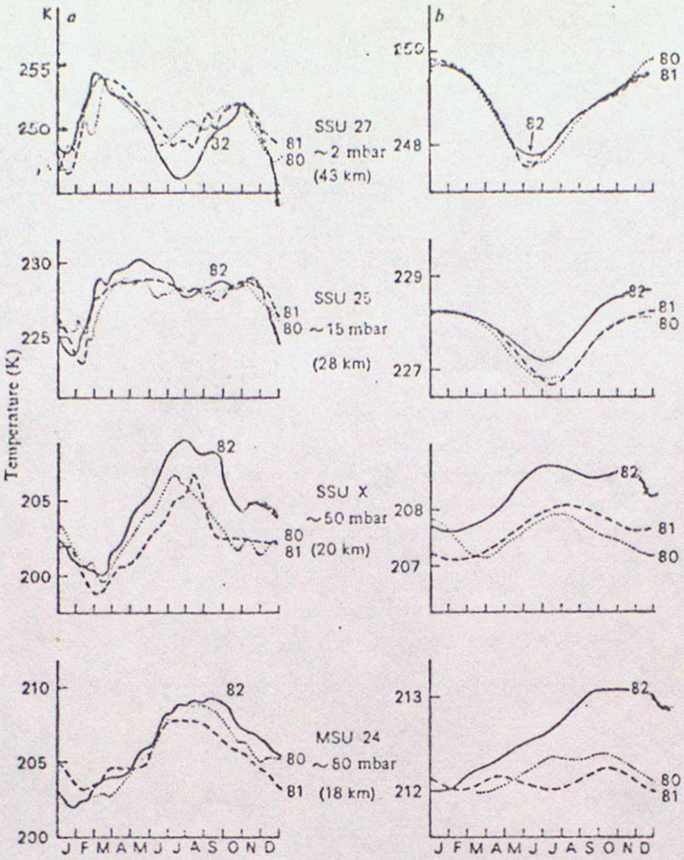

FIG 3.17A

Tropical (*a*) and global mean temperatures (*b*), 1980–82. Values are based on temperatures derived from NOAA 6 Stratospheric Sounding Unit and Microwave Sounding Unit radiance channels which have vertical resolution of ~15 km.

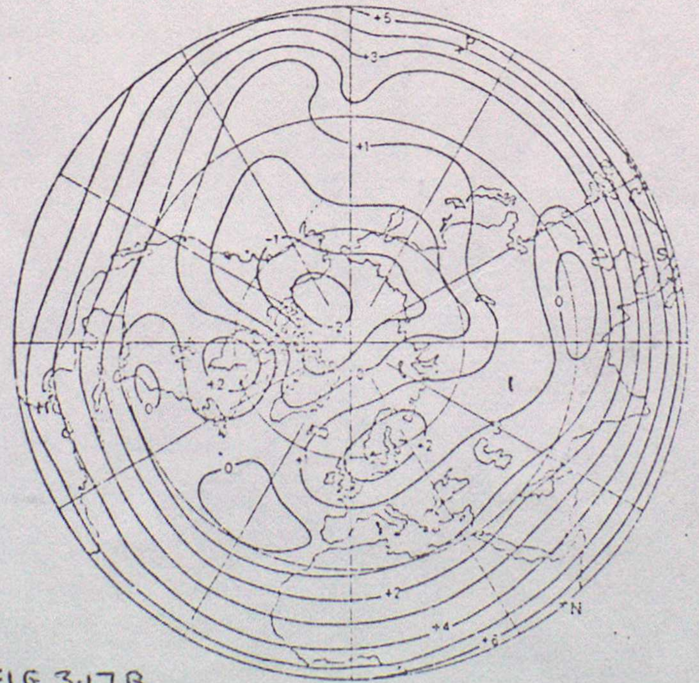

FIG 3.17B

30 mbar temperature differences (K) from normal, August 1982. H, Howard Air Force Base; N, Nairobi; P, Ponape; S, Singapore.

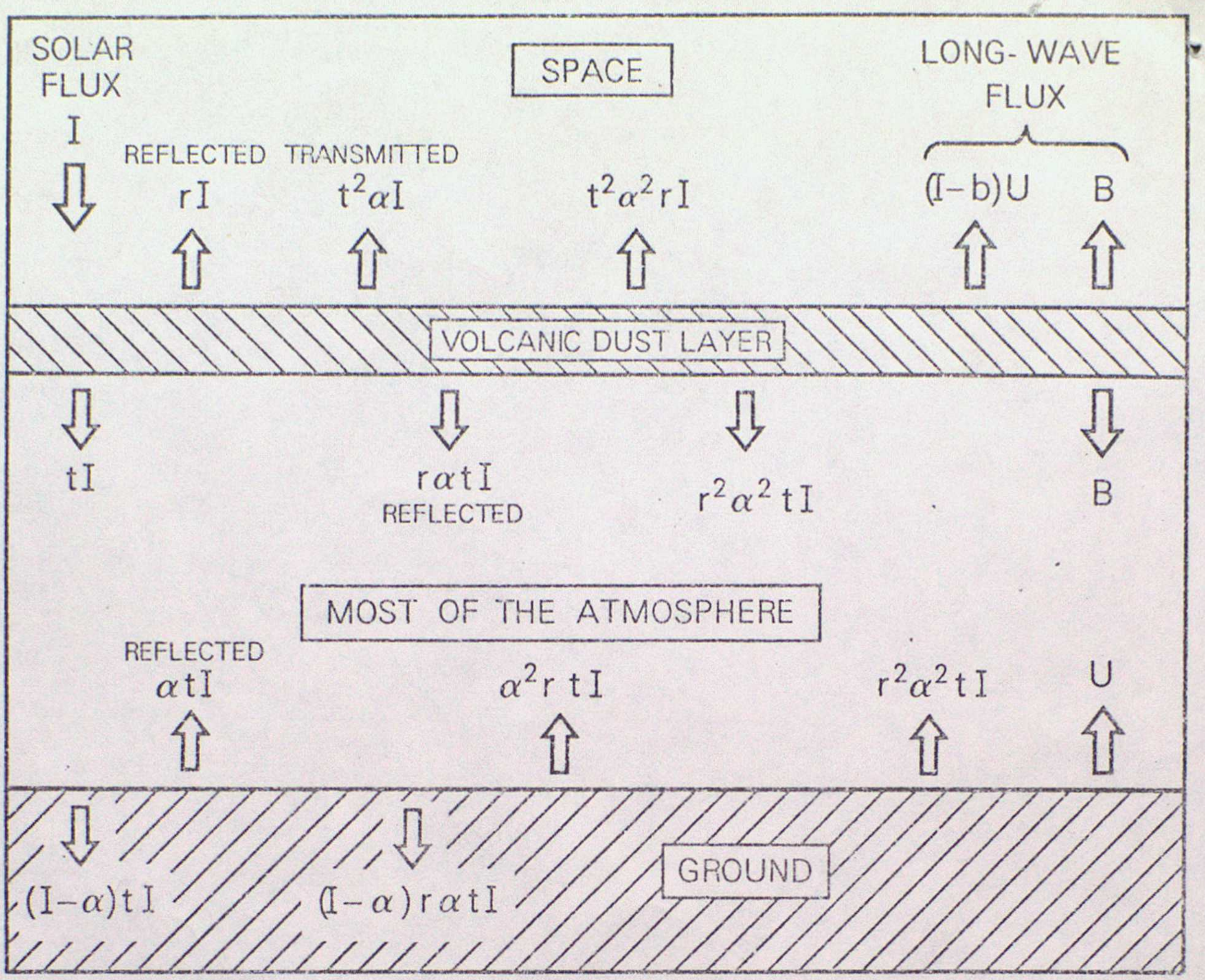
SOLAR FLUX
I
SPACE
LONG-WAVE FLUX
REFLECTED
rI
TRANSMITTED
$t^2\alpha I$
$t^2\alpha^2 rI$
$(I-b)U$
B
VOLCANIC DUST LAYER
tI
$r\alpha tI$
REFLECTED
$r^2\alpha^2 tI$
B
MOST OF THE ATMOSPHERE
REFLECTED
αtI
$\alpha^2 r tI$
$r^2\alpha^2 tI$
U
GROUND
$(I-\alpha)tI$
$(I-\alpha)r\alpha tI$

Fig. 3.18 Simple model of the effect of volcanic dust on surface radiation balance.

DO 3723

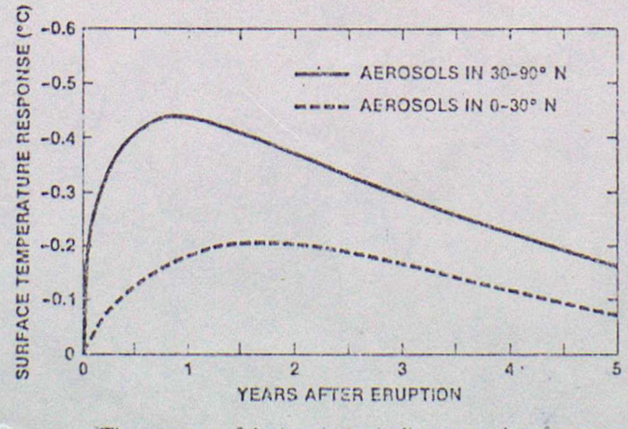

FIG 3.19 The response of the hemispherically averaged surface temperature to a uniform distribution of aerosols in the 30–90°N region (solid curve) and in the 0–30°N region (broken curve). The optical thickness of the aerosols is the same as in Fig. 7 of Ref (20)

FOR LOAN TO M.O. STAFF ONLY

METEOROLOGICAL OFFICE
145728
- 7 MAY 1985
LIBRARY

ADVANCED LECTURE NO 4

CLIMATE FORCING AND FEEDBACK PROCESSES II

PART 1 - SOIL MOISTURE AND ALBEDO

4.1 Introduction

In this lecture we consider the possible role of persistent variations of soil moisture and albedo (where the latter are not due to snow - see Appendix 1 to the set of lectures). A general introduction to the problem of the effects of soil moisture and albedo on climate is followed by a selection of results from AGCM experiments which will be referred to again in Lectures 7 and 8.

Charney (1975) (1) wrote a famous paper which contained a simple dynamical model of drought-albedo feedback. This stimulated increased interest in the likelihood of an influence of large-scale anomalies of the albedo of the ground on regional climate fluctuations. Subsequently, it became clear that soil moisture anomalies were just as likely to be important as albedo anomalies but it has long been known that there is a link between the soil moisture of the ground and its albedo. If the ground dries up sufficiently it tends to increase in albedo; albedo is increased further if the vegetation browns or dies back, especially if the drought is long lasting. Charney noted that the Sahara and its overlying atmosphere not only had a high albedo but appeared to be a net radiation sink even in the summer (Fig 4.1). The 1968-1973 Sahel drought, (which as Lecture 1 mentioned, has continued to a new peak of severity this year), stimulated Charney to consider whether it might have been partly caused by an increased albedo of the ground which may have been partly man-induced. This could occur through over population, overgrazing by man's animals as well as through the direct effects of drought. Charney considered that if the albedo of dry ground increased, then the radiation available for heating the ground would decrease and this would result in a decline in sensible heating of the atmospheric column above, which should therefore cause the overlying atmosphere to cool. To compensate, large-scale upper convergence followed by sinking motion in the middle troposphere should occur. Sinking would make convection even more difficult and so prolong the drought. One problem with this idea is that if soil moisture before the drought is not zero or there is initially considerable cloudiness and precipitation due to large-scale convergence, then a small increase in albedo might initiate some sinking motion but this would tend to remove some of the existing cloud. So solar heating would increase, perhaps offsetting the effects of the reduced albedo and preventing further development of anomalous sinking motion. In any case there is the distinct possibility that a change of albedo is much less important in prolonging a drought than a deficiency of local soil moisture.

4.1.2 A general discussion of the effect of soil moisture variations on precipitation

Why should we think that soil moisture variations could be important to regional precipitation? Evaporation of water from the ground surface is complex but essentially depends on three factors:-

ORGS UKMO
National Meteorological Library
FitzRoy Road, Exeter, Devon. EX1 3PB

3 8078 0007 8123 9

(a) The difference in vapour pressure between the soil surface and a representative level above the soil; the vapour pressure at the soil surface is usually taken as the saturation vapour pressure of water at the temperature of the soil surface and thus evaporation depends on ground temperature.

(b) The wind velocity measured at a convenient level near the ground.

(c) The availability of soil water or "soil moisture deficit".

A simple version of Penman's evaporation formula developed in 1956 (2) expresses the first two factors:-

$$E_p = 0.35\ (e_s - e_a)\ (0.5 + 0.53v)$$

where e_s equals saturation vapour pressure at the prevailing surface temperature, e_a = average vapour pressure of the air, v = wind speed at a height of 2 m

E_p is known as the potential evaporation and is nominally the actual evaporation over a flat, fresh-water, surface. However the actual evaporation from a ground surface, E', is often less than E_p when S, the soil water content, falls below a certain value. Thus a resistance to evaporation build up as the surface soil layers dry out and the soil water is evaporated from deeper layers. In some AGCM's

$$E' = \frac{E_p S}{KS_o}$$

Where S = soil water content (the equivalent depth of water in cm existing in the soil), S_o = the maximum soil water content of the soil or its "field capacity" and K = a constant; $\frac{Ep}{KSo}$ is sometimes called β.

This formula is a gross oversimplification for vegetated surfaces but has often been used in AGMS and expresses the most important variations of evaporation rate. For a discussion of evaporation formulae and the water balance of the world, see the authoritative references (3) and (4).

4.1.2.1 A schematic demonstration of the importance of soil moisture on anomalies

Fig 4.2 shows an idealised picture of the exchange of energy between the ground surface and the atmosphere involving soil moisture and evaporation. Imagine there is no horizontal motion and that cloudiness is fixed. (I am grateful to Dr P Rowntree for the basis of this section). Consider the heat balance of the bottom half of the atmosphere ie that part below 500 mb, which we shall assume to be affected by ground surface processes. The heat balance of the atmosphere can be expressed by:-

$$\frac{MC_p\ dT}{dt} = H + LP - LE \quad \ldots(1)$$

Where E = the evaporation rate, P = the precipitation rate, H = the sensible heating rate, M = the mass of the atmosphere between the surface and 500 mb, per unit area (taken as 1 cm^{-2}), C_p is the specific heat of air and L is its latent heat. In AGCM's and in the real atmosphere precipitation tends to depend on a relative humidity, r, of about 100% (at some level) being reached. Thus changes is the rate of change of relative humidity of an air mass placed over an evaporating land surface are a crude measure of changes in the time it will take for precipitation to form when convection is important.

Now we can write $\frac{dr}{dt} = \frac{d}{dt}\left[\frac{Q}{Q_s}\right]$

Q - Specific humidity integrated through the column of atmosphere between the surface and 500 mb

Q_s = saturation specific humidity in the same column

Thus $$\frac{dr}{dt} = \frac{1}{Q_s}\frac{dQ}{dt} - \frac{Q}{Q_s^2}\frac{dQ_s}{dt} \qquad \ldots(2)$$

Now $\frac{dQ}{dt} = E - P$ by definition

Furthermore $\frac{dQ_s}{dT} = \frac{\delta Q_s}{\delta T}\frac{dT}{dt}$ and we can put (approximately)

$\frac{\delta Q_s}{\delta T} = \alpha Q_s$ where α is a constant, and $Q = rQ_s$.

So $$\frac{dr}{dt} = \frac{E-P}{Q_s} - \alpha r\frac{dT}{dt}$$

From equation (1)

$$\frac{dT}{dt} = \frac{1}{MC_p}\left[H + L(P - E)\right]$$

We can put H + LE = K, a constant, if the total rate of heating of the ground due to fixed incident radiation remains constant even though the rate of evaporation may vary due to a reduction in soil moisture. It is easily found that

$$\frac{dr}{dt} = (E - P)\left[\frac{1}{Q_s} + \frac{2\alpha Lr}{MC_p}\right] - \frac{\alpha rK}{MCp}$$

The total heating rate in reasonably sunny conditions in June in S England is the equivalent of 5 mm of evaporation each day ie about 0.5 g day $^{-1}$ cm^{-2}. Now α = 0.07 (approx) from tables (or Clausius-Clapeyron equation); L = 2500 Jg^{-2}; MC_p = 500 J cm^{-2} $^{\circ}$K^{-1} for a 500 mb depth of atmosphere: Q_s is typically about 3 gm cm^{-2} for the lowest 500 mb.

If $\frac{Q}{Q_o} = 0.75$ then $\frac{dr}{dt} = 4.1\,(E - P)$ day^{-1}

If E = 3 mm/day and P = 0 then $\frac{dr}{dt} = 0.124$ day^{-1}

ie RH = 12.4% day^{-1}. If E = 1 mm/day in drought conditions ie where evaporation is much below the "potential rate",

$$\frac{dr}{dt} = -0.02\ (E - P)\ \text{day}^{-1} \text{ or } - 2\% \text{ per day, if } P = 0.$$

So the likelihood of precipitation is much increased by a wet ground surface. In fact most of the evaporation into a mass of air occurs by day (thus E reaches twice the values indicated above for part of the day); consequently an air mass need only remain over a soil moisture anomaly for about 12 hours for its relative humidity to be effected by the amount calculated. With typical advecting winds of 10 ms^{-1}, the horizontal scale of the soil moisture anomaly need only be about 400-500 km to appreciably affect the humidity of an air-mass.

4.1.3 Three examples of the sensitivity of climate to albedo (α) and S as shown by AGCM experiments

Mintz (1984) (5) provides a very good summary of 11 AGCM experiments carried out up to 1981. The examples below are chosen to help give a feel for the problem so they are not always the most elaborate experiments.

4.1.3.1 Experiments with α fixed with different anomaly and control S

(From Shukla and Mintz) (1981) (6)
This experiment used the global GLAS AGCM.

(a) Control - land-surface evaporation was everywhere set at the potential rate E_p (ie where $E = \beta E_p$; β always 1). So the soil was wet everywhere and albedo varied according to a standard climatology. Initial conditions were for the 15 June of a specific year.

(b) Anomaly - no evaporation was allowed anywhere (dry soil). Otherwise initial conditions were identical.

The results shown are averages for the following "July". Fig 4.3 shows the precipitation fields for both anomaly and control, Fig 4.4 shows the ground surface temperatures and Fig 4.5 the PMSL fields. Precipitation is greatly reduced over most of the continents in the anomaly experiment except near the ITCZ and in parts of Asia, though Sahel rainfall, itself a product of the ITCZ, is also reduced in this experiment. Furthermore, in the anomaly experiment, there is some reduction of overall precipitation over the oceans. The most dramatic effect of stopping evaporation over land in the summer half of the world and in the tropics is to greatly increase the surface temperature of the ground. Part of this increase in temperature is due to decreased cloudiness as is shown by Fig 4.6; here R_s, the solar heating rate, increases due to lower cloudiness and less latent heating. Not surprisingly, long-wave radiation losses from the ground are larger and of course the sensible heating vastly increases. Fig 4.5 shows that, on the whole, pressure falls over the continents and rises over the oceans, giving a strong global monsoon circulation component to the anomalous atmospheric response. No estimates of statistical significance are given but a qualitative response of the kind shown is physically reasonable and is shown in other similar AGCM experiments, even where experimental design is more complex. Of course the computed changes in evaporation are unrealistically large. (See the results of a more realistic experiment in Lecture 8).

4.1.3.2 Different values of α the same values of S

(Charney et al) (1977) (7)

Here we look at a restricted but interesting aspect of Charney et al's results; the Sahel drought follows as a theme through this series of lectures and we will look at the energy balance over the Sahel when α is changed.

(a) Control - where the continents are ice and snow free they are given an albedo of 0.14 though where true deserts are observed the albedo is set to 0.35 (Fig 4.7).

(b) Anomaly - same conditions except that the albedo is changed from 0.14 to 0.35 in the "Sahel", in Rajputana (India) and also in the Western Great Plains (USA), all adjacent to true deserts (see Fig 4.7). Table 4.1 shows detailed results for the energy balance of Sahel which are very instructive, given Charney's original paper of 1975. The main points are:

(1) The evaporation rate βE_p is fixed at 0.51 E_p in both experiments.

(2) The solar heating rate, R_s, increases slightly as α decreases; this paradoxical result arises because the model cloudiness, N, decreases greatly from 0.7 to 0.46, more than necessaray to offset the effects of a reduced value of α.

(3) Evaporation decreases in the anomaly experiment, though only by 1 mm-day.

(4) Sensible heating increases in the anomaly experiment.

(5) In the anomaly experiment long-wave radiation increases due to clearer skies and less humid air.

(6) Net radiation, R_n, becomes less positive.

(7) Surface temperature falls in the anomaly experiments but only very slightly. (T_a).

(8) The convergence of water vapour in the anomaly experiment decreases very strongly by 3.4 mm of precipitation per day

(9) Precipitation falls considerably in the anomaly experiment -mostly because of the decreased moisture convergence rather than because of the decreased evaporation.

So the dynamical effect of decreased convergence from more distant locations is dominant when α is reduced, but surface temperatures hardly alters, even though the availability of soil moist water is fixed (as effectively assumed in Charney's original model). Such results clearly depend on the model used but show the fascinating complexity of the problem. They do not prove however that an increase in albedo is necessarily the chief (local) cause of the Sahel drought as the next section will suggest.

4.1.3.3 Fixed α, but different time-dependent soil moisture variations - West Africa only

(Walker and Rowntree) (1977) (8)

The model used was a restricted area 11-level AGCM. Because of this, it may not properly represent changes in large scale moisture convergence. Nevertheless the experiment is instructive as soil moisture was allowed to vary through the experiments as P and E varied.

1. Case 1 - initial S = 0 in the latitudes 14-32°N; initial S = 100 mm in zones 6-14°N and 32-36°N

   Case 2 - initial S = 100 mm over all land regions.

In this model, $\beta = 1$ when S is > or = 50 mm and the maximum S = 150 mm (run off immediately occurs for greater values). Fig 4.8 shows the variation of precipitation and soil moisture for days 1-10 (case 1 experiment) and similar maps for days 1-20 (case 2 experiment). In case 1, where the soil was initially dry it remains dry. There is very little water transport into the dry region and practically no precipitation. The wetter soil regions to the south of 14°N have a variable precipitation rate as wave-like model disturbances move across these regions; however total precipitation is quite considerable. In case 2, the initially moist Sahara rapidly develops rainfall which persists. The Saharan soil moisture at first declines but steadies after 10 days. Coastal precipitation and soil moisture vary markedly on short timescales due to transient wave disturbances but precipitation is quite high. Although the integrations were very short, this simple model appeared to give two solutions to the Sahara/Sahel climate that looked distinctly "intransitive", though strong seasonal variations in circulation in this region would make this an unlikely possibility in the real atmosphere. Despite the simplicity of the model it shows that a Sahel drought, in a given season, could easily be made worse due to changes in circulation that initially tend to reduce the soil moisture which might then provide a powerful feedback on the rainfall. Changes in albedo may not be necessary (and have probably been modest over the Sahel region in the last 15 years).

Summary

4.1.4 The results of this section suggest that soil moisture, especially, may provide a new source of potential predictability on the stream 1 (1-2 months) and possibly stream 2 timescales of the World Climate Research Programme.

REFERENCES

1. CHARNEY, J G (1975) Dynamics of deserts and drought in the Sahel. Q J Roy Met Soc, 101, pp 193-202.

2. PENMAN H (1956) Estimating Evaporation. Trans Amer Geophys Union, 37(1), pp 43-46.

3. BAUMGARTNER A AND REICHEL E (1975) The World Water Balance: Mean annual global, continental and maritime precipitation, evaporation and run-off. Elsevier.

4. KORZUN V I (Ed) World Water balance and water resources of Earth. Studies and Reports in Hydrology, Vol 25, Unesco Press, Paris.

5. MINTZ Y (1984) The sensitivity of numerically simulated climates to land-surface boundary conditions. The Global Climate, pp 79-105. Ed: J T Houghton, Cambridge University Press.

6. SHUKLA J AND MINTZ Y (1981) Influence of land-surface evapotranspiration on the earth's climate. Science, 215, pp 1498-1501.

7. CHARNEY J G et al (1977) A comparative study of the effects of albedo change and drought in semi-arid regions. J Atmos Sci, 34, pp 1366-85.

8. WALKER J M AND ROWNTREE P R (1977) The effect of soil moisture on circulation and rainfall in a tropical model. Q J Roy Met Soc, 103, pp 29-46.

ADVANCED LECTURE NO 4

PART II - SEA SURFACE TEMPERATURE (SST)

4.2.1 Introduction

SST varies quite substantially through the seasons in many regions and it is well-known that differences in temperature between land and sea play an important role in shaping the observed seasonal variations in atmospheric circulation. Fig 4.9 shows the mean range of air temperature and SST over the globe between the coldest and warmest months. It is not, at first sight, completely obvious that variations in SST that occur in addition to the mean seasonal variations could be important in climate variability. In this lecture we concentrate mainly on the effects of SST anomalies on the 1-2 month timescales with an eye to the long range forecasting problem. We leave discussion of longer timescales (with one exception) to Lectures 5 and 8. Lecture 5 will discuss the ENSO phenomenon so little mention will be made here.

4.2.2 What size of SST anomaly is important?

The arguments used here are reminiscent of those used by Sawyer (1965) (1). At the most elementary level, imagine the temperature of the air to be changed over a large area by 1°C throughout the depth of the troposphere (up to say 200 mb) with no change elsewhere. If there was no immediate dynamically induced response from the surrounding atmosphere other than to accept an inflow at higher levels of excess warm air, the density of the warm air, using Boyle's law, would fall by roughly $^{1}/_{T}$ where T is the air temperature ie roughly $^{1}/_{300}$. So PMSL would fall by approximately 0.8 ($^{1000}/_{300}$) mb or about 3 mb. We could imagine an SST anomaly of 1°C producing this change. To be effective in altering large scale circulation, we could imagine that in middle latitudes that the horizontal scales of the SST anomaly might have to exceed about $^{1}/_{4}$ of a typical Rossby wave length - say 1000 km. Then the anomalous rate of heat transfer that would initially occur if the anomaly was suddenly "switched on" is given adequately by the sum of the anomalous sensible and latent heating that would be produced:-

$$\begin{aligned} \text{ie } \Delta Q &= \Delta H + \Delta E \\ &= 3.7\ U\ \Delta\ (e_a - e_s) + 2.4\ U\ \Delta\ (T_a - T_s) \quad \mathrm{Wm^{-2}} \end{aligned}$$

from standard formulae. e_a = vapour pressure of the air, e_s is the saturation vapour pressure at the sea temperature, U = wind speed in $\mathrm{ms^{-1}}$.

If we assume that the initial relative humidity = 80% and T = 15°C and that it is mid-latitude winter with $\dot{U} = 10\ \mathrm{ms^{-1}}$ then we find $\Delta Q = 70\ \mathrm{Wm^{-2}}$ approximately when T_s changes by 1°C. Although this calculation somewhat exaggerates ΔQ this amount is about 20% of the effective annual mean solar insolation warming the ocean (about 0.7 x 340 $\mathrm{Wm^{-2}}$) suggesting that a reasonably large scale winter mid-latitude SST anomaly of 1°C might be significant in regions of strong winds and strong cold advection. In summer, when mean wind speeds are typically half the winter values, the anomalous heat transfer would (approximately) also be halved. Fig 4.10 shows the annual average heat flux, including net radiation, from the

Atlantic Ocean to the overlying atmosphere, given that the sign of the values shown is reversed. Near the ITCZ, heat is transferred to the atmosphere by deep convection. A similar analysis shows that for SST of 29.5°C (the average in the warmest regions) an increase of SST by 1°C would produce a similar anomalous heat transfer when the mean wind speed was only 5 ms^{-1}, a typical value. This amount is comparable to the average heat transfer in tropical regions. It is difficult to determine the areal size of the anomaly that will be significant however. So anomalies of 1°C or more that last say 2 months or so and cover at least 1 x 10^6 km^2 could significantly in affect sequences of climate "regimes" in a number of regions.

4.2.3 What SST anomaly (SSTA) variations actually occur?

Fig 4.11(a) (b) show the standard deviation of January and July SST derived from MOHSST (Version 3) for the period 1951-80. Areas of high inter-annual variability shown in these figures include the tropical, Central and East Pacific, the Central Pacific and the Kuro and Shio and Gulf Stream regions. Fig 4.12 gives a rather better measure of the persistence of SSTA and shows areas of the world where a 1°C 10° x 10° anomaly (a) occurs and (b) on average persists (taking all seasons together).

(a) The tropical C and E Pacific

(b) The Eastern, Northern and Northwestern extratropical Pacific.

(c) The South east Tropical S Atlantic

(d) Several parts of the western Indian Ocean

(e) The tropical Central N Atlantic

(f) The North West Extratrapical Atlantic

(g) Isolated areas of the Extratropical S Pacific, most notably west of Chile though analyses are not very reliable here.

Further analyses show that although the Tropical W Pacific generally exhibits small anomalies, they are likely to be particularly persistent. The above information is taken from Newman and Storey (1985) (2).

4.2.4 Effects of Extra Tropical SSTS on atmospheric circulation

Smagorinsky (1953) (3) carried out the first physically realistic analysis, using a baroclinic model of the perturbations in the extratropics of a zonally symetric wind flow by imposed diabatic heating rates that varied along latitude circles. Fig 4.13 is representative of his results. Smagorinsky defined a sinusoidal heating function so that in Fig 4.13 the maximum diabatic heating, Q_{max}, was 209 Wm^{-2} relative to the minimum heating, Q_{min}. The wavelength of the heating function was 160° and in Fig 4.13 the maximum heating is placed at 40° relative longitude and the minimum heating at -40°. Smagorinsky designed the wavelength of this heating variation to correspond roughly with the variation in surface heating in winter due to the distribution of land and sea in the N American sector. He showed (which can be deduced from Fig 4.13) that the Iceland low at the surface should be placed about 20-30° longitude East of the 500 mb Canadian trough in the winter. In Fig 4.13, D is the meridional wavelength of the heating, h is the height of maximum heating (which includes the effects of latent heat release): for our purpose D = 35° is quite appropriate (Fig 4.13(a),(b)). This value corresponds to an appreciable positive (or negative) heating anomaly that occupies at least 10° of latitude. Fig 4.13 suggests that the maximum PMSL response would be of magnitude 1 mb/20 MW cm^{-2} of forcing and the maximum 500 mb height response would be about 1 dm/30 MW cm^{-2}.

We can apply these ideas to work carried out by Ratcliffe and Murray (1970) (4) who showed from observations an association between N Hemisphere PMSL anomalies and SSTA in the previous month south east of Newfoundland. Fig 4.14 shows the SSTA pattern, in a generalised way, and Fig 4.15(a), (b) the response of the PMSL to warm and cool anomalies; their pattern is reminiscent of Smagorinsky's results. Concentrating on February PMSL response, the magnitude of the PMSL anomalies is roughly the same for both cool and warm SSTA though the patterns are not the inverse of each other, suggesting analysis difficulties or non-linearity in the response of PMSL to SSTA. Nevertheless in February, U is approximately 12 m sec^{-1} south east of Newfoundland, T_s = approximately 10°C so a mean maximum SSTA of 1.5°C might give a maximum heating anomaly of about 80-90 Wm^{-2}. Fig 4.13 suggests a PMSL response downstream of this SSTA value of about 4 mbar, quite similar to RM's value for positive SSTA, though the observed PMSL anomaly for cold SSTA is rather displaced from its expected position. In summer the general shape of the PMSL anomaly pattern is similar but anomalies are about half those observed in February. This seems reasonable as on average U will be about half the value observed in February.

Recently, these results have been recalculated for winter by Palmer and Sun (5) using the Meteorological Office 5-level AGCM supported by an observational analysis employing better SST data than was available to RM (from the MOHSST (Version 3) data set). The modelling study used warm and cold SSTA whose maximum magnitude just exceeded 3°C ie double that used by RM; these anomalies are still realistic and correspond to the maximum observed anomalies. The model was initialised from real November atmospheric data and used winter radiation. Four pairs of anomaly (warm SST) and control (cold SSTA) runs were made. December climatological mean SST was used away from the anomaly. The difference in model 1000 mb height and 500 mb height is shown in Fig 4.16 (a)-(b); in each diagram the difference is averaged over the four pairs of integrations for model days 21-50. The patterns are reminiscent of those of RM but the (statistically significant) high and low centres are further apart. Other details of the model response are given in the paper including the anomalous tracks of depressions.

The observational study consisted of a calculation of PMSL and 500 mbar height differences between winter months (Nov-Feb) having a warm SSTA (> about 0.9°C) and those having a cool SSTA (< about 0.9°C) in the region 40°-60°W, 40°-50°N. The epoch 1951-80 was studied first and gave similar results to those of the AGCM though with a slightly shorter wavelength between high and low centres at both levels, when monthly mean SSTA, PMSL and 500 mb height were calculated for the same month. The analysis was repeated for 1901-30 and gave similar results. Fig 4.17 is an example of results for 1951-80. However a puzzling and as yet unresolved result was that when PMSL was allowed to lag one month behind SSTA the relationships did not hold up well nor did they agree well with those of RM - low pressure anomalies were indicated stretching across the Atlantic when months following warm SSTA were subtracted from those following cold SSTA.

Rowntree (6) has summarised a number of AGCM experiments carried out in the Atlantic and Pacific on mid-latitude SSTA; Fig 4.18 shows his summary diagramatically; the overall conclusions are surprisingly consistent and broadly in harmony with the ideas of Smagnorinsky and with the results of RM. Rowntree provides another useful review of AGCM extratropical SST forcing experiments in reference (7); Maryon (1981) (8) provides a detailed review of observational studies and some AGCM studies of extra-tropical and tropical SSTA - atmospheric forcing (or associations).

4.2.5 Tropical SSTA

The mechanism of Tropical SSTA forcing are different. Typically, warm tropical waters are associated with a low level tropospheric trough and an overlying upper tropospheric ridge. Anomalous tropical heating gives rise mainly to anomalous vertical motion so the most direct result of warm tropical SSTA forcing is that an anomalous warm upper high is forced near the SSTA anomaly ie anomalous high-level anticyclonic vorticity is created. Simmons (1982)(9) has, amongst others, used a relatively simple baroclinic model to show that the anomalous vorticity forcing gives a Rossby wave-like response in the extratropics which is associated with the stimulation of barotropic instability in the climatological mean upper flow (initially imposed in the model). The response in the winter is largest when the vorticity forcing is placed in certain tropical regions, if the climatological mean upper flow, including its mean troughs and ridges, is used rather than a zonally averaged mean flow. Simmons suggests that the effects of tropical vorticity forcing propagate into mid latitudes more easily when the forcing is overlain by upper westerly winds. For anticyclonic vorticity forcing, propagation is favoured when forcing coincides with a climatological upper ridge as in the tropical W Pacific in winter. Fig 4.19 shows a few of Simmon's results at 500 mb using a January mean 500 mb height climatology where vorticity is forced in different tropical regions (SST forcing was not explicitly used). Fig 4.19 shows the strongest extratropical response that Simmons found for forcing centred at 135°N, 150°E. Notice that the 500 mb height response is quite large near UK.

Palmer and Mansfield (1985) (10) have used the Meteorological Office 11-level AGCM to explore the impact of tropical W Pacific SSTA on winter atmospheric circulation. They found that an anomaly with a maximum of just over 1°C centred on the equator in the tropical W Pacific (see Fig 4.20(a)) produces a strong wave-like response at 500 mb (Fig 4.20(b)). The response is qualititatively similar to that of Simmons though the path of their 500 mb height anomalies across polar regions is appreciably different. In a companion paper (Palmer (1985) (11)) it is argued that the atmospheric response to tropical vorticity forcing may be non-linear; vorticity forcing from positive SSTA anomalies mainly results from the anomalous release of latent heat which appears to increase non-linearly with increasing SSTA. So it might be expected that a negative SSTA of given magnitude would produce a smaller response. Palmer has provided evidence for a similar response and gives reasons but it remains to be seen to what extent such results depend in the AGCM used. A contributory reason for the very strong atmospheric response to anomalies of SSTA over the W Pacific is that a given SSTA produces a large anomaly of latent heating than elsewhere because the saturation vapour pressure of ocean water rises faster as temperature increases. Typical tropical W Pacific SST's exceed 29°C; at the time of writing (mid-February 1985) SST maxima exceed 31°C quite close to the position of the maximum anomaly used by Palmer and Mansfield.

Fig 4.21 shows the response of a steady state linear model (from (9)) to an isolated positive heating anomaly near the equator. To the west of the heating maximum, the low level winds tend to be westerly and the upper level winds easterly, a similar situation to that in the real atmosphere west of the heating maximum created by the SE Asian monsoon/W Pacific region in northern summer (see Lecture 2). To the east of the heating maximum the winds are reversed: ie the upper winds are westerly and the lower winds easterly. If we consider the well-defined SST minimum near the equatorial S American coast, sinking motion should occur and connect the upper westerly flow to the lower easterly flow that occurs to the east of the W Pacific SST maximum.The closed circulation that results is just like the Walker circulation discussed in Lecture 2: the mechanism underlying Fig 4.20 probably explains a good part of the Pacific Walkere circulation and perhaps, similar circulations near the equator in other longitudes.

Rowntree (1976) (11) carried out experiments using the Met Office 5-level AGCM which indicated, in winter, that north of a positive SST anomaly in the tropical NE Atlantic a surface low was formed, with an upper high almost over the anomaly. North of the low but at middle latitudes and longitudes a high anomaly was found. Fig 4.22 shows the model response for selected experiments compared to central integrations. The SST anomaly was based on that observed at the beginning of the very cold 1962-63 NW European winter but it remains unclear to what extent the model results "explain" that winter.

Hastenrath (12) has also carried out interesting observational studies of tropical Atlantic SSTA and circulation anomalies in the region around Brazil.

4.2.6 Another way in which SSTA can influence climate

SSTA can affect climate in maritime regions by directly cooling or warming the overlying air and thus the downwind land air. Consider a fixed atmospheric circulation pattern: Parker (1984) (13) has shown an interesting correlation between decadal averages of temperature in Central England during Lamb "westerly" circulation types (see Lecture 1 for discussion of Lamb types) and decadal averages of SST calculated over the whole N Atlantic north of 35°N (Fig 4.23). The correlation was 0.67 for the decades 1861-1870 to 1971-1980. Although this correlation could arise from the influence of a third factor, the relationship is physically reasonable because SST has varied in a similar way over most of the N Atlantic on these time scales (Newman personal communication). SSTA vary by larger amplitudes on shorter time scales so turning to a moment to the long-range forecast problem it seems worthwhile investigating, for suitable fixed air masses, relationships between regional air temperature anomalies over UK and SSTA in the surrounding seas.

REFERENCES

1. SAWYER, J S (1965) Notes on the possible causes of long-term weather anomalies. WMO Tech Note, No 66, pp 227-48, Geneva.

2. NEWMAN, M and STOREY, A M (1985) A preliminary study of intermonthly changes in sea surface temperature anomalies throughout the world ocean. Proc 16th Liege Conf on Ocean Hydrodynamics (in Press).

3. SMAGORINSKY, J (1953) The dynamical influence of large-scale heat sources and sinks on the quasi-stationary mean motions of the atmosphere. Q J Roy Met Soc, 79, pp 342-366.

4. RATCLIFFE, R A S AND MURRAY, R (1970) New lag associations between N Atlantic sea temperatures and European pressure applied to long-range weather forecasting. Q J Roy Met Soc, 96, pp 226-246.

5. PALMER, T N AND SUN-Z (1985) A modelling and observational study of the relationship between sea surface temperature in the North West Atlantic and the atmospheric general circulation. (Presently unpublished, available from Met O 13).

6. ROWNTREE, P R (1984) A survey of ocean surface temperature anomaly experiments for the N Hemisphere winter. Met O 20 Technical Note II/220.

7. ROWNTREE, P R (1979) The effects of changes in ocean temperature on the atmosphere. Dynamics of Atmospheres and Oceans, 3, pp 373-390.

8. MARYON, R M (1981) A review of recent studies into the forcing of the atmosphere circulation by sea-surface temperature anomalies. Met O 13 Branch Memo No 116.

9. SIMMONS, A J (1982) The forcing of stationary wave motion by tropical diabatic heating. Q J Roy Met Soc, 108, pp 503-504.

10. PALMER, T N AND MANSFIELD, D (1984) Response of two atmospheric general circulation models to sea-surface temperature anomalies in the tropical East and West Pacific. Nature, 310, pp 483-485.

11. ROWNTREE, P R (1976) Response of the atmosphere to a tropical Atlantic ocean temperature anomaly. Q J Roy Met Soc, 102, pp 607-626.

12. HASTENRATH (1984) Interannual variability and annual cycle: Mechanisms of circulation and climate in the tropical Atlantic sector. Mon Weath Rev, 112, pp 1097-1107.

13. PARKER, D E (1984) Met O 13 Discussion Note No 82.

	Case	Energy balance							Water balance				
		(1)	(2)	(3)	(4)	(5)	(6)	(7)	(8)	(9)	(10)	(11)	(12)
Region	No.	β	$(1-\alpha)$	R_S	R_L	R_N	LE	H	N	T_A	E	$(-\overline{\nabla \cdot qv})$	P
Sahel (16-20°N	2a	0.51	0.86	169	58	111	107	4	0.70	26.0	3.7	3.7	7.4
17.5°W-37.5°E)	3a	0.51	0.65	177	84	93	81	12	0.46	25.7	2.8	1.2	4.0

Table 4.1 Components of the energy and water budgets, in experiment of Charney et al. (1977)

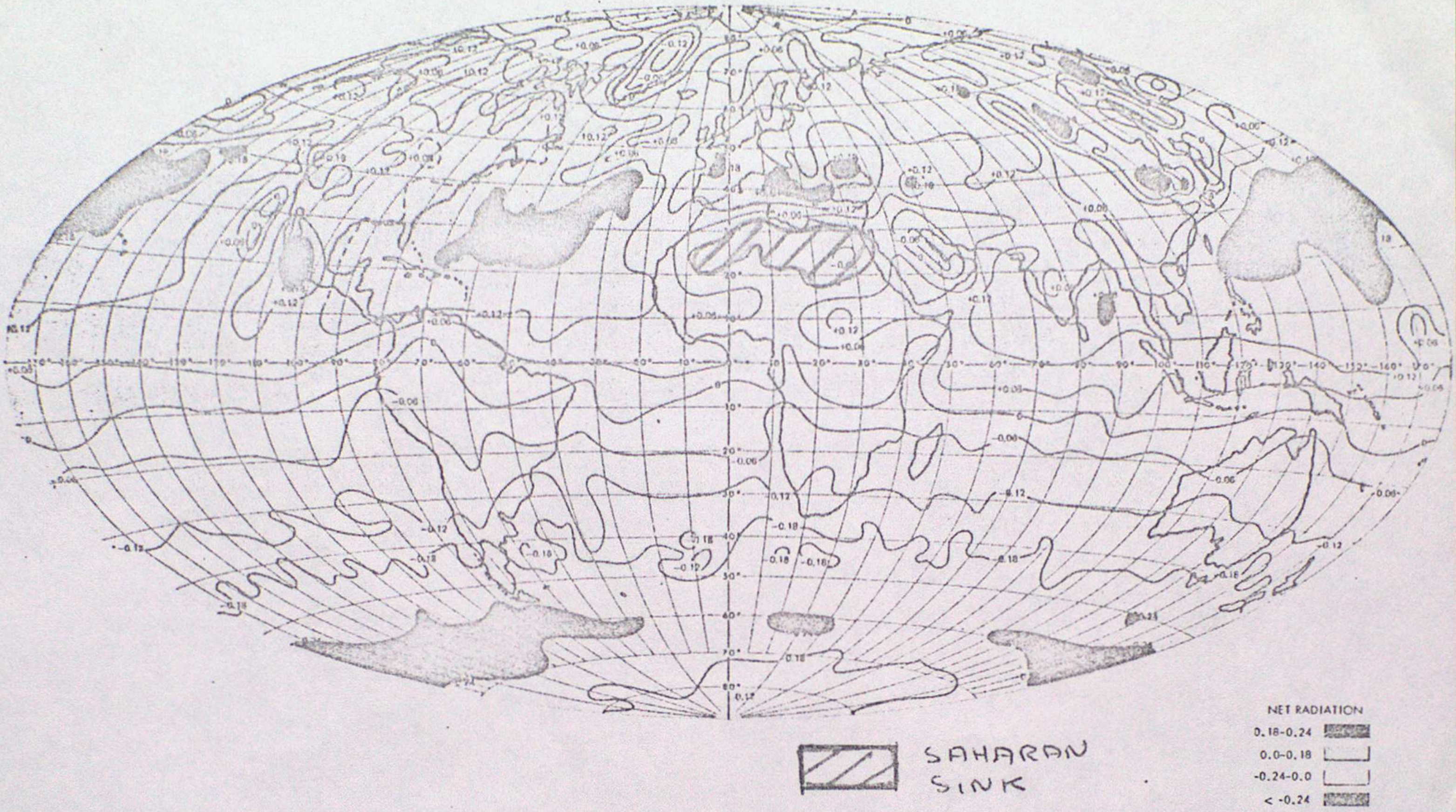
NET RADIATION
0.18-0.24 ▨
0.0-0.18 ☐
-0.24-0.0 ☐
< -0.24 ▨
SAHARAN SINK

Figure 4.1 Net radiation at the top of the atmosphere (cal/cm^2/min) measured from Nimbus III, 1–15 July 1969.

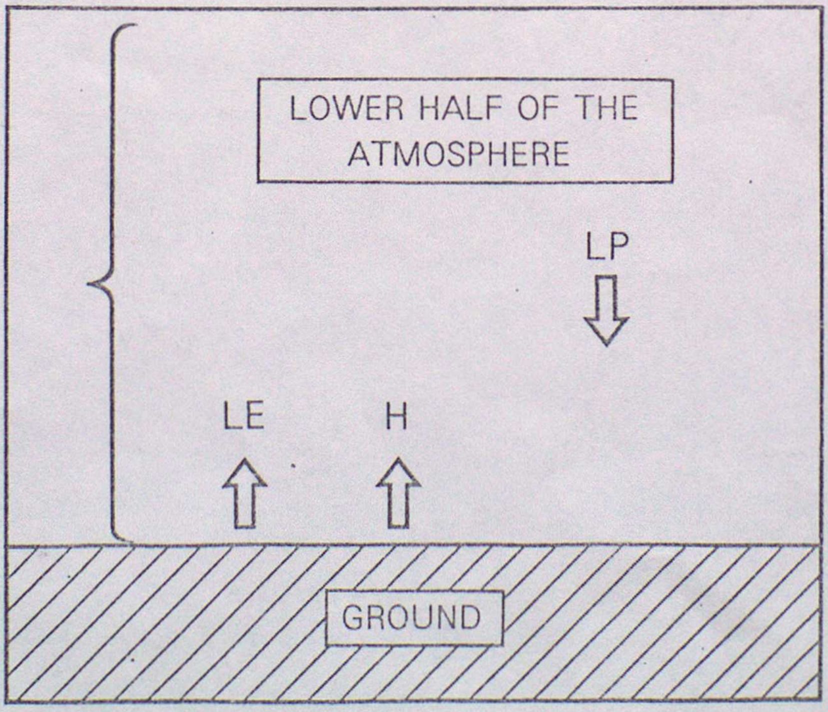
LOWER HALF OF THE ATMOSPHERE
LP
LE
H
GROUND

Fig. 4.2 Precipitation and soil moisture anomalies

Precipitation (mm/day) in wet-soil case (top) and dry-soil case (bottom), in experiment of Shukla & Mintz (1981). (Precipitation greater than 2 mm/day is shaded.)

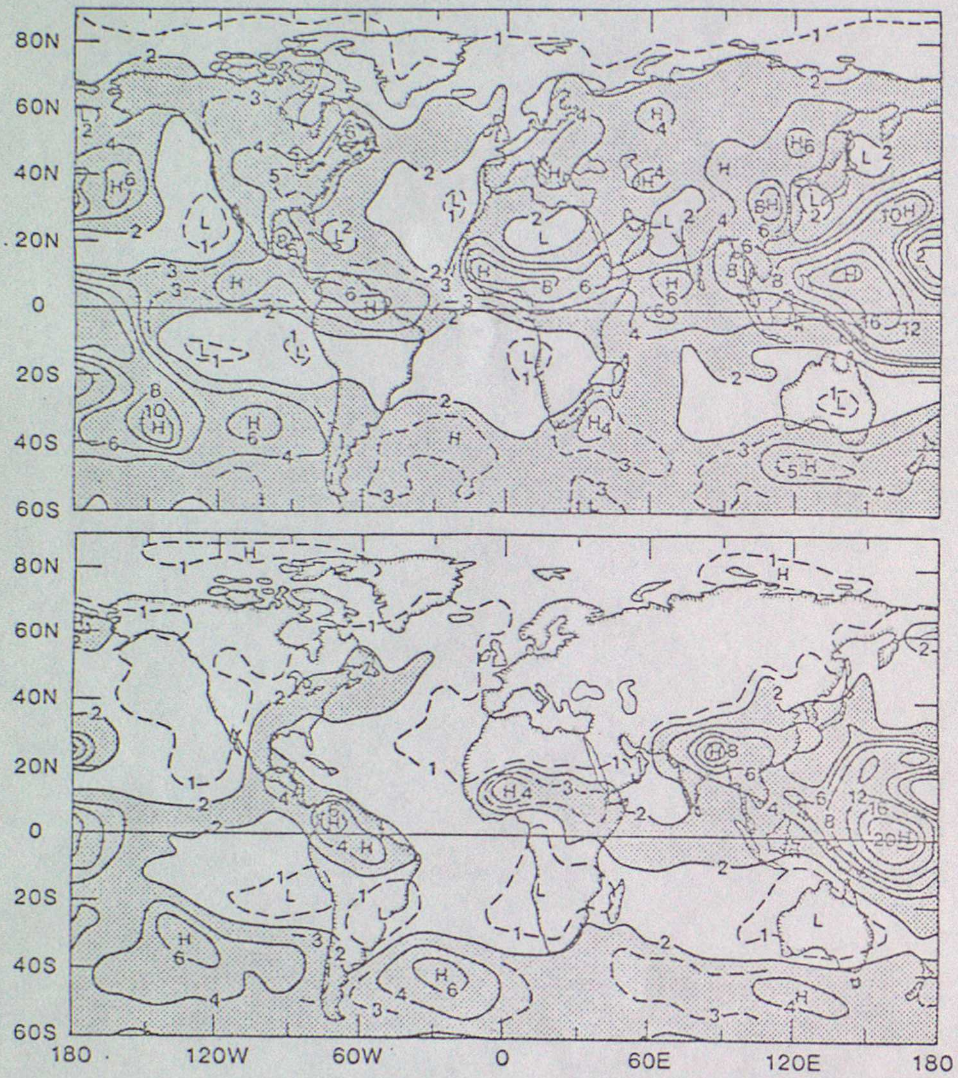
80N
60N
40N
20N
0
20S
40S
60S
180
120W
60W
0
60E
120E
180

FIG 4·3

Ground-surface temperature (°C) in wet-soil case (top) and dry-soil case (bottom), in experiment of Shukla & Mintz (1981).

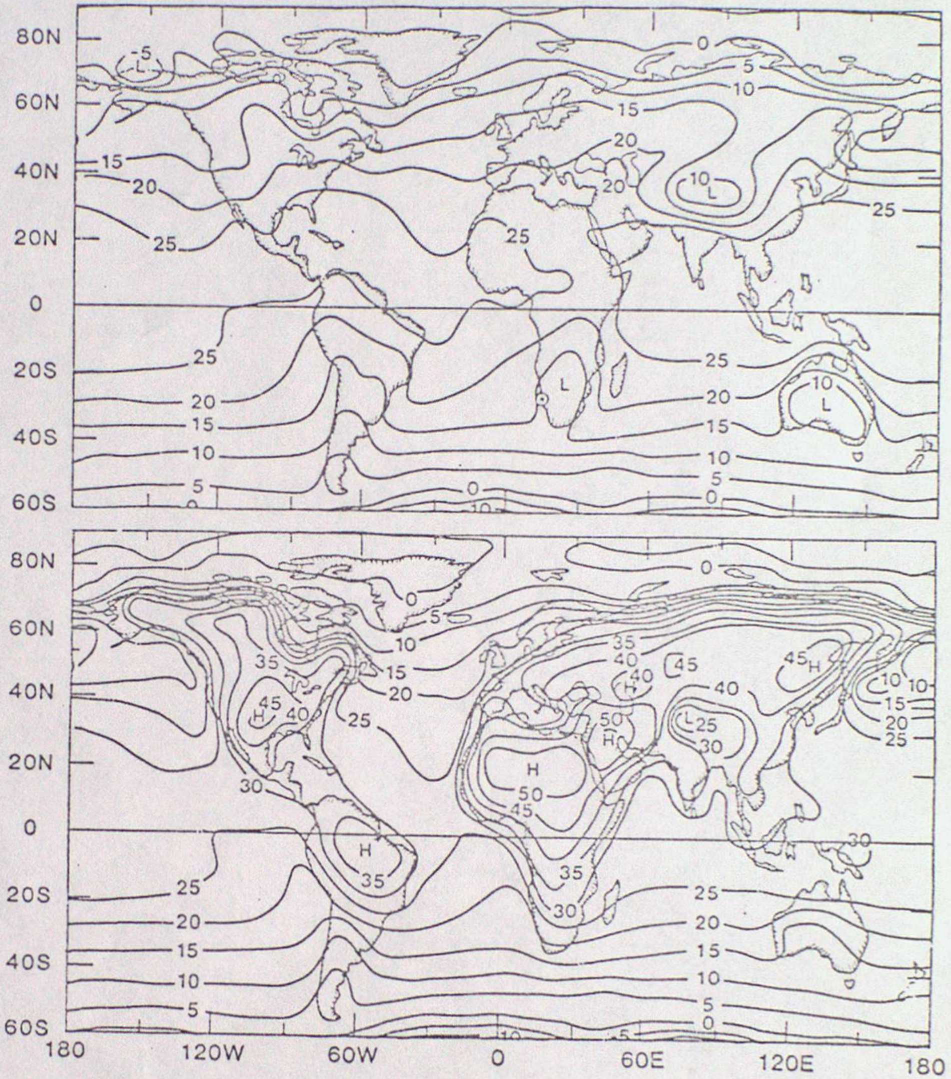
80N
60N
40N
20N
0
20S
40S
60S
180
120W
60W
0
60E
120E
180

FIG 4·4

Surface pressure reduced to sea level (mb minus 1000) in wet-soil case (top) and dry-soil case (center), in experiment of Shukla & Mintz (1981). Bottom map show the difference between the two surface pressures (mb).

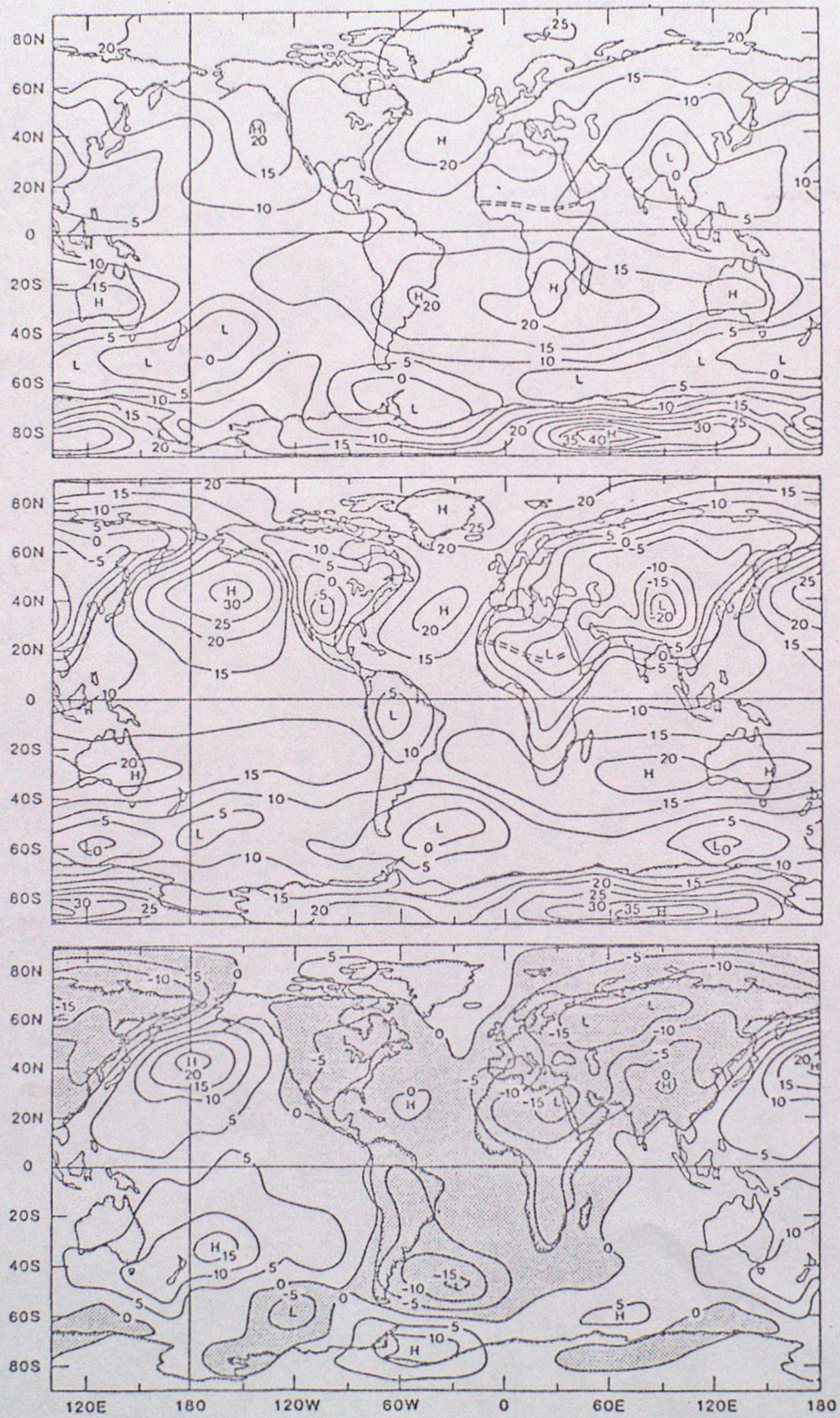
80N
60N
40N
20N
0
20S
40S
60S
80S
120E
180
120W
60W
0
60E
120E
180
H
L

FIG 4·5

Surface energy transfers (watt/m²) averaged for the continents between 20°S and 60°N, in experiment of Shukla and Mintz (1981).

R_S solar raditional heating of the ground.
R_L long wave radiational cooling of the ground (difference between radiation emitted by ground and radiation absorbed by ground).
$R_N = (R_S - R_L)$ net (all-wavelength) radiational heating of the ground.
LE latent heat transfer from ground to atmosphere (evaporative cooling of the ground).
H conductive-convective heat transfer from ground to atmosphere.

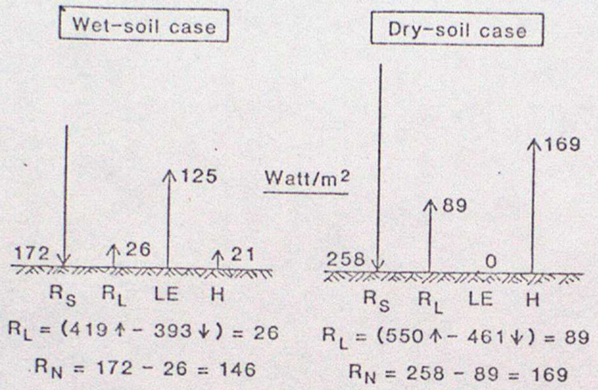
Wet-soil case
Dry-soil case
Watt/m²
172
26
125
21
258
89
0
169
R_S R_L LE H
R_S R_L LE H
R_L = (419↑ − 393↓) = 26
R_N = 172 − 26 = 146
R_L = (550↑ − 461↓) = 89
R_N = 258 − 89 = 169

FIG 4·6

Bottom panel: the assigned albedos in experiments of Charney *et al.* (1977). Unshaded land areas have an albedo of 0.14 in all cases, and dot-shaded areas have an albedo of 0.35 in all cases. In the cross-ruled areas the albedo was changed from 0.14 (in cases 2a and 2b) to 0.35 (in cases 3a and 3b). Top panel: precipitation (mm/day) in case 3b.

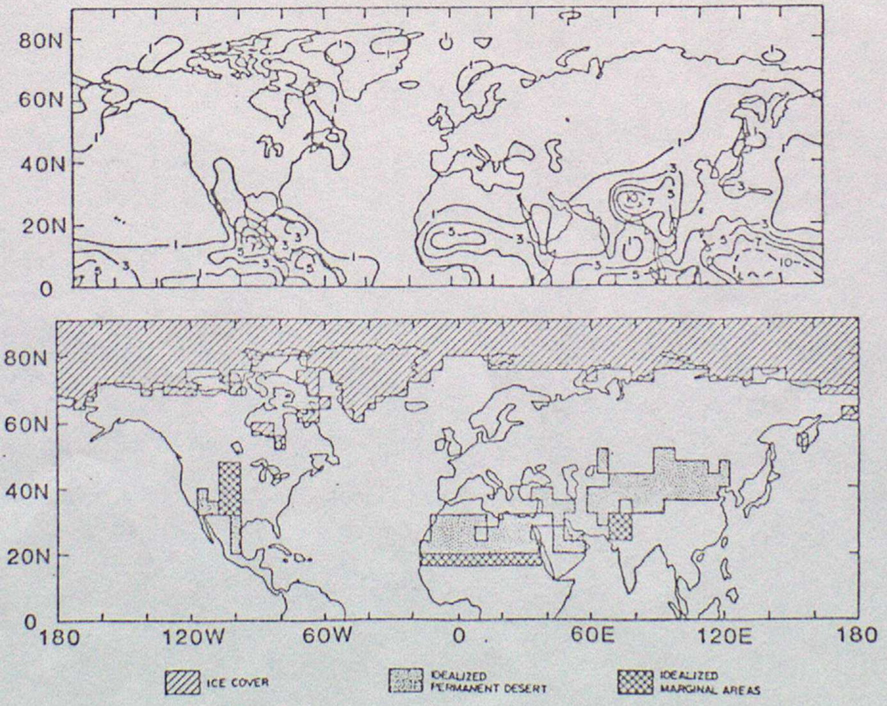
80N
60N
40N
20N
0
180
120W
60W
0
60E
120E
180
ICE COVER
IDEALIZED PERMANENT DESERT
IDEALIZED MARGINAL AREAS

FIG 4·7

. Variation with time of the zonally averaged precipitation (top) and soil moisture (bottom) in the case where, initially, the soil in the Sahara is completely dry. (Experiment of Walker & Rowntree, 1977.)

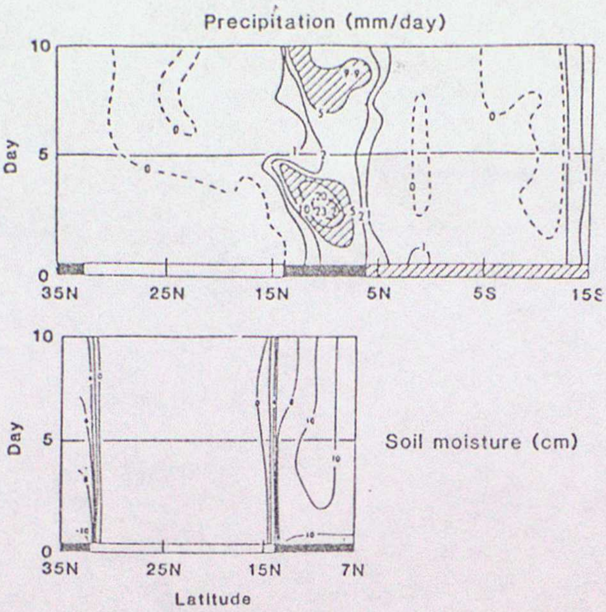

Variation with time of the zonally averaged precipitation (top) and soil moisture (bottom) in the case where the initial soil moisture in the Sahara is 100 mm. (Experiment of Walker & Rowntree, 1977.)

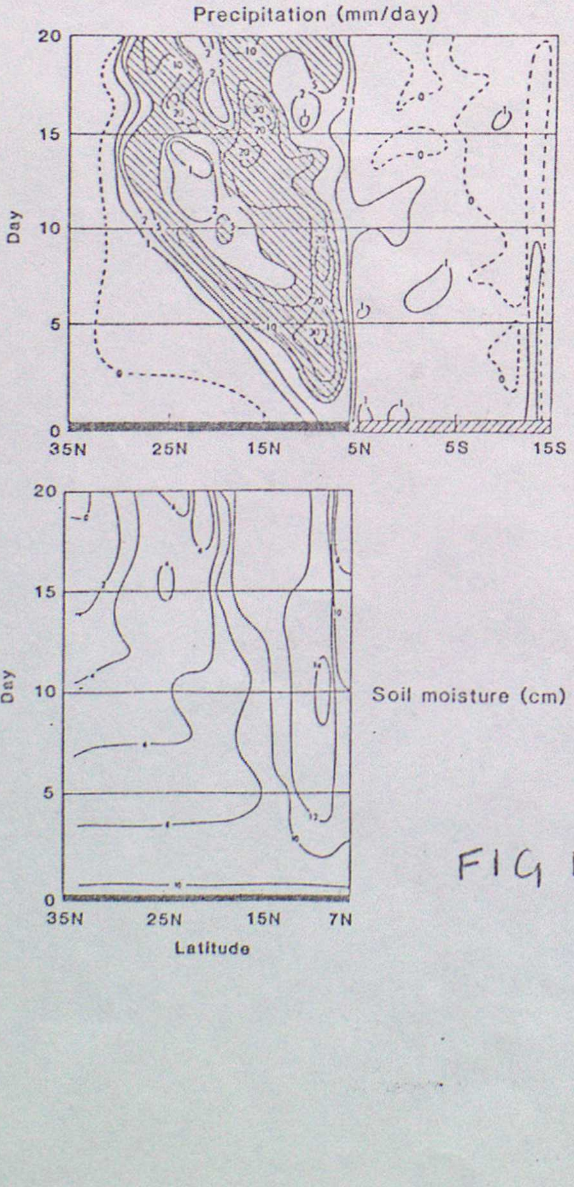

Variation of the zonally averaged precipitation and soil moisture with time, in selected latitude zones across north Africa, in the case where the initial soil moisture in the Sahara is 100 mm. (Experiment of Walker & Rowntree, 1977.)

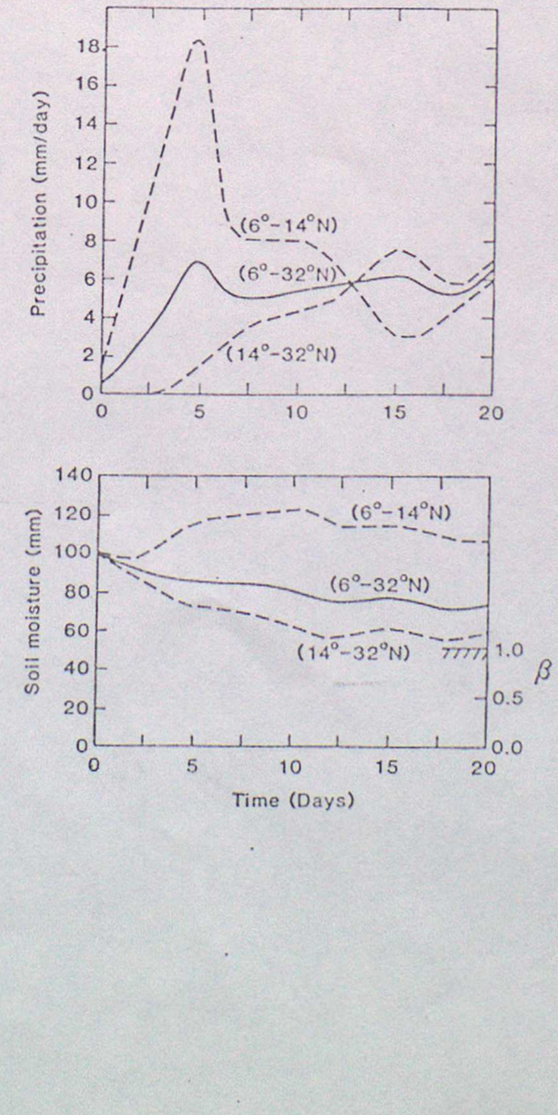

FIG 4·8

.. The world map of annual range of surface temperature.
(After Monin 1975.)

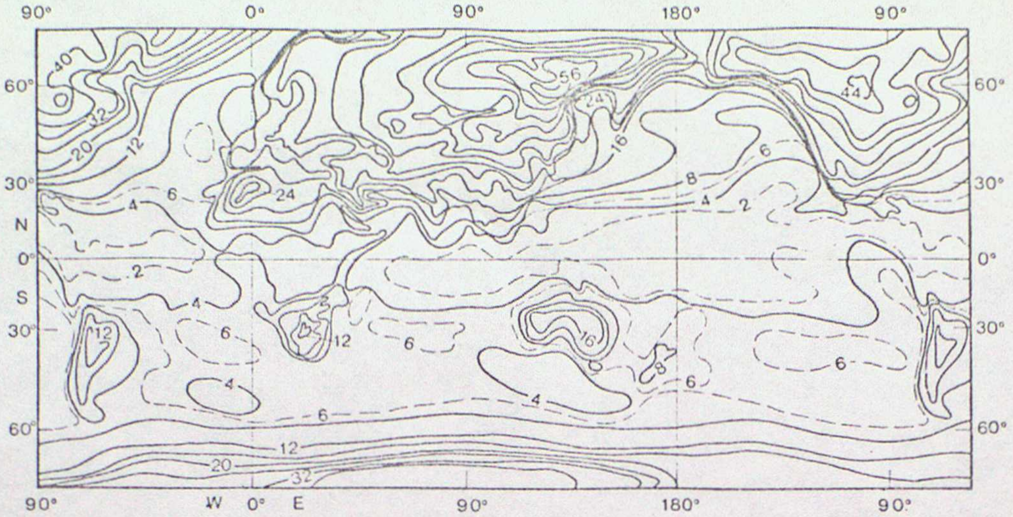
90°
0°
90°
180°
90°
60°
30°
N
0°
S
30°
60°
W 0° E
40
32
20
12
56
24
44
16
6
8
4
2
24
6
4
2
4
6
12
6
16
8
6
6
4
4
6
12
20
32

FIG 4·9

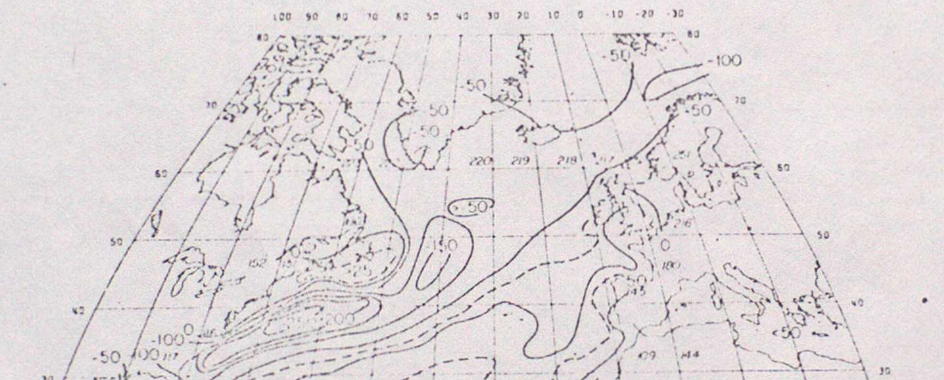
100 90 80 70 60 50 40 30 20 10 0 -10 -20 -30
-50
-100
-50
-50
-50
-50
220
219
218
>50
150
-100
-50
0
>25
0
-20
50
50
50
>75
<25
50
50
50
100
100
100
100
50
50
50
50
100
150
100
-100
-100
-50
0
>25
-50
-25
0
489
488
486
485
482
481
480
515
514
513

The annual average net surface heat flux into the ocean (W m^{-2}). [According to Bunker (1980, Fig. 18)].

FIG 4·10

FIG 4·11

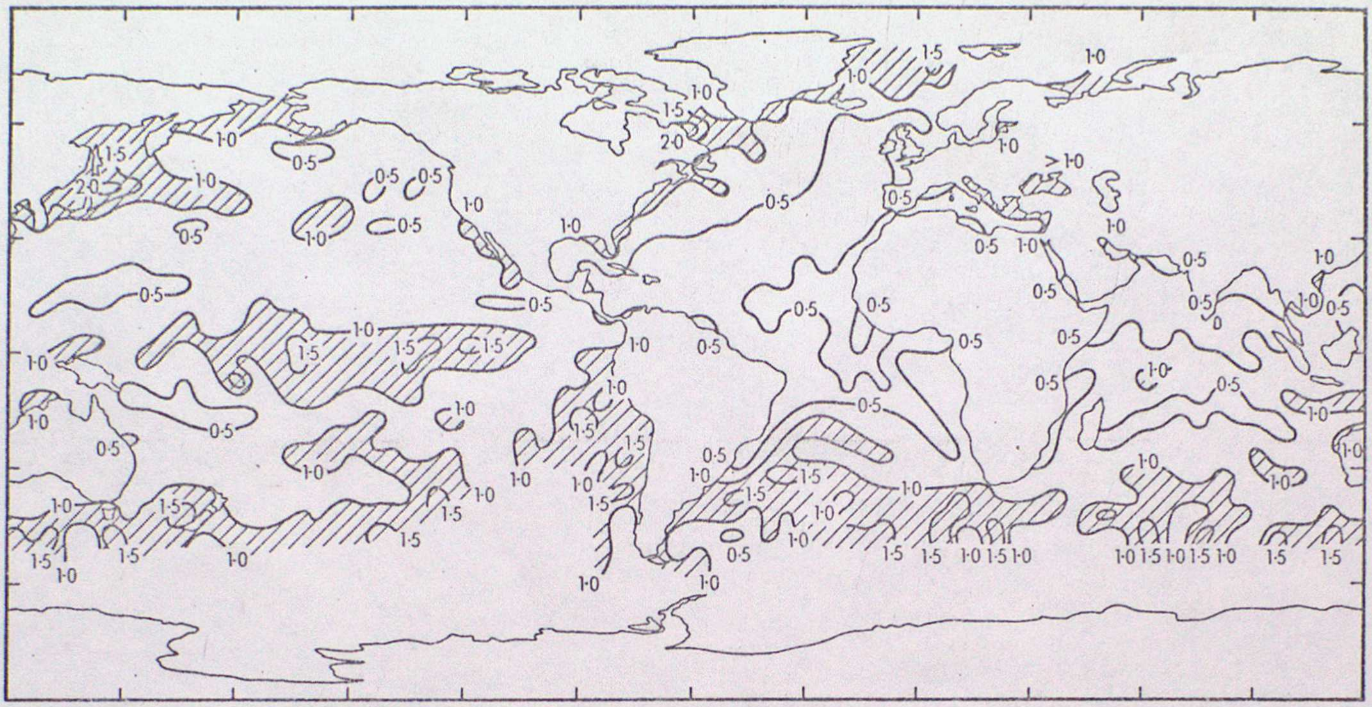
1·5
1·0
1·0
1·5
2·0
1·5
2·0
1·0
0·5
1·0
0·5
0·5
0·5
1·0
0·5
1·0
1·0
0·5
0·5
0·5
1·0
1·0
>1·0
1·0
0·5
1·0
0·5
0·5
1·0
0·5
0·5
1·0
1·5
1·5
1·5
1·0
0·5
0·5
0·5
0·5
1·0
1·0
0·5
1·0
1·0
1·5
1·5
0·5
1·5
1·0
1·0
1·0
1·5
1·0
0·5
1·0
1·5
1·0
1·5
1·0
1·0
0·5
1·0
1·0
1·0
1·5
1·0
1·5
1·5
1·5
1·0
1·0
1·5
1·5
1·0 1·5 1·0
1·0 1·5 1·0 1·5 1·0
1·5
1·5
0·5
1·0
1·0

Standard deviation of sea surface temperature, January. (Based on MOHSST 3)

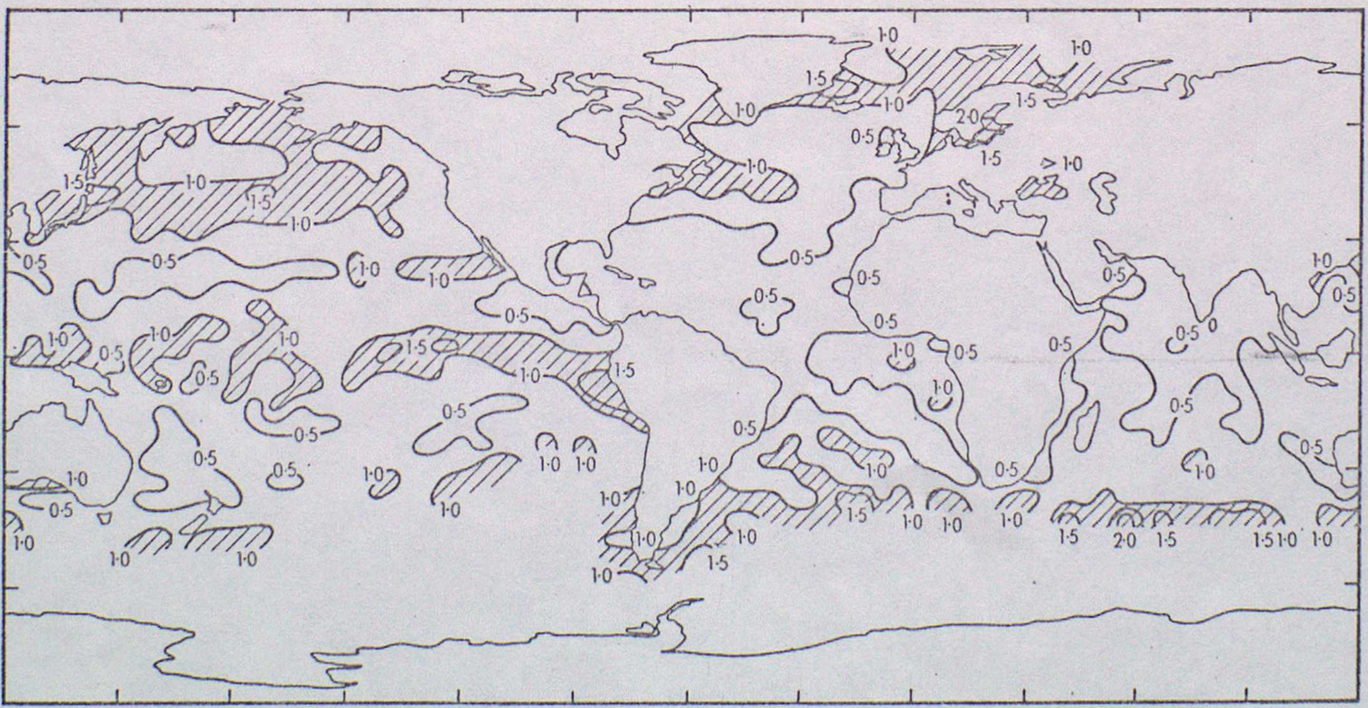
1·0
1·0
1·5
1·0
1·5
1·0
0·5
2·0
1·5
1·5
1·0
>1·0
1·5
1·0
1·5
1·0
0·5
0·5
1·0
1·0
0·5
0·5
1·0
0·5
0·5
0·5
1·0
0·5
1·0
0·5
1·0
1·0
0·5
1·5
1·0
1·5
1·0
0·5
0·5
0·5
0·5
0·5
0·5
0·5
1·0
1·0
1·0
1·0
0·5
1·0
0·5
0·5
1·0
0·5
1·0
0·5
1·0
1·0
1·0
1·0
1·0
1·0
1·0
1·5
1·0
1·0
1·0
1·5
2·0
1·5
1·5 1·0
1·0
1·0
1·0
1·0
1·0
1·0
1·5
1·0

Standard deviation of sea surface temperature, July. (Based on MOHSST 3)

FIG 4·12

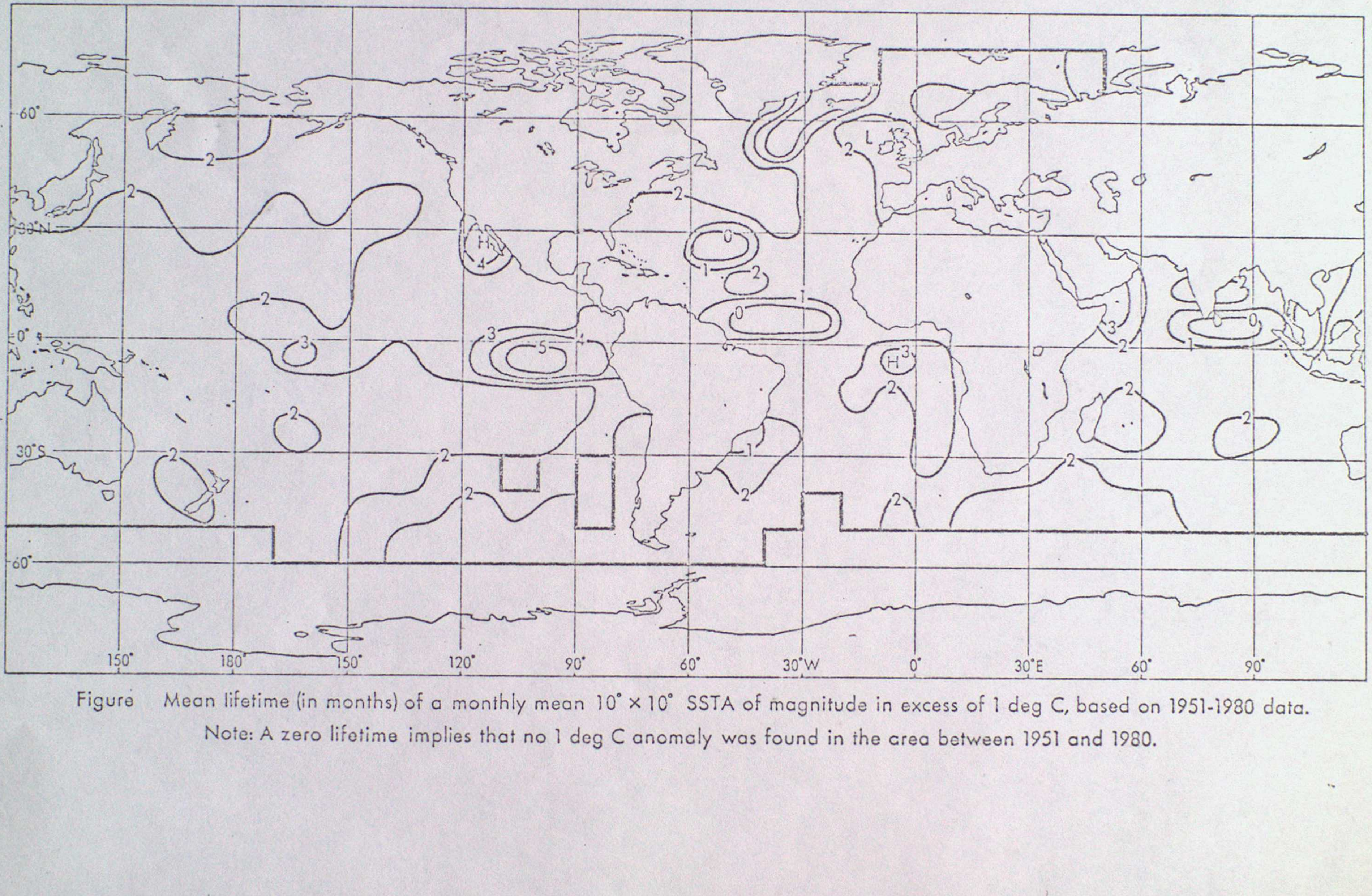
60°
30°N
0°
30°S
60°
150°
180°
150°
120°
90°
60°
30°W
0°
30°E
60°
90°
2
0
1
3
4
5
H
L

Figure Mean lifetime (in months) of a monthly mean 10° × 10° SSTA of magnitude in excess of 1 deg C, based on 1951-1980 data.

Note: A zero lifetime implies that no 1 deg C anomaly was found in the area between 1951 and 1980.

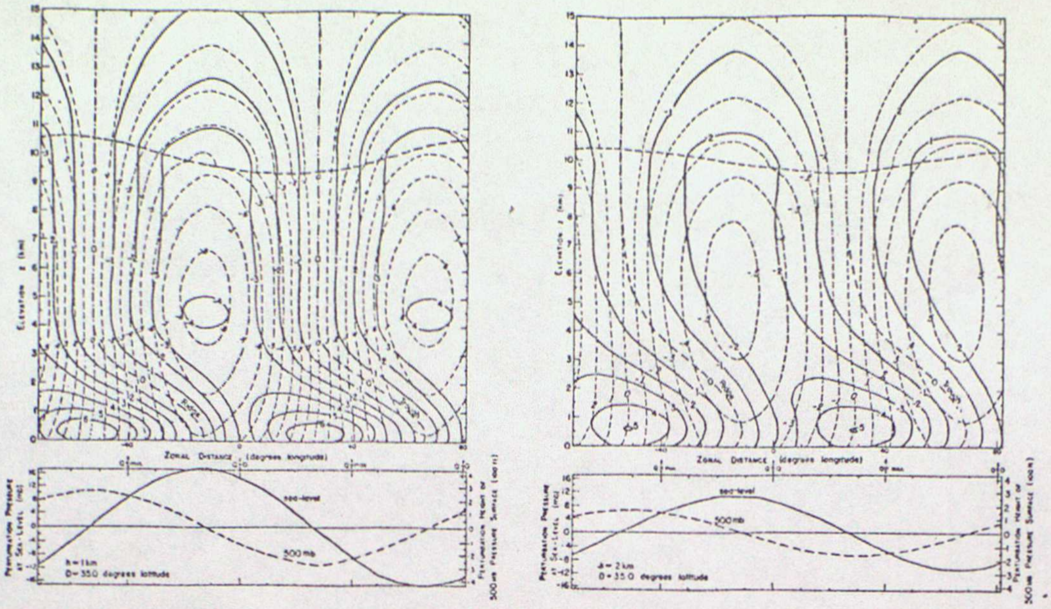

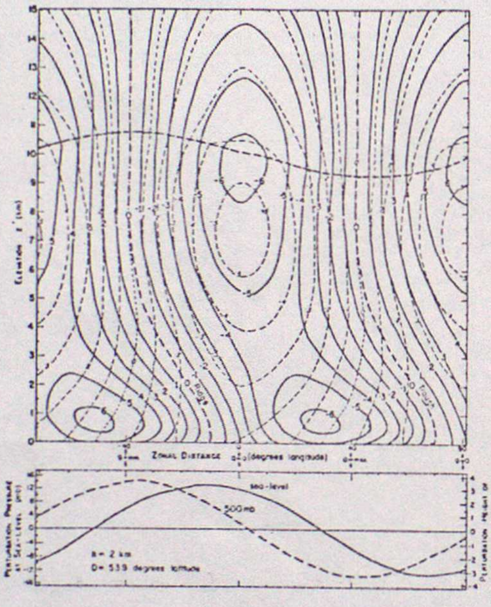

FIG 4·13

General baroclinic model with surface friction, at latitude of maximum heating and cooling. Stable stratosphere taken into account. Upper part : zonal section of perturbation meridional velocity v (solid lines) in m sec^{-1} and perturbation vertical velocity w (dashed lines) in cm sec^{-1}. Lower part : zonal profile of perturbation pressure at sea level (solid lines) and perturbation height of 500-mb pressure surface (dashed lines).

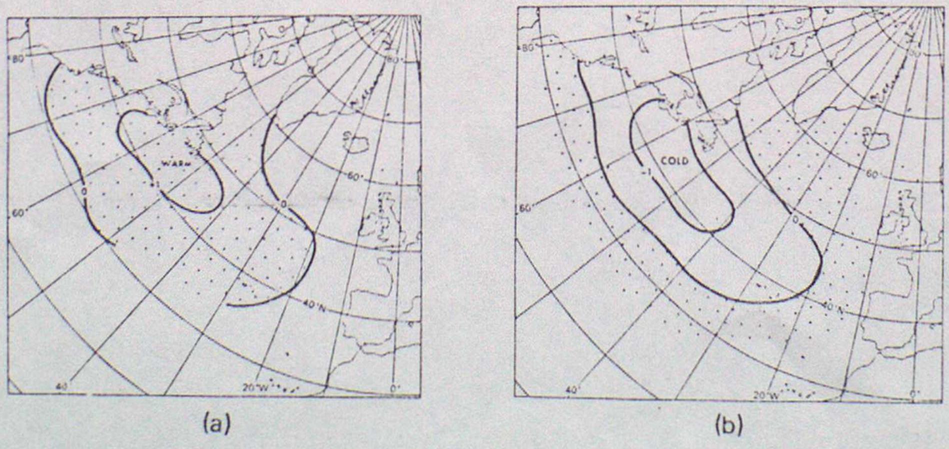

(a) (b)

FIG 4·14

Generalized sea surface temperature anomaly distributions (°C):
(*a*) Type here designated as 'warm sea' cases.
(*b*) Type here designated as 'cold sea' cases.

FIG 4·15a

Pressure anomalies (mb) averaged for the following months:

(*a*) Octobers, given 'warm sea' (fig. 10.6(*a*)) in September.

(*b*) Februarys, given 'warm sea' in January.

(*c*) Mays, given 'warm sea' in April.

(*d*) Julys, given 'warm sea' in June.

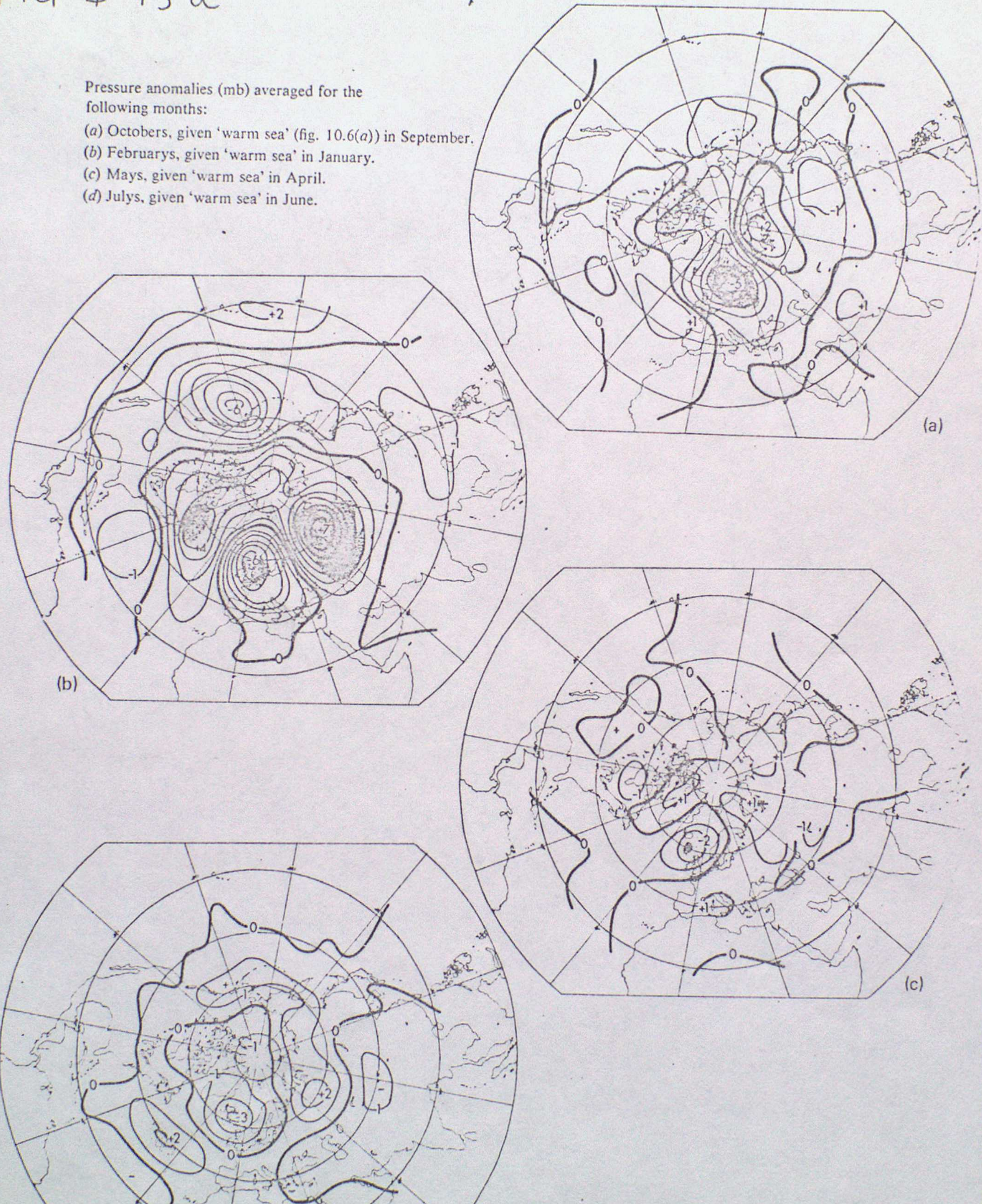

FIG 4.15 G

Pressure anomalies (mb) averaged for the following months:

(*a*) Octobers, given 'cold sea' (fig. 10.6(*b*)) in September.

(*b*) Februarys, given 'cold sea' in January.

(*c*) Mays, given 'cold sea' in April.

(*d*) Julys, given 'cold sea' in June.

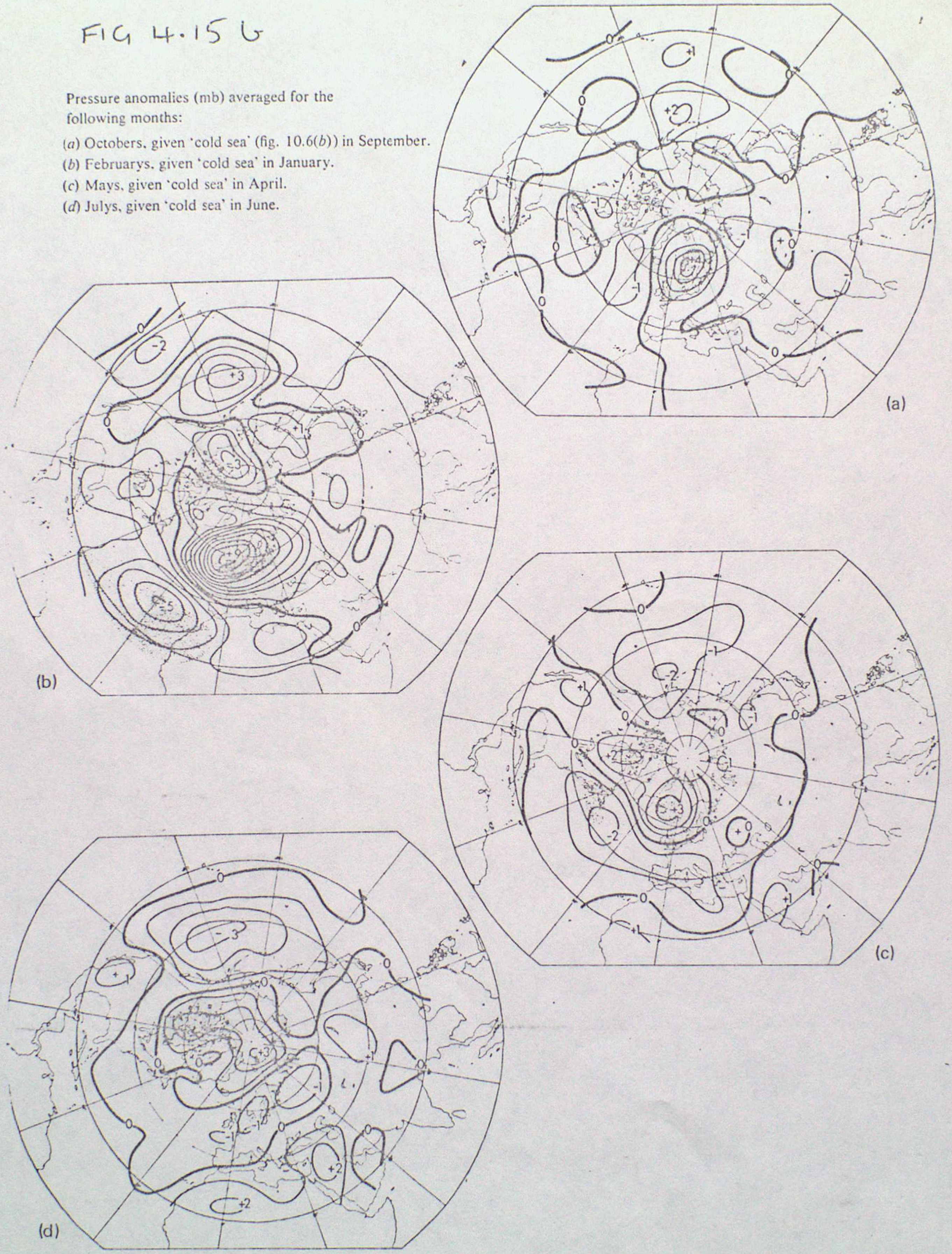
(a)
0
+1
+2
-1
+4
(b)
0
-2
+3
+1
-3
+9
-5
(c)
0
-1
-2
+1
+2
-3
(d)
0
-3
+1
+3
-1
+2

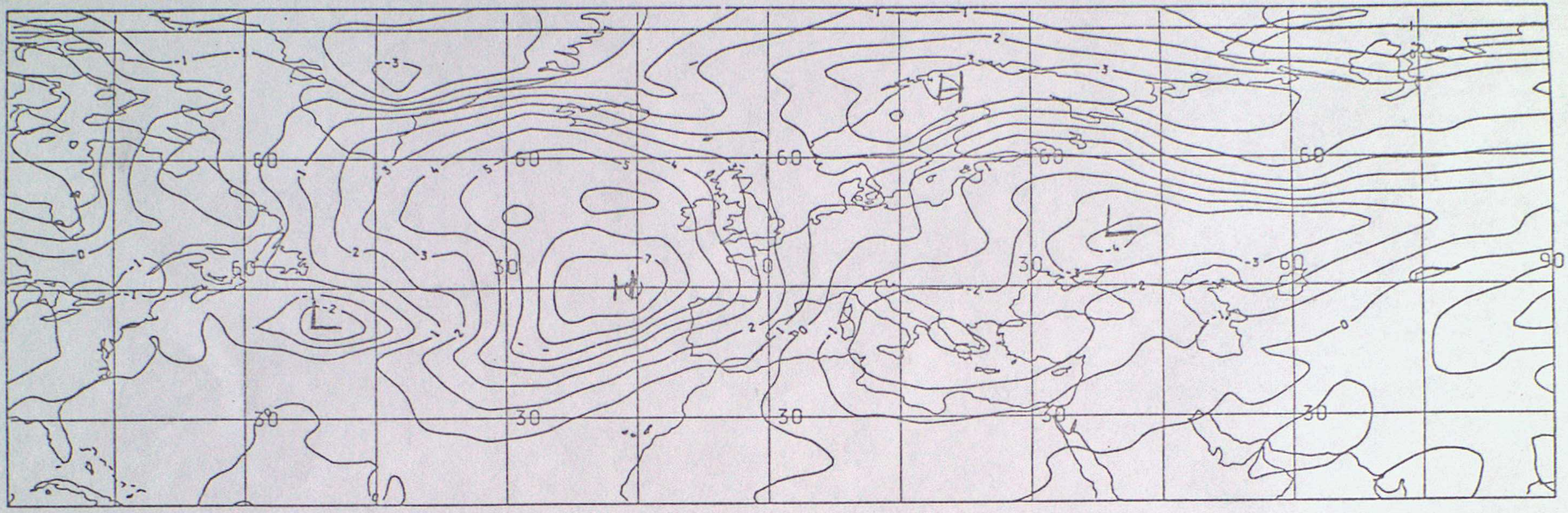
H
L
L
H
60
30
0
90

A 1000 MB

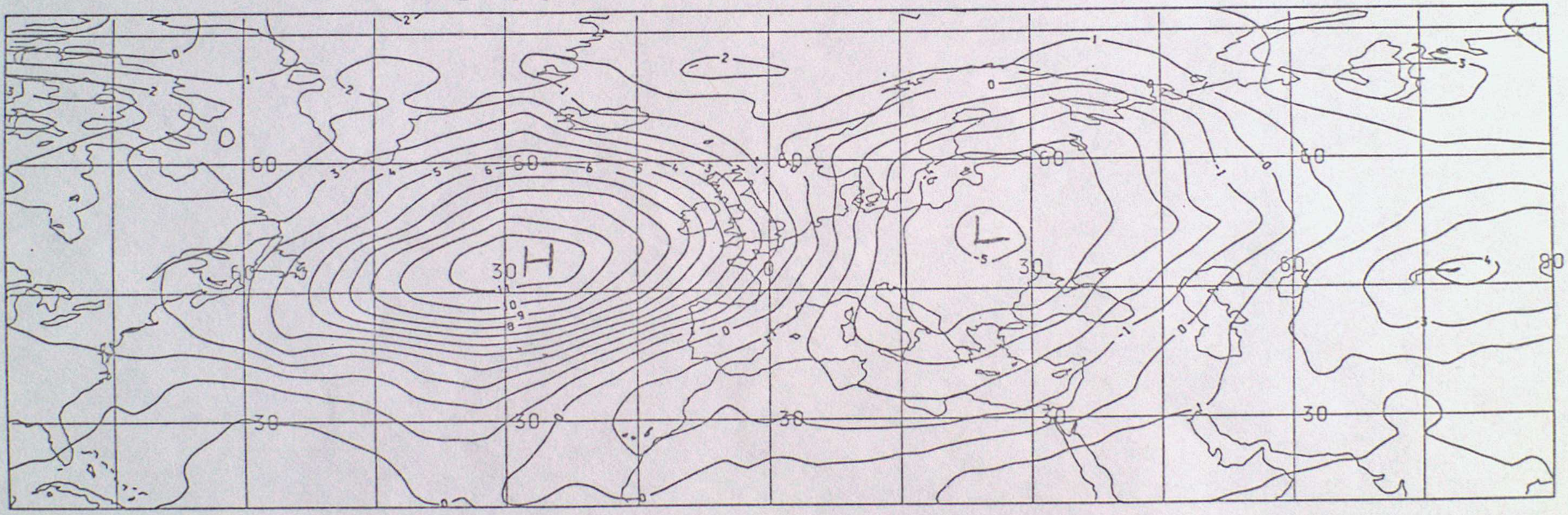

500 MB

FIG 4-16

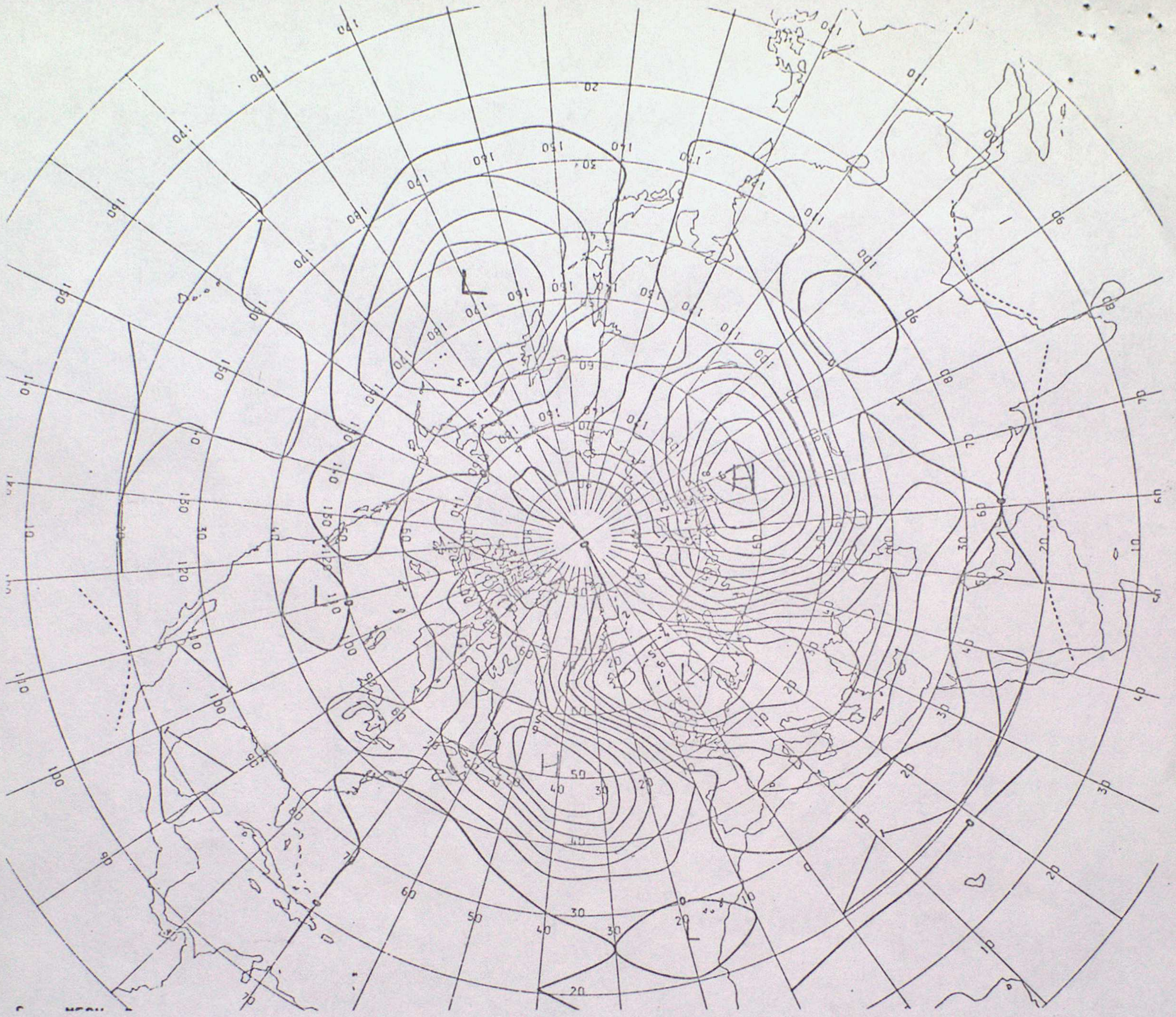
L
H
L
H
L
20
30
40
50
60

FIG 4·17 PMSL DIFFERENCE FOR (WARM-COLD) "RATCLIFFE REGION" SSTA - SAME MONTH, AVERAGED FOR NOV-FEB

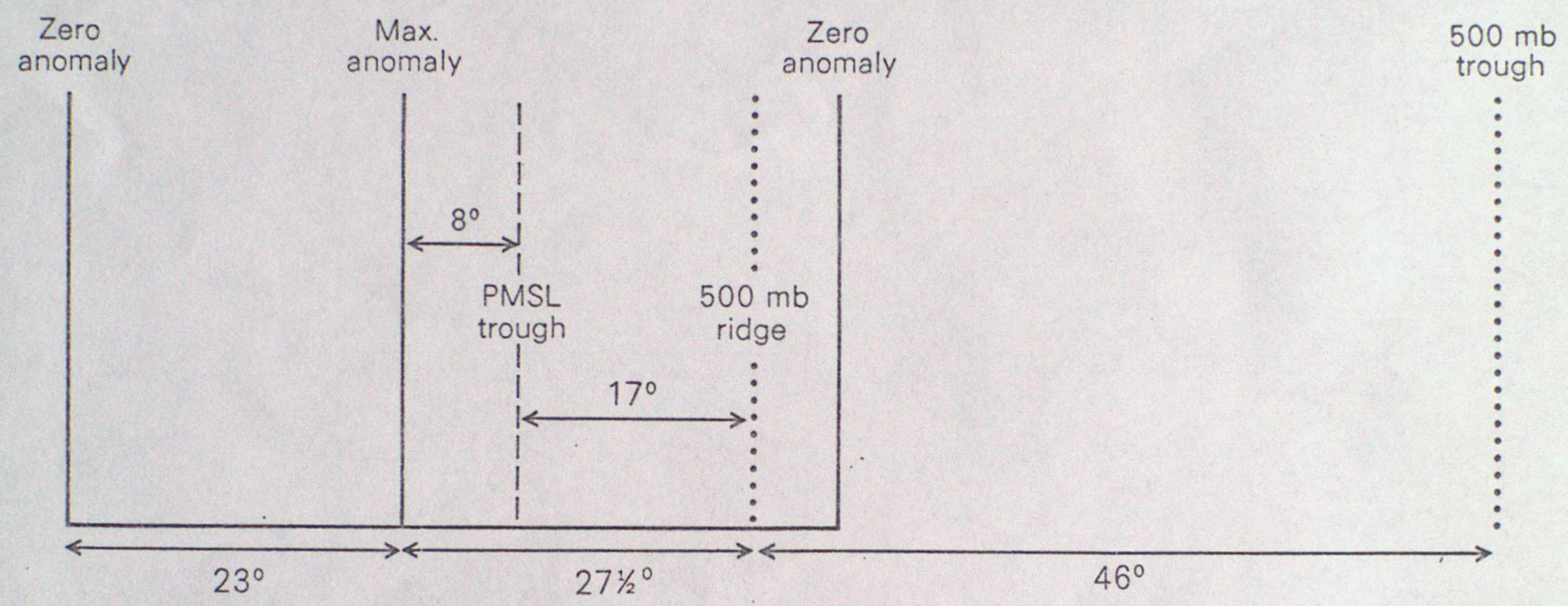
Zero anomaly
Max. anomaly
Zero anomaly
500 mb trough
8°
PMSL trough
500 mb ridge
17°
23°
27½°
46°

Fig. 4.18 Summarised effects of warm mid-latitude SST anomalies on PMSL and 500 mb height (from Rowntree 1984)

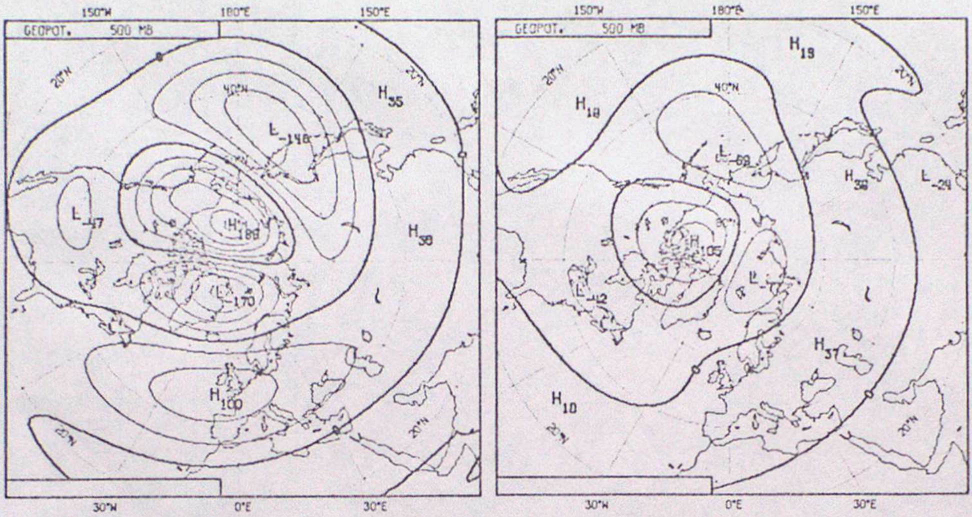
GEOPOT. 500 MB
150°W
180°E
150°E
120°W
90°W
60°W
30°W
0°E
30°E
120°E
90°E
60°E
20°N
40°N
L-148
H35
L-47
H189
H38
L-170
H100
H19
H18
L-69
H38
L-24
H105
L-12
H37
H10

15°N forcing

25°N forcing

FIG 4.19 500MB HEIGHT PERTURBATIONS

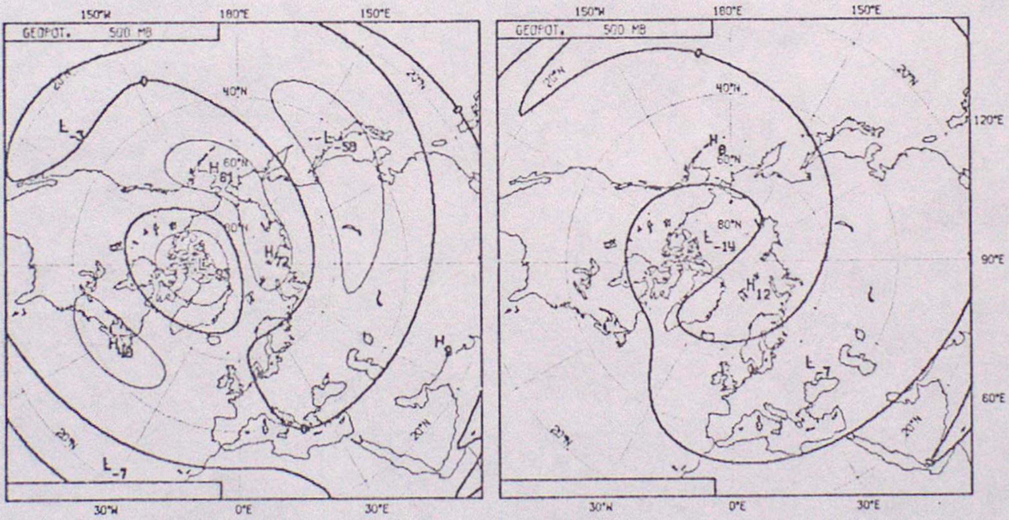
GEOPOT. 500 MB
150°W
180°E
150°E
120°W
90°W
60°W
30°W
0°E
30°E
120°E
90°E
60°E
20°N
40°N
60°N
80°N
L-3
L-58
H61
H72
L-93
H18
H9
L-7
H8
L-14
H12
L-7

5°N forcing

15°S forcing

500 mb height perturbations for heatings centred at 135 °E and various latitudes.

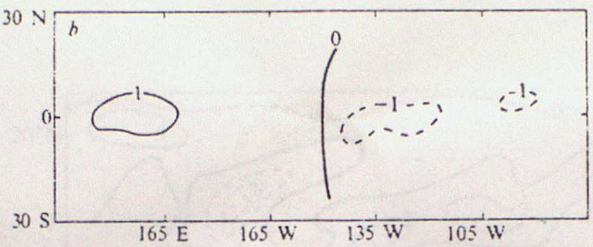

SST anomaly (K). *a*, Expt 1; *b*, expt 2 (having a maximum value of 1.3 K in the West Pacific).

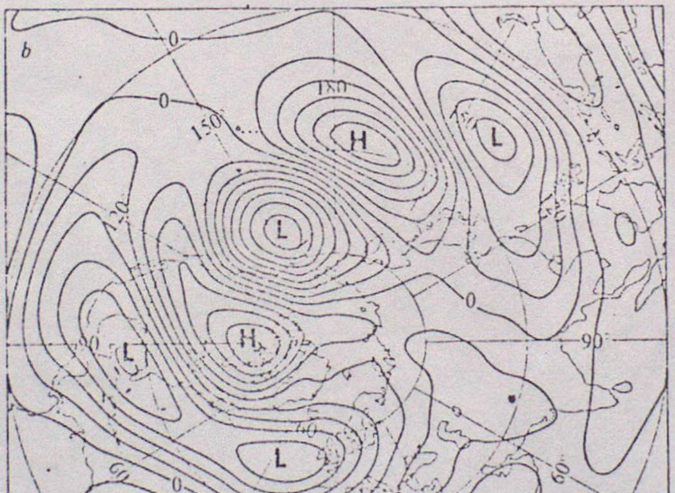
b
0
150
180
H
L
L
H
L
L
120
90
60
60
30 N
30 W
30 E
0

FIG 4·20 500-mbar streamfunction anomaly averaged over days 1–150. *a*, Expt 1; *b*, expt 2. Contour interval is $2\times10^6\ \mathrm{m^2s^{-1}}$.

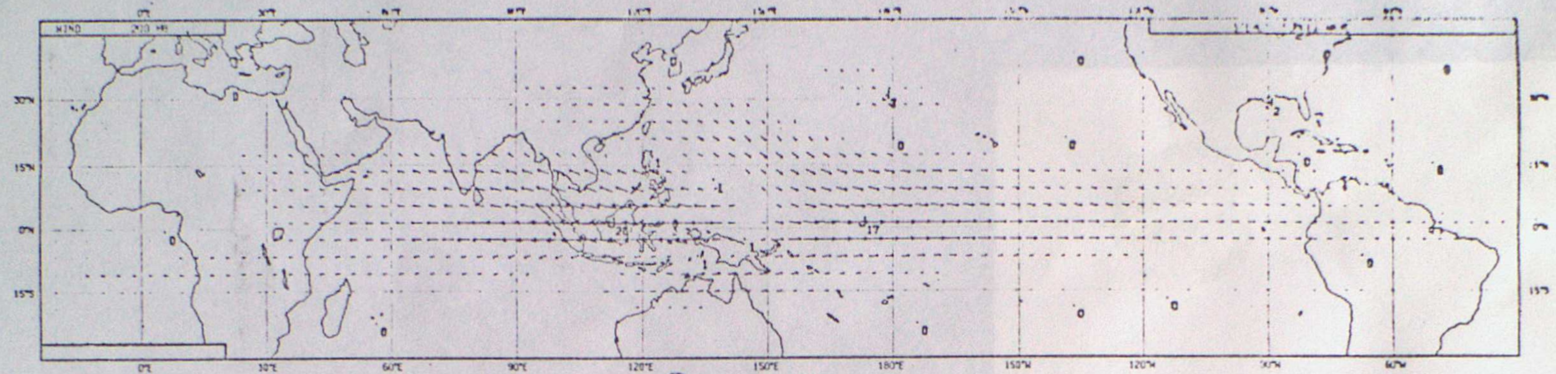
WIND
200 MB
30°N
15°N
0°N
15°S
0°E
30°E
60°E
90°E
120°E
150°E
180°E
150°W
120°W
90°W
60°W
17

200 MB

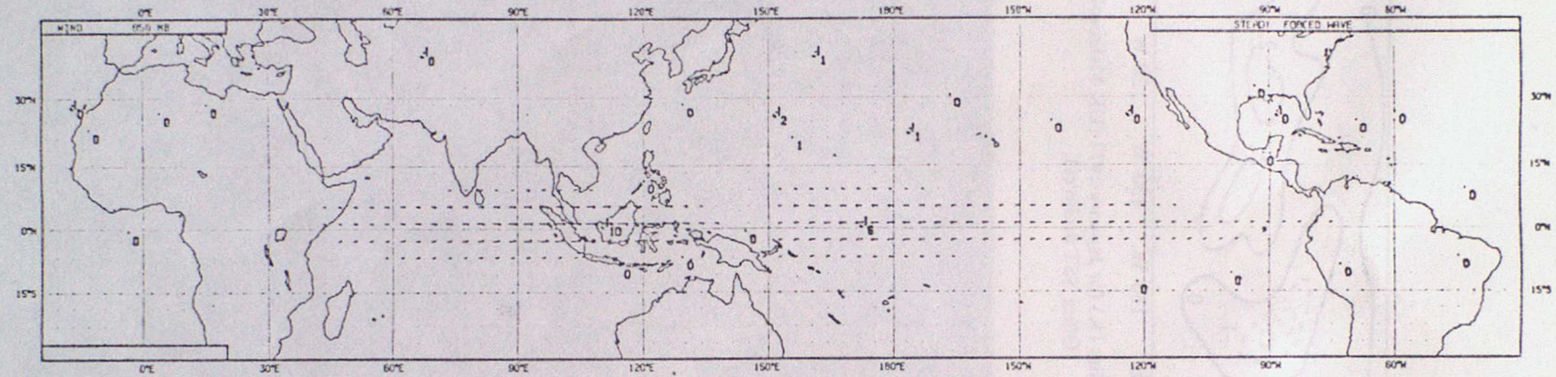
WIND
850 MB
STEADY FORCED WAVE
30°N
15°N
0°N
15°S
0°E
30°E
60°E
90°E
120°E
150°E
180°E
150°W
120°W
90°W
60°W
10

850 MB

FIG 4·21

Perturbation winds at 200 mb and 850 mb for a heating centred on the equator at 135 °E. Velocity maxima (in m s^{-1}) are marked. Other details are specified in the text

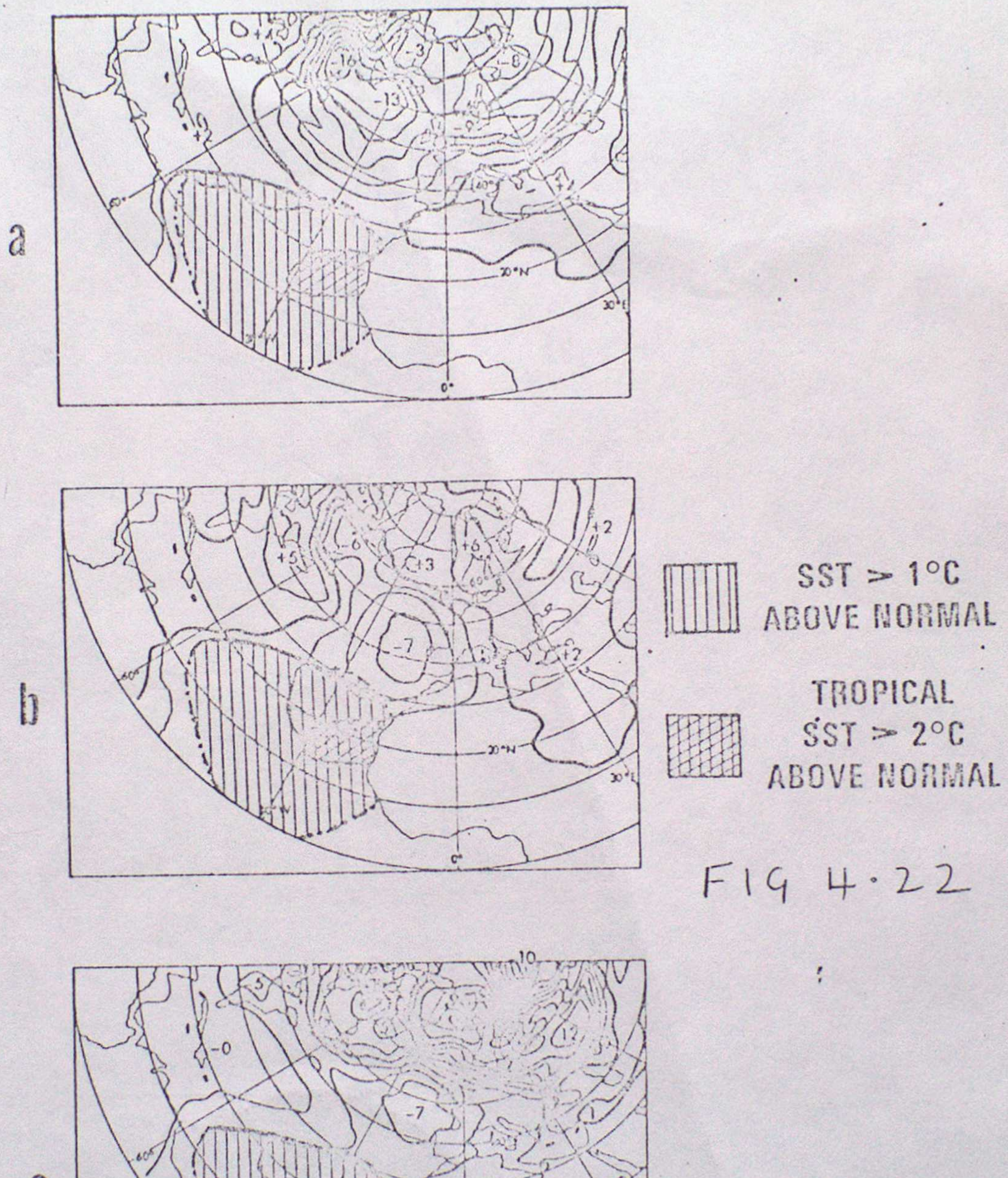
a
-16
-13
-3
-8
30°N
30°E
0°
b
+5
-6
+3
+6
+2
-7
30°N
30°E
0°
SST > 1°C ABOVE NORMAL
TROPICAL SST > 2°C ABOVE NORMAL
c
10
-0
-7
≤4
≤2
30°N
30°E
0°

FIG 4·22

Difference in mean surface pressure (mb) averaged over days 41–80 of model integrations between surface pressure obtained with tropical Atlantic warming and the control experiment without the warming. (a) experiment 1 using isothermal initial data, (b) experiment 2 using initial real data, and (c) experiment 3 also using initial real data. Both (b) and (c) use initial data for 29 December 1965. SST averages taken from US Naval Oceanographic Office data.

Decadal anomalies of Central England Temperature on days with pure "W" Lamb type,
SST for the Atlantic north of 35°N (with instrumental corrections as in (4)).

FIG 4·23

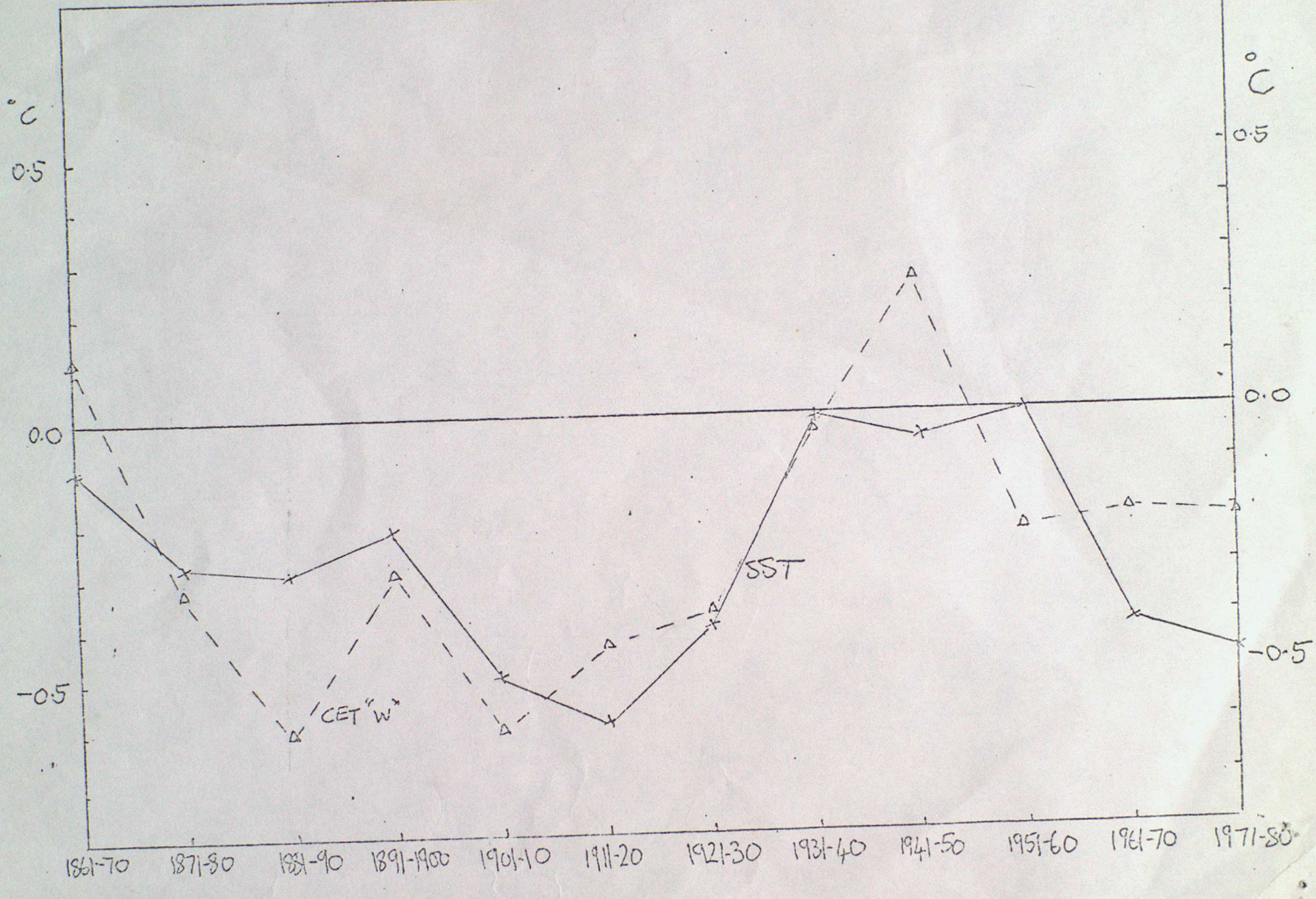

FOR LOAN by Met. Office Staff only

METEOROLOGICAL OFFICE
145729
- 7 MAY 1985
LIBRARY

RECURRING NON-SEASONAL CLIMATE VARIATIONS.

LECTURE 5 - PART I - QUASI-BIENNIAL OSCILLATION

C K FOLLAND AND D E PARKER

5.1 Introduction

A brief description is given of this curious lower-stratospheric phenomenon which was discovered almost simultaneously by Ebdon (of Met O 13) (1) and Reed (2) who both first published in 1960. The QBO is the only quasi-periodic process of reasonably regular behaviour known in the climate system whose time scale lies between the annual and ice-age time scales. (The next most regular process is the ENSO phenomenon discussed in Pt II). Although the links between QBO and surface climate are tenuous, (though often suggested), we justify its inclusion here:-

(a) to provide a background to the description of volcanic dust and climate in lecture 3; the QBO affects our ability to interpret and detect the effects of volcanic dust on stratospheric temperature and thus to unravel the physical properties of volcanic dust

(b) because of the possibility of a link with the ENSO events

5.2 Description

QBO shows up most prominantly as a quasi-biennial oscillation of wind direction, speed and temperature in the tropical lower stratosphere within 15° of the equator. Fig 5.1A shows the monthly mean 30 mb winds above Canton Island (central Pacific) 1954-1967, Gan (Central Indian Ocean) 1967-75, Singapore 1976-81 and Changi 1981 onwards. Corresponding 50 mb winds are shown in Fig 5.1B. The associated temperature changes between 50 mb, and 150 mb (where they have disappeared) are shown in Fig 5.2. It is possible to form composite series from such widely-separated stations because the QBO occurs on a global scale in the tropics with very little time-lag between different longitudes. The period of the oscillation is not constant: it varies from less than 2 years to about 3 years, and averages 2 years and 3 months. Periods close to either 2 or 3 years tend to be favoured, and there are also favoured seasons for reversal of the 50 mb or 30 mb wind directions (Parker 1976) (3). A downwards phase propagation of the oscillation occurs, so for example, changes in the 50 mb wind vector lag several months behind changes in the 30 mb wind vector (Fig 5.3).

The discovery of the tropical stratospheric QBO has been followed by widespread reports of quasi-biennial behaviour in local tropospheric climate and circulation parameters. Parthasarathy and Mooley (1978) (4) found a quasi-biennial oscillation in Indian Monsoon rainfall, but this was not strong and regular enough to be used for forecasting. Ebdon (1975) (5) documented differences in the mean Northern hemisphere midlatitude surface pressure and 500 mb geopotential patterns, and in zonal winds aloft that varied, according to the phase of the tropical QBO. Figure 5.4 illustrates the mean sea level pressure anomaly in the extratropical N Hemisphere for Julys with a westerly tropical QBO wind mode. The anticyclonic anomaly near the British Isles was found to be statistically significant at about the 5% level. In addition, not only Ebdon (1975) but also Angell and

ORGS UKMO
National Meteorological Library
FitzRoy Road, Exeter, Devon. EX1 3PB
3 8078 0007 8113 0

Korshover (1977) (6) observed that the circumpolar upper-tropospheric vortex was smaller during the westerly phase of the QBO particularly in winter with an associated increase of tropospheric temperature of several tenths °C in midlatitudes. Consequent possible associations with, for example, summer temperature and sunshine in the United Kingdom, were noted by Ebdon and also by Folland (1977) (7). Holton and Tan (1980) Fig 5.5 (8) have demonstrated that there may be a 50 mb and a 1000 mb quasi-biennial oscillation in the geopotential and temperature of the northern polar regions. The two atmospheric levels are in phase but the effect is weaker at 1000 mb. It must be emphasised that observations of QBO outside the tropical stratosphere have only been associated statistically with the tropical stratospheric QBO at this stage. Physical associations have not been established.

The physical causes of the tropical stratospheric QBO were studied in a quite convincing paper by Holton and Lindzen (9) but since then evidence has mounted which casts serious doubt on their hypothesis and currently much research is going on. So we will not describe the theories here.

The mechanisms by which the tropical lower stratospheric quasi-biennial oscillation might affect the rest of the atmosphere are completely uncertain. It is just possible that the associated temperature changes near the tropical tropopause (Fig 5.3) may affect the strength of tropical convection where it is most powerful eg the tropical W Pacific, and thereby influence the Hadley or Walker cells and subsequently the rest of the circulation. It is known that tropospheric air almost certainly regularly enters the stratosphere in this region (10).

5.3 Angular momentum considerations

It is worth mentioning that in N Hemisphere summer the difference in the axial angular momentum of the N Hemisphere atmosphere contributed to by a westerly phase of QBO compared to an easterly phase may sometimes be 5%-10% of the total N Hemisphere axial angular momentum (allowing for phase lags of the QBO with height). In any case the development of a westerly phase of QBO represents an increase in the axial momentum of the atmosphere where it is already by definition a maximum. So small, compensating changes in atmospheric circulation that preserve axial angular momentum should occur somewhere else (in either hemisphere). Note that this momentum cannot be transmitted to and temporarily stored or released in earth's rotation in a direct way though this could occur indirectly through a tropospheric circulation change.

REFERENCES

1. EBDON, R A (1960) Notes on the wind flow at 50 mb in tropical and sub-tropical regions in January 1957 and January 1958. Q J Roy Met Soc, 86, pp 540-42.

2. REED, R J (1960) The circulation of the stratosphere. Paper presented at the 4th Ann meeting of the American Met Soc, Boston, Mass.

3. PARKER, B N (1976) The quasi-biennial oscillation in tropical stratospheric winds: a method of forecasting. Meteorol Mag, 105, 134-143.

4. PARTHASARATHY, B AND MOOLEY, D A (1978) Some features of a long homogeneous series of Indian summer monsoon rainfall. Mon Weather Rev, 106, 771-781.

5. EBDON, R A (1975) The quasi-biennial oscillation and its association with tropospheric circulation patterns. Meteorol Mag, 104, 282-297.

6. ANGELL, J K AND KORSHOVER, J (1977) Variation in size and location of the 300 mb north circumpolar vortex between 1963 and 1975. Mon Weather Rev, 105, 19-25.

7. FOLLAND, C K (1977) Recent work on some quasi-cyclic fluctuations of meteorological parameters affecting British climate. Weather, 32, pp 336-342.

8. HOLTON, J R AND TAN, H-C (1980) The influence of the equatorial quasi-biennial oscillation on the global circulation at 50 mb. J Atm Sci, 37, pp 2200-2208.

9. HOLTON, J R AND LINDZEN, R S (1972) An updated theory for the quasi-biennial cycle of the tropical stratosphere. J Atm Sci, 29, pp 1076-1080.

10. NEWELL, R E AND GOULD-STEWART, S. A stratospheric fountain? J Atm Sci, 38, pp 2789-2796.

ADVANCED LECTURE NO 5 PART II

THE EL NINO - SOUTHERN OSCILLATION (ENSO)

5.2.1 Introduction

The term El Nino (The "Christ Child") was originally given to a weak warm coastal current which commences around Christmas and flows southwards along the coast of Ecuador and Peru during each Southern Hemisphere summer. Every few years the near-coastal warming associated with the current becomes particularly intense (4-7°C); during the following 12 months the entire Central and Eastern tropical Pacific Ocean warms typically by 1-3°C. In 1982-83, the warming in the open ocean near 130°W, 5°S, caused SST to reach almost 6°C above normal in December 1982,an amount which can usefully be compared with the annual cycle of SST for the world shown in Lecture 4, Fig 4.9

Fig 5.6 shows the observed SST in the Pacific and Fig 5.7 the observed sea surface temperature anomaly (SSTA) during the N Hemisphere winter of 1982-83 and near the most intense phase of one of these tropical Pacific warmings (Quiroz) (1). The term 'El Nino' is now generally used by climatologists to describe the widespread ocean warming and not the local coastal warming. Fig 2.5, Lecture 2, shows mean January SST for 1951-80; it can be seen that the normal east-west gradient of tropical Pacific SST has not only nearly disappeared in Fig 5.6 but that the absolute maximum SST in the period between Dec 1982-Feb 1983 was placed about 60°E of its normal position. The 1982-83 El Nino will be discussed below; Quiroz gives a very good observational account.

High surface temperatures are only one aspect of the anomalous behaviour of the Tropical Pacific Ocean during an El Nino: the entire thermal and dynamic structure of the upper ocean is different from normal (Gill and Rasmusson 1983) (2) (see later). The presence of such a large anomalous heat source at the lower boundary of the tropical atmosphere can be expected to affect the atmospheric general circulation and it has become clear over the last 20 years that a near global scale PMSL sea-saw known for half a century as the Southern Oscillation (SO) is linked to El Nino.

The possible existence of a large-scale interannual PMSL fluctuation was first hinted at by a Swede, Hildebrandsson, in 1897 who found an out-of-phase relationship between PMSL at Sydney, Australia and Buenos Aires, Argentina. Lockyer and Lockyer uncovered the worldwide scale of the PMSL fluctuation in 1902-6 but Walker and Bliss (1923-37) provided the first detailed analyses of the companion temperature and rainfall fluctuations and were the first to name the phenomenon the "Southern Oscillation". See Rasmusson and Carpenter (RC) (1982) (3) for historical detail and references. Fig 5.8 shows the correlation between annual PMSL anomalies at Easter Island and many other stations distributed worldwide produced by Berlage (1959) (4), confirmed several times since Berlage's paper. Djakarta, Java and Easter Island are 140° of longitude (15,000 km) apart and all investigations agree on a negative correlation of -0.9 or so between their annual or even seasonal mean PMSL values. Fig 5.9 shows the average January PMSL in the Pacific (1961-76) and the position of some of the "key" stations that will be used in the description. The SO fluctuations are usually monitored by an SO index (SOI) which has been defined in many ways; Fig 5.8 indicates that the simplest and best index might be simultaneous values of (Easter Island - Djakarta) PMSL. Returning to relationships between SO and Argentinian climate, Fig 5.10 shows superimposed time-series of the level of the great Parana river and an SO index about a century AGO (correlation 0.56) (6). However due to better data quality and availability Tahiti and Darwin PMSL have often, if less satisfactorily, been used to provide an SO index. Fig 5.11 shows the normalised pressure difference between Tahiti and Darwin updated from Parker (1983) (5) and Fig 5.12 shows a time series of seasonal SSTA for 1856-1984 (from 1951-60 average) calculated for the Tropical E Pacific (170°E - S American coast, 20°N-20°S) an area of about 45 x 10^6 km^2, taken from Folland et al (1984) (7). The correlation between 3 month seasonal mean Tropical E Pacific SSTA and SO indices between 1935-80 is about -0.65 ie warm SSTA is associated with a negative SO index. The tropical E Pacific SSTA variations are (in the main) part of a worldwide fluctuation of SSTA. This is most readily shown in Fig 5.13 which shows the second (correlation matrix) eigenvector (EOF2) of worldwide SSTA (from (6)) calculated for each season and for available 10° x 10° areas between 1901-80. The time series of the amplitude of EOF2 is shown in Fig 5.14 together with that of the tropical E Pacific SSTA variations; the two time series of EOF2 are strongly correlated. EOF2 does not allow for systematic developments in the shape of the worldwide SSTA patterns which might occur as "ENSO events" develop, or real differences in pattern between events. Despite these limitations a strong, consistent, warming of the Indian Ocean and the NE Pacific and a similar tendency for simultaneous negative SSTA in the NW Paqcific when the tropical C and E Pacific are warm is apparent. (Values of the terms of EOF2 of magnitude about 40 or over (Fig 5.13) reflect a reasonably consistent relationship with tropical E Pacific SSTA). Fig 5.15 shows a spectrum of seasonal tropical E and W Pacific SSTA and marine air temperature for 1861-1980 from (6) and shows the time scales of variation. The E Pacific (basically El Nino variations) occupy the 2.5-16 year time scales. The W Pacific spectrum is distinctly different, being much "whiter".

5.2.2 Global temperature variations associated with El Nino

5.2.2.1 SSTA

Newman (1984) (8) has carried out a detailed analysis of the typical worldwide SSTA variations associated with the various phases of El Nino over about the last century. The years quoted below are usually the first of the consecutive years that were affected by El Nino (the first is called year (0)). The 17 El Nino events identified were: 1880, 1896, 1899, 1902, 1905, 1918, 1930, 1939, 1940, 1941, 1951, 1957, 1965, 19659, 1972, 1976 and 1979. 1982 was certainly an El Nino year but data was not available for Newman's study. 1877-78 was an El Nino year but with too few data for analysis. Composite monthly global SSTA charts are shown for April, August and December of year (0) and March of year (+1) (Fig 5.16(a)-(d)).

The early stages in the development of an El Nino, during which the warming is confined to S American coastal waters, is not well represented because the 5° x 5° area resolution used was too coarse. By April of year 0, the S Pacific near the western coast of South America as far south as 35°S shows a distinct warming. A tongue of positive SSTA extends westwards from the South American coast along the Equator, reaching 130°W in May and 170°E by July. The SSTA pattern intensifies, so by September a large proportion of the Tropical Pacific is warmer than normal and by up to 2°C in the east. In December the warming is at its peak with maximum mean SSTA of 2°C to 3°C. In year (1) SSTA decline. Both Indian and Tropical Atlantic Oceans warm during El Nino, starting in late summer of year (0). By March of year (+1) much of the Atlantic from 30°N to 30°S is warmer than normal by between .2° and .5°C. The Indian Ocean exhibits maximum mean SSTA of up to .6°C in January of year (+1).

By contrast, in April of year (0) an area in the central N Pacific, centred near 30°N, is weakly cool; then the negative SSTA spread northwards and strengthen, giving mean anomalies of −.8°C in some areas near 40°N between July and October. From November of year (0) to March of year (+1) negative SSTA persist, but are generally weaker. In the North East extratropical Pacific an area of anomalous warmth spreads northwards near the North American coast in October. This warm area persists until after March of year (+1). From October to December of year (0), the north east Atlantic, polewards of 35°N, is weakly cool with a suggestion of cool SSTA south of 40°S, common to much of the southern ocean. The data is too sparse to be certain, however.

RC used SSTA measured between 1953 and 1974 along 6 ship routes in the area 20°N to 20°S, 70°W to the dateline, to investigate the growth and movement of tropical Pacific SSTA during El Nino. The most common time scales of SSTA fluctuations associated with El Nino (in the area and for the period defined above) were found to be between 36 and 43 months. Cross spectral analysis of SST data at different longitudes indicated that the large scale positive SSTA which initially appear off the coast of Peru about December (eg at Puerto Chichama see Fig 5.9) spread westward along the Equator, reaching 170°W in 3-6 months. They also noted that SSTA appeared to modestly increase almost simultaneously near the equator at about 170°W. The average westward propagation of SSTA has a speed of of .5-1.0 m s^{-1}. RC also noted a warming of the ocean west of Chile in the year (-1) preceding El Nino in latitudes 30-35°S.

El Nino's vary considerably in character and in the time intervals between them (eg 3 years between 1969 to 1972, but nine years from 1942-51). This variability may prove crucial to our understanding. For example: the Tropical Pacific west of the dateline was markedly warmer in 1976 than 1972; in the 1982 event the Tropical E Pacific warmed before the S American coast, which warmed most at the *end* of the ENSO event, in April-June 1983. The Tropical E Pacific remained warm well into autumn 1983, ie year (+1), and widespread warming of the Indian Ocean exceeded 1.5°C. In 1976, the warming of the Indian Ocean area was weak. The years between 1972 and 1982 during which there were 4 El Ninos (3 of them strong) contrasts with the periods 1942-50 and 1879-1887 when there were none while between 1907 and 1938 El Nino's were few or very weak (Fig 5.12).

5.2.2.2 Atmospheric Temperature Variations

Pan and Oort (1983) (9) have given a zonal mean latitude height cross section for northern winter of mean temperature differences between three pairs of years having warm and cool East Pacific SST respectively (Fig 5.17). The tropical troposphere as far as 45°N and S warmed by upto

1°C at 400 mb, presumably due to increased moist convection in the tropics. Note also the cooling at middle and high latitudes of about -0.5°C in the Northern Hemisphere, which matches the underlying SST changes fairly well.

Pan and Oort also showed that specific humidity rose where air temperature rose and also, fell slightly in high latitudes. It is interesting that a tropical forcing (warming)from below has warmed the global troposphere as a whole but that the atmospheric circulation has changed so as to provide a weak cooling in high latitudes. This is rather unexpected, perhaps.

5.2.3 Atmosphere Variations

5.2.3.1 General Description

There is now a considerable literature on aspects of the general circulation associated with ENSO or suspected to have a connection with it: RC and Wyrtki (1975) (10) have both shown that ENSO is associated with variations in the Pacific trade wind circulations and the latter author, sea level fluctuations in the Pacific. Chen (1982) (11) and Horel and Wallace (1981) (12) have indicated links with the Northern Hemisphere mid-latitude circulations; van Loon et al (1981) report associations with the stratospheric circulation and Angell (1981) reports associations with ozone over North America and water vapour content of the low stratosphere; Keeling and Bacastow (1981) note a link with tropospheric CO_2 content. ENSO has been proposed as a long range forecasting trool for the Indian monsoon by Shukla and Paolino (1983) and has been used to help make long range forecasts in the USA and New Zealand. Tropical Pacific SST variations (now defined separately in the Central and East Pacific) have recently been introduced, usefully, as a factor in a statistical long range forecasting technique used in Met O 13 (Maryon and Storey) (1985). Newman (1984) gives details of unnumbered references.

5.2.3.2 Tropical Atmosphere Variations

The tropical atmosphere is perturbed during ENSO in a complex way as indicated by RC and other authors. In the winter and summer (S Hemisphere) preceeding El Nino, the south east trade winds between 120°N and the dateline are usually abnormally strong giving wind stresses over the tropical S Pacific 50-80% above normal. Relaxation of this stress to below normal levels in the tropical W Pacific in the next summer is followed by the start of El Nino - sometimes the wind stress is reversed ie the winds become westerly. The reason for the weakening is not known, though wind stress is usually less in summer in this region. During year (0) of El Nino the easterly component of wind stress reaches a minimum but increases once more later in year (0). By contrast, near the equator, between 90°W and about 130°W, the E to SE trades increase in strength to reach a peak during year (0).

The spatial distribution of surface wind anomalies reflects changes in the positions of the Inter-Tropical Convergence Zone (ITCZ) and the South Pacific Convergence Zone (SPCZ) (see Lecture 2). The convergence zones are important in determining the areas of active convection and hence areas of latent heating in the middle and upper troposphere and the rain falling on the "desert" islands of the equatorial Pacific (Lecture 2).

Changes in the trade wind circulation also reflect changes in the intensity of the Indonesian Low and Easter Island High, which as described above, are often used to indicate the phase of the SO.

Figs 5.18(a)-(c) show the anomalous mean tropical Pacific surface winds in an El Nino composite study carried out by RC here shown for August-October (-1), March-May (0) and December (0) - February (+1). In autumn of year (-1) surface wind anomalies are generally small, except to the north-east of Australia, where anomalous northwesterlies tend to occur and SPCZ is displaced to the southwest of its normal position. The South Pacific High then weakens but the Indonesian Low changes little. Wind anomalies increase from November (-1) to March (0) with a strong anomalous westerly component (not always giving abso lute westerlies) developing north of the Equator and south of 10°S from 170°E to 170°W, reflecting a reduction in strength of the south-east trades. The Indonesian Low fills while the Easter Island High continues to decline. From March to May (0) the same trends in the pressure field continue. Between 110°W and 170°E, ITCZ is now displaced south of its normal position with anomalous northerlies on its northern side. The anomalous westerly component just south of the Equator now reaches 160°W and there is a strengthening of the south-south east trades in the latitude band 30°S to 10°S from East of Australia to the dateline.

During the remainder of year (0) the anomalous features noted above intensify. In particular the ITCZ continues to be placed south of its climatological position and the SPCZ now becomes located north east of its usual location, reducing the size of the equatorial dry zone (centred near the dateline) between them. During August-October of year (0) the equatorial westerly anomalies are at their strongest exceeding 2 ms^{-1} over much of the Tropical Pacific west of 160°W and an anomalous surface wind convergence is centred near 150°W close to the equator. The Pacific High begins to build again about July followed by a deepening of the Indonesian Low about November. As the El Nino year progresses, the surface wind convergence maximum moves eastwards to near 130°W, the westerly anomaly decreases and the south east trades strengthen between 140-180°W ie west of the wind convergence.

Pan and Oort (9) correlated SST in a key area near 2.5°S, 130°W (assumed to represent the entire Tropical E Pacific, a reasonable assumption in view of SSTA analyses presented in Section 5.2.2.1) with global fields of 850 mb and 200 mb wind components and 500 mb vertical velocity.

Warm SST (El Nino) is associated with:-

i. Anomalous ascent of air over Central and much of the Eastern Equatorial Pacific, with anomalous descent of air east of 120°W, over the western Pacific between 110°E and 150°E, and over the subtropics.

ii. An increase in the 200 mb subtropical westerlies in both hemispheres near 25° latitude, with anomalous 200 mb easterlies over the Equatorial Pacific, roughly west of the main SSTA maximum.

iii. A weakening of surface and 200 mb westerlies near 60°N.

Pan and Oort note that these observations are consistent with Bjerknes' pioneering (1969) explanation of ENSO; Bjerknes suggested (13) that the normal nearly east-west equatorial Pacific Walker cell, in which air ascends in the convectively active area around Indonesia and descends over the Eastern Pacific near 90°W, is weakened during El Nino. Fig 5.19 shows this cell in more detail (from (5)). See Lecture 2 for "Walker" cells.

The warm ocean causes the Hadley cell to intensify, leading to stronger 200 mb subtropical jets. In Section 5.2.2.1 it was noted that all three tropical oceans warm during El Ninos, which is consistent with the intensification of subtropical jets at all longitudes. A decrease in the westerlies at 60°N is seen by Pan and Oort as evidence for a stronger than normal Northern Hemisphere Ferrel cell.

Selkirk (1984) (14) has provided an up-to-date analysis of the 200 mb flow associated with El Nino and usefully discusses the fluctuations in the light of predictions made by linear models eg that of Simmons (Fig 4.19) which shows how the 200 mb and lower tropospheric winds might respond to an anomalous (here C or E Pacific) heat source.

5.2.3.3 Extra Tropical Relationships with El Nino Events

Many authors have found that the El Nino is associated with changes in extratropical circulations, though teleconnections are less well defined than in the tropics.

Chen (1982) correlated seasonal values of the Tahiti-Darwin SOI with Northern Hemisphere 700 mb geopotential height between 1950 and 1979. He also carried out a composite analysis of the 700 mb data stratified according to SOI. The simultaneous correlations are shown in Figure 9. The winter pattern is quite similar to the 'Pacific North America (PNA)' teleconnection pattern found by Horel and Wallace (Fig 5.21) with three centres of response situated at 40°N, 145°W, (high positive correlation), Canada near 125°W (large negative correlation) and near Florida extending towards Spain (high positive correlation). Correlations between the height field and SOI of later seasons drop sharply and also as the lag of SOI behind the 700 mb fields increases. By contrast, correlations reach a maximum when SOI leads the 700 mb fields by one or two seasons, the response pattern staying broadly similar. However, only in winter with SOI leading the 700 mb data by one or two seasons is statistical significance at the 95% level unequivicably obtained.

The composite analyses of Chen (1982) enable non-linearity in the Northern Hemisphere 700 mb atmospheric response to variations in SOI to be studied. Chen finds that 700 mb height anomalies over the Atlantic are more pronounced with high SOI (low E Pacific SST) (Fig 5.20(a), (b)).

5.2.3.3 Rainfall Variations

Equatorial rainfall anomalies are an important aspect of El Nino events because of their obvious implications for Pacific 'weather' and because they indicate the position and anomalous intensity of convective activity associated with El Nino. Figure 5.22 shows annual rainfall at several Pacific Islands near the dateline; there are very large increases during El Nino events. These local changes may be put in a global context using satellite data as reported by Newman (1984). Figure 5.23 shows the percentage cover of cloud tops with radiative temperatures less than 235K on a 5° x 5° space scale for some recent northern hemisphere spring and winter seasons. This index is thought to give a good measure of convective activity. The data is not completely homogeneous in time but is probably spatially reasonably homogeneous. The relative minima in convection over the East Pacific are the result of the descending branch of the Walker cell. However by March-May 1983 highly anomalous heavy rainfall was reported from the Galapagos Islands which turned green as a result; high SSTA persisted and even strengthened again in this region after the earlier mid summer peak around December/January 1982-3. Wright (1977) (15) is also a useful reference for a number of observational aspects of SO.

5.2.4 AGCM Experiments

Is it physically reasonable that the global atmosphere could respond to El Nino? If so, how? Several experiments using AGCM's have been carried out using El Nino SST forcing; their results broadly support the idea of a widespread tropical response like that observed but give much more variable results in the extratropics (most of the experiments have concentrated on N Hemisphere teleconnections). The first N Hemisphere winter AGCM experiment, carried out by Rowntree (1972), indicated, like most subsequent experiments that a pair of low-level low pressure anomalies are forced on either side of the equator near the maximum tropical SSTA (probably nearer the local maximum absolute SST) with upper level anticyclones overlying the low pressure centres. Further north, a nearly equivalent barotropic response occurs with a low anomaly forced well to the north of the tropical anomaly (about 35-50°N). The general result is to strengthen the Aleutian low. Palmer (1985) has recently carried out extensive experiments on El Nino using the Met Office 11-level AGCM for perpetual winter time conditions. Two of his experiments are discussed below:

5.2.4.1 Experiment 1 "Composite" El Nino SSTA

Palmer used a composite of the observed SSTA (Fig 5.23a) associated with several El Ninos obtained by RC appropriate to December but doubled in intensity with climatological SST elsewhere. Palmer carried out an anomaly experiment with this SSTA and a control experiment without it. Each experiment was continued for 540 model days using "perpetual" January radiation. Anomaly and control experiments both started from real atmospheric data for 28 December 1972, and the model incorporated "envelope" orography whereby mountains are enhanced in height.

Fig 5.23b shows the average difference in 200 mb height (anomaly minus control) for these experiments. The "PNA" pattern of Horel and Wallace is evident and was found to be present at all levels. Tropical lows were overlain by tropical highs as expected (see Lecture 4 for a description of this upper level anticyclonic "vorticity" forcing). Tests showed that the extratropical Rossby wave-like response was highly statistically significant.

5.2.4.2 Experiment 2 - December 1982 SSTA

The maximum of this real SSTA was to the east of the composite SSTA and simpler in shape (Fig 5.24a) Palmer used two versions of the 11-level AGCM integrated for perpetual winter conditions as before.

(a) Anomaly and control integrations using "envelope" orography, starting from 28 December 1972 atmospheric data.

(b) Anomaly and control integration for a model with "standard" orography, same starting date.

"Envelope" orography has higher mountains than "standard" orography. Both pairs of experiments were integrated for 540 model days.

Fig 5.24b show the difference between the anomaly and control experiments for (a) and (b). Neither figure shows a recognisable PNA pattern which was not, in fact, observed in 1982-83. Both models do show a Rossby wave-like anomaly response and in both pairs of experiments the response is highly statistically significant - but nevertheless different. In the "standard" orography experiment the anomaly wavelength is longer and the pattern is distorted compared to the "envelope" orography experiment. This is not surprising as the climatological mean flow of the "standard" orography model is much more westerly than that of the "envelope" model in winter, the "envelope" model being thought more realistic.

Conclusion from these experiments (and those of other workers could be:-

(1) The wintertime extratropical response to El Nino may be quite strong but vary from event to event eg with the longitude or shape of the SSTA or position of the resulting absolute maximum tropical Pacific SST.

(2) The response of an AGCM will depend on its climatology. A realistic, local response, as required for long-range forecasting, may demand a realistic representation of the structure of the mean flow.

5.2.5 Oceanographic aspects

Gill and Rasmusson (2) have discussed the oceanographic aspects of the 1982-83 El Nino using a model of the response of the mixed layer of the tropical Pacific Ocean to the observed weakening of the trade winds near 160°E during early 1982. They assume a pre-existing (much as actually measured) gradient of sea surface topography with higher sea-level in the W Pacific than in the E Pacific (the east-west difference is typically observed to be about 1 m before El Nino and results from the wind stress imparted by the preceding, strong, SE trade winds). Fig 5.25 shows the longitude-time plots of eastward wind stress anomaly used in the model experiment (the anomalies represent westward stresses), Fig 5.26A shows the computed change of surface elevation of the sea from a pre-existing condition where the height is greater in the west and Fig 5.26B shows the resulting eastward currents. These tend to oscillate in direction on a time scale of about 9 months as a result of the prediction of an eastward moving 'Kelvin' wave in the mixed layer which which is partially reflected from the S American coast as a form of planetary wave. Fig 5.27 shows the observed anomalies along the equator of (a) rainfall (measured by anomalies of outgoing long-wave radiation (b) westerly wind (c) values of absolute SST (d) climatological avereage SST values. The model produced a very good simulation of the observed change of sea-level topography during SSTA; this tends to rise first near the S American coast but the main warming propagates eastwards from the W toward the central Pacific, though warming is initiated simultaneously near S America too. So there is much more to be understood about El Nino as this behaviour, though correct for 1982-3, is not necessarily typical.

Conclusion

The ENSO event represents the most important non-seasonal, if irregularly recurring, event in the climate system on time scales between the annual cycle and the ice ages tha has yet been properly identified. The factors that initiate the El Nino/ENSO sequence remain elusive. Some of the physical processes that occur in the ocean during ENSO have been isolated, however.

REFERENCES

1. QUIROZ, R S (1983). The climate of the "El Nino" winter of 1982-82 -a season of extraordinary climatic anomalies. Mon Weath Rev, 111, pp 1685-1706.

2. GILL, A E AND RASMUSSON, E M. The 1982-83 climate anomaly in the equatorial Pacific. Nature, 306, pp 229-234.

3. RASMUSSON, E M AND CARPENTER, T H (1982). Variations in tropical sea surface temperature and surface wind fields associated with the Southern Oscillation/El Nino. Mon Weath Rev, 110, pp 354-384.

4. BERLAGE, H P AND DE BOER, H J (1959). On the extension of the Southern Oscillation throughout the world during the period July 1 1949-July 1 1957. Geofis pure appl, 44, pp 287-295.

5. KOUSKY, V E ET AL (1984). A review of the Southern Oscillation: oceanic-atmosphere circulation changes and related rainfall anomalies. Tellus, 36A, pp 490-504.

6. PARKER, D E (1983). Documentation of a Southern Oscillation index. Met Mag, 112, pp 184-188.

7. FOLLAND, C K ET AL (1985). Worldwide marine temperature fluctuations on the season-to-century time scale. Proc 9th Climate Diagnostics Conf, Corvallis, Oregon, 22-26 Oct 1984.

8. NEWMAN, M. Observational aspects of the El Nino and the atmospheric response. Met O 13 Branch Memo 148.

9. PAN, Y H AND OORT, A H (1983). Global climate variations connected with sea surface temperature anomalies in the eastern equatorial Pacific Ocean for the 1958-73 period. Mon Weath Rev, 111, pp 1244-1258.

10. WYRTKI (1975) El Nino - the dynamic response of the equatorial Pacific Ocean to atmospheric forcing. J. Phys. Ocean, 5, pp 572-584.

11. CHEN, W Y (1982). Fluctuations in northern hemisphere 700 mb height field associated with the Southern Oscillation. Mon Weath Rev, 110, pp 808-823.

12. HOREL, J D AND WALLACE, J M (1981). Planetary scale atmospheric phenomena associated with the southern oscillation. Mon Weath Rev, 109, pp 813-829.

13. BJERKNES, J (1969). Atmospheric teleconnections from the equatorial Pacific. MWR, 97, pp 163-172.

14. SELKIRK, (1984). Seasonally stratified correlations of the 200 mb tropical wind field to the Southern Oscillation. J Clim, 4, pp 365-382.

15. WRIGHT P B (1977) The southern oscillation - patterns and mechanisms of the teleconnections and the persistence. Grant OCE-76-23173, University of Hawaii.

16. ROWNTREE, P R (1972). The influence of tropical east Pacific Ocean temperatures on the atmosphere. Q J Roy Met Soc, 98, pp 290-321.

17. PALMER, T N (1985). A General Circulation Model's response to sea surface temperature anomalies in the tropical Pacific Ocean. Proc 16th Liege Conf on Ocean Hydrodynamics (in Press).

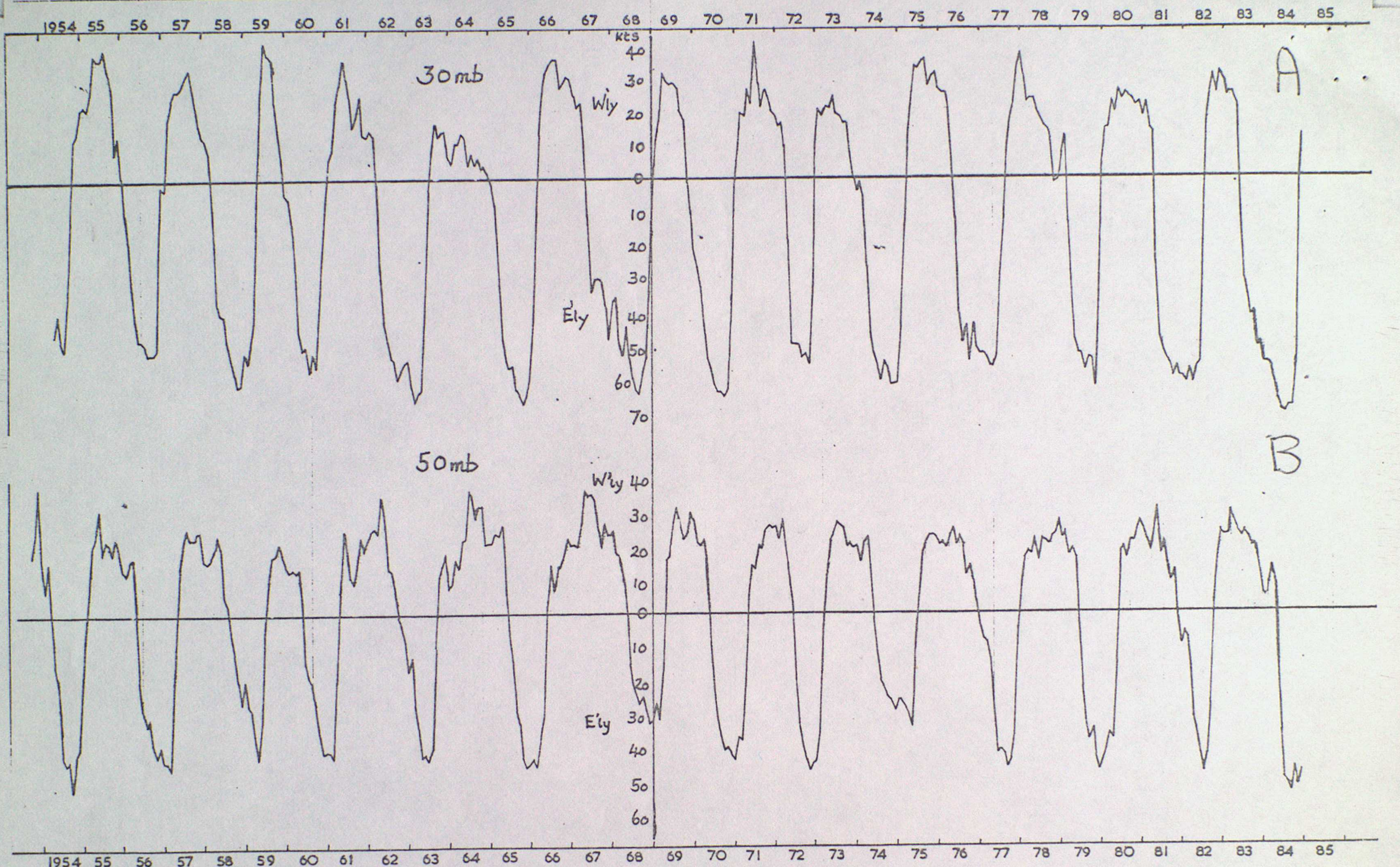

Monthly mean zonal wind components at 50 & 30 mb for Canton Island (2°46'S 171°43'W) from Oct 1953 - Aug 1967 & for Gan (00°41'S 73°09'E) from Sept 1967 to Dec 1975 & for Singapore (1°22'N 103°55'W) from Jan 1976 to June 1981 & for Changi (1°22'N 103°59'W) from Jul 1981 FIG 5.1

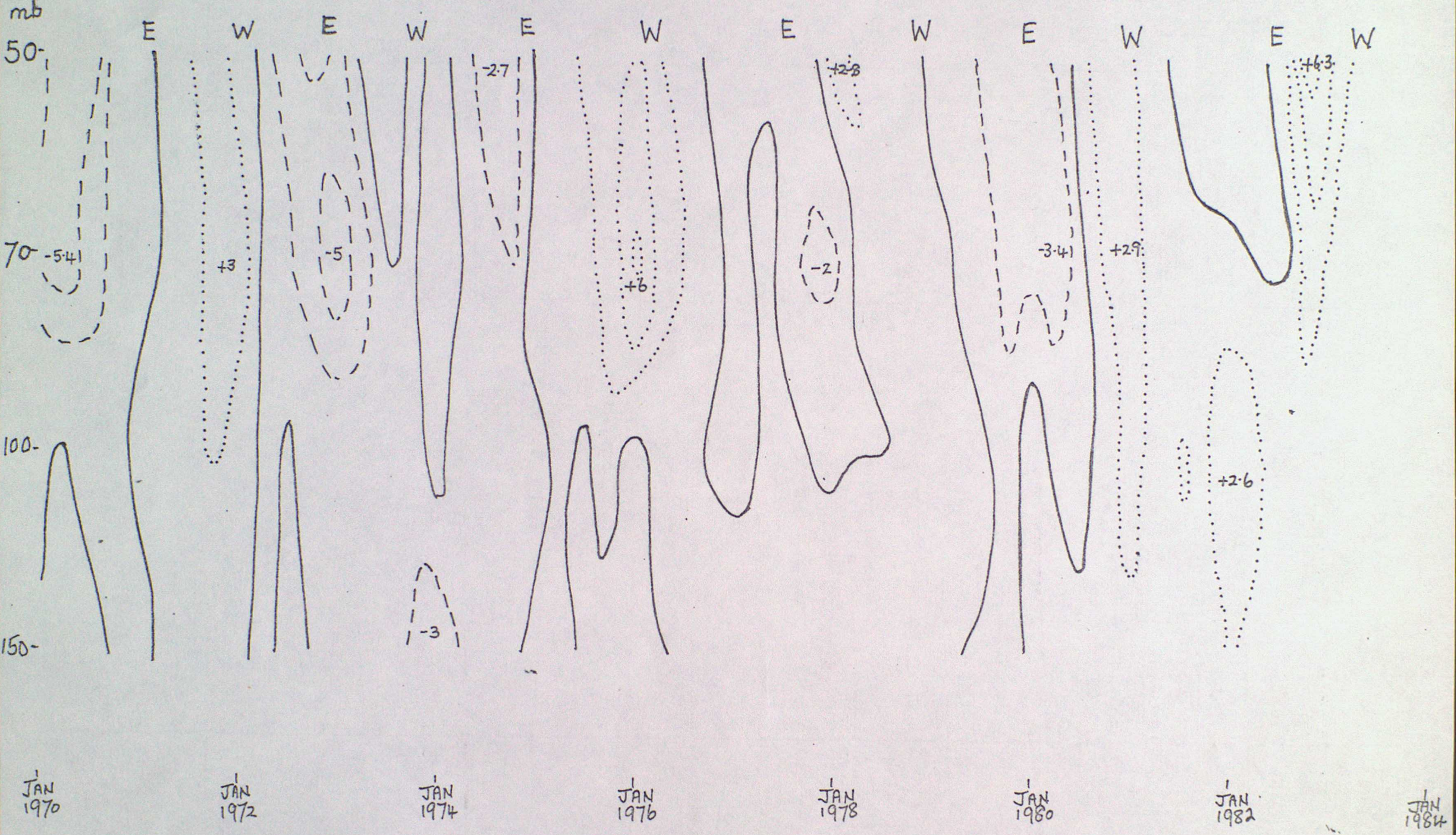

FIG5.2 Temperature anomalies (w.r.t. 1971-80) over Singapore.
Isotherms at 2°C intervals.

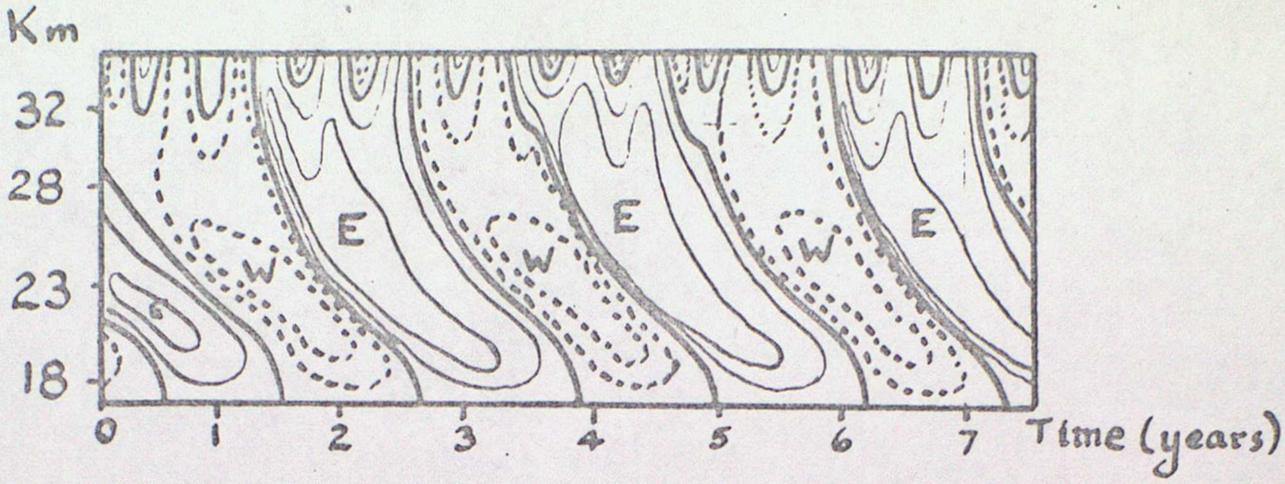

a) from the model of Holton & Lindzen (1972)

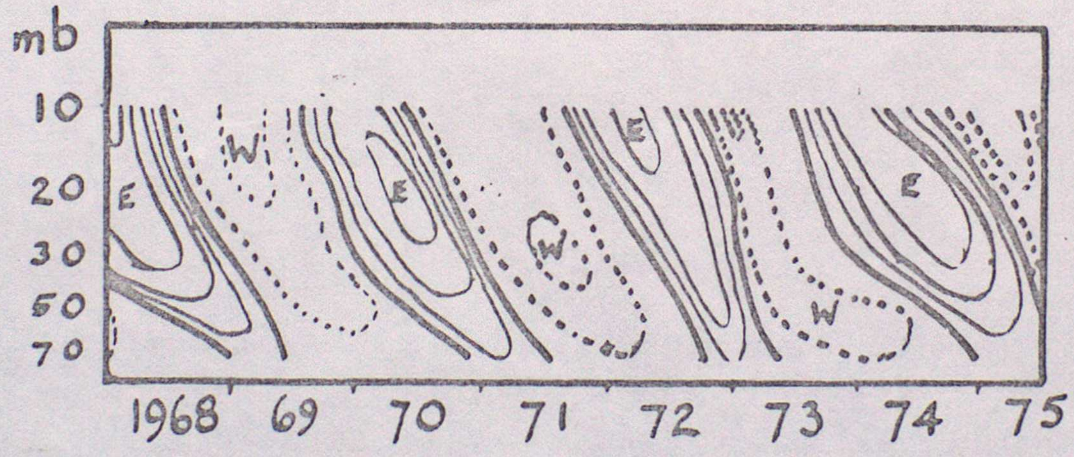

b) from data for Gan

TIME-HEIGHT SECTIONS OF MEAN ZONAL WIND

FIG 5·3

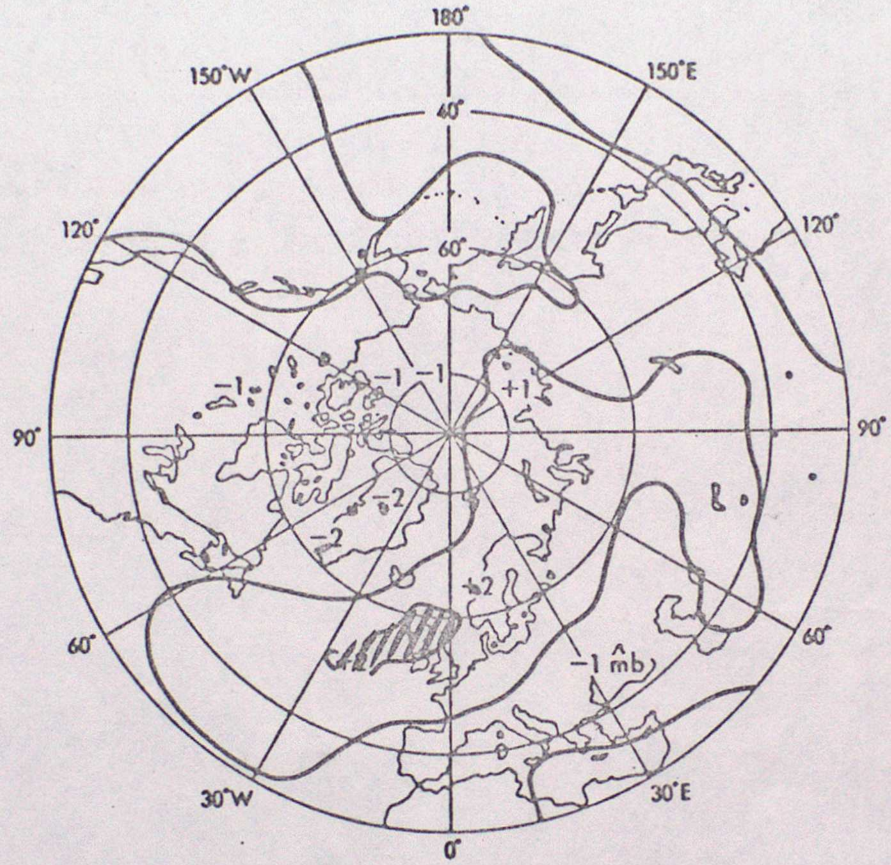
180°
150°W
150°E
40°
60°
120°
120°
90°
90°
60°
60°
30°W
30°E
0°
−1
−1
−1
+1
−2
−2
+2
−1 mb

Figure 5.4 Surface pressure anomaly from 1951–70 average, July.
After Ebdon (1975).
Mean of eight Julys with westerly phase of QBO at 30 mb.

FIG 5.5a

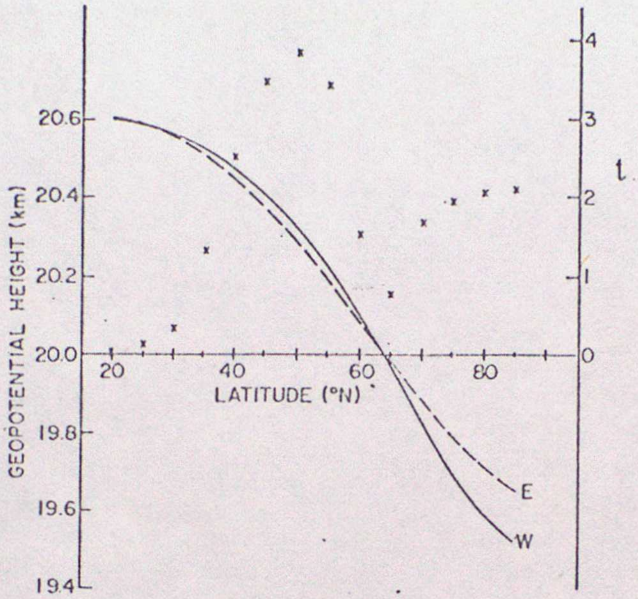

FIG. 4. Composite meridional profiles of the zonal mean 50 mb geopotential height for November–December. W and E denote westerly and easterly categories, respectively. Crosses denote Student's t values (right hand scale). t values of 2.15, 3.00 and 4.14 correspond to significance levels of 5, 1 and 0.1%, respectively (14 degrees of freedom).

FIG 5.5b

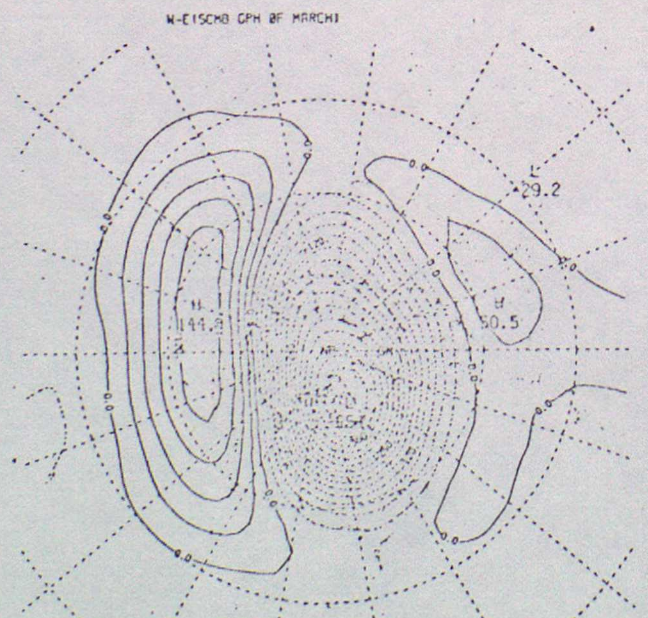
W-E(50MB GPH BF MARCH)
L
-29.2
H
144.9
H
50.5

FIG. 2. (*Continued*)

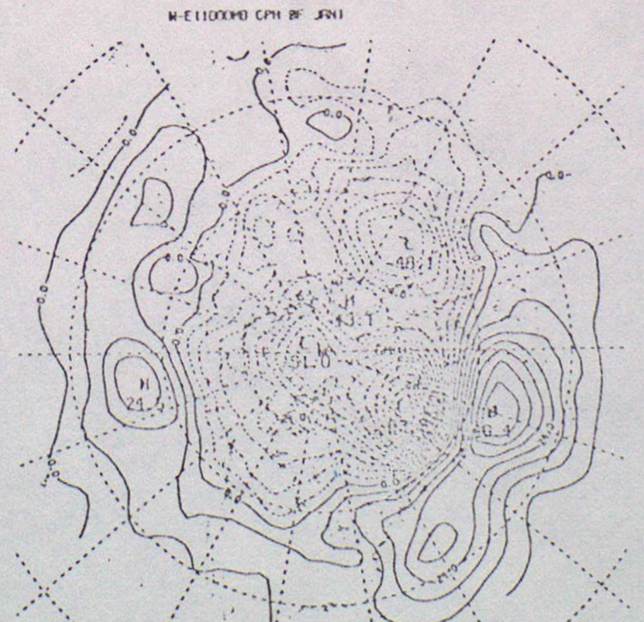
W-E(1000MB GPH BF JAN)
H
21.1
H
L
-48.1

FIG. 3. January mean 1000 mb geopotential height difference (westerly category minus easterly category). Units: geopotential meters.

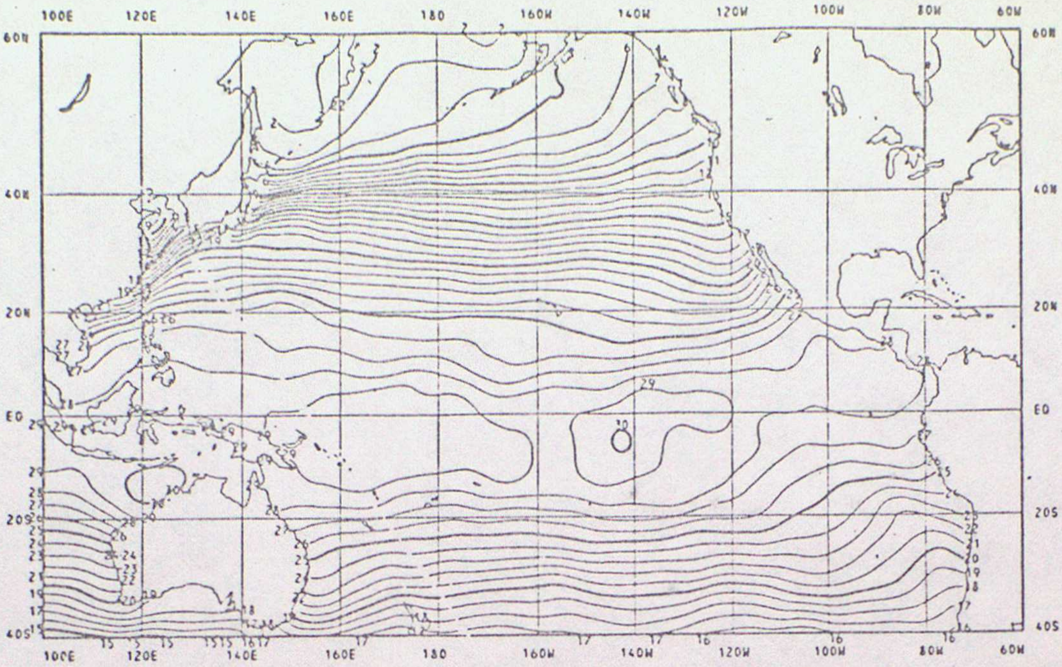
100E
120E
140E
160E
180
160W
140W
120W
100W
80W
60W
60N
40N
20N
EQ
20S
40S
29
30

FIG 5·6

SEASONAL NMC SST MEAN FIELD (CAC ANALYSIS) DEC JAN FEB 1983

. Sea surface temperature over the Pacific Ocean for winter 1982–83.

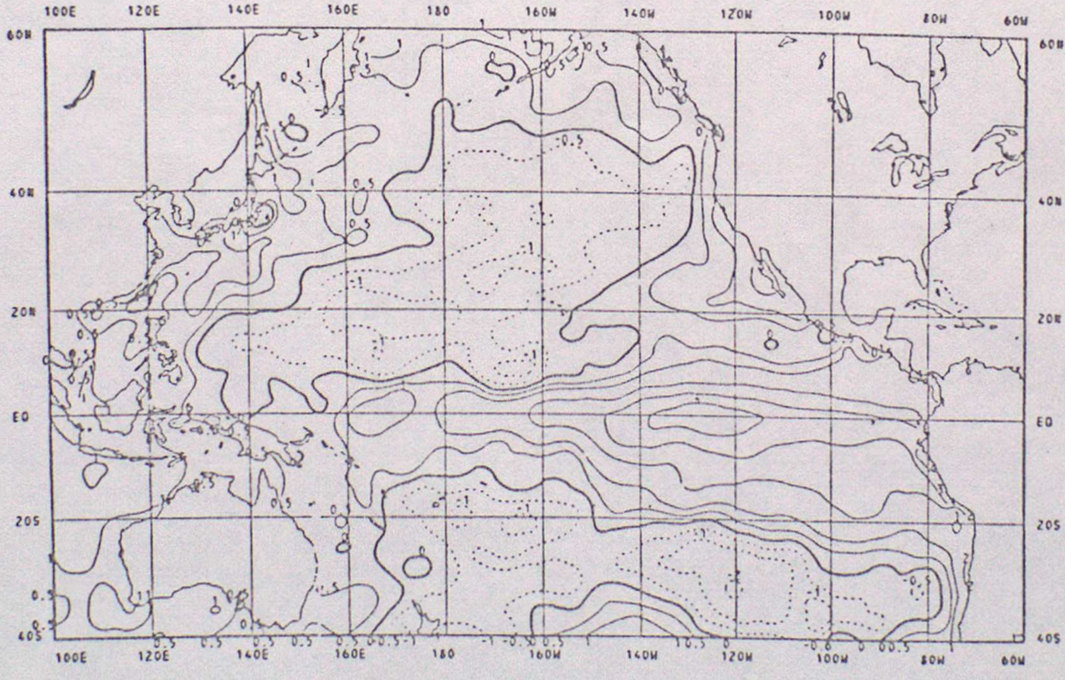
100E
120E
140E
160E
180
160W
140W
120W
100W
80W
60W
60N
40N
20N
EQ
20S
40S
0.5
-1

SEASONAL SST ANOMALIES (CAC ANALYSIS, NCC CLIMATE) DEC JAN FEB 1983

Sea surface temperature (°C) for winter 1982–83 over the Pacific Ocean. Dashed lines portray negative anomalies, thin solid lines indicate positive anomalies, and the heavy solid line is the zero line. Anomalous isotherms are at 1°C intervals except for 0.5°C between +1 and −1°C.

FIG 5·7

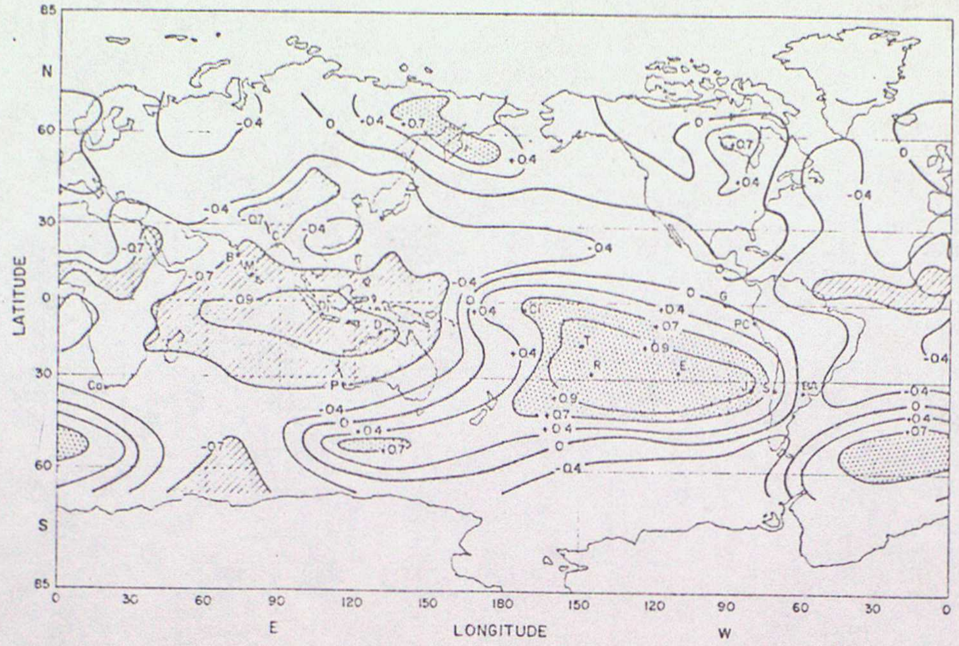

85
N
60
30
0
30
60
S
85
LATITUDE
0
30
60
90
120
150
180
150
120
90
60
30
0
E
LONGITUDE
W

Isolines of correlation coefficients of sea level pressure anomalies using Easter Island (E) as the reference station. Adapted from Berlage and de Boer (1959).

FIG 5·8

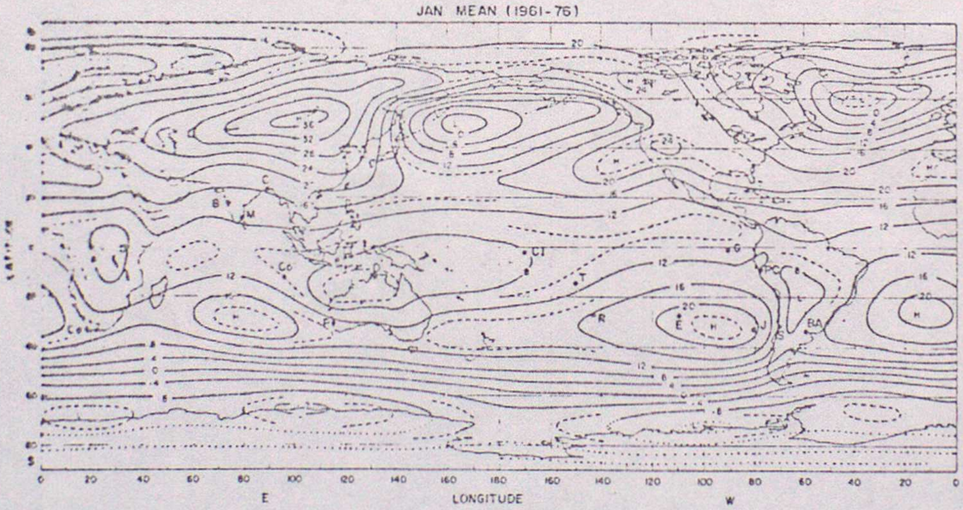

JAN MEAN (1961-76)
0
20
40
60
80
100
120
140
160
180
160
140
120
100
80
60
40
20
0
E
LONGITUDE
W

January mean sea level pressure (1961–76). Adapted from Godbole and Shukla (1981). Stations commonly referred to as being key stations in the Southern Oscillation and indicated in the figure are: Capetown (Ca), Bombay (B), Madras (M), Calcutta (C), Djakarta (Dj), Darwin (D), Perth (P), Cocos Island (Co), Canton Island (CI), Papaete, Tahiti (T), Rapa (R), Easter Island (E), Juan Fernandez Island (J), Galapagos Islands (G), Puerto Chicama (PC), Santiago (S) and Buenos Aires (BA).

FIG 5·9

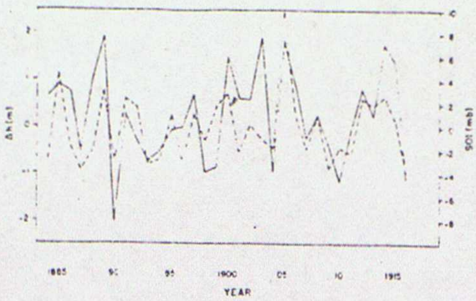

FIG 5·10

The mean Parana river level anomalies (m). for April–September. at Rosario. Argentina (dashed line) and a Southern Oscillation Index (SOI) (solid line) calculated by taking the sum of the pressure anomalies (mb) at Bombay. Madras. Djakarta. Calcutta. Darwin. Perth and Cape Town for the period of October–March. The SOI values are plotted in the year corresponding to the January–March period. and are taken from Berlage (1966). The Parana river level anomalies are taken from Mossman (1924)

FIG 5·17

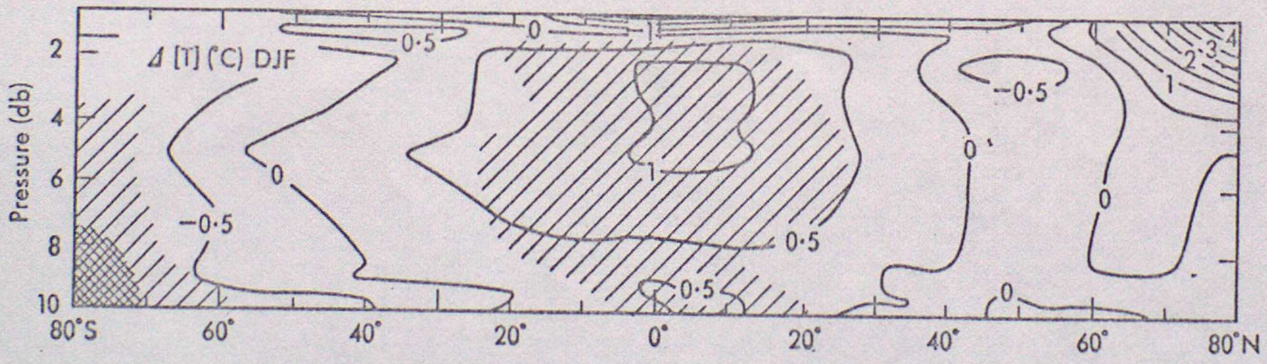

Zonal mean cross section of the average temperature difference (°C) between cases when the winter mean surface temperatures at 2·5°S, 130°W was relatively warm and cases when it was relatively cool. (After Pan & Oort, 1983).

Normalised seasonal southern oscillation index (Tahiti minus Darwin)

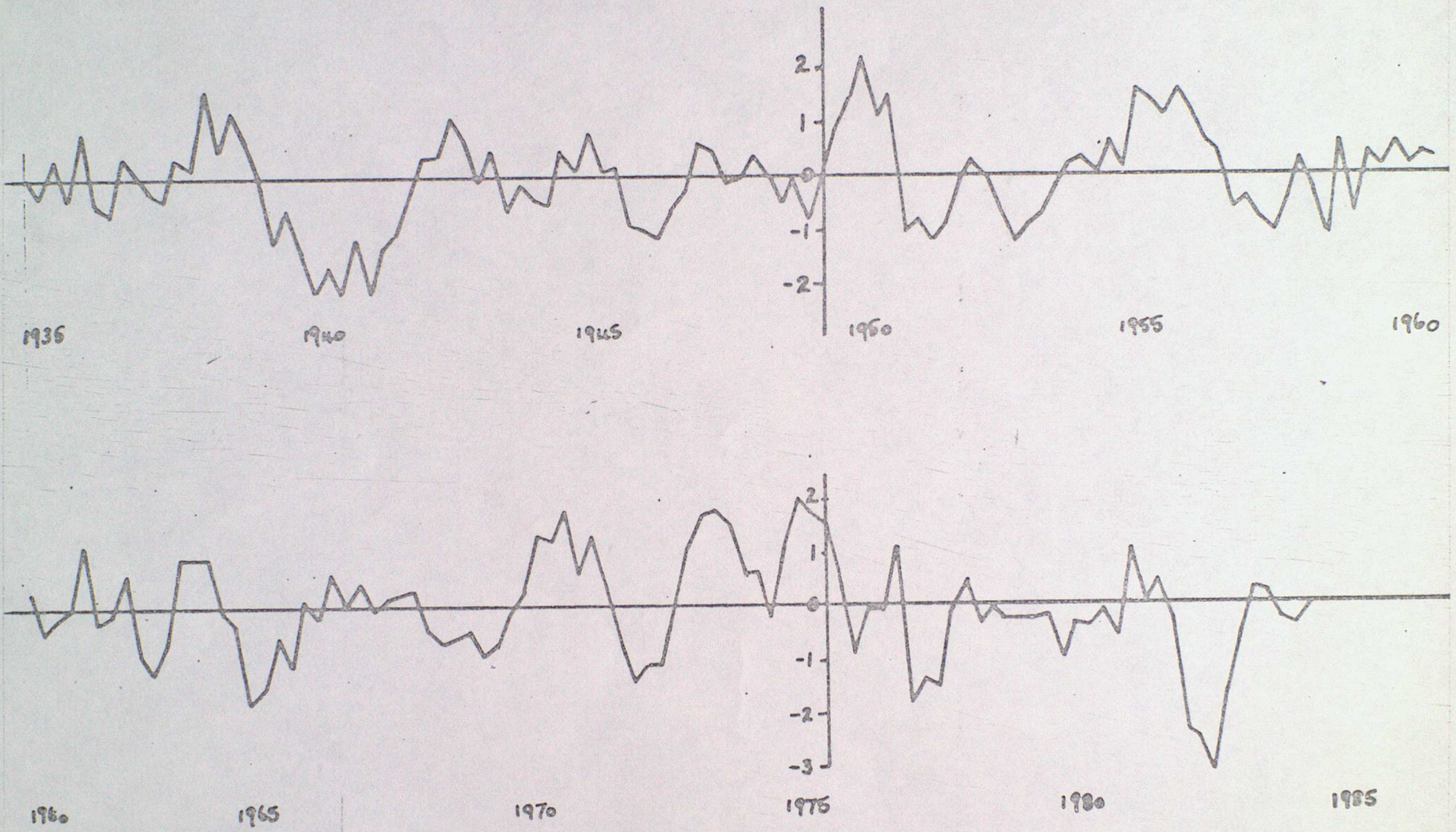

FIG 5·11

Seasonal SST (---) & MATN anomalies from 1856 with respect to 1951-60 means over the East Tropical Pacific

FIG 5·12

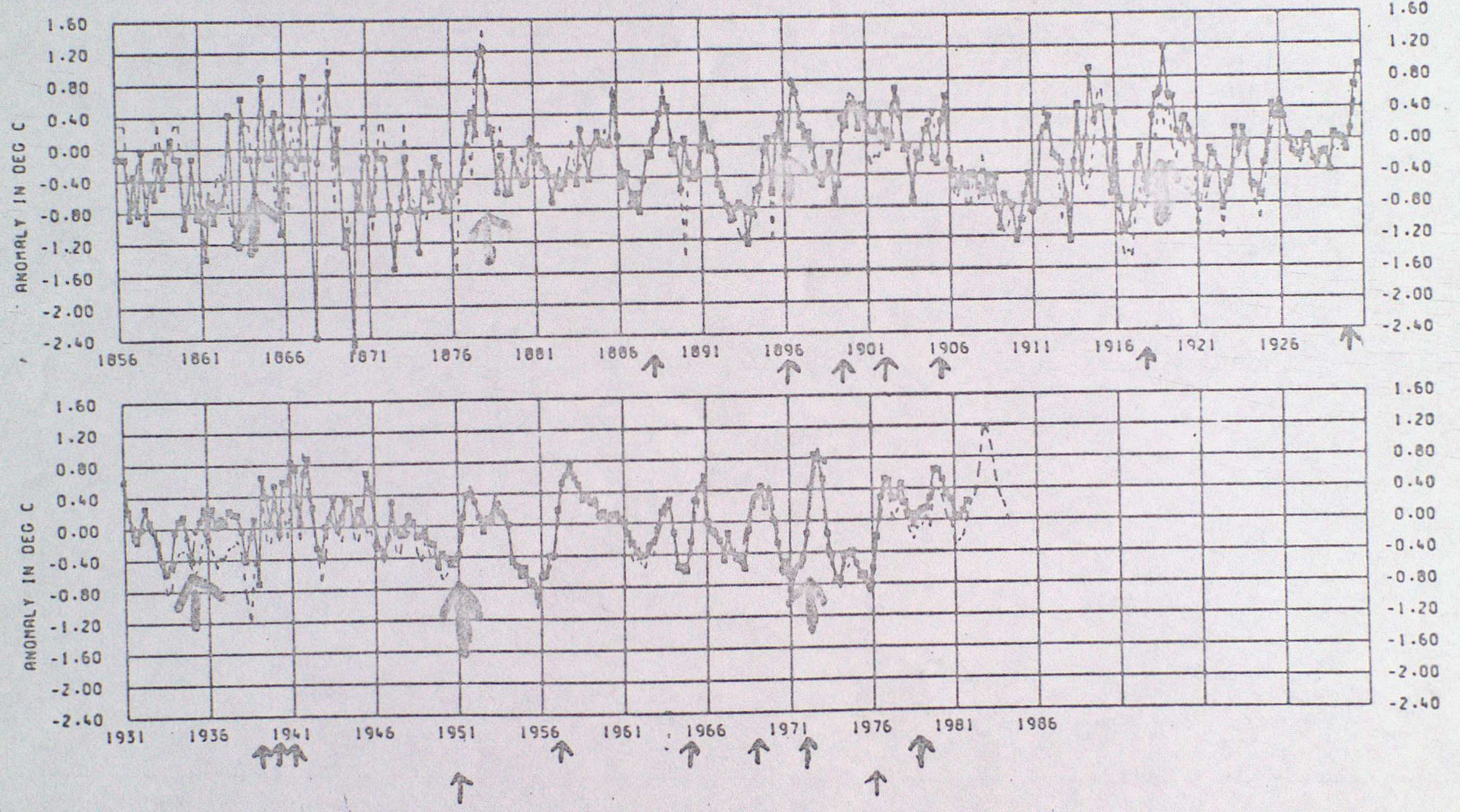

EOF2 Global SST (10° squares 1901-80) FIG 5.13

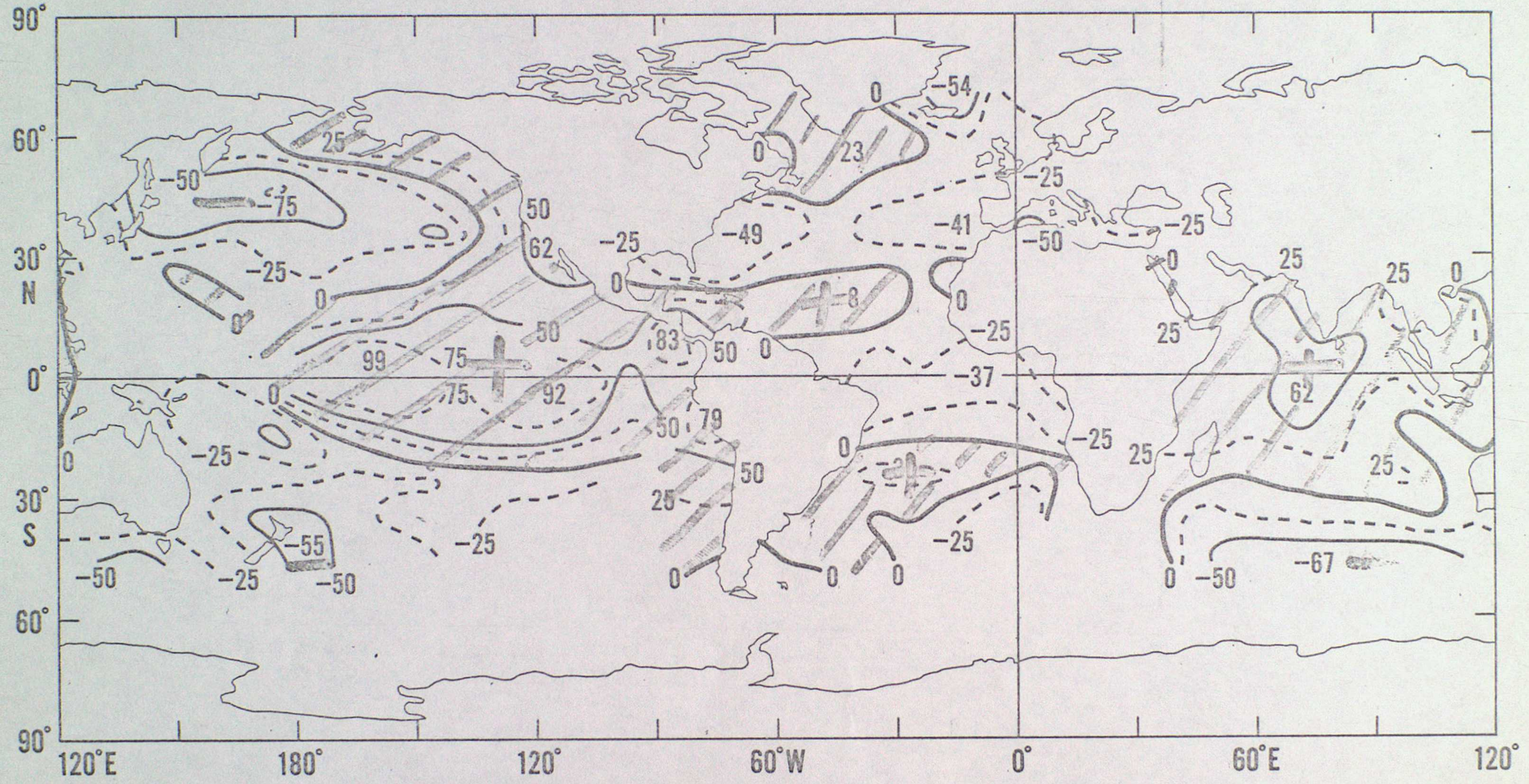
90°
60°
30° N
0°
30° S
60°
90°
120°E
180°
120°
60°W
0°
60°E
120°
25
-50
-75
50
62
-25
0
99
75
-50
83
92
79
50
-55
-25
-50
0
23
-54
-49
-41
-25
-50
8
-37
-25
0
25
62
-67
-50

DO 3631

FIG 5.14

Comparison between EOF2 and Tropical East Pacific SST Anomaly Time Series

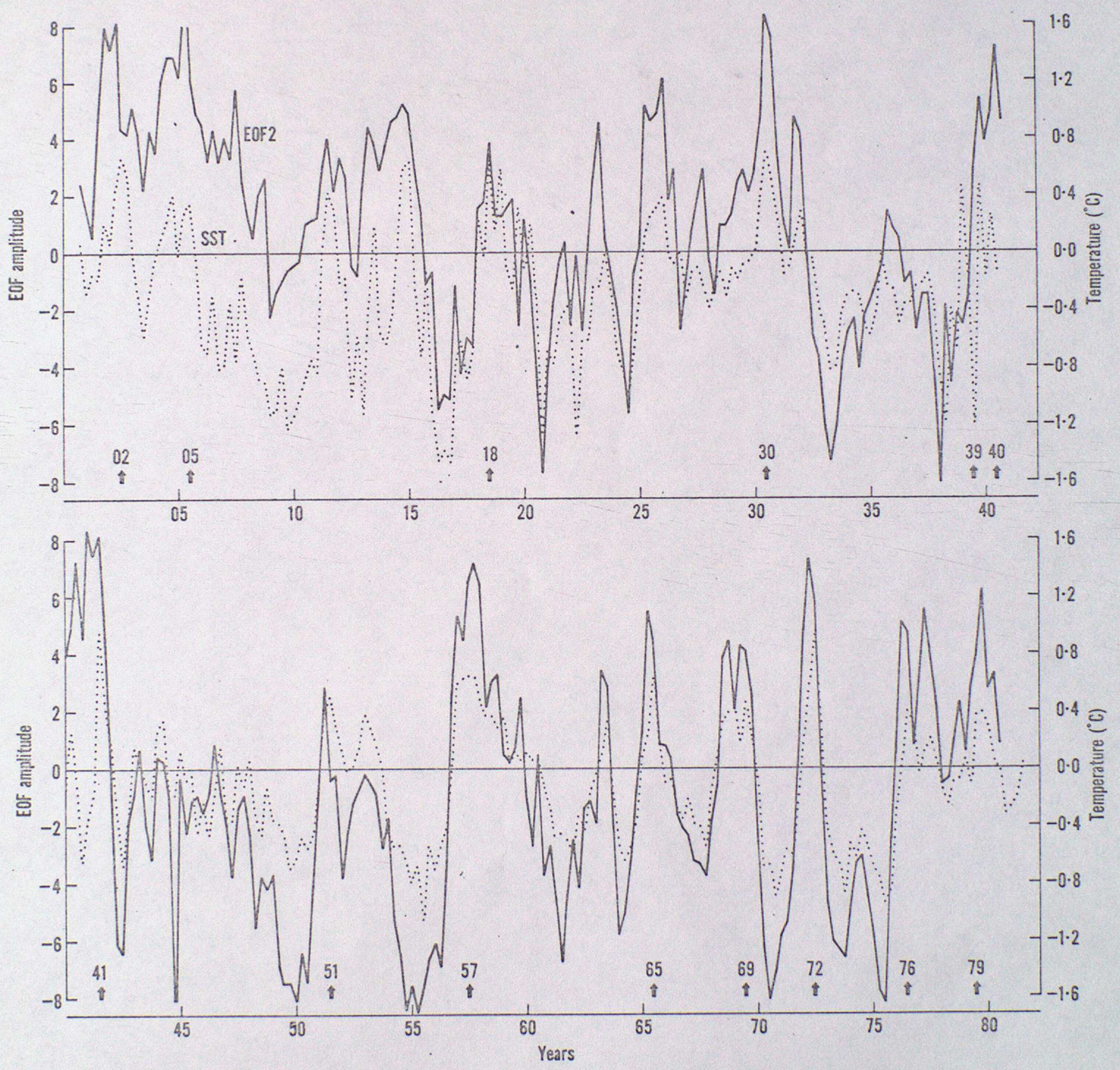

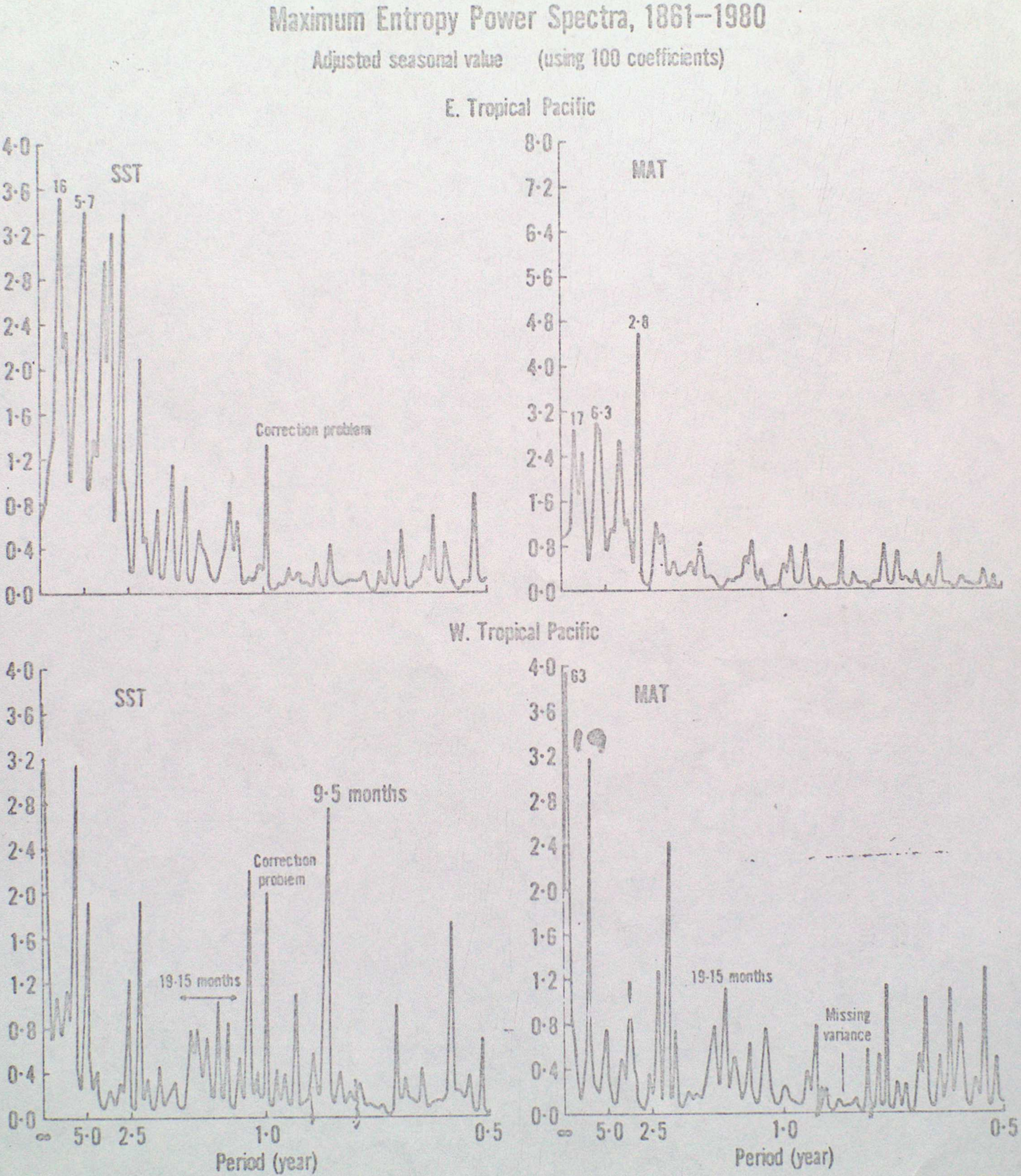
Maximum Entropy Power Spectra, 1861–1980
Adjusted seasonal value (using 100 coefficients)
E. Tropical Pacific
SST
16
5·7
Correction problem
MAT
17
6·3
2·8
W. Tropical Pacific
SST
9·5 months
Correction problem
19-15 months
MAT
63
19
19-15 months
Missing variance
4·0
3·6
3·2
2·8
2·4
2·0
1·6
1·2
0·8
0·4
0·0
8·0
7·2
6·4
5·6
4·8
4·0
3·2
2·4
1·6
0·8
0·0
∞
5·0
2·5
1·0
0·5
Period (year)
DO 343

FIG 5.15

FIG 5·16a

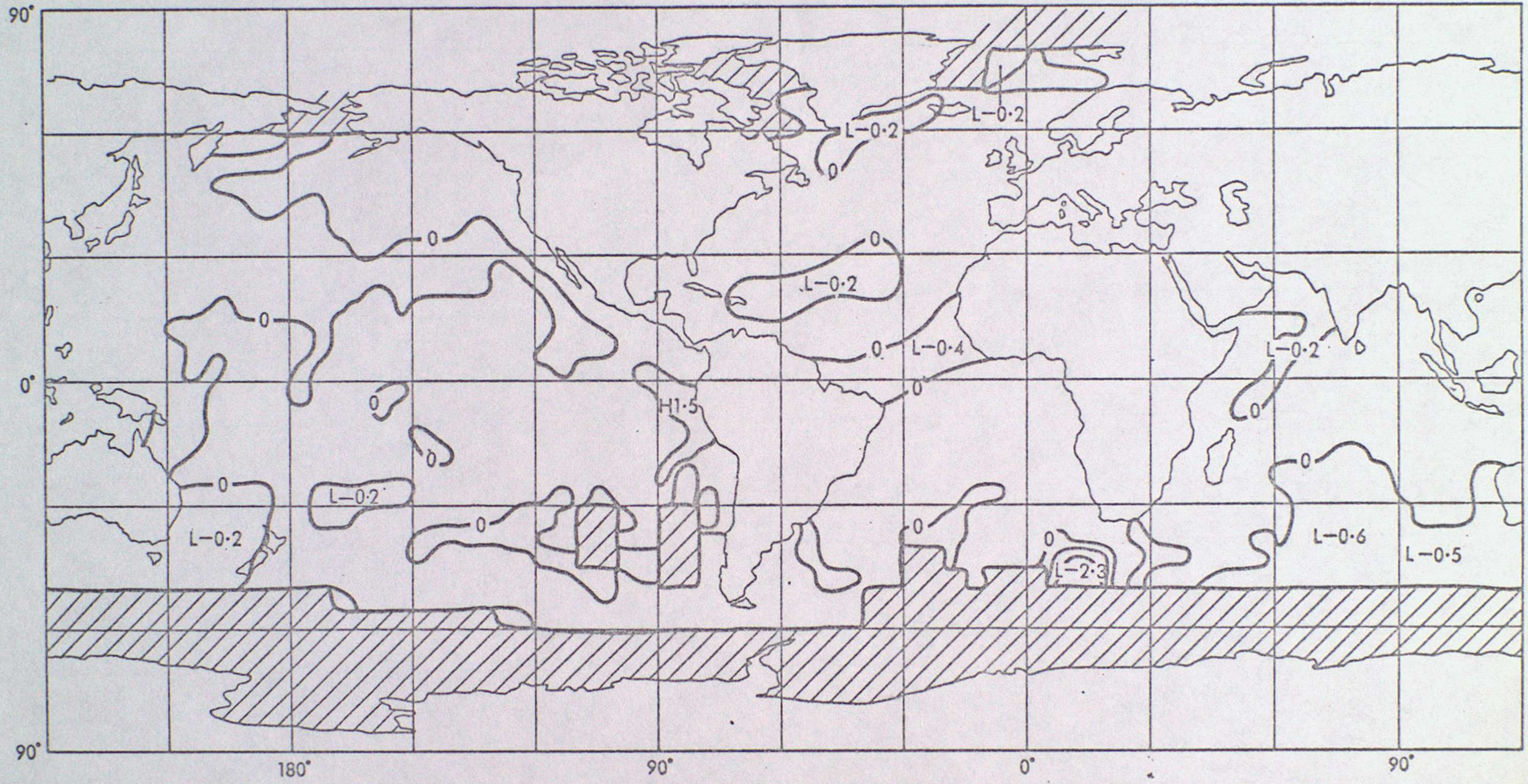
90°
0°
90°
180°
90°
0°
90°
L-0·2
L-0·2
0
0
L-0·2
0
L-0·4
0
0
L-0·2
0
0
H1·5
0
0
0
L-0·2
L-0·2
0
0
L-2·3
L-0·6
L-0·5

El-Nino sea surface temperature anomaly composite. April, Year (0)

FIG 5·16 G

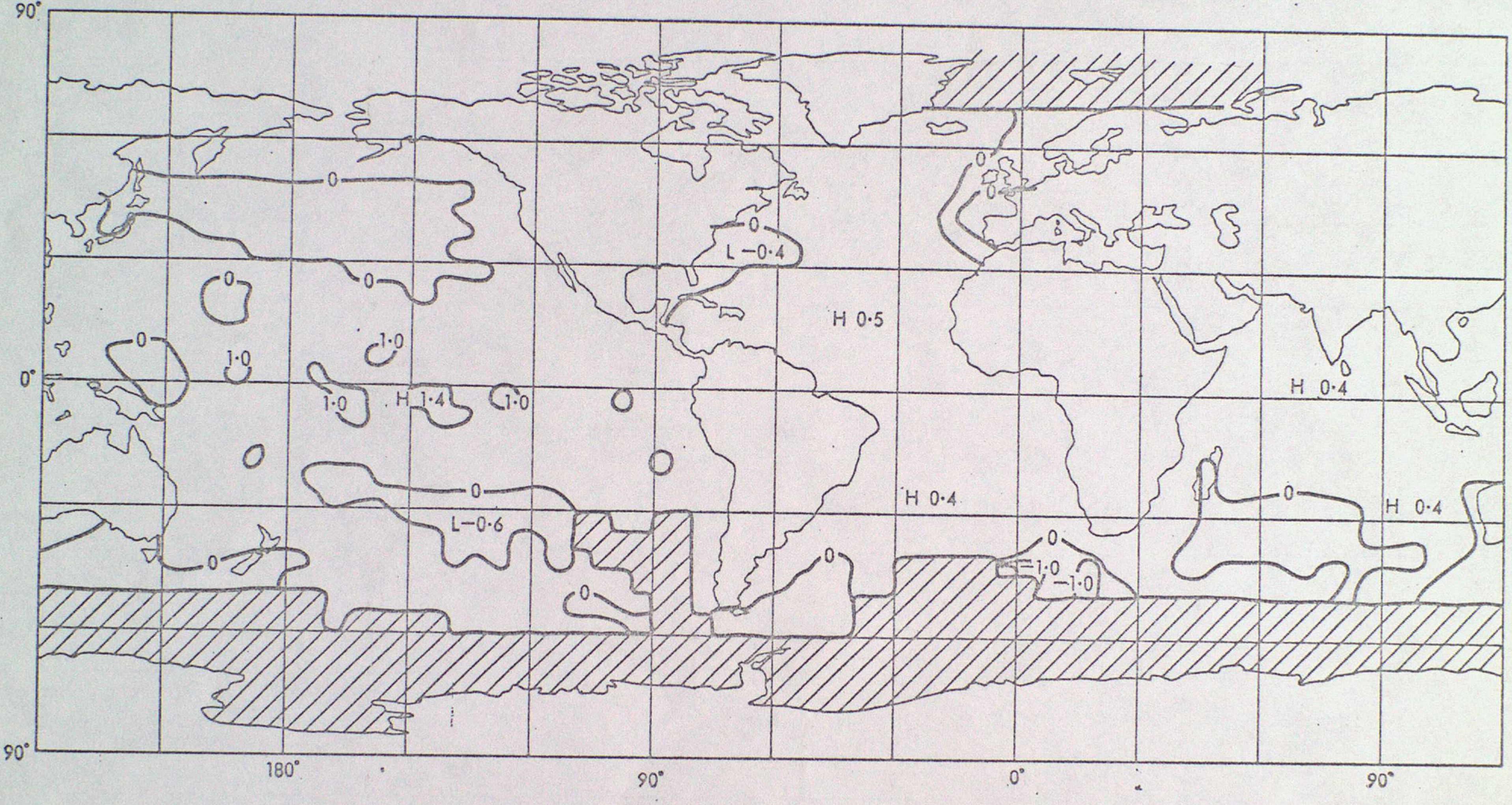
90°
0°
90°
180°
90°
0°
90°
0
0
0
L −0·4
H 0·5
0
1·0
0
1·0
1·0
H 1·4
1·0
0
L−0·6
0
0
0
H 0·4
0
−1·0
−1·0
H 0·4
0
H 0·4

El-Nino sea surface temperature anomaly composite. March, Year (+1)

FIG 5-16 c

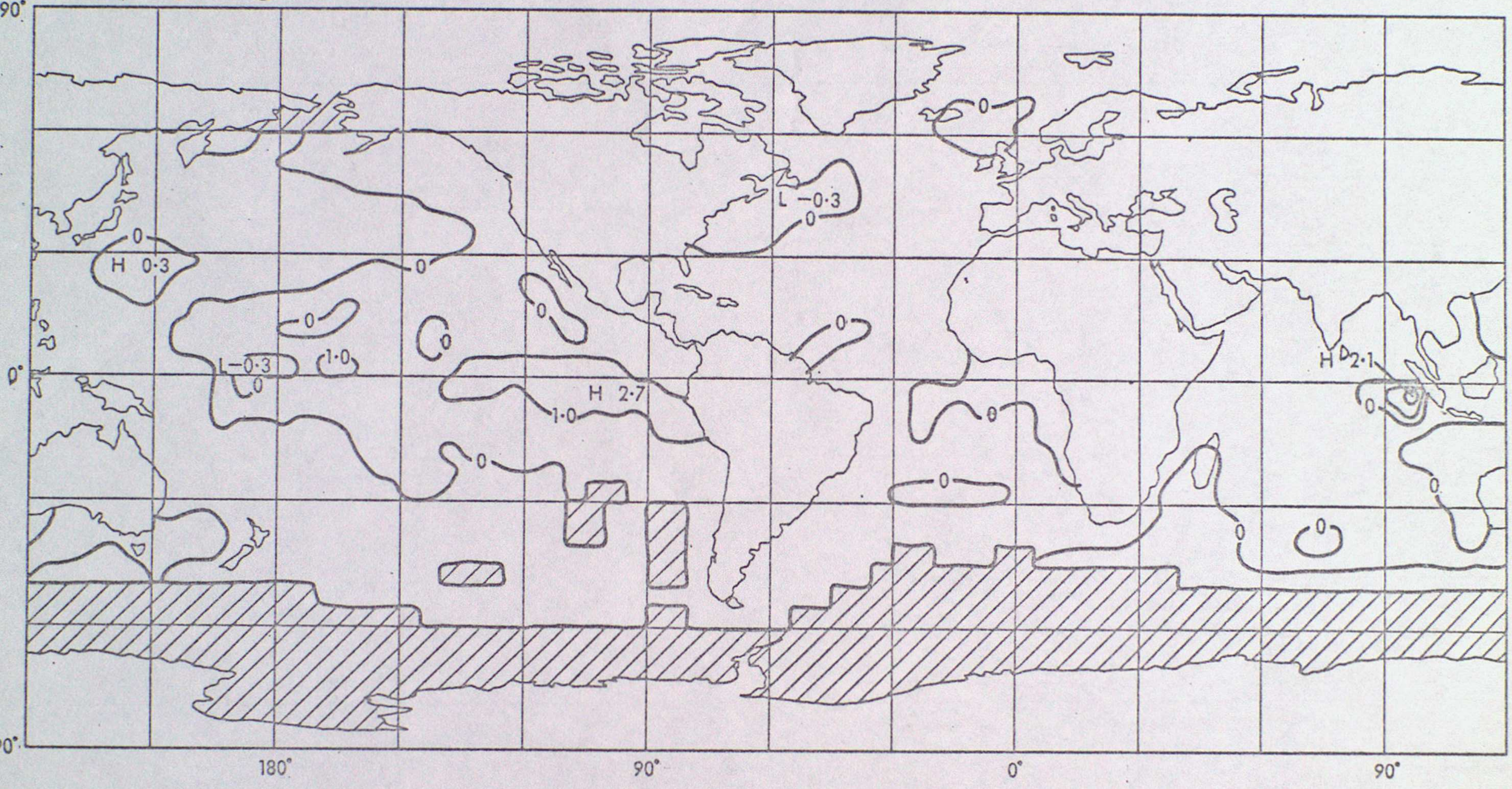
90°
0°
90°
180°
90°
0°
90°
0
H 0·3
0
0
L−0·3
0
1·0
0
0
1·0
H 2·7
0
L −0·3
0
0
0
0
0
H 2·1
0
0
0
0

El-Nino sea surface temperature anomaly composite. August, Year (0)

FIG 5.16d

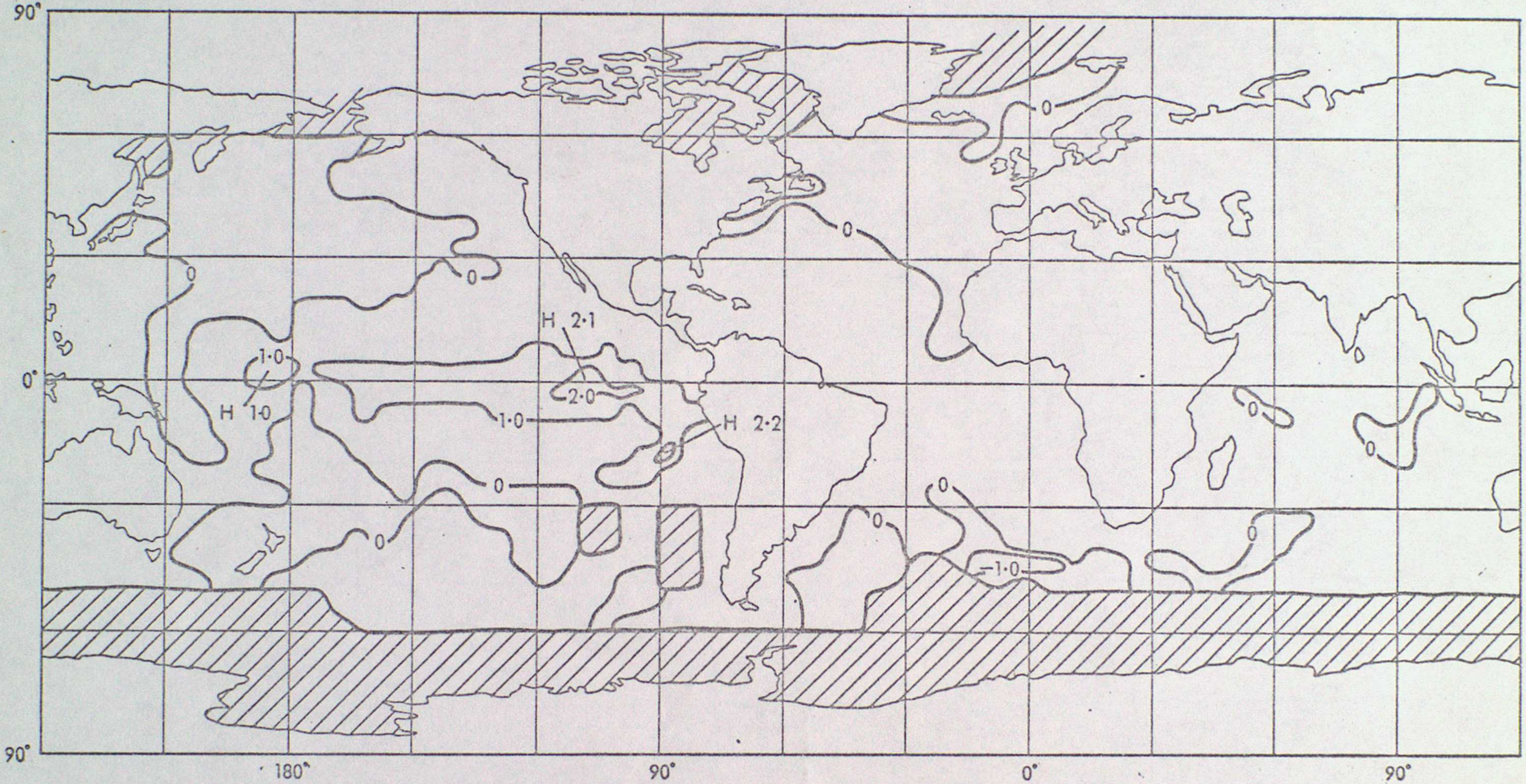
90°
0°
90°
180°
90°
0°
90°
0
0
0
0
0
0
0
0
0
1·0
H 1·0
H 2·1
2·0
1·0
H 2·2
−1·0

'El-Nino sea surface temperature anomaly composite. December, Year (0)

FIG 5·18a

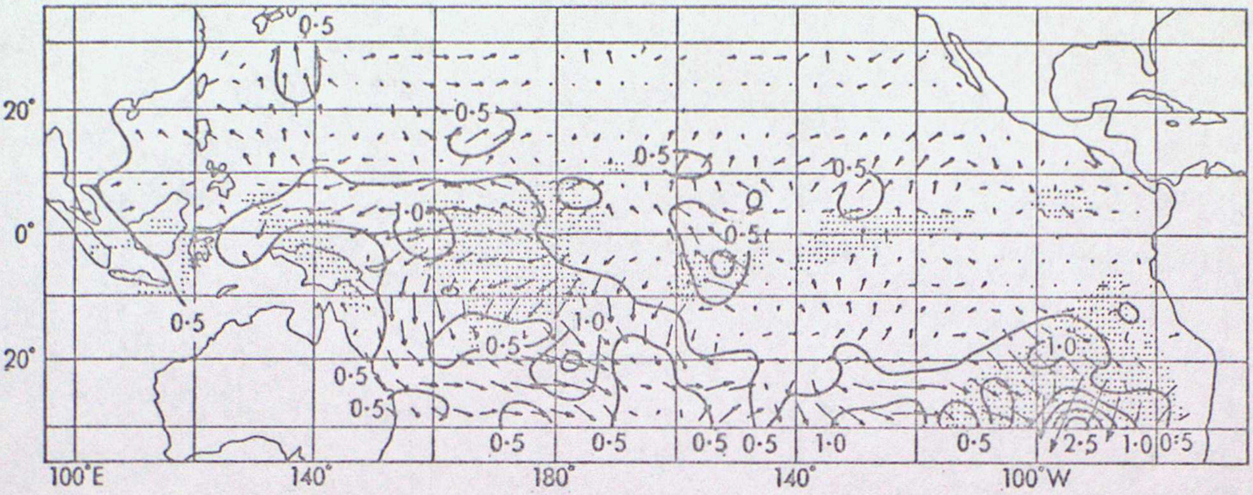
20°
0°
20°
100°E
140°
180°
140°
100°W
0·5
1·0
2·5

August—October Year (−1)

FIG 5·18b

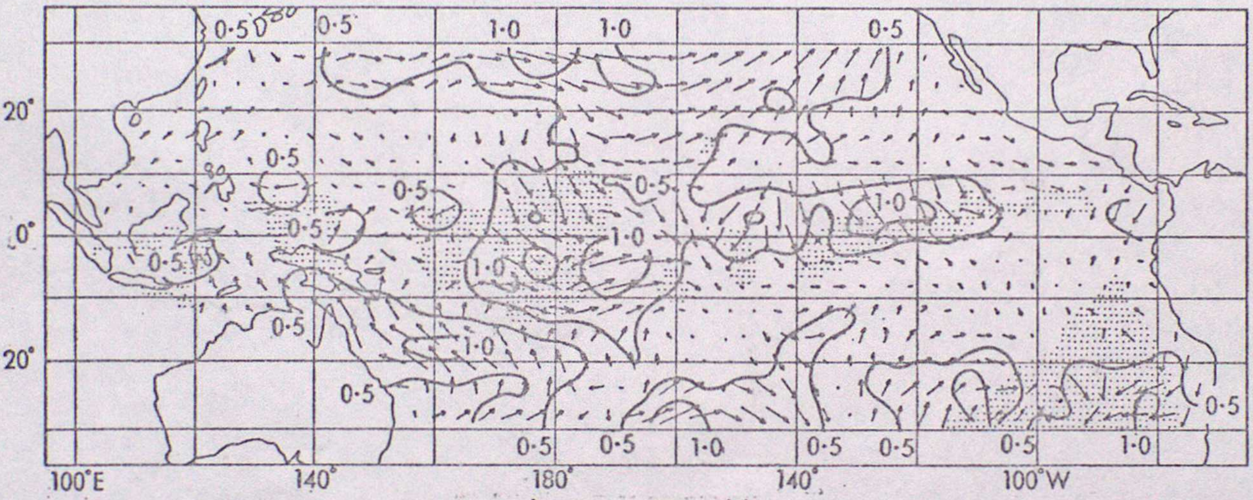
20°
0°
20°
100°E
140°
180°
140°
100°W
0·5
1·0

March—May Year (0)

FIG 5·18c

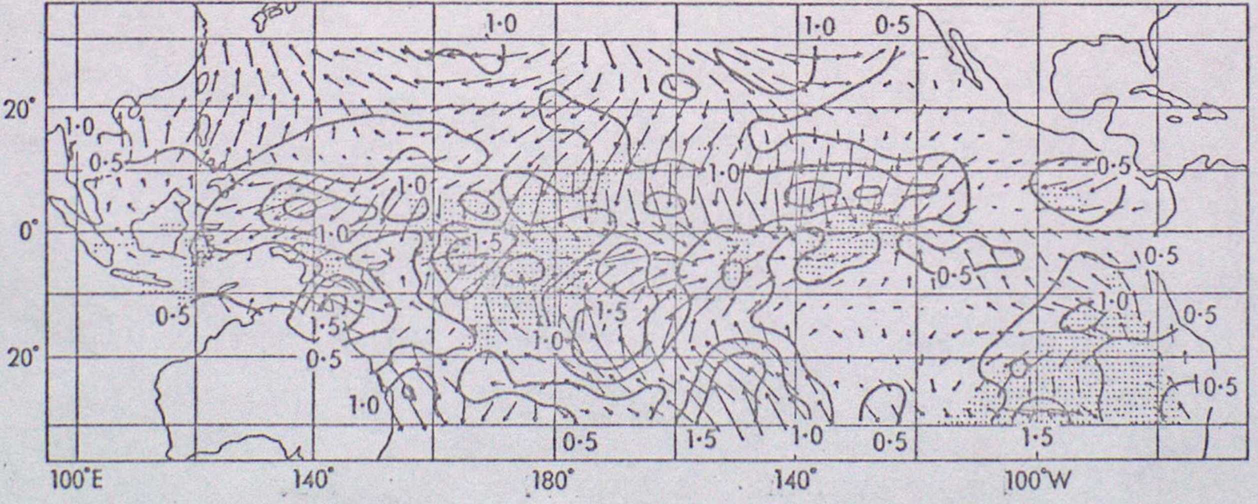
20°
0°
20°
100°E
140°
180°
140°
100°W
0·5
1·0
1·5

December Year (0) — February Year (+1)

El-Nino surface wind anomaly composites (units m s^{-1}).
Areas in which the number of observations average less than 10 in a two degree square are shaded on the wind composite. (After RC 82)

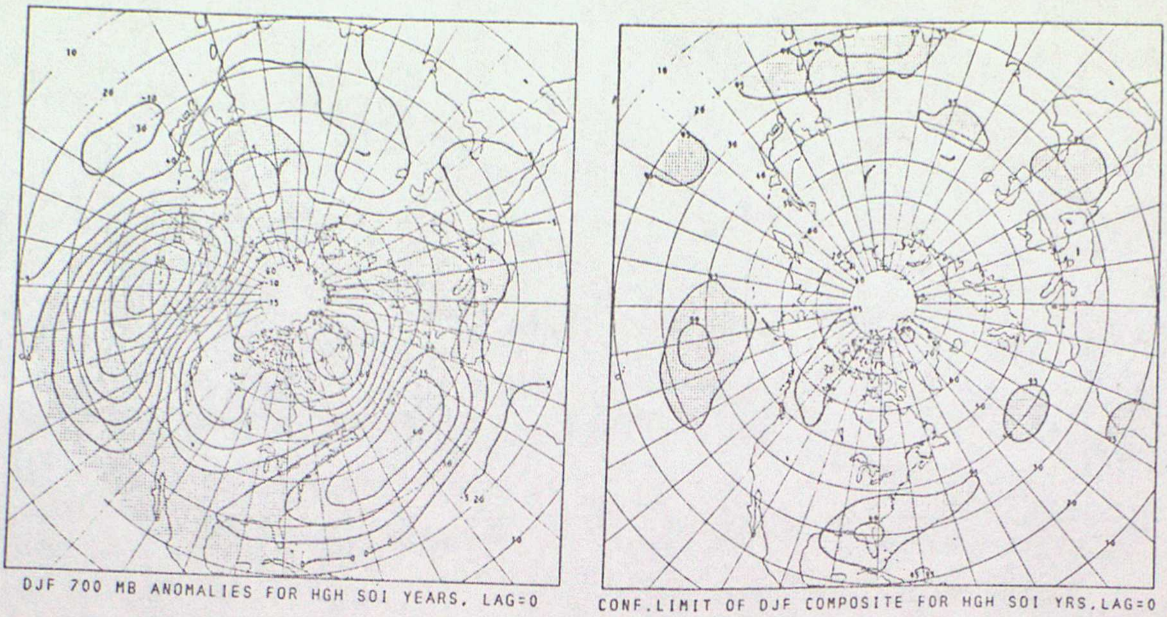

DJF 700 MB ANOMALIES FOR HGH SOI YEARS, LAG=0

CONF.LIMIT OF DJF COMPOSITE FOR HGH SOI YRS,LAG=0

FIG 5·20a

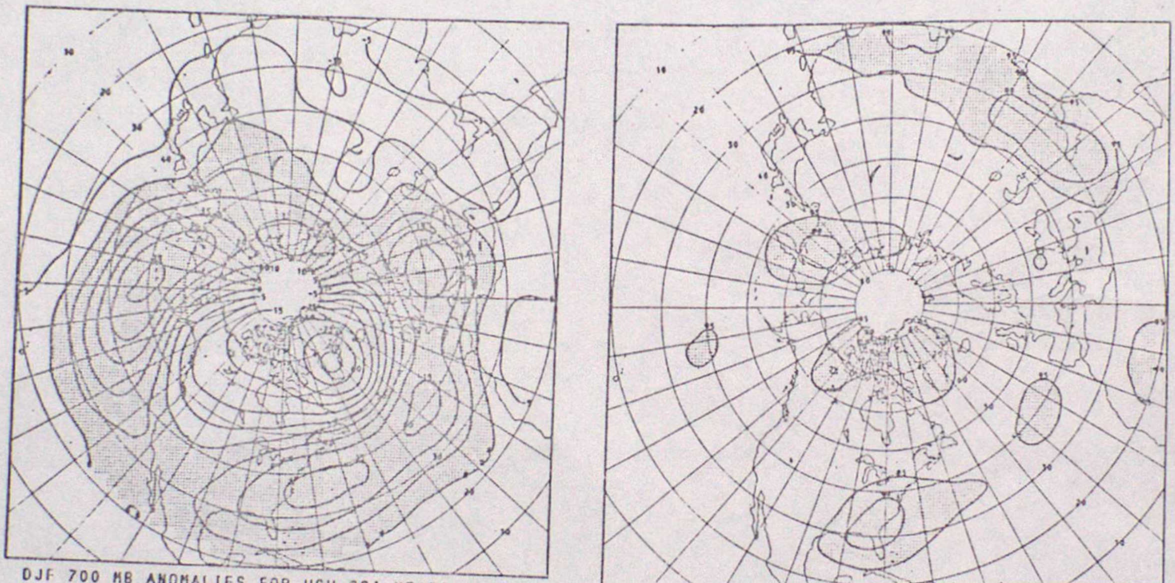

DJF 700 MB ANOMALIES FOR HGH SOI YEARS, LAG=1

CONF.LIMIT OF DJF COMPOSITE FOR HGH SOI YRS,LAG=1

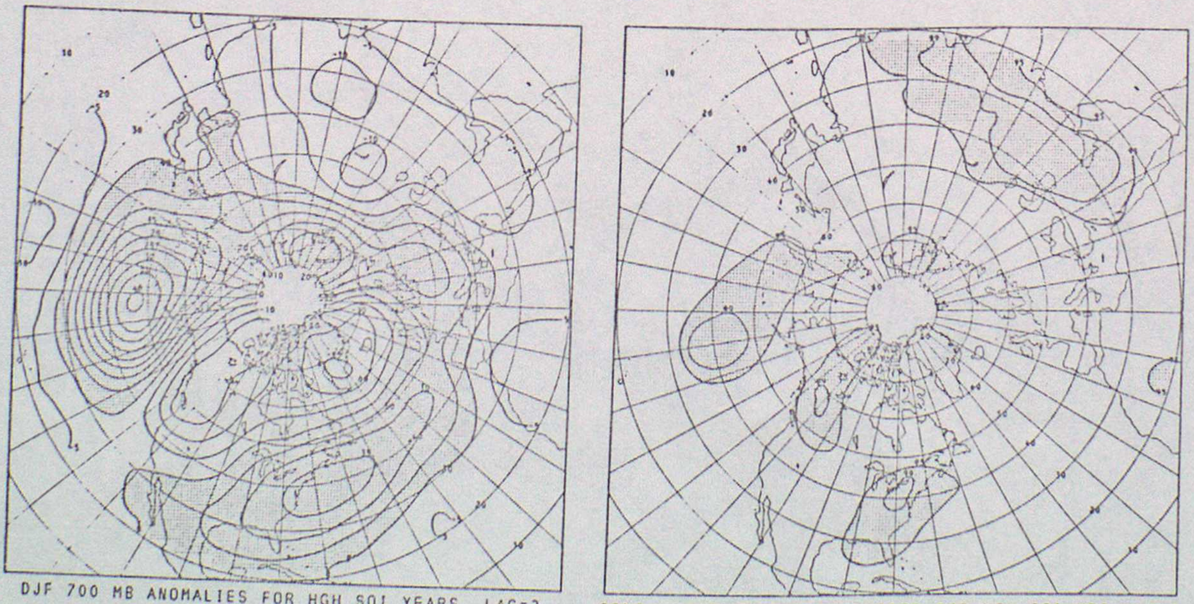

DJF 700 MB ANOMALIES FOR HGH SOI YEARS, LAG=2

CONF.LIMIT OF DJF COMPOSITE FOR HGH SOI YRS,LAG=2

.. Winter composites associated with high SOI values with the latter leading the height field by various seasons. The shaded areas are positive and the contour interval is 5 m. Confidence limits of the anomalies are presented on the right.

FIG 5·19

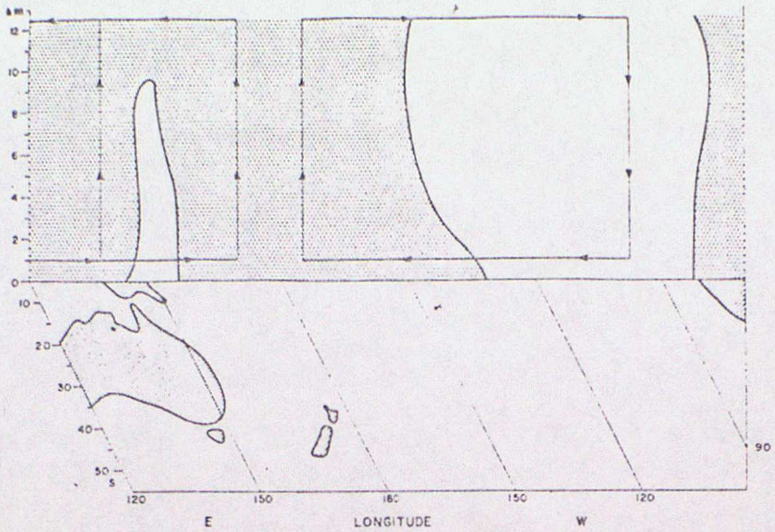

. Schematic diagram of the Pacific Walker Circulation. Shaded regions are areas of rising motion. The circulation pattern shown is the January mean for 1979–81 and is taken from Fig. 9.

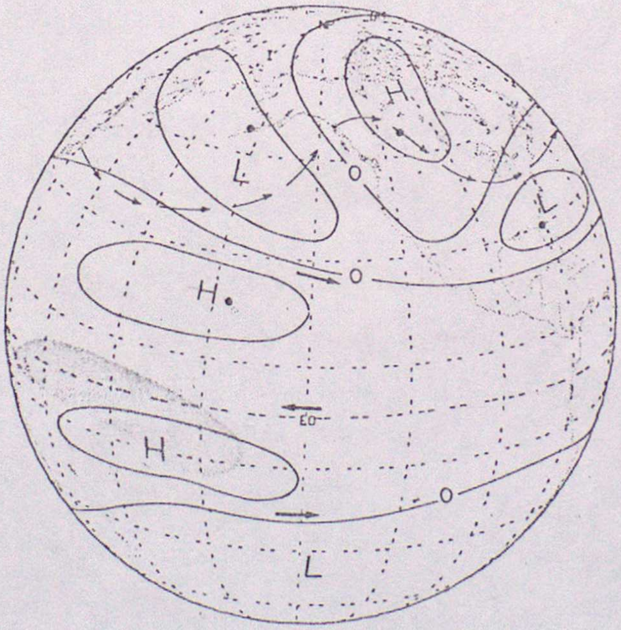

. Schematic illustration of the hypothesized global pattern of middle and upper tropospheric geopotential height anomalies (solid lines) during a Northern Hemisphere winter which falls within an episode of warm sea surface temperatures in the equatorial Pacific. The arrows in darker type reflect the strengthening of the subtropical jets in both hemispheres along with stronger easterlies near the equator during warm episodes. The arrows in lighter type depict a mid-tropospheric streamline as distorted by the anomaly pattern, with pronounced "troughing" over the central Pacific and "ridging" over western Canada. Shading indicates regions of enhanced cirriform cloudiness and rainfall. For further details see Section 7. The locations of the stations used in Table 4 are indicated by dots.

FIG 5·21

FIG 5·20b

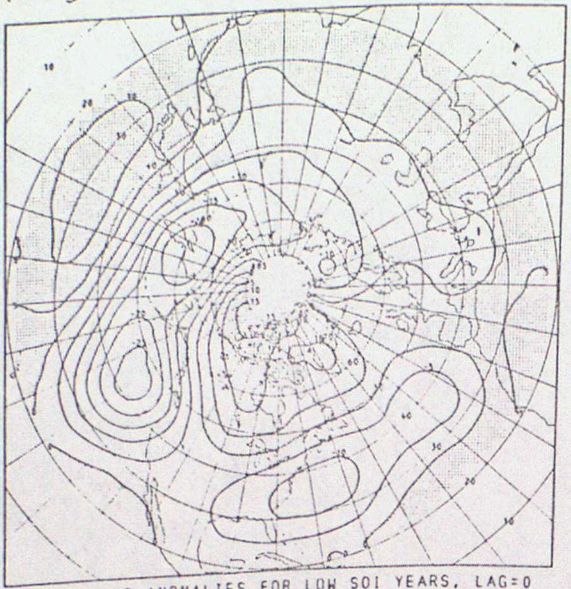

DJF 700 MB ANOMALIES FOR LOW SOI YEARS, LAG=0

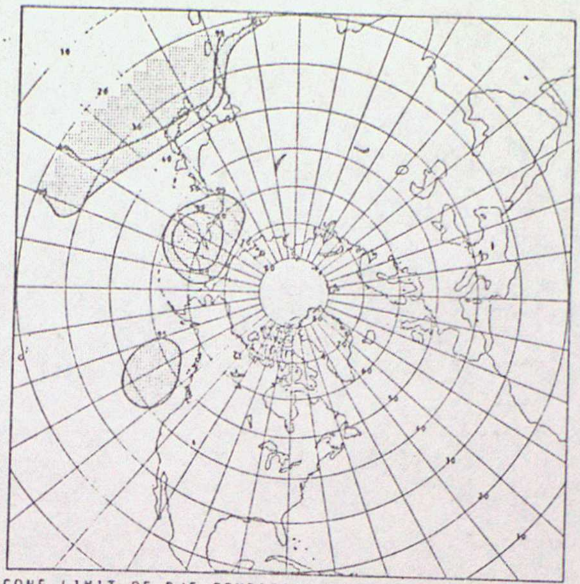

CONF.LIMIT OF DJF COMPOSITE FOR LOW SOI YRS,LAG=0

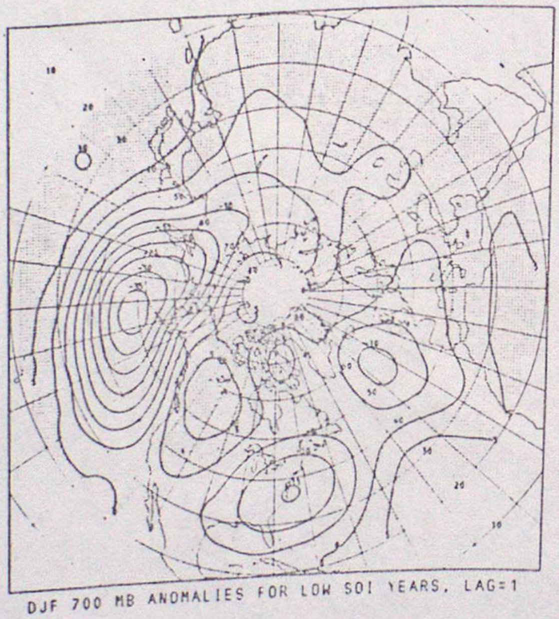

DJF 700 MB ANOMALIES FOR LOW SOI YEARS, LAG=1

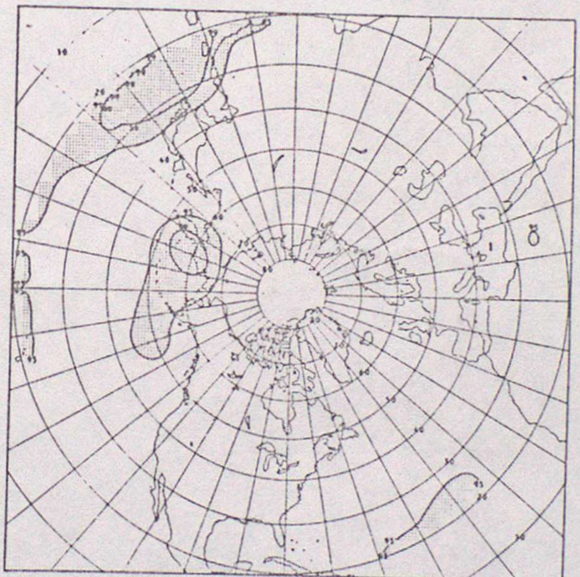

CONF.LIMIT OF DJF COMPOSITE FOR LOW SOI YRS,LAG=1

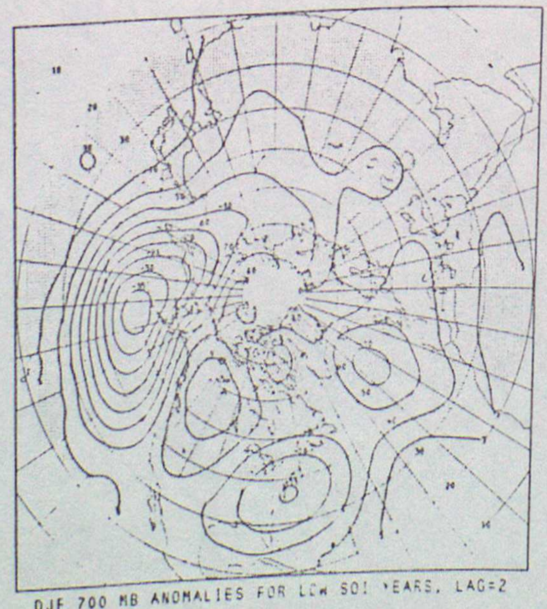

DJF 700 MB ANOMALIES FOR LOW SOI YEARS, LAG=2

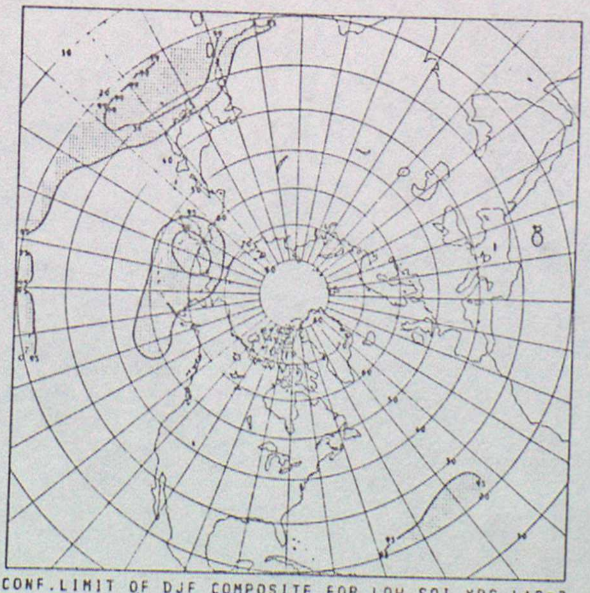

CONF.LIMIT OF DJF COMPOSITE FOR LOW SOI YRS,LAG=2

, associated with low-SOI values.

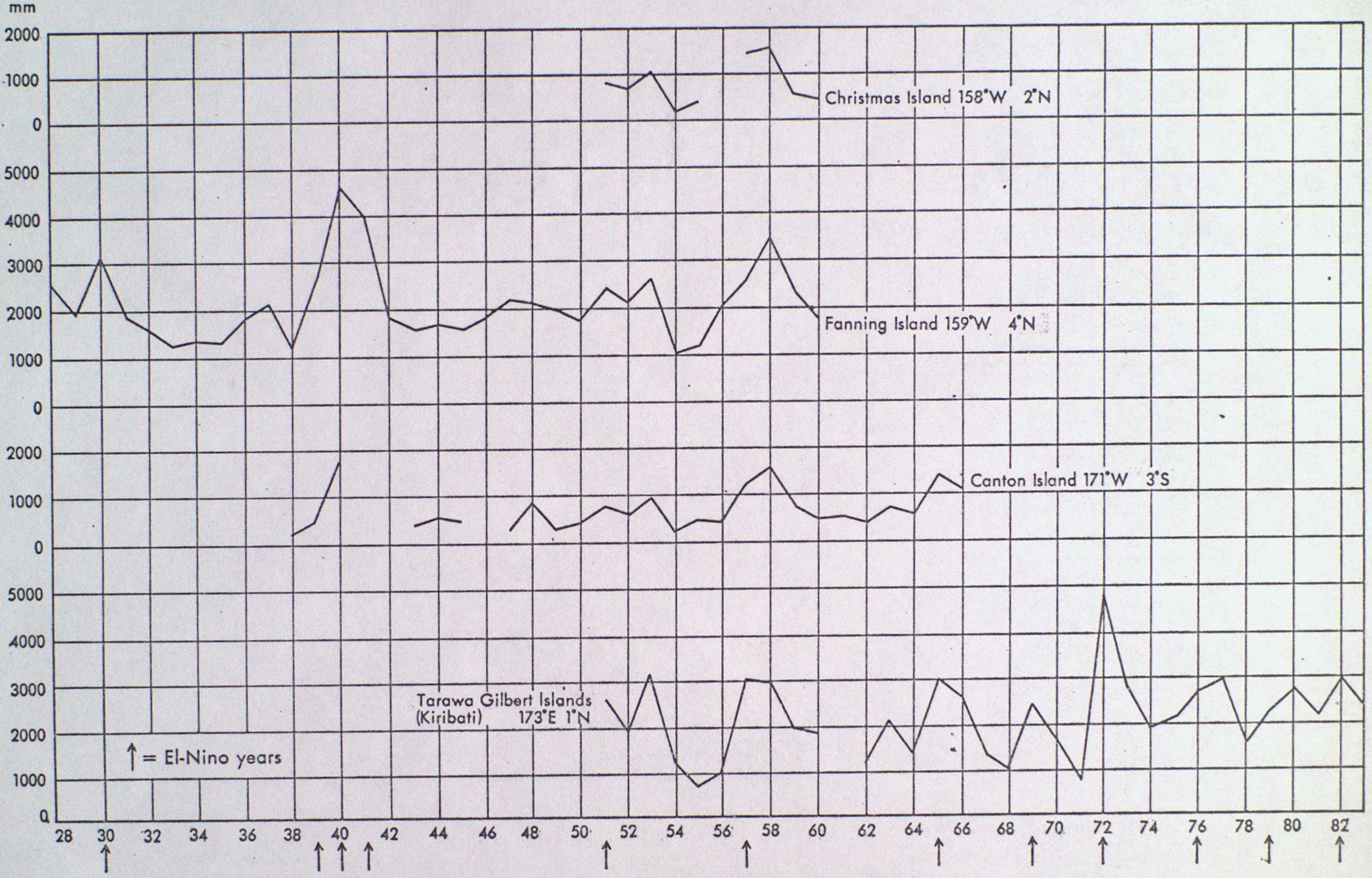

FIG 5·22

Annual rainfall at selected Pacific islands

FIG 5.23 a

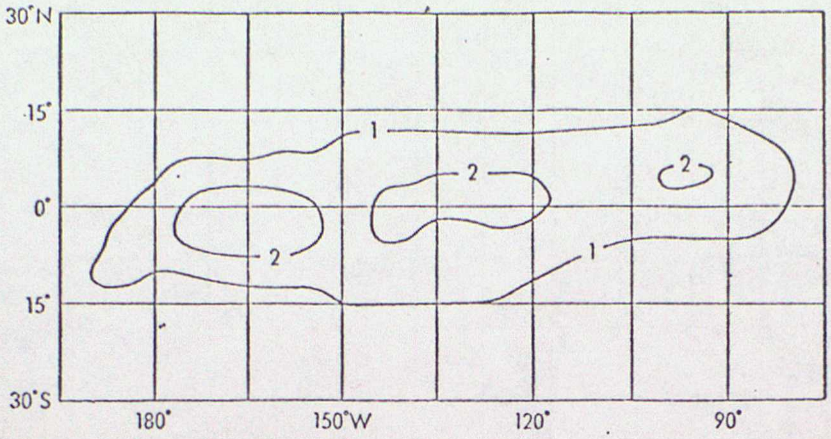
30°N
15°
0°
15°
30°S
180°
150°W
120°
90°
1
2
2
2
1

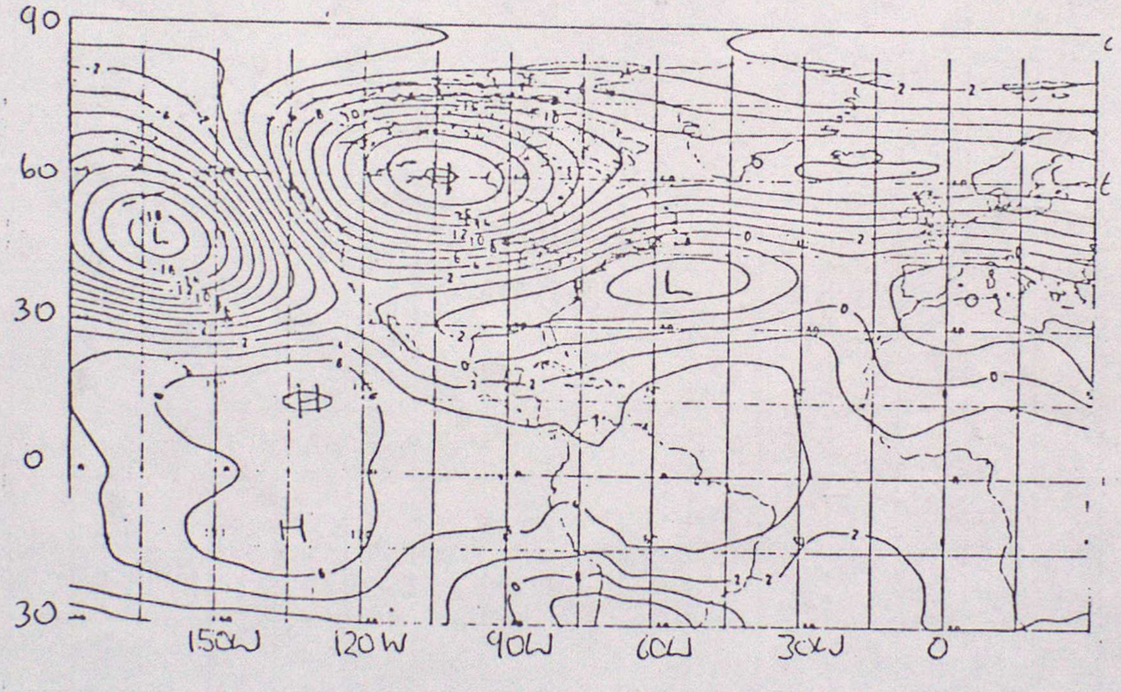
90
60
30
0
30
150W
120W
90W
60W
30W
0
L
L
H
2
0

Anomalous 200mb height (dm) for CEN.

FIG 5.23 b

FIG 5·24a

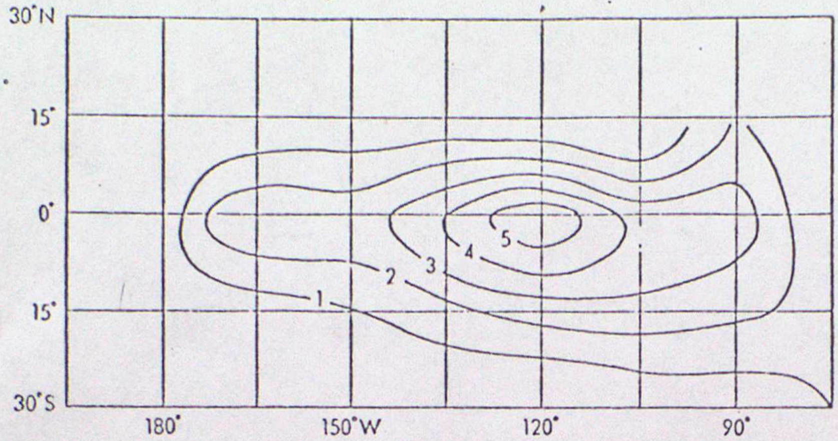
30°N
15°
0°
15°
30°S
180°
150°W
120°
90°
1
2
3
4
5

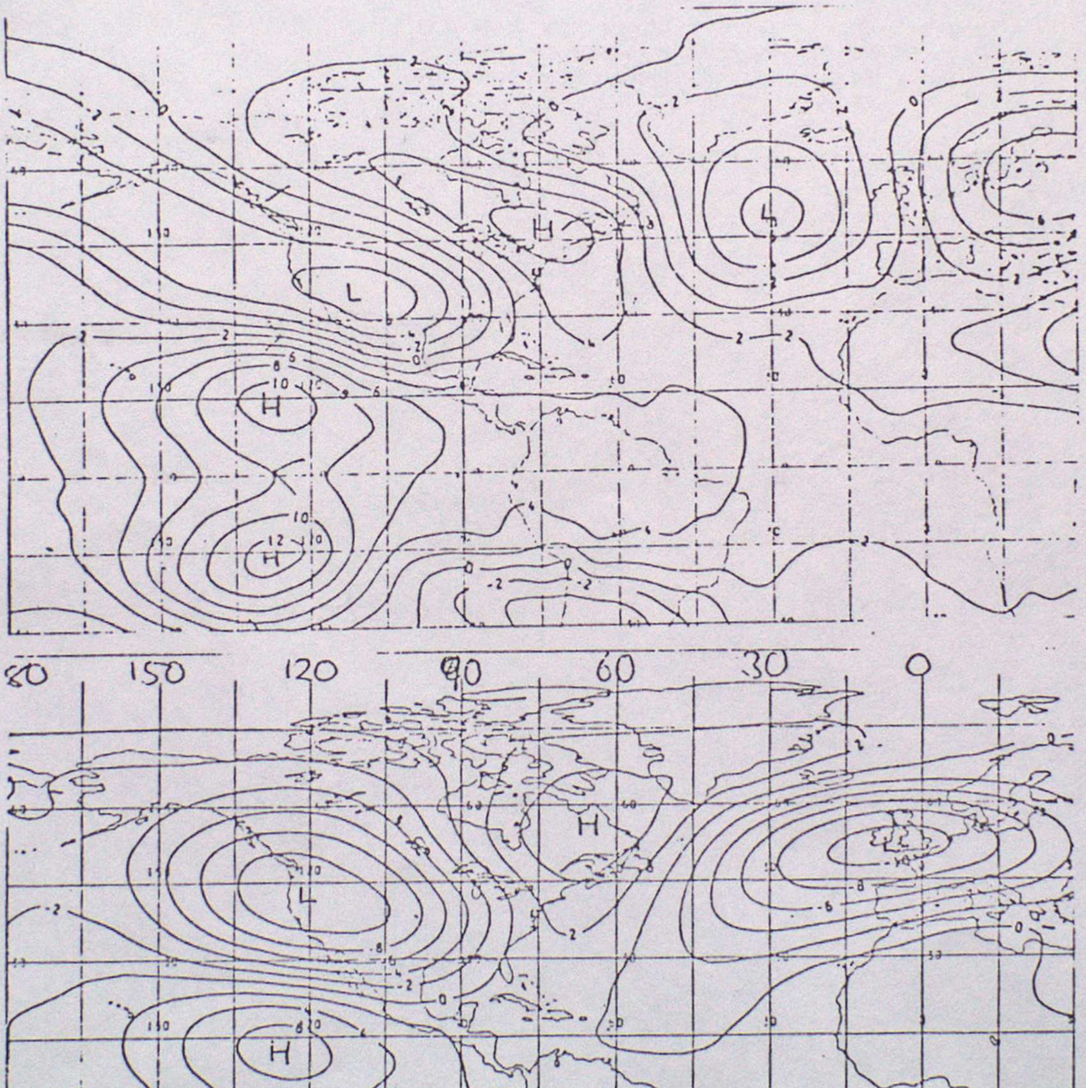
H
L
L
H
H
-2
0
2
6
8
10
12
180
150
120
90
60
30
0
H
L
H
H
-2
0
2
-6
-8

FIG 5·24b

Anomalous 200mb height (dm) for EP a) with envelope orography b) with standard orography.

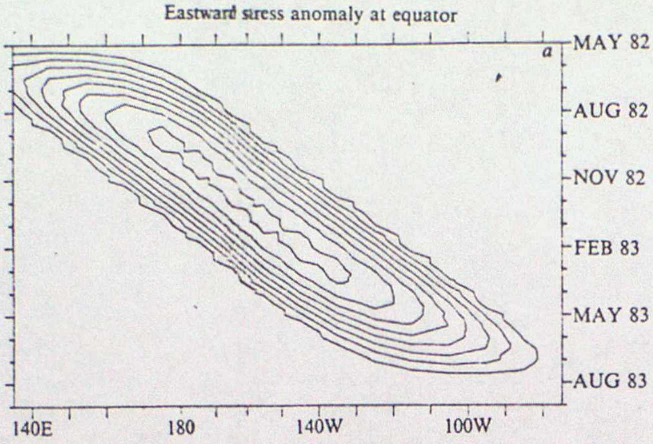

FIG 5·25

Fig. 6 Longitude–time plots along the Equator of *a*, eastward stress anomaly, *b*, surface elevation and *c*, zonal surface current. Values are averages between 5° S and 5° N. *b* and *c* are the results of a model calculation in which *a* is the forcing function. Solid contours represent positive values and broken contours negative values.

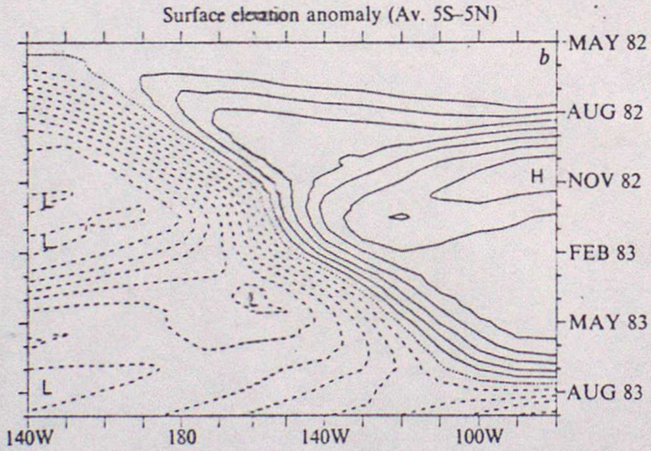

a FIG 5·26

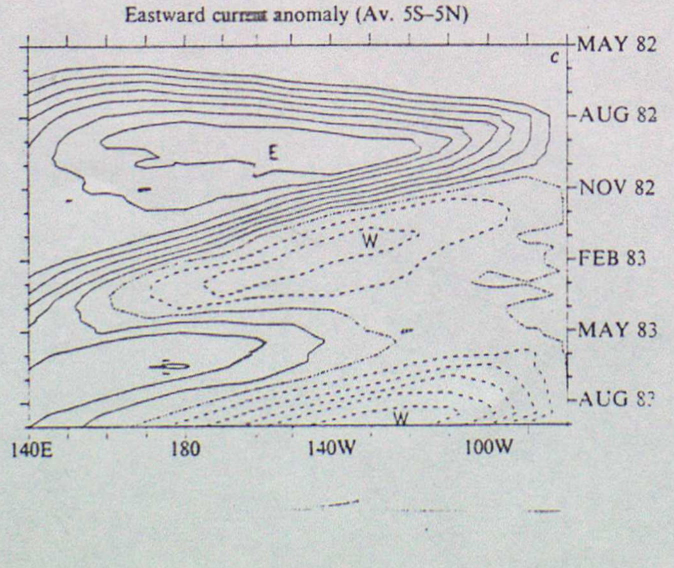

b

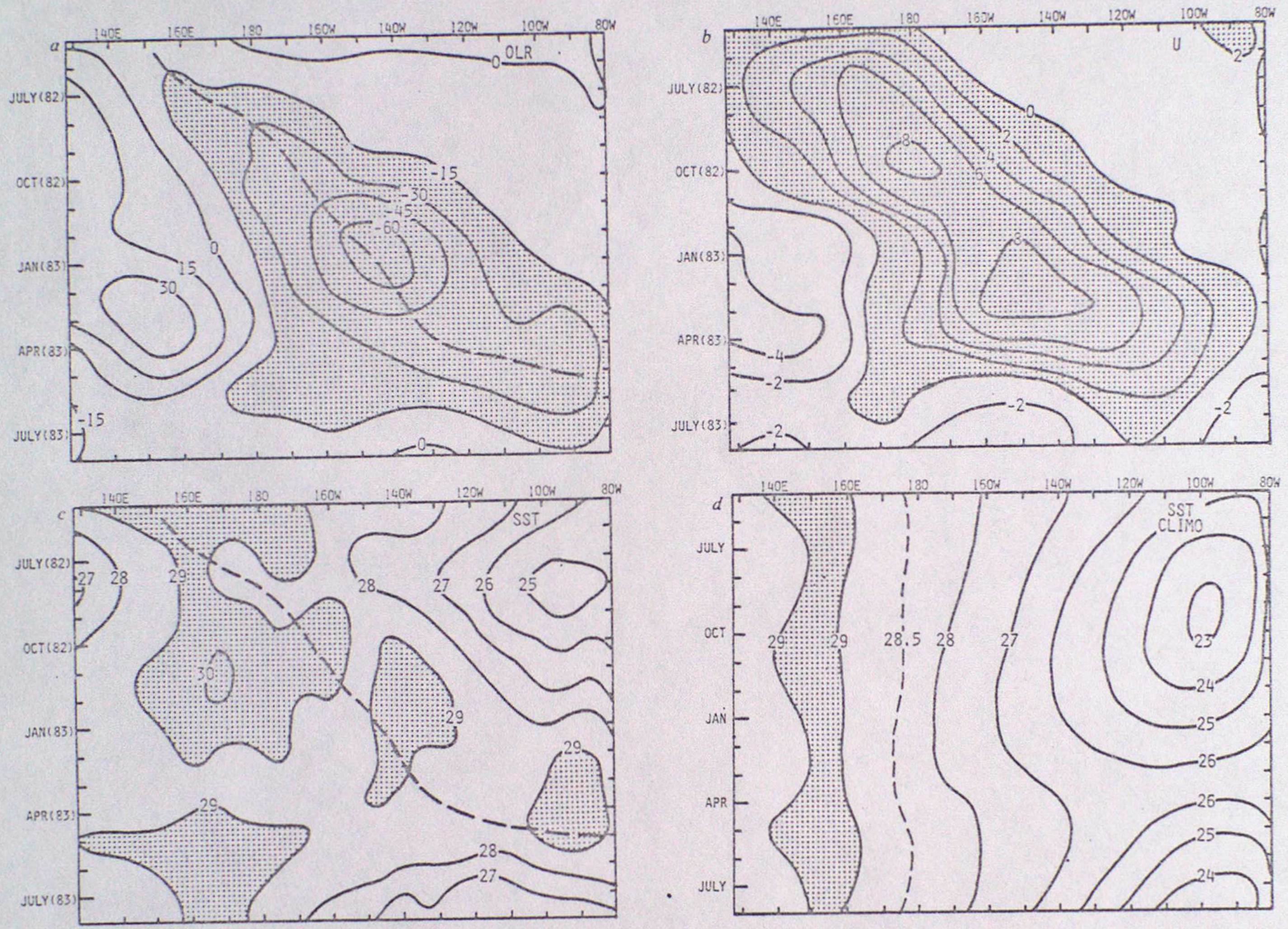

Longitude–time plots along the Equator of monthly mean values of *a*, OLR anomaly during 1982–83 in Wm^{-2}. *b*, Westerly wind anomaly (5° S–5° N) during 1982–83 in ms^{-1}. *c*, SST (4° S–4° N) during 1982–83. *d*, SST climatological mean values (from ref. 33, slightly smoothed). The dashed line in *a*, *c* follows the peak OLR anomaly.

FIG 5·27

FOR LOAN to Met Office Staff only

METEOROLOGICAL OFFICE
145729
- 7 MAY 1985
LIBRARY

ADVANCED LECTURE NO 6

CLIMATES OF THE PAST I - FROM THE EARLY EARTH TO THE PLEISTOCENE ICE AGES

6.1 Summary

Lectures 6-8 are concerned with the history of the Earth's climate. The key reference is Lamb (1977) (1). The subject is vast and I shall concentrate on selected aspects which are either particularly interesting or where our knowledge is most secure. The standards of proof for past climates can never be as high as for today's climate and many of the deductions depend on bringing together disparate strands of evidence, bound together sometimes by a measure of circular argument. The recent, limited, use of AGCM's to study specific aspects of past climates has tended to support recent empirical reconstructions; so the joint use of observations and models points the way to improvements in our understanding of the remarkable changes of climate that have occurred during the long history of the earth.

6.2 Introduction and the Faint Sun paradox

The further one goes back into the past, the more fragmented the evidence for past climates becomes and it is difficult to establish whether the evidence for a particular climatic feature is really synchronous in time.

Fig 6.1, from Lamb, shows characteristic time-scales over which some influences on climate operate. The first difficulty one meets is that of solar variability. Astronomers are convinced from theory and observation of other stars that solar luminosity has increased in the way shown in Fig 6.2. The age of the sun is placed near 4.7 billion years (b.y.) and the age of the earth at 4.5-4.65 b.y. An increase of solar constant, Q, of about 15% since the first recorded ice-age at 2,200 m.y. (million years ago) is embarassingly large. Fig 13, Appendix I to this set of lectures, which is derived from an energy-balance model, suggests that the early Earth should have been covered in ice and should not yet have escaped this fate(?). Compensating mechanisms that would increase the surface temperature include a changed composition of the Earth's atmosphere ie less oxygen and much more carbon dioxide. A much increased transport of heat from equator to pole or an increased flux of geothermal heat would presumably provide less favourable conditions in high latitudes for the onset of glaciation. The latter possibility is not now thought to be significant.

Endal and Schatten (1982) (2) used a simple energy-balance climate model due to North (See Appendix I to this set of lectures) to see if an ice-covered earth having today's atmospheric composition could be avoided if they increased a parameter D that is used in North's model to represent eddy diffusion of heat across latitude circles. Fig 6.3 shows some results which have some complex features; concentrating on D = infinity, an ice-free earth is just possible for $Q/Q_0 = 0.81$ (Q_0 = today's solar constant). The slope of the line $D = \alpha$, (and adjacent lines), is negative so once ice forms, the model solution jumps to a completely ice-covered earth. The addition of an atmospheric greenhouse effect would obviously

ORGS UKMO
National Meteorological Library
FitzRoy Road, Exeter, Devon. EX1 3PB

3 8078 0007 8125 4

help to increase temperature but would have to be (a) very large 2,000 million years ago (b) have declined since that time at a rather precise rate to have avoided a later "white" earth catastrophe.

6.3 Evidence for climate of the Earth 2500-200 m.y.

Fig 6.4, taken from Lamb lists the geological eras, their divisions into periods and their sub-divisions into epochs. Fig 6.4 also summarises some opinions about past climates. Fig 6.5 gives a simpler summary of the likely times of ice-age cycles.

6.3.1 Dating ancient rocks - how do we know when geological features were formed?

Dating past rock formations is complex and a main preoccupation of geology. In the ancient past, the relative ages of rocks can be estimated by studying the order in which they were laid down (stratigraphy). Absolute dating requires measurements of the proportions of various radio-active isotopes existing in the rocks, so that use of a specific method would depend on whether a given chemical element exists in the rock. Two examples are given:-

(1) The decay of the radio active isotope of potassium ^{40}K to ^{40}A has a half-life of 1.3×10^9 years. So measurements of the amount of argon gas trapped in the rock expressed as a ratio of the amount of ^{40}K still remaining can be used to date some ancient rocks. Extremely old rocks can sometimes be dated using the decay of ^{87}Rb to ^{87}Sr (the rubidium-strontium method); the half-life of this decay is very long: 53×10^9 years. For details of other methods and references see Lamb, pp 70-72.

6.3.2 Earliest evidence of past climate

The first half of the Earth's history has left rather little evidence in its rocks but the second half is increasingly rich in indications of past conditions. For most of the Earth's more recent history the climates have been warmer than now but there is much evidence that from that time to time the climate has cooled, at least in some parts of the world. The earliest record of glaciation is the Huronian of about 2250 million years ago (3) discovered in the USA in the region of Lake Huron. There is little evidence of glaciation in the next 1000 million years but the Precambrian period of 950-650 million years ago produces evidence of (perhaps) three widespread glaciations down to quite low latitudes.

Harland and Herod (3) discuss the Precambrian glaciations but it is difficult to make reliable deductions as the relative proportions and extent of the continents at that time are not well known. However, Harland and Herod believe that the Precambrian ice-sheets have at least approached the equator so there is a possibility that a close approach (surely not reached!) to a "white" Earth occurred at that time.

6.3.3 Cambrian (500 m.y.) to Permian (200 m.y.) times

Understanding of this period of Earth's history has been revolutionised in the last few decades by the ideas of continental drift and plate tectonics. A lively account is given by Tarling and Tarling (4). Some details remain controversial, but the crucial step that converted speculations about the meaning of remarkable geometrical fits between various continents (especially if their shapes were measured near the edges of the continental shelves) into an almost universally accepted theory of continental drift involved the measurement of remanent palaeomagnetism in ancient rocks. When rocks containing iron cool, they retain a remanent magnetism that reflects the local earth's magnetic field at that time (ie the angle of dip, magnetic north vector etc). From time to time, geologically very sudden changes in the direction of the remanent magnetic field occur, usually by 180°. This indicates a recurring total reversal of earth's magnetic field. These reversals can be followed in many continental rocks; The last reversal occurred dc 730000 years ago. Even more convincingly, these ancient magnetic fields are preserved with great clarity in the basaltic ocean floors as a series of magnetic stripes so that each stripe is reversed in polarity by 180° with respect to adjacent stripes. These observations indicate that the ocean floor is continually being formed by spreading out from the observed volcanically active (submerged) mid-ocean ridges. The convective cells in the Earth's mantle that caused the sea-floor spreading also provide the energy to move the continents or at least individual continental blocks known as "plates". So it is possible to fix the latitudes of the plates in ancient times by measuring the remanent palaeomagnetic vectors using a magnetometer, and assuming that Earth's magnetic poles were always near the geographical pole.

Fig 6.6(a) and (b) give reconstructions of the continents 500 m.y., 340 m.y., 250 m.y. and 50 m.y. as illustrated by Lamb. The changing positions of the continents are likely to affect climate:-

(a) Locally, as the latitude of a given location changes eg Fig 6.6 shows that England both "existed" and was probably near 15°S at 340 m.y., 15°N at 250 m.y. and 40°N at 50 m.y.

(b) Because the global proportion of land in higher and lower latitudes progressively changes.

(c) As a result, the meridional heat flux (equivalent to D in Fig 6.3) should change with the changing ocean currents and atmospheric circulation.

Fig 6.7, taken from Sellers and Meadows (1975) (5), shows how the broad pattern of ice ages shown in Fig 6.5 is reflected in variations in the fraction of land estimated to have occupied latitudes higher than 60°N or 60°S. So a large land surface may be required in high latitudes whose albedo can be increased by snow and eventually by ice but some mechanism for delivering large quantities of precipitation to these surfaces over long periods would also be needed.

Figs 6.8 and 6.9 show two reconstructions of past glaciations:-

(a) Ordovician times (about 400 m.y.)

(b) In Permo-carboniferous times (about 250 m.y.)

The Ordovician ice age affected the Sahara and parts of S America. Before the widespread acceptance of continental drift, this glaciation posed a severe problems to climatologists who had to invent a climate with both an equatorial ice cap and no high latitude ice caps. Brooks (1949) (7) proposed an elaborate theory of a world containing an ice cap in equatorial regions only. The evidence for the Ordovician ice age is strong, with eroded but recognisable geological features which are widespread in parts of the dry Sahara eg in the Tibesti Mountains; the remnants include U-shaped valleys, glacial morains etc. The subsequent Permo-carboniferous ice age affected Antarctica, Australia and S India. In fact Antarctica has propably remained quite close to the S Pole since that time (Fig 6.6) and given the difficulty of obtaining evidence from Antarctica, it is not absolutely clear whether deglaciation has ever been complete since Permo-carboniferious times. Finally both glacial periods show signs of interglacials, as in the recent ice age, but the geological evidence is only capable of showing gross fluctuations.

6.3.4 Cosmic theories of ice ages

The apparent rhythmic nature of the 3 or 4 Ice Age epochs since the late Precambrian has prompted theories about their possible cosmic origins. Cosmic factors would now be regarded as additional to those involving continental drift.

One theory due to Urey (see 8) suggests that the sun varies in its radiation output as it goes round the Galaxy. This would produce variations on time scales of 250 million years. Another theory (due to McCrae),which would produce solar radiation variations on the same time-scale, concerns the fact that as the solar system orbits the centre of our galaxy, it passes through galactic dust clouds which reduce the solar constant (8). We are currently in a glacial period and these dust clouds are not now evident so the theory seems to assume that the most recent ice age epoch has finished.

6.4 The Mesozoic and Cenozoic Eras, excluding the Pleistocene Epoch (200-3 m.y.)

6.4.1 Mesozoic era

This era was the heyday of the dinosaurs. Fig 6.6 indicates that both Poles were open or virtually open to the global ocean circulation and no evidence of glaciation has yet been found but considerable evidence of warm climates has been found. This is a period when limestone rocks were laid down, many of which show a banded structure with depth; evidence has started to accumulate that these structures are associated with Milankovitch radiation variations but this idea is very recent and on the face of it puzzling in the absence of a glaciation-deglaciation cycle. Interested readers should refer to the two volumes on "Milankovitch and Climate" published in 1984 which are referenced later in this lecture. The latter part of this period is mysterious; quite suddenly the dinosaurs and many other animals died out in what appeared to be mass extinctions. There is accumulating geological evidence of a volcanic or meteoric "glassy" layer in the rocks in several parts of the world dated at about 65 m.y. So it is possible that massive volcanism or an impact with a giant meteorite may have occured, perhaps causing mass extinctions via the "nuclear winter" effect. If so, the climate did not change for long enough for the evidence to have survived, and no ice-age resulted.

6.4.2 Cenozoic Era - Tertiary period

The Tertiary provides the first quantitative evidence for the values of ocean temperatures. The main tool is the measurement of the quantity the isotope of oxygen ^{18}O in marine foraminifera, which are types of plankton whose ancient shells are found on the ocean bed. Appendix I to this lecture describes the oxygen isotope method of measuring palaeo-temperatures. The shells are made of calcium carbonate and Fig 6.10 shows an example: the species globorotalia menardii. We shall discuss these types of measurement in the next section, but remark here that the ^{18}O method requires measurement of the ratio of $^{18}O/^{16}O$ in the calcarious shells. Unfortunately, this ratio depends not only on ocean temperature but whether the ratio in the oceans themselves changes. Such changes would occur if glaciers formed on land when ^{18}O would rise in the oceans as the glaciers developed. The USA Deep-Sea Drilling Project has provided over the last 30 years many deep-sea sedementary cores containing these shells. Because the length of the cores that can be extracted from the ocean bed is currently limited to about 20 m areas of the deep ocean which have a very low sedementation rate are required for measuring temperature profiles through the long time interval encompassed by the Tertiary. Dating of these cores can sometimes be done using the magnetic reversals mentioned before. In addition, the relative proportions of different planktonic species in the sediments and whether certain species are present or not can be used as a guide to past sea temperatures. However this gets more difficult in the Tertiary as some species have changed since that time. The sea temperatures which the planktonic shells represent depend of course on the depth at which the plankton lived. Some lived near the surface but other forms lived at great depths and these must be correctly identified. Fig 6.11 is a generalised picture of the variation of worldwide tropical ocean temperatures deduced by several workers from such cores. This interpretation has been challenged (9) and alternative explanations of these measurements include a period of low tropical SST with no ice or a period of high tropical SST with a considerable amount of land ice. Fig 6.12 shows other evidence of climate variations through the Tertiary which suggests a gradual reduction in temperatures towards the present. About 30 m.y., Antarctica and S America drifted far enough apart so that the Drake Passage between them opened up sufficiently for a free flow of water. This is thought to have changed the ocean circulation and helped give rise to a gradual reduction in ocean bottom water temperatures. There is considerable evidence of glaciation in Antarctica from about 17 m.y. (10) and it is now thought that Antarctica has remained partially or wholly glaciated since that time.

6.5 The Quaternary (Pleistocene) Ice Ages (from about 3 m.y.-15000 BP)

Imbrie and Imbrie (1) contains an easy-to-read account of the history of the evidence and ideas about the Ice Ages. In the last decade there have been two major developments in ideas:-

(1) Evidence is now strong that the ice age/Interglacial oscillations have been almost regular on a 100000 year time scale for the last 800 k.y. and possibly for considerably longer. This regularity has been shown to be related to the Milankovitch radiation variations discussed in Lecture 3. So theories that require random internal variations of the climate system to be the prime initiators of ice ages do not seem to be correct, even if "random changes" play a subsidiary role.

(2) Recent calculations using GCM's suggest that Milankovitch radiation variations are of sufficient size to strongly affect the integrations. However it has not yet been possible to work out the causes of the formation and destruction of the ice age continental ice sheets in any detail, though a number of "simple" models of ice sheets have been constructed, giving a variety of results.

So although many influences have undoubtedly been at work, the Milankovitch radiation variations can probably be regarded as the "pace-makers" of the ice ages. The evidence for this contention will be briefly reviewed, one or two major difficulties highlighted and a couple of GCM integrations carried out for Ice Age radiation conditions are discussed which that sum up the problems and prospects.

6.5.1 Empirical evidence for Milankovitch effects

6.5.1.1 The Wrong Evidence

Until fairly recently, a major problem was that crucial observational evidence concerning the timing of past ice ages was wrongly interpreted (Imbrie and Imbrie (11)). Fig 6.13 shows a diagram of the four Pleistocene ice ages which you may have heard about at school - the Mindel, Riss, Gunz and Wurm ice ages which were worked out by Penck and Bruckner early this century (Imbrie (12)). It has been shown that, except for the Wurm ice age, the other ice ages simply did not exist. The timing of the Wurm ice age was roughly coincident with what is now known to have been the timing of the last glacial maximum but this is regarded as Imbrie as an accident! The four glaciations were derived from a study of glacial deposits in the Alps; not only have the dates ascribed to the earlier glacial deposits been shown to be incorrect, but the stratification of these glacial deposits has been shown, apparently, to result from tectonic movements and has had nothing to do with climate change at all!.

6.5.1.2 A breakthrough

The initial breakthrough probably came in 1973 when Shackleton and Opdyke (13), following pioneering work by Emiliani (see 11 for references), produced convincing estimates of the fluctuating volume of ice on the global continents over much of the last million years. This evidence was deduced from a study of plankton shells in a deep sea core in the equatorial Pacific using the oxygen isotope method. (Please see Appendix

I for a description of the oxygen isotope method). Absolute dating of deep sea cores is difficult unless palaeo-magnetic field reversals can be detected. Shackleton and Opdyke chose a core which could provide detail on much less than a 10,000 year timescale but which nevertheless extended beyond the most recent known magnetic field reversal horizon, known as the Brunhes-Matuyama magnetic reversal. This reversal is now dated at about 730,000 k.y., and its detection in the core allowed the age of different sections of the core to be fixed reasonably well. It is known that deep-ocean sedimentation rates vary in time and cores can be compressed at depth; so this core by itself did not provide an absolute age for most of the temperature variations deduced from the oxygen isotope method. However, it turned out that the relative ages could be deduced quite well given the one measurement of absolute age described above as sedimentation rates do not vary greatly (see Fig 6.14). In Fig 6.14 the ups and downs in $\delta\ ^{18}O$ should be (mainly) a record of the changes of ice volume; thus less negative values of $\delta\ ^{18}O$ correspond to more ice and/or lower sea temperature. Seven quasi-regular major peaks and troughs can be seen with superimposed higher frequency fluctuations. This (and previous cores) suggested that seven ice ages occurred at roughly equal intervals back to 730,000 k.y., because the record of $\delta\ ^{18}O$ from any one core should be mainly a record of variations in the worldwide volume of ice on land. It was found possible to match this long core to many previously analysed, shorter, cores obtained elsewhere in the ocean and it began to seem that major ice ages tended to recur at almost fixed intervals of 100,000 years. Spectral analysis of the core in figure 6.14 suggested strongly that periods of roughly 41,000 and about 22,000 years were present in addition to a 100,000 year peak; these time scales correspond to those of variations in "Milankovitch" northern and southern hemisphere seasonal radiation as described in Lecture 3, shown now in spectral form for several latitudes and months in Fig 6.15. Fig 6.16 shows a later deep sea core (using similar analytic methods) that seemed to support Shackleton and Opdyke's results, together with its spectrum. (See Reference 11 for more details). Lecture 3 showed some of the solar insolation variations as recalculated by Berger and Pestiaux (14); please refer there. A puzzle however was that no spectral peak of 100,000 years exists in the Milankovitch radiation variations, even though this time scale is dominant in the cores. Nevertheless the amplitudes of the higher frequency seasonal radiation peaks are amplitude modulated on the 100,000 year time scale by variations in the eccentricity of earth's orbit.

6.5.1.3 Strong Confirmation of the Ice-Age Milankovitch Link

In 1982, Imbrie et al presented a key paper at a special conference held in USA to debate the Milankovitch radiation variations and their effect on climate. This paper brings together the five most reliably analysed deep-sea ocean cores and their $\delta\ ^{18}O$ records, three of which are long enough to reach the Brunhes-Mutuyama magnetic reversal (15). The locations of these cores are shown in Fig 6.17, while Fig 6.18 shows the $\delta\ ^{18}O$ data filtered on the obliquity (41,000 year) and precession (19000 -23000 year) time scales separately, together with similar curves for the amplitude and phase of the astronomical variations of obliquity and precession. Both pairs of curves are normalised to the same vertical scale and small, constant, offsets between the astronomical and $\delta\ ^{18}O$ curves have been removed. The match in amplitude and phase between the $\delta\ ^{18}O$ and astronomical curves is striking as this type of test is quite a sensitive one. However it must be pointed out that this excellent match does reflect several artificial adjustments to the data which chiefly affect the phase match. It is still difficult to explain, in terms of the Milankovitch radiation variations, the dominant 10^6 year cycle in the deep sea cores as 10^6 year amplitude modulation of the shorter time scales turnsout not to be a convincing explanation because it is not consistent in magnitude. Many tentative explanations have been given of this cycle relating to the dynamics of ice-sheets and the time it takes for the sheets to form and to melt. Another factor is that when ice sheets form, the rocks beneath sink and when the ice sheets melt it can take a long time for the rocks to recover. So, if for example, an extensive area of land above a certain altitude in a critical geographical situation was required for glaciation to start during a summer radiation minimum, it could take many thousands of years after the ending of a previous glacial period before this altitude was again reached. At the moment ideas are changing about the time scales involved, which could be much longer than hitherto supposed for an area of millions of km^2 occupied by say the N American ice sheet.

6.6 Conditions at the glacial maximum

(We shall use "BP" = "Before present" for ages here).

An interdisciplinary project called CLIMAP (Climate Long-Range Investigation Mapping and Predictions) has attempted to reconstruct the geography of the Ice Age ice sheets and the values of surface ocean temperatures for each month of the year for about 18,000 BP. Evidence was derived from land geology measurements of $\delta\, ^{18}O$, and most importantly, the distribution of species of surface-dwelling plankton found in deep-sea cores which were used as palaeo thermometers. If we know the current distribution of different kinds of plankton and can relate these to variations of sea temperature, then for a period as recent as 18,000 BP for which evolution of species is not a problem, we can reconstruct past distributions of SST. A complex, multivariate analysis scheme was used to estimate worldwide calendar monthly ocean temperatures. Fig 6.19 shows the reconstructed global SST, together with the extent of the land and ocean ice sheets for August 18,000 BP. Fig 6.20 shows, for the North Atlantic, an estimate of the change of SST from modern values; this ocean cooled most. See Reference (11) for further details and references.

6.7 Numerical model experiments

6.7.1 Manabe and Broccoli (1984) (17)

MB used a coupled mixed ocean-layer spectral AGCM. They set out to determine what the physical effects of the land ice sheets existing at 18,000 BP on SST might be. The model was integrated for 20 model years and the last 5 years of the integrations averaged. So all months of the year were modelled.

(a) Control experiment

Modern continental ice, today's radiation conditions.

(b) Anomaly experiment

CLIMAP continental ice, today's radiation conditions (at 18000 BP the radiation conditions happened to be similar to today's, as the summer minimum and winter maximum in the N Hemisphere ~~was~~ WERE several thousand years previous to this time).

Fig 6.21 shows the difference between anomaly and control experiments and also the difference between the SST values reconstructed by CLIMAP for 18,000 BP and today's values in February and in August. In the N Hemisphere, SST's in the anomaly experiment are much lower in both months in the N Atlantic and N Pacific, and these changes agree quite well with the CLIMAP reconstructions. In the S Hemisphere the differences in SST between anomaly and control experiments are mostly positive so that S Hemisphere SST was mostly warmer in the anomaly experiment, ie at 18000 BP. The CLIMAP reconstruction shows that some areas by the S Hemisphere were warmer but many areas were substantially colder than now. The model results suggest, therefore, that the presence of the N Hemisphere ice sheet may have little effect on SST in the S Hemisphere. The reason (in the model) appears to be that although the S Hemisphere reflected more incoming solar radiation at 18,000 BP, this was almost exactly compensated by a lower emission rate of long wave radiation. So an insignificant change in net hemispheric heat exchange occurred to balance the heating difference. Thus some other mechanism may be needed to provide the observed cooling of the S Hemisphere. MB suggest that recent measurements (see Lecture 9) that show a lower concentration of carbon dioxide in the atmosphere at that time might provide the missing physical effect. So it is still something of a puzzle as to why both hemispheres suffered glaciation at the same time; radiation was of course near a maximum in the southern summer at this time, rather like now.

6.7.2 Royer et al (1984) (18)

Royer et al studied the annual cycle of climate at 125,000 BP when N Hemisphere radiation was at a maximum and at 115,000 BP when N Hemisphere radiation was at minimum. The earlier date coincided with the last interglacial, now known as the Eemian. The orbit of the earth was highly eccentric at both times (e = 0.05) so an especially large change in N Hemisphere summer radiation occurred between these two dates. The experiment was rather short, the model being integrated only through one annual cycle. In both cases the modern distribution of land ice and modern values of SST were assumed. We shall highlight only one aspect of the results - does the model provide evidence that ice might preferentially form in eastern Canada in 115000 BP where the largest of the continental ice sheets in fact developed in recent Ice Ages (Fig 6.20). Fig 6.22 shows the difference in simulated annual mean surface temperature 115000 BP-125000 BP. The largest cooling in the N Hemisphere at 115000 BP is indeed in Eastern Canada. Furthermore model soil water content, which includes the effect of snow accumulation, also increased in this region. Fig 6.23 shows the differences in PMSL. It was found that the model maintained colder conditions in most of the year in Eastern Canada partly due to higher pressure in winter at 115,000 BP (despite increased winter radiation) but also due to cloudier summers which of course were accompanied by less solar insolation. So the results of these experiments, although tentative, are encouraging.

APPENDIX I LECTURE 6

OXYGEN ISOTOPE METHOD FOR DEDUCING GLOBAL ICE VOLUME, OCEAN TEMPERATURE AND AN INDEX OF AIR TEMPERATURE OVER LARGE LAND GLACIERS

A(1) δ in polar ice

Consider the evaporation of water from the ocean surface (Fig 6AI). There are three oxygen isotopes ^{16}O, ^{17}O, ^{18}O, of which ^{17}O can be neglected. The average ratio of $^{16}O:^{18}O$ in today's oceans is 998:2. The vapour pressure of (A) $H_2\,^{18}O$ is less than that of (B) $H_2\,^{16}O$; the ratio $^A/_B = 0.99$ at 0°C and 0.992 at 25°C and the difference continues to reduce at higher temperatures. So there is always a lower fraction of ^{18}O in atmospheric water vapour than in the ocean. Now, $H_2\,^{18}O$ vapour preferentially condenses into the liquid or solid form as its vapour pressure is lower than that of $H_2\,^{16}O$. The ratio A/B above suggests that condensation will produce relatively more ^{18}O in rain and snow at lower temperatures than at high temperatures. This effect is offset at higher latitudes by (a) the fact that the water will have been derived from cooler seas (mainly sub-tropical or mid-latitude) so less ^{18}O is evaporated than in the tropics and (b) most importantly, condensation and precipitation at higher latitudes and altitudes will be from water vapour already further depleted in ^{18}O by preferential condensation and precipitation of $H_2\,^{18}O$ vapour at lower latitudes and lower altitudes. The process becomes impossibly complex to unravel if precipitation falls on land and is re-evaporated and reprecipitated so measurements of ^{18}O in frozen precipitation on ice sheets only have a (rough) meaning if the precipitated vapour is (mostly) derived directly from the oceans. The amount of ^{18}O is measured by δ:-

$$\delta = 1000 \left(\frac{^{18}O/^{16}O\text{ (sample)} - ^{18}O/^{16}O\text{ smow}}{^{18}O/^{16}O\text{ smow}}\right)$$

smow = standard mean ocean water. In one set of measurements (Dansgaard (1964)) quoted by Lamb (1);the following was found ($\delta_p = \delta$ in precipitation:)

At Valentia $\delta_p = -6$ annual mean surface air temp $T_a = 11$°C
At Upenowsk (Greenland) $\delta_p = -18$ " " " " " " $= -7$°C
At South Pole $\delta_p = -49$ " " " " " " $= -49$°C

Dansgaard gives a formula relating T_a to δp.

$$0.7\,T_a = \delta_p + 13.6$$

The δ values are preserved in glacier ice and show substantial seasonal conditions. The sesonal variations are easily detected in some ice samples as δ can be measured with a standard error of about ± 0.2 , considerably less than the seasonal variations. We shall consider measurements of δ in ice sheets in Lecture 7.

AII δ in the shells of plankton and global ice volume

Shells made of calcium carbonate contain more ^{18}O than sea water. The equilibrium amount depends on water temperature; the ratio $^{18}O_{SHELL}/^{18}O$ SEA ($^{18}O_S/^{18}O_W$) varies from 1.025 at 0°C to 1.021 at 25°C. So δ_S becomes more positive as sea temperature falls. In practice the δ_S values have a further "constant" offset from calculated equilibrium values by an amount which depends on the specific plankton species (of foraminifera usually). An equation often used is

$$T = 16.9 - 4.38\,(\delta_S - \delta_W) - 0.10\,(\delta_S - \delta_W)^2$$

where δ_W is the δ of ambient sea water (relative to smow), when the plankton was alive.

It used to be thought that $\delta - \delta_W$ in deep sea cores mostly varied with temperature, ie δ_W did not change much through time eg through the ice ages at a specific location. This is now known not to be true. δ_W rises if large quantities of land ice form as land ice contains less ^{18}O than the ocean, as shown in Section 1 AO. So the presence of continental ice sheets increases the concentration of ^{18}O in the ocean. The amount of the increase depends mainly on the change in the volume of land ice relative to that of the oceans and, appreciably, on the sea and air temperatures prevailing when the land ice was formed. Observations of δ in ice sheets and in deep sea cores show that δ_W varies considerably more than $\delta_S - \delta_W$, under most conditions. It is then easy to show that δ_S represents the changes through time of δ_W, rather than those of T, ie the changes mainly represent the changes in global ice volume.

So, from δ measurements in ice sheets, δ_S can be calibrated to measure the approximate changes in the volume of worldwide land ice, in km^3 (roughly 1‰ change of δ per $30 \times 10^6\ km^3$ of ice). However the effect of sea temperature on δ_S is not always negligible, and global ice volume changes can only be monitored semi-quantitatively unless additional geological evidence is at hand. If we assume an ice free world, as some authors do for the Tertiary epoch, quite large changes in sea temperature can be deduced from δ_S measurements which would be exaggerated if land ice volume, in reality, changed appreciably.

LECTURE 6

REFERENCES

1. LAMB, H H (1977). Climate: present, past and future Vol 2. Methuen.

2. ENDAL, A S AND SCHATTEN, K W (1982). The faint young sun-climate paradox: continental influences. J Geophys Res, 87, C9, pp 7295-7302.

3. HARLAND, W B AND HEROD, K N (1975). Glaciations through time. Ice Ages Ancient and Modern. pp 189-216. Seal House Press, Liverpool.

4. TARLING, D H AND TARLING, M P (1974). Continental Drift. Penguin Books.

5. SELLERS, A AND MEADOWS, A (1975). Long term variations in the albedo and surface temperature of the earth. Nature, 254, p 44.

6. VARIOUS PAPERS IN "Ice ages ancient and modern". (1975). Seal House Press, Liverpool.

7. BROOKS, C E P (1949). Climate through the ages. Benn, London 2nd Ed.

8. OPIK, E J (1965). Climatic change in cosmic perspective. Icarus N-1, 4, pp 289-307.

9. MATTHEWS, R K AND POORE, R Z (1980). Tertiary $\delta^{18}O$ record and glacio-eustatic sea-level fluctuations. Geology, 8, pp 501-504.

10. FRAKES, L. (1978) The long-term climate record. In Climate Change and Variability - a Southern Perspective. Ed: A B Pittock et al. Cambridge Univ Press.

11. IMBRIE, J AND IMBRIE K P (1979). Ice Ages - Solving the Mystery. MacMillan, London.

12. IMBRIE, J (1982). Astronomical theory of the Pleistocene Ice Ages: A brief historical review. Icarus, 50, pp 408-422.

13. SHACKLETON, N J AND OPDYKE, N D (1973). Oxygen isotope and paleomagnetic stratigraphy of equatorial Pacific core V28-238: oxygen isotope temperature and ice columns on a 10^5 and 10^6 year scale. Quarternary Research, 3, pp 39-55.

14. BERGER, A AND PESTIAUX, P (1984). Accuracy and Stability of the Quaternary Terrestrial Radiation. Milankovitch and Climate, Pt I. Ed: A Berger et al, pp 83-111.

15. IMBRIE, J ET AL (1984). The orbital theory of Pleistocene Climate: Support from a revised chronology of the marine $\delta^{18}O$ record. Ibid, pp 269-305.

16. PELTIER, W AND HYDE, W (1984). A model of the ice age cycle. Ibid, Pt 2, pp 565-580.

17. MANABE, S AND BROCCOLI, A (1984). Influence of the CLIMAP ice-sheet on the climate of a general circulation model: implications for the Milankovitch theory. Ibid, Pt 2, pp 789-799.

18. ROYER, J ET AL (1984). A sensitivity experiment to astronomical forcing with a spectral GCM: simulation of the annual cycle at 125000 BP and 115000 BP. Ibid, pp 733-764.

FIG 6·1

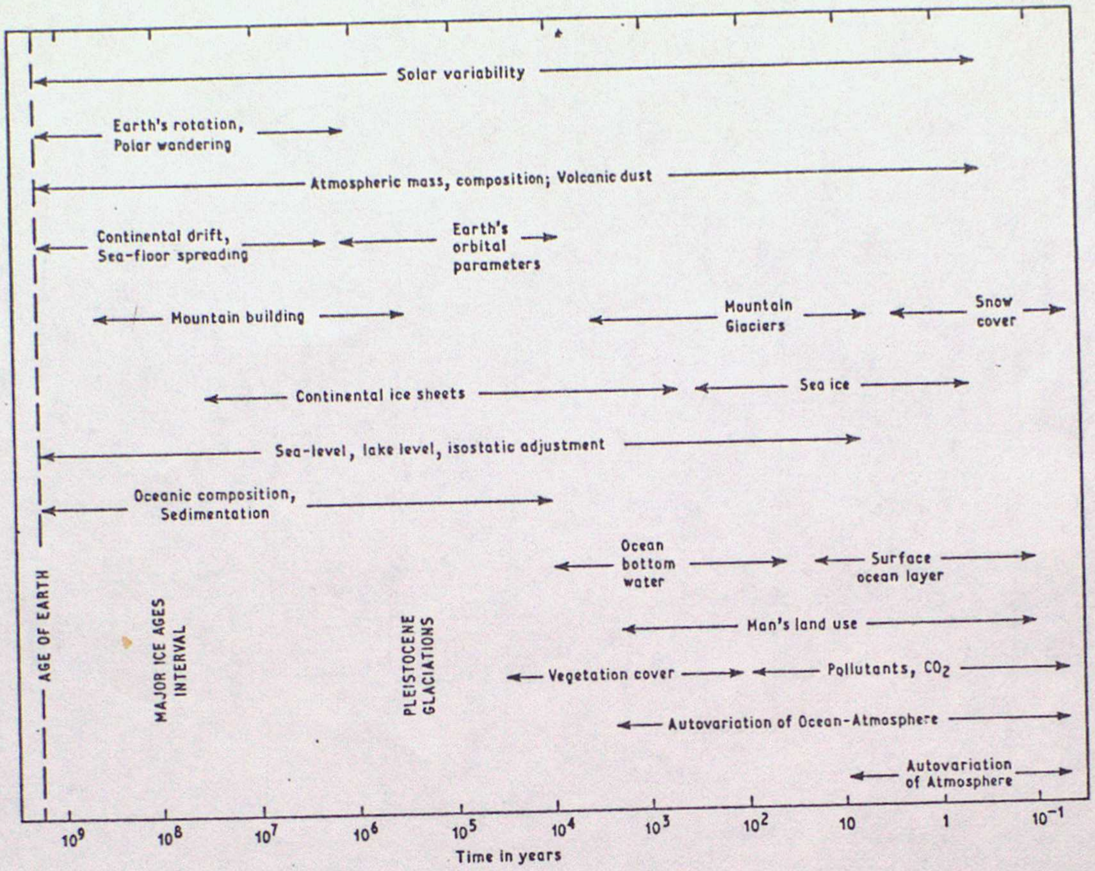
Solar variability
Earth's rotation, Polar wandering
Atmospheric mass, composition; Volcanic dust
Continental drift, Sea-floor spreading
Earth's orbital parameters
Mountain building
Mountain Glaciers
Snow cover
Continental ice sheets
Sea ice
Sea-level, lake level, isostatic adjustment
Oceanic composition, Sedimentation
Ocean bottom water
Surface ocean layer
Man's land use
Vegetation cover
Pollutants, CO2
Autovariation of Ocean-Atmosphere
Autovariation of Atmosphere
AGE OF EARTH
MAJOR ICE AGES INTERVAL
PLEISTOCENE GLACIATIONS
10^9
10^8
10^7
10^6
10^5
10^4
10^3
10^2
10
1
10^-1
Time in years

FIG 6·2

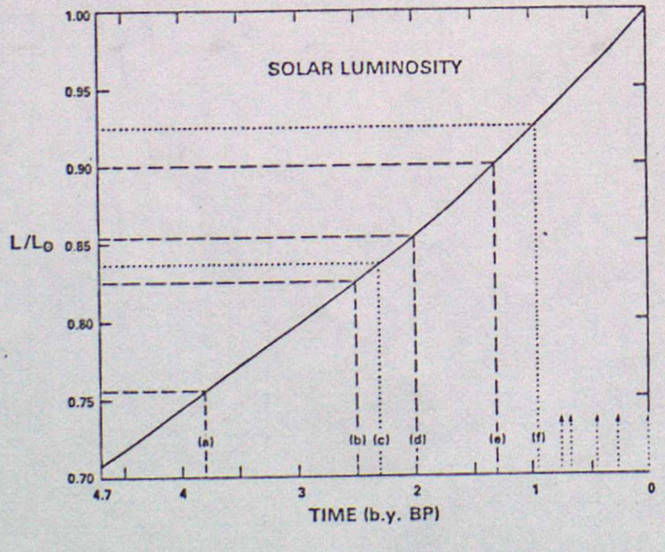

FIG 6·3

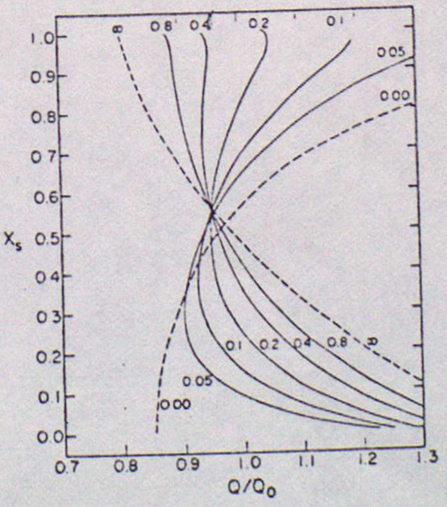

Table App. V.1 Geological eras and their subdivisions, with time scale

Era	*System or Period*	*Series or Epoch*	*Notes on climate, fauna and flora*	*Radiometric age*
Cenozoic (Kainozoic)	Quaternary	Holocene or Recent (post-glacial)		*c.* 10 000 years ago
		Pleistocene	Glaciations and Interglacial ages alternating. *Homo sapiens* emerged about mid last glacial (40 000 years ago). Earliest forms of Man in early Pleistocene.	1–3 million years ago
	Tertiary	Pliocene	Becoming colder. Large carnivorous animals.	*c.* 10 million years ago
		Miocene	Warm to moderate. Whales, apes and grazing animals.	*c.* 25 million years ago
		Oligocene	Warm. First monkeys and man-like apes.	*c.* 40 million years ago
		Eocene	Moderate becoming warm.	*c.* 60 million years ago
		Palaeocene	Becoming warmer. Early horses, elephants, etc. Most modern genera of flora present, but world distribution different.	*c.* 70 million years ago
Mesozoic	Cretaceous		Some evidence of a cold, but not glacial phase towards end. Ichthyosaurus became extinct; many other extinctions about end of Cretaceous to early Tertiary including among phytoplankton, marine turtles, dinosaurs.	*c.* 130 million years ago
	Jurassic		First birds and small mammals. Dinosaurs' heyday. First crocodiles and flying reptiles.	*c.* 180 million years ago
	Triassic		First dionosaurs, ichthyosaurus, etc.	

Table App. V.1 – continued

Era	*System or Period*	*Series or Epoch*	*Notes on climate, fauna and flora*	*Radiometric age*
				c. 230 million years ago
Palaeozoic	Permian		Glacial at first, later moderate. Conifers abundant.	*c.* 270 million years ago
	Carboniferous		Warm at first, becoming glacial in some regions. First winged insects. First spiders. Climax of seed ferns and clubmoss trees; great coal forests. First coniferous trees.	*c.* 350 million years ago
	Devonian		Moderate, becoming warm. First insects. First trees. Fish abundant.	*c.* 400 million years ago
	Silurian		Warm. First known land plants and animals.	*c.* 440 million years ago
	Ordovician		Moderate to warm. First corals. First fishes.	*c.* 500 million years ago
	Cambrian		Climates becoming warm. First foraminifera, starfish, snails (mollusks), bivalve shells.	*c.* 600 million years ago
Precambrian	Proterozoic (first period with life forms)		First algae, radiolaria and worms. Evidence of some ice ages, perhaps severe enough to cover the whole Earth.	
	Azoic or Archaean		Before the dawn of life.	> 3000 million years ago

FIG 6·4

FIG 6·5

Figure 2. The Geological Time Scale

(millions of years).

2250 B.P.	Huronian Ice Sheet
950-650 B.P.	Pre-Cambrian Ice Ages
450 B.P.	Ordovician Ice Age
300 B.P.	Permo-Carboniferous Ice Age
50 B.P.	Start of cooling
2 ? B.P.	Start of Quaternary Ice Age

FIG 6.6a

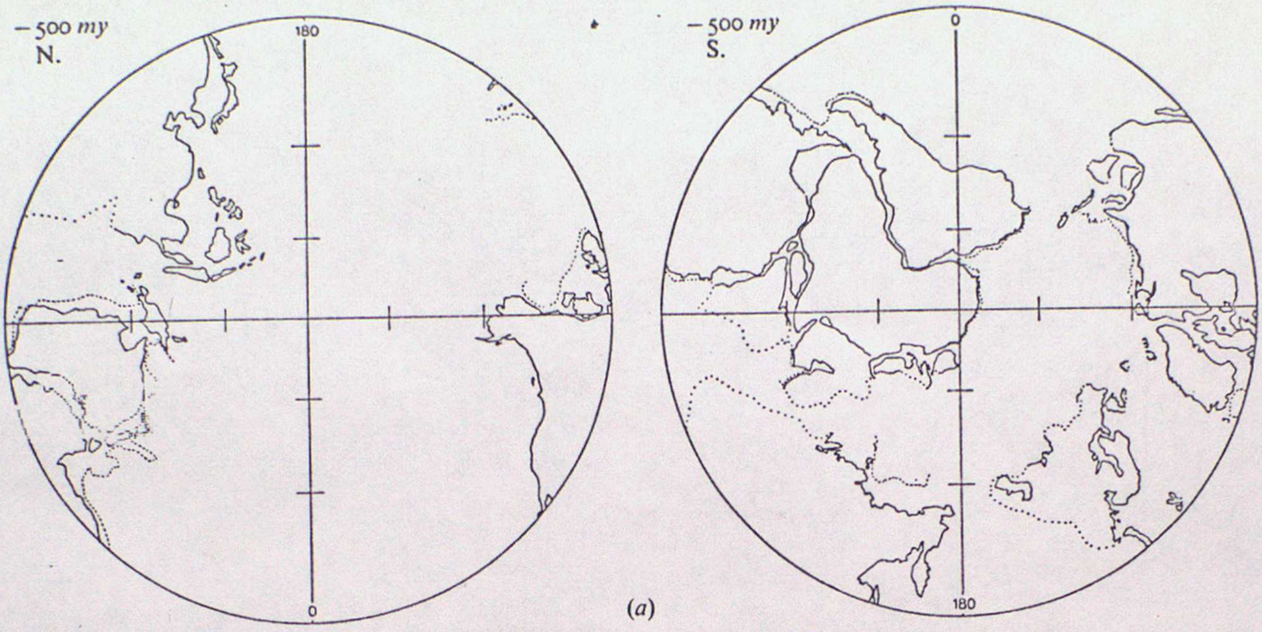
−500 *my*
N.
180
0
−500 *my*
S.
0
180

(*a*)

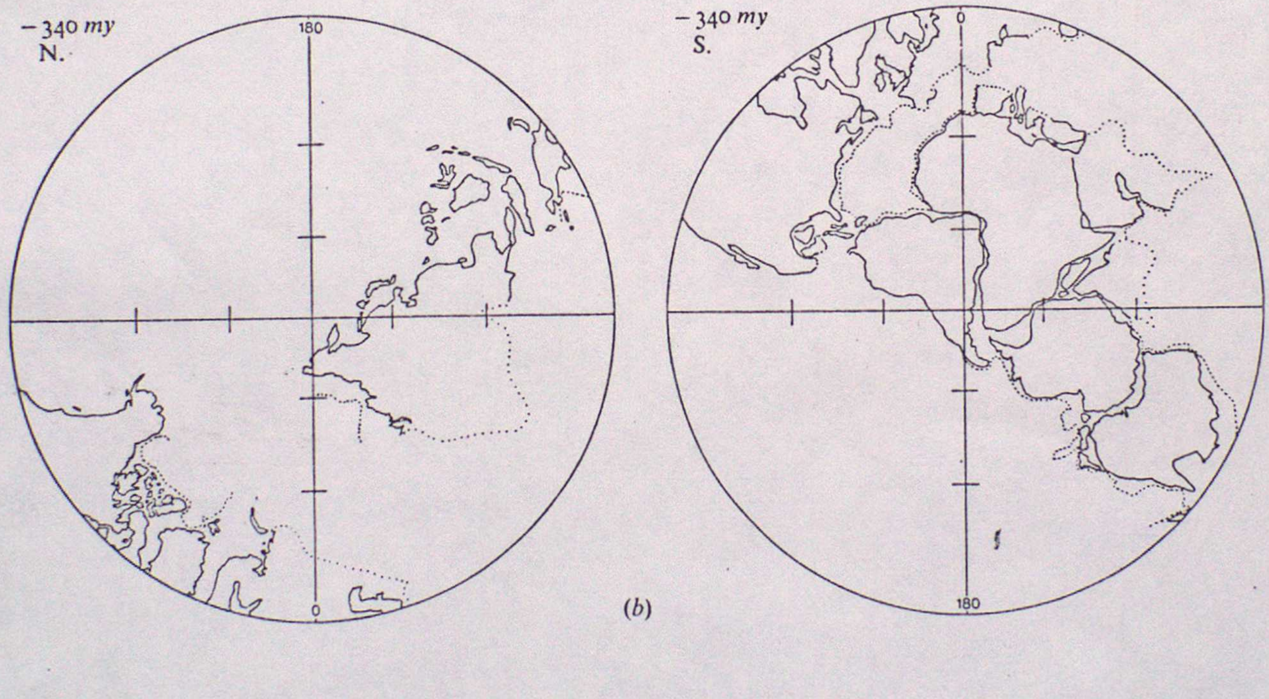
−340 *my*
N.
180
0
−340 *my*
S.
0
180

(*b*)

FIG 6·6b

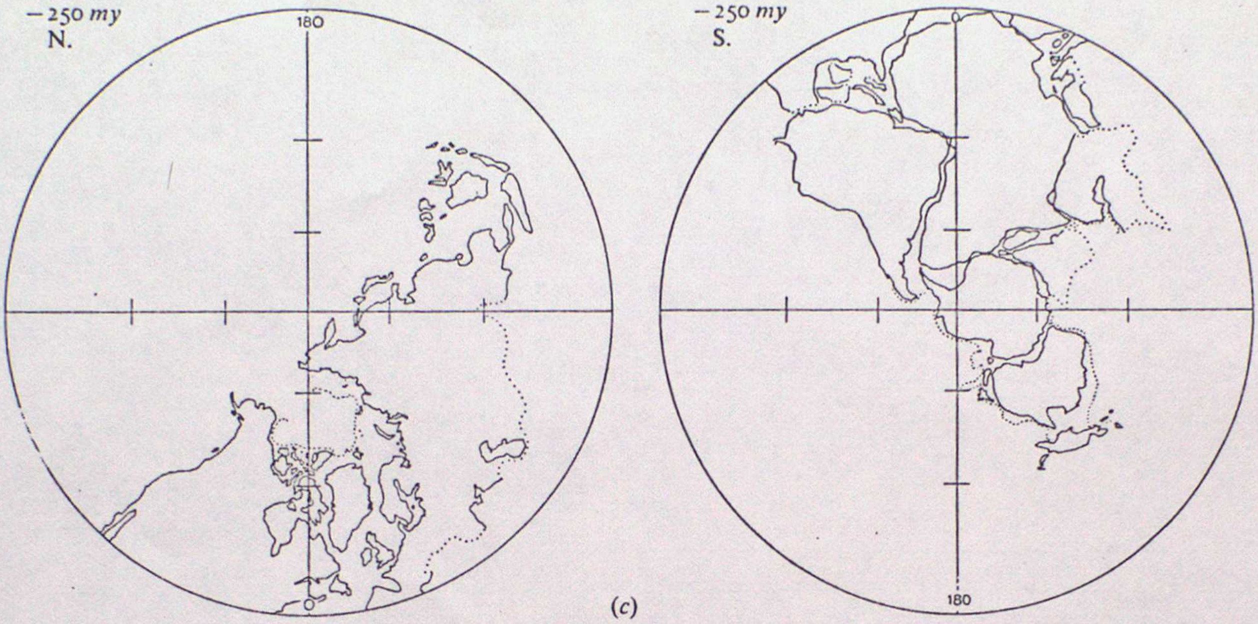
−250 my
N.
180
0
−250 my
S.
0
180

(c)

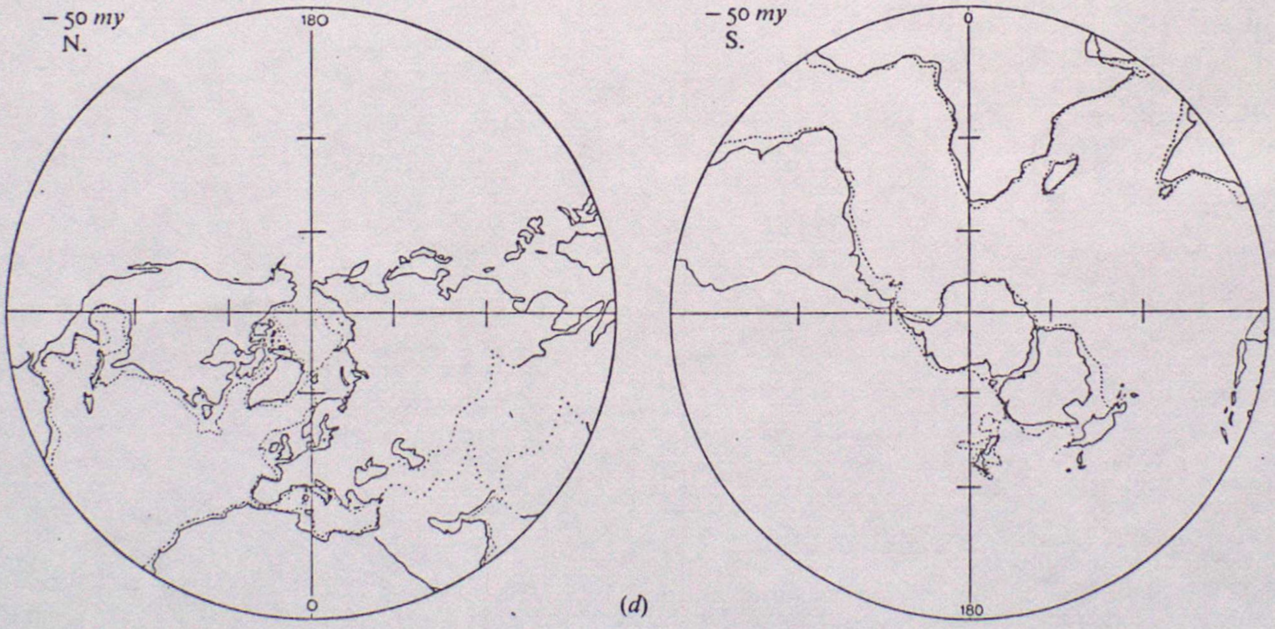
−50 my
N.
180
0
−50 my
S.
0
180

(d)

FIG 6·7

Nature Vol. 254 March 6 1975

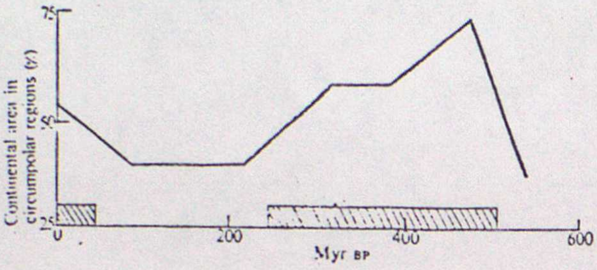

FIG 6·10

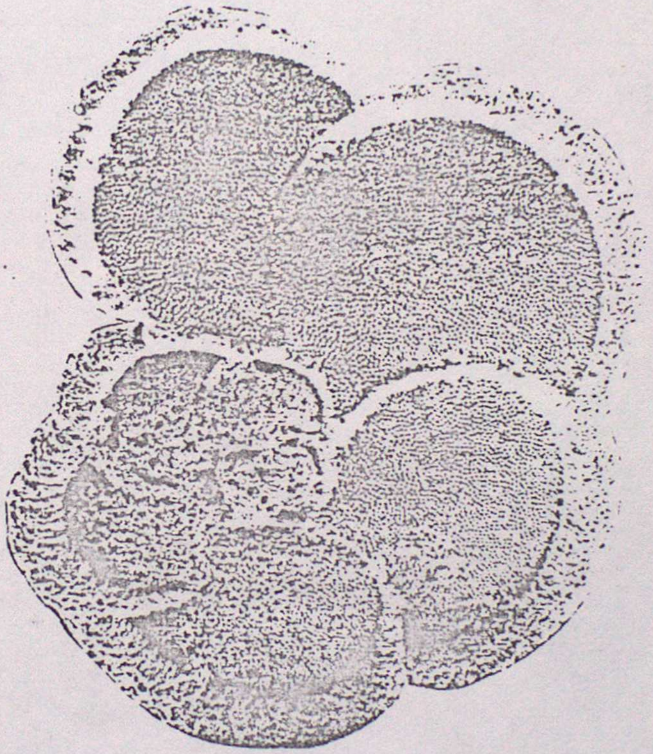

FIG 6·11

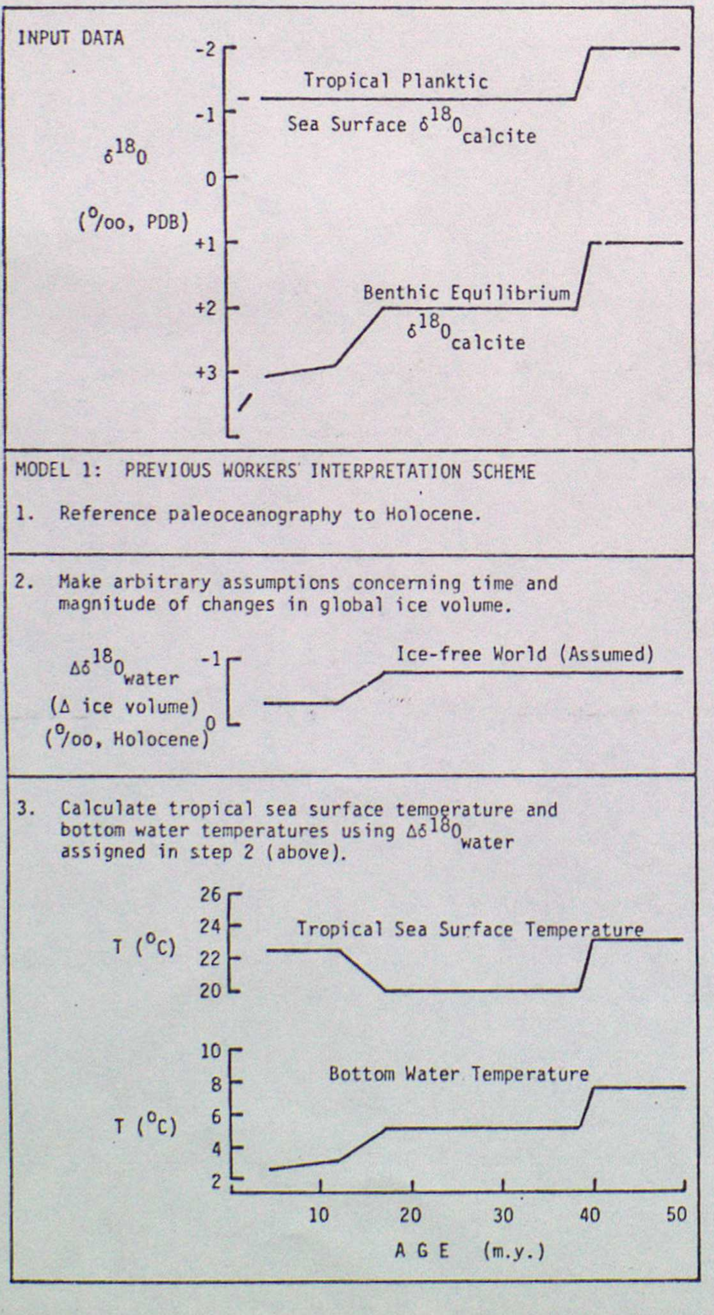

MODEL 1: PREVIOUS WORKERS' INTERPRETATION SCHEME

1. Reference paleoceanography to Holocene.
2. Make arbitrary assumptions concerning time and magnitude of changes in global ice volume.

3. Calculate tropical sea surface temperature and bottom water temperatures using $\Delta\delta^{18}O_{water}$ assigned in step 2 (above).

FIG 6·8

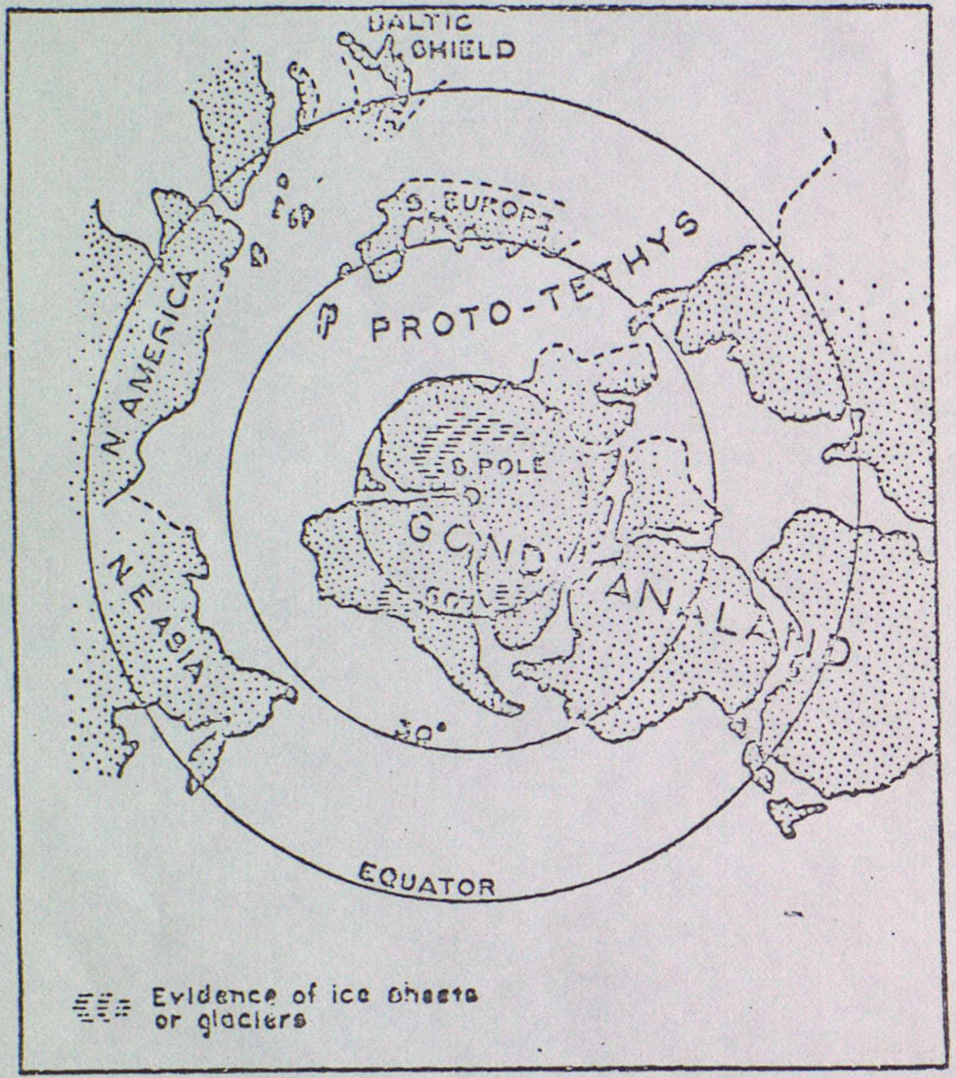
BALTIC SHIELD
S. EUROPE
PROTO-TETHYS
N. AMERICA
N.E. ASIA
S. POLE
GONDWANALAND
30°
EQUATOR
Evidence of ice sheets or glaciers

FIG 6·9

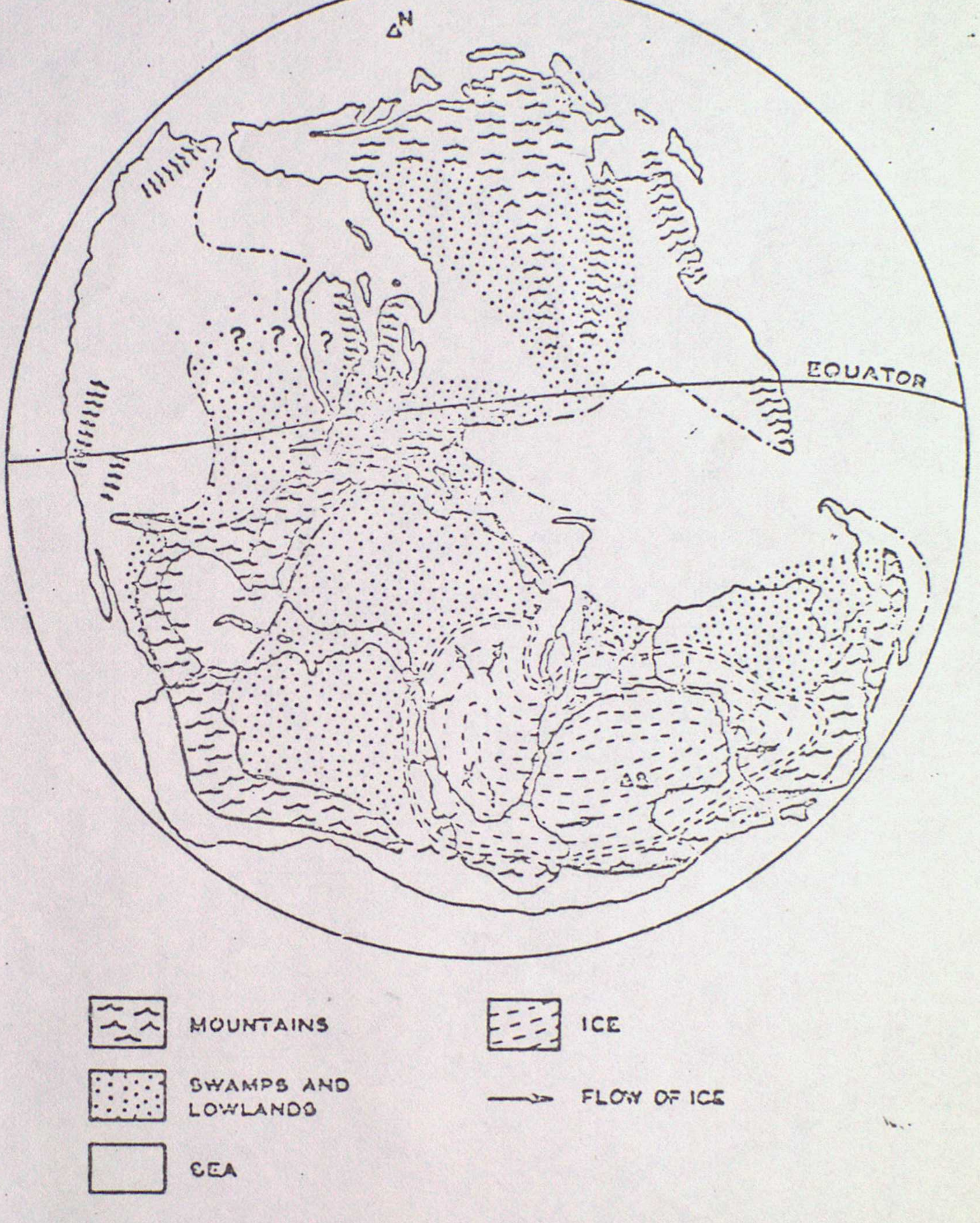
N
EQUATOR
?
?
?
MOUNTAINS
SWAMPS AND LOWLANDS
SEA
ICE
FLOW OF ICE

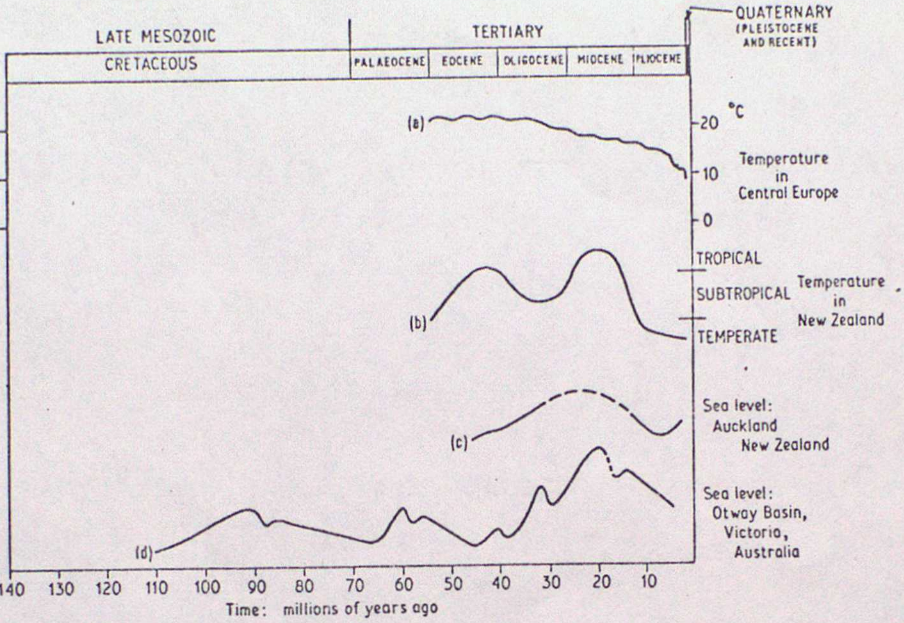

FIG 6·12

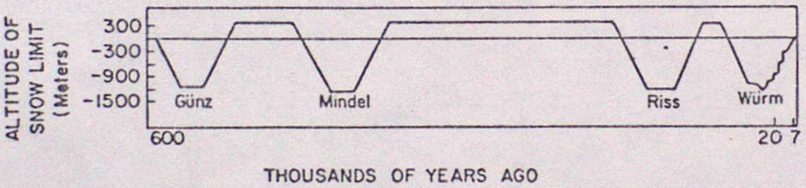

FIG 6·13

FIG 6·14

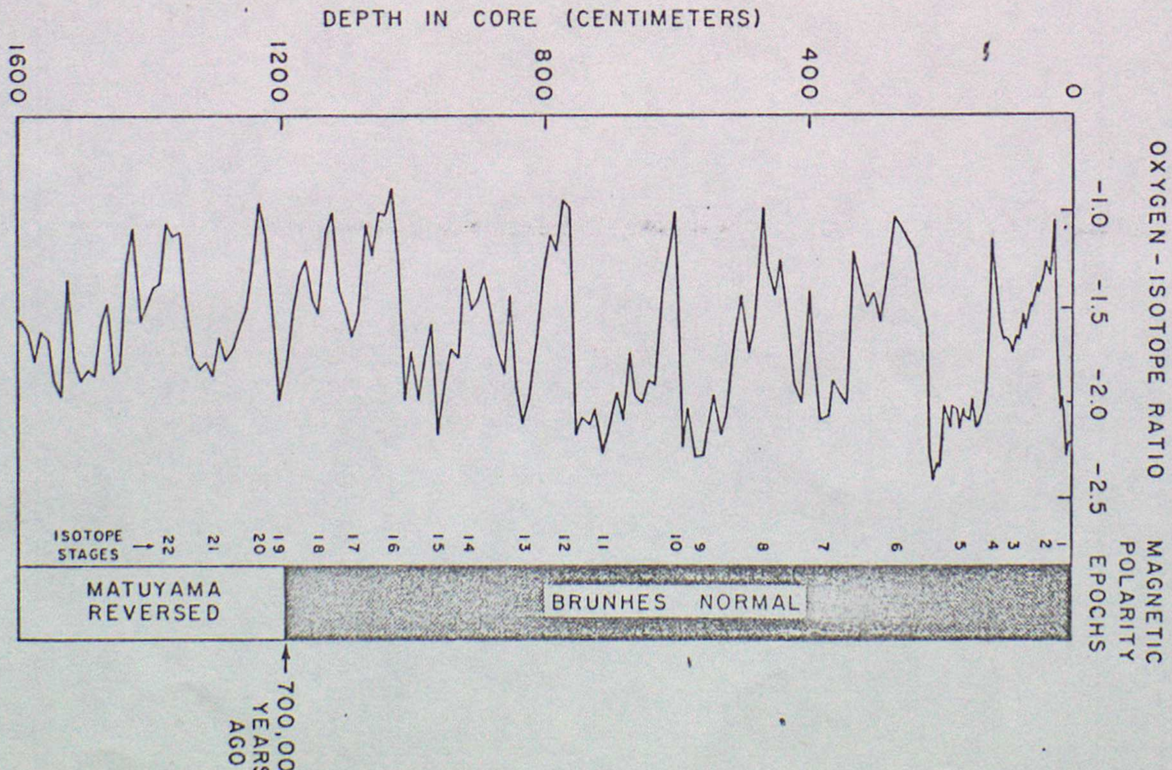

FIG 6·15

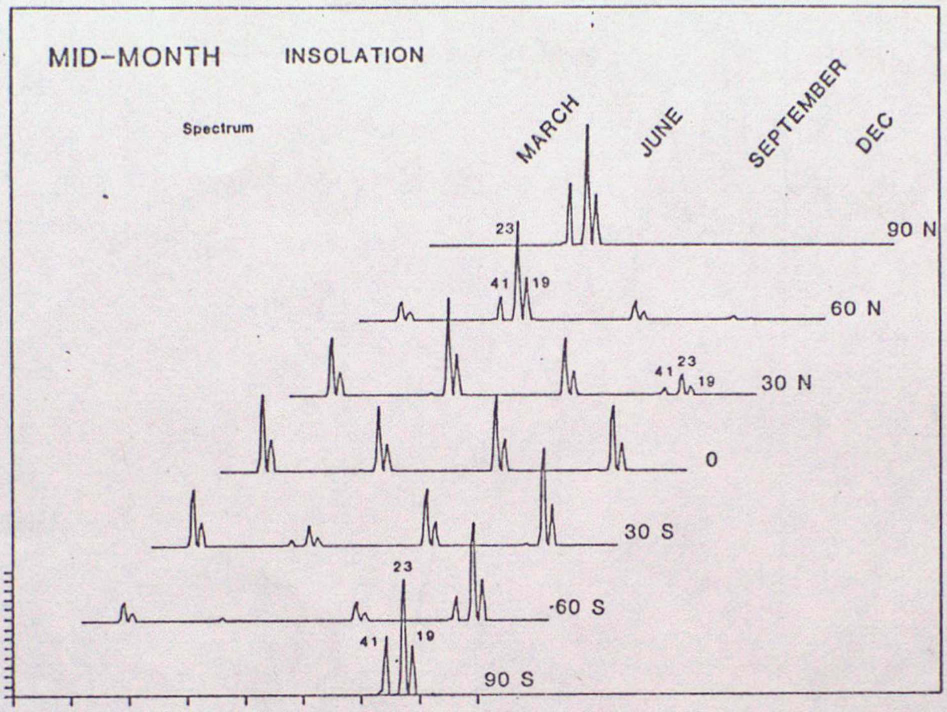

FIG 6·17

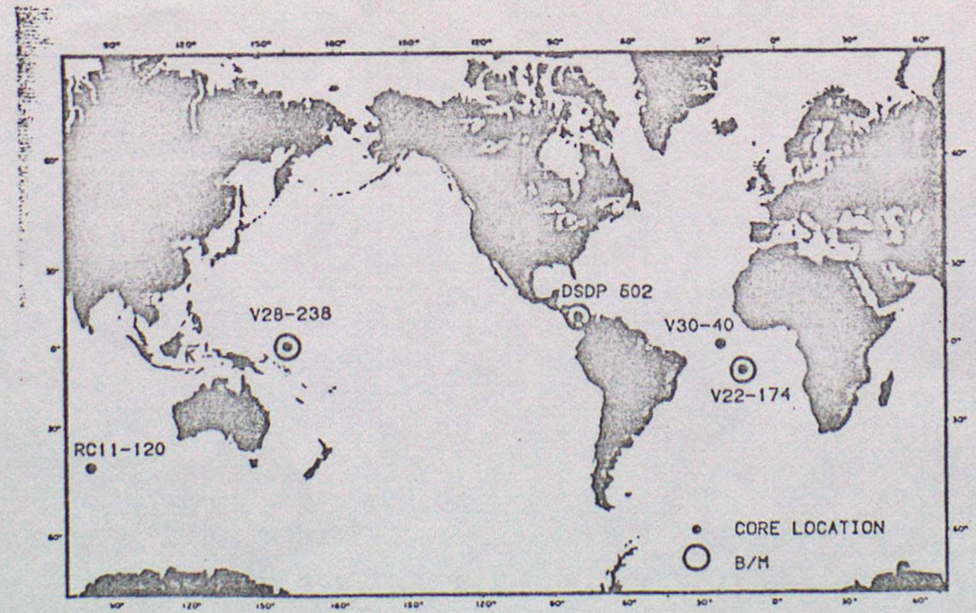
DSDP 502
V28-238
V30-40
V22-174
RC11-120
● CORE LOCATION
○ B/M

FIG 6·16

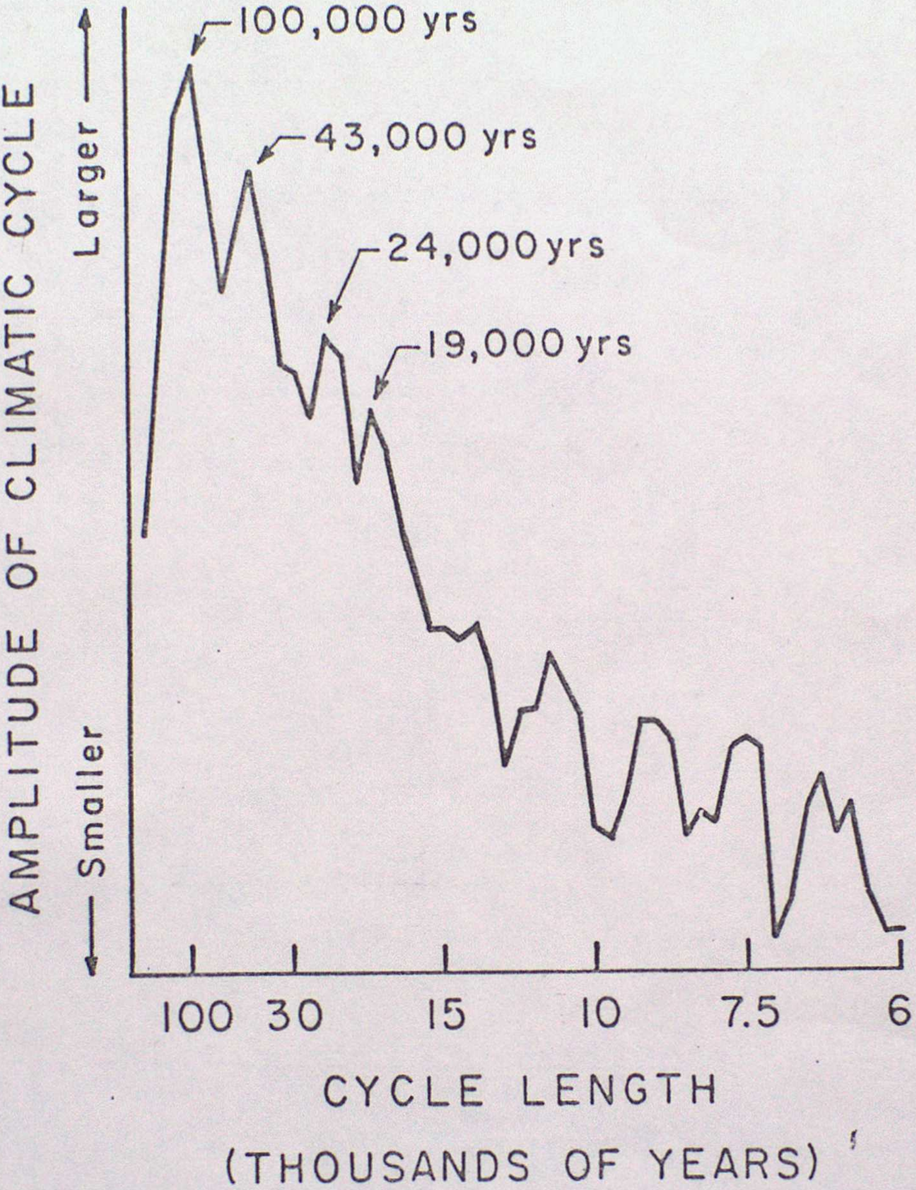

100,000 yrs
43,000 yrs
24,000 yrs
19,000 yrs
AMPLITUDE OF CLIMATIC CYCLE
Smaller
Larger
100
30
15
10
7.5
6
CYCLE LENGTH
(THOUSANDS OF YEARS)

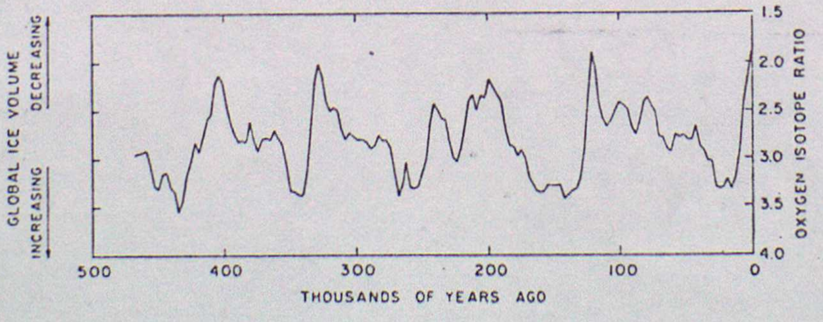

GLOBAL ICE VOLUME
INCREASING
DECREASING
OXYGEN ISOTOPE RATIO
1.5
2.0
2.5
3.0
3.5
4.0
500
400
300
200
100
0
THOUSANDS OF YEARS AGO

FIG 6·18

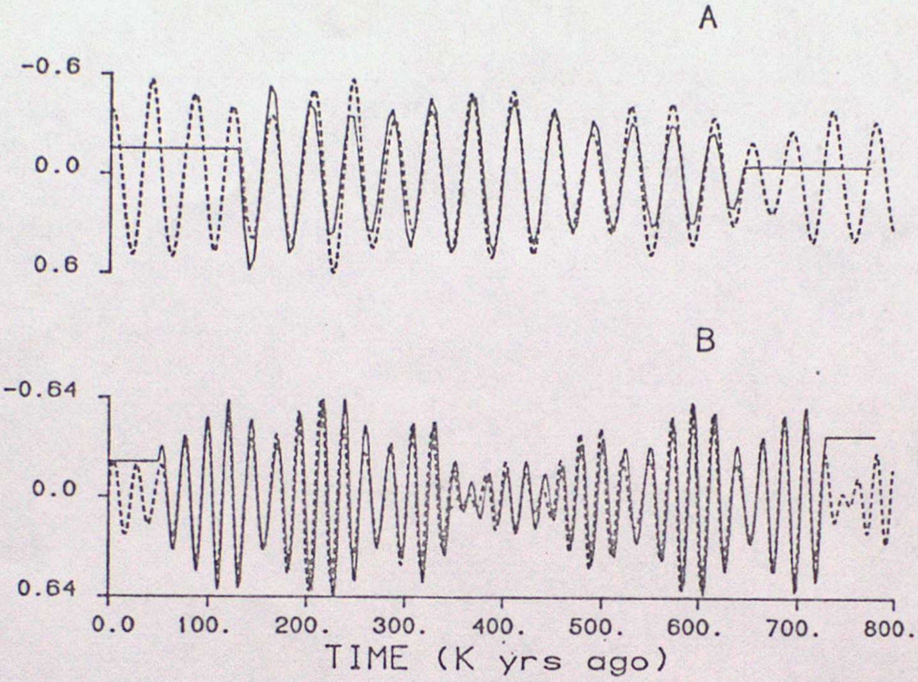

FIG 6·19

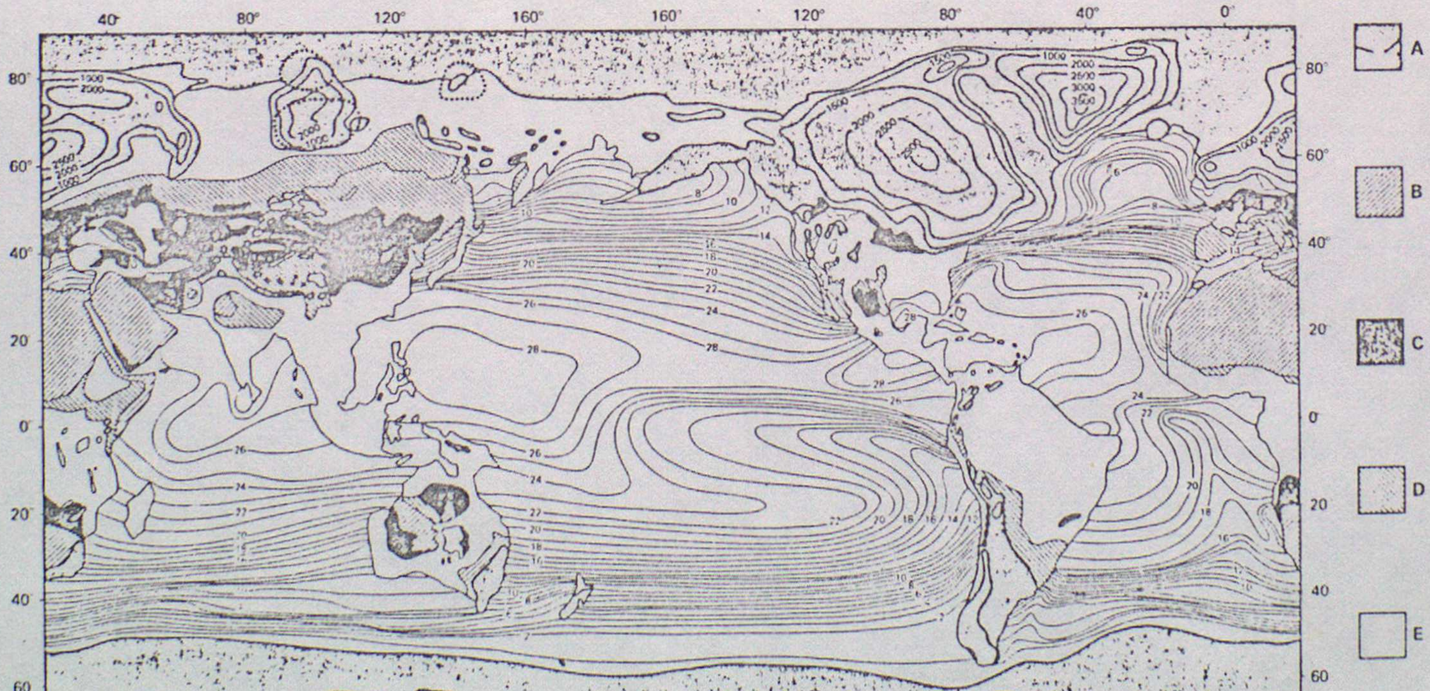
40°
80°
120°
160°
160°
120°
80°
40°
0°
80°
60°
40°
20
0°
20
40
60
80
A
B
C
D
E
F
1000
2000
3000
28
26
24
22
20
18
16
14
12
10
8

FIG 6·20

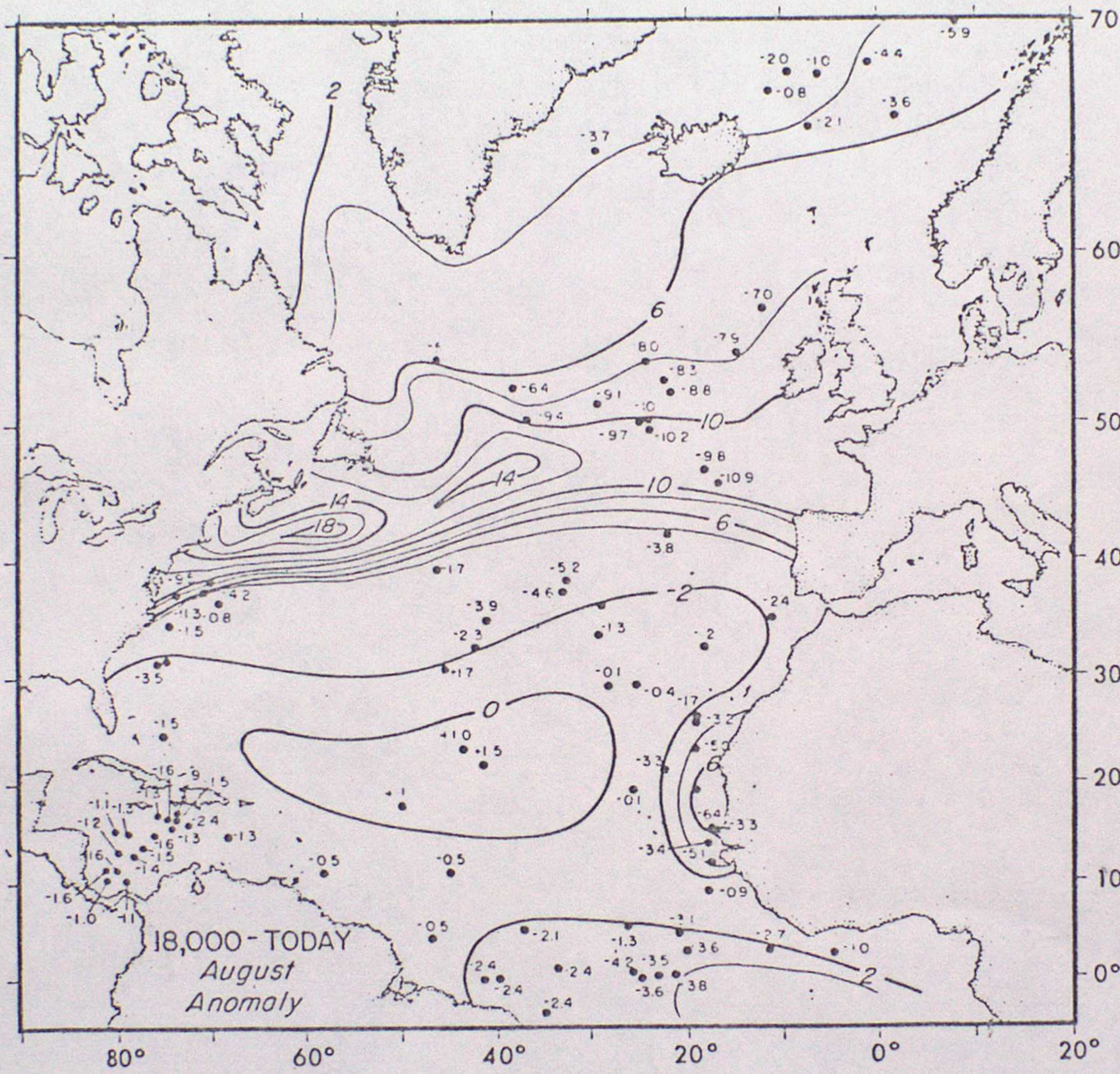
18,000 - TODAY
August
Anomaly
70°
60°
50°
40°
30°
20°
10°
0°
80°
60°
40°
20°
0°
20°
2
6
10
14
18
14
10
6
-2
0
6
2

FIG 6·21

SEA SURFACE TEMPERATURE DIFFERENCE (ICE SHEET EXP. – STANDARD EXP.)

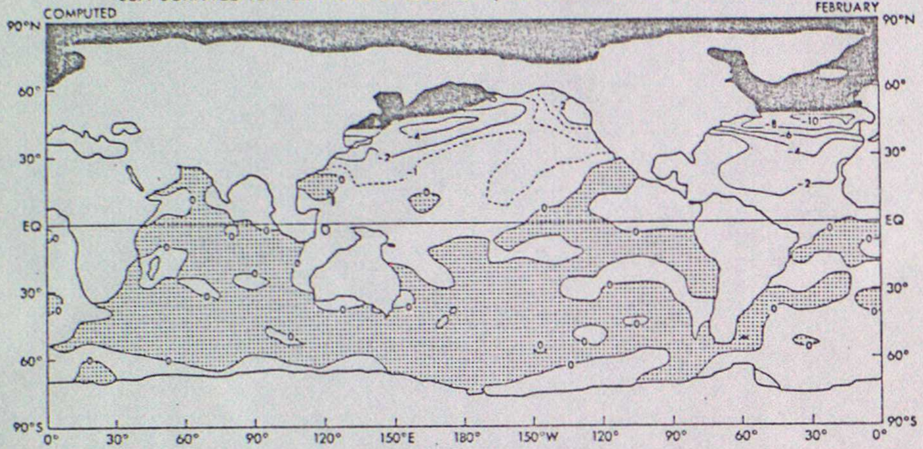
COMPUTED
FEBRUARY
90°N
60°
30°
EQ
30°
60°
90°S
0°
30°
60°
90°
120°
150°E
180°
150°W
120°
90°
60°
30°
0°

SEA SURFACE TEMPERATURE DIFFERENCE (ICE SHEET EXP. – STANDARD EXP.)

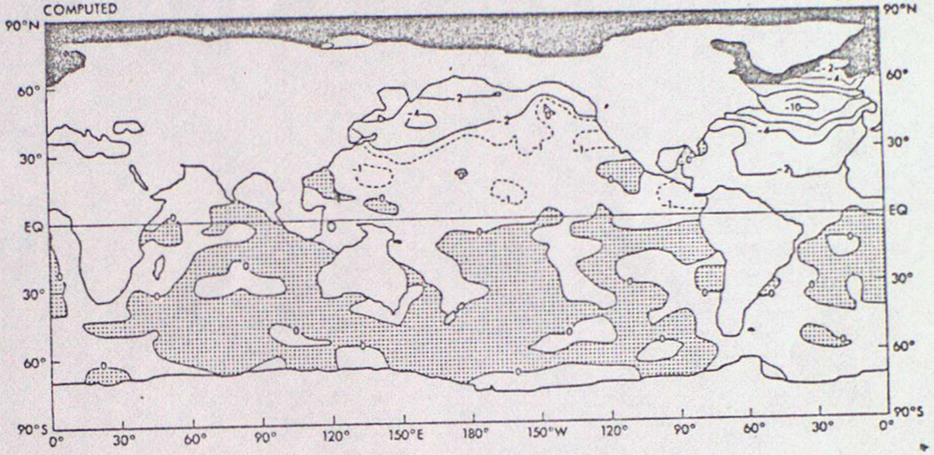
COMPUTED
AUGUST
90°N
60°
30°
EQ
30°
60°
90°S
0°
30°
60°
90°
120°
150°E
180°
150°W
120°
90°
60°
30°
0°

SEA SURFACE TEMPERATURE DIFFERENCE (ICE AGE–MODERN)

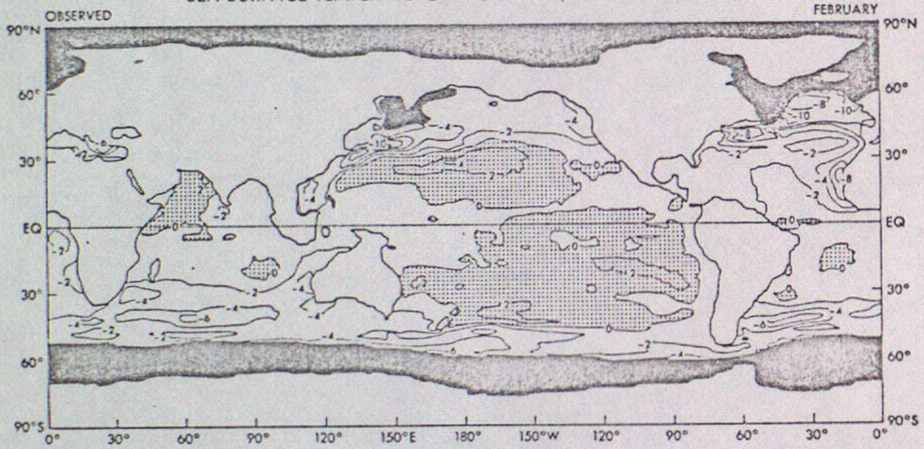
OBSERVED
FEBRUARY
90°N
60°
30°
EQ
30°
60°
90°S
0°
30°
60°
90°
120°
150°E
180°
150°W
120°
90°
60°
30°
0°

SEA SURFACE TEMPERATURE DIFFERENCE (ICE AGE–MODERN)

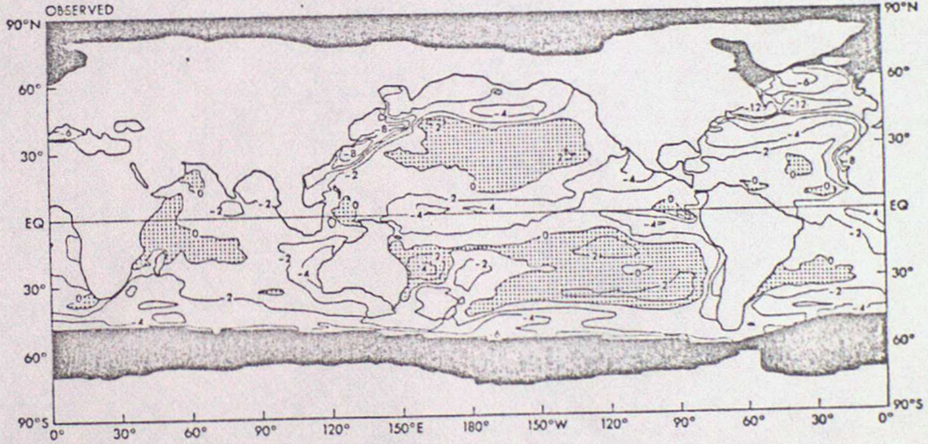
OBSERVED
AUGUST
90°N
60°
30°
EQ
30°
60°
90°S
0°
30°
60°
90°
120°
150°E
180°
150°W
120°
90°
60°
30°
0°

FIG 6·22

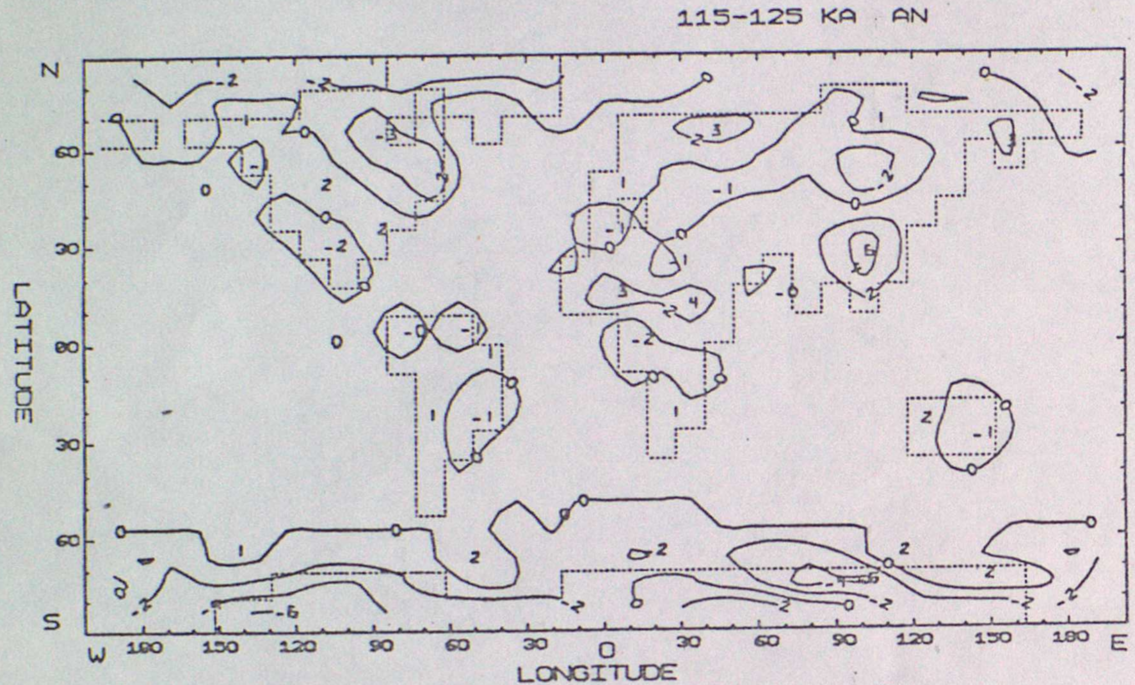
115-125 KA AN

N
S
W
E
LATITUDE
LONGITUDE
60
30
0
180
150
120
90

TEMPERATURE DU SOL -DEG C-

FIG 6·23

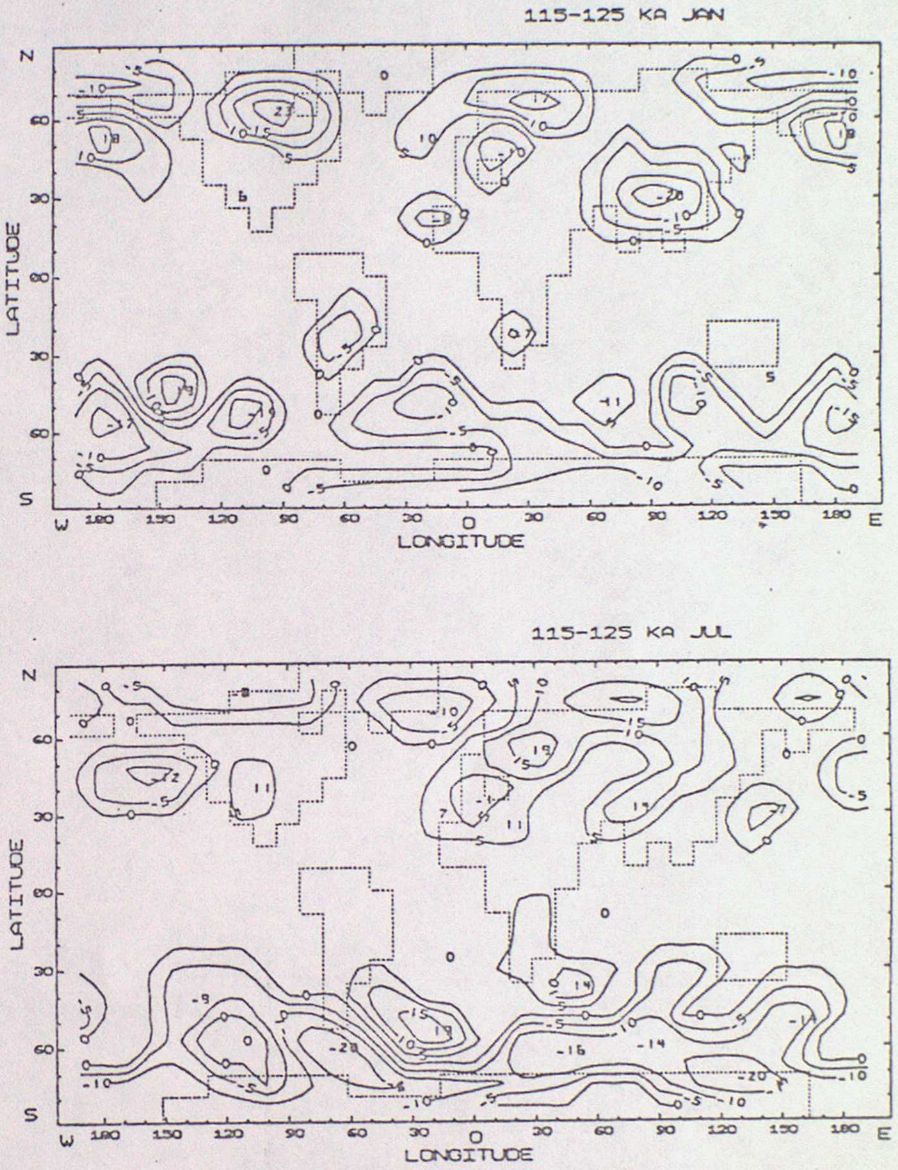
115-125 KA JAN

115-125 KA JUL

N
S
W
E
LATITUDE
LONGITUDE
60
30
0
180
150
120
90

PRESSION MER -MB-

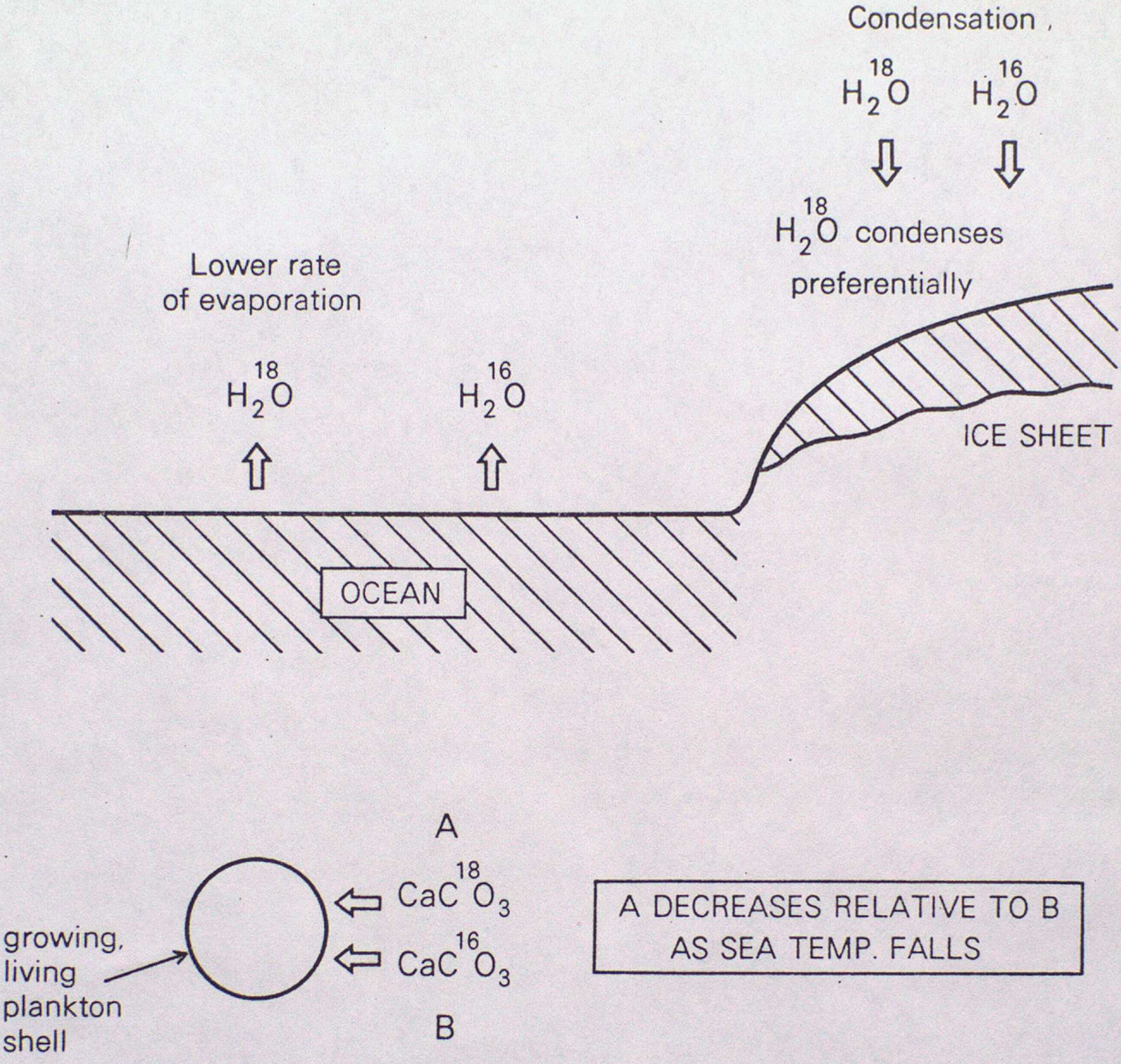
Condensation ,
$H_2{}^{18}O$
$H_2{}^{16}O$
$H_2{}^{18}O$ condenses preferentially
Lower rate of evaporation
$H_2{}^{18}O$
$H_2{}^{16}O$
ICE SHEET
OCEAN
A
$CaC{}^{18}O_3$
$CaC{}^{16}O_3$
B
growing, living plankton shell
A DECREASES RELATIVE TO B AS SEA TEMP. FALLS

Fig. 6A.1 Oxygen isotope method

65 copies

FOR LOAN to Met. Office Staff only

METEOROLOGICAL OFFICE
145730
- 7 MAY 1985
LIBRARY

KW/34

ADVANCED LECTURE NO 7

CLIMATES OF THE PAST II - LATE GLACIAL TO LITTLE ICE AGE (c 15000 BP to 200 BP)

7.1 SUMMARY

After pausing to recap the physical processes likely to influence climate change, we shall briefly discuss some of the "proxy" techniques used to reconstruct Holocene climate prior to the historical period. We shall then try to link the Holocene to previous epochs by considering the variations of global sea-level that have been deduced which provide (perhaps) the best evidence of climatic change of worldwide significance.

Climate change in the Holocene is discussed with emphasis on the period about 9000 BP when the last Milankovitch radiation maximum occurred. After about 6000 BP the evidence for climate variation is considerable but localised, difficult to synthesise, and indicates relatively small changes. The situation is little better in the historical period, even though documentary evidence becomes available. We concentrate on evidence for a climate deterioration between about 1300 and 1800 AD, the "Little Ice Age".

7.2 Physical Processes in Climate Change

Fig 7.1 (from Lamb (1977) (1)) provides a useful summary of physical processes and their time scales, some of which we have already studied. On time scales of 10^3 - 10^4 years many processes compete: the dynamics and time constants of ice sheet development and decay and the longest time-scale oceanic processes become very important i.e. those that may involve the interchange of ocean bottom waters with the surface circulation. Over the last few thousand years man's effect on the land surface has been considerable - in clearing forests, draining marshes and inadvertantly extending deserts. Fluctuations in carbon dioxide are also increasingly seen to have occurred. As we approach century and lesser time-scales, many of the ocean circulation processes are likely to occupy a leading position in influencing climate variability. The role of truly external forcing (e.g. solar variability, volcanic dust) is unclear. Finally, on the shortest time scales relevant to climate (and possibly on longer ones as suggested in fig 7.1) internally-caused variations in the atmosphere-ocean system may become important (like ENSO, soil moisture variations etc).

7.2.1 Transitivity, intransitivity and almost-intransitivity

A particular problem, raised by Lorenz (1968) (2), is whether the climate is internally stable. Non-linear systems far simpler than the atmosphere display a tendency to fluctuate in an irregular manner between two or more internal states (fig 7.2). In a transitive system, a climate state B will approach a new state A after the climate system has been forced by new boundary conditions appropriate to state B. So given boundary conditions correspond to a given climate. In an intransitive system B stays unchanged despite the forcing. (e.g. the "white earth" stays white (lecture 6) even when solar constant increases by reasonable amounts). A third type of

ORGS UKMO
National Meteorological Library
FitzRoy Road, Exeter, Devon. EX1 3PB

3 8078 0007 8121 3

behaviour is one where the system stays in state B despite the new forcing but after some time it starts to shift toward A where it might remain - or perhaps spontaneously shift back to B. This "flip-flop" behaviour is called "almost intransitive". Until recently, at least, many climatologists considered that ice-age-interglacial fluctuations were quite likely to have been the result of an almost intransitive process of this kind.

7.3 Methods of Studying Post Glacial Climates

Lamb gives an extensive description while Critchfield 1983(3) and Crane (1981) (4) provide a useful summary. The subject is vast. I shall list and describe a few of the main techniques, but see lecture 6 for some other methods. Fig 7.3 is a diagrammatic summary of some of the techniques.

(1) RADIOMETRIC METHODS FOR DATING

These involve the decay of radioactive isotopes contained in the material being studied; the ratio of the concentration of a radioactive to a non radioactive isotope of a given element is a measure of the age of a sample. The most usual method for dating Holocene organic material uses the decay of ^{14}C to ^{14}C. ^{14}C is continually created in the atmospheric carbon dioxide by cosmic rays (but not at quite a constant rate due to the variable effects of solar-caused interplanetary magnetic fields). Fig. 7 gives an idea of the accuracy of this technique. The technique is not very useful for young samples (less than 150 years old) partly because of the long half-life of ^{14}C (5700 years) and partly because man has changed the proportion of ^{14}C in the atmosphere, and thus in organic samples, through fossil fuel burning.

Other methods include (1) the protoactinium-ionium method (the decay of ^{231}p to ^{230}Th, an isotope of thorium known as ionium), whose standard error of dating is about ± 1000y for ages 7000 BP - 30000 BP: this decay process has been used occasionally to date deep-sea cores. (2) The uranium -thorium method: this includes several radioactive decay techniques one of which involves the decay ^{234}U to ^{230}Th (ionium) with a half life of 75000 years; the method has been used to date fossil coral reefs which provide important evidence of past sea-level fluctuations.

(2) VARVE CHRONOLOGY - DATING AND CLIMATIC EVIDENCE

Varves are annual layers of silt and clay deposited on the bottom of certain lakes and ponds which are subject to freezing in winter and thawing in summer. In winter, ice prevents other than fine sediments from settling to the bottom of the lake; in summer a flux of fresh water brings in coarse sediments. Successive years will exhibit different thicknesses of coarse sediment when a core is taken through the sediments. If the varves are of climatic origin, parallel dating of lake beds in a region is possible through matching of varve thickness. (fig 5). When the lakes are buried under glaciers, no varves are formed so a comparison of varves in lake beds can indicate when and where glaciers retreated in a region if parallel dating of the varves can be successfully done. Nearly absolute dating is occasionally possible, depending on more recent climate variations and on a lack disturbance to the varves by burrowing creates, floods etc. Lake varves provide powerful evidence for the geography and timing of the retreat of the Scandinavian ice-sheet in the early Holocene.

(3) GROWTH OF LICHENS - LICHENOMETRY

Lichens reaching newly exposed rock-faces after glacier retreat exhibit (after an initial growth flush) remarkably constant growth rates. Measurements of the sizes of the largest lichens present provide evidence of the timing of glacier retreat (for the last few hundred years only).

(4) POLLEN DATING, SOIL CHANGES AND EVIDENCE FOR PAST CLIMATES

Pollen dating is a technique for use on land whose approach parallels the study of changes in the species of foraminifera in lecture 6. By studying the present relationships (ranges and limits) of trees, flowers and shrubs to climate and the density of (very durable) fossil pollen grains left in the soil beneath, it is possible to guess at previous climates by extracting, in widespread locations, cores of soil and identifying and dating the fossil pollen grains. The method is not easy to use as trees may take a long while to migrate after a climate change, disease may strike widely and trees and plants compete in complex ways, even in a constant climate. Nevertheless, with the aid of ^{14}C dating and the study of associated past changes in soil type, such as drying out of peat bogs or their re-establishment, it has been possible to construct detailed pictures of Holocene climate variation in many parts of the world using this technique.

(5) LEVELS OF OLD LAKES

Geological evidence of past lake shorelines can register changes in the balance between local precipitation and evaporation, given no past tectonic changes and that the geography of supply and outlet channels has not altered. Dating can be done using ^{14}C techniques or by studying old varves etc.

(6) DENDROCHRONOLOGY - "TREE RINGS"

This technique is based on the observed annual increment of tree growth, the tree ring, and has been mainly used in middle and high latitudes (fig 7.5). A close relationship between annual rainfall or temperature and growth rings of trees under climatic stress was demonstrated by A E Douglas, an American, early this century. This relationship includes the longest living of all trees, the bristlecone pine of SW USA (oldest specimens 6-8000 years old). Recently the technique has been extended to forest trees like oak living in W. Europe, where tree rings reflect (mainly) May-September climatic conditions but in a complex way. Dendrochronology is controversial as complex statistical procedures are needed to allow for many non-climatic factors like ageing of the tree, disease, competition, "weather" factors like isolated late frosts, and the fact that the remaining climatic response itself is often complex. The chief reference work is Fritts (1976) (5). Dendrochronology has now been extended to other aspects of tree growth, such as the amount of ^{18}O in a tree ring which can be used, with care, as a paleothermometer.

(7) BEETLES

It is believed by some workers that insects react quickly to climate change; their ancient remains in soils can be very numerous and can be ^{14}C dated. Beetles have apparently shown almost no tendency to evolution over the last 250000 years or so. By studying today's distribution of beetles, past temperatures (mainly summer temperatures) can be inferred from the past distribution of the remains of different beetle species.

(8) RAISED BEACHES AND CORAL REEFS

It is sometimes possible to date raised beaches and, especially, old coral reefs. Corals only grow at or down to about 20-30 m below sea-level. If slow tectonic movements steadily raise reefs, a past, constant sea level is indicated as an extended almost horizontal growth of the reef; rapid falls in sea level will produce rapid downward growth from this level. If the rate of tectonic movement is just correct, a series of stepped surfaces will be created above the changing shore-line. Fig 7.6 shows the most famous example, in New Guinea, which has been used to support the timing of the ice-age-interglacial cycles inferred from deep-sea cores and the Milankovitch radiation cycles.

7.4 Sea-level Variations

Fig 7.7 (a) shows a reconstruction (Lamb, p114) of sea-level variations from the mid Tertiary (20 m.y) to the present. The glacial-interglacial cycles are indicated (some are omitted). A long-term fall in sea level seems to be superimposed on the glacial-interglacial cycles; Lamb suggests that this fall may be due to crustal sinking under the ocean floor. The rise at the end of the curve of about 100 m is consistent with the total volume of ice that is believed to have melted since 18000 BP. Fig 7.7 (b) shows a more detailed reconstruction of sea-level over the last 200000 years while fig 7 (c) gives details of changes in Holocene sea-level, from diverse indicators, due to Fairbridge (6).

Holocene sea-level reached a maximum globally (corrected for tectonic movements) about 4000 BP and has declined by about 4 m since then. There are suggestions of mid-Holocene fluctuations to levels at or below the present level. Fairbridge claims that the sea-level fluctuation about 4900 BP (during the regions of the early Pharoahs of Egypt) was abrupt with a 5 m increase in perhaps 250 years. If true, this corresponds to a melting of more ice than currently exists on all mountain glaciers (excluding the Greenland and Antarctic Ice caps).

7.5 Post-Glacial Climate Fluctuations and the Melting of the Laurentide (N. American) and Scandinavian Ice Sheets

7.5.1 General Scheme of temperature Fluctuations

The details of the Holocene warming are best known in the N. Hemisphere and there is no guarantee for example of a global synchroneity in temperature change. Fig 7.8 (a) shows an interpretation of the evidence for the timing of temperature changes in Central England (Lamb, p232). The warming was not apparently, continuous but interrupted by at least one major cooling c.

10000-11000 BP (others have been suggested). The prior, warm, stage at about 12000-11000 BP is known as the Allerod and the cold period afterwards (about 10800-10200 BP) is called the Younger Dryas. In the Allerod summers of Central England, beetle evidence suggests a mean temperature of 18°C or so i.e.probably warmer than now. Going far afield, there is only a little evidence of the Allerod/Younger Dryas oscillation from the New Guinea mountains (fig 7.8 (b)) though warming occurred up to 11600 BP and after 11600 BP a small glacial advance occurred on Mt Carstenz (1500m), West Irian, Indonesia (where glacier snouts currently reach down to 4300 m). However fig 7.8 (b) taken from (7), is striking in that it indicates a large warming from 18000 BP - 5000 BP when the CLIMAP SST reconstruction (lecture 6) suggests that SST at 18000 BP was only about 1.5-2.0°C below todays values. Equally, large, roughly contemporary, high mountain warnings have also been inferred by several workers in the equatorial Andes. However an increase of 2°C in SST could give rise to nearly double that increase at 4000 m near the equator as equivalent potential temperature, rather than air temperature should perhaps have changed uniformly with height i.e. the lapse rate probably changed (a modern example is given in lecture 5, Pt II of the fluctuations of tropical troposphere temperatures and lapse rate associated with ENSO described by Pan and Oort). There is support for the Allerod-Younger Dryas temperature oscillation in two Greenland Ice cores (8), at Dye 3 and Camp Century; (see fig 7.9 (a) and look at the area between "3" and "2" also shown in lecture 6).

A fluctuation from wet (Allerod) to dry (Younger Dryas) conditions in the Colombian Cordillera (5°N, 2850 m) is reported in Flohn (1978) (9); a hint of a decrease of temperature and a strong indication of a decrease of CO_2 (by about 100 ppm) is reported for the same period from the Antarctic "Dome C" ice core (Delmas et al) (1980) (fig 7.9 (b)). This core also shows a rise in CO_2 (trapped in the ice) from 15000 BP -13000 BP (dates uncertain by say ±1000) of about 100 ppm, (from 190 ppm to 300 ppm) suggesting that the waxing and waning of world-wide temperature was accompanied by quite large changes in CO_2 on more than one time scale. Fig 7.10 shows a reconstruction of mid-latitude tree lines, 13000 BP to now. Fig 7.11 summarises the current rather vaguely understood picture of the broad changes in mid-latitude N. Hemisphere temperatures on several time scales (Lamb, P334) including the Holocene (10000 year) time scale.

7.5.2 The recession of N. Hemisphere ice sheets in the early Holocene

This description is mostly taken from Lamb. Figs 7.12 (a) - (c) show reconstructed positions of the ice sheets for (a) 18000 BP, (b) the Allerod warm phase and (c) the Younger Dryas. Ice had nearly disappeared from Scotland by the end of the Allerod but then strongly readvanced for a few hundred years in the Younger Dryas (known as the Loch Lomond Readvance), an advance that has left many traces in old moraines etc and which occurred near the N. Hemisphere Milankovitch radiation maximum. Fig 7.13 shows a reconstruction of the stages in the contraction of the Scandinavian Ice Sheet; the associated emergence of the Baltic is shown in fig 7.14 (a) - (d) (a lot of the evidence comes from old shore lines). At first the Baltic was probably a fresh water lake (fig 7.14 (a)) then as sea-level rose it became the salt "Yaldia Sea", connected now with the Atlantic. The land continued to rise ("isostatic uplift") as the burden of ice disappeared the Baltic became fresh again (8000 BP). As sea-level rose further, due to melting of the Laurentide ice sheet, the Baltic became salt again. At present the land is rising by up to 1 m a year in the northern Gulf of Bothnia (near 65°N) so widespread re-emergence of land may occur there in the next 1-2 thousand years unless global sea-level rises. Fig 7.15 shows an old, but apparently acceptable reconstruction of the geography of Britain and NW Europe 1000-2000 years before sea-level rose high enough to turn Britain into an island. Fig 7.16 shows isochrones of the withdrawal of the Laurentide ice sheet. Remnants still exist on Baffin Island (Barnes Ice Cap). A slowing of the retreat in the Younger Dryas period is suggested.

7.6 The Holocene Milankovitch Raidation Maximum - the Sahara and the Sahel

There is considerable evidence of increased rainfall in the southern Sahara and the Sahel about 4000-9000 years ago. Cave and rock paintings of many species of savannah animals (being hunted or farmed) are found from the latter part of this time (an excellent example in Lockwood, p121 (10)). Widespread evidence of expanded lakes occurs in the region (11), including an enormously extended Lake Chad (Lake Megachad), and other equatorial African and Sahel lakes were larger too (fig 7.17). Kutzbach and Guetter (KG) (1984) (12) have carried out two AGCM experiments for radiation conditions for 9000 BP to determine if a high resolution model (the NCAR Community Climate model) indicates that a more vigorous African and Asian Summer monsoon was likely. KG carried out two types of anomaly-control experiments:-

(a) Perpetual January and July experiments with 9000 BP radiation, retaining an extensive Laurentide ice sheet. 9000 BP radiation was used in anomaly experiments, present day radiation and ice in the control experiment.

(b) Similar, but no Laurentide ice sheets at 9000 BP.

Climatological-mean SST is believed to have been similar averaged over the year but with a slightly larger annual range (perhaps 1°C); the model was given modern climatological mean SST in all experiments however. Each experiment was run for 120 days and the final 90 days averaged. The main results - global maps of the differences between anomaly and control experiments - are shown in fig 7.18 (a) - (c) (surface temperature) and 7.19 (a) -(c) PMSL.

In winter, N.Hemisphere land at higher latitudes is simulated to be colder at 9000 BP as a result of the reduced winter radiation but in summer the land is much warmer as radiation is larger i.e. the seasonal range increases (by 3°C over N. Hemisphere land as a whole). In summer, the presence of the Laurentide ice sheet only affects temperatures just downstream (over the N. Atlantic); just upstream, (fig 7.18 (b)) its presence does not change the surface temperature, which is considerably warmer than now in summer. In winter the Laurentide ice sheet reduces PMSL considerably over the N. Atlantic/W. European region, inducing a large lee trough. In summer, the 9000 BP monsoon circulation over N. Africa and S. Asia is considerably enhanced (fig 7.19 (b)). Precipitation increases in the area from 30°E - east Asian coast and south of 40°N by 20% according to KG. Fig 7.20 summarises zonally-averaged precipitation changes. In July increased precipitation associated with the ITCZ at 9000 BP is shown; the vertical bars represent 1 standard deviation of the control integrations (1050 model days were available for modern (control) conditions). So given the archaeological evidence as well it is very likely that summer rainfall was larger in the Sahel/Sahara at 9000 BP than now and probably for some time after.

7.7 Holocene maximum (hypsithermal)

Figs 7.10, 7.11 suggested that rather modest changes of worldwide climate have occurred since 5000 BP (3000 BC), at least up to 1000 AD. Details are difficult to unravel but about 3000-3500 BC there is evidence of a short cooling (Piora Oscillation) in the N. Hemisphere. The details of Holocene climate are currently being pieced together for the whole globe by COHMAP, (Cooperative Holocene Mapping Project) in USA. Many proxy techniques are being used including pollen analysis and deep-sea core analysis. It is hoped to reconstruct a mean picture of climate about every 3000 years since 18000 BP. Fig 7.21 is an example of vegetation mapping in N. America for 10000 BP, 6000 BP and 1500 AD (13). Note the reconstructed close approach of forest to the Laurentide Ice Sheet at 10000 BP.

About 4000 BP (2000 BC), the advanced Harrapan culture of the now Thar Desert in Rajastan declined and disappeared. Fig 7.22 suggests this was due to a strong reduction of summer monsoon rainfall towards current conditions. The climatic evidence has mostly been obtained from pollen cores drilled beneath the beds of former lakes that occupy positions between sand dunes.

Subsequently there is evidence that about 500 BC a sharp cooling occurred (the so-called sub-Atlantic pessimum) when temperature may have declined widely by about 2°C and the mountain glaciers advanced. In Roman times the climate was probably rather like nowadays but in early Rome climate was probably cooler. About 800 AD, possibly later, there is evidence of a climatic warming in the middle and high N. Hemisphere latitudes. This was the time (870-950) of the settlement of, first, Iceland and then, Greenland, by the Norse. In the High Middle Ages vineyards were common in England and good quality wines were produced where wine growing is hazardous nowadays. This was the so-called Little Optimum (at least in W. Europe) and shows well on the graph of temperatures of the last 1000 years (fig 7.11). However it is not clear whether the Little Optimum represents a regional or a more widespread change in climate. Growth of some of the Bristlecone pines in south-west USA when near the tree line is believed to be controlled by summer temperature. Fig 7.23 (from two locations in California) shows slight evidence of the Piora temperature oscillation, the 1000 BC - 500 MB cooling and the cooling since the Medieval Optimum, which latter period does not show as a peak but rather as a halt in a steady decline of temperature. The Alpine tree-line curve (fig 7.2.3) is broadly similar in shape except it shows a more definite medieval climatic optimum, and it does not extend back to the Piora oscillation.

7.8 Little Ice Age

As will be shown in lecture 8, it is not necessarily true that if one hemisphere cools or warms that the other responds similarly. Furthermore, changes in the structure of the mid-latitude long waves can give an impression of global warmth or coldness if sampling is longitudinally restricted. Having said this, the evidence for a "Little Ice Age" is quite good, but not all areas were necessarily colder than now as superimposed changes in circulation patterns would probably have occurred. Fig 7.24 shows the results of a survey of historical documents and weather records in Europe and Japan that attempts to summarise the changing frequency of cold winters in these two areas 120° of longitude apart. The diagram suggests that Japanese winter temperatures have fluctuated largely out of phase with those of European winters. However there is geographically widespread evidence for a cooler climate, worldwide, from after 1400 AD until about 1850 or before. Fig 7.25 shows evidence of century time-scale temperature variations from New Zealand, (accuracy of reconstruction unclear) while the Greenland Ice cores also support a cooler climate (the dating should be excellent), though Dome C only gives slight support. It is possible to use ^{18}O measurements in the wood of oaks to determine past changes of temperature, at least in a relative sense. Dating is done by counting tree rings and the ^{18}O concentration is measured in the individual rings. Fig 7.26 shows such a reconstruction for some trees in Germany. Freezing of rivers and canals also became more frequent in Europe around 1600-1800. Most impressive are the results of widespread investigations of the moraines left by mountain glaciers (fig 7.27 gives examples). In many parts of the world there is increasingly strong evidence that the glaciers on many mountains were the most advanced since the Younger Dryas around 1600-1800 AD. (Ladurie gives an excellent description for the Alps (15)).

There is no doubt that conditions in the Iceland-Greenland area became much colder after 1200 AD and especially after 1550 AD. In lecture 3 we showed a diagram of the reconstructed variation of sea-ice around Iceland in weeks/year; the period around 1800 seems to have been the worst for sea-ice. The Norse colony in S. Greenland established around 900 AD probably died out in the fifteenth century as conditions became worse, sea ice prevented access (from Iceland and Europe) and crops failed (16). Fig 7.28 shows the variation of ^{18}O in a Greenland ice core; absolute dates are probably not accurate but a tendency to cooling after about 1100-1200 AD is clearly shown as is the rise in temperature at the beginning of the twentieth century. Remember that temperature increases to the right on these diagrams. Lamb also describes documentary evidence of observations of extensive ice flows around the Faeroe Islands in a few winters in the seventeenth century and once or twice, ice floes reached the Shetland Isles while eighteenth century travellers frequently mention permanent snowbeds in the Cairngorms. In recent years lichenometry has been used to indicate that certain hollows in the Scottish mountains might well have been permanently filled with snow for lengthy periods up to the middle of the last century.

Despite this evidence, more research is required to show whether the period 1600-1800 was cold worldwide. However the latter part of the Little Ice Age overlaps with the instrumental period so we can pursue this problem a little more in the next lecture.

REFERENCES (LECTURE 7)

1. LAMB, H H (1977) Climate: Present, Past and Future Vol 2. Methuen.

2. LORENZ, E N (1968) Climatic Determinism.
In 'Causes of Climatic Change' Ed: J M Mitchell, Jr, Met Monograph 8, pp 1-3. Boston: Amer. Met. Soc.

3. CRITCHFIELD, H J (1983) General Climatology.
4th Edition. Prentice-Hall.

4. CRANE, A J (1981) Techniques for reconstructing Past Climates. In 'Climatic Variations and Variability: Facts and Theories'. Ed:- A Berger Reidel.

5. FRITTS, H C (1976) Tree rings and climate. Academic Press.

6. FAIRBRIDGE, R N (1978) Models of Climate Change. In 'Climatic Change and Variability - a Southern Perspective' Eds: A Pittock et al. Cambridge Univ. Press.

7. BOWLER ET AL (1976) Late Quarternary Climates of Australia and New Guinea. Quaternary Res., 6, pp 359-394.

8. DANSGAARD W et al (1982) A new Greenland Ice Core. Science, 218, pp1273-1277.

9. FLOHN H (1978) Abrupt events in climatic history. In: 'Climate Change and Variability - a Southern Perspective'. Ed: A Pittock et al, Cambridge University Press.

10. LOCKWOOD, J G (1979) Causes of Climate. Edward Arnold, London.

11. NICHOLSON, S E AND FLOHN, H (1980) African environmental and climatic changes and the general atmospheric circulation in Late Pleistocene and Holocene. Climatic Change, 2, pp 313-348.

12. KUTZBACH, J E AND GUETTER, P J (1984) The sensitivity of monsoon climates to orbital parameter changes for 9000 years BP: Experiments with the NCAR general circulation model.
Milankovitch and Climate, Vol 2, pp 801-820.

13. KERR, R (1984) Report in Research News, Science, Oct 19 1984 "Climate since the ice began to melt".

14. LAMB, H H (1982) Climate, history and the modern world. Methuen.

15. LE ROY LADURIE, E (1971) Times of Feast, Times of Famine: A History of Climate since the year 1000.
Trans. B Bray; Douleday.

16. DANSGAARD, W ET AL (1975) Climatic changes, Norsemen and modern man. Nature, 255, pp 24-28.

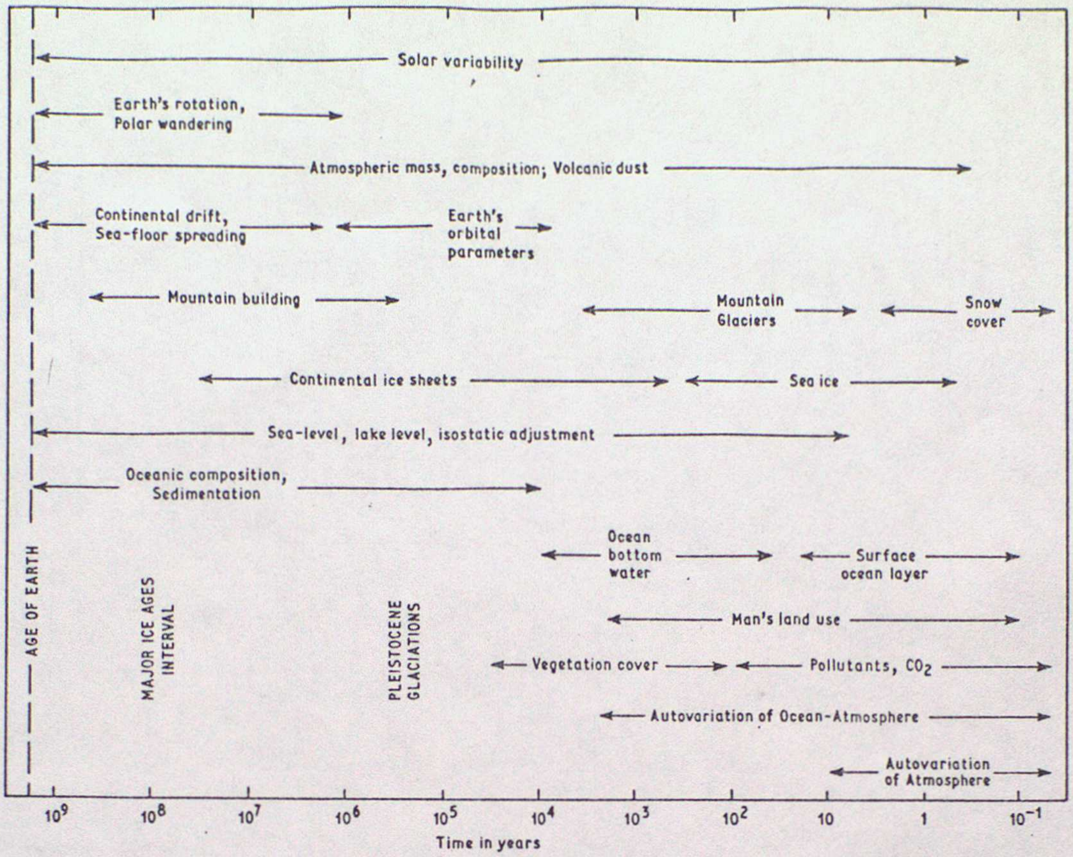

Summary diagram to show the characteristic time-scales over which changes in various influences upon the global climate operate.
(*Adapted from a diagram by* W. L. GATES.)

FIG 7·1

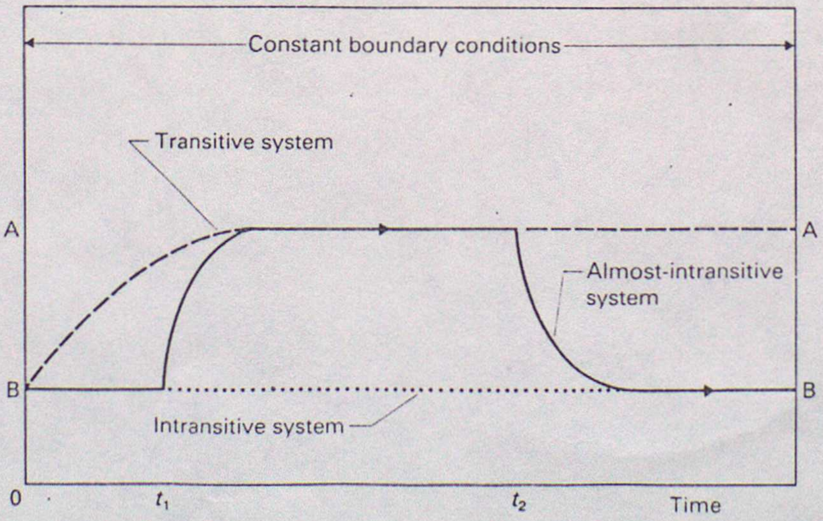
Constant boundary conditions
Transitive system
A
A
Almost-intransitive system
B
B
Intransitive system
0
t1
t2
Time

Illustration of the behaviour of transitive, intransitive and almost-intransitive climatic systems with respect to an initial climatic state B. The climatic state A is an alternative bistable state under the same boundary conditions (*after US National Academy of Sciences, 1975*).

FIG 7·2

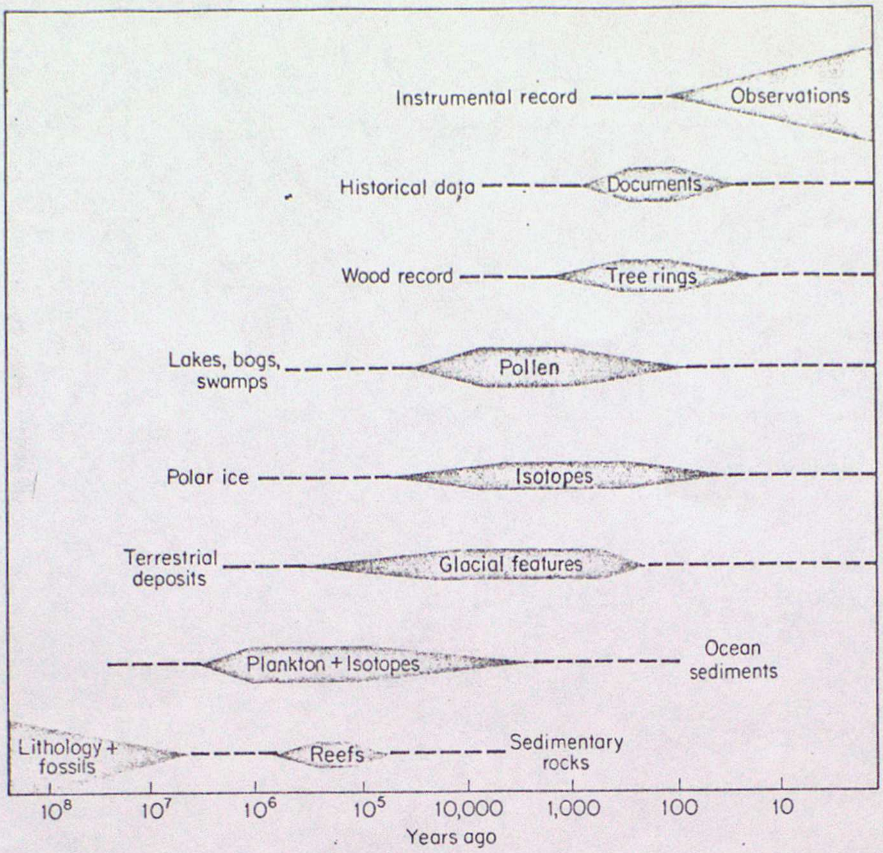

Types of evidence for climatic change and their approximate time scales.
(After Bernabo, *EDIS*.)

FIG 7·3

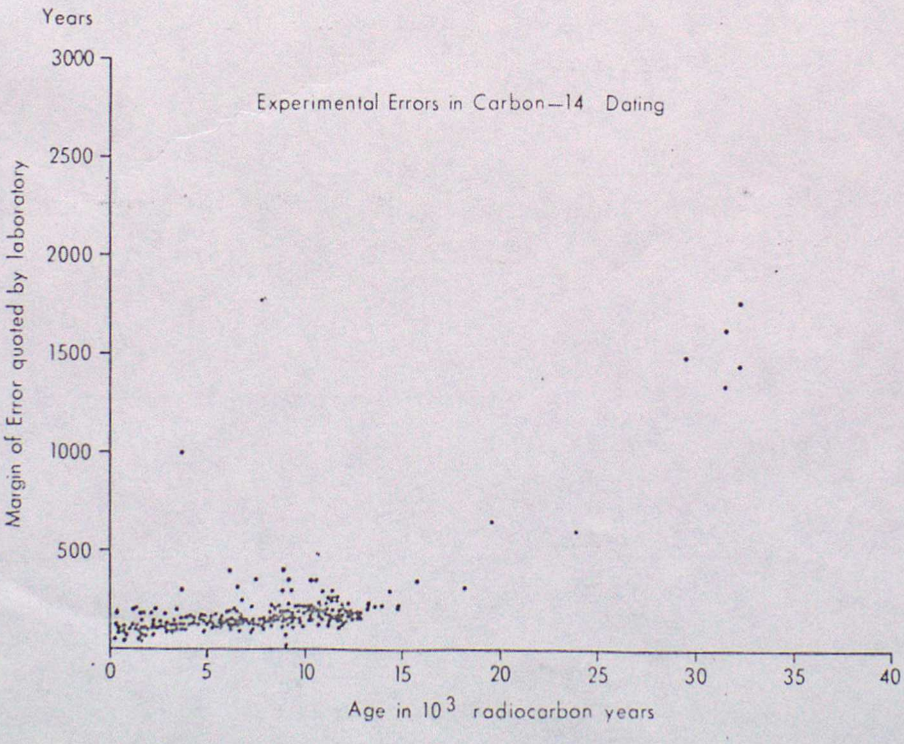

Experimental errors (i.e. random error) in radiocarbon dating.
The plotted points are estimates of one sigma error published with the age results of measurements made in the Cambridge, Copenhagen and Washington University radiocarbon laboratories between 1959 and 1968.
(*From Radiocarbon, vols. 1–10.*)

FIG 7·4

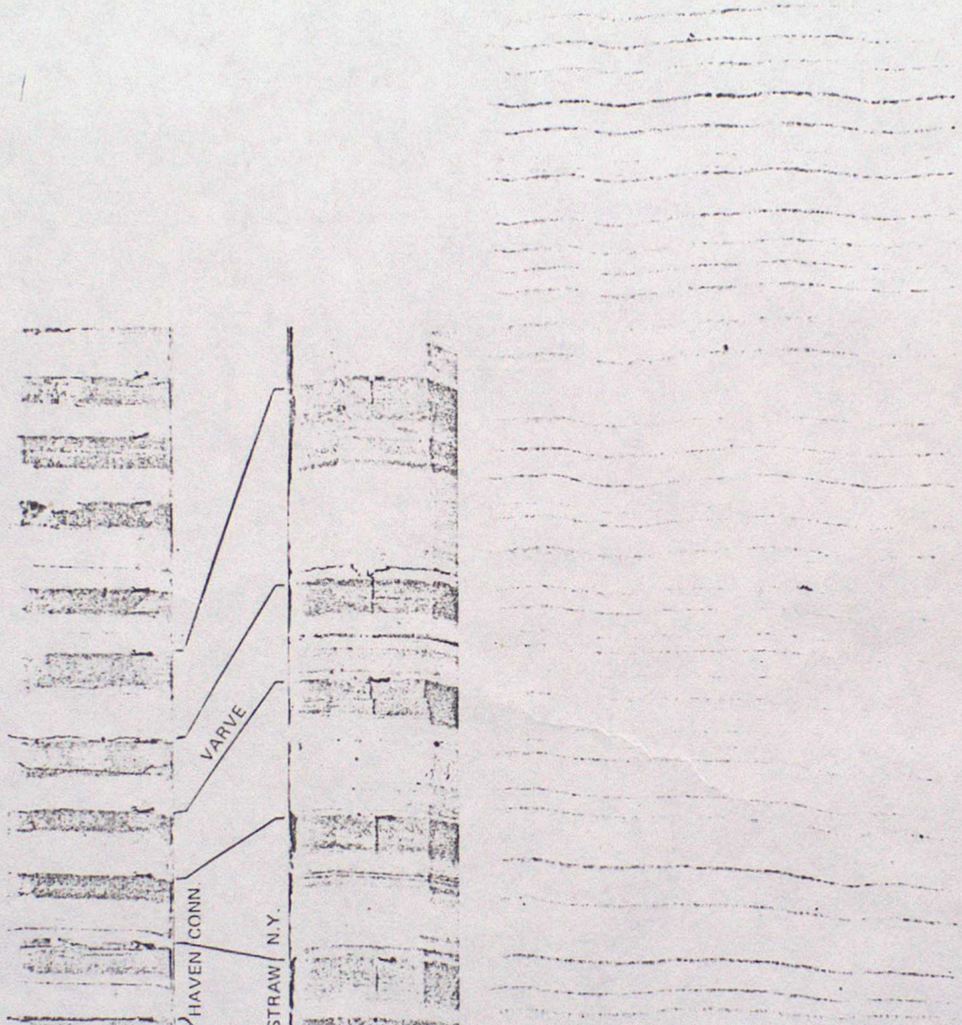

Examples of proxy evidence for geochronology. Varve correlations on the left are from sites near New Haven, Connecticut, and Haverstraw, New York. The tree-ring cross section on the right indicates variations in annual growth of a New Zealand conifer. (Varve photograph courtesy The American Museum of Natural History; tree-ring photograph courtesy Peter Dunwiddie, Quaternary Research Center, University of Washington.)

FIG 7·5

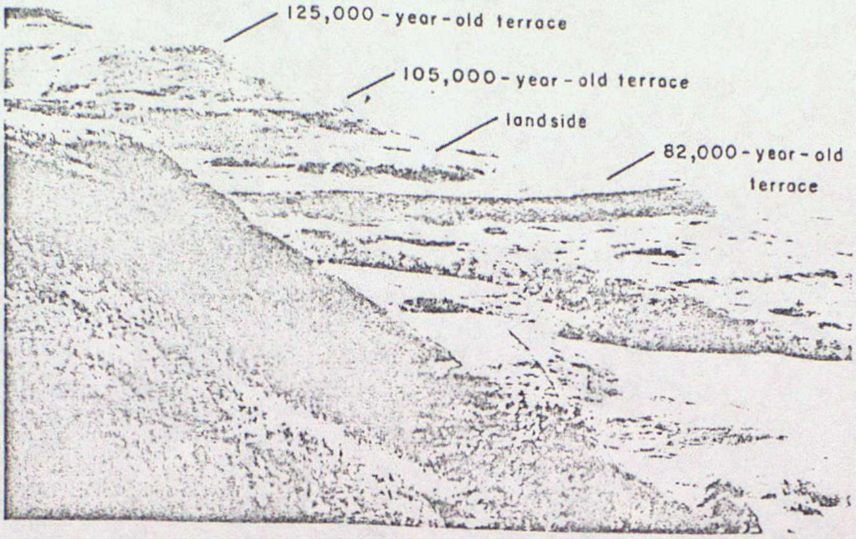
125,000-year-old terrace
105,000-year-old terrace
landside
82,000-year-old terrace

Reef terraces on New Guinea. A view along the north coast of the Huon Peninsula, showing uplifted terraces formed by Pleistocene coral reefs. Terraces similar to these were first dated on the Caribbean island of Barbados. (Courtesy of A. Bloom.)

FIG 7·6

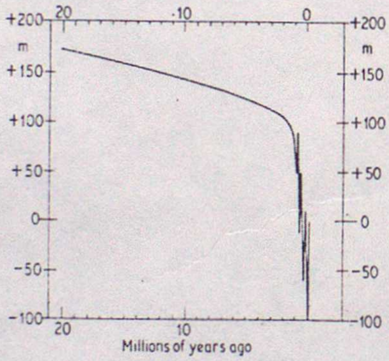

World sea level changes since the late Tertiary (Miocene).

(Ice-age-interglacial variations only schematically indicated – in reduced numbers).

FIG 7·7a

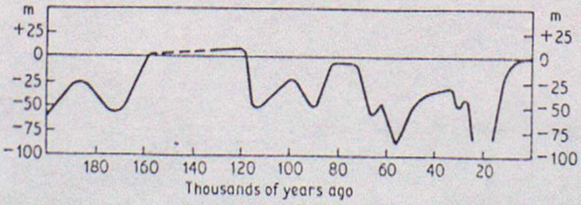

History of world sea level over the last 200 000 years, according to VEEH and CHAPPELL (1970).

FIG 7·7b

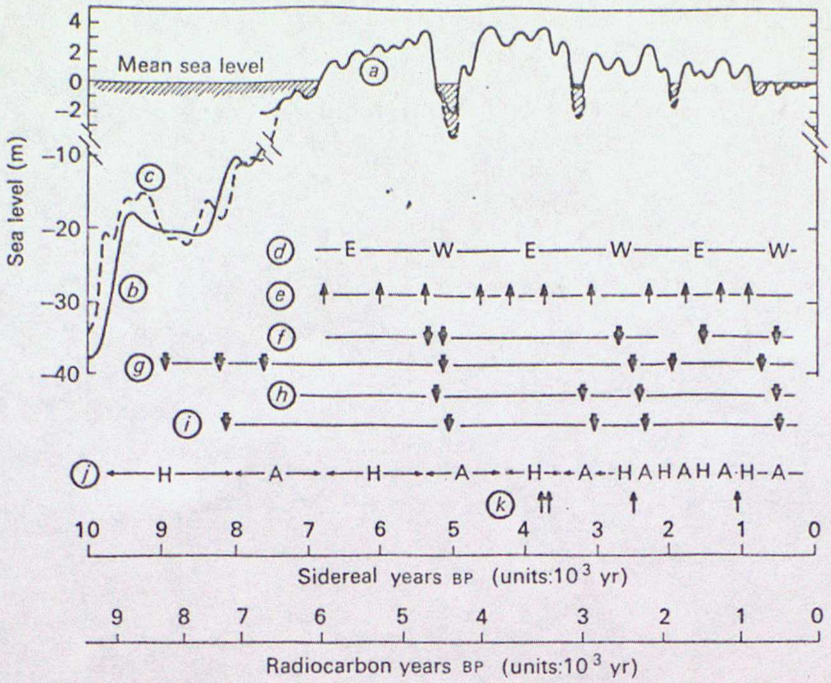

. Trace of eustatic sea level over the last 10,000 years, as indicated (*a*) by an example from Brazil (Fairbridge, 1976), based on radiocarbon-dated beach deposits, coral reefs and Indian middens, for the last 7,000 years, and for the previous 3,000 years by data (*b*) from Scandinavia (Mörner, 1969), and (*c*) elsewhere (Fairbridge, 1961). Note that time is given in both sidereal and radiocarbon years. Comparisons are presented (from top to bottom) with (*d*) the magnetic declination cycle (approximately 2,850 years) with its E–W inflections; (*e*) the $^{18}O/^{16}O$ isotope ratio peaks from Greenland (Dansgaard *et al.*, 1971) indicative of maximum warming; the glacial readvances (*f*) from New Zealand (Burrows, 1973, 1975), (*g*) from Greenland (Ten Brink & Weidick, 1974), (*h*) from Alaska and (*i*) from Lapland (Denton & Karlén, 1973); (*j*) the Sahara climates (Geyh & Jäkel, 1974) where H denotes humid, and A denotes arid; and (*k*) maximum flood levels of the Nile (Fairbridge, 1962, and pharonic inscriptions). Note that imperfections in the datings exist that might present false impressions of one region 'leading' another.

FIG 7.7c

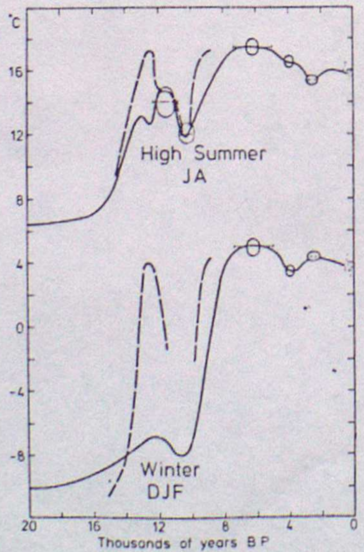

Probable course of prevailing temperatures in central England over the last 20 000 years.

Full lines = mainly from botanical evidence.

Broken lines = amendment suggested by analysis of the beetle fauna.

Ovals = margins of uncertainty of the dating and temperature values derived.

Horizontal bars = apparent duration of the conditions from which the temperature values were derived.

Dots = mean temperature values derived for individual centuries of the last millennium from reported weather or actual temperature measurements (see fig. 6.6, Volume 1, p. 236).

FIG 7.8a

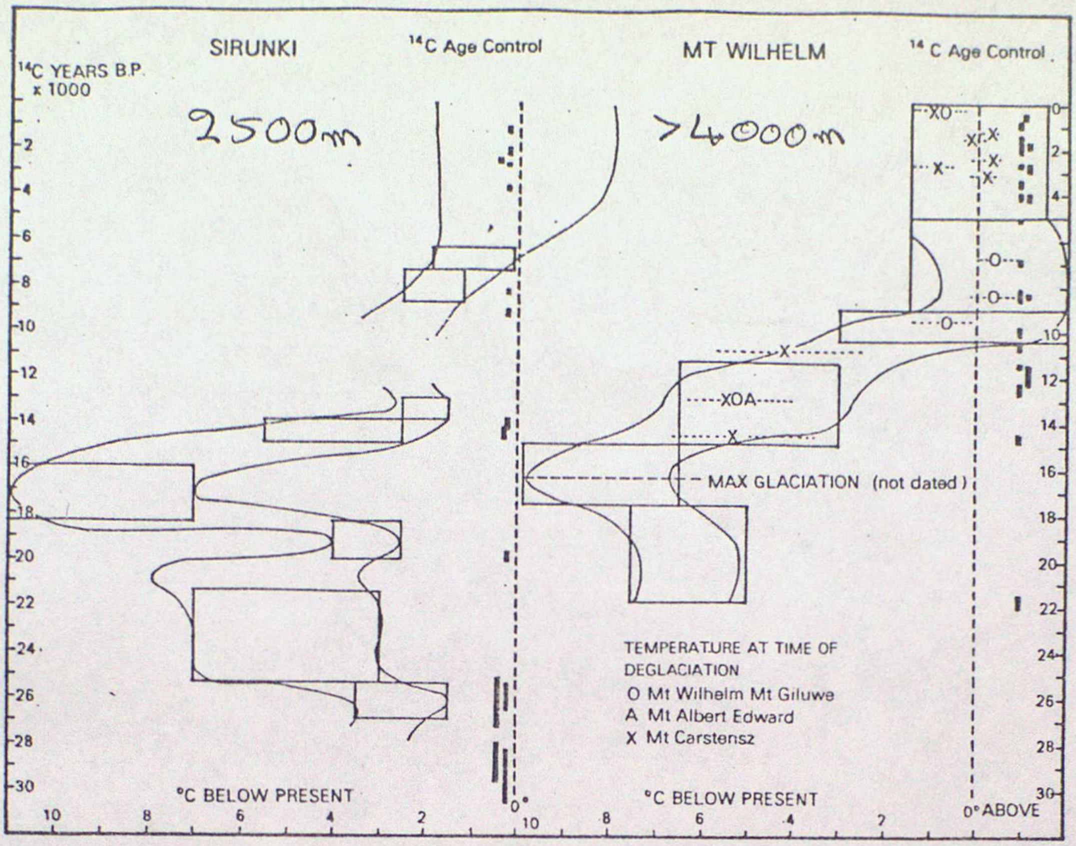

Limits of temperature variation through the past 28,000 years at two sites in the highlands of New Guinea derived from pollen analysis, with estimates of temperature indicated by glacial stages on four mountains.

FIG 7.8b

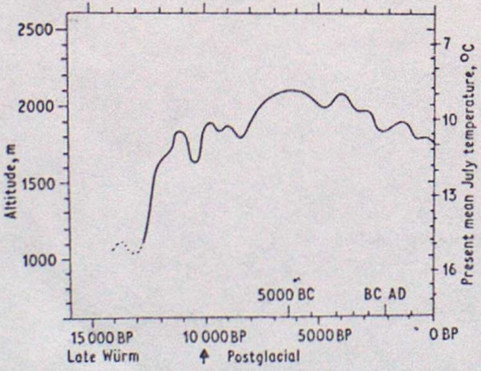

Generalized graph of height changes of the upper tree line in the Alps and other temperate mountain regions over the last 15 000 years.

(From MARKGRAF *(1974), p. 71; reproduced by kind permission.)*

The secondary climatic optimum or Little Optimum (in the European Dark Ages and Early Middle Ages)

FIG 7.10

(FIG 7.9 CAN BE FOUND WITH FIG 7.15)

FIG 7·11

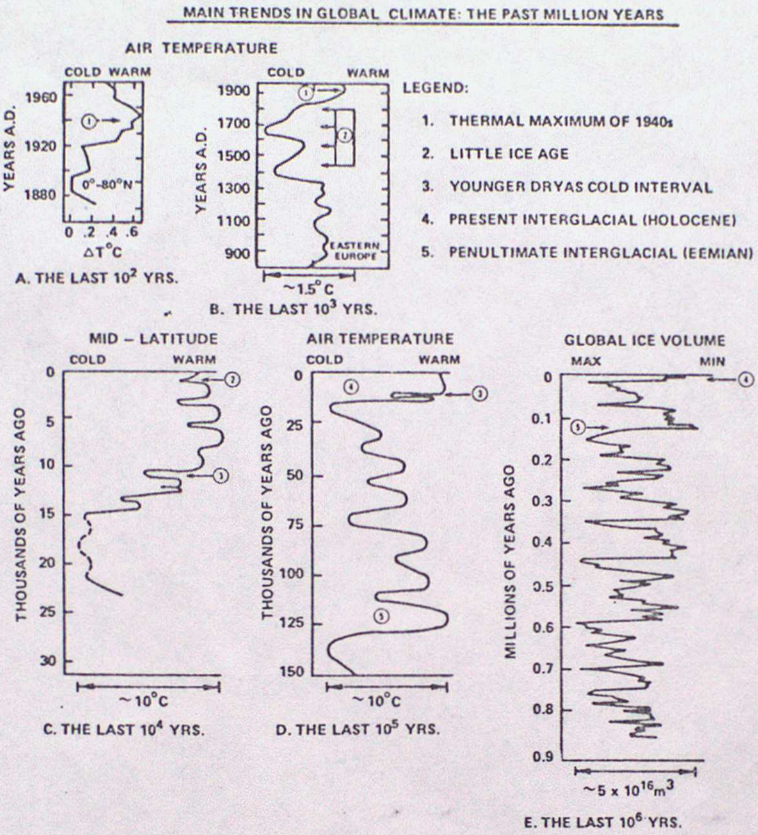

Indicators of global temperature change: different time spans compared.

(*a*) Successive 5-year mean observed surface air temperatures, last 100 years (MITCHELL *1963*).

(*b*) Winter severity index for Europe near 50°N 35°E, last 1000 years (LAMB *1969*).

(*c*) Generalized temperature changes in middle latitudes of the northern hemisphere, from tree line studies, last 10 000 years (LAMARCHE *1974*).

(*d*) Middle latitudes northern hemisphere air temperature variations, from diagnosis of sea temperatures and from pollen records on land, last 100 000 years (compiled by W. L. GATES from the curves in fig. 15.10).

(*e*) Global ice volume changes from isotope measurements on plankton in a Pacific Ocean sediment core, last million years (as in fig. 15.4).

(*Diagram kindly supplied by Drs* W. L. GATES *and* J. S. PERRY *with the permission of the U.S. National Academy of Sciences.*)

FIG 7·12 a

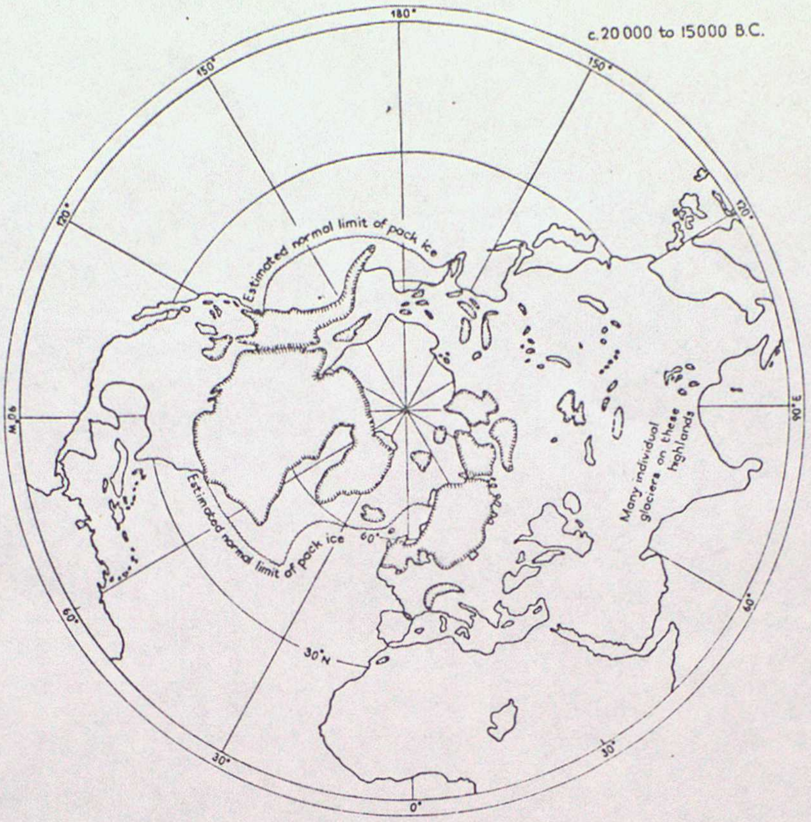
c. 20 000 to 15000 B.C.
180°
150°
150°
120°
120°
90°W
90°E
60°
60°
30°
30°
0°
Estimated normal limit of pack ice
Estimated normal limit of pack ice
60°
30°N
Many individual glaciers on these highlands

Northern hemisphere geography at the time of the last climax of glaciation about 18 000 years ago.

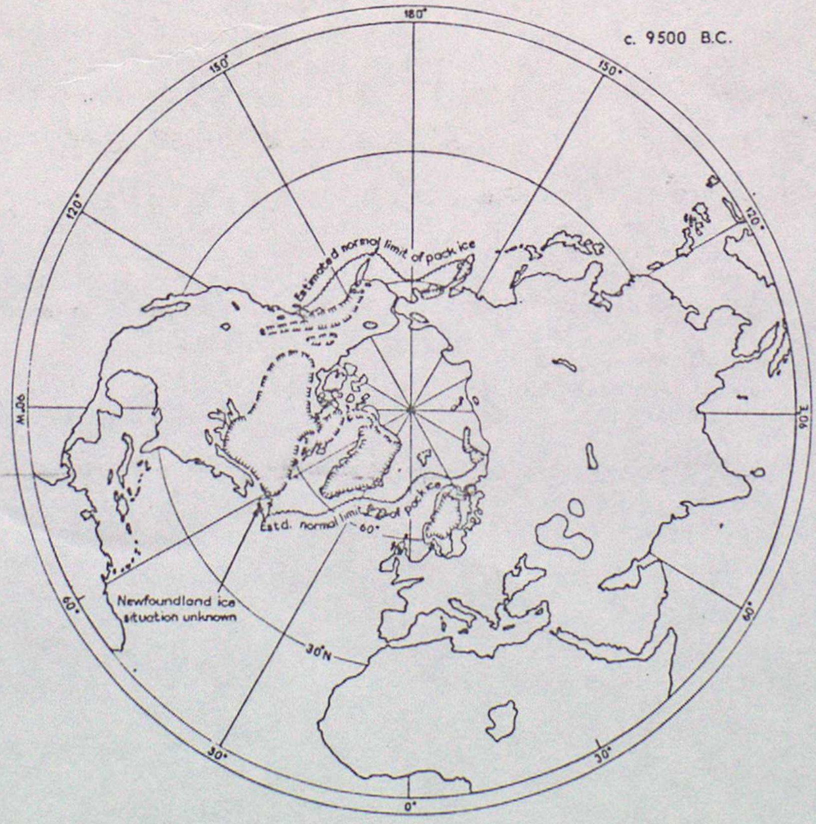
c. 9500 B.C.
180°
150°
150°
120°
120°
90°W
90°E
60°
60°
30°
30°
0°
Estimated normal limit of pack ice
Estd. normal limit of pack ice
60°
30°N
Newfoundland ice situation unknown

Northern hemisphere geography at the time of the Allerød (warm) interstadial 11 000–12 000 years ago.

FIG 7·12 b

FIG 7·12 c

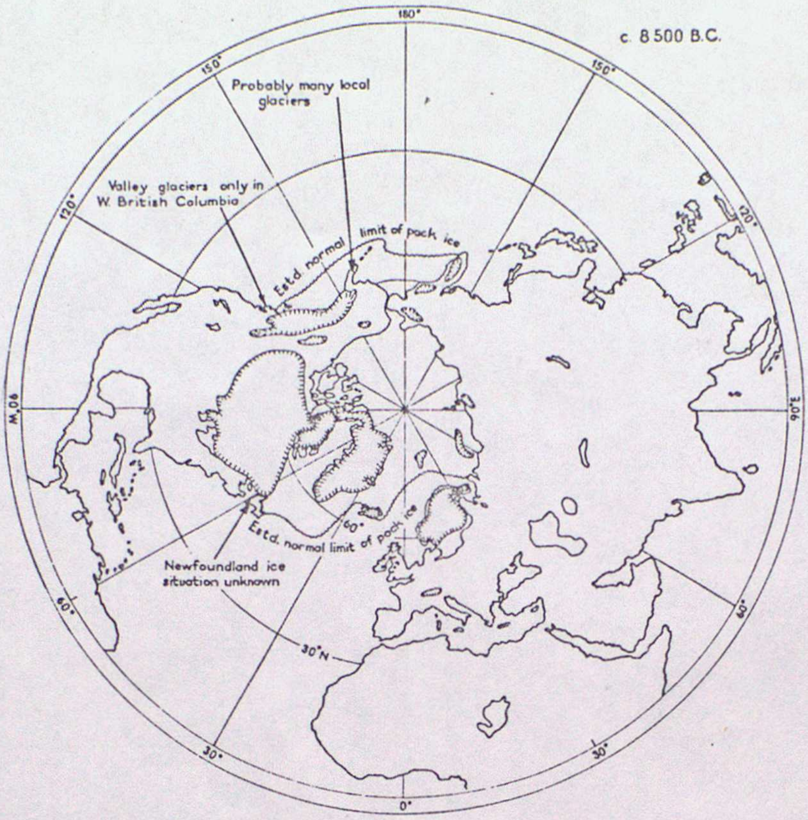
c. 8 500 B.C.
180°
150°
150°
120°
120°
90°W
90°E
60°
60°
30°
30°
0°
30°N
60°
Probably many local glaciers
Valley glaciers only in W. British Columbia
Estd. normal limit of pack ice
Estd. normal limit of pack ice
Newfoundland ice situation unknown

Northern hemisphere geography during the post-Allerød cold time between about 10 200 and 10 800 years ago.

FIG 7·13

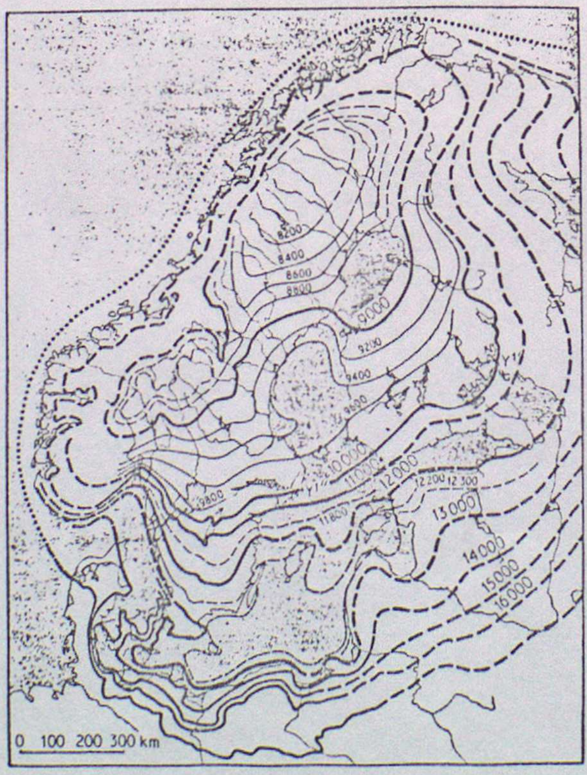
8200
8400
8600
8800
9000
9200
9400
9600
9800
10 000
11 000
11 800
12 000
12 200
12 300
13 000
14 000
15 000
16 000
Y1
Y1
0 100 200 300 km

Positions of the retreating edge of the main north European ice sheet from about 17 000 to 8200 years ago. Dates based on Swedish varve chronology.

(*After* DE GEER *1954*.)

FIG 7.14

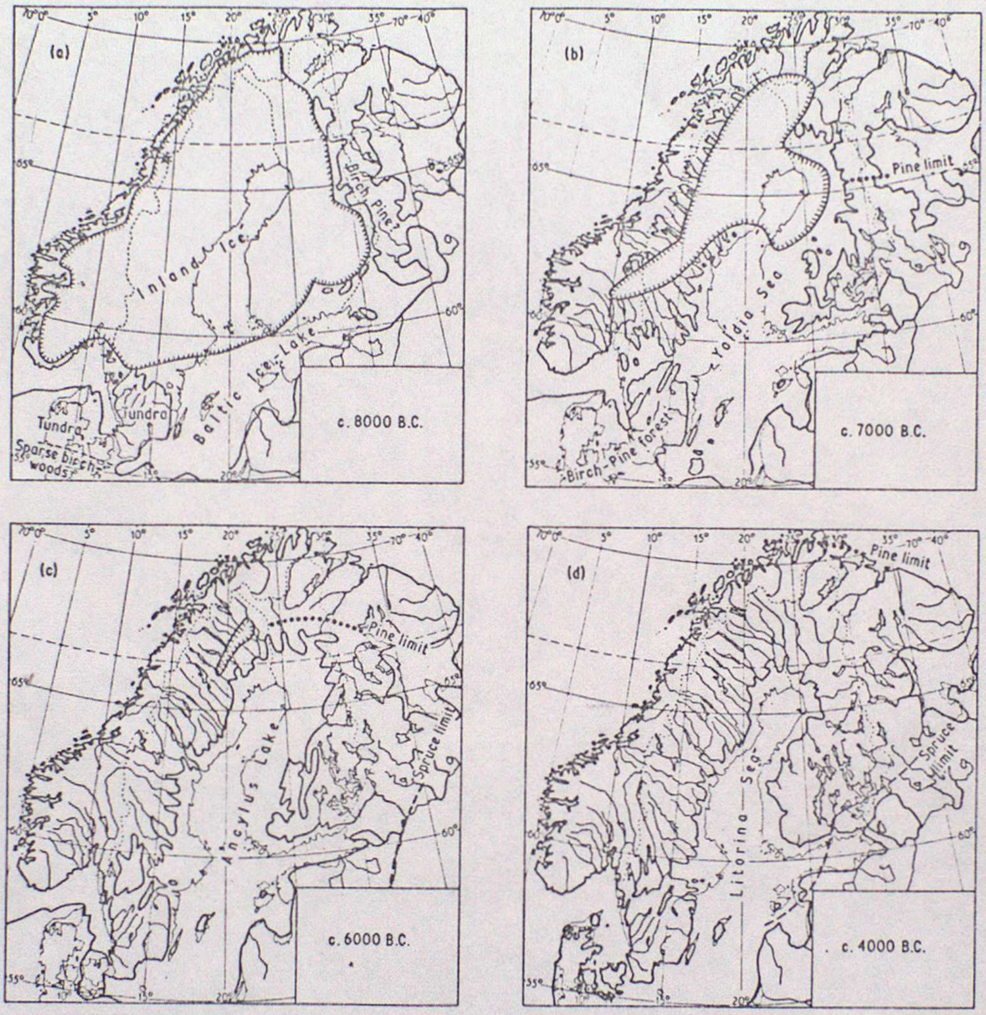
a
b
c
d
(a)
Inland Ice
Birch pine?
Baltic Ice-Lake
Tundra
Tundra
Sparse birch woods
c. 8000 B.C.
(b)
Pine limit
Yoldia Sea
Birch-Pine forest
c. 7000 B.C.
(c)
Pine limit
Ancylus Lake
Spruce limit
c. 6000 B.C.
(d)
Pine limit
Spruce limit
Litorina — Sea
c. 4000 B.C.
70°
0°
5°
10°
15°
20°
35°
40°
65°
60°
55°

The postglacial development of the Baltic. (*a*) 8000 B.C. (*b*) 7000 B.C. (*c*) 6000 B.C. (*d*) 4000 B.C.
(*After* HULTÉN *1971*.)

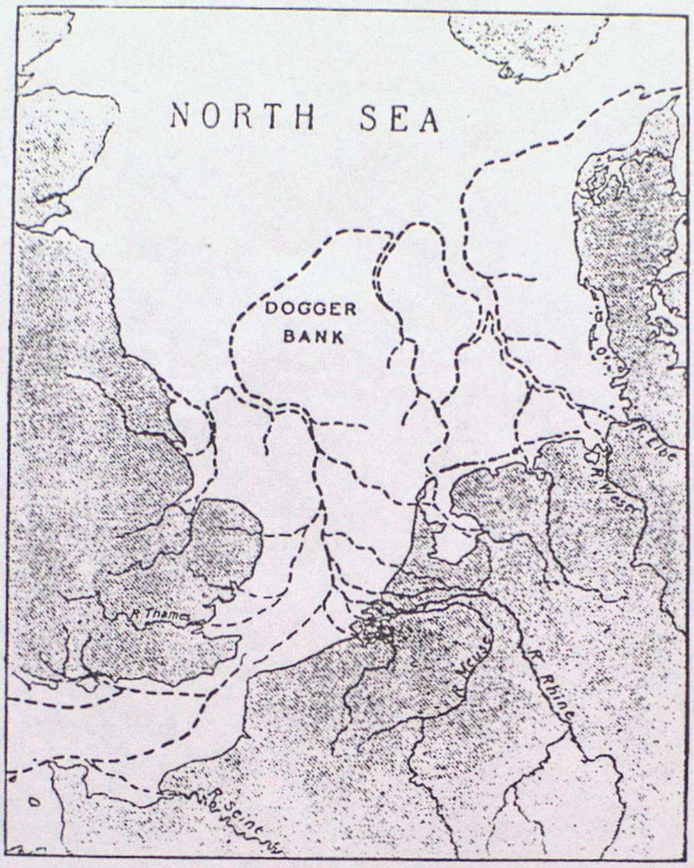
NORTH SEA
DOGGER BANK
R. Thames
R. Rhine
R. Seine
R. Elbe
R. Weser

FIG 7.15

The geography of Northsealand about 7000 B.C. (*first published by* CLEMENT REID *in 1902; also in* GODWIN *1956.*)

FIG 7.9 a

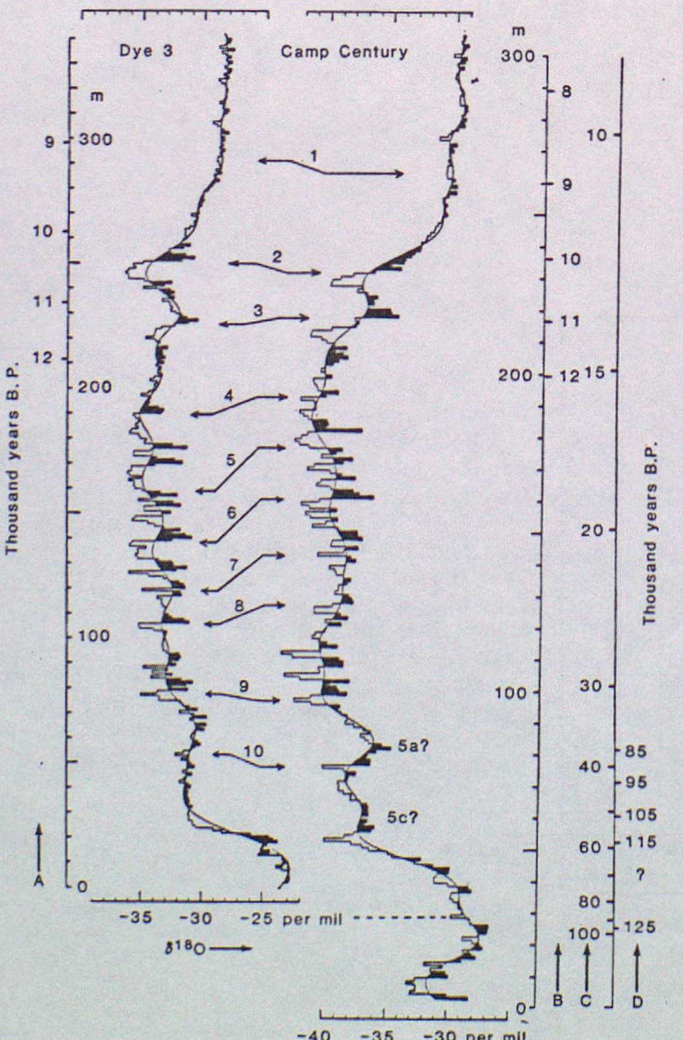

FIG 7.9 b .. Evidence from an Antarctic ice core that the atmospheric CO_2 concentration (dots) was half the present value at the peak of the last glaciation 18000 years ago. The change of ocean volume as the ice melted (15000–10000 years ago) is shown by the change in $^{18}O:^{16}O$ ratio (continuous curve). (Based on Delmas, Ascencio & Legrand 1980.)

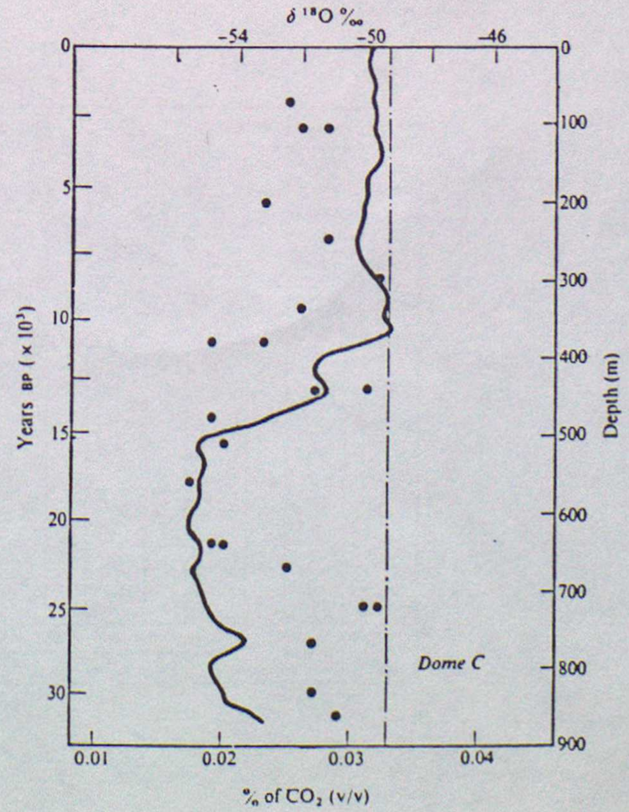

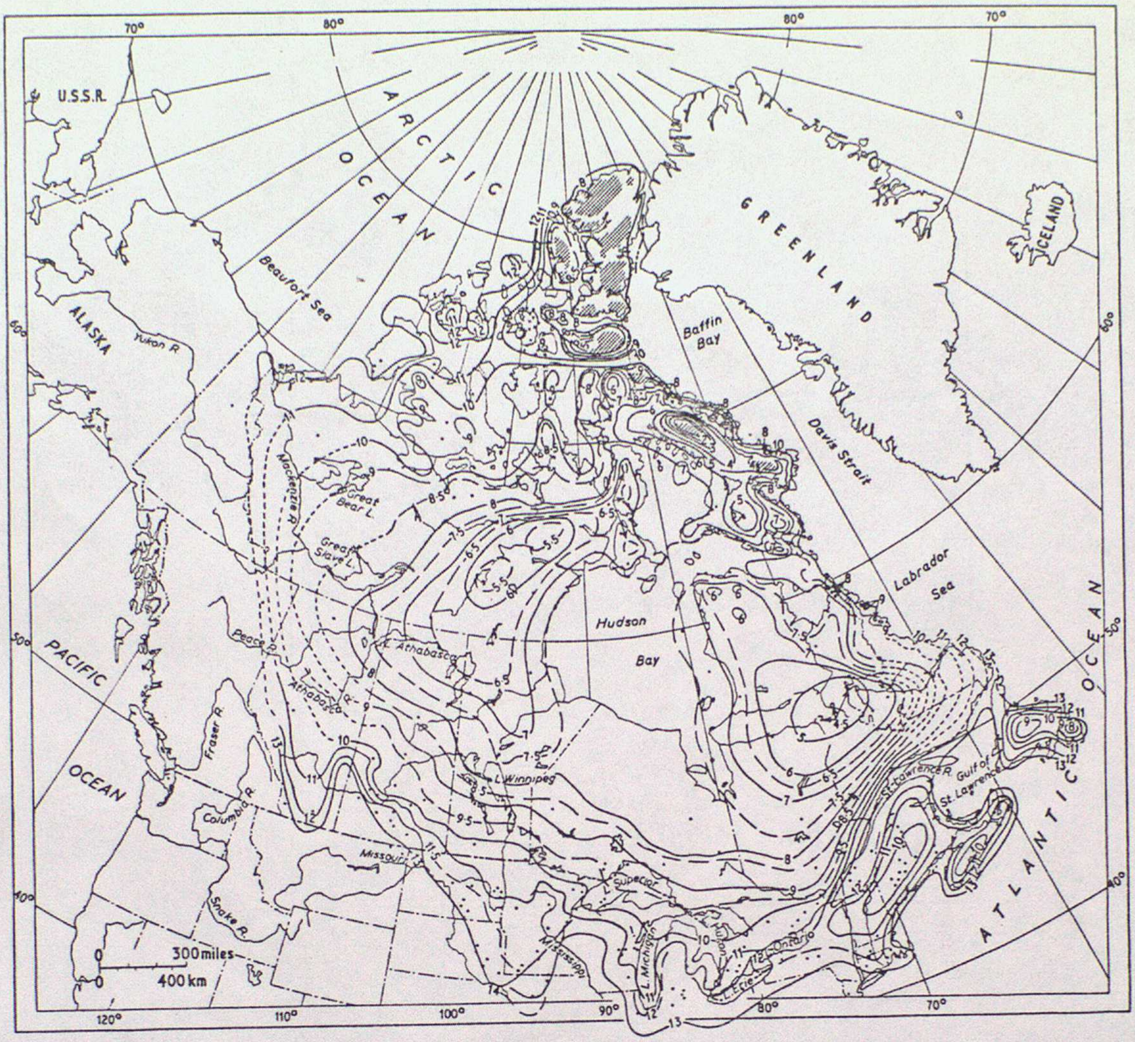
U.S.S.R.
ARCTIC OCEAN
GREENLAND
ICELAND
ALASKA
Yukon R.
Beaufort Sea
Baffin Bay
Davis Strait
Labrador Sea
Hudson Bay
Great Bear L.
Great Slave L.
Mackenzie R.
L. Athabasca
Athabasca
Peace R.
PACIFIC OCEAN
ATLANTIC OCEAN
Fraser R.
Columbia R.
Snake R.
Missouri
Mississippi
L. Winnipeg
L. Superior
L. Michigan
L. Huron
L. Erie
L. Ontario
St. Lawrence R.
Gulf of St. Lawrence
300 miles
400 km
70°
80°
120°
110°
100°
90°
60°
50°
40°

Isochromes of the withdrawal of the North American (Laurentide) ice sheet.
All dates B.P. (before present).
Dots show where radiocarbon dates have been established.
Moraines, coastlines and all other available field evidence used.
(*Reproduced from* BRYSON *et al.* (*1969*); *by kind permission.*)

FIG 7·16

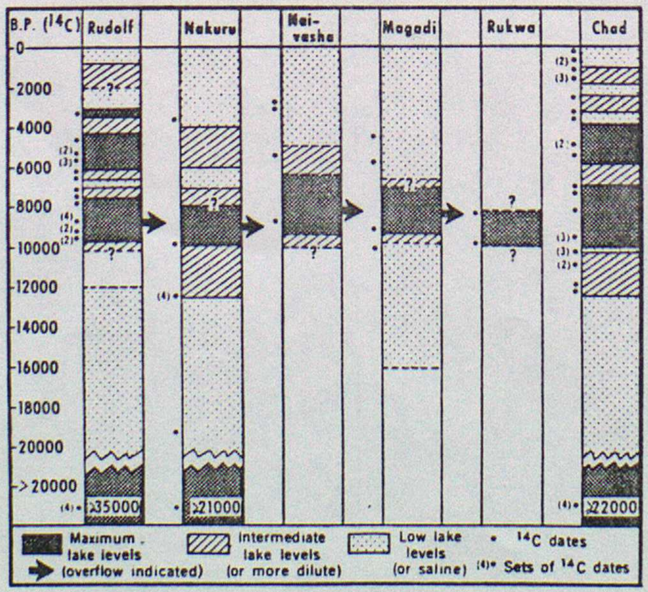

Lake levels in equatorial and tropical Africa.
Radiocarbon dated high stands and low stands.

Lake Rudolf	(4°30′–2°20′N 35°50′–36°40′E)
Lake Nakuru	(0°20′S–36°05′E)
Lake Naivasha	(0°50′S 36°20′E)
Lake Magadi	(1°55′S 36°15′E)
Lake Rukwa	(8°S 32°20′E)
Lake Chad	(approx. 13°N 13°E)

(*From* BUTZER *et al. 1972; reproduced by kind permission of the authors and of* Science.)

FIG 7·17

FIG 7·18

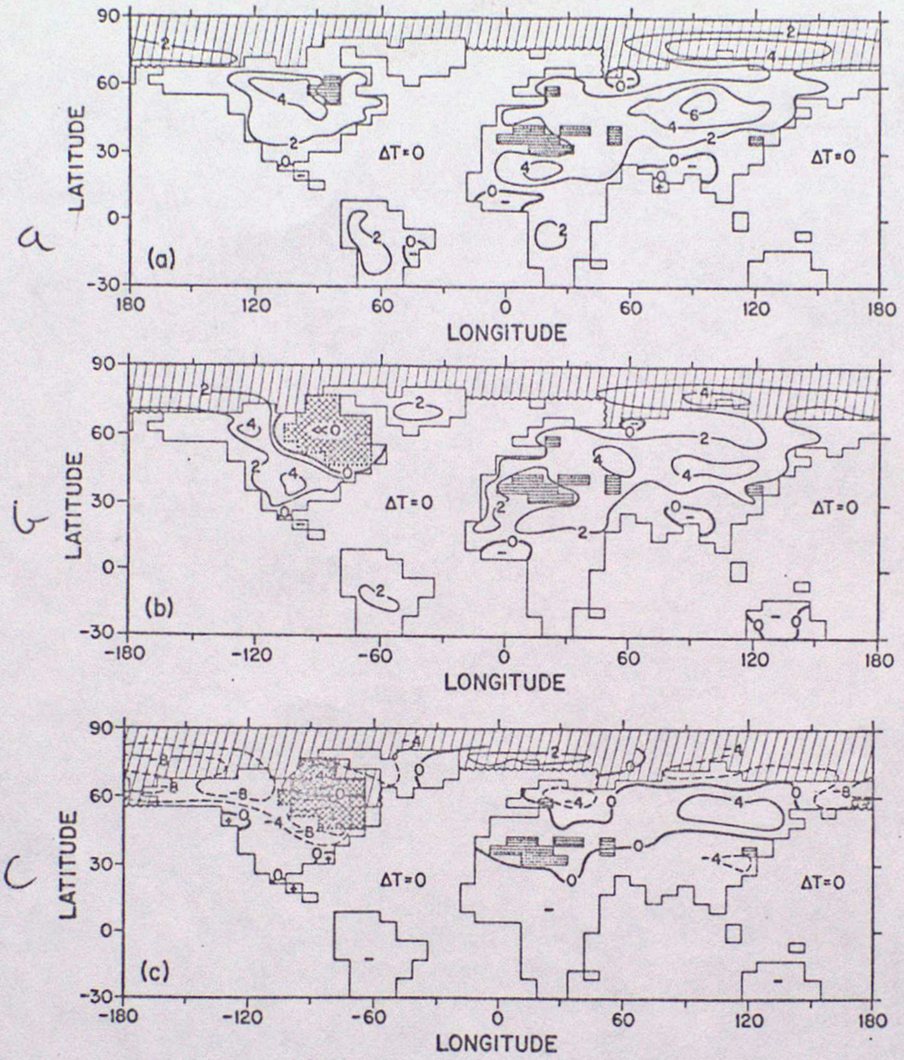
a
b
c
(a)
(b)
(c)
LATITUDE
LONGITUDE
90
60
30
0
-30
180
120
60
0
60
120
180
-180
-120
-60
ΔT=0
2
4
6
0
-4
-8
<<0

Simulated land surface temperature (K) differences (9 kyr BP minus present) for a) an experiment with solar radiation for July 9 kyr BP, present July ocean surface temperature, and no North American ice sheet ; b) same as (a) except with North American ice-sheet ; c) same as (b) except for January. Temperature difference is prescribed to be zero at ocean gridpoints and at interior sea gridpoints (wavey lines) but not over sea ice (hatched). The area covered by the North American ice sheet is indicated with cross-hatching. Results of the simulation for the region south of 30° s are not shown because the number of land gridpoints is small.

FIG 7·19

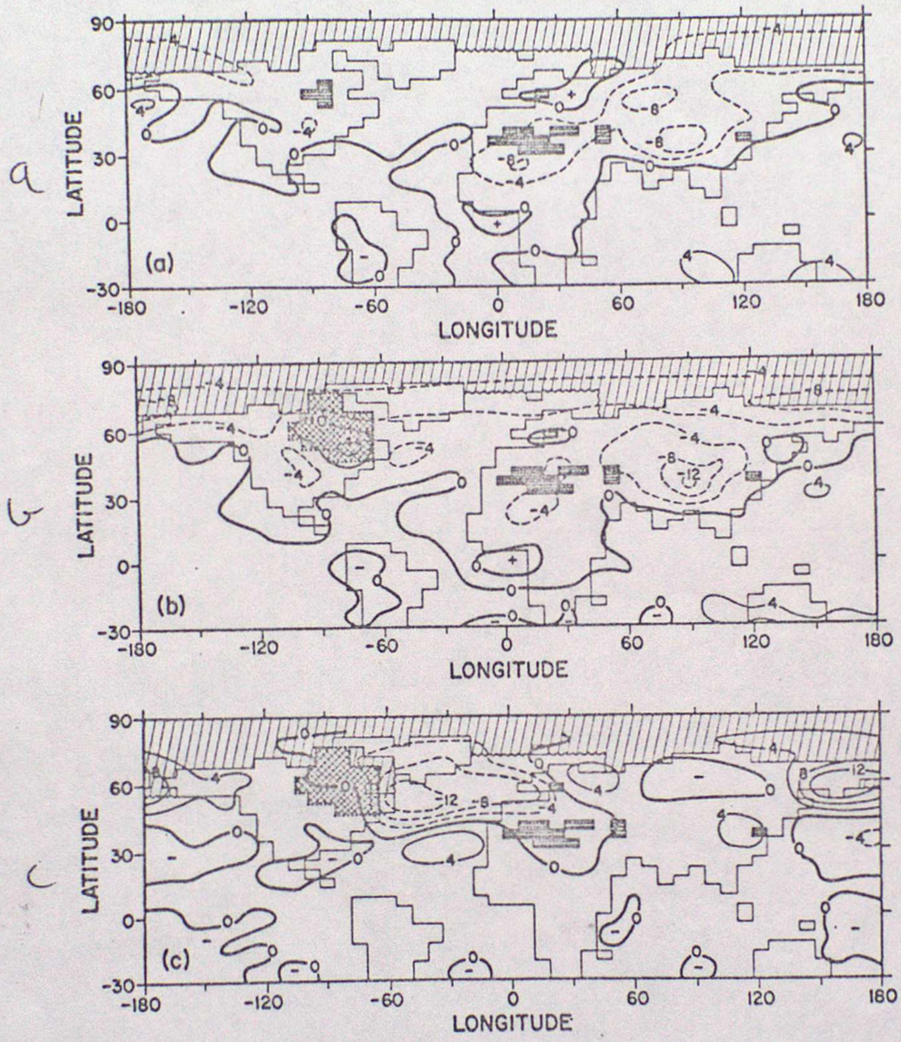

a
b
c
(a)
(b)
(c)
LATITUDE
LONGITUDE
90
60
30
0
-30
-180
-120
-60
0
60
120
180
0
4
-4
-8
-12
12
8
+
-

Simulated sea-level pressure (mb) differences (9 kyr BP minus Present) for : a) an experiment with solar radiation for July 9 kyr BP, present July ocean surface temperature, and no North American ice-sheet ; b) same as (a), except with North American ice-sheet ; c) same as (b), except for January.

FIG 7·20

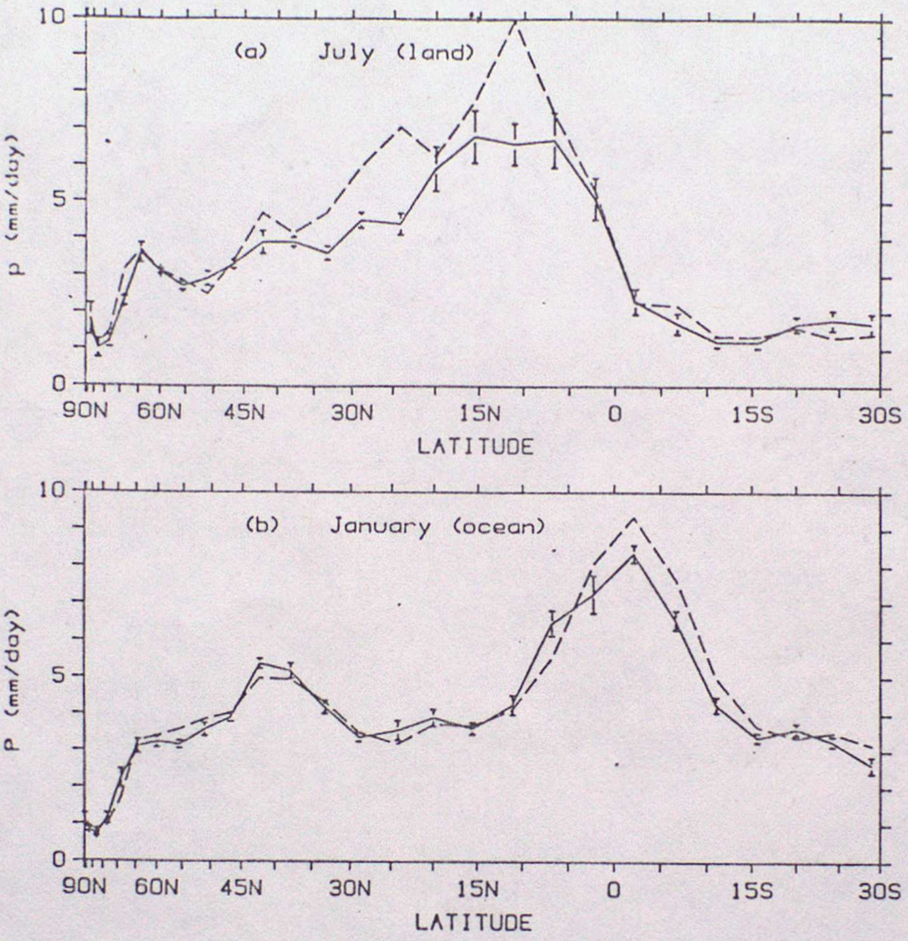

Latitudinal average of simulated precipitation (mm/day) as a function of sine of latitude : a) July--land precipitation; the control simulation (solid line) and the experiment with 9 kyr BP solar radiation and with the North American ice sheet (dashed line) ; b) January--ocean precipitation ; the control simulation (solid line) and the experiment with 9 kyr BP solar radiation and with the North American ice-sheet (dashed line). Vertical bars indicate one standard deviation about the modern control simulation.

FIG 7·21

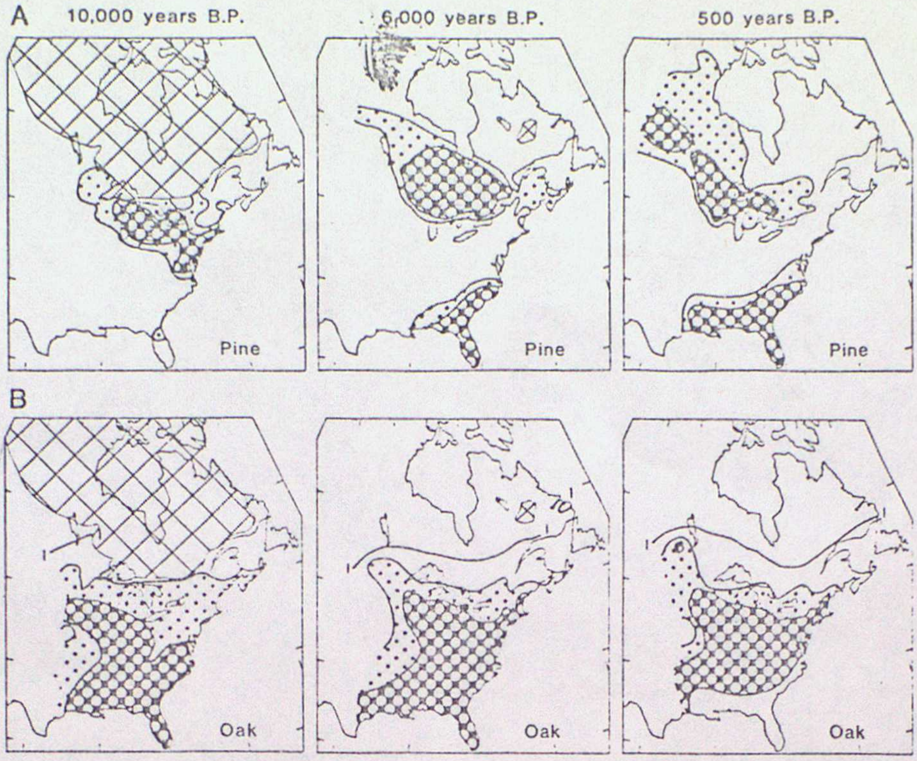

Pollen clues to shifting Holocene climate

These maps illustrate the continuing adjustment of plants to changing climate. A decrease in summer solar radiation and the withdrawal of the cold ice sheet (crosshatch) combined to withdraw the oak and northern pine forests to the north and then to develop the southern pine forest. Light stippling is 5 to 20 percent oak or 20 to 40 percent pine; heavy stippling is greater than 20 percent oak or greater than 40 percent pine.

FIG 7·22

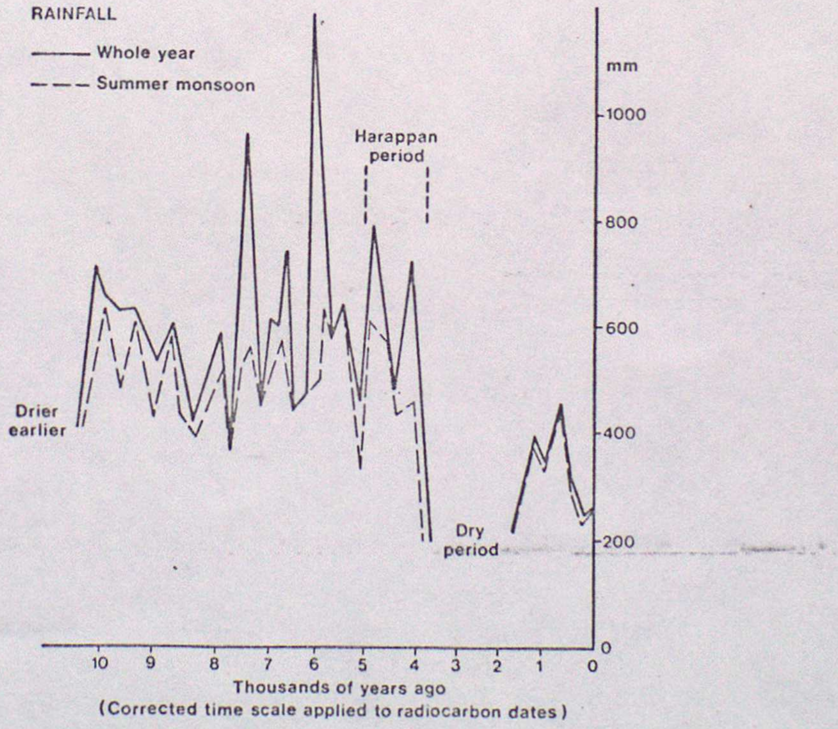

Estimated variations of the rainfall in Rajasthan, northwest India over the last 10,000 years, from lake levels and botanical (pollen analysis) evidence. (Adapted from a diagram by R. A. Bryson, based on the work of G. Singh)

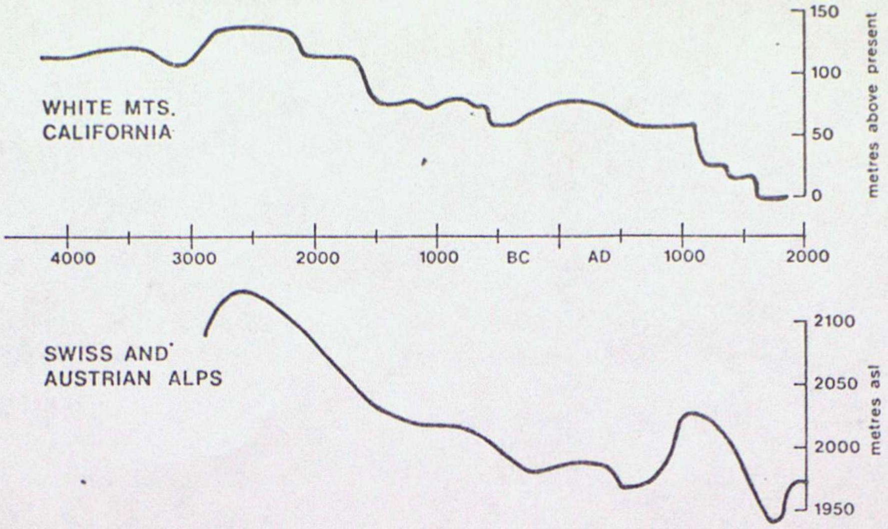

Changes in the height of the upper tree line in two areas in the White Mountains, California and in the Alps in Switzerland and Austria. (From work by V. C. La Marche and V. Markgraf)

FIG 7·23

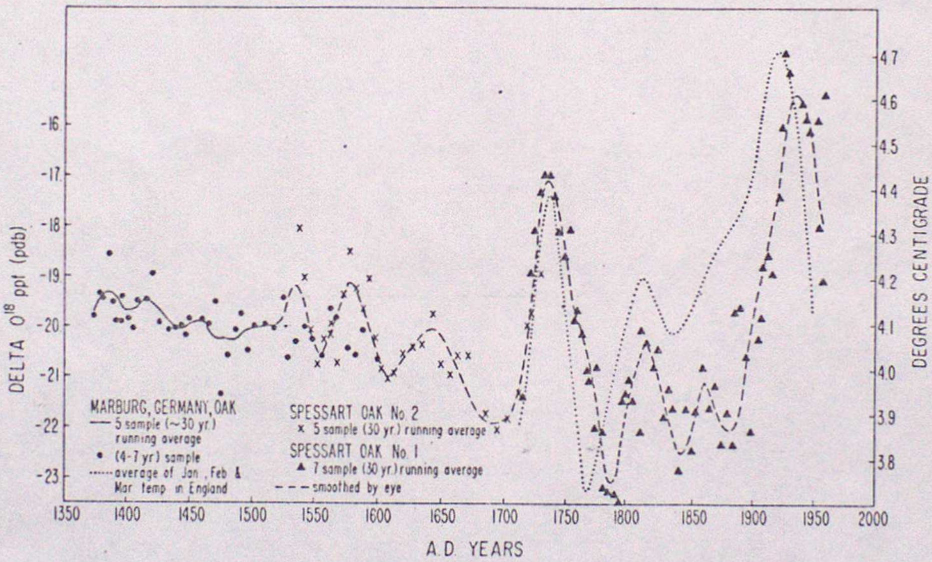

Composite record made up of the oxygen isotope ratio anomaly measured in the (tree-ring-dated) wood of oak trees in two areas of Germany (Marburg: 50°49′N 8°45′E) and Spessart (around 50°N 9°30′E).

Internal consistency/continuity of the record is suggested by the overlap.

Calibration against the last 270 years of winter temperatures (average for January, February and March) observed in England is suggested by the dotted curve.

Note: The very low dot plotted about 1480 would fit much better with other data for the 1430s, and it seems that the overlap with Spessart would fit equally well if there were about a 50-year dating error in the Marburg tree.

(*Diagram kindly provided while measurements were still incomplete by Dr* LEONA M. LIBBY *and reproduced with her permission.*)

FIG 7·26

FIG 7·24

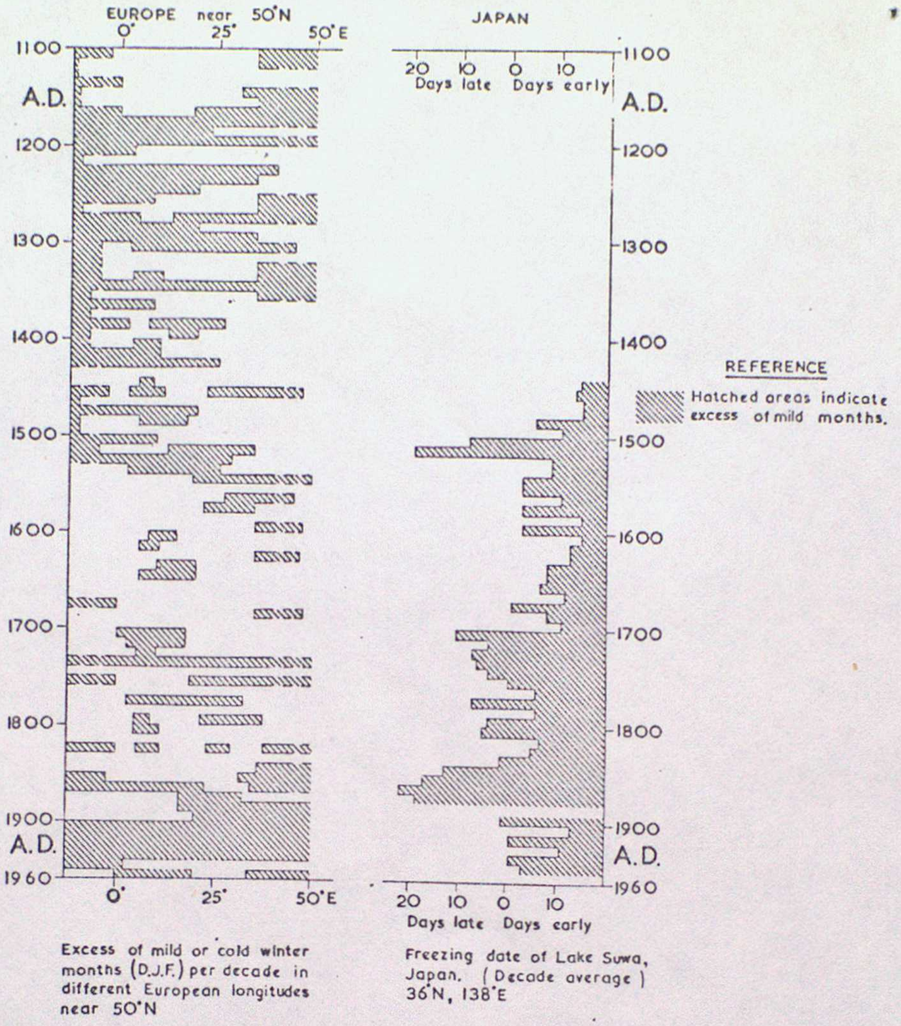

Excess of mild or cold winter months (D.J.F.) per decade in different European longitudes near 50°N

Freezing date of Lake Suwa, Japan. (Decade average) 36°N, 138°E

Survey of historical weather records by decades in Europe and Japan.

Left-hand side: Predominance of winter mildness (shaded) or severity (clear) in different European longitudes near 50°N

Right-hand side: Variations of average freezing date of a small lake in central Japan, decade by decade, from the overall mean date.

Europe: decades from A.D. 1100.

Japan: decades from A.D. 1440.

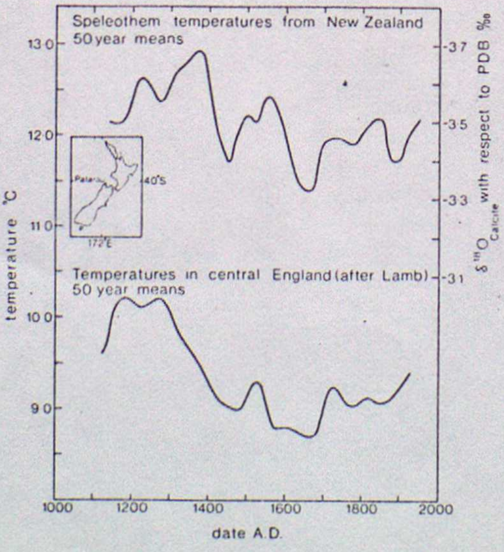

Course of the 50-year mean temperatures in the Nelson area, South Island, New Zealand, since A.D. 1100, derived from oxygen isotope measurements on a stalagmite in a cave at Patarau.

Temperatures derived by LAMB for Central England, as shown in Volume 1, p. 236, are repeated here for comparison.

(Adapted from the original diagram kindly supplied by Professor A. T. WILSON.)

FIG 7·25

FIG 7·27

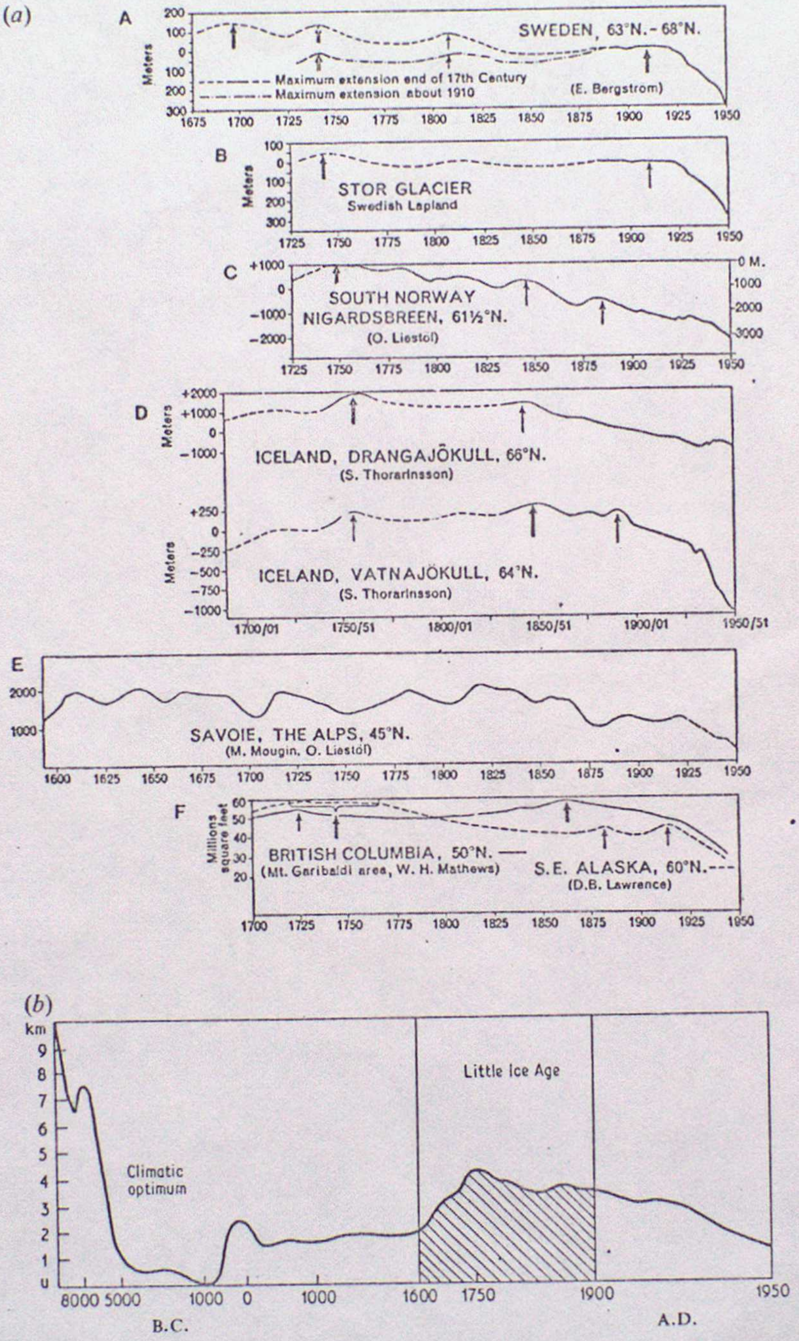

(*a*) Variations of glacier termini since A.D. 1600.

(*b*) Variations in the length in km of the glaciers in Iceland and Norway since 10 000 B.C.

(*After* H. W. AHLMANN *1953*.)

FIG 7.28

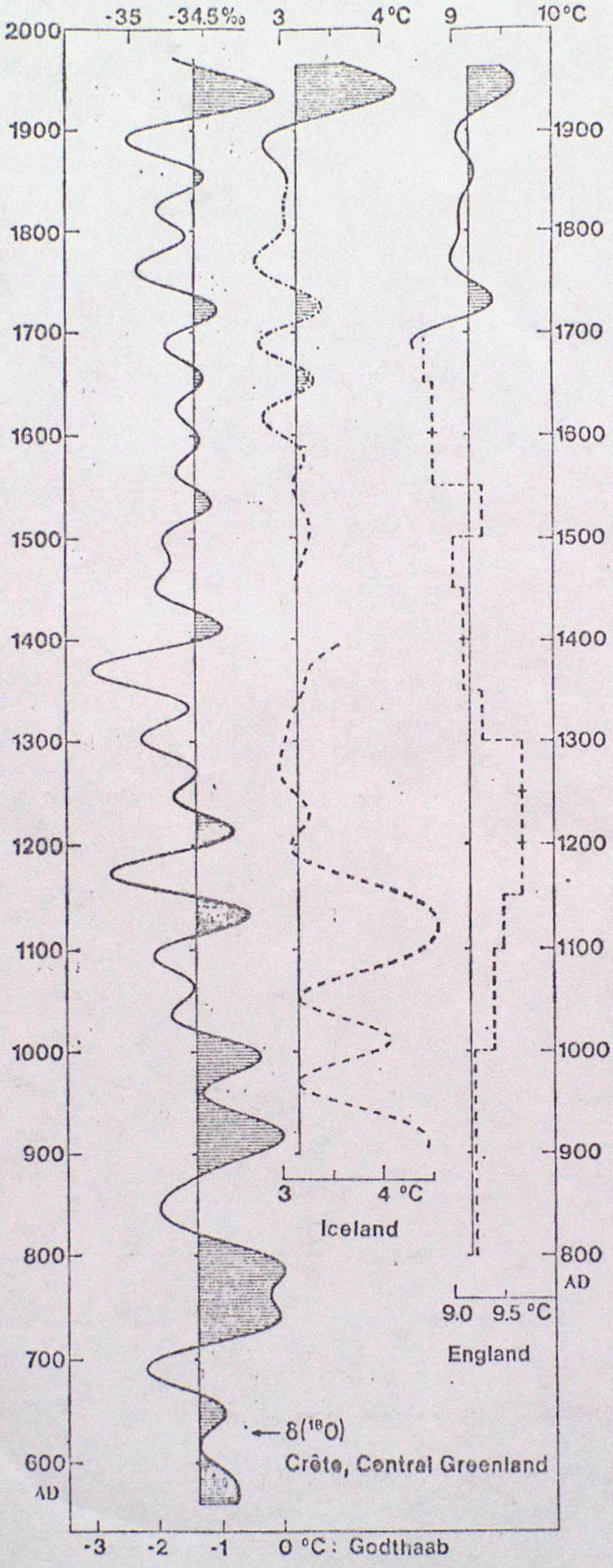

Comparison between the ^{18}O concentration (left) in snow fallen at Crête, Central Greenland, (δ scale on top), and temperatures for Iceland and England. The curves are smoothed by a 60-yr low pass digital filter, except for England 800–1700 AD. The full curves are based on systematic, direct observations, the dashed-dotted part of the Iceland record is estimated from systematic ice observations[9], whereas the dashed curves depend on indirect evidence[9,14].

FOR LOAN to Met. O. Staff only

METEOROLOGICAL OFFICE
145730
- 7 MAY 1985
LIBRARY

ADVANCED LECTURE No 8

CLIMATES OF THE PAST III - INSTRUMENTAL ERA

8.1 SUMMARY

The reality and nature of fluctuations in climate in the last 300 years are discussed in the light of the quality and quantity of instrumental data. Emphasis is placed on trying to link the "Little Ice Age" fluctuations with the modern era and on evidence for climate variation over the most recent century.

8.2 INTRODUCTION

This lecture covers climatic fluctuations on time scales from a decade to a few centuries and bridges the gap between studies of interannual variability and paleoclimatology. The approach to climatic fluctuations in the instrumental period has traditionally differed from the approach to interannual variability, with necessary emphasis on a few long well-documented local or global time-series of data, mainly those of temperature and PMSL rather than on statistical and physical links between atmospheric behaviour in different parts of the globe. This bias remains in this lecture.

8.3 OBSERVATIONS OF CHANGES IN TEMPERATURE

The beginning of the instrumental period (say the early eighteenth century) coincides with the latter part of the "Little Ice Age" and part of the problem that must be tackled is whether temperature (and atmospheric circulation) have really varied appreciably since that time. Referring back to fig 7.26, lecture 7, ^{18}O measurements from tree rings in W. Europe at least suggest a rise of winter/early spring temperature since the late seventeenth century exceeding 1°C up to 1940. Of equal interest is a marked increase in temperature in 1720-1740 which quickly reversed. Fig 7.26 also showed temperatures for January - March in Central England for the period after 1700. Central England temperature (CET) is the longest available, mostly instrumental, temperature series and we shall now look at CET in detail.

8.3.1 CENTRAL ENGLAND TEMPERATURE AND THE PROBLEMS OF HOMOGENISING ANCIENT THERMOMETER READINGS

A fundamental problem in constructing a local time-series is to ensure that the data are as temporarily homogeneous as possible: in other words, that a given meteorological reality has always resulted in the same value in the series. Only to the extent that this is true can the series be used to make reliable deductions about local climatic fluctuations. A time series of temperature in a restricted locality may, however, indicate fluctuations of climate on a larger scale as temperature is sensitive to changes in circulation.

Manley (1974)(1) constructed a monthly temperature series for Central England and an updated series (Storey and Folland (1985)(2)) is shown in Figure 8.1. Manley chose to represent an area, rather than to reduce his series to a single point, because of the scattered locations of most of the early observations, and because the only concentrated observations were in London and thus were eventually affected by heating resulting from urban expansion. He adjusted the monthly data to compensate for the following variables:

ORGS UKMO
National Meteorological Library
FitzRoy Road, Exeter, Devon. EX1 3PB
10
3 8078 0007 8117 1

i) Times of observation: the traditional mean temperature computed as $\frac{1}{2}$ (max + min) differs from eg the mean of 8 am and noon, by amounts which vary with season but can be estimated from modern data.

ii) The change of calendar in September 1752 when 11 days were omitted in that month. Daily data facilitated this adjustment.

iii) Housing of thermometers: in the 18th Century this was often an unheated north-facing room attached to a house; in later years, use was often made of either north-wall observations, or of Glaisher screens, which preceded Stevenson screens. The problem of changing thermometer screens may be a serious problem which has probably never been adequately investigated.

iv) Types of thermometer: pressure corrections were needed for early thermometers which consisted of a U-tube with one open end. Also different scales had to be converted to modern units. Unreliable instruments were excluded from Manley's compilation.

v) Geographical region and site: Manley found from modern data that so long as frost-hollows and other unrepresentative sites are excluded, the monthly deviations from a normal, or the successive differences between months of the same name, are almost uniform for English inland stations. Thus he could work with temperature differences rather than absolute temperature values, and produce a single series from overlapping records at sites scattered through much of England. This technique also aided cross calibration of early temperature scales and the effects of changing observing time and instrumentation.

Manley checked his compilation against a series for Utrecht (Holland) and found good agreement. Also, in periods of sparse data he noted observations of wind direction and snowfall.

It can be seen from Manley's series (fig 8.1) that, except in summer, much of the 20th Century in Central England has been warmer than the previous 250 years: the peak warmth was in the mid-20th Century except in winter when it was earlier. The late 17th Century was particularly cold corresponding to the supposed peak of the "Little Ice Age". There was notable warmth in the 1720's and 1730's however. These features are also found in instrumental temperature series for Utrecht and for other locations in Northwest Europe. Other major features are the warming in October between 1890 and 1975 and the sharp cooling in April in the past 25 years.

Fig 8.2(a) shows a power spectrum analysis of the unsmoothed annual mean CET data from 1659-1975. The most significant peak is labelled 76 years and mainly reflects the temperature fluctuations between about 1890 and 1975 and between about 1700 and 1770. (bottom diagram of fig 8.1). Fig 8.2(b) shows a power spectrum reported by Lamb (3), ~~due to~~ Siren, of tree-ring widths in N. Finland which mainly reflect summer temperature (it is thought). The shape of figs 8.2(a) and 8.2(b) are surprisingly similar with more power in fig 8.2(b) at the 70-200 year time scale presumably because of the longer (497 year) data series. The 23 year peak is like the 76 year peak, statistically significant (using an "F" test) and has sometimes been linked with the "double sunspot" cycle of magnetic activity on the sun. (The double sunspot cycle is constructed from the sunspot series shown in lecture 3 by reversing the sign of the values in the sunspot series between alternate sunspot cycles.) Fig 8.3 (Folland (1983)(4)) shows that a band-pass filtered time series of annual CET whose filter function is centred on the 23 year time scale bears no long-term consistent phase relationship with the double sunspot cycle. Indeed the 23 year peak disappeared after 1880 whereas the double sunspot cycle increased slightly in amplitude. Nevertheless the origin of this CET fluctuation and its disappearance is of interest. The meaning of power spectra such as fig 8.2 can only be gradually uncovered by a worldwide study of temperature and circulation fluctuations if improved data and physical understanding permit this. A clue to some of the variations of CET may come from the diagram shown at the end of lecture 4; there it was suggested that a century-time scale fluctuation in the temperature of Lamb westerly types in Central England over the last century may be related to parallel fluctuations in N. Atlantic SST (see also section 8.8).

Fig 8.4 shows an attempt (Lamb (1972)(5)) to estimate Central England temperatures back to the beginning of the Medieval "climatic optimum" including assessments of their uncertainties. Prior to 1680 the temperatures have been derived from a mixture of botanical and documentary evidence. A clear minimum in mean annual and winter CET is suggested around 1600 - 1700 with winter temperatures in the period 1900-1950 similar to those during the "Medieval optimum".

8.4 POSSIBLE EFFECTS OF URBAN HEATING ON TEMPERATURE RECORDS

The possible effect of urban heating on long time series of temperature, mostly avoided by Manley, is illustrated for Paris in figs 8.5(a) and (b) (after Dettwiller (1978)(6). Central Paris has warmed by 1°C since 1900 when its temperature is compared with that of the surrounding countryside; much of the warming has been in the minimum temperatures as is typical of urban heating. Studies like that of Dettwiller can only be used to correct urban data if long series of homogeneous rural data exist. The problem of urbanisation is serious as many long temperature series have been kept in what are now large cities; fig 8.6 compares a long time series of annual mean temperature for Vienna with that for an observatory on a low mountain in S. Germany (Hohenpeissenberg) 600 km to the west. (Angell and Gruza (1984))(7)A relative warming of Vienna since 1920 appears to have occurred but it is not easy to determine if urbanisation is the main cause. The higher frequency fluctuations tend to be in phase however and a very long period temperature fluctuation with a flat minimum around 1880-1890 is common to both series; the period around 1800 is relatively warm though, unlike Central England.

8.5 HEMISPHERIC TEMPERATURE FLUCTUATIONS

Hemispheric scale air temperature variability, mainly over land, has received increased attention in recent years despite the problems cited above. Fig 8.7 shows the variations in mean annual N. Hemisphere air temperature (mainly but not wholly over land - but no ship data is included) from two authors: Vinnikov et al 1980(8) for 1881-1978 and Jones, Wigley and Kelly (1982)(JWK) for 1881 - (9) 1981. Vinnikov et als' analysis only extends to 17.5°N. However the correlation between the two hemispheric series is 0.97 (Angell and Gruza). Of interest is the fact that the interannual variability of hemispheric temperature is much less than that for local series like Vienna, Hohenpeissenberg or the unsmoothed Central England series (mean year to year variation of hemispheric temperature is about 0.15°C compared to 0.8°C in the Vienna and Hohenpeissenberg series). Despite this, the (decadally-averaged) century time-scale fluctuations are comparable, being in the range 0.5°C - 1°C. The reality of a coherent long time-scale N. Hemisphere temperature fluctuation this century is suggested by figs 8.8(a) and (b), taken from Jones and Kelly (1983)(10). The warming between 1917-1939 is quite coherent over mid and higher latitudes (fig 8.8b); also the Arctic series is rather like that for the N. Hemisphere as a whole but with larger amplitudes of fluctuation.

Groveman and Landsberg (1979)(11) used regression formulae relating a near-hemispheric grid-point data series of N. Hemisphere air temperature which had been previously constructed by Borzenkova et al, (1976)(12) to temperature values constructed for a few very long-period stations. These series had to be based on a mixture of botanical and documentary data in the pre-instrumental era. In this way a continuous N. Hemisphere temperature series was estimated back to 1579 (fig 8.9). Confidence limits for the series are shown and are comparable to the magnitude of the climatic changes suggested by the series. Nevertheless a cold period around 1600-1700 is suggested in common with European series, with a hint of warmth in the 1730's. The large temperature fluctuation in the first half of the nineteenth century is less expected while the early twentieth century warming (based on instrumental data) is clearly visible and comparable in magnitude with that of JWK or Vinnikov et al.

8.6 CAN WE BELIEVE THE EVIDENCE CONCERNING LAND SURFACE TEMPERATURE CHANGES: THE ASSOCIATED CIRCUATION FLUCTUATIONS

8.6.1 ATLANTIC SECTOR

The chief evidence for circulation fluctuations in the last few hundred years comes from the Atlantic sector and is to be found in:-

(a) diaries kept by careful observers of wind direction and weather
(b) since the eighteenth century, we have many measurements of pressure at station level. One of the most interesting and lengthy series of type (a) was put together by Lamb (11), if of necessity rather subjectively (fig 8.10), and shows variations in the frequency of south westerly winds in S.E. England.

A relatively low frequency of south westerly winds during much of the 17th century and a peak in the 1730's is in accord with the variations in CET (i.e. outside the summer season; in summer, the level of CET is not well-related to the frequency of south westerly winds.) A minimum frequency of south westerly winds has been confirmed for a few years in the late 18th century by Kington (1980) (13) who has constructed daily weather maps for the period 1781-86. At this time, due to a briefly successful international cooperation, a well-distributed network of pressure observations was made in Europe. Lamb and Johnson (1966) have also constructed monthly-mean PMSL charts for the N. Atlantic for January and July since 1750, and in later years, for much of the N. Hemisphere (see reference 3). The most convincing evidence of a circulation fluctuation (in winter) in the N. Atlantic sector over the last century is probably provided by fig 8.11(a). The data from the two stations shown are of good quality have been carefully scrutinised (Parker D.E. personal communication) and both are situated near sea-level. They provide an index of Atlantic circulation where the strength (or location) of the mid-latitude N. Westerlies is reflected by the size of the difference in PMSL between the Azores and Iceland. The long-term trend in this index in winter roughly parallels the trend of Manley's CET; greatest warmth in the winter parallels the strongest westerlies earlier in this century, but correspondence is somewhat poorer in the late 19th Century. Fig 8.11(b) shows variations in a more subjective index: that of Lamb "Westerly" types over UK which were introduced in Lecture 1 (from Lamb (1977)). Allowing for differences in the location and definition of the indices, (UK is 30°E of Azores and Iceland) fig 8.11(b) is acceptably similar to fig 8.11(a) though some details do differ. Focussing on a shorter period, fig 8.12 shows the difference in PMSL over the N. Hemisphere between 1951-70 and 1901-30 taken from Folland, Parker and Newman (1985)(14). Some of the difference will not be reliable but those over the N. Atlantic between 20°N and 75°N should be. In the period 1901-30, a very strong mid-latitude south westerly wind anomaly (of magnitude 3-4 m/s over Scotland) existed in January relative to 1951-70. Scrutiny of fig 8.1 (where the 20 year running mean of CET is plotted against the last year of the 20 year period) shows that between 1901-30, January CET averaged about 1.2°C higher than in the latter period. 1.2°C is a large change in mean temperature; e.g. during the recent 30 year period (1951-80) a month with an anomaly of 1.2°C from the mean is just enough to place that month into the top 20% of the January temperature probability distribution. The larger warming in October between 1890 and 1975 can be shown to be partly due to an increase in the frequency of south westerly winds in that month. The warming is so large that a very mild month (top 20% of the ranked distribution of October temperatures in the period 1870-1900) could easily have the same temperature as a rather cold month (bottom but one 20% of the 30 year ranked distribution of October temperature) in the period 1951-80. The sharp cooling in April since 1961 has been associated with a strong increase in blocking and thus in east-north-east winds in that month. So (mainly) as a result, there have been no very warm Aprils in Central England since 1961.

8.6.2 EVIDENCE OF CIRCULATION VARIATIONS ON THE GLOBAL SCALE

A comprehensive analysis of available quality-controlled PMSL data on land and at sea has yet to be carried out. However the potential value of such analyses is suggested by fig. 8.13 taken from Chang and Yasunari (CY) (1983)(13). CY analysed July PMSL over much of the globe using station, including island, data but excluding the Atlantic Ocean sector 0-60°W. The data was analysed into a grid point format. Fig 8.13 (a) shows the first two eigenvectors (EOFs) of an EOF analysis of 11 year running mean PMSL data; this averaging time-scale was chosen to highlight the long time-scale variations. The first EOF (31% of the variance) is negative north of about 20°N and positive to the south; the time series suggests a progressive reduction of PMSL in the S. Hemisphere relative to the extratropical N. Hemisphere over the last century with a halt to this tendency between about 1900 and 1930. Fig 8.13(b) shows the second EOF 19% of the variance), a variation of PMSL between the Pacific and Indian Ocean on the one hand and the surrounding continental areas on the other. Relatively low pressure over land and high pressure over the areas is suggested in the late nineteenth century and mid-twentieth century, with a reversed pattern around 1900-1920. Both eigenvectors are clearly dominated by century time-scale variations. Could these PMSL eigenvectors reflect century-time scale fluctuations in relative air temperature between continents and oceans or even between whole hemispheres? It must be emphasised though that away from the mid latitude N Atlantic region most existing grid point data sets of PMSL must be viewed with great caution. Parker (16) has shown that substantial disagreements exist, especially over the N. Pacific, between several well-known N. Hemisphere PMSL data sets, (CY's data set was not tested), of sufficient magnitude to obscure past real circulation changes in some regions unless they have been large. Other authors have shown that PMSL data sets have been subject to sudden, unrealistic, changes in the mean value of derived PMSL over some mountainous regions and are quite unreliable over the Canadian and Siberian Arctic prior to 1930.

8.7 CHANGES IN TROPOSPHERE AND STRATOSPHERE TEMPERATURES

These data series are generally too short to indicate much about climate change; the series are presently much more useful for studying interannual variability, especially the effects of El Nino, for which the data have yet to be fully exploited. Radiosonde data are unfortunately subject to severe problems of changing instrumental biases, especially upper atmosphere temperature measurements; biases vary between countries and therefore may be geographically variable. This problem results from a combination of changes in instrumentation and changes in correction procedures. The main difficulty has been the need to compensate adequately for solar heating of radiosonde thermometers; the problem is acute in the lower stratosphere. Fig 8.14(a) shows time series of fluctuations in tropospheric and stratospheric temperature reported by Angell and Gruza; the N Hemisphere stratospheric changes at 26-55 km are far too large to be due to the influence of carbon dioxide. It is possible that a careful synthesis of these data and surface data may become feasible in the next few years.

8.8 A RECENT STUDY OF CLIMATE VARIATION USING WORLDWIDE SST AND NIGHT MARINE AIR TEMPERATURE (NMAT) OBSERVATIONS

The first reasonably comprehensive analysis of worldwide SST and MAT, including attention to the problems of data quality, especially problems due to changing measurement biases has been carried out by Folland, Parker and Kates (1984)(17) and Folland, Parker and Newman (14). They used the Meteorological Office Historical Sea Surface Temperature data set (MOHSST)(see reference in lecture 5) and the corresponding night marine air temperature data set (MOHMAT)(Parker 1984) (18). Reference (17) discusses the problems of the changing biases in the SST and MAT observations; the biases in the latter were reduced by only using night-time observations of air temperature, thereby eliminating most of the problems due to heating of the ship's fabric in bright sunshine. Despite the fact that problems are known to still exist with this data, the apparent reasonable agreement between variations in SST and in MAT on many time and space scales has suggested that useful information about climate change over the oceans can be obtained from them. Fig 8.15(a) indicates the amount of data available and fig 8.15(b) gives an idea of the worldwide SST (or NMAT) data coverage in the 1870's; nowadays data is reasonably complete on a seasonal time scale north of 45°S except west of Chile and in parts of the Tropical central Pacific.

8.8.1 MAIN RESULTS OF THE MARINE ANALYSIS

Fig 8.16(a)-(d) shows the main results on the global space scale. Fig 8.15(a) shows the SST and NMAT time series before correction; the data are expressed as anomalies from a 1951-60 average. The main correction to the NMAT data concerned compensation for a progressive increase in the heights of screens above the ocean surface as ships have become larger. In addition, pre-second world war SST data were too cold due to the predominant use of canvas or leather buckets to collect sea water which suffer from evaporative cooling. Fig 8.16(b) shows the series after correction. A century time-scale fluctuation in SST and NMAT is shown of range about 0.5°C - 0.6°C; part of the superimposed "noise" is related to the influence of El Nino (see lecture 5). Fig 8.16(c) shows that the SST and NMAT anomalies have a remarkably similar shape in all calendar seasons (or months); this is similarly true for most regions of the world. The occurrence of El Nino tends to be locked to the seasonal cycle and the increased interannual variance of global SST and NMAT between October and March in fig 8.15(c) would be expected as a result. Fig 8.16(d) shows a comparison of corrected NMAT averaged over the N. Hemisphere and a digitised version of Vinnikov et al's land surface temperature data. After 1890 the agreement is very good, surprisingly so perhaps as:-

(a) the data are completely independent in origin and
(b) largely independent in the areasthey represent
(c) the surface ocean air temperatures show the same interannual and long-time scale magnitudesof variation as those on the land, a result not expected by some authors due to the thermal inertia of the oceans.

Fig 8.17(a) shows zonally and decadally averaged changes in SST between 1856-1980 (anomalies expressed from a 1951-60 average). Relatively warm conditions at most latitudes are suggested around 1861-1875 (data was sparse but widely spread) followed by a slow cooling. A more rapid cooling followed in the N. Hemisphere between 1891-1910, especially in middle and sub-tropical N. Hemisphere latitudes. Warming then commenced in all lattitudes with peak warmth around 1950. After 1951-60, cooling occurred in the N. Hemisphere until 1971-80 but further slight warming is evident in the S. Hemisphere Interestingly when compared to fig 8.13(a), the S. Hemisphere was relatively coldest compared to the N. Hemisphere around 1871-1880 and relatively warmed until about 1891-1900 with only slow relative warming thereafter. About 1951-60, further relative warming started. Despitethe limitations of both fig 8.17(a) and the non-global coverage of fig 8.13(a), a link between the SST and PMSL changes is possible as relative warming of one hemisphere should cause its PMSL to fall relatively to the other hemisphere. Fig 8.17(b) shows the worldwide SST anomalies in the coolest decade, 1903-12, compared to 1951-60, which was (probably) the warmest decade. The worldwide nature of the century-time scale SST fluctuation is brought out, with smallest changes in the Tropical central and W. Pacific and largest (reliable) changes in the tropical and sub-tropical Atlantic.

Fig 8.18(a) showsthe first correlation eigenvector, EOF1, of seasonal $10^\circ \times 10^\circ$ area SST anomalies calculated between 1901-1980. This eigenvector accounts for about 11% of the variance of SST on the $10^\circ \times 10^\circ$ space scale measured in all areas; fig 8.18(b) compares the time series of this eigenvector to that of the global, seasonal, SST anomalies shown in fig 8.16(b). The correlation is over 0.9. (The arrows point to years judged to experience on El Nino warming events). EOF1 indicates that to the local variance of SST, the largest long time scale changes in SST have occurred in the tropical and subtropical Atlantic, in the N. Indian Ocean and near Japan. Only a small region near Greenland has fluctuated with a weak opposite phase to that of the remainder of the world, i.e. the long-term variations have probably been truly worldwide. In fact individual time series of most individual $10^\circ \times 10^\circ$ areas show a long time scale SST or NMAT fluctuation which has a similar phase in all seasons.

Fig 8.19(a)(b) show maximum entropy power spectra of SST and NMAT for the Northern and Southern hemispheres for 1861-1980. The dominant peak in the N. Hemisphere represents the century time-scale fluctuation; in the Southern hemisphere this peak is large but shorter time scale fluctuations in the period range 2.5-10 years are more prominent - mainly related to El Nino. The peak near 17 years (SST) or its equivalent near 20 years in NMAT is unexplained but merits investigation. Fig 8.19(c) shows a spectrum of global SST between 1951-80 when long-time scale fluctuations (averaged over the globe as a whole) are not very evident. ENSO-related fluctuations dominate the spectrum though the 8-10 year time scale fluctuations, prominent in the original time series, are not clearly only the result of successive ENSO events. Fig 8.20 highlights the relative changes in S. and N. Hemisphere SST (effectively on a 5-10 year time scale). The relative warming of the Southern Hemisphere since about 1960 is shown and currently exceeds 0.3°C or over half the range of the long term trend in global SST.

Fig 8.21(a) and (b) suggests a possible link between the long term trend in land and ocean surface temperatures and recent fluctuations of some European glaciers, despite the complexity of the climatic factors that influence individual glacier advances and retreats. Fig 8.21(a) and (b) shows that the percentage of advancing and retreating glaciers in Switzerland (apparently derived from a large sample) (quoted by Untersteiner (1984)(19)) and variations in N. Atlantic SST north of 35°N seem to be related. Autumn was chosen as being the most critical season affecting glacier advances and retreats though in the N. Atlantic all seasons show broadly similar SST fluctuations. The advance of the Swiss glaciers in the early twentieth century seems to correspond with the cool period in the N. Atlantic (and over the globe) around 1900-1915; the subsequent retreat peaked around 1950 again seems to be nearly phase locked to the variations of SST. Most convincing is the recent advance that corresponds well with the fall in N. Atlantic SST up to about 1980. The changes in SST may not of course be the direct cause of the glacier fluctuations - both may be the result of a third common factor.

8.9 THE SAHEL DROUGHT

The Sahel drought has been a special theme of these lectures. So it is perhaps fitting that we should complete the trilogy of lectures on climatic variations with recent evidence that the drought is not just a regional phenomenon but seems to be related to lage scale changes in atmospheric circulation and (possibly of SST). Fig 8.22 repeats for convenience the graph, due to P J Lamb, of west Sahel rainfall anomalies shown in lecture 1. Fig 8.23(a) and (b) shows for July and August separately maps of PMSL differences for the N. Hemisphere derived from the Met 013 grid point PMSL data set for the most recent wet Sahel period (1951-60) minus the dry period (1968-84). The two maps are remarkably similar and the areas of difference that are statistically significant at the 5% level (within the dotted lines) cover similar areas. These areas total about 25-35% of the N. Hemisphere north of 20°N, the southern limit of the analysis. The chance area is about 5-7% PMSL. Except near the Himalayas, the central N. Pacific and over Greenland, the PMSL changes should mostly be reliably measured. The largest changes occur near Scotland; as a result, rainfall averaged over England and Wales (EW) in July and August has been declining since about 1955-1960 with a small reduction in June also. Fig 8.23 shows unsmoothed (EW) rainfall totals for July and August since 1767. The possible link between the Sahel drought and UK drought is heightened by the fact that since 1975 four of the 11 driest summers (June-August) recorded in EW since 1767 have apparently occurred. The EW series used is due to Wigley et al (1984)(20). The summers include the driest (1976) and second driest (1983). (1984 was probably the sixth driest). At present it is unclear whether recent hemisphere scale SST changes (which have been considerably larger in the N and S Atlantic sector) are related to the Sahel drought. This possibility is currently being explored using the Meteorological Office 11-level AGCM. Rowntree and Bolton (1983) (21) during an investigation of the effects of large scde soil moisture deficits over W. Europe in summer have provided some evidence from experiments with the Meteorological Office 5-level AGCM of a possible positive feedback between dry conditions over W. Europe and over the Sahel (the fundamental cause of dryness in either region would have to lie elsewhere however). The feedback is conceivable as a dryer than normal origin of the N.E. trade winds that converge toward the W. African ITCZ near 20°N in July and August could play a part in further suppressing deep convection there.

8.10 CONCLUSION

The nature, even the existence, of climate change and variation in the instrumental era is only now being exposed. As yet, except for the role of El Nino, there are few convincing explanations of the observed fluctuations. Meanwhile a wide-ranging critical review of current evidence for climate change in the instrumental period has been prepared by Ellsaesser, MacCracken and Walton (1985)(22); it is recommended as providing an excellent summary,

REFERENCES

1. Manley, G. (1974) Central England temperatures: monthly means 1659-1973. Quart. J. Roy. Met. Soc., 100, 389-405.

2. Storey, A.S. and Folland, C.K. (1985) A homogeneous archive of daily Central England Temperature 1772-1984 and new monthly averaged values 1974-1984. Met 013 Branch Memo No. 107.

3. Lamb, H.H. (1977) Climate Present, Past and Future Vol. 2 Methuen.

4. Folland, C.K. (1983) Regional-scale interannual variability of climate - a north-west European perspective. Met. Mag., 112, pp 163-183.

5. Lamb, H.H. (1972) Climate Present, Past and Future Vol. 1. Methuen.

6. Dettwiller, J. (1978) L'evolution seculaire de la temperature a Paris. La Meteorologie, VI, 13,95-130.

7. Angell, J.K. and Gruza G.V. (1984) Climate Variability as estimated from atmospheric observations. In "The Global Climate" Ed: J.T. Houghton pp25-36. Cambridge University Press.

8. Vinnikov K. Ya et al (1980) Present day climatic changes in the northern hemisphere. Meteorol. i Gidrol., 6, pp5-17

9. Jones, P.D., Wigley, T.M.L. and Kelly, P.M. (1982) Variations in surface air temperature. Part I, Northern Hemisphere 1881-1980. Mon. Weath. Rev., 110, pp 59-70.

10. Jones, P.D. and Kelly, P.M. (1983) The spatial and temporal characteristics of Northern Hemisphere surface air temperature variations. J. Clim., 3, pp 243-252.

11. Groveman, B.S. and Landsberg, H.E. (1979) Reconstruction of Northern Hemisphere temperature: 1579-1880. Univ. Maryland Met. Program, Publ.79-181.46 pp + 59 pp of data appendices in separate volume.

12. Borzenkova, I.I., Vinnikov, K.Ya., Spirina, L.P. and Stechnovskii, P.I. (1976) Variations of Northern Hemisphere air temperature from 1881 to 1975. Met. i Gid, 7,27-35.

13. Kington, J. (1980) Daily weather mapping from 1781: a detailed synoptic examination of weather and climate during the decade leading up to the French Revolution. Climatic Change, 3, p7.

14. Folland, C.K., Parker, D.E. and Newman, M. (1985) (1985) Worldwide marine temperature fluctuations on the season to century timescale. Proc. 9th Climate diagnostics Conf., Corvallis, Oregon 22-26 Oct. Amer. Met. Soc.

15. Chang, T. and Yasunari, T. (1983) Fluctuations of Global Surface Pressure Patterns during the past 100 years and their relation to the Asian monsoon Part I. Northern Summer (July). J. Met. Soc. Japan, 60, No 5, pp 1132-1142.

16. Parker, D.E. (1980) Climatic change or analysts' artifice? - a study of grid-point upper-air data. Met. Mag., 109, 129-152.

17. Folland, C K, Parker, D.E. and Kates, F. (1984) Worldwide marine temperature fluctuations 1856-1981. Nature 310, pp 670-3.

18. Parker, D.E. (1984) The Meteorological Office Historical Marine Air Temperature Data set (MOHMAT). Met O13. Branch Memo 138.

19. Untersteiner, N. (1984) The cryosphere. In "The Global Climate" Ed: J T Houghton pp 121-140. Cambridge Univ. Press.

20. Wigley et al (1984) Spatial patterns of precipitation in England and Wales and a revised homogeneous England and Wales precipitation series. J. Clim., 4, pp 1-25.

21. Rowntree, P R and Bolton J.A. (1983) Simulation of the atmospheric response to soil moisture anomalies over Europe. Q.J. Roy Met Soc., 109, pp 501-526.

22. Ellsaesser, H.W., MacCracken, M.C. and Walton, J.W. (1985) (1985) Global Climatic trends as revealed by the recorded data. Rev. Geophys. and Space Phys. (in Press).

FIG 8.1 CENTRAL ENGLAND TEMPERATURE 1659 TO 1983
FILTERED SERIES REVISED SERIES 1974 ONWARD

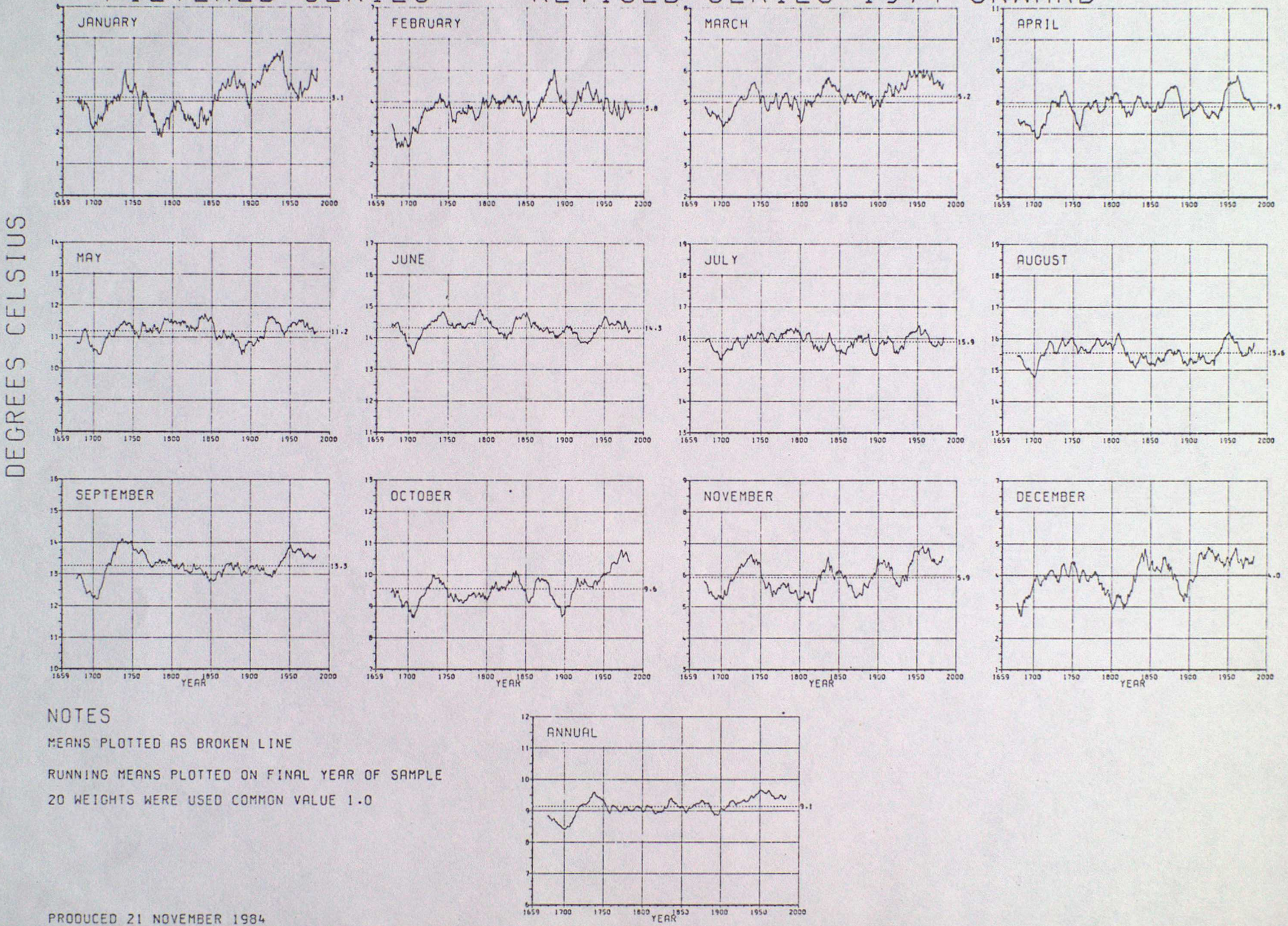

NOTES

MEANS PLOTTED AS BROKEN LINE

RUNNING MEANS PLOTTED ON FINAL YEAR OF SAMPLE

20 WEIGHTS WERE USED COMMON VALUE 1.0

PRODUCED 21 NOVEMBER 1984

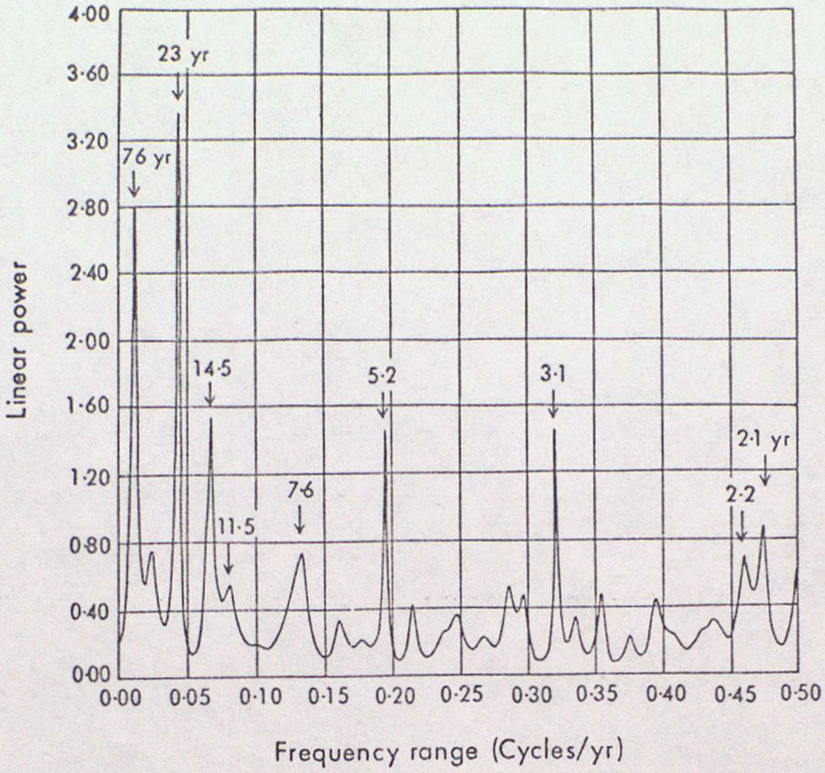

FIG 8·2(a) Power spectrum of the Manley record of Central England temperatures with the long-term trend removed.

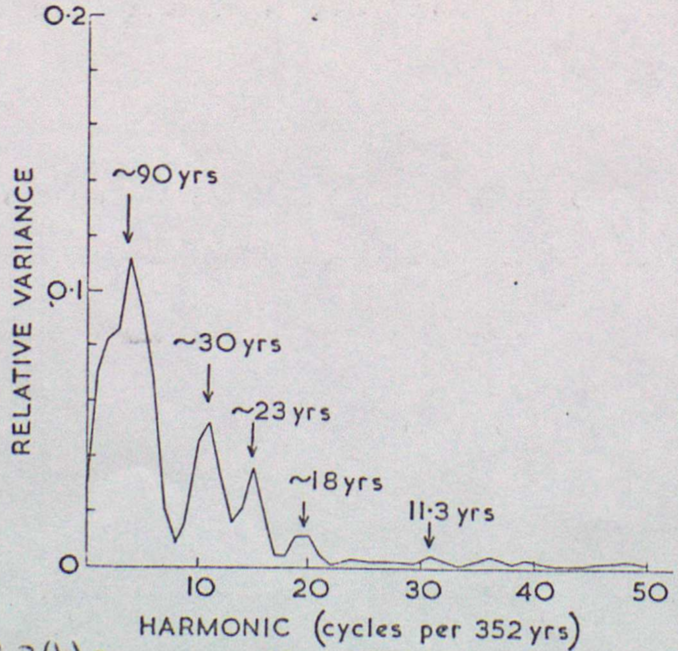

Fig. 8. 2(b) Power spectrum of SIRÉN's (1961) Lapland tree-ring index from 1463 to 1960, which is believed to register mean temperatures of the high summer period in northern Finland. (*Kindly supplied to the author by* J. M. MITCHELL *and reproduced by permission.*)

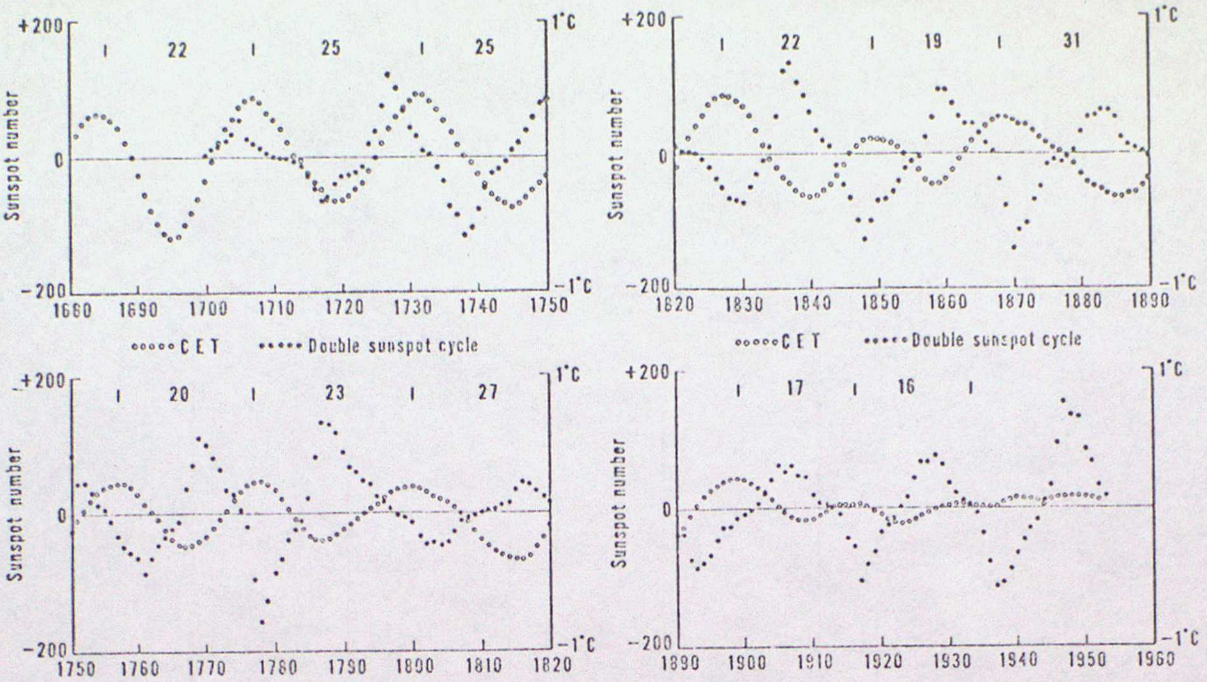

FIG 8.3 The '23-year' wavelength band-pass filtered series of annual mean Central England Temperature and the 'Hale' or double-sunspot cycle. (from Folland 1983)

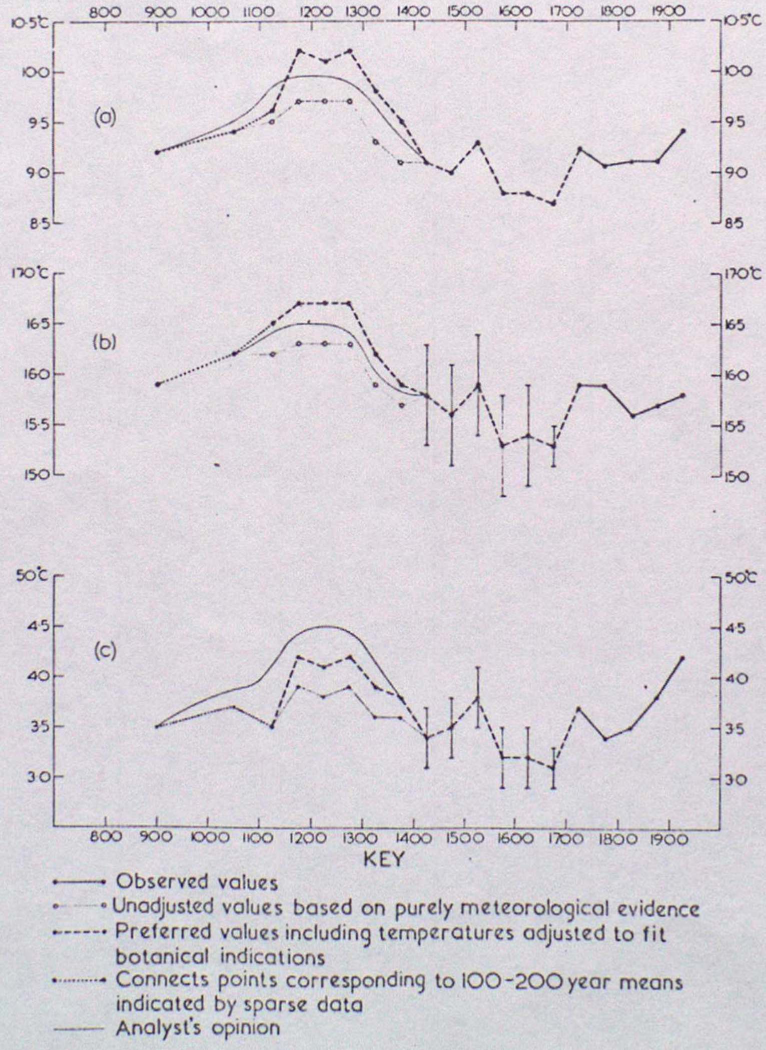

Fig 8.4. Temperatures (°C) prevailing in central England, 50-year averages:

(*a*) Year

(*b*) High summer (July and August)

(*c*) Winter (December, January and February).

Observed values from 1680, as standardized by MANLEY. Values for earlier periods as derived by LAMB (1965). The ranges indicated by the vertical bars are three times the standard error of the estimates.

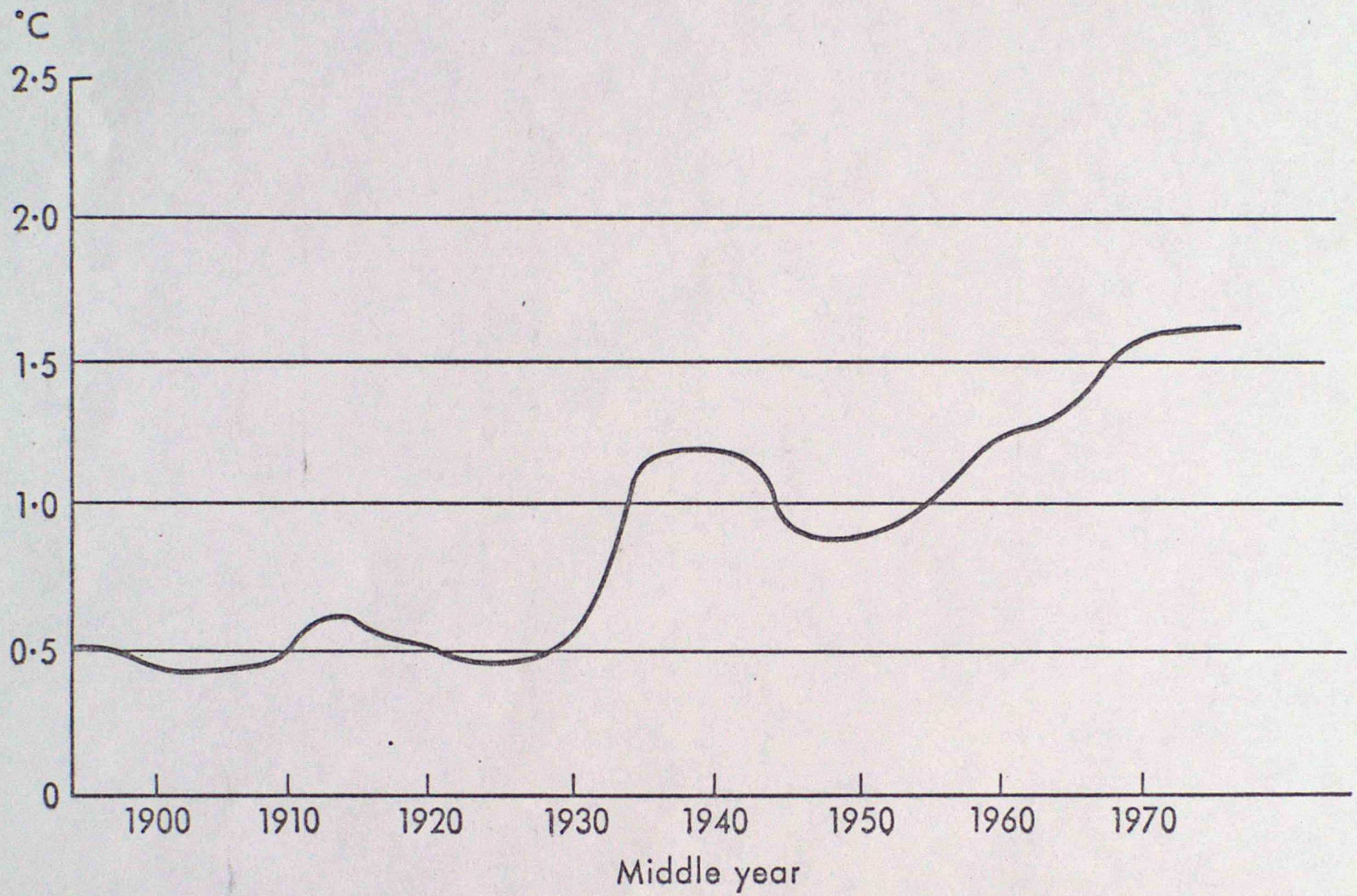

FIG 85 (A) ANNUAL MEAN TEMPERATURE DIFFERENCE, PARIS— MONTSOURIS MINUS BESANCON (AFTER DETTWILLER 1978). Values are 10-year running means.

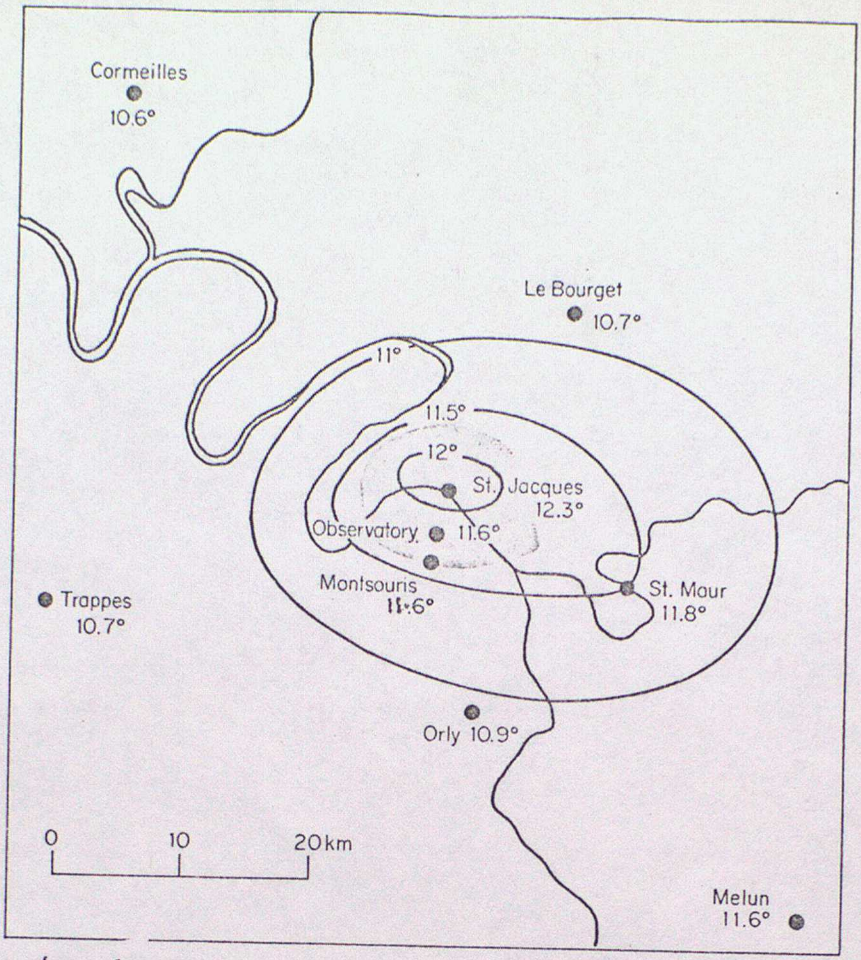
Cormeilles
10.6°
Le Bourget
10.7°
11°
11.5°
12°
St. Jacques
12.3°
Observatory
11.6°
Montsouris
11.6°
St. Maur
11.8°
Trappes
10.7°
Orly 10.9°
0
10
20 km
Melun
11.6°

Fig 8.5 (b) Mean annual surface temperatures of Paris and vicinity, °C. (After Dettwiller.)

Fig 8.6 Variation in mean-annual temperature at Vienna and Hohenpeissenberg.

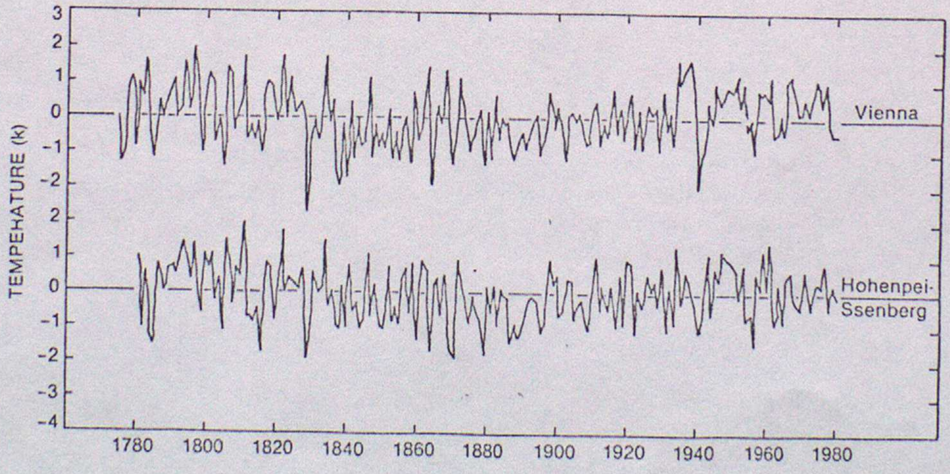

FIG 9.7 Variation in mean-annual NHST according to Vinnikov *et al.* (analysis only to 17.5°N), and Jones, Wigley & Kelly. The volcanic eruptions of Krakatoa and Agung are indicated.

NORTHERN HEMISPHERE SURFACE TEMPERATURE

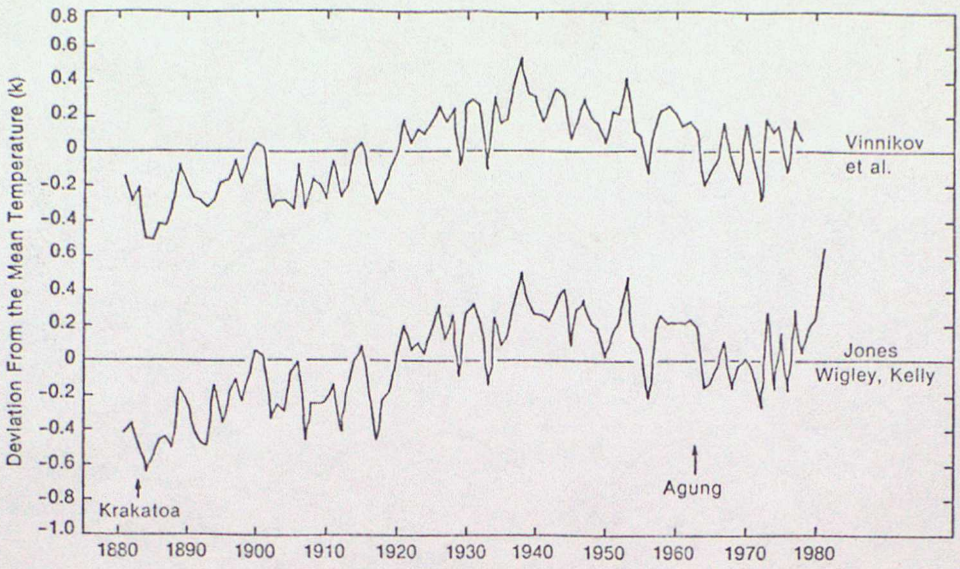

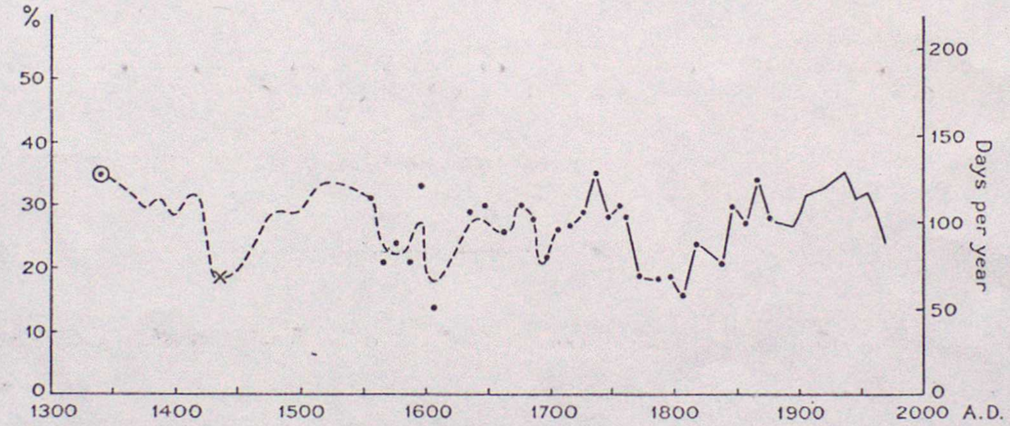

Fig 8.10 Frequency of SW'ly surface winds in southeastern England since A.D. 1340. Approximately 10-year average values and estimates.

Composite record derived directly from daily observations near London since 1670 (the earlier part worked up from manuscript sources by MANLEY, the later part since 1811 from observations in the archives of the Meteorological Office). Estimates for periods before 1670 provisionally derived from indirect evidence including weather diaries kept in various parts of England and neighbouring parts of Europe.

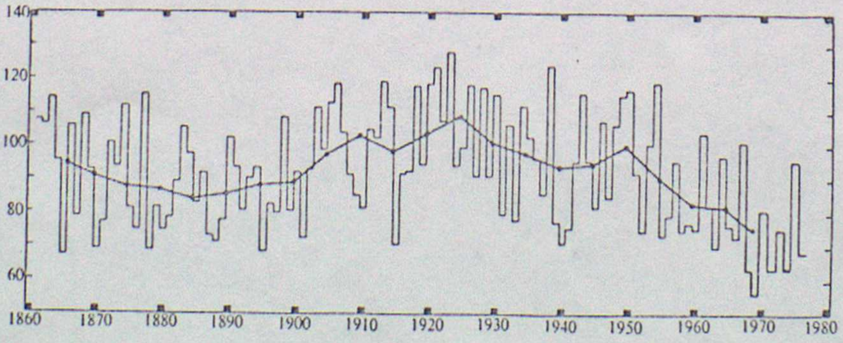

Fig. 8.11 (b) Number of days each year of general W'ly type over the British Isles: 1861 to 1975. (The number of W'ly type days in 1976 was 59.)

Individual years and 10-year means at 5-year intervals.

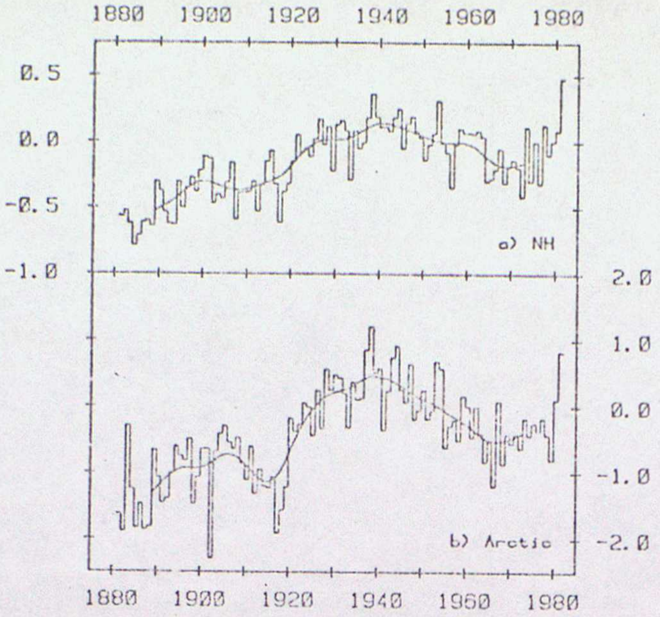

8·8(a) Annual means of surface air temperature for the Northern Hemisphere and for the Arctic (expressed as departures in °C from the 1946–1960 reference period). Data for 1981 are included in this figure but have not been analyzed. The smoothed curves show the data smoothed with a binomial filter designed to suppress variations on time scales of less than 20 years

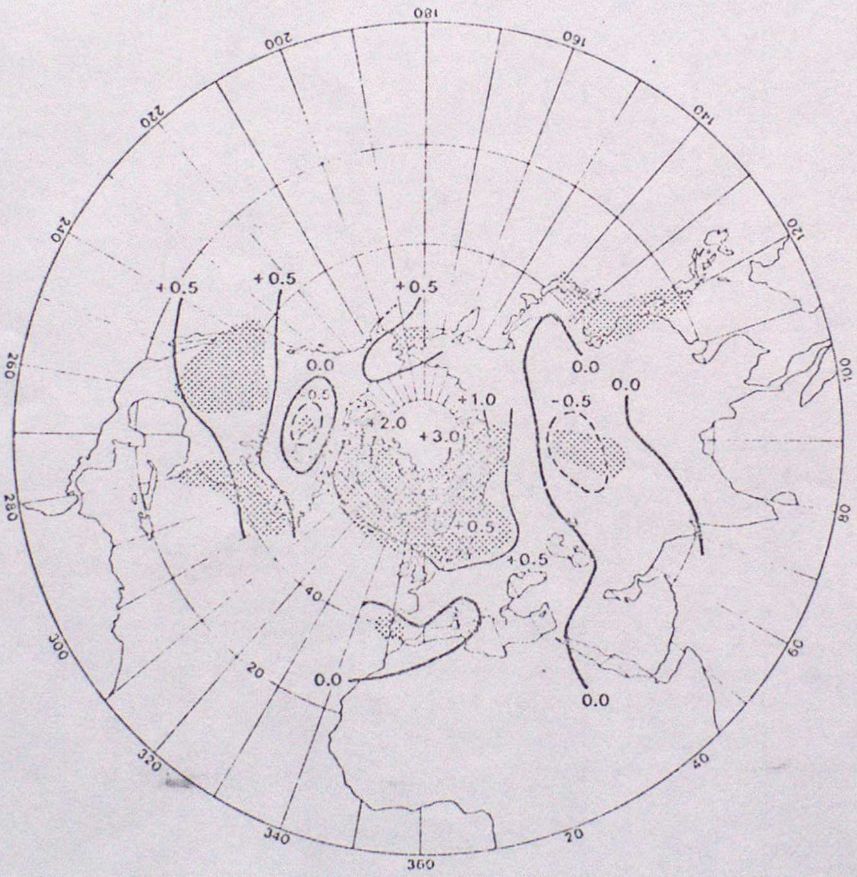
180
160
140
120
100
80
60
40
20
360
340
320
300
280
260
240
220
200
+0.5
+0.5
+0.5
0.0
-0.5
+1.0
+2.0
+3.0
0.0
-0.5
0.0
+0.5
+0.5
40
20
0.0
0.0

8·8(b) Linear trend of gridpoint temperatures over the period 1917–1939 (°C/y×10^{-1}). Shaded areas are significant at the 5 per cent level

(from Jones and Kelly 1983)

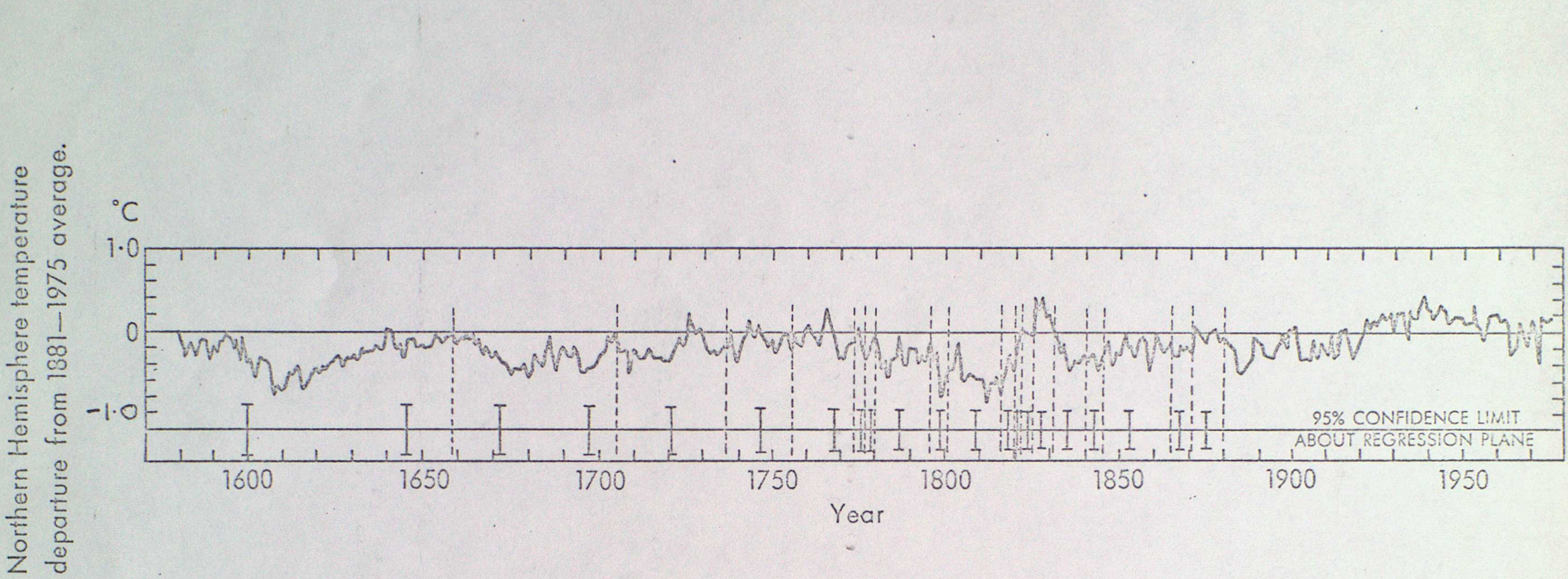

FIGURE 8.9 RECONSTRUCTED ANNUAL TEMPERATURE DEPARTURES (1579—1880) FOR THE NORTHERN HEMISPHERE FOLLOWED BY DATA OF BORZENKOVA et al., (1976). AFTER GROVEMAN AND LANDSBERG (1979). Confidence limits of regressions at bottom of graph.

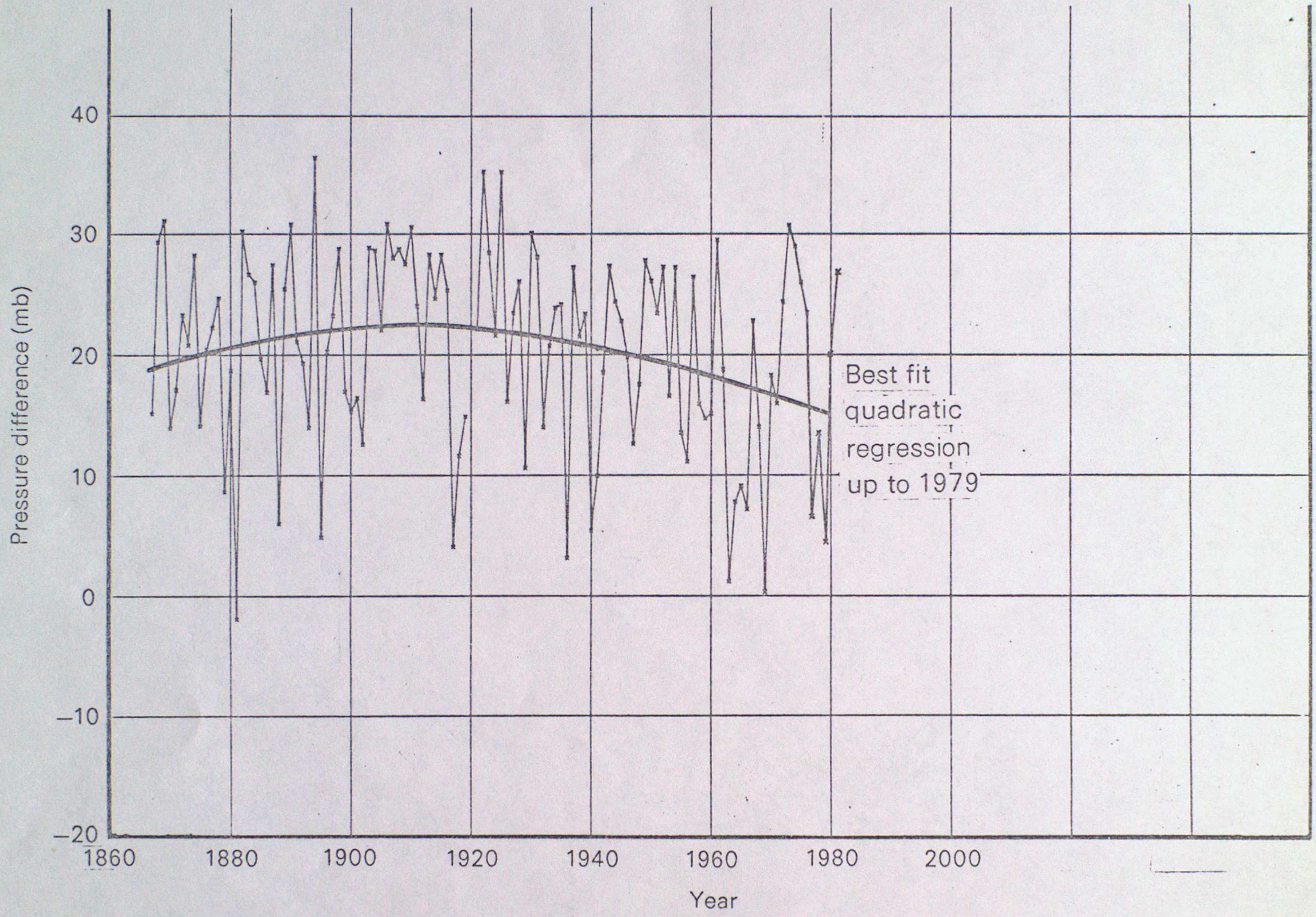

Fig 8.11(a) TIME SERIES OF AZORES (PONTA DELGADA) MINUS ICELAND (STYKKISHOLMUR) SEA LEVEL PRESSURE IN WINTER, 1867–1981. ["NORTH ATLANTIC OSCILLATION"]

JANUARY 1901-30 MEAN SURFACE PRESSURE ANOMALY (1951-70 BASE PERIOD)

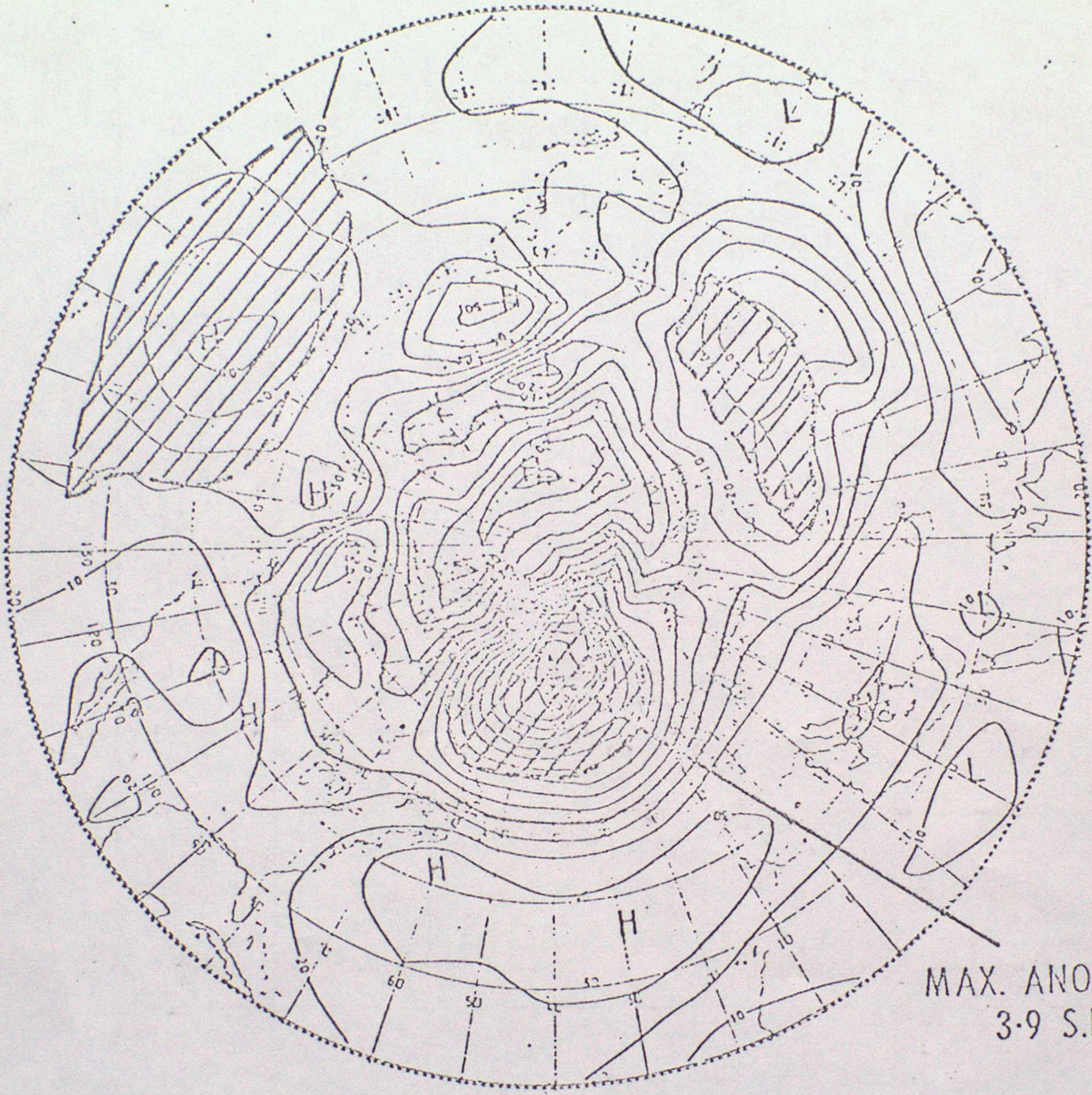

MAX. ANOMALY
3·9 S.E.,

anomaly mb x 10

▨ Areas of 5% significant difference using "t" test (approx assessment)

NB Other areas of large anomaly not shaded as data too doubtful

Fig 8·12

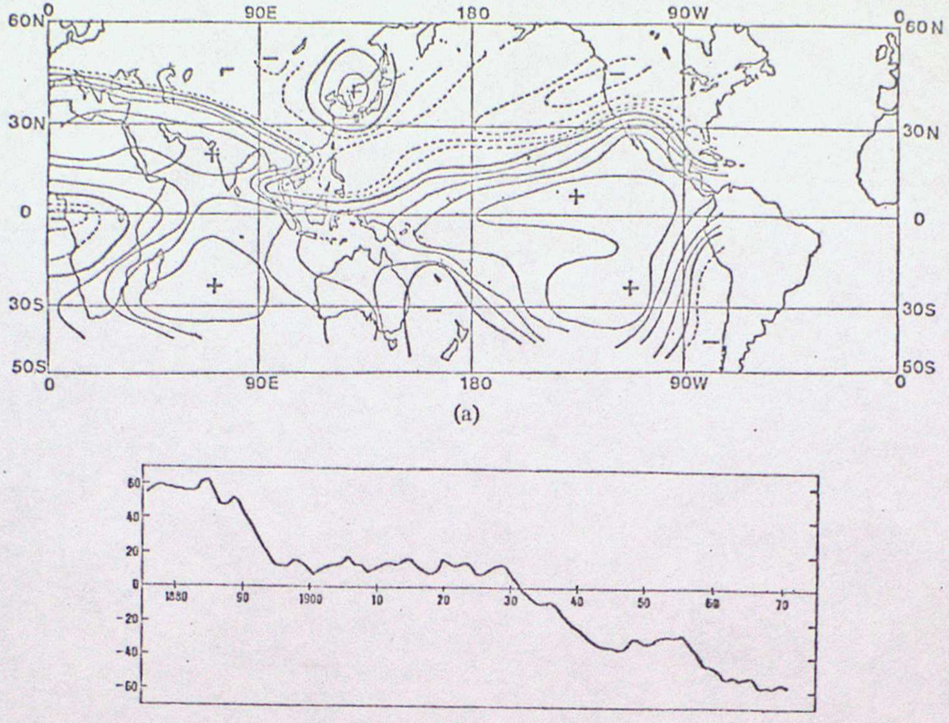
60N
30N
0
30S
50S
0
90E
180
90W
+
-
60
40
20
0
-20
-40
-60
1880
90
1900
10
20
30
40
50
60
70

(a)

(b)

FIG 8.13(a) (a) Spatial pattern of the first component deduced by the EOF analysis of the 11-year moving smoothed pressure. Dashed contours are negative values. Units are 0.2. (b) Time coefficients of the first component.

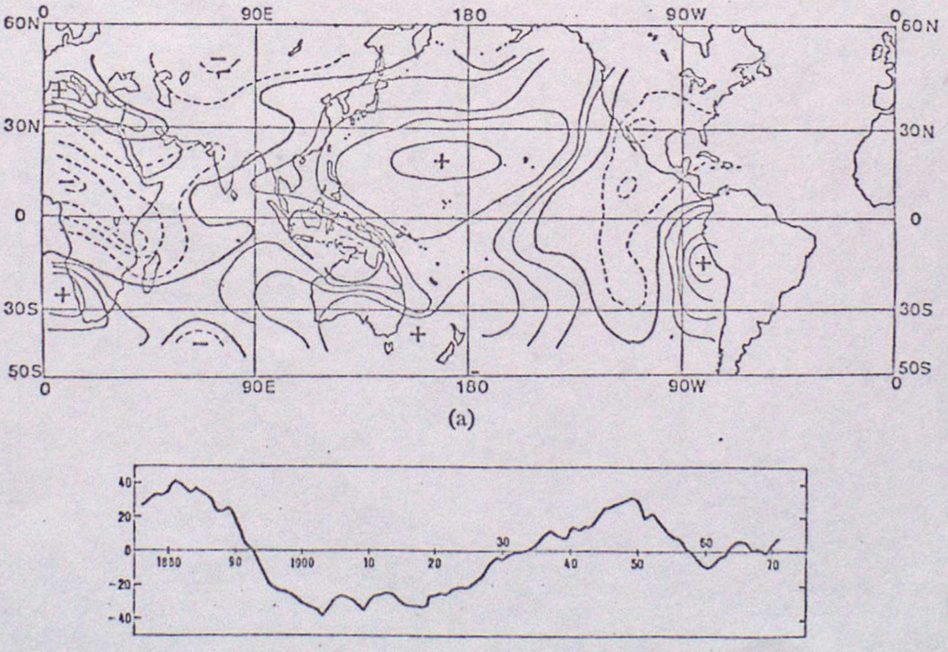
60N
30N
0
30S
50S
0
90E
180
90W
+
-
40
20
0
-20
-40
1880
90
1900
10
20
30
40
50
60
70

(a)

(b)

FIG 8.13(b) (a) Same as Fig. 2(a) but for the second component. (b) Same as Fig. 2(b) but for the second component.

FIG 8.14 (a) . Variation in surface temperature, and mean temperature in the 85–30 kPa layer, in the five climatic zones. A 1–2–1 weighting (divided by 4) has been applied twice to successive seasonal values, except at the beginning and end of the record (northern spring of 1982) where a 1–1 weighting (divided by 2) has been applied twice.

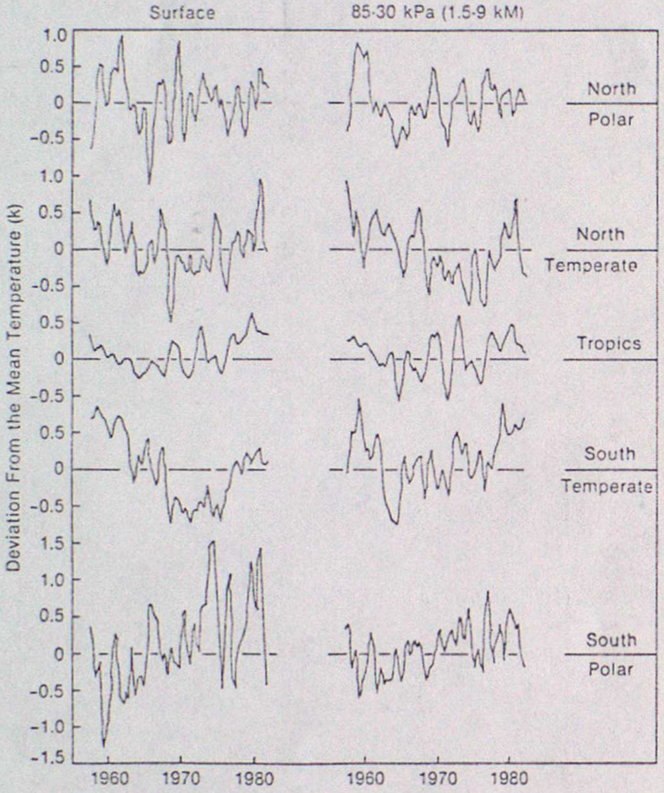

8.14(b) Variation in temperature in given height layers of northern and southern hemispheres. The temperatures for the 26–55 km layer of the northern hemisphere are based on rocketsonde data mostly in the western quadrant. Note the change in ordinate scale at left. Otherwise, see Fig. 3.7, caption.

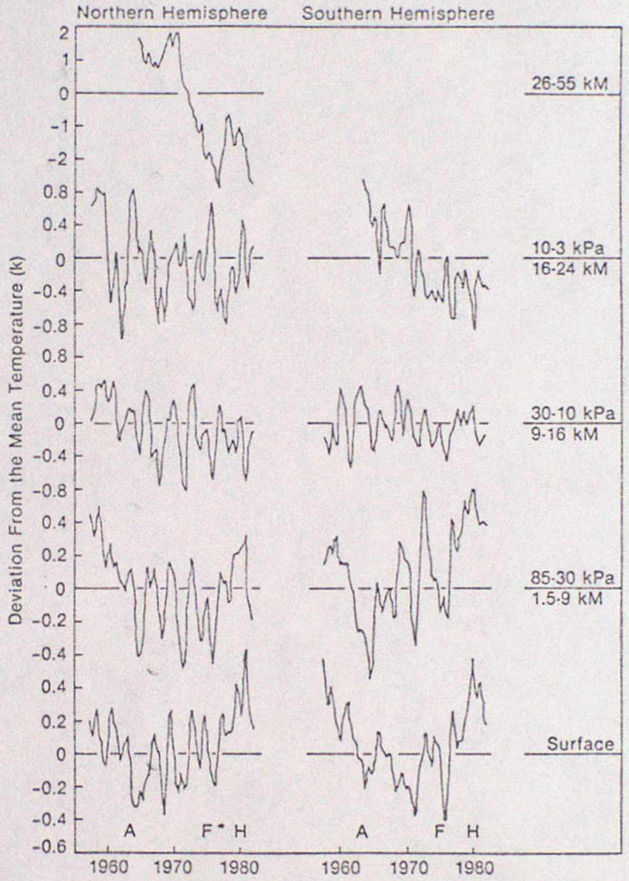

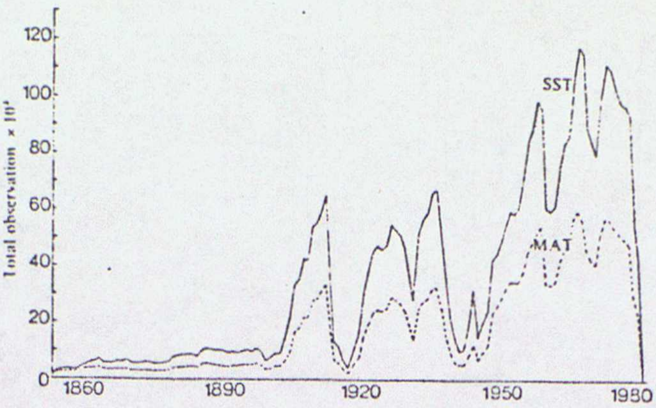

FIG 8.15: Annual numbers of marine temperature observations for the globe. SST, sea-surface temperature; MAT, nighttime marine air temperature.

(from Folland, Parker and Kates)
(1984)

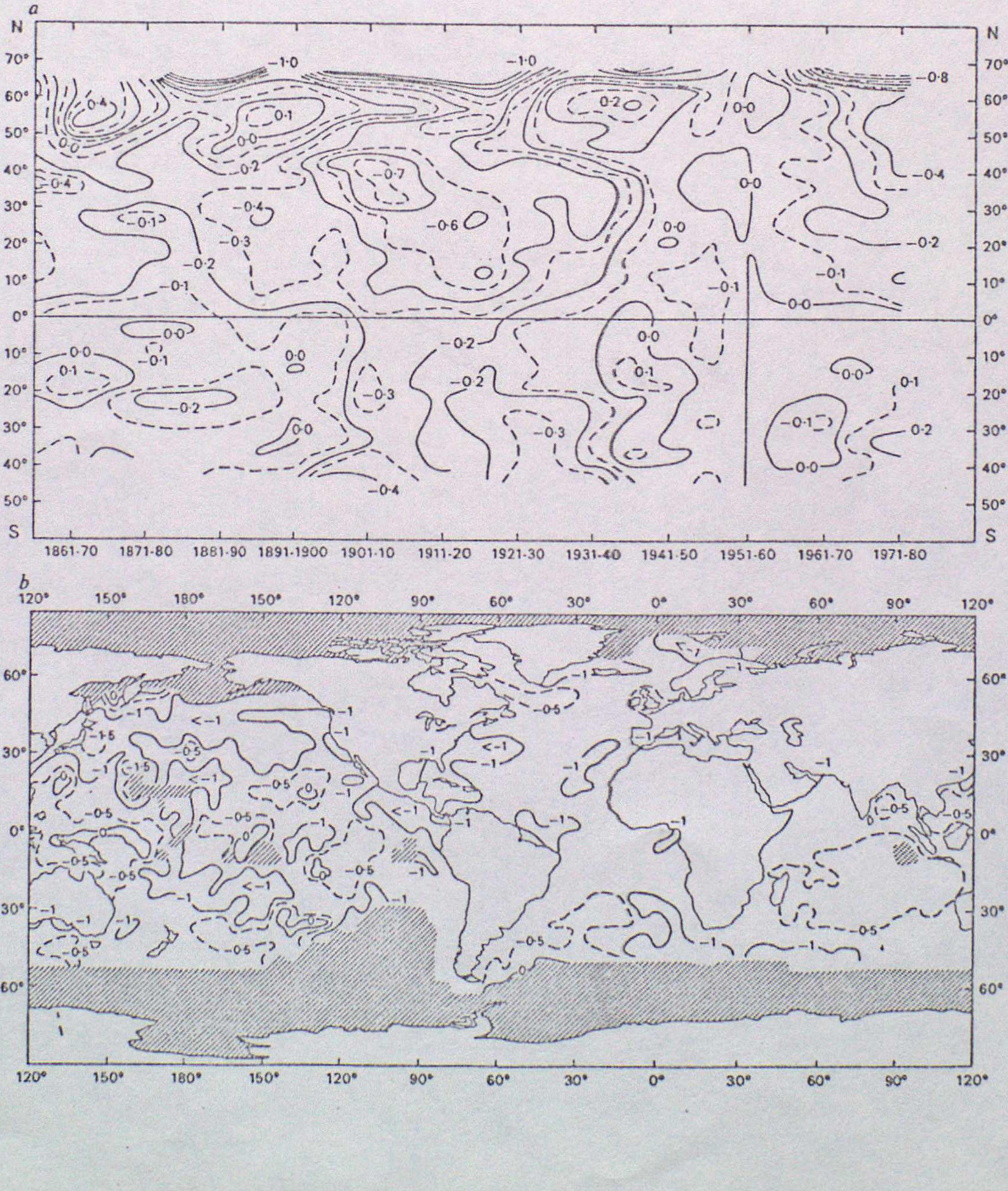
a
N
70°
60°
50°
40°
30°
20°
10°
0°
10°
20°
30°
40°
50°
S
−1·0
−0·8
−0·4
−0·2
−0·1
0·0
0·1
−0·3
−0·6
−0·7
0·2
1861-70
1871-80
1881-90
1891-1900
1901-10
1911-20
1921-30
1931-40
1941-50
1951-60
1961-70
1971-80
b
120°
150°
180°
150°
120°
90°
60°
30°
0°
30°
60°
90°
120°
−1
−0·5
−1·5
<−1

Fig. 8.17 *a*, Zonally-averaged sea-surface temperature anomalies (relative to 1951–60) (°C). Values are for 5-yearly overlapping decades and are corrected for instrumental changes. *b*, Corrected decadal sea-surface temperature for 1903–12 relative to 1951–60 (°C). Hatching denotes missing data.

COUNT OF SEASONS WITH DATA IN MOHSST (3)
YEARS 1871 TO 1880

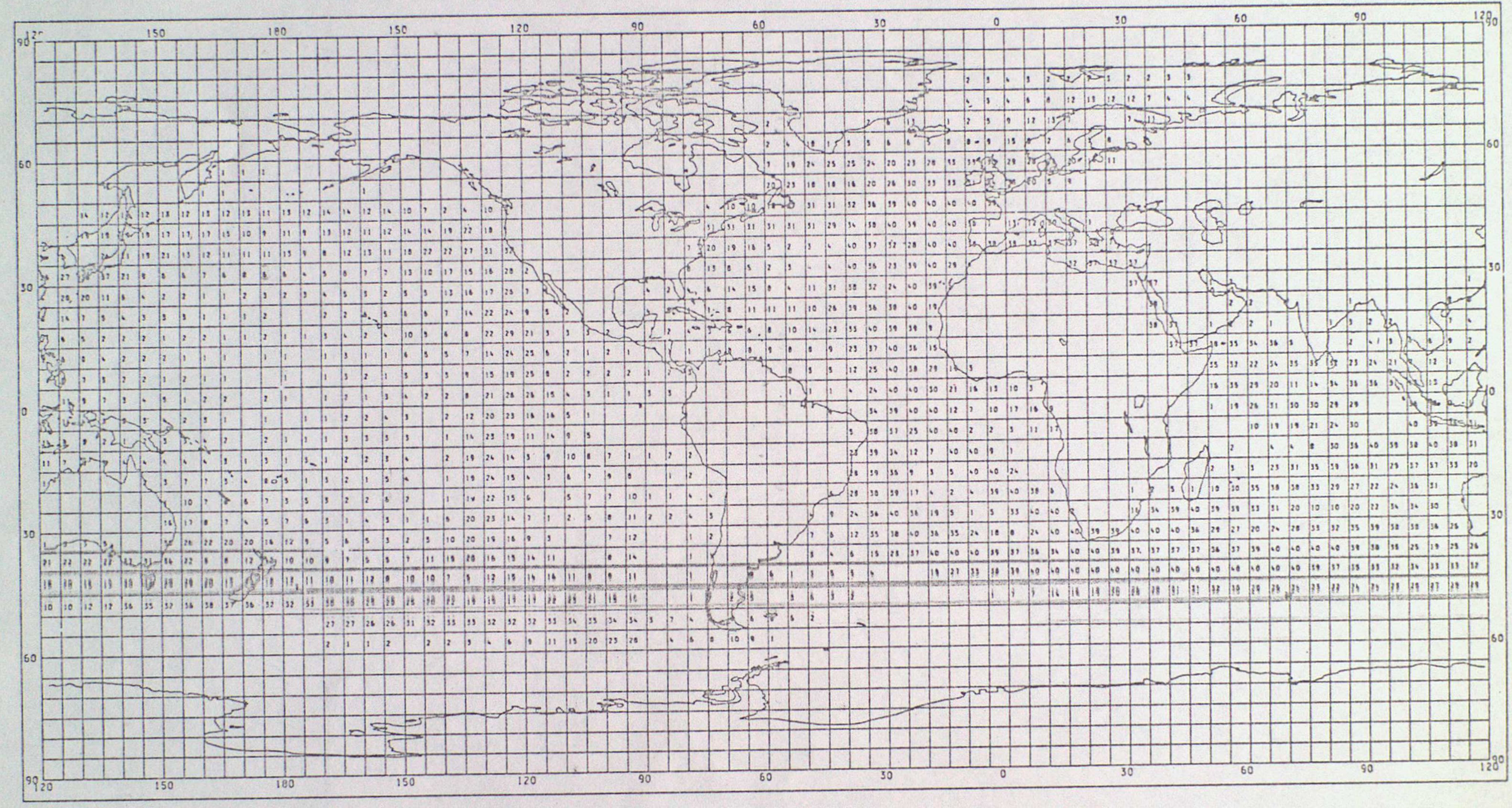
120
150
180
150
120
90
60
30
0
30
60
90
120
90
60
30
0
30
60
90

FIG 8.15(b)

FLAGS SET TO :11111

[MAXIMUM NUMBER OF SEASONS = 40]

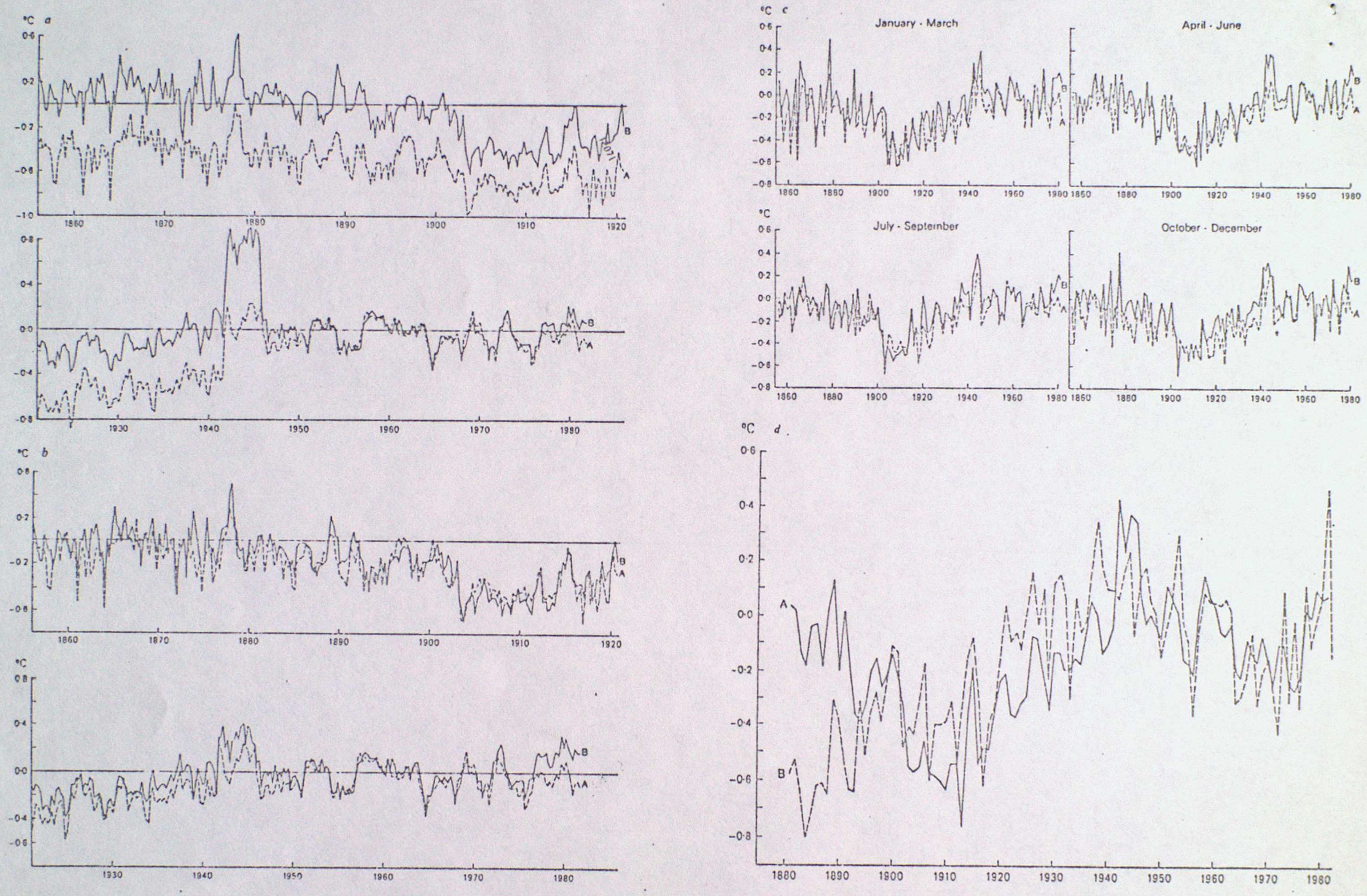

FIG 8·16 *a*, Uncorrected anomalies (relative to 1951–60) of: A, global sea-surface temperature; and B, nighttime marine air temperature. *b*, Corrected anomalies (relative to 1951–60) of: A, global sea-surface temperature; and B, global nighttime marine air temperature. *c*, Corrected anomalies (relative to 1951–60) of: A, global sea-surface temperature, and B, global nighttime marine air temperature, for the seasons taken separately. *d*, Annual anomalies (relative to 1951–60) for the Northern Hemisphere of: A corrected nighttime marine air temperature; and B, mainly land temperature after ref. 17.

EOF1 Global SST (10° squares 1901-80)

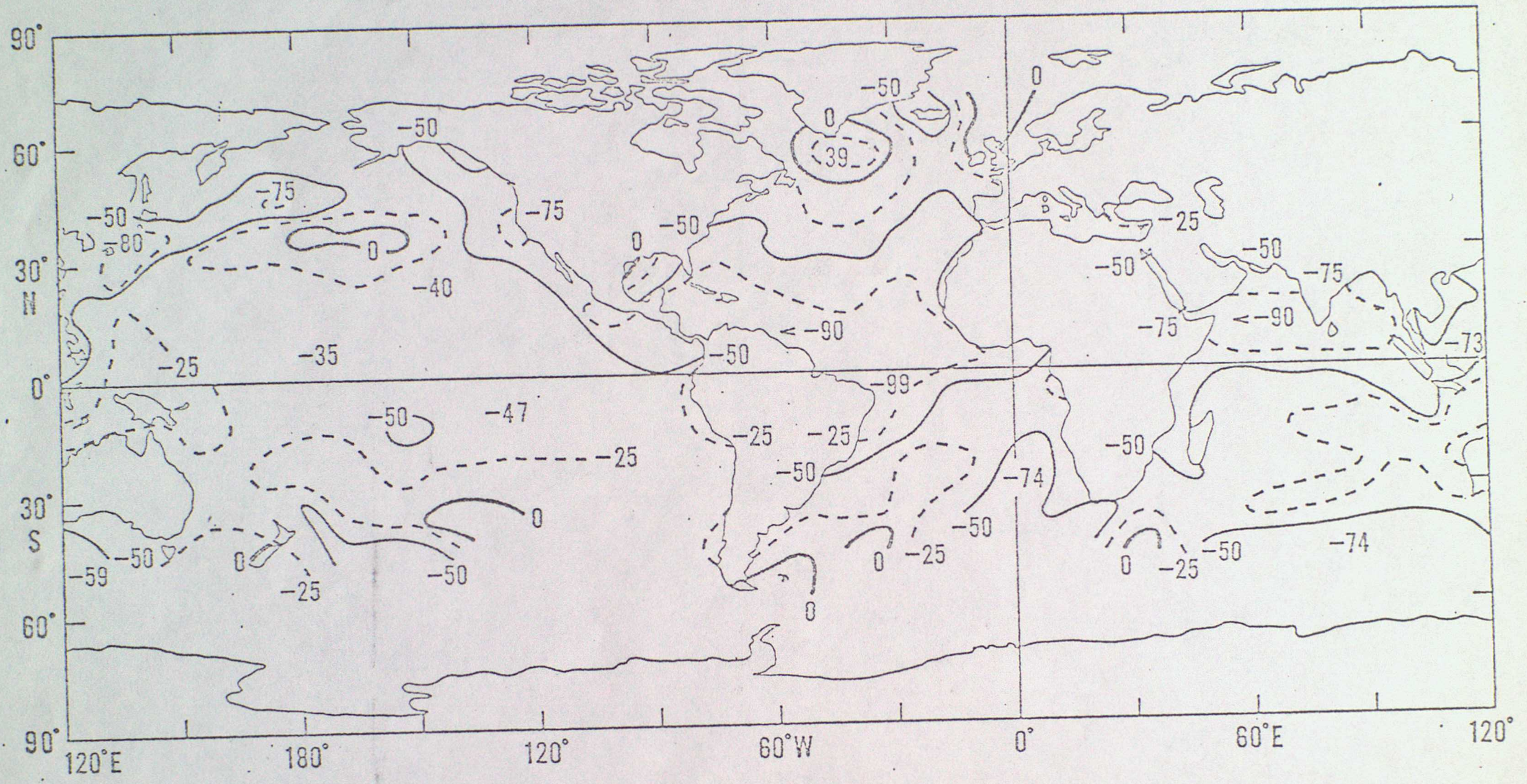
90°
60°
30° N
0°
30° S
60°
90°
120°E
180°
120°
60°W
0°
60°E
120°
-50
0
-39
-50
0
-75
-50
-75
-50
-80
0
-40
-50
-25
-50
-75
-90
-75
-90
-73
-25
-35
-50
-99
-50
-47
-25
-25
-25
-74
-50
-74
-50
0
-50
-25
-59
0
-25
-50
0
-25
0
-25
-50

FIGURE 8.13 (a)

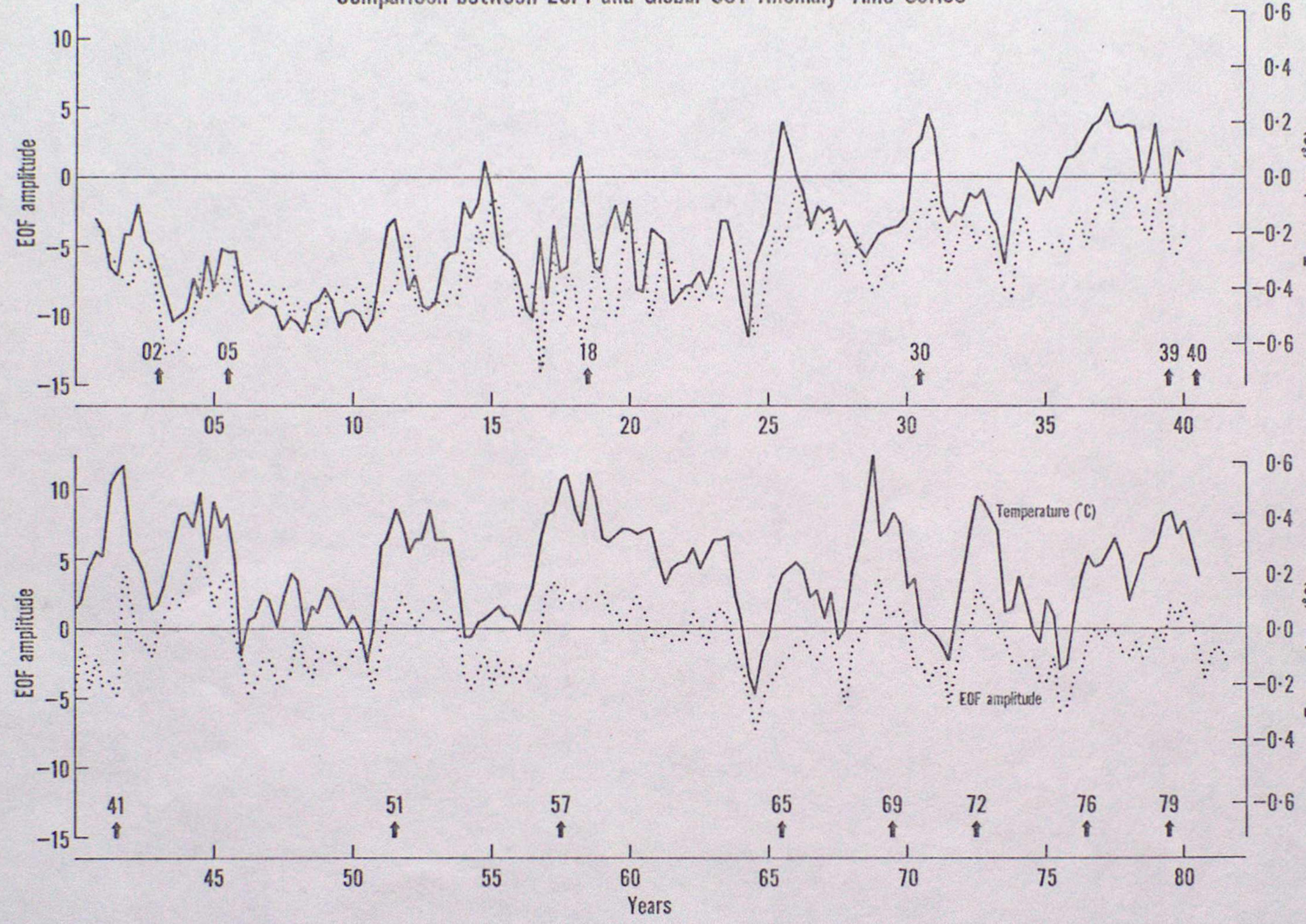
Comparison between EOF1 and Global SST Anomaly Time Series

FIG 8·18b

FIG 8.19 (a)

Maximum Entropy Power Spectra, 1861–1980

Adjusted seasonal values (using 100 coefficients)

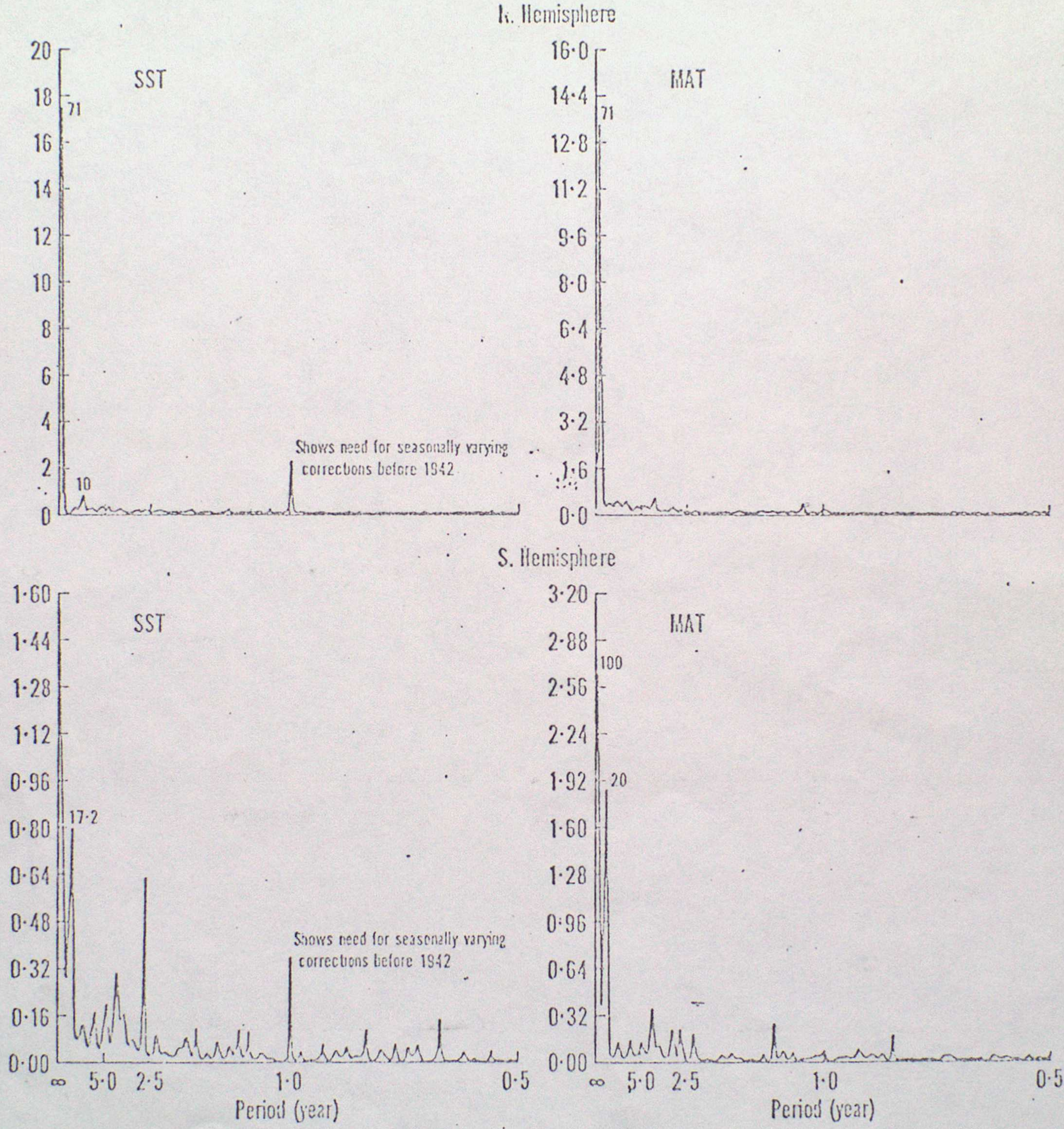

FIG 8.19 (b)

SST ANOMALIES FOR GLOBE 1951-80

NYQUIST FREQUENCY=1.00 PER MONTIME STEP=0.50. START = 0.00. STEP = 0.00.
NO.OF DATA POINTS=360..
NO.OF COEFFICIENTS=80.
NO.OF FREQUENCY POINTS=1000..
POWER SPECTRAL DENSITY.MEM.CALC.VALUE.

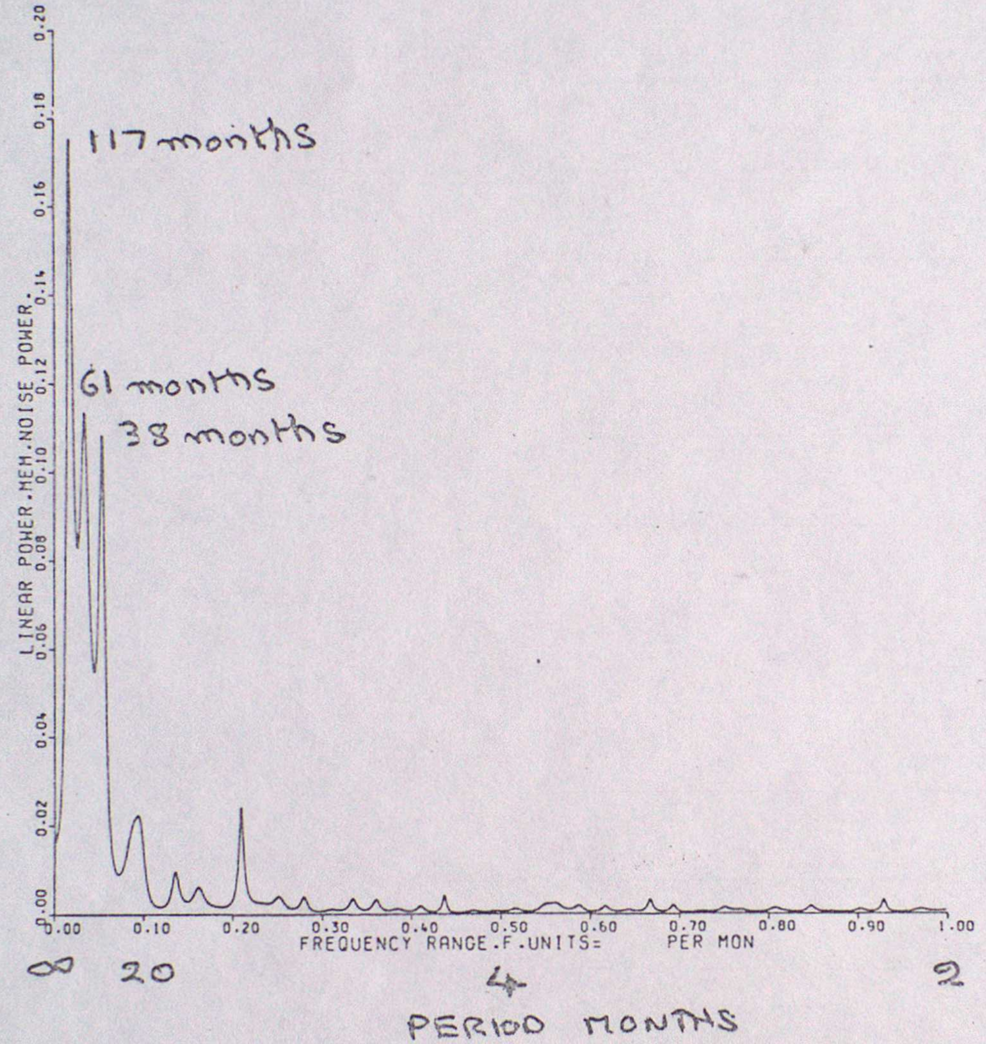

FIG 8·20 "FILTERED SST ANOMALIES IN THE N. AND S. HEMISPHERE 1856-1984"

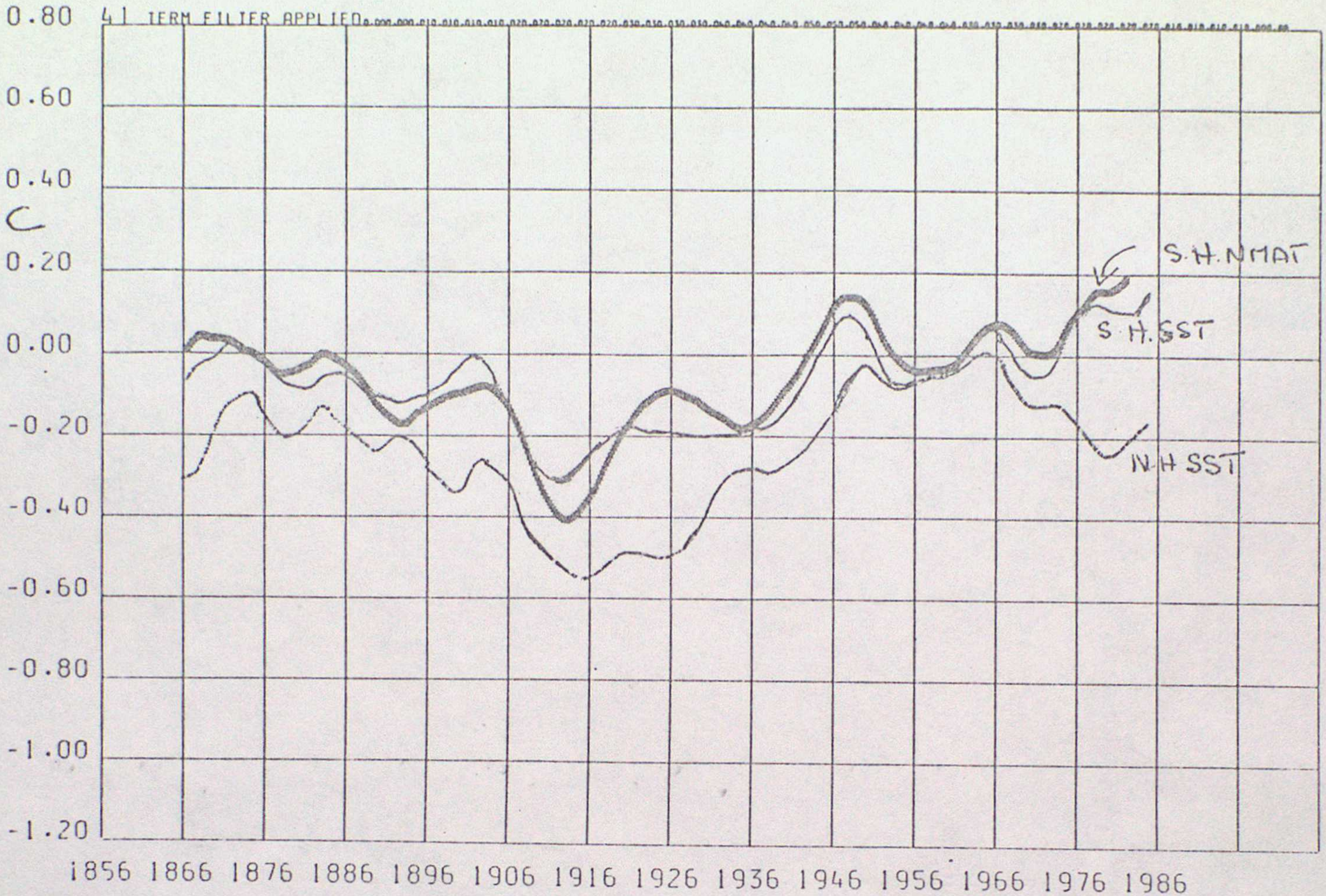

Fig 8.21(a)

Percentage of advancing and retreating glaciers in Switzerland, 1891–1975, showing the increase of advancing glaciers since the mid-twentieth century. (From Kasser & Aellen, 1981.)

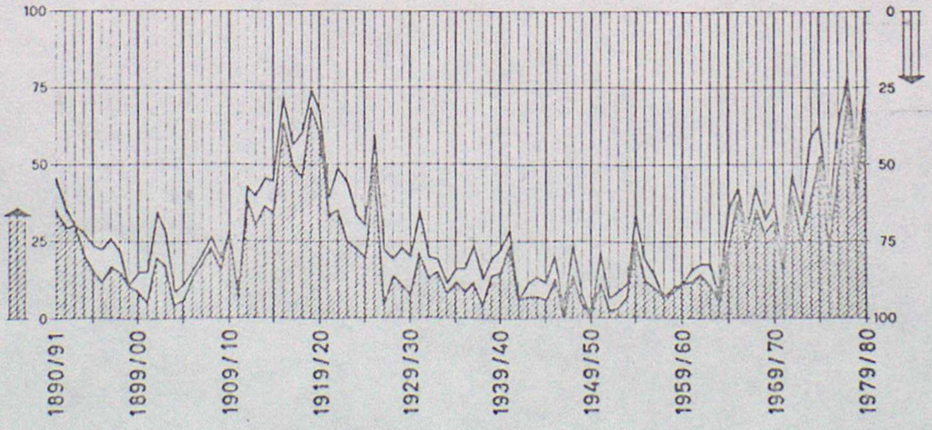

FIG 8.21 (b)

ANOMALY FOR YEARS 1856 TO 1981 AVERAGED OVER THE ATLANTIC N OF 35N (NORTHERN AUTUMN(OND) ONLY)
INSTRUMENTAL CORRECTIONS APPLIED PLOTTED FOR CENTRAL YEAR OF 10 YEAR PERIOD.
SOLID LINE IS NIGHT MAT ANOMALY WRT 1951-60 INCLUDING DATA TYPES ABCD
DASHED LINE IS SST ANOMALY WRT 1951-60 INCLUDING MIT DATA
VALUES AVERAGED SEASONALLY (JFM ETC) OVER 5 DEG X 5 DEG AREA THEN SPATIALLY
SPATIAL AVERAGING USES COS(LAT) AND PROPORTION OF LAND IN 5 DEG X 5 DEG AREA
10 YEAR RUNNING MEAN SMOOTHING APPLIED

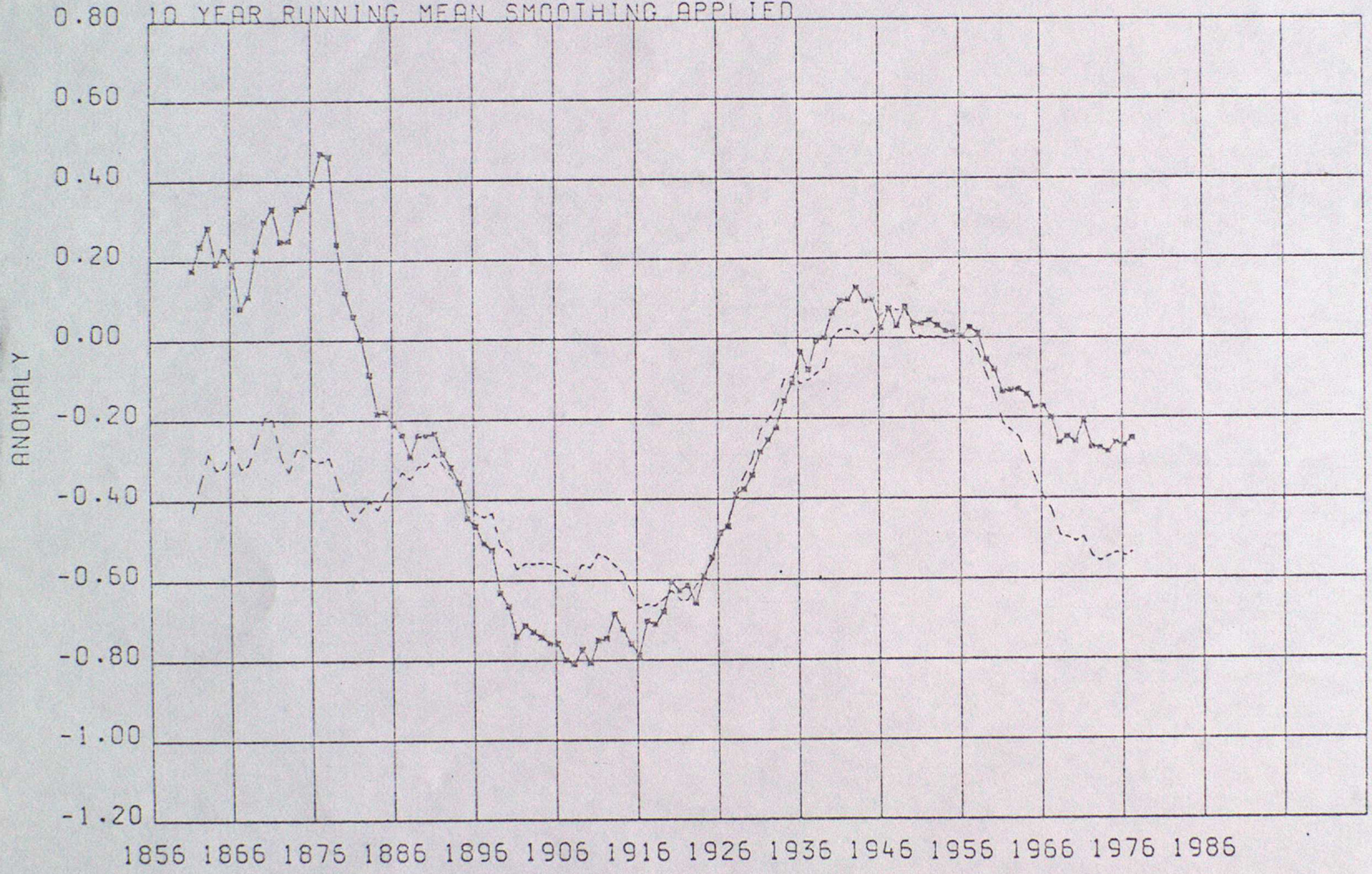

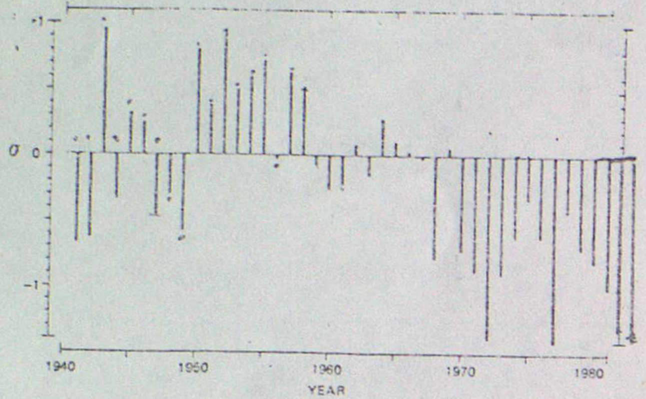

1941–81 time series of the yearly average of the normalized rainfall departures (σ) for 14–20 Subsaharan stations west of 9°E. Kraus[13], and Faure and Gac[19] suggest that the largely dry epoch at the start of the time series (1941–49) commenced no more than a year or two earlier. The 1969 value of +0.06 is a correction of the −0.11 value published earlier[21].

FIG 8·22

ENGLAND & WALES RAINFALL FOR HIGH SUMMER (JA)

DATA FROM WIGLEY ET AL (J. CLIMATOLOGY 4(1984) PP 1-25) TO 1980

DATA FROM MET 013 FROM 1981.ADJUSTED BY DIFFERENCE IN 1971-80 NORMALS

VALUES IN MM

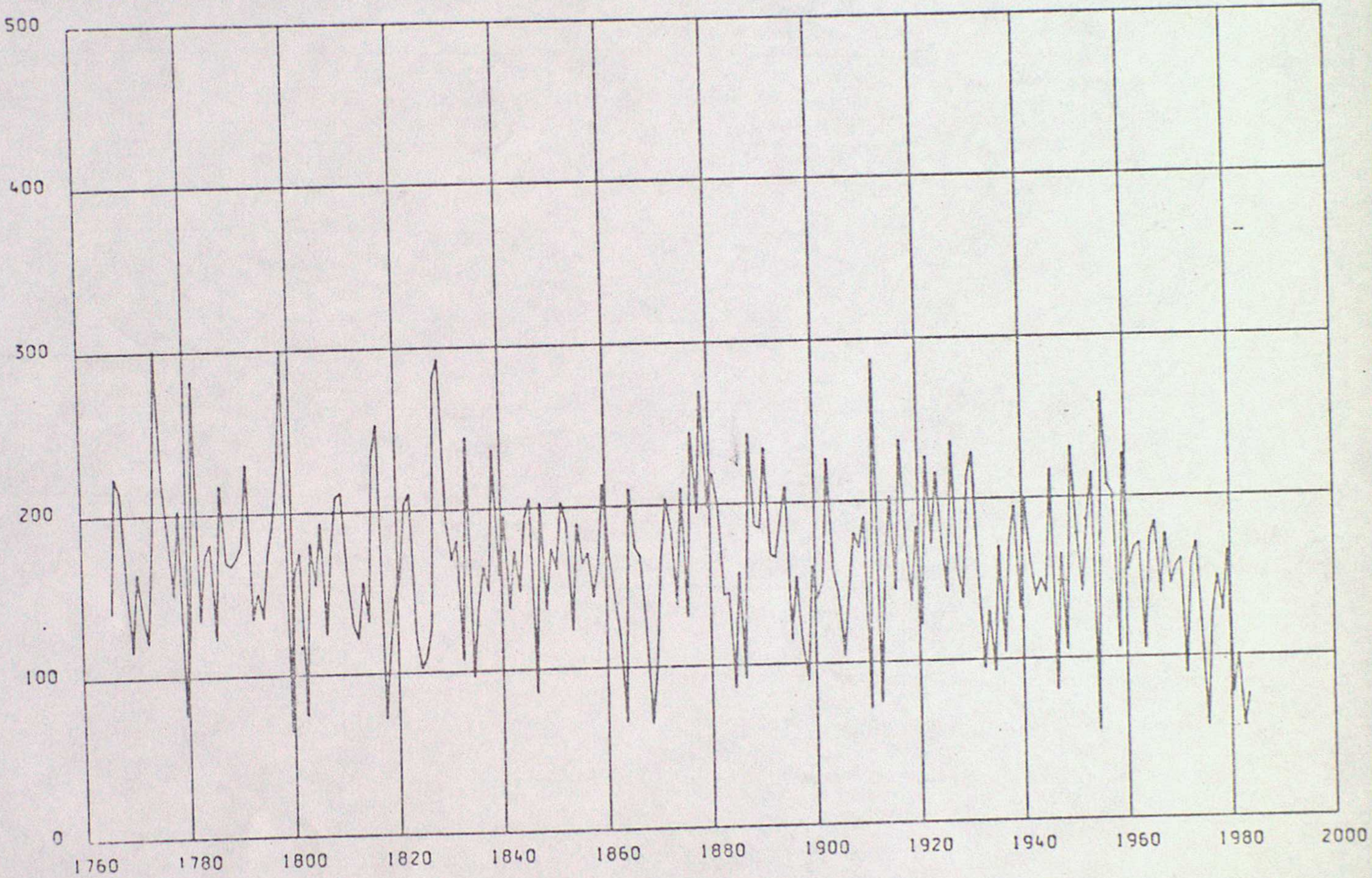

FIG 8-24

FRAME 002

04/03/85 1745Z

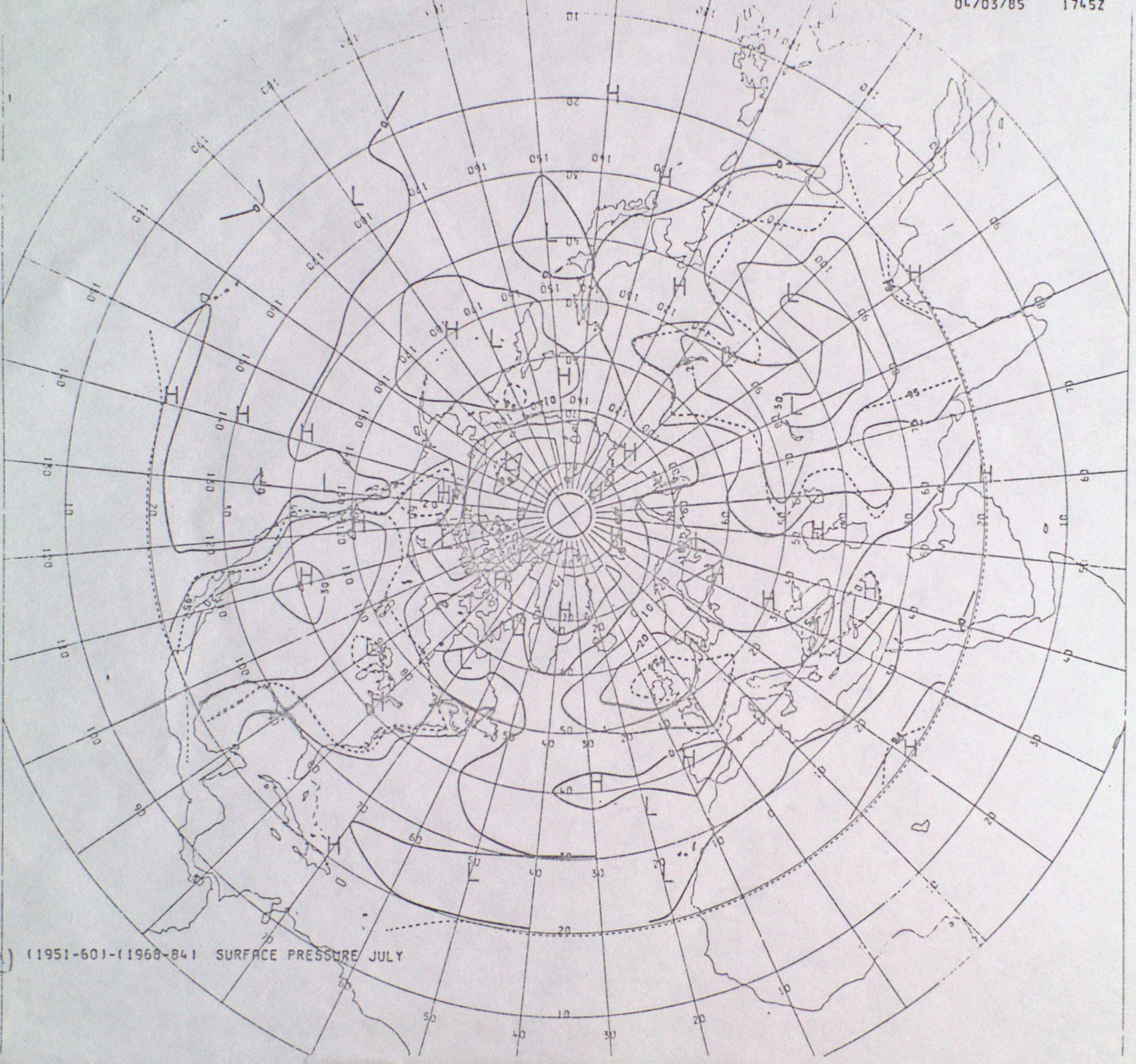

Fig 8.23(i) (1951-60)-(1968-84) SURFACE PRESSURE JULY

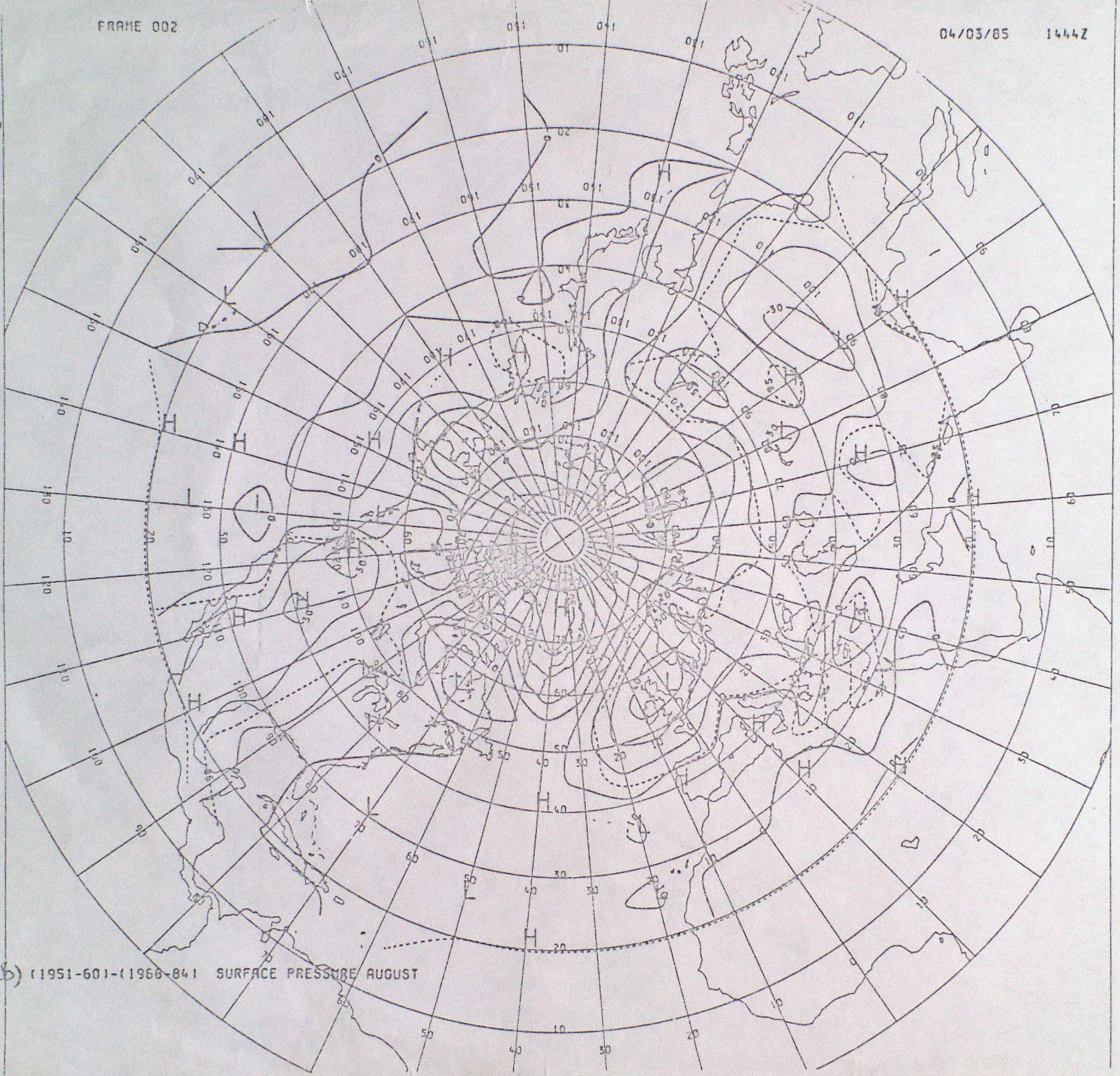
FRAME 002
04/03/85 1444Z

FIG 8.23(b) (1951-60)-(1960-84) SURFACE PRESSURE AUGUST

FOR LOAN to Met. Office Staff only.

METEOROLOGICAL OFFICE
145731
- 7 MAY 1985
LIBRARY

ADVANCED LECTURES 1985

LECTURE 9 - CARBON DIOXIDE AND CLIMATE VARIATION

by D E Parker and C K Folland

1. INTRODUCTION

The evidence is reviewed for the possible past and future impact of changing atmospheric carbon dioxide (CO_2) levels on climate. The influence of other radiatively active gases is also considered.

2. EVIDENCE FOR INCREASING ATMOSPHERIC CARBON DIOXIDE

Direct and reliable measurements of the amount of CO_2 in the atmosphere are available only from 1958, and show (Figure 9.1) an increase from 315 parts per million (ppm) to over 340 ppm. Until the early 1980's it was generally thought, on the basis of earlier, less accurate measurements, that the pre-industrial concentration was about 290 ppm. However recent measurements of carbon-13 in tree-rings, and of carbon dioxide concentration in air bubbles trapped in polar ice, yield estimates in the range 260 to 280 ppm (see for example Barnola et al (1983)). The basis of the carbon-13 method is that changes in the size of the biosphere, which are likely causes of past changes of atmospheric CO_2 concentration, introduce tiny changes in the atmospheric carbon-13/carbon-12 ratio because organic materials are about 1.8% deficient in carbon-13 relative to the nominal concentration of carbon 13 in atmospheric carbon dioxide. Possible difficulties with these methods include contamination with present day air (which would cause estimates of past CO_2 concentration to be too high), more diffusion than expected of carbon-13 in the tree rings or of carbon dioxide locked in polar ice layers.

Analysis of air bubbles in polar ice has been used to extend the record of atmospheric CO_2 concentration back for more than 30,000 years. Figure 9.2 shows the results: of particular note is the low concentration in the late Pleistocene and the rapid (possibly sudden) increase when the ice-sheets melted after the Allerod-Younger Dryas oscillation around 10,000 years ago (Siegenthaler and Wenk (1984). This increase is likely to have accelerated the global warming during the early Holocene (Sarmiento and Toggweiler 1984)). See also lecture 7.

Estimates of CO_2 input to the atmosphere, as a result of man's activities, yield a rate of increase of atmospheric concentration around double that observed. The discrepancy can largely be accounted for by oceanic absorption processes (Broecker et al (1979)), though a small part of the difference may result from increased photosynthesis in the biosphere because of the increased atmospheric carbon dioxide concentration (Schiff (1981)).

ORGS UKMO
National Meteorological Library
FitzRoy Road, Exeter, Devon. EX1 3PB

3 8078 0007 8157 7

3. THE RADIATIVE EFFECTS OF INCREASING ATMOSPHERIC CARBON DIOXIDE

3.1 DIRECT EFFECTS

In the 3rd Lecture, a very simple explanation of the greenhouse effect was provided. Figure 9.3, along with Table 3.14 of Kondratyev (1969), illustrates the fact that CO_2 absorbs perhaps 2 to 3 times more outgoing long wave terrestrial radiation than radiation reaching the Earth from the sun: some absorption of the longer solar wavelengths also occurs. There is not, at present, 100% absorption of long wave radiation in the wavelengths affected by CO_2 (Figure 9.4): therefore, as the concentration of CO_2 increases, the absorption of outgoing long-wave radiation will increase: absorption is given by

$$I\lambda = I_{\lambda o} \exp\left(- \int_{o} K\lambda\rho dz \right) \qquad (1)$$

at any given wavelength λ, where $I_{o\lambda}$, I_{λ} are the outgoing beam intensities at the surface ($Z = 0$) and the top of the atmosphere ($Z = \infty$) respectively; k is the absorption coefficient of the gas, ρ is its density, and integration is with respect to height z, from the surface to the top of the atmosphere (see also Lecture 4). Because CO_2 is distributed throughout the depth of the atmosphere, and because there is a temperature lapse with height, the "effective" re-emission of terrestrial radiation to space will be at intensities corresponding to the temperature at the atmosphere's "centre of mass" of emission (roughly half-way up through the mass of the atmosphere) rather than at the higher intensities corresponding to the higher temperature of the surface. Lecture 3 shows that if α, the albedo of the earth-atmosphere system remains unchanged, the outgoing radiation to space from the earth-atmosphere system remains unchanged. Thus for $e = 1$ (perfectly absorbing "glass"), the outgoing radiation B is still equal to the ingoing solar radiation I. However the fluxes within the earth-atmosphere system change, giving a changed vertical temperature profile within the atmosphere (with the aid of convective and dynamical processes) and a net increase in incident radiation at the surface of the earth.

3.2 INDIRECT EFFECTS

Lack of radiative equilibrium at the earth's surface caused by increasing atmospheric CO_2 will cause the ocean surface, as well as the land surface, to warm. As a result, the mixing ratio of atmospheric water vapour will, on a global average, increase. This increase will enhance surface warming because of the increased downard flux of long-wave radiation provided by the extra water vapour in the troposphere (Figures 9.3 and 9.4) ie the 'glass' becomes more opaque so its emissivity increases. Radiative-convective models indicate that the effect of the additional water vapour on the long-wave flux is markedly greater than the direct effect of the additional CO_2 on the long-wave flux (see Figure 9.3 and eg Lal and Ramanathan (1984)).

An increase of global surface temperature might be expected to result in a decrease in the area covered by snow and ice. Since both snow and ice have a larger albedo than water or land, the amount of solar radiation reflected back into space will decrease, further enhancing the global surface warming. The temperature rises are likely to affect atmospheric circulation and, therefore, cloud, providing further potential influences on the earth's radiation budget. Clouds both reflect insolation (encouraging cooling) and absorb terrestrial radiation (encouraging warming) and in a given situation the balance between these two depends intricately on cloud level, cloud thickness and water content, though low clouds tend to cause cooling and cirrus clouds warming. Because of the complex factors involved, and the rudimentary treatment of clouds in atmospheric general circulation models, varying results have been obtained by different modellers who have attempted to simulate the effects of changes in cloud amount when atmospheric CO_2 concentration is increased.

Not all the indirect effects of increased CO_2 need enhance surface warming. For example, Choudhury and Kukla (1979) suggest that increased atmospheric absorption of solar radiation resulting from an increase in atmospheric CO_2 concentration will hinder the melting of snow, given that the surface air temperature is low enough (snow slowly melts in bright sunshine even when air temperature is below 0°C). So the warming of water surfaces eg the ocean, by direct solar heating may also slightly decrease. These effects would tend to offset, to a small extent, the surface warming that would result from an increased flux of long-wave radiation.

3.3 A CAUTIONARY TALE

By considering the energy balance at the surface a few authors (eg Newell and Dopplick (1979) (ND), Idso (1982)) have deduced that a doubling of atmospheric CO_2 concentration would result in a global warming of $^1/_4$°C or less, in conflict with the consensus range of 1.5°C to 4°C obtained by general circulation models and vertical profile (radiative-convective) models. Cess and Potter (1984) have demonstrated that, despite the undoubted uncertainties that remain with AGCM results, the results of ND and of Idso, can unfortunately be shown to be based on violations of the first law of thermodynamics. ND did not take into account the response of the depth of the atmosphere (considered the they surface in isolation), while Idso implicitly regarded the atmospheric feedbacks as part of the initial forcing.

The global annual average surface energy balance may be expressed, as:-

$$F + LH + SH = Q \qquad (2)$$

F and Q denote the net upward infrared and net downward solar radiation fluxes at the surface, while LH and SH are the net upward latent and sensible heat fluxes from the surface. Let the surface energy balance be perturbed by an amount ΔG resulting from a change in the radiation fluxes F and Q (Figure 9.3), all other terms being kept fixed and no feedbacks due to changes in cloudiness etc being considered. When equilibrium is reached, the total change in the energy balance, allowing for feedbacks etc is:-

$$\Delta F_D + \Delta F_I + \Delta LH + \Delta SH = \Delta Q_D + \Delta Q_I \qquad (3)$$

where subscript D denotes direct effects in the fluxes F and Q and I the indirect effects that result from feedback processes (ΔQ_I, for example, might result from changes in cloudiness or changes in ice cover). Now $\Delta G \equiv \Delta Q_D - \Delta F_D$, the direct change in net radiation and ΔLH and ΔSH are by definition, special cases of indirect effects of the changes in net radiation. Substituting $\Delta G = \Delta Q_D - \Delta F_D$ yields:-

$$\Delta G = \Delta F_I + \Delta LH + \Delta SH - \Delta Q_I \qquad (4)$$

ie the indirect changes in energy flux at the surface are balanced by the direct change in net radiation at the surface when equilibrium is attained.

Let $\lambda(T_s)$ be a surface temperature function defined by

$$\frac{dT_s}{dG} = \lambda(T_s)$$

So $\lambda(T_s)$ is the rate of change of surface temperature due to the change (a) in imposed flux of net radiation or (b) the net change in indirect radiative and surface energy fluxes.

From (4):-

$$\frac{1}{\lambda(T_s)} = \frac{dF_I}{dT_s} + \frac{d(LH)}{dT_s} + \frac{d(SH)}{dT_s} - \frac{dQ_I}{dT_s} \qquad (5)$$

(T_s is surface temperature, not air temperature). Equation (5) describes the sensitivity of T_s to the terms of the surface energy balance. These terms are forced to change by ΔF_I, ΔLH, ΔSH and $-\Delta Q_I$ respectively when CO_2 increases. If a surface temperature change ΔT_s occurs then from (4)

$$\frac{1}{\lambda(T_s)} = \frac{\Delta F_I}{\Delta T_s} + \frac{\Delta LH}{\Delta T_s} + \frac{\Delta SH}{\Delta T_s} - \frac{\Delta Q_I}{\Delta T_s}$$

or $$\Delta T_s = \lambda(T_s) \times \Delta G \qquad (6)$$

Equations (4), (5) and (6) are statements of the first law of thermodynamics (change in surface heating = change in internal energy of the surface layer + work done by the surface). Note that the definition of λ refers to the equilibrium response of each part of the climate system including all feedbacks and so is a sum of total derivatives of the fluxes.

Now ND ignored indirect changes in Q, (ΔQ_I) and also assumed a constant atmospheric temperature-height and water vapour content-height profile during the response of the climate system. This latter assumption corresponds to replacing the total derivatives of LH and SH within equation (5) by their partial derivatives, ie ND's surface temperature response function, (λ_{ND}), is given by

$$\frac{1}{\lambda_{ND}(T_s)} = \frac{dF_D}{dT_s} + \frac{\delta(LH)}{\delta T_s} + \frac{\delta(SH)}{\delta T_s} \qquad (7)$$

Since $d(LH)/dT_s$ and $d(SH)/dT_s$ include the inhibiting effects on the upward surface energy flux of the moistening and warming of the overlying atmosphere whereas $\delta(LH)/\delta T_s$ and $\delta(SH)/\delta T_s$ do not, the total derivatives of LH and SH imply reduced rates of change of the upward fluxes, compared with the partial derivatives, eg

$$\frac{d(LH)}{dT_s} < \frac{\delta(LH)}{\delta T_s} \qquad (8a)$$

and

$$\frac{d(SH)}{dT_s} < \frac{\delta(SH)}{\delta T_s} \qquad (8b).$$

In fact many models give $d(SH)/dT_s < 0$ whereas the partial derivative is strongly positive. Thus equation (7) tends to give a value of λ smaller than does the thermodynamically-consistent equation (5), and ND's calculated response would be too small. Of course if ΔF_I was sufficiently negative and ΔF_I smaller than expected then small values of λ are possible - but not for the reason stated by ND. The essential point is that one cannot consider the surface in isolation: the whole troposphere-surface system must be taken into account. According to Kiehl and Ramanathan (1982) the doubling of CO_2 concentration will only cause an equilibrium increase of 0.55 Wm^{-2} in downward long wave radiation at the surface, whereas there will be an equilibrium increase of 3.99 Wm^{-2} in downward long wave radiation at the tropopause. The difference results from a modelled change in emissivity near the tropopause larger than that near the surface. As a result, the radiative heat balance of the upper troposphere relative to that of the surface will change and the upper troposphere will tend to warm more than the surface; equilibrium will be maintained by changes in convection. ND's equations do not take changes in the vertical distribution of water vapour into account, whereas in fact changes in moist convection are likley to occur and affect surface relative humidity, air-sea temperature difference, surface wind speed etc. Table 9.1 summarises Cess and Potter's analysis of ND's results.

Idso (1982) carried out a very simple calculation: proceeding from one assumed equilibrium state (a 254.4K earth surface with no atmosphere) to a second equilibrium state (the present earth-atmosphere system), he calculated a change of downward infrared surface flux from an initial value of zero to 348 Wm^{-2} for a 33.6°C surface temperature increase. He equated the 348 Wm^{-2} to the forcing ΔG, ie the DIRECT change in net radiation, whereas the downwards flux at the surface of 348 Wm^{-2} in fact includes the net effect of both forcing and response (feedback), ie the sum of the direct and indirect changes. Thus Idso's λ, (about 0.1), calculated using (6) with ΔT_s = 33.6°C, was much too small.

4. NUMERICAL MODELLING RESULTS

Numerical models may be used to make detailed studies of the above feedbacks and terms in the energy balance equation. The present discussion will concentrate on the results of Mitchell and Lupton (ML) (1983). We begin with a brief summary of CO_2 induced changes of temperature predicted by several general circulation models.

Table 9.2 summarises the basic properties of and predicted global-mean carbon surface warmings due to carbon dioxide from 11 GCM experiments. Note that the predicted global-mean surface warming is in the region of -2°C-3°C for a doubling of atmospheric CO_2 and that warming is likely to be greater in polar latitudes, partly because of the ice-albedo feedback effect. A further common feature is a predicted stratospheric cooling (see eg Manabe and Wetherald (1980), Mitchell (1983)), of about 5°C to 10°C. The stratosphere cools because its emissivity, just like that of the troposphere, increases as the concentration of carbon dioxide increases within it but unlike the tropopshere the extra absorption of long-wave radiation above the stratosphere is insufficient to offset the increased emission. It is more difficult to find common changes of atmospheric circulation, regional precipitation etc between the GCM results but there is a general tendency to reduce soil moisture in midlatitudes in summer largely because of increased evaporation in the warmer climate. So concern over possible effects of an increase in atmospheric CO_2 on crop growth in mid-latitudes has been expressed.

The AGCM experiment of Mitchell and Lupton (1983), where CO_2 is increased by a factor of four above present levels, differs from other work reported in Table 9.2, in that a separate calculation of predicted changes in surface heat fluxes appropriate to a quadrupling of carbon dioxide was used to estimate a time-invariant but latitudinally-varying sea-surface temperature (SST) anomaly from a climatology appropriate to today. This perturbed SST distribution was applied as a fixed external boundary condition. Using results from Mitchell (1983) where SST was increased by a fixed 2°C in one set of experiments and CO_2 was doubled, without an increase of SST, in another set, zonally averaged changes in net surface heat flux due to those changes (Figure 9.5) were estimated and averaged over one or more annual cycles for bands of latitude 15° wide. It was then assumed (probably justifiably) that the response of model variables was linear with change in sea surface temperature and logarithm of carbon dioxide concentration. Then separate estimates were made, for each latitude band, of the increase in the flux of heat from the atmosphere to the ocean due to quadrupling carbon dioxide, (F), and the increase in the flux of heat, H, from the ocean to the atmosphere due to a 1°C increase of SST. The SST change in a given latitude band produced by a quadrupling of CO_2 concentration was then assigned the value F/H. So it was assumed effectively that a local response in SST balances local changes in surface heat flux; this is not quite true, of course because of advective effects. The assumption was relaxed at higher latitudes though, because a marked increase in the advection of atmospheric heat and moisture from low latitudes, could not be neglected. Thus poleward of 40° latitude, the estimated SST changes F/H were replaced by annually averaged changes in ocean mixed layer temperature found by Manabe and Stouffer (1980) (MS). A further increase in SST was imposed at some latitudes because of changes in prescribed sea-ice, and the resulting values smoothed (Figure 9.6). One might add that the above method also assumes that systematic changes of $^F/_H$ with longitude are not very important, such as might result from large-scale longitudinal variations in average SST. These reach 6°C–8°C in the S Pacific between 0° and 15°S (Lecture 2).

Figures 9.7a and 9.7b show ML's calculated changes in zonal average atmospheric temperature for quadrupled CO_2 averaged for June to August and December to February for quadrupled carbon dioxide. Stratospheric cooling is evident but its small value is not to be taken as significant, because the model has only 5 layers, each about 200 mb thick. Enhanced surface warming at high latitudes is mainly a winter phenomenon.

ML present a variety of results inducing changes in zonal-mean zonal winds, upper tropospheric transient eddy kinetic energy, poleward moisture fluxes, and precipitation minus evaporation. The latter is reproduced here as Figure 9.8 and shows the expected enhanced evaporation relative to precipitation over land in summer at midlatitudes.

The radiation scheme in ML's model has recently been found to underestimate downward longwave radiation fluxes in the lower troposphere by a global average of 13 Wm^{-2}, and by 20 Wm^{-2} over the oceans. So, an improved radiation scheme has been devised (Slingo and Wilderspin (1984)), in which absorption and emission spectra are temperature-dependent and the treatment of the water vapour continuum and its overlap with the carbon dioxide 15 μm band is refined. As a result, there may in future be a slight reduction in the sensitivity of the model's global surface temperature to changes in atmospheric CO_2 concentration.

5. THE DELAYING ROLE OF THE OCEANS

The necessarily over-rudimentary treatment of the oceans by ML and by most other modellers highlights the need to develop fully interactive ocean-atmosphere-cryosphere models, despite their computational expense. Initial attempts have been made by Spelman and Manabe (1984) and others, which indicate that the oceans should produce a delay of several decades in CO_2-induced warming as a result of their thermal capacity. In reality, the magnitude of the delay depends on the extent to which the deep and abyssal waters are connected with surface waters. Fig 2.5, Lecture 2, shows that in the tropics the regions of cool ocean water that result from large-scale upwelling are quite extensive. So, the effect of upwelling ocean waters is likely to be important in the transient response of the climate system to changes in CO_2 concentration. Further observational studies are required to clarify this important point.

Observations of ocean and atmospheric temperature suggest that the oceans have already substantially delayed any CO_2-induced warming. Theoretically, the (approximately) 25% increase in CO_2 concentration observed since 1870 should have given a mean global warming of SST of about $^1/_2$°C. However Figure 9.9, which is a smoothed update of the results of Folland et al (1984) (Lecture 8) indicates that present day (1975-84) marine temperatures when averaged worldwide may be only a little (about 0.1°C) higher than in 1860-1880, and that there has been a substantial globally-averaged fluctuation of order 0.5°C between these dates, with coldest conditions around 1910 and warmest conditions around the 1940-1950. This fluctuation may itself have resulted in part from atmosphere-ocean interactions due to presently unknown mechanisms. Figure 9.9 clearly indicates the substantial magnitude of the 'noise', in addition to short-term weather and ENSO-related fluctuations, against which the 'signal' of CO_2-induced global warming remains to be detected.

6. EFFECTS OF OTHER RADIATIVELY ACTIVE GASES ON ATMOSPHERIC TEMPERATURE

The trace gases of interest include nitrous oxide (N_2O), methane (CH_4), chlorofluorocarbons ($CFCl_3$ and CF_2Cl_2), sulphur dioxide (SO_2), ozone (O_3), and stratospheric water vapour from aircraft. The effects on surface temperature of changes in the concentrations of these gases is summarised by Mitchell (1984): for likely changes, he finds that the total effect of these gases on surface temperature may be considerably less than that resulting from a doubling of carbon dioxide, though not negligible by comparison. Lacis et al (1981), on the other hand, find that, between 1970-1980, the equilibrium warming for the measured increments of CH_4, chlorofluorocarbons and N_2O was probably between 50% and 100% of that for carbon dioxide for the same period. The subject is considered in detail by WMO (1982): their compilation of the climatic effects of increases in trace gas concentration is reproduced as Table 9.3.

REFERENCES

Barnola, J.M., Raynaud, D., Neftel, A. and Oeschger, H.	1983	Comparison of CO_2 measurements by two laboratories on air from bubbles in polar ice. Nature, 303, 410-413.
Broecker, W.S., Takahashi,T., Simpson, H.J., and Peng, T.-H.	1979	Fate of fossil fuel carbon dioxide and the global carbon budget. Science, 206, 409-418.
Cess, R.D. and Potter,G.L.	1984	A commentary on the recent CO_2 climate controversy. Climatic Change 6, 365-376.
Choudhury, B. and Kukla, G.	1979	Impact of CO_2 on cooling of snow and water surfaces. Nature, 280, 668-671.
Folland, C.K., Parker, D.E., and Kates, F.E.	1984	Worldwide marine temperature fluctuations 1856-1981. Nature, 310, 670-673.
Hansen, J., Johnson, D., Lacis, A., Lebedeff, S., Lee, P., Rind, D., and Russell, G.	1981	Climate impact of increasing atmospheric carbon dioxide. Science, 213, 957-966.
Houghton, J.T.	1979	Greenhouse effects of some atmospheric constituents. Phil. Trans. R. Soc. Lond. A.290, 515-521.
Idso, S.B.	1982	A surface air temperature response function for Earth's atmosphere. Boundary Layer Met., 22, 227-232.
Kiehl, J.T. and Ramanathan, V.	1982	Radiative heating due to increased CO_2: the role of H_2O continuum absorption in the 12-18 μm region. J. Atm. Sci., 39, 2923-2926.
Kondrabyer, K.Ya	1969	Radiation in the atmosphere. International Geophysics series, Vol. 12. Academic Press, New York and London. 912 pp.
Lacis, A., Hansen, J., Lee, P., Mitchell, T., and Lebedeff, S.	1981	Greenhouse effect of trace gases, 1970-1980. Geoph. Res. Lett., 8, 1035-1038.
Lal, M. and Ramanathan, V.	1984	The effects of moist convection and water vapour radiative processes on climate sensitivity. J. Atmos. Sci., 41, 2238-2249.

Manabe, S. and Stouffer, R.J.	1980	Sensitivity of a global climate model to an increase of CO_2 concentration in the atmosphere. J. Geoph. Res., 85, 5529-5554.
Manabe, S. and Wetherald, R.T.	1975	The effects of doubling the CO_2 concentration on the climate of a general circulation model. J. Atm. Sci., 32, 3-15.
Manabe, S. and Wetherald, R.T.	1980	On the distribution of climate change resulting from an increase in CO_2 content of the atmosphere. J. Atm. Sci., 37, 99-118.
Mitchell, J.F.B.	1983	The seasonal response of a general circulation model to changes in CO_2 and sea temperatures. Quart. J.R. Met. Soc. 109, 113-152.
Mitchell, J.F.B.	1984	The effects of pollutants on global climate. Met. Mag. 113, 1-16.
Mitchell, J.F.B. and Lupton, G.	1983	A 4 x CO_2 experiment with prescribed changes in sea surface temperatures. Met O 20 Tech. Note II/198. Unpublished. (Presented at EEC Symposium on 'Interactions between climate and the biosphere', Osnabruch, 21-23 March 1983).
Newell, R.E. and Dopplick, T.G.	1979	Questions concerning the possible influence of anthropogenic CO_2 on atmospheric temperature. J. Appl. Met., 18, 822-825.
Newell, R.E., Kidsen, J.W., Vincent, D.G. and Boer, G.J.	1974	The General Circulation of the Tropical Atmosphere and Interactions with Extratropical Latitudes. 2 Vols. MIT.
Sarmiento, J L and Toggweiler, J R	1984	A new model for the role of the oceans in determining atmospheric P CO2. Nature, 308, 621-624.
Schiff, H.I.	1981	A review of the carbon dioxide greenhouse problem. Planet. Space Sci., 29, 935-950.

Siegenthaler, U and Wenk, Th	1984	Rapid atmospheric CO_2 variations and ocean circulation. Nature, 308, 624-626.
Slingo, A. and Wilderspin, R.C.	1984	Development of a revised long wave radiation scheme for a general circulation model. Met O 20 DCTN14. Unpublished.
Spelman, M.J. and Manabe, S.	1984	Influence of oceanic heat transport upon the sensitivity of a model climate. J. Geoph. Res., 89, C1, 571-586.
Washington, W.M. and Meehl, G.A.	1983	General circulation model experiments on the climatic effects due to a doubling and quadrupling of carbon dioxide concentration. J. Geoph. Res., 88, C11, 6600-6610.
Wetherald, R.T. and Manabe, S.	1981	Influence of seasonal variation upon the sensitivity of a model climate. J. Geoph. Res., 86, C2, 1194-1204.
WMO	1982	Report of the Meeting of Experts on Potential Climatic Effects of Ozone and other Minor Trace Gases, Boulder, Colorado, 13-17 September 1982. WMO Global Ozone Research and Monitoring Project, Report No. 14.
WMO/UNEP/ICSU	1981	Papers presented at the WMO/ICSU/UNEP Scientific Conference on Analysis and Interpretation of Atmospheric CO_2 data. (Bern, 14-18 September 1981). WCP-14, Geneva.

Table 9.1. Effects of a doubling of atmospheric CO_2 (from the 2-dimensional model of Cess and Potter (1984))

Quantity	Value
ΔT_s	1.87°C
ΔG	1.69 Wm^{-2}
$\frac{dF}{dT_s}$	5.87 Wm^{-2} $°C^{-1}$
$\frac{dF}{dT_s}$	−0.24 Wm^{-2} $°C^{-1}$
$\frac{dQ}{dT_s}$	−0.39 Wm^{-2} $°C^{-1}$
$\frac{d(LH)}{dT_s}$	1.11 Wm^{-2} $°C^{-1}$
$\frac{d(SH)}{dT_s}$	−0.35 Wm^{-2} $°C^{-1}$
$\frac{\delta(LH)}{\delta T_s}$	51.64 Wm^{-2} $°C^{-1}$
$\frac{\delta(SH)}{\delta T_s}$	18.26 Wm^{-2} $°C^{-1}$

TABLE 9.2

Model Characteristics	MW75	MW80	MS80	$WM81_1$	$WM81_2$
Domain	$0^\circ<\lambda<120^\circ$ $0^\circ<\phi<81.7^\circ$	$0^\circ<\lambda<120^\circ$ $0^\circ<\phi<90^\circ$	Global	$0^\circ<\lambda<120^\circ$ $-90^\circ<\phi<90^\circ$	
Land-ocean distribution	Ocean for $60^\circ<\lambda<120^\circ$ $0^\circ<\phi<66.5^\circ$	Ocean for $60^\circ<\lambda<120^\circ$ $0^\circ<\phi<90^\circ$	Realistic	Ocean for $60^\circ<\lambda<120^\circ$ $0^\circ<\phi<90^\circ$	
Ocean	Swamp$^+$	Swamp$^+$	Mixed layer	Mixed layer	
Seasonal variation	No	No	Yes	Yes	No
Cloud Feedback	No	Yes	No	No	
Horizontal resolution	About 500 km on a Mercator projection	5° in long 4.5° in lat	Spectral models with max zonal wavenumber 15	Spectral models with max zonal wavenumber 15	
Global mean surface temp rise (K)	2.9	3.0	2.0*	2.4*	3.0*
Surface temp rise at lat 70°	About 7	About 6	About 4*	About 4*	About 6*

Table 9.2 . Summary of characteristics of GCMs. ALso given are the global mean temperature rise (K) and the zonal mean temperture rise at 70° latitude (mean of 70°N and 70°S where appropriate) for a doubling of CO_2 concentration. An asterisk implies that the value given is half the value obtained in a CO_2-quadrupling experiment. The models are those of Manabe and Wetherald (1975) -MW75; Manabe and Wetherald (1980) - MW80; Manabe and Stouffer (1979 and 1980) - MS80, Wetherald and Manabe (1981) $WM81_1$ and $WM81_2$; Hansen et al (1981) - H1 and H2; Washington and Meehl (1983) - WWGM; Spelman and Manabe (1984) - SM; Mitchell (1983) - M83; Mitchell and Lupton (1983) - ML83.

+ A 'swamp' ocean has zero heat capacity but an unlimited supply of moisture for evaporation.

Table 9.2 (continued)

H1	H2	WWGM	SM	M83	ML83
Global	Global	Global	$0^\circ < \lambda < 120^\circ$	Global	Global
Realistic	Realistic	Realistic	Ocean for $60^\circ < \lambda < 120^\circ$	Realistic	Realistic
Mixed layer	Swamp[†]	Swamp[†]	Coupled with currents	Climatological SST +2°C	Climatological SST + °C (see text)
Yes	No	No	No	Yes	Yes
Yes	Yes	Yes	No	No	No
10° in long. 8° in lat.	10° in long 8° in lat.	Spectral with max. zonal wavenumber 15	Spectral with max. zonal wavenumber 15	330 Km	330 Km
3.5	3.9	1.3	About 2.6*	2.25 but 2.9 over land	2.3*
Unavailable	Unavailable	1.4	About 4.5*	Similar to global value	About 4*

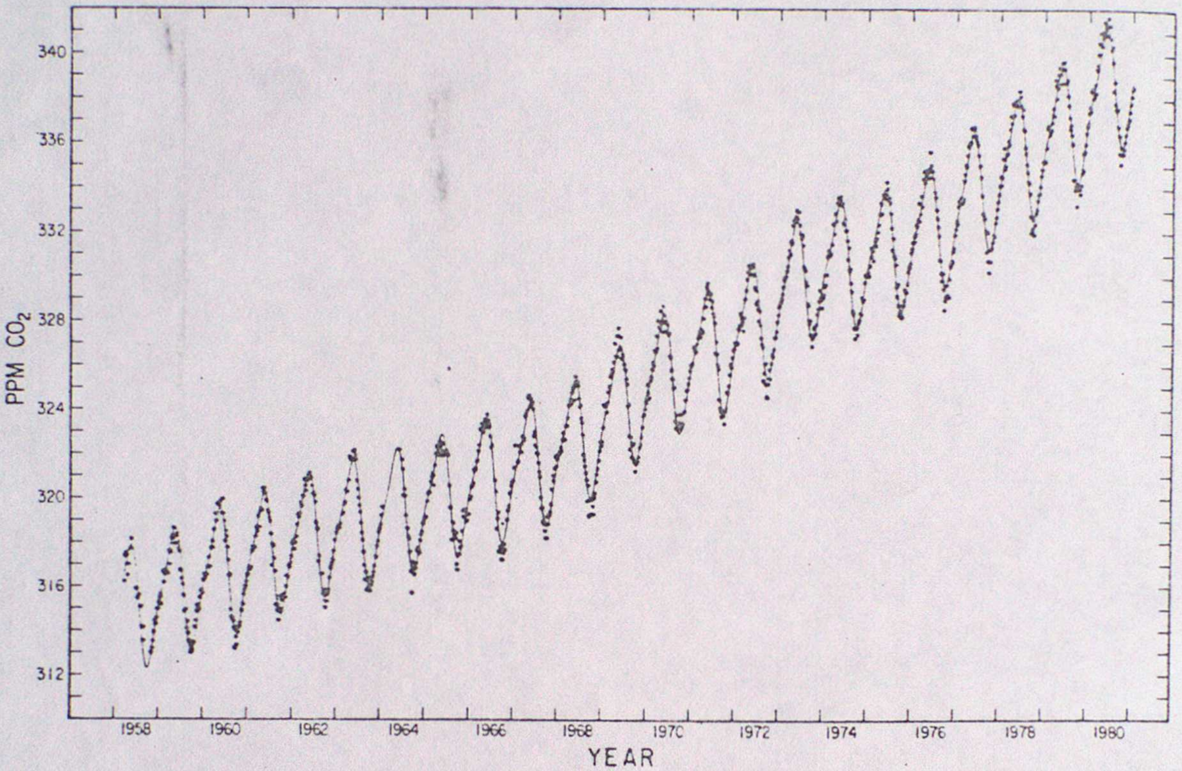

Figure 9.1 Concentration of atmospheric CO_2 at Mauna Loa Observatory, Hawaii, 19.5° N, 155.6° W. Dots are seven day averages of daily averages of blue-lined data (see text). (After WMO/UNEP/ICSU(1981))

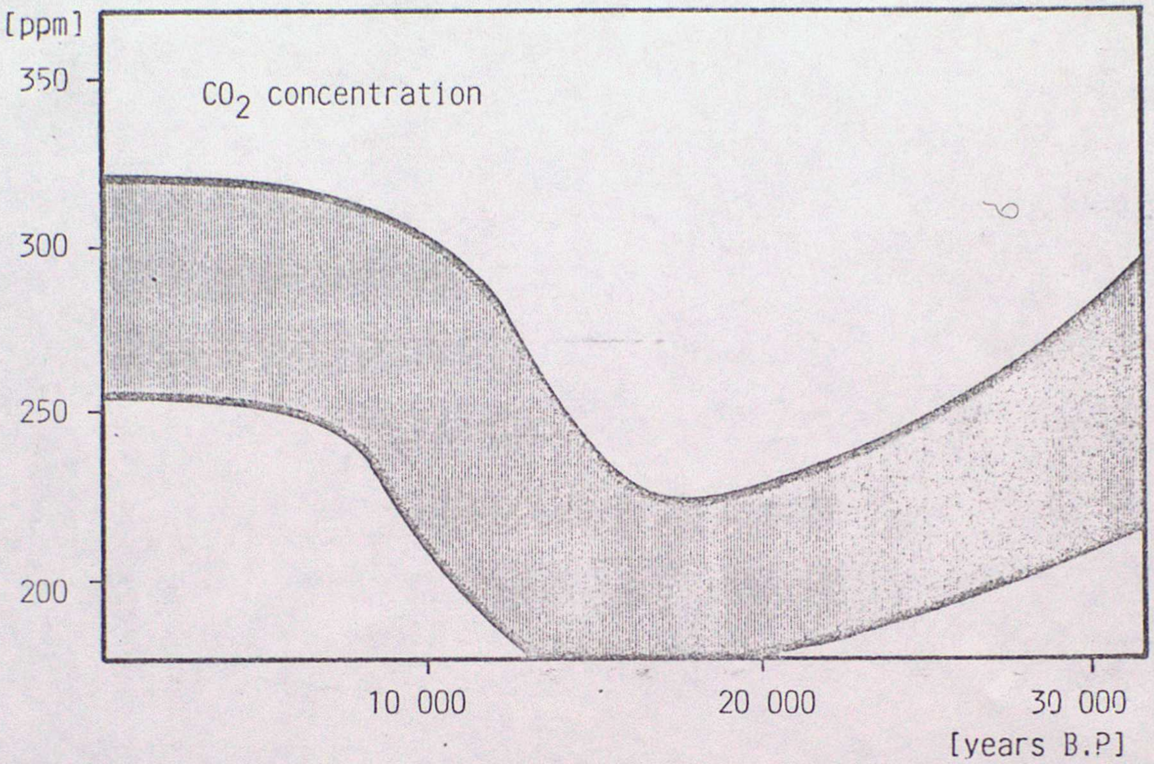

Figure 9.2 Estimated range of atmospheric CO_2 concentrations during the past 40,000 years. From WMO/UNEP/ICSU (1981)

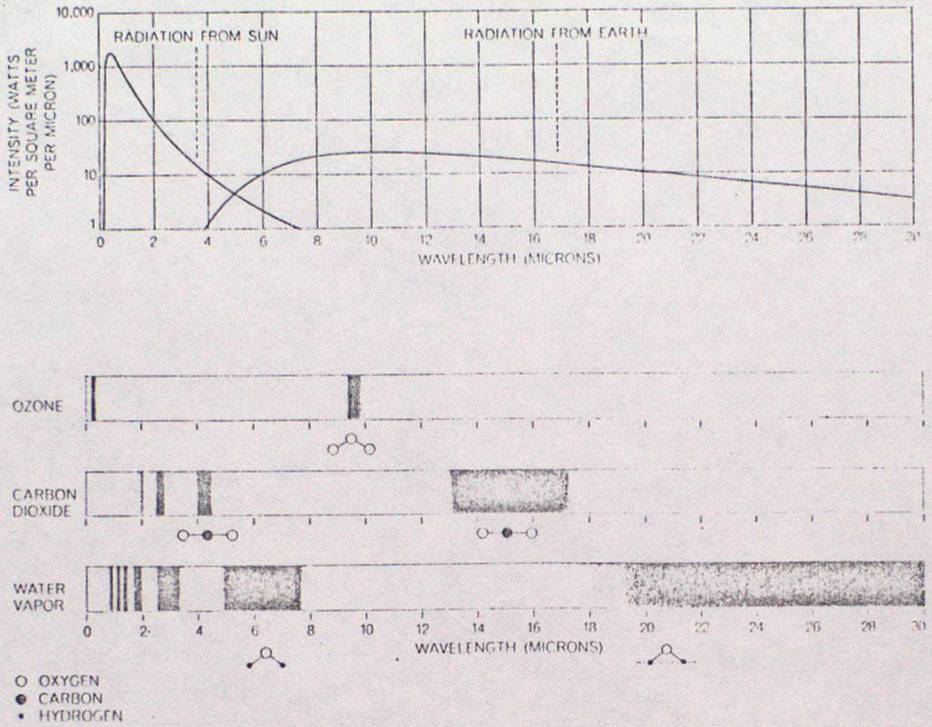

Fig.9.3 Schematic representation of the solar and thermal radiation spectrum and of the absorption lines and bands of ozone, carbon dioxide, and water vapor. (From *Scientific American* 210, no. 3:68.) (After Newell et al (1974))

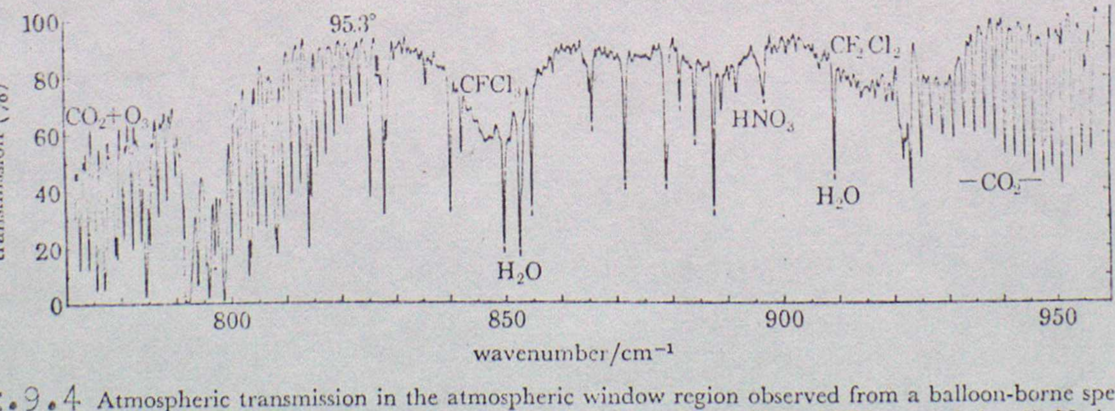

Fig.9.4 Atmospheric transmission in the atmospheric window region observed from a balloon-borne spectrometer from a height of 30 km along a limb path at 95.3° to the zenith by Williams *et al.* (1976). Notice the absorption bands of $CFCl_3$ and CF_2Cl_2. Resolution is 0.2 cm^{-1}. (From Houghton (1979))

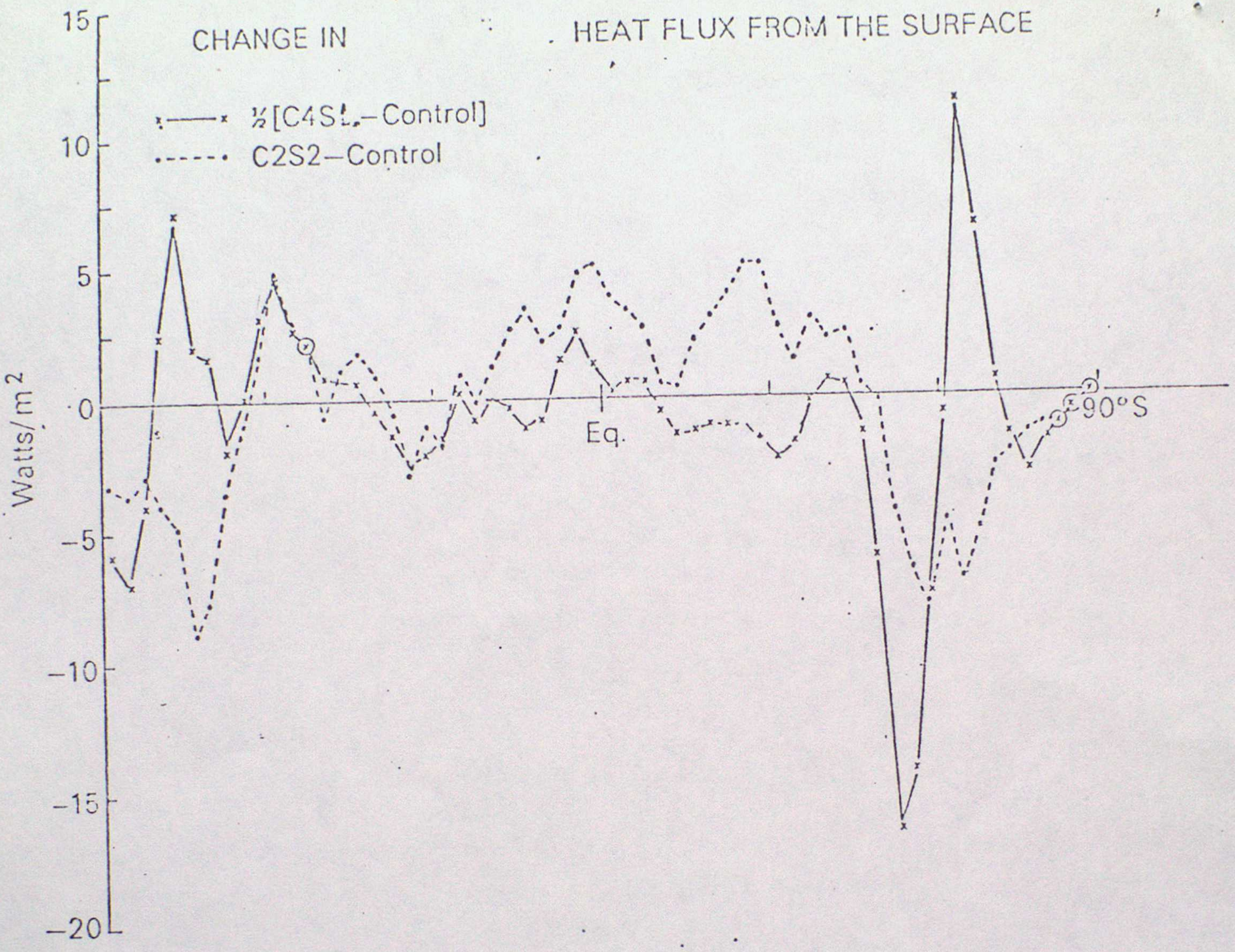

Fig.9.5 (From Mitchell and Lupton (1983))

Changes in Sea Surface Temperature

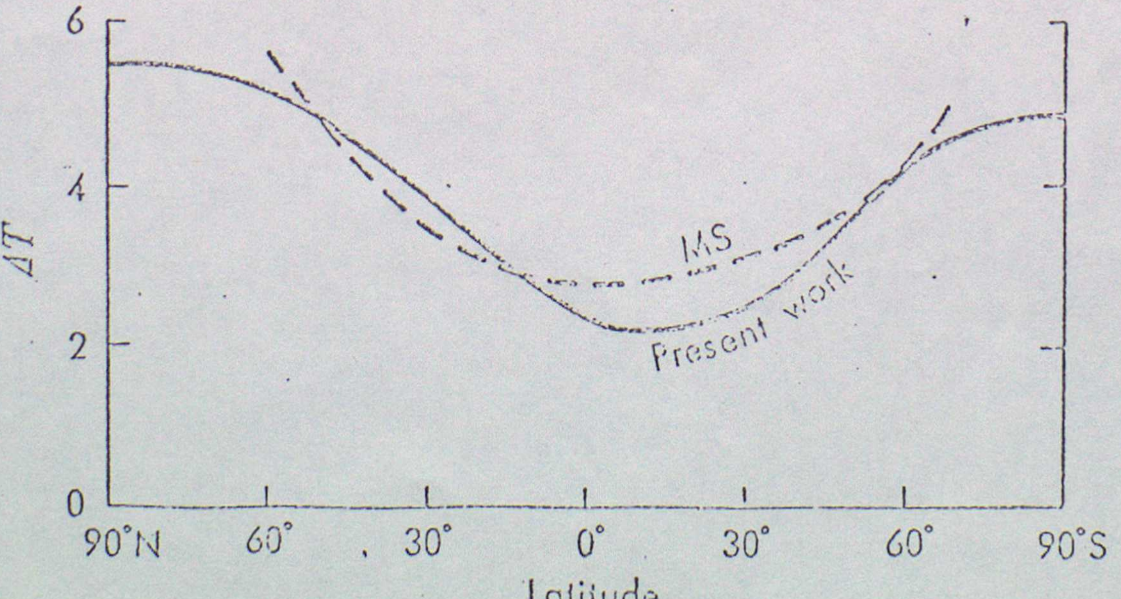

Fig.9.6 (From Mitchell and Lupton (1983))

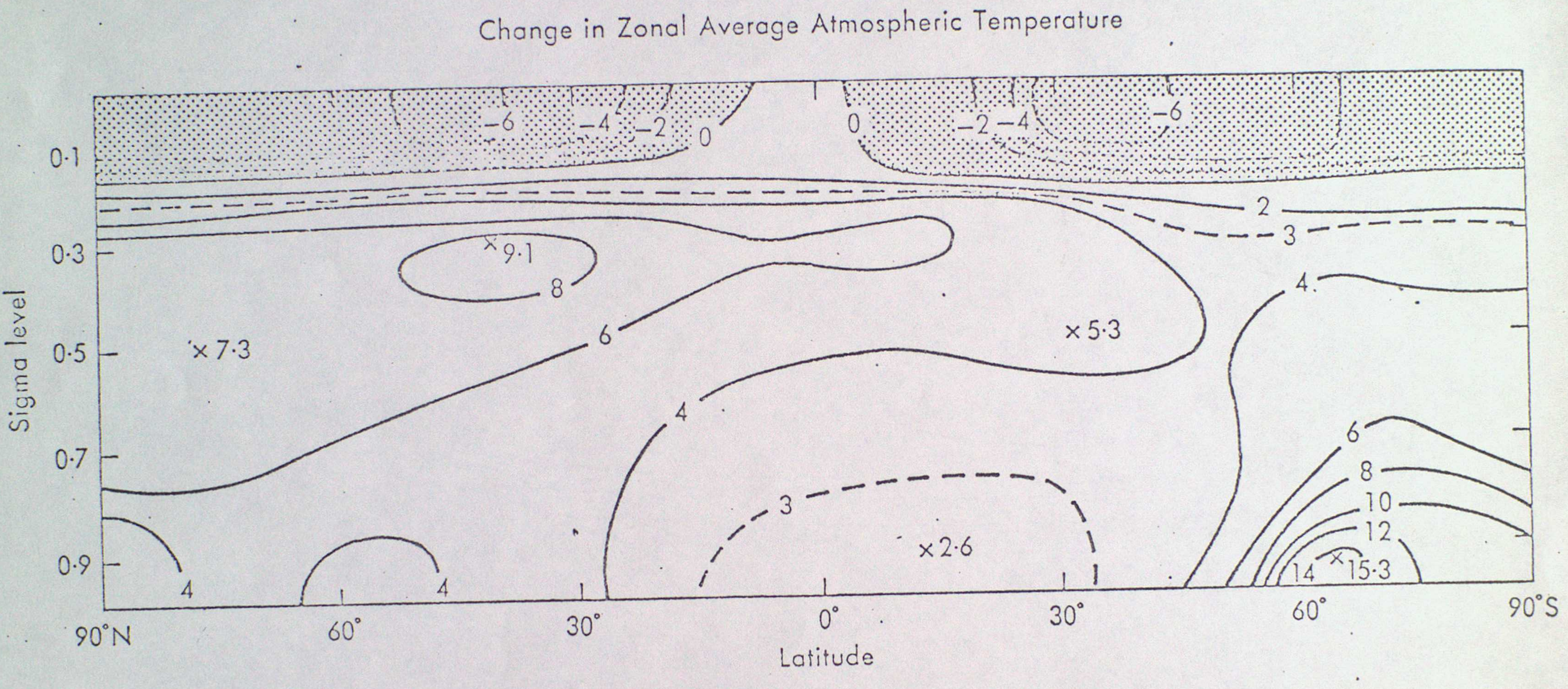

Fig.9.7 (a) June to August (C4SL – Control) (From Mitchell and Lupton(1983))

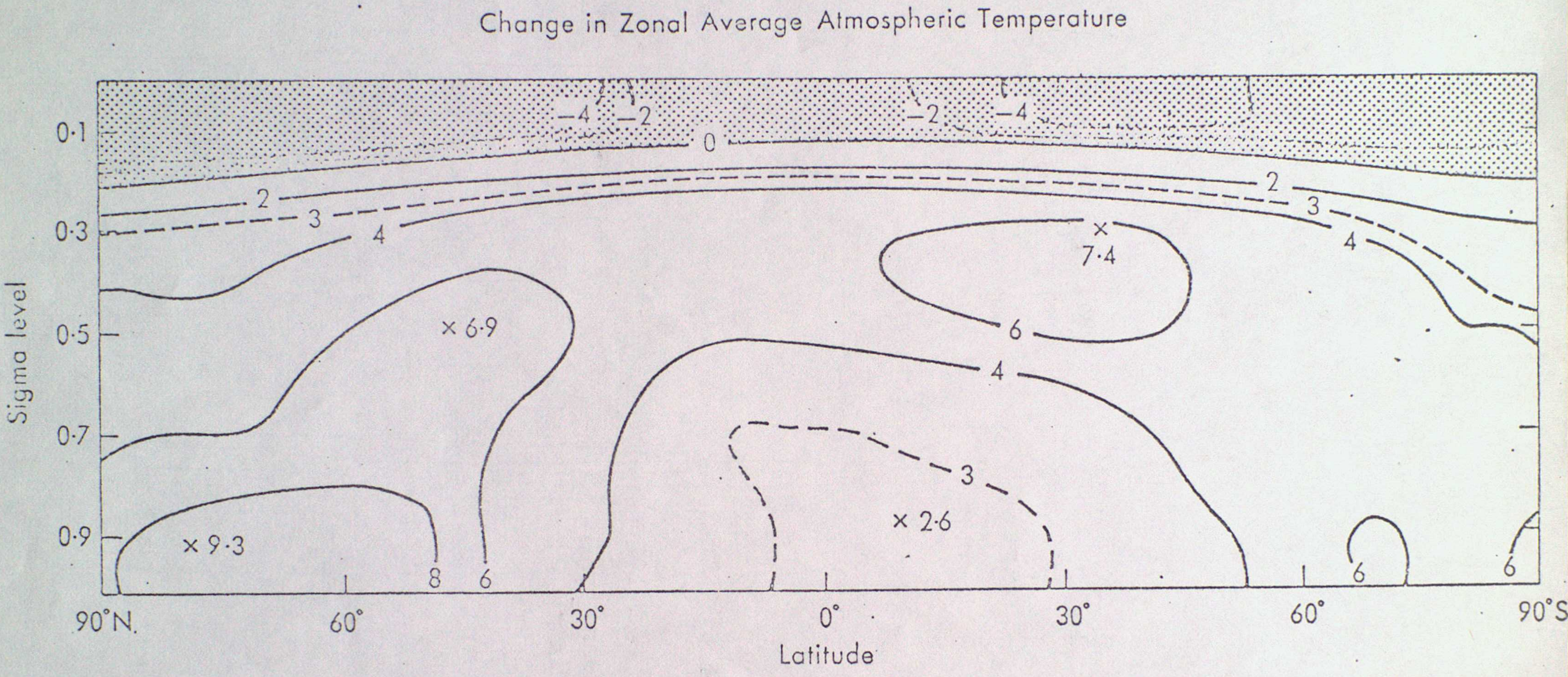

Change in Zonal Average Atmospheric Temperature

Fig.9.7 (b) December to February (C4SL – Control) (From Mitchell and Lupton (1983))

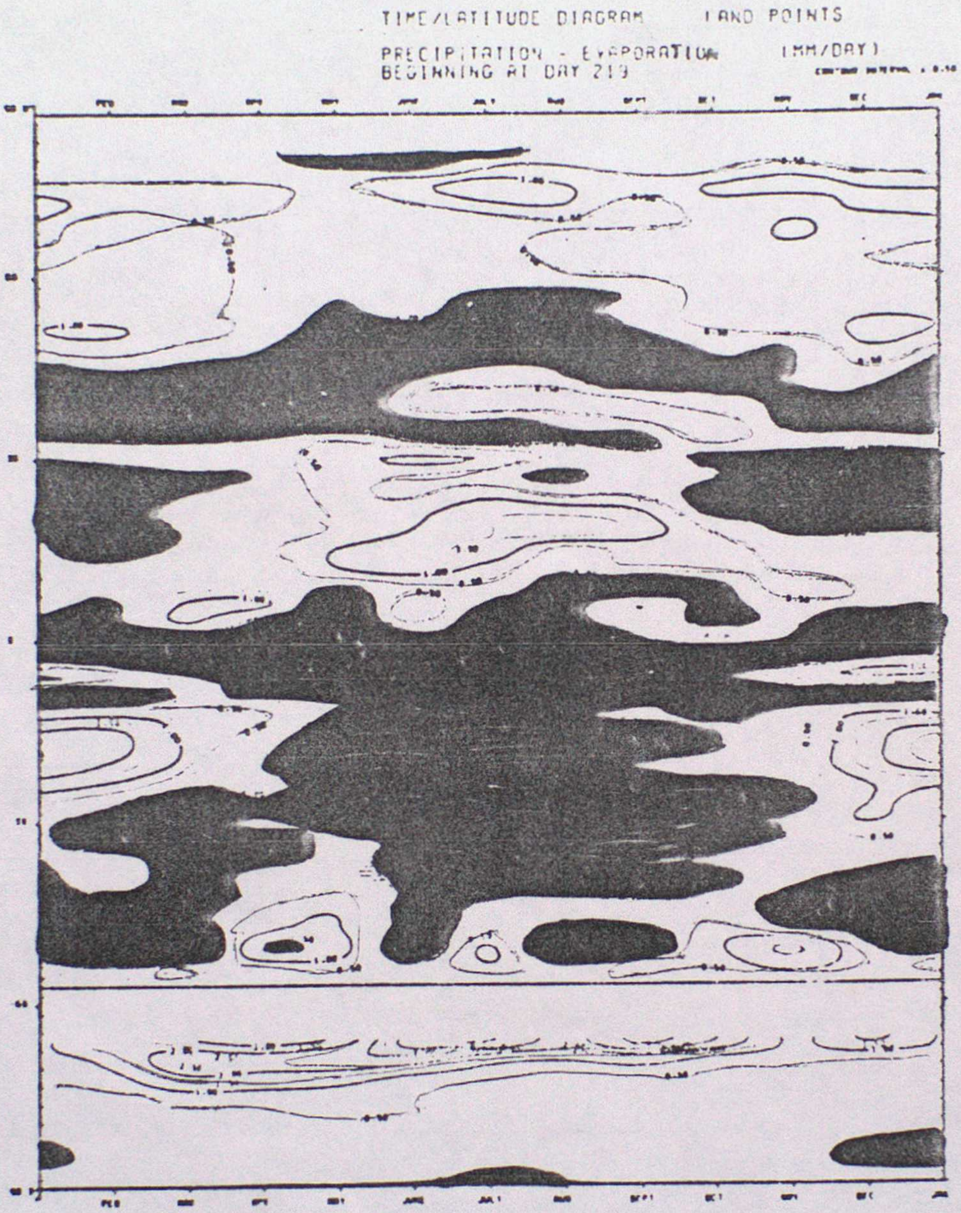

C4SL - Control FIG 9.8

PRECIPITATION MINUS EVAPORATION CHANGES OVER LAND WHEN CO_2 WAS QUADRUPLED. SHADING IS NEGATIVE

(A BETTER DIAGRAM WILL BE PRODUCED IN THE FUTURE)

FIGURE 9.9

ANOMALY FOR YEARS 1856 TO 1981 AVERAGED OVER THE GLOBE

INSTRUMENTAL CORRECTIONS APPLIED GLOBALLY AS IN FOLLAND ET AL NATURE 1984 BUT 0.03,0.04 FOR 1971-5,1976-81 MAT

SOLID LINE IS NIGHT MAT ANOMALY WRT 1951-60 INCLUDING DATA TYPES ABCD

DASHED LINE IS SST ANOMALY WRT 1951-60 INCLUDING MIT DATA:(OPERATIONAL DATA FROM 1982)

VALUES AVERAGED SEASONALLY (JFM ETC) OVER 5 DEG X 5 DEG AREA THEN SPATIALLY

SPATIAL AVERAGING USES COS(LAT) AND PROPORTION OF LAND IN 5 DEG X 5 DEG AREA

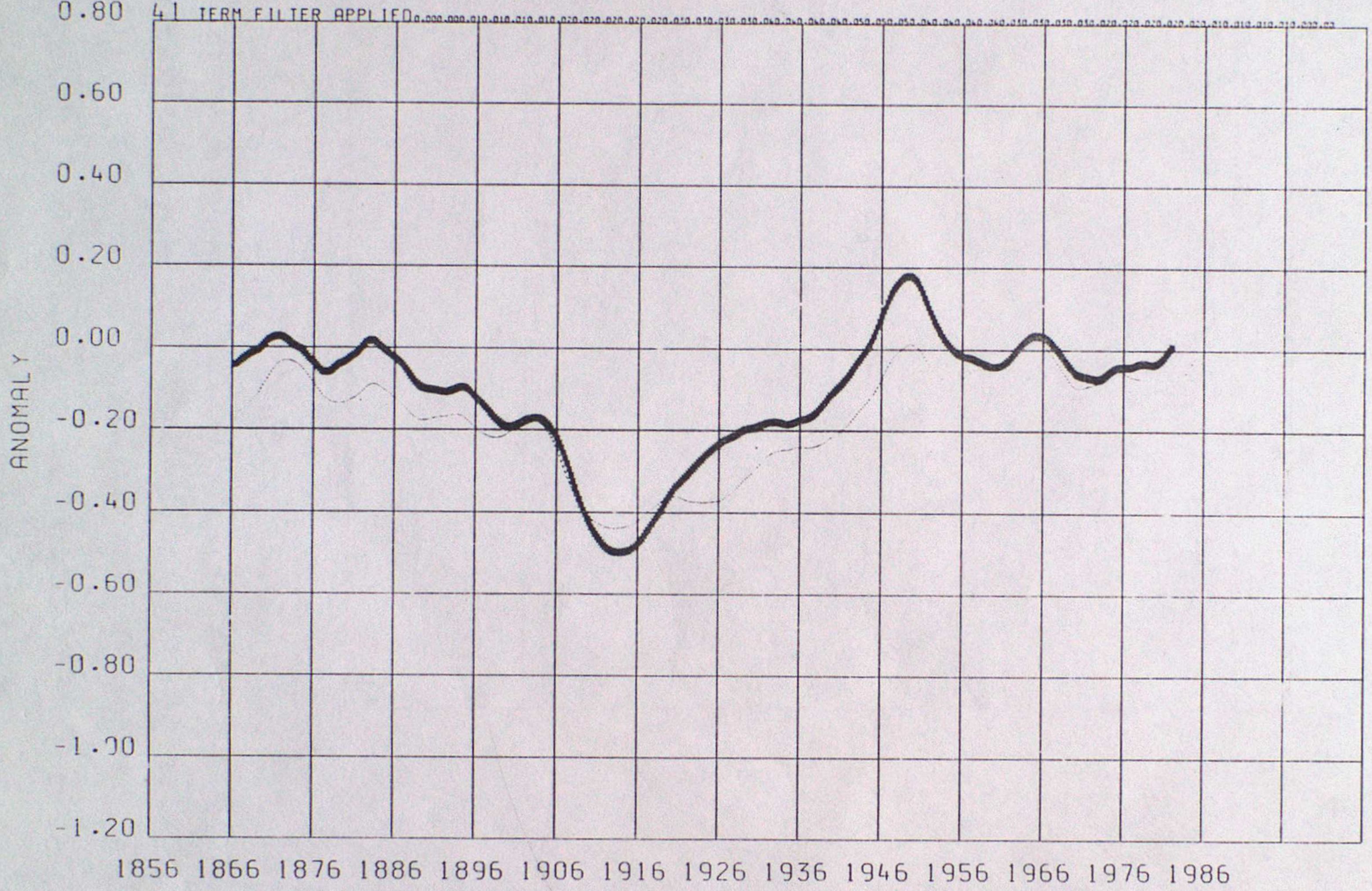

Plotting is at end of filter interval

METEOROLOGICAL OFFICE
145728
- 7 MAY 1985
LIBRARY

APPENDIX I

TO 1985 ADVANCED LECTURES ON CLIMATE OF THE WORLD

Simple Energy - balance Climate Models

by

FOR LOAN to Met Office Staff only

D J Carson

(A lecture presented during 1982 Advanced Lectures on climate of the world)

1. Introduction

An increasing awareness of man's vulnerability to climate variations and a growing belief that his activities may have a significant influence on the climate have led, over the past decade, to the World Climate Conference in 1979 (WMO, 1979) and to the formulation of the World Climate Programme (WMO, 1980), one component of which is the programme for research on climate change and variability, the World Climate Research Programme (WCRP). One of the main elements in the WCRP is the development and evaluation of climate models to be used for the study of climate predictability and climate sensitivity.

There is as yet no comprehensive theory of climate to explain its variability, nor are there, at this juncture physical-dynamical models which can simulate adequately the subtleties and complexities of the full climate system. Indeed there exists an almost continuous spectrum of types of so-called climate model, ranging from simple, one-dimensional, equilibrium representations of the vertical radiative processes in the atmosphere to the full complexity of the three-dimensional, time-dependent, global general circulation models. The latter, in which the effects of large-scale disturbances in the atmosphere are included explicitly, are sometimes referred to as comprehensive models in contrast to the simple models in which many more dynamical and physical processes have to be parametrized. There is of course debate about the advantages and deficiencies of each class of model but at present it is probably fair to claim that each type has a rôle to play in furthering our understanding of the real climate system. It should be obvious, for example, that some of the time scales of interest in climate modelling make it both economically and practically impossible to apply the fully comprehensive models in many studies and so the simpler, usually less realistic, models have to be used.

The Meteorological Office has a major commitment to develop its atmospheric general circulation models to produce, ultimately, a comprehensive, coupled atmosphere - land - ocean - cryosphere climate model. The structure and performance of such general circulation models have been discussed, for example, by Dr A Slingo in the complementary lecture series on The General Circulation of the Atmosphere. The aim of this lecture is not to review the state of the art of simple climate modelling (there exists too large a body of literature!) but rather it is to introduce the reader to the concept of such models and to the assumptions made in the simplest examples. Their application to climate-related problems and the somewhat surprising properties of their solutions will also be discussed.

Before describing the models it is worth introducing some terms which are likely to be encountered, increasingly without being explained, in the literature concerned with the design of climate models and their application to sensitivity and predictability studies.

Predictability of Different Kinds

Consider the two questions:

(1) Is climate predictable in some sense or another and at some time range ?

(2) Are man's activities influencing the climate in any way ?

~~FG2~~
ORGS UKMO

3 8078 0007 8118 9

Different modelling methodologies are required to tackle the two, generally distinct, aspects of climate predictability embodied in these questions. Lorenz (1975) recognised these as questions of predictability of the first and second kind, respectively.

Predictability of the First Kind

This is defined as the prediction of the natural variations of the climate system i.e. it is effectively long-range forecasting using the present state of the climate system as an initial condition.

In principle this includes variations from the synoptic scale limit of predictability of a few weeks up to the epochs of glaciations. The nature of climate predictability of the first kind is not understood anywhere in its range. Indeed, a major open question is whether there are any characteristics of the circulation that retain predictability in the range of several weeks to several years. Even if climate predictability of the first kind is possible in principle it remains to be determined how the problem can be approached. The long-range forecasting for a month to a season ahead, which is being researched in the Synoptic Climatology branch (Met O 13), comes into this category at the short-period end of the range. Because such relatively short periods (in climate terms) of prediction are involved at present in such studies, then fully comprehensive general circulation models can be used.

Predictability of the Second Kind

This is defined as the determination of the response of the climate system to changing external influences which might be prescribed or predicted in terms of other dynamical and physical considerations. Such predictions are not concerned directly with the chronological order of occurrence of atmospheric states, but rather with the long-term average statistical properties of the climate (or model).

Most applications of atmospheric general circulation models to climate problems are necessarily predictability studies of the second kind i.e. the typical set of control and perturbation integrations to determine the sensitivity of a simulated climate to prescribed changes in external forcing. A topical example is the study of the impact on the simulated climate of doubling the amount of CO_2 in the atmosphere (see, for example, Mitchell (1981)). It is still an unresolved question whether predictability of the second kind is a meaningful concept or not.

Transitivity, Intransitivity and Almost Intransitivity

An important issue of climate theory is whether the causes of most climate fluctuations are external to the climate system or internal to it, i.e. have past changes been caused, for example, by fluctuations in solar emissions or changes in the earth's orbital parameters (the so-called Milankovich Theory of climate change), or can these changes be explained to a large extent by the intrinsic internal variability within the system, which needs only an external trigger ? This question has been given a more precise mathematical formulation by Lorenz (1968, 1970, 1975) who introduced the concepts of transitivity, intransitivity and almost intransitivity, taken from ergodic theory.

Transitivity. If the very long-term averaged statistics of a climate system (or climate model) are independent of the initial state, then that climate (or model) is said to be transitive.

Intransitivity. If no unique set of such equilibrium climate statistics exists then the climate (or model) is called intransitive, i.e. there are two or more sets of statistical properties and some initial states lead to one set while others lead to another.

Almost Intransitivity. If the climate system (or model) is transitive for statistics taken over an infinite period and yet contains shorter-period self-fluctuations that might be interpreted as climate changes indicative of an intransitive climate system, then it is called almost intransitive. An almost intransitive system could be mistaken for a truly intransitive one if the statistics over long but finite times were identified as those over an infinite period. For example, the existence of glacial and interglacial periods raises the possibility that the climate system is almost intransitive.

There exists the possibility that for fixed external conditions, very different climate states may be implied by finite-interval time averages owing solely to intransitivity or almost intransitivity. The association of a particular climate with a given external state requires an assumption (as yet unfounded) of transitivity of the climate. With any climate model it is very important to determine the sensitivity of its equilibrium state statistics to variations of internal (e.g. initial) conditions. It will be discussed below that some of the simplest climate models are intransitive and do in fact support two steady state solutions corresponding to glacial and interglacial climates.

2. Radiative-convective Thermal Equilibrium Models (Vertical Column Energy-balance Models)

2.1 Introduction

This class of one-dimensional models computes the annually and horizontally averaged, global, surface and atmospheric temperatures. The temperature profile is determined essentially from a balance between the incoming short-wave (or solar) and the outgoing long-wave (alternatively called terrestrial, infrared or thermal) radiative fluxes, which, in turn, depend upon specified surface properties and vertical distributions and optical properties of clouds, aerosols and of the most important of the optically active gases such as water vapour, carbon dioxide and ozone. A method of convective adjustment is used to ensure that realistic vertical temperature profiles are obtained.

The first radiative-convective models for the earth's atmosphere were developed by Manabe and Strickler (1964) and Manabe and Wetherald (1967). Further variations of the approach have also been developed and are discussed in the comprehensive review by Ramanathan and Coakley (1978). Radiative-convective modelling is a technique commonly employed in studies of stellar and planetary atmospheres.

The paper by Manabe and Wetherald (1967) is to some extent a repeat of the computation of radiative-convective equilibrium of the atmosphere which was discussed in the earlier paper by Manabe and Strickler (1964). The main difference is that Manabe and Wetherald specify a given distribution of relative humidity instead of a given distribution of absolute humidity as used in Manabe and Strickler. The former assumption is thought to be the more realistic. The prime objective in both cases was to formulate and test a method to incorporate radiative transfer into a general circulation model.

Note that with respect to the formulation of the radiative transfer processes in the single column the radiative-convective models are not necessarily simple. Because so much else is parametrized in such a simple way the combination of high vertical resolution and the small demand made on computing resources enables the radiative processes to be modelled in a very detailed fashion. It is not the purpose of this lecture to examine the subtleties and complexities of the actual schemes used by Manabe and his colleagues; for this information the reader is referred to the original papers.

Further objectives of such modelling were:

(1) To determine the influence of various factors such as the solar constant, cloudiness, surface albedo and the various atmospheric absorbers in maintaining the existing thermal structure of the atmosphere.

(2) To determine the rôles of the above factors in maintaining the observed climate at the earth's surface.

2.2 Model assumptions and structure

a. Pure radiative equilibrium

In order to prepare for the study of thermal equilibrium with convective adjustment, calculations were first done for the simple case of purely radiative equilibrium, in which the equilibrium state was approached as an asymptotic steady state of an initial value problem. Equilibrium is considered to have been reached when the temperature change at each level over the time-step used in the model is less than a specified small value.

The following constraints are also satisfied in the equilibrium state:

(1) At the earth's surface, the net upward flux of long-wave radiation is equal to the net downward flux of solar radiation. This guarantees radiative equilibrium at the surface.

(2) At the top of the atmosphere the net upward flux of long-wave radiation is equal to the net downward solar radiation. This guarantees the radiative equilibrium of both the atmosphere and the earth as a whole.

The unrealistic temperature profiles which result when radiation alone is acting have been described by Dr A Slingo in the complementary lecture series on the General Circulation of the Atmosphere and so there is no need to discuss them further here.

b. Radiative-convective equilibrium

The procedure of convective adjustment is to modify the lapse rate to the critical lapse rate whenever that critical lapse rate is exceeded in the course of the integration. The critical lapse rate generally adopted is 6.5 K km^{-1} which was assumed to be a reasonably realistic value for the observed tropospheric lapse rate of temperature. The process of convective adjustment will transfer heat energy from the surface into the atmosphere and thereby permit more realistic temperatures to occur throughout the troposphere.

The requirements for radiative-convective equilibrium are:

(1) At the top of the atmosphere, the net incoming solar radiation should be equal to the net outgoing long-wave radiation.

(2) No temperature discontinuity should exist.

(3) Free and forced convection, and mixing by large-scale eddies, prevent the lapse rate exceeding a critical value of 6.5 K km^{-1}.

(4) Whenever the lapse rate is subcritical, the condition of local radiative equilibrium is satisfied.

(5) The heat capacity of the earth's surface is zero.

(6) The atmosphere maintains the given distribution of relative humidity. (This is a requirement introduced in Manabe and Wetherald (1967)).

Figure 1 gives a simple schematic representation of the iterative procedure used to obtain the state of radiative-convective equilibrium. Both 18 and 9 atmospheric levels were used in the computations such that the pressure thickness of the layer is thin both near the surface and near the top of the atmosphere.

Mathematical Note: r (the humidity mixing ratio) = $\dfrac{0.622\,e}{p-e}$

where e is the water vapour pressure, p is the atmospheric pressure.

h (the relative humidity) = $\dfrac{e}{e_s}$

where e_s is the saturation water vapour pressure.

Therefore, r can be written

$$r = \frac{0.622\,h\,e_s(T)}{p - h\,e_s(T)}$$

where e_s as a function of temperature, T, can be evaluated from the Clausius-Clapeyron relationship,

$$\frac{de_s}{dT} = \frac{0.622\,L\,e_s}{R_d T^2}$$

where L is the latent heat of evaporation and Rd is the specific gas constant for dry air.

c. Details of the radiation scheme

The reader is referred to Manabe and Strickler (1964) for details of:

(1) The computation of the flux of long-wave radiation.

(2) The computation of the depletion of solar radiation.

(3) The determination of mean absorptivity and emissivity.

d. Assumptions made about standard distributions of atmospheric absorbers

The following constituents and their vertical distributions are adopted unless otherwise specified.

Water vapour	The relative humidity is assumed to be a linear function of pressure throughout most of the atmosphere, as illustrated in Figure 2. The line was chosen to fit the data quoted in the Figure legend and a constraint of a minimum value of the humidity mixing ratio of 3×10^{-6} is enforced.
Carbon dioxide	The mixing ratio of carbon dioxide in the atmosphere is assumed constant at 0.0456 % by weight (300 ppm by volume).
Ozone	The adopted vertical distribution of ozone is shown in Figure 3.

The verticaldistributions of gaseous absorbers are those appropriate for 35°N in April. Insolation is assumed to be the annual mean value for the hemisphere.

Clouds The characteristics of the clouds implied in the model are listed in Table 1. The albedo of the earth's surface is assumed to be 0.102.

Cloud	Height (km)	Amount	Albedo
High	10.0	0.228	0.20
Middle	4.1	0.090	0.48
Low: Top	2.7	0.313	0.69
Bottom	1.7		

Table 1. Cloud characteristics used in the radiative-convective equilibrium model of Manabe and Wetherald (1967).

2.3 Some results from radiative-convective equilibrium models

Figure 4, from Manabe and Wetherald, shows the purely radiative equilibrium profile obtained with the assumption of fixed absolute humidity (as used by Manabe and Strickler) and that obtained with the assumption of fixed relative humidity. Note that with fixed relative humidity there is a very sharp decrease with height near the surface and that the temperature of the troposphere is generally much lower than that obtained with fixed absolute humidity. The radiative-convective equilibrium profile for the case with fixed relative humidity is also shown and demonstrates quite clearly the role of convective adjustment in establishing and maintaining the existing distribution of atmospheric temperature (Cf. Figure 6 of Slingo (1982)).

Figure 5, from Manabe and Strickler, shows the approach to pure radiative equilibrium and radiative-convective equilibrium from both initially warm and initially cold isothermal states, respectively. This figure indicates that the final states may be regarded as steady states.

A wide range of experiments has been done to examine the sensitivity of the radiative-convective equilibrium temperature profiles obtained, for example, with different values of the solar constant and the surface albedo and different combinations and vertical distributions of the main atmospheric absorbers such as water vapour, CO_2, O_3 and clouds. Of particular, topical interest are the experiments of Manabe and Wetherald which examined the response of the surface temperature to changes in the atmospheric CO_2 content.

Figure 6, from Manabe and Wetherald, shows the vertical distributions of equilibrium temperature corresponding to three different CO_2 contents, viz. 150, 300 and 600 ppm. Note:

(1) The larger the mixing ratio of CO_2 the warmer is the equilibrium temperature of the earth's surface and troposphere. This results primarily from an enhanced absorption of the surface long-wave radiation by the tropospheric CO_2 but is also partly due to the effective increase in downward radiation emitted by stratospheric CO_2.

(2) The larger the mixing ratio of CO_2, the colder is the equilibrium temperature of the stratosphere. This results from the increase in long-wave radiation emitted to space by CO_2 in the stratosphere.

(3) Relatively speaking, the dependence of the equilibrium temperature of the stratosphere on CO_2 content is much larger than that of the tropospheric temperature.

Tables 2 and 3 show the equilibrium temperature of the earth's surface corresponding to different CO_2 contents and also the change of the equilibrium surface temperature corresponding to the specified changes in CO_2. Values for both fixed absolute humidity and fixed relative humidity cases are given. Note that the equilibrium temperature of the latter is almost twice as sensitive to the change in CO_2 as that of the former due to the adjustment of water vapour content to the temperature variation of the atmosphere. The changes resulting from doubling the CO_2 content are in reasonable agreement with those obtained in subsequent experiments with general circulation models. Table 4, from Mitchell (1981), gives a comparison of estimates of the change in global mean surface temperature obtained for specified changes in the CO_2 content from single-column, radiative-convective equilibrium models (including the results of Manabe and Wetherald (1967)) with the changes obtained from corresponding general circulation model integrations.

	Average cloudiness		Clear	
CO_2 content (ppm)	Fixed absolute humidity	Fixed relative humidity	Fixed absolute humidity	Fixed relative humidity
150	289.80	286.11	298.75	304.40
300	291.05	288.39	300.05	307.20
600	292.38	290.75	301.41	310.12

Table 2. Equilibrium temperature of the earth's surface (K) for different values of the CO_2 content of the atmosphere, from Manabe and Wetherald (1967).

Change of CO_2 content (ppm)	Fixed absolute humidity		Fixed relative humidity	
	Average cloudiness	Clear	Average cloudiness	Clear
300 ⟶ 150	-1.25	-1.30	-2.28	-2.80
300 ⟶ 600	+1.33	+1.36	+2.36	+2.92

Table 3. Change of equilibrium temperature of the earth's surface corresponding to various changes of CO_2 content of the atmosphere, from Manabe and Wetherald (1967).

2.4 Limitations of the radiative-convective equilibrium models

(1) The most important limitation is that results from these models are mostly of academic interest, since they do not give any information about regional and latitudinal temperature changes.

(2) Many of the model parameters (cloud amounts, surface albedo, relative humidity, critical lapse rates, etc) are prescribed on the basis of present day conditions which may not apply for large departures from present day conditions. Radiative-convective models cannot be applied for large perturbations from present conditions.

(3) The model results depend very critically on the details of the parametrizations. Also like many other models, particularly the simpler models, these models are probably too deterministic.

It is of course very important that the limitations of all the models, especially the simpler, cruder models, be borne in mind when their results are being interpreted.

3. Horizontally Varying Energy-balance Models

3.1 Introduction

In contrast to the radiative-convective equilibrium models of the previous section, this class of one-dimensional, energy-balance models treats the vertical structure with much less detail than the horizontal structure. There exist many types of model of varying degrees of complexity within this class but here we shall concentrate on those which presume to compute the zonally-averaged surface temperature as a function of latitude only, obtained effectively as a balance between incoming solar and outgoing terrestrial radiation. Budyko (1969) and Sellers (1969) are generally acknowledged as having proposed independently the first such models and it is now common practice to refer to the class of derivatives and extensions of their approaches as Budyko - Sellers type models.

Table 4. Estimates of global mean changes in temperature and precipitation due to increasing atmospheric carbon dioxide.

Source	3-dimensional model							
	Topography	Solar Radiation	Cloud	Ocean	CO_2	PPTN	T*	1-D model T*
Manabe and Wetherald, 1975	Idealized	Annual mean	Fixed	Swamp	2	7%	2.93	2.36 †
Manabe and Wetherald, 1980	Idealized	Annual mean	Model Dependent	Swamp	2	7%	3.0	2.0
					4	12%	5.9	4.1
Manabe and Stouffer, 1980	Realistic	Seasonal	Fixed	Fixed depth	4	6.7%	4.1	
Present work								
(a) 2 x CO_2 + 2K	Realistic	Seasonal	Fixed	Present day + 2K	2	5%	2.25	
(b) Estimate assuming no change in global mean net surface heat balance				Present day + 1.65K	2	3.5%	1.9	1.7

† Manabe and Wetherald(1967)

This table is taken from Mitchell (1981).

There is incontrovertible evidence of the existence of large fluctuations in past climate. There is also debate that the impact of man's activities may possibly initiate a significant response in the climate system. Therefore there is concern about and interest in the question of the stability of the global climate to small perturbations of any sort. This led Budyko (1969) and Sellers (1969) to develop their simple models of the earth's climate, based on the mean annual balance of heat entering and leaving latitudinal strips of the earth-atmosphere system, for the purpose of testing the sensitivity of the equilibrium state of the climate to changes in the solar radiative heating.

Schematically, the heat balance for the i-th strip in equilibrium may be written:

$$\begin{Bmatrix}\text{Absorbed solar}\\ \text{radiation}\end{Bmatrix}_i - \begin{Bmatrix}\text{Outgoing infrared}\\ \text{radiation}\end{Bmatrix}_i = \begin{Bmatrix}\text{Horizontal divergence of}\\ \text{thermal energy flux}\end{Bmatrix}_i$$

Each of the above terms is parametrized by some theoretical or semi-empirical formula, usually in terms of the sea-level temperature field. All of the equations are then solved simultaneously to give the surface temperature field. Note that the balance equation assumes that there is no heat or moisture storage in the oceans, land or atmosphere and hence no long-term climatic trend. There is also the gross assumption that the character of the climate of the whole column of the earth-atmosphere system is embodied in a single variable, the surface temperature. Although the various particular studies differ in the exact details of their parametrizations of the above components of the balance it is generally believed that they are at least qualitatively equivalent.

Although these models are highly simplified their solutions to particular problems have a rather complicated structure. Indeed it will be shown that a multiplicity of solutions is obtained for the present value of the solar constant. The interesting and, arguably, unexpected character of such solutions, their mathematical stability properties and the consequent implications for our appreciation of climate are the main reasons why an increasingly large amount of study has been devoted to this class of simple climate model since the appearance of the papers by Budyko (1969) and Sellers (1969).

3.2 The model of Budyko (1969)

In the first instance let us consider the model and results of Budyko (1969). The simplified, integrated thermodynamic energy equation for the whole earth-atmosphere system is represented in terms of annually and zonally averaged variables and equations, thus

$$R + \mathrm{div}\,\underset{\sim}{F} = 0 \tag{1}$$

where R is the net radiation for a column of the earth-atmosphere system at a given latitude and $\mathrm{div}\,\underset{\sim}{F}$ represents the net gain or loss of heat, i.e. it represents the divergence of the net energy flux, as a result of the atmospheric and hydrospheric circulations for that latitude

The net radiation is expressed as

$$R = Q\,(1-\alpha) - I \tag{2}$$

where Q is the annual mean solar radiation at the outer boundary of the atmosphere, α is the planetary albedo (or reflectivity) and I is the net terrestrial radiation to space, all for a given latitude.

An analysis of radiation and temperature data led Budyko to propose and use the empirical formula

$$I = a + BT_0 - (a_1 + B_1 T_0)\, n \qquad (3)$$

where I is the outgoing radiation in kcal cm^{-2} month^{-1},
T_0 is the temperature at the earth's surface in $^{\circ}$C,
n is the cloudiness in fractions of unit, and
a, B, a_1, B_1 are dimensional coefficients with values
$a = 14.0$, $B = 0.14$, $a_1 = 3.0$ and $B_1 = 0.10$.

For the earth as a whole (i.e. with div $\underset{\sim}{F} \equiv 0$) Budyko found that with $n = 0.50$ and constant $\alpha = 0.33$, a change of solar radiation by 1% results in a temperature change of 1.5K. He cites a corresponding estimate from Manabe and Wetherald (1967) as giving a 1.2K change in surface temperature as a result of a solar radiation change of 1%. Budyko argues that the long time-scales involved in any climate response resulting from radiation variations require that changes in the earth's albedo should be taken into account which are due to the expansion or reduction of the ice-cover at the surface. The parametric coupling that results between α and T_0 provides a strong positive feedback between ice-cover and temperature and we shall see later that it is this empiricism which is responsible for many of the surprising results.

The flux divergence term in Equation (1) is also specified empirically. Budyko derived a relationship which enabled him to represent this term quite simply in terms of the difference between the local zonal mean and the planetary mean temperature, thus

$$\operatorname{div} \underset{\sim}{F} = -\beta\,(T_0 - T_p). \qquad (4)$$

where T_p is the globally averaged, annual mean surface temperature and β is an empirically derived coefficient equal to 0.235 kcal cm^{-2} month^{-1} K^{-1}.

From (1) - (4) we obtain the following equations:

$$T_0 = \frac{Q(1-\alpha) - a + a_1 n + \beta T_p}{\beta + B - B_1 n} \qquad (5)$$

$$T_p = \frac{Q_p(1-\alpha_p) - a + a_1 n}{B - B_1 n} \qquad (6)$$

where Q_p, α_p are the corresponding planetary values of incident radiation and albedo, respectively. Budyko used these to derive the average latitudinal annual mean temperatures corresponding to present climatic conditions for the Northern Hemisphere. Q and Q_p were computed corresponding to a solar constant of 1.92 cal cm^{-2} min^{-1}. In the calculation, the influence on the temperatures of deviations of cloudiness values from the mean planetary value of 0.50 is neglected.

Based on observational data Budyko chose the following specification of albedo:

$$\alpha = \begin{cases} 0.32 & 0 \leq \varphi \leq 60^\circ \quad (\varphi \text{ is latitude}) \\ 0.50 & \varphi = 70^\circ \\ 0.62 & \varphi = 80^\circ \end{cases}$$

Budyko's calculation of contemporary average latitudinal distribution of temperature is shown in Figure 7. The computed values of T_0 are in good agreement with the observed values, T, and this encouraged Budyko to use his model to study the effects of variations in the radiation on the Earth's thermal regime and glaciations.

Budyko asserts that the southern boundary of the Arctic ice corresponds to a mean latitude of 72°N and adopts an ice-albedo-temperature coupling such that the ice-cap expands or contracts to coincide with the surface whose temperature is less than or equal to the temperature observed now at 72°N i.e. about -10°C. The -10°C isotherm therefore determines the extent of the ice-covered area which is given an albedo of 0.62 with a discontinuity and drop to 0.50 at its southern boundary. Budyko then computed the zonal mean temperatures and hence the position of the edge of the ice-sheet for effectively different values of the solar constant. The results are shown in Figure 8 where the lines $T_{1.0}$ and $T_{1.5}$ correspond to the temperature distributions for a 1% and a 1.5% decrease in the incoming solar radiation. It is assumed that the relative decrease in radiation is the same at all latitudes. Figure 9 shows the values obtained for the mean planetary temperature, $\overline{T_p}$ and the mean latitude to which glaciation extends, φ_0, as a function of the relative radiation changes.

The most striking feature of Figure 9 is the implication that only a small per cent (about 1.6%) drop in the solar constant is required for the earth to ice over completely. When radiation decreases by 1.6% the ice-cover reaches the mean latitude of about 50°N after which it starts shifting towards lower latitudes up to the equator as a result of self-development. Simultaneously, $\overline{T_p}$ drops sharply to values several tens of degrees below zero.

3.3 The model of Sellers (1969)

Sellers' starting point is also the integrated energy-balance equation for the earth-atmosphere system for a given latitude belt. His dependent variable is the average annual sea-level temperature, T_s, in each 10° latitude belt. Again, as in Budyko (1969), several empirical and relatively crude relationships are involved in the model. Using the same definitions and notation as was used above for Budyko's model, the components of Sellers' model can be expressed as follows:

Net terrestrial radiation to space:

$$I = \sigma T_s^4 \left[1 - m \tanh\left(19 T_s^6 \times 10^{-16}\right)\right] \tag{7}$$

where σ is the Stefan-Boltzmann constant $(1.356 \times 10^{-12}\ ly\ s^{-1}\ K^{-4})$, and m is an atmospheric attenuation coeffient, taken to be 0.5 for present conditions. Equation (7) is based on an empirical fit to data.

Albedo:

$$\alpha = \begin{cases} b - 0.009 T_0 & T_0 < 283.16K \quad (8a) \\ \alpha_d = b - 2.548 & T_0 \geqslant 283.16K \quad (8b) \end{cases}$$

with the constraint that $0.25 \leq \alpha \leq 0.85$ for all T_0 ,

where $T_0 = T_s - 0.0065Z$ is the average surface temperature, Z is the average surface elevation in metres, and b is an empirical coefficient. Values of Z and b are tabulated by Sellers for each latitude belt of 10° latitudinal span.

As in Budyko's model, it is assumed that variations in α are associated mainly with variations in surface snow cover and Equation (8a) is valid only as long as $T_0 < 10^\circ$C and $\alpha < 0.85$. The planetary albedo α_d of (8b) is used for higher temperatures i.e. in the absence of snow or ice cover. Equation (8a) implies an increase in α by 0.009 for every 1K drop in T_0 . The coefficient b was selected so that the equation would fit observed data. The effects of variations in cloud cover on albedo were ignored.

The flux-divergence term:

Sellers identifies three separate components making up the total net flux of heat out of the belt at a given latitude. They are due to, respectively, the net fluxes of water vapour and sensible heat by the atmospheric circulation and sensible heat by ocean currents.

Let F_o be the meridional sensible heat transport due to ocean currents,
F_A the corresponding sensible heat transport due to atmospheric motion,
and F_q the meridional transport of latent heat energy (q is specific humidity),

then Sellers adopts a parametrization which relates these fluxes to the horizontal mixing by large-scale eddies and to a vertically integrated mean meridional wind $\langle v \rangle$ which, in turn, is parametrized as an empirically determined function of the North-South temperature gradient, thus

$$F_o \propto -K_o \frac{\partial T_s}{\partial y} \qquad (9a)$$

$$F_A \propto -K_A \frac{\partial T_s}{\partial y} + \langle v \rangle T_s \qquad (9b)$$

$$F_q \propto -K_q \frac{\partial q(T_s)}{\partial y} + \langle v \rangle q(T_s) \qquad (9c)$$

where K_o, K_A and K_q are effective eddy diffusion coefficients.

An implicit important assumption here is that average atmospheric temperatures and specific humidities and ocean temperatures are proportional to their respective sea-level values. Further the actual specific humidity is replaced by the saturation specific humidity which enables it to be related to the temperature through the Clausius-Clapeyron relationship (see, for reference, the Mathematical Note of Section 2.2b). The poleward transport of water vapour and sensible heat (equations (9b) and (9c)) are assumed to consist of two parts, one associated with a mean meridional motion and the other with large-scale eddies or cyclones and anticyclones. The inclusion of the mean meridional motion is necessary in order to avoid having to deal with negative diffusivities. Values of the K's are tabulated by Sellers at 10° intervals for each latitude circle.

Sellers' system of equations leads to a second-order equation, effectively in T_0 , with only one of the roots giving realistic temperatures. The model was first used to reconstruct the present state of the earth-atmosphere system. The reader is referred to Sellers (1969) to verify that the model specifies present conditions very well. Sellers then applied his model to several different problems, two of which are considered here.

a. Modification of the polar ice caps

A number of different combinations fo albedo were used, with α at one or both poles (70 - 90°) being set equal to and held fixed at either 0.50 or 0.40 (with the exception of 70 - 80°S where a minimum value of 0.44 was imposed). The results, shown in Figure 10, have a number of interesting features, viz,

(1) Cases 1 and 2. Removal of north polar ice results in an increase in temperature poleward of 70°N by at most about 7K. Temperature would rise by about 1K in the tropics and 1-3K near the South Pole.

(2) Cases 3 and 4. Removal of antarctic ice produces a temperature increase there of 12-15K with a rise in the Arctic of about 4K.

(3) Cases 5 and 6. Removal of both polar ice-caps yields temperature increases of 7-10K in the Arctic and 13-17K in the Antarctic. Tropical warming does not exceed 2K.

Therefore albedo changes at either pole have global repercussions. An interesting result, comparing the curves for Cases 1 and 3, is that reducing the albedo south of 70°S to 0.50 would, according to this model, produce a larger temperature rise in the Arctic than would a reduction of the albedo north of 70°N to 0.50. The greater effects of changes to the albedo in the Antarctic than in the Arctic are simply the result of the Antarctic's higher initial albedo. Others have argued that the extent of sea-ice in the Southern Hemisphere has a much more significant effect on the global circulation than the extent of sea-ice in the Northern Hemisphere.

b. Variations in the solar constant

Sellers examined the sensitivity of his models to variations in the solar constant and his calculations corroborate, qualitatively at least, the implications from Budyko's model that a slight reduction in the solar constant (or, for example, increase in global dust contamination) would be sufficient to initiate another ice age. In Figure 11 the global mean sea-level temperature, T_{sp} , is plotted as a function of the solar constant, S , currently assumed to be 2.00 ly min^{-1} (cf. Budyko used 1.92 ly min^{-1} as the current value !) The present value of T_{sp} is about 14.0°C. Three analyses were carried out, two with α allowed to vary according to $\alpha = b - 0.009\,T_0$ and $\alpha = b - 0.005\,T_0$, respectively, and the other with α held fixed at its assumed current values. There are no very dramatic events when α is kept fixed at the present values and S allowed to vary. However with a realistic albedo-temperature coupling a decrease of about 2% in the solar constant is sufficient to create another ice-age with ice-caps extending equatorward to 50° (i.e. where $T_0 = -10°$C). Any further drop in the solar constant is accompanied in the model by a rapid transition to an ice-covered earth with albedo of 0.85 (cf. Equation (8a)) and an equilibrium temperature of -100°C. With the weaker dependence of α on surface temperature and ice-cover (i.e. 0.005 used in place of 0.009 and b adjusted accordingly) a severe ice-age would not occur until the solar constant decreased by about 5 - 6%.

Sellers also reports a few sensitivity studies where he has kept the solar constant fixed but has increased or decreased the effective diffusion coefficients in his model. He concludes that a relatively small change in the ability of the system to transfer heat poleward could conceivably offset any increase or decrease in the intensity of solar radiation. Hence the obvious caution about allowing only one variable to change without being able to allow for consequent changes in the others. Nevertheless Sellers' model implies quite conclusively that a decrease in the solar constant of less than 5% would be sufficient to start another ice-age.

3.4 The sensitivity of time-dependent Budyko-Sellers type models

Schneider and Gal-Chen (1973) examined the sensitivity of time-dependent models of the Budyko-Sellers type to changes in initial as well as external conditions. The problem is then formulated as an initial value problem in which the basic equations are integrated from a given initial state until a final asymptotic equilibrium state is obtained.

The time-dependent version of the zonally averaged, vertically integrated heat balance equation for the earth-atmosphere system is

$$C \frac{\partial T_0}{\partial t} = R + \mathrm{div}\, \underset{\sim}{F} \tag{10}$$

where C is a prescribed thermal inertia coefficient for a zonal column through the land-ocean-atmosphere system. R is defined as in Equation (2) with I the net infra-red cooling to space given by

$$I = c(\varphi)\, \sigma T_0^4 \left[1 - m \tanh\left(19 T_0^6 \times 10^{-16}\right)\right] \tag{11}$$

with $m = 0.5$. Note that with $c(\varphi) = 1$ (and ignoring the distinction between T_0 and T_s) this formula is identical to that used by Sellers (1969). Scheider and Gal-Chen claim to be using the zonally averaged 1000-mb temperature which has been written here as T_0, the notation used previously for the surface temperature. Their numerical scheme requires that the 'consistency factor' $c(\varphi)$ be adjustable over a small range of values close to unity.

Schneider and Gal-Chen examined four different versions of the model, defined by different formulations of $\mathrm{div}\, \underset{\sim}{F}$ and α.

(1) Labelled (S), is the formulation of Sellers (1969) with respect to $\mathrm{div}\, \underset{\sim}{F}$ and α.

(2) Labelled (SV), is exactly as (S) but with $\langle v \rangle \equiv 0$.

(3) Labelled (B), uses α as defined in (S) but has the Budyko (1969) formulation for $\mathrm{div}\, \underset{\sim}{F}$ as in Equation (4).

(4) Labelled (FG), is as (S) with respect to $\mathrm{div}\, \underset{\sim}{F}$ but uses a formulation for α attributed to Faegre (1972) such that

$$\alpha = 0.4860 - 0.0092\,(T_0 - 273)$$

$$0.25 \leq \alpha \leq 0.85 \quad \text{for all values of } T_0$$

ie. α is a function of temperature everywhere.

The asymptotic equilibrium climate from the time-dependent version was shown to exhibit the same sensitivity to small changes in the solar constant as experienced with the steady-state models. Figure 12 shows the results of Schneider and Gal-Chen for their version (S) of the Sellers (1969) approach. Again with a decrease in solar constant of more than 1.6% a planetary mean temperature of 174.65K was obtained corresponding to an entirely ice-covered earth. Calculations for a 1% decrease in solar constant and Sellers-type energy fluxes with, (S), or without, (SV), mean meridional motion gave quite similar results both in the global average amount of temperature decrease and in the latitudinal distribution of the temperature decrease. The results for the Budyko parametrization, (B), are qualitatively similar to those of (S) and (SV) for the global average. However the corresponding latitudinal distribution of temperature decrease differs significantly from that of Sellers. The particular form used for $\mathrm{div}\,\underset{\sim}{F}$ does appear to be significant for determining the details of the latitudinal distribution of temperature.

The stability of the (B) and (S) solutions to various perturbations of the initial temperatures were examined and the results are summarised in Table 5. It was found in both cases that the respective steady-state control climates could be recovered exactly if the temperature perturbation was positive. Perturbations of 2K and 16K were tried and in both energy-balance requirements alone produced a return to the control climate ie. the control climates appear to be unique, fully stable and transitive. For an initial temperature decrease of magnitude not exceeding 18.3K the apparent slight intransitivity in the equilibrium climates has been attributed to computer rounding errors. The models then show that the asymptotic equilibrium climate is extremely insensitive to changes in the initial conditions. However for initial temperature decreases greater than about -18.3K both models lead to an ice-covered earth solution similar to curve D in Figure 12. Thus it takes a very large negative perturbation to the initial temperatures to lead to the highly intransitive alternative ice-covered earth regime of these models. The insensitivity of the model to decreases in the initial temperature conditions of less than 18K follows from an unchanged albedo in equatorial latitudes.

Initial Temperature Perturbation (K)	Mean Planetary Temperature (K)	
	Sellers (S)	Budyko (B)
0	287.06	287.09
$0 < P < 16$ for all φ	287.06	287.09
$-18.3 < P \leq 0$ for all φ	286.67	286.87
$P < -18.3$ for all φ	175.58	175.44
$\left.\begin{array}{l} -22 \text{ for } \lvert\varphi\rvert \geq 20^\circ \\ 0 \text{ for } \lvert\varphi\rvert < 20^\circ \end{array}\right\}$	286.67	286.87

Table 5. Asymptotic steady-state global average temperatures resulting from various perturbations to the initial temperature distributions for two of Schneider and Gal-Chen's (1973) parametrizations. This table is taken from the review of climate modelling by Schneider and Dickinson (1974).

The implication from these experiments is that even when ice-cover exists down to temperate latitudes but if the solar constant and the tropical albedos are unaltered then there is still sufficient energy available to the tropics to provide a poleward heat transport to melt the ice and restore the equilibrium climate to near the present-day value. If the equatorial temperature is reduced into the range of the positive feedback temperature-albedo coupling then climate instability is triggered, and an ice-covered earth results. This hypothesis was tested (see Table 5) by introducing a very large negative perturbation in the initial temperatures, viz. -22K, for all $|\varphi| \geqslant 20^\circ$ only. In both models there was a return to near the present-day climate.

The model, (FG), which adopts Faegre's (1972) formulation for α is very sensitive to negative perturbations in both solar constant and initial conditions. The interpretation is that with the temperature-albedo coupling for all temperatures and at all latitudes then a slight negative perturbation in either initial temperature or solar constant can cause a decrease in energy input to the tropics thereby enhancing the albedo-temperature positive feedback at all latitudes. Experiments with such energy-balance models suggest that the stability of the climate may be quite dependent on the functional relationship between the albedo and the surface temperature.

3.5 Multiple solutions and their stability

We have seen from the numerical perturbation studies of Schneider and Gal-Chen (1973) that more than one solution is admissable in the Budyko-Sellers models with the present value of the solar constant ie. the system appears to be intransitive. North (1975) studied the latitude of the ice-line as a function of the solar constant by using a model, described as intermediate between that of Budyko and that of Sellers, which yielded exact analytical solutions. His results, summarised in Figure 13, show a multiplicity of solutions for the present-day value of the solar constant; indeed, there are no less than five solutions for the present value of the solar constant! Other studies with models of this type, but with different formulations for the individual terms, give results qualitatively similar to these. Lowering the solar constant by a few per cent leads to a catastrophic plunge to an ice-covered planet but more than a 30% increase is needed to yield an ice-free earth as the only solution.

North (1975) performed a linear stability analysis about the equilibrium solutions on branches I, II and III and confirmed that the present climate (I) and the ice-covered earth (III) solutions are stable (shown numerically by Schneider and Gal-Chen (1973)) while the intermediate solution (II) with the earth about two-thirds covered with ice is unstable and therefore of no physical significance.

Several other authors, including Held and Suarez (1974), Su and Hsieh (1976), Ghil (1976), Drazin and Griffel (1977), North (1977) and Cahalan and North (1978), have established a general stability theorem applicable to a wide variety of specific models within the general class. The slope stability theorem states that

$$\frac{dx_s}{ds} > 0 \Longrightarrow \text{Stability},$$

$$\frac{dx_s}{ds} < 0 \Longrightarrow \text{Instability},$$

where x_s is the sine of the latitude of the ice-line.
The validity of this theorem for a large class of models is important, since it has implications for those branches of the solutions nearest to that corresponding to the present climate, viz. they are unstable and therefore unphysical. Their instability also explains why they were not located by the earlier approaches of Budyko, Sellers and Schneider and Gal-Chen.

One interesting point is that the slope stability theorem implies that if a cusp near $x_s = 1$ exists in a model solution (as, for example, in Figure 13) then small ice-caps are unstable. However the existence of such a cusp appears to depend very crucially on the details of the parametrizations adopted. Budyko-Sellers type models may be too simple to examine such a point This is unfortunate since whether small ice-caps are stable or not is an important issue if one recalls the concern over rising levels of CO_2 in the atmosphere and the possible effects of melting ice on the sea-level.

3.6 Further studies with Budyko-Sellers type models

The basic concept of the Budyko-Sellers type models has been extended and made more realistic and much more complicated in a great variety of ways. The comprehensive review by Schneider and Dickinson (1974) and the more recent reviews by North (1979), North et al (1980) and Hunt (1980) are recommended as sources for further study.

REFERENCES

Note: References which occur only in Figures or Tables are deemed to be of secondary interest and if required should be consulted in the papers of origin cited below.

Budyko, M.I.	1969	'The effect of solar radiation variations on the climate of the Earth', Tellus, 21, 611-619.
Cahalan, R.F. and North, G.R.	1978	'A stability theorem for energy-balance climate models', J. Atmos. Sci, 36, 1178-1188.
Drazin, P.G. and Griffel, D.H.	1977	'On the branching structure of diffusive climatological models', Ibid, 34, 1696-1706.
Faegre, A.	1972	'An intransitive model of the earth-atmosphere-ocean system', J. Appl. Meteorol., 11, 4-6.
Ghil, M.	1976	'Climate stability for a Sellers-type model', J. Atmos. Sci., 33, 3-20.
Held, I.M. and Suarez, M.J.	1974	'Simple albedo feedback models of the ice caps', Tellus, 26, 613-629.
Hunt, B.G.	1980	'Numerical modelling of climate', Aust. J. Phys., 33, 897-910.
Lorenz, E.N.	1968	'Climatic determinism', Meteorol,Monogr., 5, 1-3.
	1970	'Climatic change as a mathematical problem', J. Appl. Meteorol., 9, 325-329.
	1975	'Climate predictability', Report of the Intl. Study. Conf. on the Physical Basis of Climate and Climate Modelling, App. 2.1, 132-136, GARP Publications Series No. 16, WMO-ICSU.
Manabe, S. and Strickler, R.F.	1964	'Thermal equilibrium of the atmosphere with a convective adjustment', J. Atmos. Sci., 21, 361-385.
Manabe, S. and Wetherald, R.T.	1967	'Thermal equilibrium of the atmosphere with a given distribution of relative humidity' Ibid., 24, 241-259.
Mitchell, J.F.B.	1981	'The seasonal response of a general circulation model to changes in CO$_2$ and sea temperatures', Unpublished Met. Office Report, Met O 20 Tech Note No II/171.
North, G.R.	1975	'Analytical solution to a simple climate model with diffusive heat transport', J. Atmos. Sci., 32, 1301-1307.
	1977	'Analytical models of the earth's macroclimate', Proc. First. Intl. Conf. on Mathematical Modelling, Vol. IV, Univ. of Missouri, Rolla, Missouri, 2291-2302.

North, G.R. 1979 'Recent work on heat balance models', Report on the JOC Study Conference on Climate Models: Performance, Intercomparison and Sensitivity Studies, Vol II, 752-765, GARP Publications Series No 22, WMO-ICSU.

North, G.R., Cahalan, R.F and Coakley, J.A. 1980 'Energy-balance climate models', Washington, N.A.S.A., Tech. Memo. 82047.

Ramanathan, V. and Coakley, J.A. 1978 'Climate modelling through radiative-convective models', Rev. Geophys. Space Phys., 16, 465-489.

Schneider, S.H. and Dickinson, R.E. 1974 'Climate modelling', Ibid., 12, 447-493.

Schneider, S.H. and Gal-Chen, T. 1973 'Numerical experiments in climate stability', J. Geophys. Res., 78, 6182-6194.

Sellers, W.D. 1969 'A global climatic model based on the energy balance of the earth-atmosphere system', J. Appl. Meteorol., 8, 392-400.

Slingo, A. 1982 'Introduction and radiative heat balance', Lecture The General Circulation of the Atmosphere, Lecture Notes, Met O 20.

Su, C.H. and Hsien, D.Y. 1976 'Stability of the Budyko climate model', J. Atmos. Sci., 33, 2273-2275.

WMO 1979 World Climate Conference, A Conference of Experts on Climate and Mankind, Geneva, Feb 1979, WMO.

1980 Outline Plan and Basis for the World Climate Programme, 1980 - 1983, WMO - No. 540.

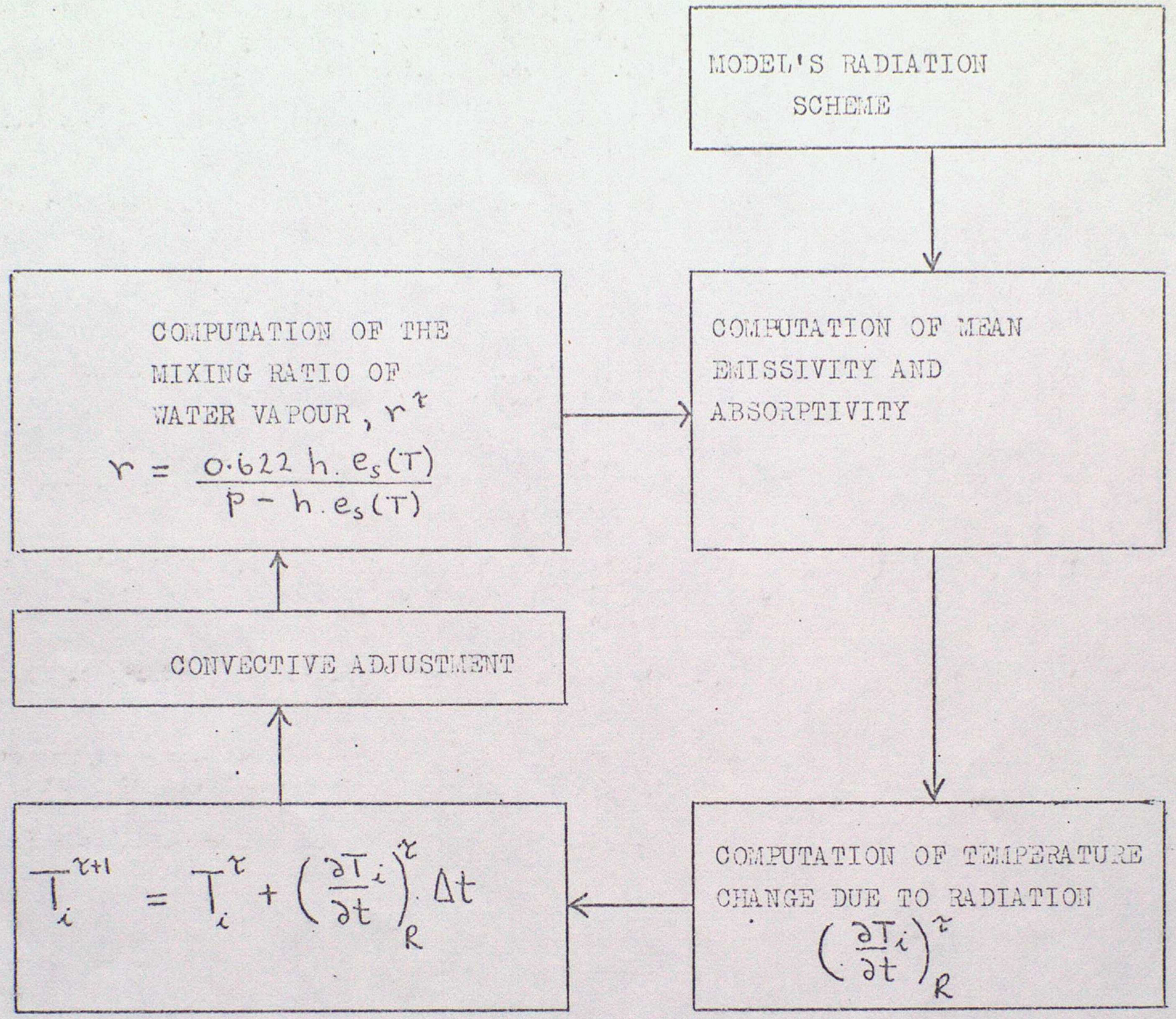
MODEL'S RADIATION SCHEME
COMPUTATION OF MEAN EMISSIVITY AND ABSORPTIVITY
COMPUTATION OF TEMPERATURE CHANGE DUE TO RADIATION $\left(\frac{\partial T_i}{\partial t}\right)_R^{\tau}$
$T_i^{\tau+1} = T_i^{\tau} + \left(\frac{\partial T_i}{\partial t}\right)_R^{\tau} \Delta t$
CONVECTIVE ADJUSTMENT
COMPUTATION OF THE MIXING RATIO OF WATER VAPOUR, r^{τ}
$r = \frac{0.622\, h.\, e_s(T)}{p - h.\, e_s(T)}$

Figure 1. Schematic representation of the iterative procedure used to obtain the state of radiative-convective equilibrium, as described by Manabe and Wetherald (1967). τ is the number of the time-step of the numerical integration. i is the index for the finite-differencing in the vertical.

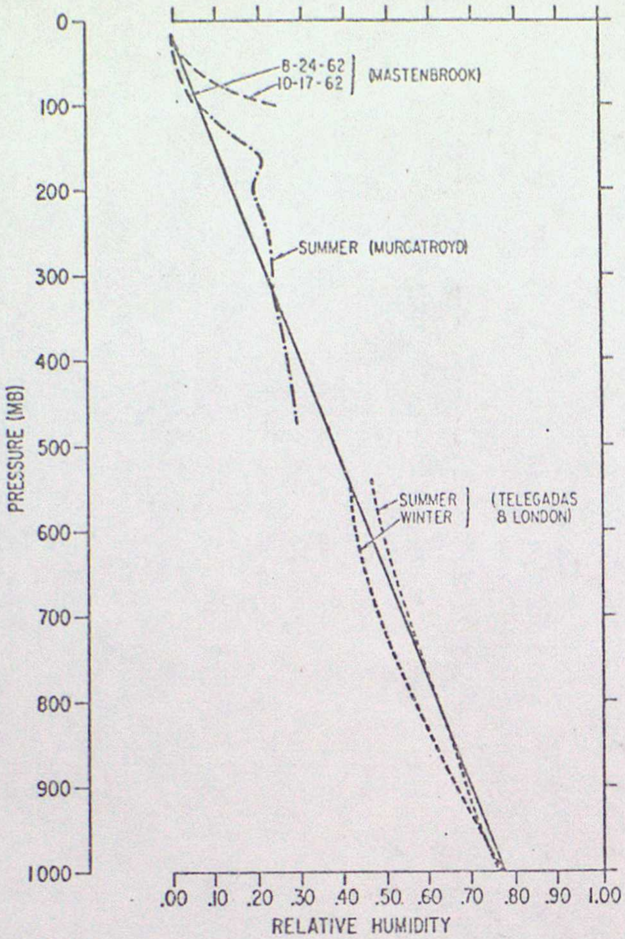

FIG. 2 Vertical distribution of relative humidity (Mastenbrook, 1963; Murgatroyd, 1960; Telegadas and London, 1954).

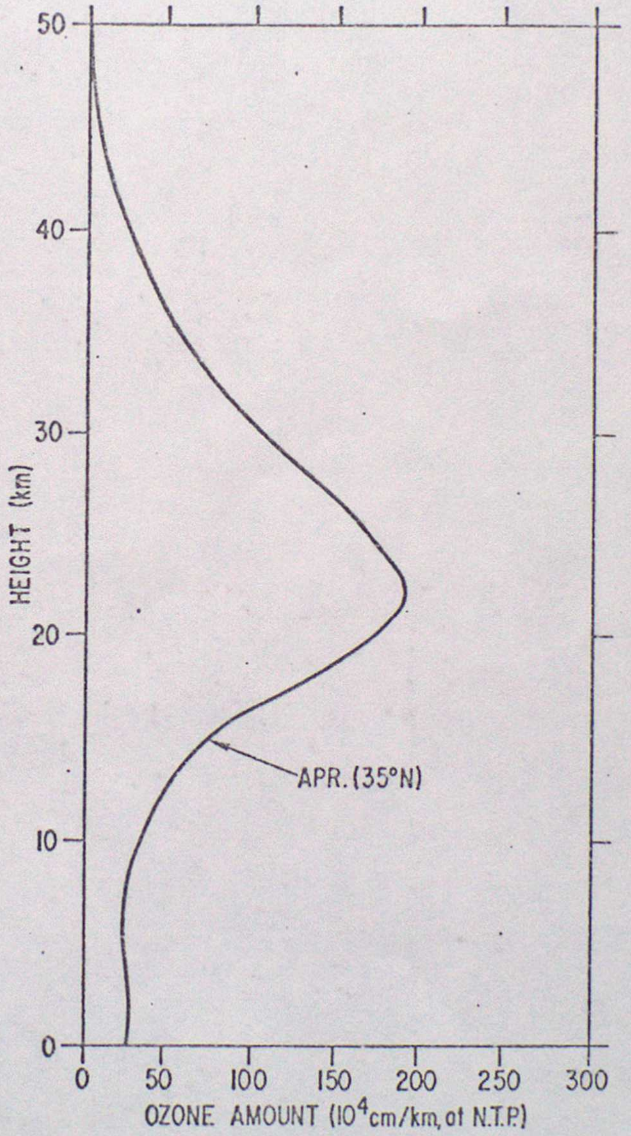

FIG. 3. Vertical distribution of ozone at 35N, April (Herring and Borden, 1965), normalized by the total amount from London (1962).

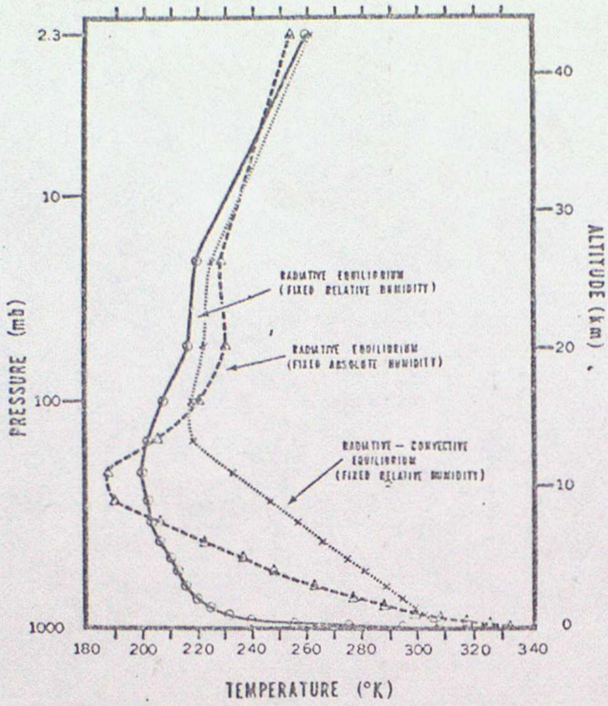

FIG. 4. Solid line, radiative equilibrium of the clear atmosphere with the given distribution of relative humidity; dashed line, radiative equilibrium of the clear atmosphere with the given distribution of absolute humidity; dotted line, radiative convective equilibrium of the atmosphere with the given distribution of relative humidity.

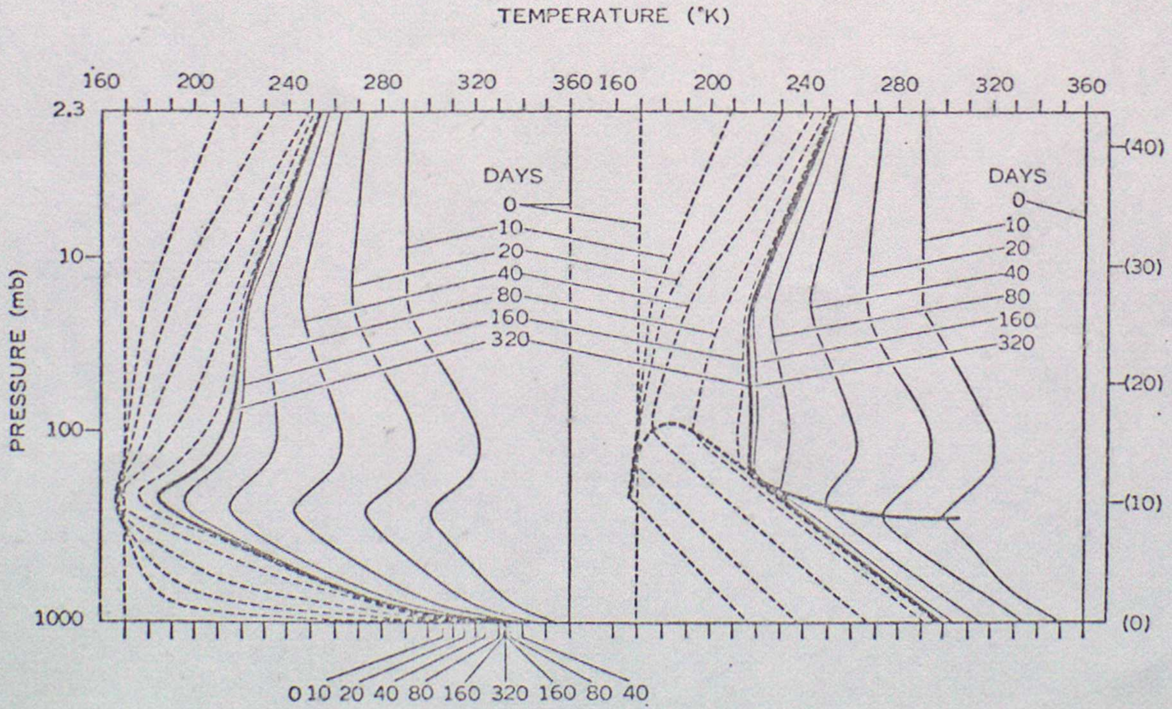

FIG. 5 The left and right hand sides of the figure, respectively, show the approach to states of pure radiative and thermal equilibrium. The solid and dashed lines show the approach from a warm and cold isothermal atmosphere.

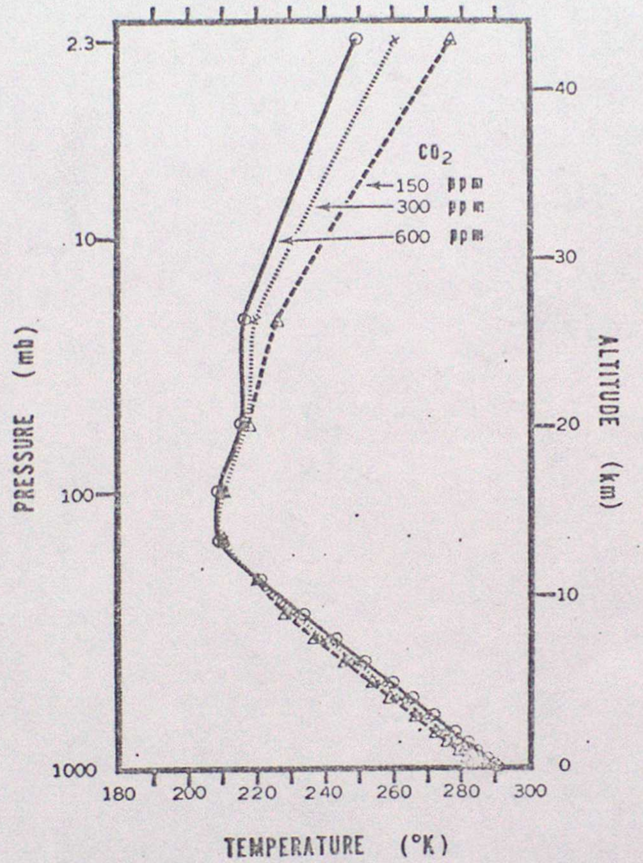

FIG. 6. Vertical distributions of temperature in radiative convective equilibrium for various values of CO_2 content.

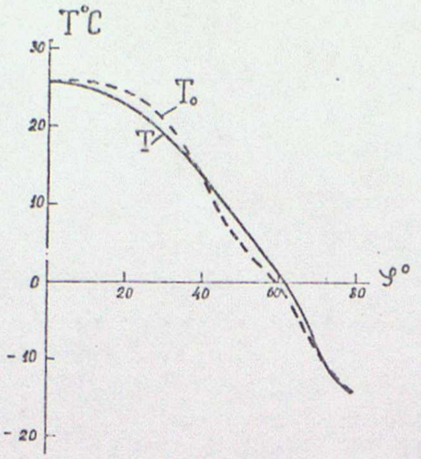

Fig. 7. The average latitudinal temperature distribution.

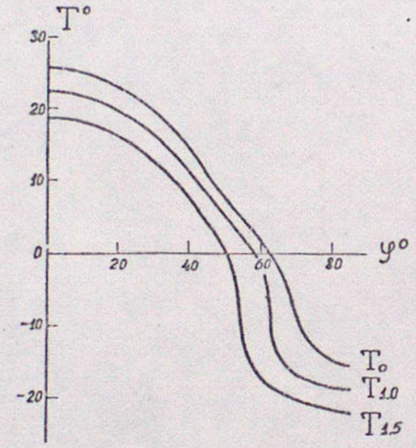

Fig. 8. The dependence of temperature distribution on radiation amount.

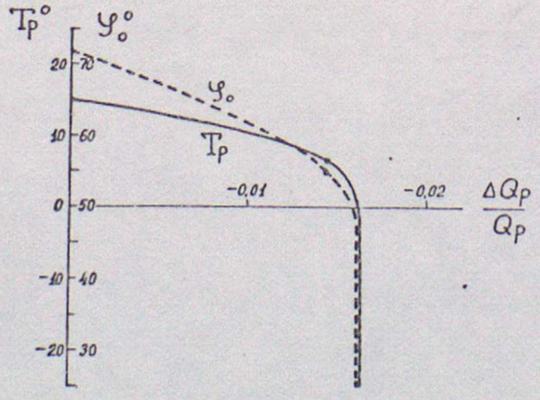

Fig. 9 The dependence of the Earth's temperature and ice cover boundary on radiation variations.

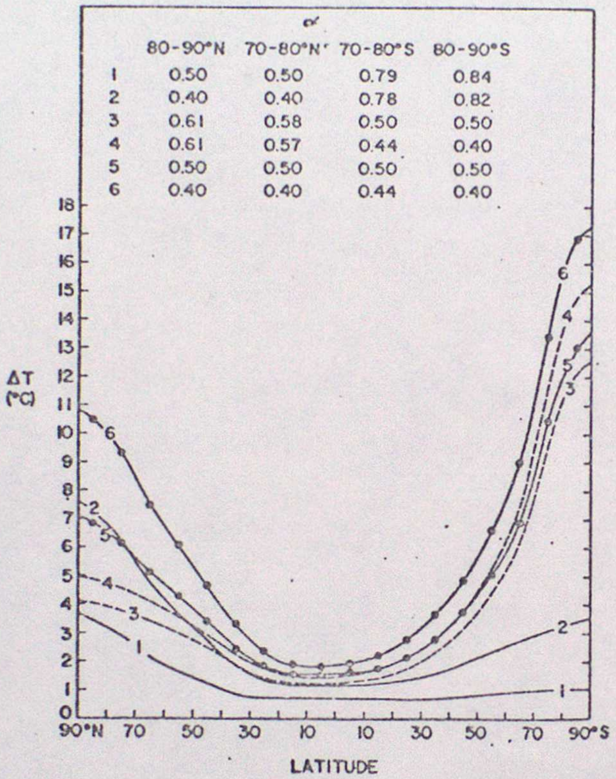

FIG. 10 Predicted latitudinal distribution of the mean annual temperature rise associated with albedo manipulation at one or both poles.

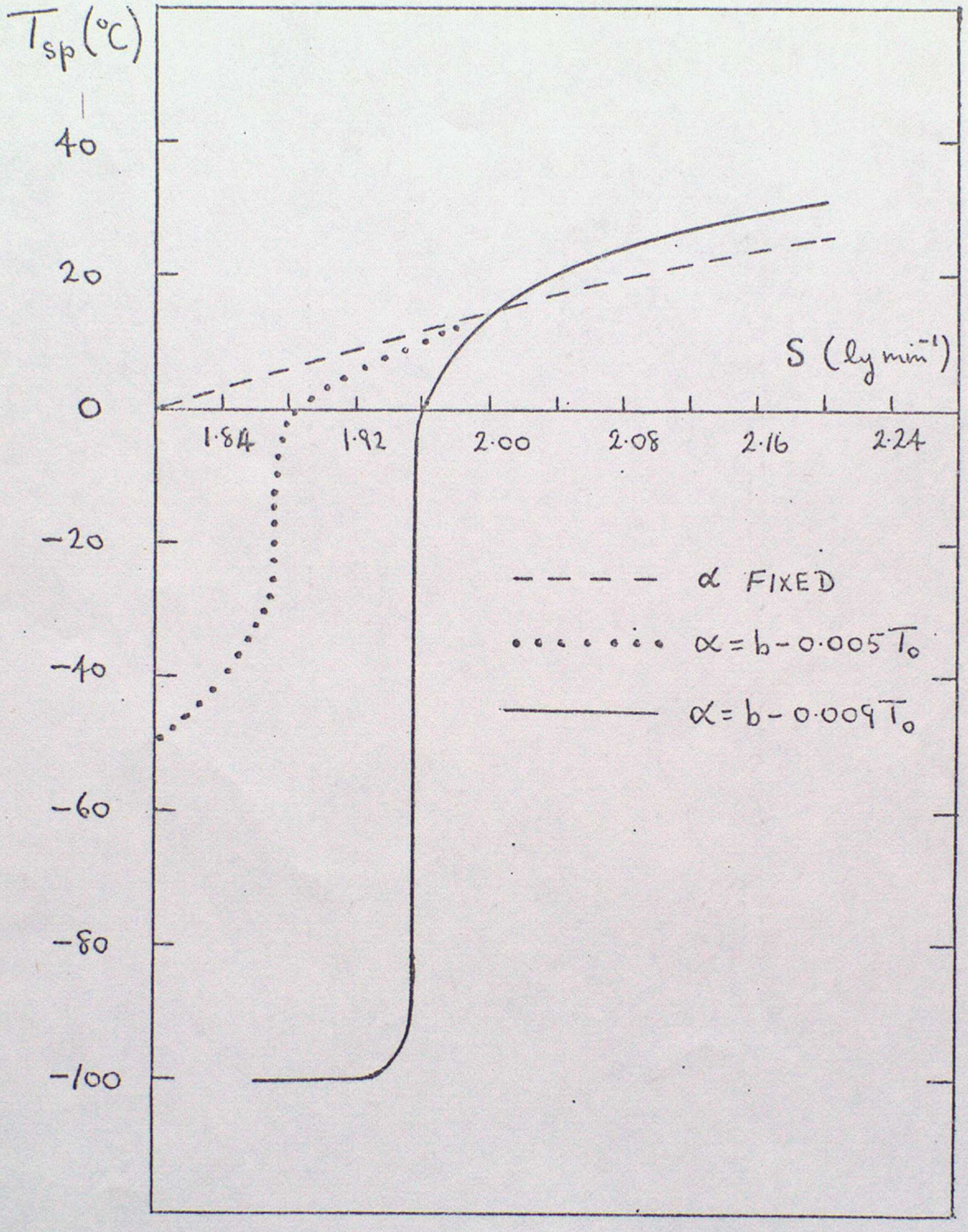

Fig. 11. The mean global sea level temperature, T_{sp}, as a function of the solar constant, S, for different specifications of the planetary albedo, α. This figure is based on the results of Sellers(1969).

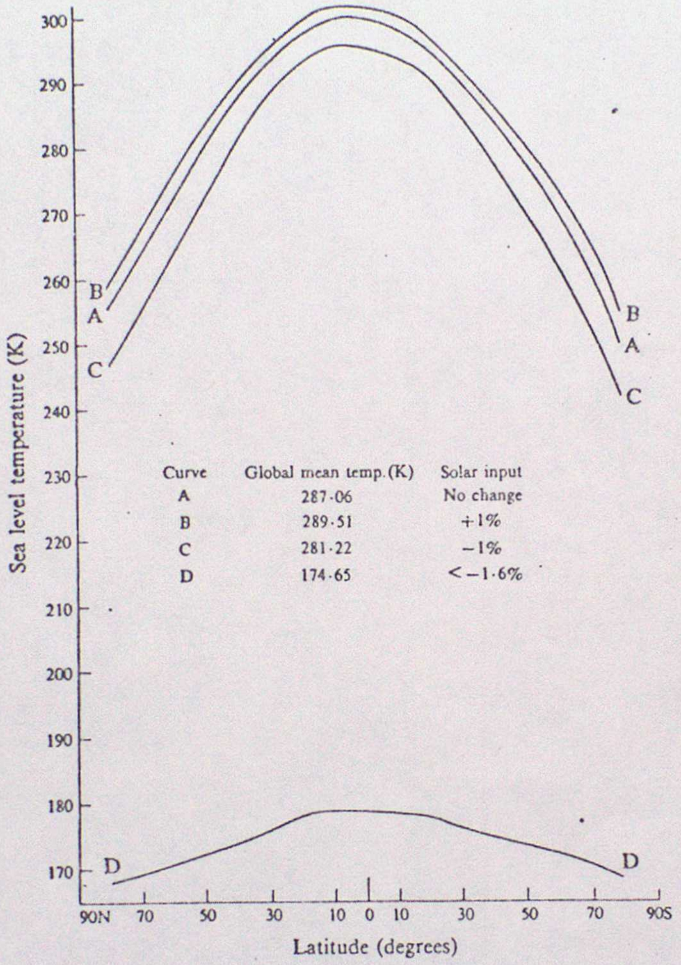

Curve	Global mean temp. (K)	Solar input
A	287·06	No change
B	289·51	+1%
C	281·22	−1%
D	174·65	< −1·6%

Fig. 12 Latitudinal temperature distribution calculated for various solar constant values. [From Schneider and Gal-Chen (1973).]

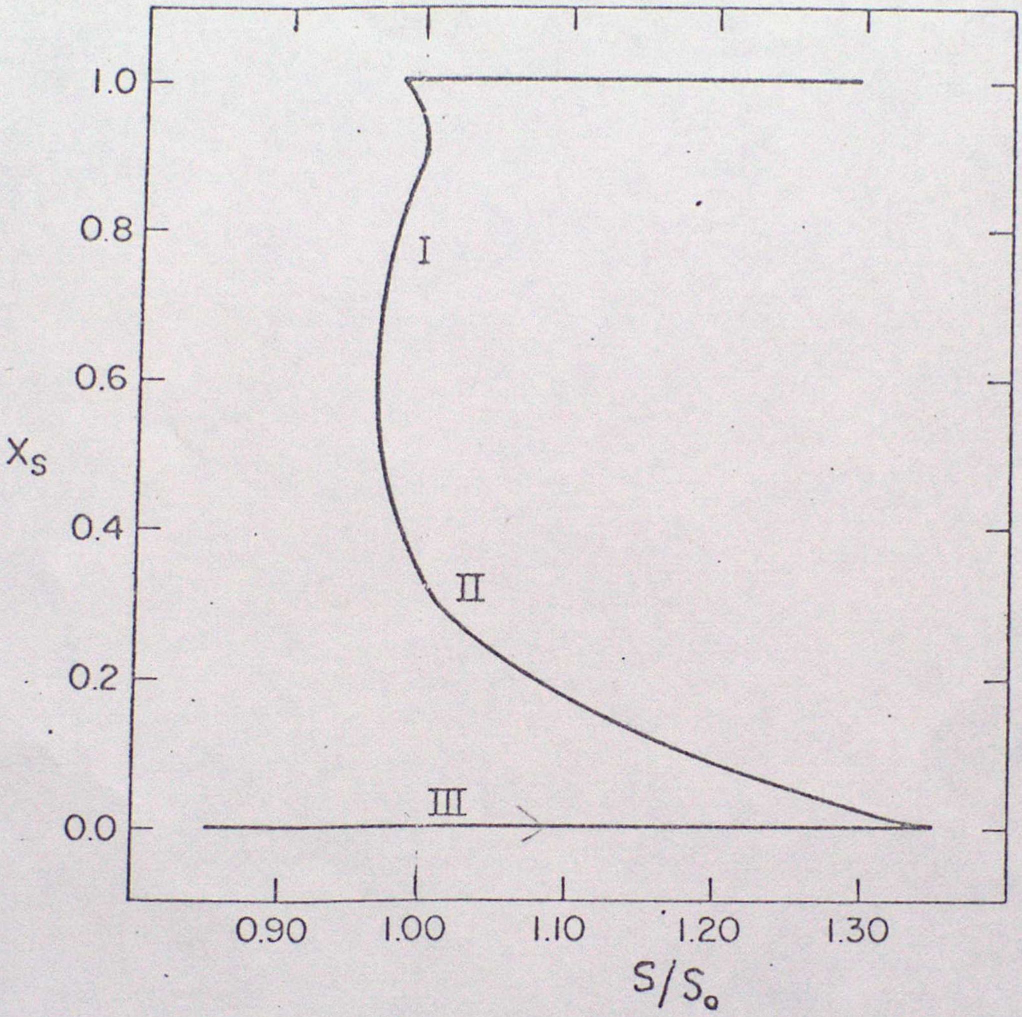

Fig. 13 A typical plot of the sine of the latitude of the ice line (X_S) versus the solar constant S/S_0 normalized to its present value. This curve is for an exact solution of a model with constant diffusion coefficient and discontinuous albedo at the ice line.

This figure is taken from North(1975).